Lucian-Constantin Ungureanu | Timo Hartmann (eds.)

EG-ICE 2020 Workshop on Intelligent Computing in Engineering

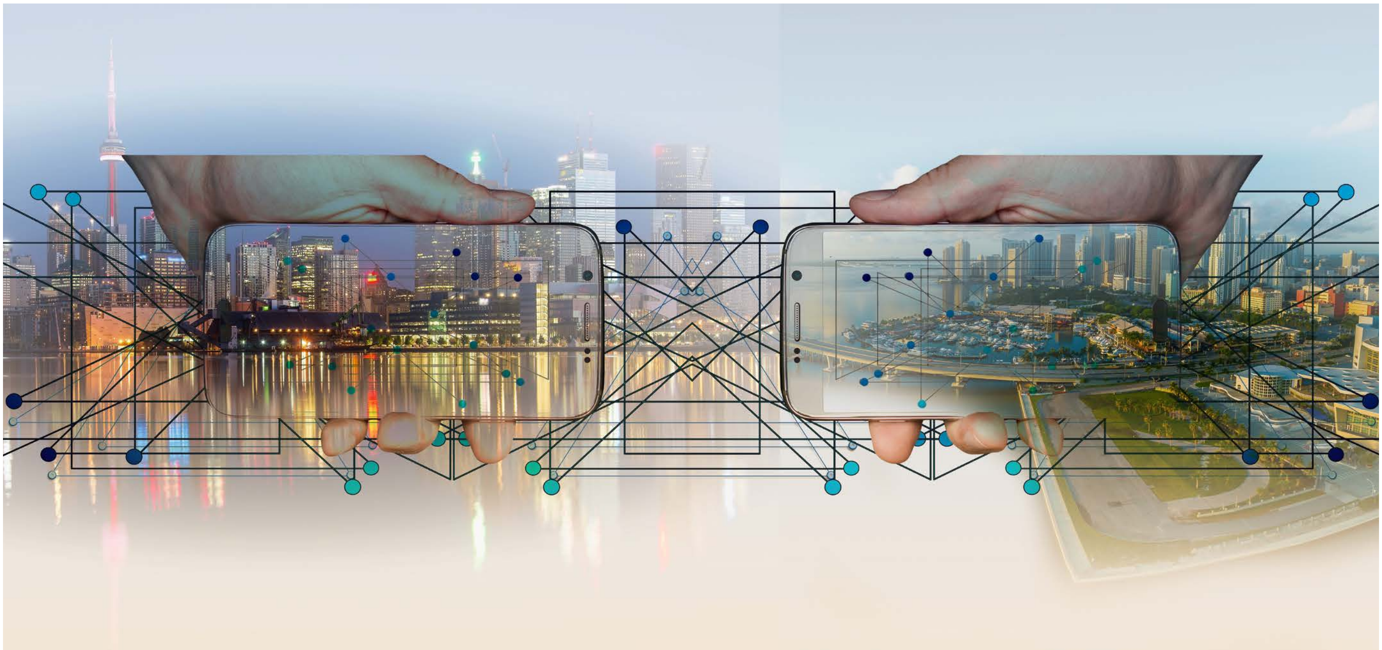

1st–4th July 2020, Online
Proceedings

Revised version

Universitätsverlag der TU Berlin

Technische Universität Berlin

Lucian Constantin Ungureanu, Timo Hartmann (eds.)
EG-ICE 2020 Proceedings

EG-ICE 2020 Proceedings:
Workshop on Intelligent Computing in Engineering

1st–4th July 2020, Online
Technische Universität Berlin

Editors:
Lucian Constantin Ungureanu
Timo Hartmann

Universitätsverlag der TU Berlin

Bibliographic information published by the Deutsche Nationalbibliothek
The Deutsche Nationalbibliothek lists this publication in the Deutsche Nationalbibliografie; detailed bibliographic data are available in the Internet at http://dnb.dnb.de/

Revised version. The paper "Modeling Geometry and Semantics of Physical Damages using IFC" by Mathias Artus and Christian Koch (pp. 144–153) has been removed for legal reasons.

Universitätsverlag der TU Berlin, 2023
http://verlag.tu-berlin.de

Fasanenstr. 88, 10623 Berlin
Tel.: +49 (0)30 314 76131

Cover image: geralt | https://pixabay.com/de/photos/stadt-panorama-smartphone-steuerung-3213676/ | Pixabay License | https://pixabay.com/de/service/license/

Layout/Typesetting: Lucian Constantin Ungureanu

Original version published as:
ISBN 978-3-7983-3155-6 (print)
ISBN 978-3-7983-3156-3 (online)

Revised version published online on the institutional repository of the Technische Universität Berlin:
DOI 10.14279/depositonce-19121
https://doi.org/10.14279/depositonce-19121

Preface

According to the report World Population Prospects 2019[1] published by the United Nations the world population will increase to 9.7 billion by 2050. This together with the increasing urban population, ageing workforce, increasing infrastructure demands, and the ageing built environment as well as increasing demands to meet the sustainability targets puts considerable pressure on the civil engineering field. In short, we have to do more with less. Current trends in computing and technologies allow us to approach these challenges from the perspective of computational support and automation, allowing today's and future's engineers to explore creative solutions with an increased speed and limited resources. Nevertheless, there are challenges when it comes to implementing such solutions.

The 27th EG-ICE International Workshop 2020 brings together international experts working at the interface between advanced computing and modern engineering challenges. Many engineering tasks require open-world resolutions to support multi-actor collaboration, coping with approximate models, providing effective engineer-computer interaction, search in multi-dimensional solution spaces, accommodating uncertainty, including specialist domain knowledge, performing sensor-data interpretation and dealing with incomplete knowledge. While results from computer science provide much initial support for resolution, adaptation is unavoidable and most importantly, feedback from addressing engineering challenges drives fundamental computer-science research. Competence and knowledge transfer goes both ways.

The papers included in this volume were presented at the 27th International Workshop on Intelligent Computing in Engineering of the European Group for Intelligent Computing in Engineering (eg-ice). What was originally planned as a face-to-face workshop meant to be held in Berlin, was quickly transformed into an online workshop due to Covid-19 pandemic. Nevertheless, while we only proposed the online format, all the thanks for making the workshop possible go to the authors of the accepted papers for embracing the proposed format and willing to disseminate their research results despite the unconventional format forced by the pandemic restrictions.

Moreover, we should not forget the tremendous effort made by reviewers on making possible the selection of the best papers for the presentation. We are grateful for their hard work on providing valuable and constructive feedback to the authors. We believe that the digital transformation, currently disrupting the architecture, engineering, construction, facility management, and operation of the built environment, can gain valuable insight from the scientific work published in this volume.

July, 2020

Lucian Constantin Ungureanu

Timo Hartmann

[1] Desa, U. N. (2019). World population prospects 2019: Highlights. New York (US): United Nations Department for Economic and Social Affairs.

Organization

Organizing Committee

Timo Hartmann (Workshop Chair)	Technische Universität Berlin, Germany
Lucian Constantin Ungureanu (Scientific Chair)	Technische Universität Berlin, Germany
Valentina Obradovic (Workshop Secretary)	Technische Universität Berlin, Germany

EG-ICE Committee

Pieter de Wilde (Chair)	University of Plymouth, UK
Philipp Geyer (Vice-chair)	Technische Universität Berlin, Germany
Timo Hartmann (Treasurer)	Technische Universität Berlin, Germany
Christian Koch (International representative)	Bauhaus-Universität Weimar, Germany
HaiJiang Li (Secretary)	Cardiff University, UK
Georg Suter (Auditor)	TU Wien, Austria
Jakob Beetz (Committee Member)	RWTH Aachen University, Germany
Bernd Domer (Committee Member)	University of Applied Sciences, HEPIA, Switzerland
Pieter Pauwels (Committee Member)	Eindhoven University of Technology, Netherlands
André Borrmann (Past Chair)	Technical University Munich, Germany
Ian Smith (EG-ICE Fellow)	Swiss Federal Institute of Technology, EPFL, Switzerland

Scientific Committee

Pieter de Wilde	University of Plymouth, UK
Philipp Geyer	Technische Universität Berlin, Germany
Timo Hartmann	Technische Universität Berlin, Germany
Christian Koch	Bauhaus-Universität Weimar, Germany
HaiJiang Li	Cardiff University, UK
Georg Suter	TU Wien, Austria
Jakob Beetz	RWTH Aachen University, Germany
Bernd Domer	University of Applied Sciences and Arts Western, Switzerland
André Borrmann	Technical University Munich, Germany

EG–ICE 2020 Programme

27th International Workshop on Intelligent Computing in Engineering

Wednesday, July 1st

Session 1.1	**Best Paper 2019** *Chair: Timo Hartmann*	page
10:00–10:20	**#93 – Felix Eickeler and André Borrmann** *Retracing Positions of Terrestrial Laser Scanners to Reinstate Legacy Point Clouds*	1–11

Session 1.2	**Monitoring and Control Algorithms in Engineering** *Chair: Timo Hartmann*	
10:20–10:30	**#29 – Yewei Ouyang, Chi Kwong Wong, and Xiaowei Luo** *Assessing Students' Hazard Identification Ability in Virtual Reality using Eye Tracking Devices*	12–21
10:30–10:40	**#24 – Jinjing Ke, Xiaowei Luo, and Hainan Chen** *Investigating Information Overload and Cognitive Correlation of Crane Operators*	22–32
10:40–11:00	*Discussions and Questions*	

Session 1.3	**Life-cycle design support** *Chair: Christian Koch*	
11:00–11:10	**#36 – Jimmy Abualdenien and André Borrmann** *Formal analysis and validation of Levels of Geometry (LOG) in building information models*	33–42
11:10–11:20	**#39 – Goran Sibenik, Iva Kovacic, and Valentinas Petrinas** *From physical to analytical models: automated geometry interpretations*	43–51
11:20–11:30	**#77 – Nan Zhu, Fangzheng Lin, Raimar Scherer, and Philipp Dohmen** *Underground Engineering Orientated Data Mapping from Construction Information Models to Structural Analysis*	52–61
11:30–11:50	*Discussions and Questions*	

* Access to this paper is blocked for legal reasons.

Session 2.3	***Advanced Computing in Engineering*** *Chair: Iva Kovacic*	
16:40–16:50	***#62 – Md Nazmus Sakib, Theodora Chaspari, Changbum R. Ahn and Amir Behzadan*** *An Experimental Study of Wearable Technology and Immersive Virtual Reality for Drone Operator Training*	154–163
16:50–17:00	***#74 – Zhengbo Zou, Suzana Duran Bernardes, Abdullah Kurkcu, Semiha Ergan, Kaan Ozbay*** *An Integrated Approach to Capture Construction Workers' Response towards Safety Alarms using Wearable Sensors and Virtual Reality*	164–174
17:00–17:10	***#37 – Sanaz Saeidi and Yimin Zhu*** *Exploring Thermally-Driven Occupant Behavioral Intention in Immersive Virtual Environment*	175–184
17:10–17:30	*Discussions and Questions*	

17:30–18:30	*Virtual Bar and Discussion Rooms*	

18:30-19:30	*EG-ICE board meeting (closed doors)*	

Thursday, July 2nd

Session 3.1	***BIM and Engineering Ontologies*** *Chair: Georg Suter*	
10:00–10:10	**#86 – Hui-Hsin Cheng and Shang-Hsien Hsieh** *A Design Evaluation Framework for Building Lifts Based on BIM and Pedestrian Simulation*	185–193
10:10–10:20	***#87 – Tarek Zaki, Abdelrahman Magdy and Khaled Nassar*** *BIM-Based Bill of Quantities Generator following POMI and NRM2 Methods of Measurement*	194–203
10:20–10:30	***#22 – Sophia Pibal and Iva Kovačić*** *Digital Design Workflow for an Algorithm Aided BIM Approach in Research Led Teaching*	204–214
10:30–10:50	*Discussions and Questions*	

Session 3.2	***Advanced Computing in Engineering*** *Chair: André Borrmann*	
10:50–11:00	***#42 – Beidi Li, John Fitzgerald and Carl Schultz*** *Modelling Co-presence in the Built Environment - a Spatio-temporal Approach to Human Perception and Movement*	215–225
11:00–11:10	***#92 – Slah Drira, Sai G.S. Pai and Ian Smith*** *Model-based multiple-occupant tracking through floor vibrations*	226–236
11:10–11:20	***#25 – Barbara Strug, Grażyna Ślusarczyk and Jakub Jas*** *Parameterized IFC-based Graph Generation for User-oriented Path Search*	237–242
11:20–11:40	*Discussions and Questions*	

Session 3.3	***Life-Cycle Design Support*** *Chair: Pieter de Wilde*	
11:40–11:50	***#65 – Manuel Jungmann, Christoph Bindal-Gutsche and Timo Hartmann*** *Developing a multi-criteria method to evaluate deep renovation options for buildings considering ecological, economic and socio-cultural factors over its lifecycle*	243–253
11:50–12:00	***#38 – Maarten Albert van Eldik, João Santos, Faridaddin Vahdatikhaki, Maarten Visser, Andre Dorée*** *BIM-based life cycle assessment framework for infrastructure design*	254–263
12:00–12:10	***#23 – Monica Pena Acosta, Faridaddin Vahdatikhaki, João Santos, Andries G. Dorée*** *A conceptual framework for more efficient simulation of the interplay between road pavements and the Urban Heat Island phenomenon*	264–274
12:10–12:30	*Discussions and Questions*	

12:30–14:00	*Break*	

14:00–15:00	*International discussions – sessions 1, 2, 3*	

Session 4.1	***Advanced Computing in Engineering*** *Chair: Ivan Mutis*	
15:00–15:10	***#47 – Ning Wang and Raja R. A. Issa*** *Natural Language Generation from Building Information Models for Intelligent NLP-based Information Extraction*	275–284
15:10–15:20	***#75 – Ruichuan Zhang and Nora El-Gohary*** *A Deep-Learning Method for Evaluating Semantically-Rich Building Code Annotations*	285–293
15:20–15:30	***#33 – Dion Moult and Thomas Krijnen*** *Compliance checking on building models with the Gherkin language and Continuous Integration*	294–303
15:30–15:50	*Discussions and Questions*	

Session 4.2	***BIM and Engineering Ontologies*** *Chair: Pieter Pauwels*	
15:50–16:00	***#28 – Christopher Rausch, Benjamin Sanchez, Chloe Edwards, and Carl Haas*** *A computational model for product cycling of modular buildings*	304–313
16:00–16:10	***#84 – Tan Tan, Grant Mills, Eleni Papadonikolaki, Weisheng Lu and Ke Chen*** *BIM-enabled Design for Manufacture and Assembly*	314–323
16:10–16:20	***#6 – Patricia Peralta Abadia, Sebastian Heine, Horst-Michael Ludwig and Kay Smarsly*** *A BIM-based approach towards additive manufacturing of concrete structures*	324–332
16:20–16:40	*Discussions and Questions*	

Session 4.3	***Advanced Computing in Engineering*** *Chair: Ian Smith*	
16:40–16:50	***#48 – Thomas Czerniawski, Jong Won Ma, and Fernanda Leite*** *Metadata-based photo filtering for facility management*	333–341
16:50–17:00	***#56 – Ying Shi, Zhe Sun, Wen Xiong, and Pingbo Tang*** *Automated Detection of Information Anomalies in Bridge Inspection Reports for Bridge Deterioration Prognosis*	342–351
17:00–17:10	***#80 – Linh Truong-Hong and Roderik Lindenbergh*** *Inspecting structural components of a construction project using laser scanning*	352–362
17:10–17:30	*Discussions and Questions*	

17:30–18:30	*Virtual Bar and Discussion Room*	

Friday, July 3rd

Session 5.1	***Life-Cycle Design Support*** *Chair: Heng Li*	
10:00–10:10	***#35 – Carl Schultz, Beidi Li, and Jochen Teizer*** *Towards a Unifying Domain Model of Construction Safety: SafeConDM*	363–372
10:10–10:20	***#4 – Tengxiang Su and Haijiang Li*** *Data exchange analysis for property valuation on sustainability perspective*	373–382
10:20–10:30	***#91 – Irem Dikmen and Timo Hartmann*** *Seeing the Risk Picture: Visualization of Project Risk Information*	383–392
10:30–10:50	*Discussions and Questions*	

Session 5.2	***BIM and Engineering Ontologies*** *Chair: Wolfgang Huhnt*	
10:50–11:00	***#60 – Tim-Jonathan Huyeng, Christian-Dominik Thiele, Anna Wagner, Meiling Shi, André Hoffmann, Wendelin Sprenger, Uwe Rüppel*** *An approach to process geometric and semantic information as open graph-based description using a microservice architecture on the example of structural data*	393–402
11:00–11:10	***#64 – Madhumitha Senthilvel, Jakob Beetz*** *A Visual Programming Approach for Validating Linked Building Data*	403–411
11:10–11:20	***#7 – Heinrich Söbke, Patricia Peralta Abadia, Dominik Heigener and Kay Smarsly*** *BIM-based sizing of reactors in processing facilities*	412–421
11:20–11:40	*Discussions and Questions*	

Session 5.3	***Advanced Computing in Engineering*** *Chair: Jakob Beetz*	
11:40–11:50	***#41 – Ana Sánchez-Rodríguez, Sebastian Esser, Jimmy Abualdenien, André Borrmann and Belén Riveiro*** *From point cloud to IFC: A masonry arch bridge case study*	422–431
11:50–12:00	***#15 – Enrico Romanschek, Christian Clemen and Wolfgang Huhnt*** *From Terrestrial Laser Scans to a Surface Model of a Building; Proof of Concept in 2D*	432–442
12:00–12:10	***#17 – Ashley Caselli, Vincenzo Daponte, Gilles Falquet and Claudine Métral*** *A Rule Language Model for Subsurface Data Refinement*	443–452
12:10–12:30	*Discussions and Questions*	

12:30–14:00	*Break*	

14:00–15:00	*EG–ICE assembly (open session)*	

Session 6.1	***Advanced Computing in Engineering*** *Chair: Carl Haas*	
15:00–15:10	***#53 – Makram Bou Hatoum and Hala Nassereddine*** *Developing a Framework for the Implementation of Robotics in Construction Enterprises*	453–462
15:10–15:20	***#66 – Leyuan Ma and Timo Hartmann*** *A Review of Wall-Climbing Robots: Technical Analysis and Potential for Indoor Building Inspection*	463–471
15:20–15:30	***#12 – Aiyu Zhu, Pieter Pauwels, and Bauke de Vries*** *Robot Construction Simulation using Deep Reinforcement Learning*	472–480
15:30–15:50	*Discussions and Questions*	

Session 6.2	***Monitoring and control algorithms in engineering*** *Chair: Fernanda Leite*	
15:50–16:00	***#43 – Yuan Zheng, Seppo Törmä and Olli Seppänen*** *An object-based conceptual model of the construction process for ICT-based situational awareness*	481–490
16:00–16:10	***#61 – David F. Bucher and Daniel M. Hall*** *Common Data Environment within the AEC Ecosystem: moving collaborative platforms beyond the open versus closed dichotomy*	490–500
16:10–16:20	***#55 – Mahmoud El Jazzar, Melanie Piskernik, Hala Nassereddine*** *Digital Twin in Construction: An Empirical Analysis*	500–510
16:20–16:40	*Discussions and Questions*	

17:30–18:30	*Virtual Bar and Discussions Room*	

Saturday, July 4th

13:00–14:00	*International discussions – sessions 4,5,6*	

14:00–15:00	*Best paper award and closing*	

Retracing Positions of Terrestrial Laser Scanners to Reinstate Legacy Point Clouds

Felix Eickeler, André Borrmann
Chair of Computational Modelling and Simulation
Technical University of Munich, Germany
felix.eickeler@tum.de

Abstract. Laser scanners provide a mostly geometric representation, but further details can be collected by analysing the recording setup. While the recording configuration is needed in post-processing, it is generally not passed on to the engineers as most scans are created by surveyors and handled by subcontractors. This disconnection between the consumer and the creator can be observed by the fact, that most laser scanned point clouds include intensity information. In day to day use, the intensity information serves as a substitute for colour as it provides contrasts between different objects in the recording. However, from the technical perspective the intensity is the result of the recording device interacting with the surface. This interaction should not be used for automation as different recording setups may result in different interactions and outcomes. Facing this problem, we propose a mechanism to enrich terrestrial laser scans by recreating original scan parameters and further converting the intensity to reflectivity - a sole property of the recorded surface.

1. Introduction

Modern workflows for urban redevelopment, redesign and construction in existing context are based on construction plans and surveys. While surveys do not provide design information or internal specifications, they capture the current state of the area and provide a unified representation. As full geometric models can be abstracted, recent survey techniques promote point clouds instead of control networks as a preferred way for data acquisition. These recordings provide high precision, accuracy and resolution and are a starting point for numerous investigations. Investigations, that can be performed before decisions on new designs need to be finalized. Exploring different variants and clearing issues early, can lead to more efficient building design and better-informed decisions. Ultimately, this results in cost and time savings.

While point clouds can be recorded with different devices, the current gold standard for precise measurements is the terrestrial laser scanner (*TLS*). Mobile laser scanner (*MLS*) have advantages in coverage and recording speed, but the recording complexity is much higher and precise control points are needed. A control network is an additional step with the recording complexity of a full *TLS* scan. With an increasing market for *TLS* surveys, the number of data formats and standards for encoding have prospered, making switches between software and vendors obnoxiously difficult. The interface between different contractors is often the reason for data loss in point clouds. If attributes are not requested and paid by the first contractor, later contractors will receive incomplete point clouds. In many recorded datasets, filters such as voxel grids, have been applied to reduce the load on systems and are steps in the post processing. Nonetheless, automatic remodeling and quality assessment tools might use all information to achieve the best possible results. Re-engineering of information may be of particular interest for the numerous buildings that were recorded in the past years. These legacy point clouds do not contain needed information as they were neither needed nor requested during the time.

The focus of this research are material properties of the underlying construction. Each material has a distinct reflection signature that can be partially measured by the laser scanner as it is encoded in the intensity (Allmen, 1987). With the correct positioning of the scanner, parts of the material properties can be estimated. However, as the positions of the scanners often are not encoded and lost after merging multiple scans to a single point cloud, the lack of scanning positions needs to be addressed first. Therefore, we will present our approach to recover *TLS* positions and assign all points to their source. In a second step, the reflectivity of the material is calculated. The developed algorithms are benchmarked using datasets consisting of artificial and real-world examples.

2. Related Work

2.1 Terrestrial Laser Scanner

Laser scanners illuminate a target with a concurrent beam and measure the time of flight to deduce the distance. *TLSs* consist of a mirror with two degrees of freedom that redirects the beam (see Figure 1), in different angles. The mirror tilts step by step providing an up-down-shift using primary axis φ and a rotation using the secondary axis θ. The resolution of the scanner relates to the number of positions of the mirror during the recording and can be described by defining the horizontal- and vertical line resolution. The resulting point pattern resembles ripples in water (see Figure 1).

The scanner is controlling the mirror with a fixed angular resolution. As a result, the point density decrease if an object is farther away. Aside from the distance measurement, determined by the speed of light, scanners usually record the signal strength known as intensity. Since *TLSs* record from fixed positions, obstructed elements are not recorded. This behaviour is similar to a point light source. To avoid shadows, multiple aligned scans are combined to a single dataset by using targets that are captured from multiple positions. Merging multiple scans blurs the radial density behaviour. Hot-spots occur close to the scanner pose and objects that are recorded by all scanners are represented with elevated density. New methods propose an adaptive scanning process, to generate a more even distribution based the recording distance (Li et al., 2019).

2.2 Intensity, Reflectivity & Accuracy

Merging multiple scans into a single point cloud has severe consequences for the intensity information. The intensity is mostly affected by the recording distance, the angle of incidence, and the reflectivity of the material. Therefore, intensity information can be considered a property of the recording vector rather than a property of the recorded point. The intensity is usually stored in dimensionless values that depend of the manufacturer of the scanner. Typical values are i $\in$\{[-1;1]; [0;1], [0;1024), (-2048; 2048)\}. The propagation of the signal strength can be described by the radar equation (Jelalian, 1992; Kaasalainen et al., 2011):

$$P_r = \underbrace{\frac{P_t D_r^2}{4\beta_t^2}}_{=constant} \frac{\sigma}{r^4} \tag{1}$$

where:

P_t is the transmitted,
P_r the received power.
D_r is the aperture of the scanner,
r the distance to the measured point,
σ the cross-section backscatter
$|\boldsymbol{p} - \boldsymbol{pos}|$ and β_t the width of the beam.

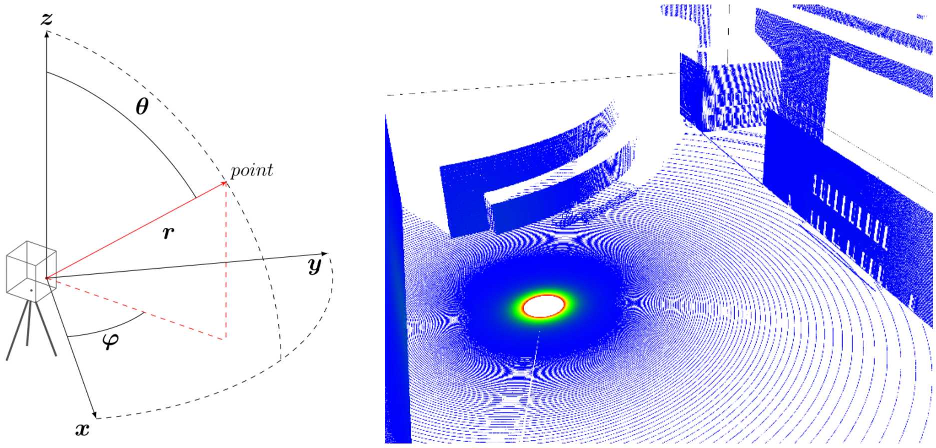

Figure 1: (**a**) **TLS System.** The scanner records in a spherical coordinate system. In post processing, all points are translated to global space. (**b**) **Simulation of a Laser Scan.** Colours reflect the density of the scan. With increasing distance, the distance between the horizontal and vertical lines is increasing (Bechtold and B. Höfle, 2016).

Under the assumption that the scan parameters were not changed during the scan, we can introduce a constant parameter c_{scan}. Since σ is proportional to the area πr^2 and the incident angle α, the relation can be simplified further:

$$\rho = \frac{r^2 P_r}{c_{scan} \cos(\alpha)} \tag{2}$$

The incident angle α can be determined using the surface normal and the recording angle. Based on different surface properties this simple model can be extended to include diffuse and specular reflections (Pfeifer et al., 2007). A benchmark of different reflection models was done by Bolkas (2019) who recommends the Torrance-Sparrow model in combination with the Trowbridge-Reitz distribution (Trowbridge and Reitz, 1975).

If the scanner position is known, such information can be leveraged for multiple applications: (1) Analysis of range precision (Pawłowicz, 2018; Schmitz et al., 2019); (2) Classification of materials(Voegtle, Schwab, and Landes, 2008); (3) Segmentation of point clouds (Bernhard Höfle and Pfeifer, 2007; Levashev, 2019); (4) Filtering & Compression (Eickeler and Borrmann, 2019; Han et al., 2017).

2.3 Edge Detection

Isolating and categorizing points is one of the major tasks in point cloud processing. In images, edges can be detected using the Sobel or Canny edge detection algorithms. For point clouds with a comparable row and column structure (e.g. depth maps), these algorithms have both been successfully implemented (Choi, Trevor, and Christensen, 2013). Known as organized points clouds, these image-like structures resemble the recording of sensors such as RGB-D cameras or single TLS frames.

If point clouds are sparse and randomly ordered, different approaches need to be taken (Hackel, Wegner, and Schindler, 2016; Weber, Hahmann, and Hagen, 2011). One of the main components of many contour detectors is the use of a principle component analysis and the resulting eigenvalues (λ_1, λ_2, λ_3).

2.4 Shape Detection in Point Clouds

Another important task is searching and identifying objects. Two general approaches are the Random Sample Consensus (RANSAC) and the Hough Transformation.

RANSAC. The algorithm is based on creating random subsets of points, fitting and testing them against a given model (Lazebnik, 2009; Strutz, 2016). If the deviation, usually root mean squared (RMS) error, is lower than our confidence interval the current set of samples are part of the identified model. Normally the consensus samples are retested and improved iteratively. Because the algorithm is evaluating many different combinations of points, it is known to be a robust and noise resistant method for identifying objects in images and point clouds.

Hough Transform. Another way of fitting a model into a set of samples is the Hough Transformation (*HT*) (Lazebnik, 2009). The underlying data is transformed to a Hough Domain, where each features of the model is parametrized and intersects in a single point. The intersection represents one set of correct parameters. The search space is dependent on the number of free parameters of the model. An example for a *HT* is shown in Figure 2.

For line detection usually the Hesse normal form is r = x cos θ + y sin θ and the search parameters is (Duda and Hart, 1972). The intersection of all considered points in the space indicate the parameters of a line. Multiple intersections indicate multiple lines, however the certainty of the line existence decreases as the “intersection to sample ratio” lowers.

During the implementation of the *HT*, the parameter space is discretized. Each sample in the dataset is mapped to the discrete parameter space and added to an accumulator. The accumulator can be thought of as bucket that collects votes on the discretized parameters. For each possible parameter, the model is evaluated and stored in that bucket. After processing all samples, the accumulator will have collected the most certain locations of the model occurring.

Ellipse Hough Transform. The concept of the *HT* can be used to identify circles and ellipses. For circles, the search space consists of 3 dimensions (*x, y, r*) hence the accumulator is also of 3 dimensions. This makes choosing the appropriate grid size complicated. One approach is separating the accumulator for each search parameter (Yuen, Princen, et al., 1989).

Extending the search to ellipses, the number of dimensions increases to 5 (Hassanein et al., 2015). Different approaches have been made to reduce the size of the accumulator. Yuen, Illingworth, and Kittler (1988) proposed a multi-stage approach, where the centre is identified independently

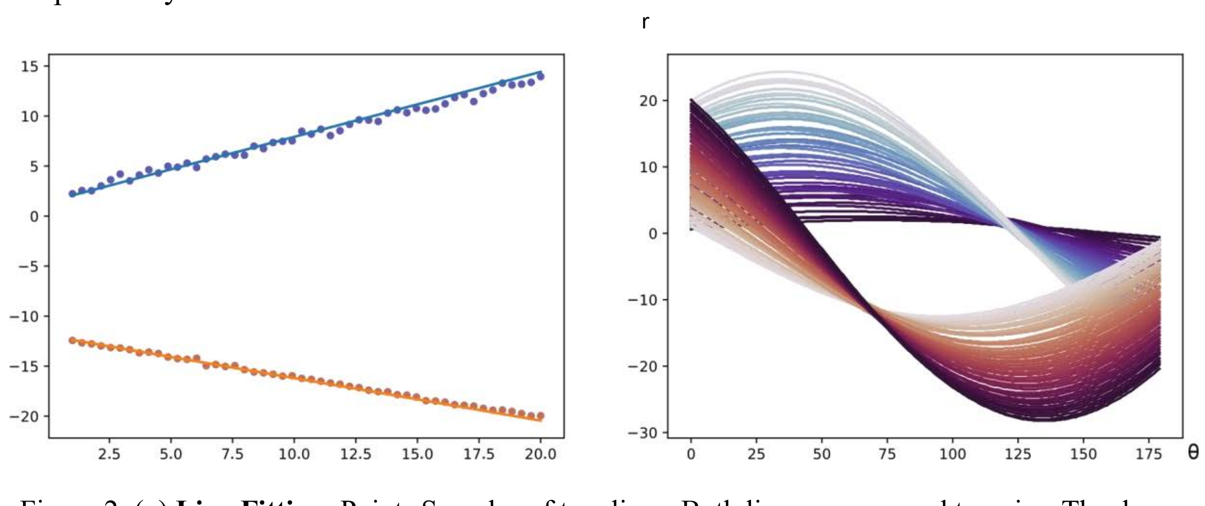

Figure 2: (**a**) **Line Fitting**: Points Samples of two lines. Both lines are exposed to noise. The drawn lines are the result of the Hough Transformation. (**b**) **Hough Space**: Each sample point votes on possible angles. The votes gather on two prominent line parameters (intersections).

from the remaining parameters. A more recent approach is the evaluation of point combinations to reduce dimensions. Similar to the RANSAC, the algorithm selects a subset of 3 samples to vote for possible ellipses. The accumulator is left to be purely 1-dimensional (Xie and Ji, 2012).

Hough Transformation in 3D. Some approaches have been made to adapt the *HT* into 3D space. One major concern is the isolation of points of interest. Some *HT* variants for plane and line detection in point clouds exists (Hulik et al., 2014; Khoshelham, 2007; Leeuwen, Coops, and Wulder, 2010; Rabbani and Heuvel, 2005). Generalized 3D curves on surfaces where detected by Torrente, Biasotti, and Falcidieno (2018). Most approaches use projections to handle the increasing complexity of 3D.

3. Methodology

Our approach to increase the value of a legacy laser scans consists of three main steps: (1) Detecting all *TLSs* recording positions; (2) Associate all points to their origin *TLS*; (3) Calculate the reflectivity with a chosen model (see Figure 3).

The only conditions posed upon the input data is that the points of the recordings where not affected by position altering filters (e.g. voxel grid).

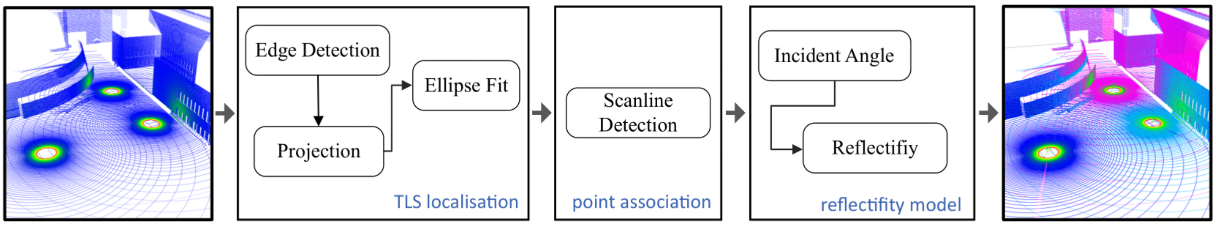

Figure 3: **Process of Enrichment.** The process starts with a non-destructive filtered point cloud. The main process is separated in three parts: Analyse, associate, calculate. First, we start the process by identifying contours of interest. We then project the reduced point cloud to the ground and find the centre of recording. In our second step we sort the points based on the recording centres and refine the search. Lastly, we enrich the data by calculating the reflectivity.

3.1 TLS Localization

The first stage of our analysis is the search for the recording positions. Each scanner has a minimal scanning angle θ_{min} where the tripod is located. In general, surveyors set up the scanner with a spirit level, which results in true horizontal and vertical scan lines. With these two boundary conditions the lowest scan line is typical circular shape on the ground. This circle has a high density due the low distance and is separable from other scan lines. Issues during detection of that circle will occur, if the soil has a gradient or is uneven. The projection of a circle on a sloped ground will form an ellipse. This is also true if the scanner was not set up correctly and the head is tilted.

Edge Detection. Since laser scans are very dense, we need to isolate characteristic shapes in the point cloud before running any parametrization. For effective filtering, a cascade of filters is applied on the second eigenvalue. Based on this eigenvalue evaluations the points with higher λ_2 are culled and outliers are removed based on the mean distance *SOR*. We then repeat this step until the change of the mean nearest neighbour radius falls under a specific threshold. This approach isolates edges with high densities and strong λ_2 such as the ellipses (see Figure 4).

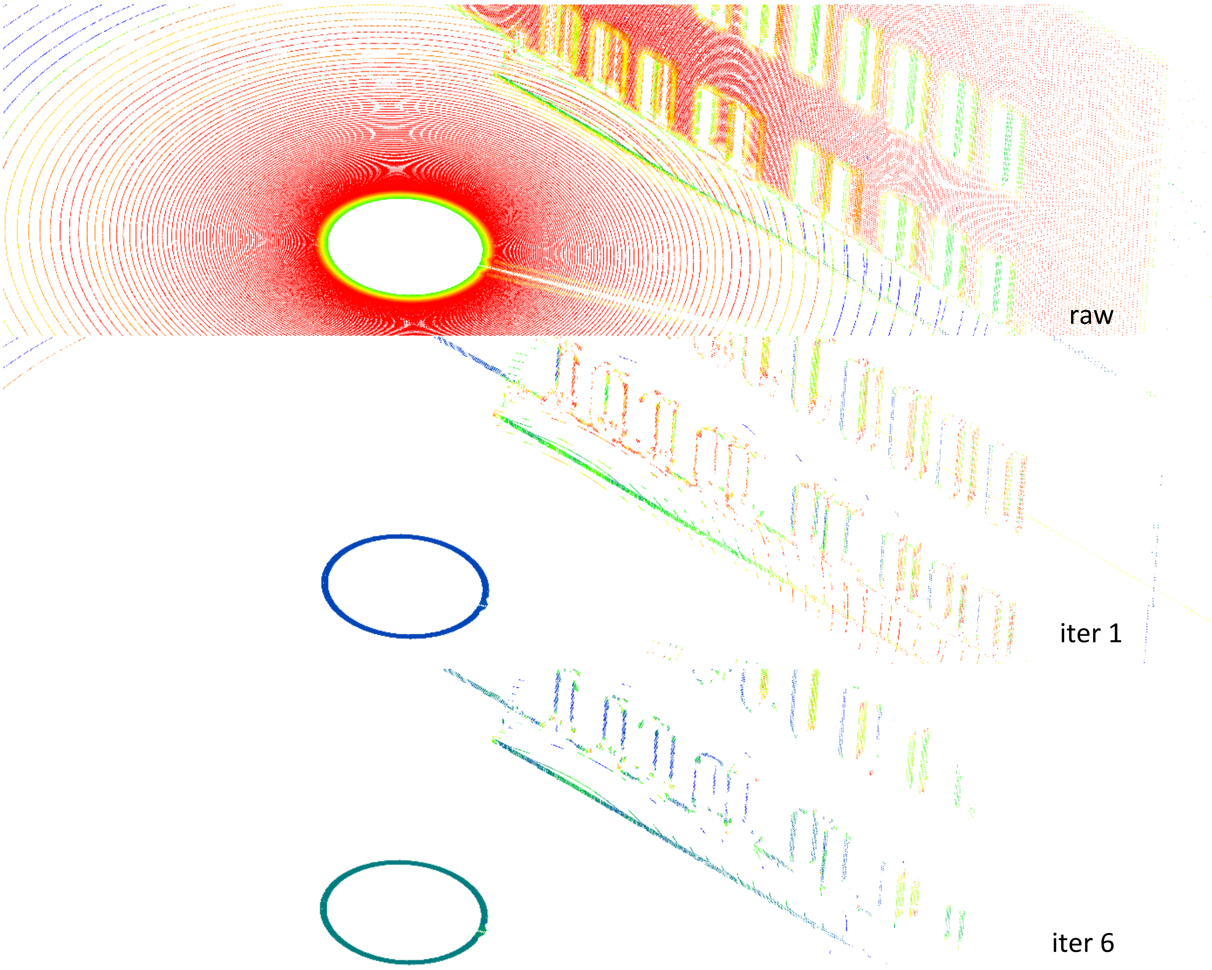

Figure 4: Edge Detection: Applied cascade of filters; |: λ_2 based filtering; outlier removal :|. The shown example is automatically executed and visualized with CloudCompare (CloudCompare, 2020).

Ellipse Hough Transform. After isolating the edges of possible ellipses, these points are projected to the XY-Plane e.g. the bottom of the bounding box. Following this projection, the 2D space is transferred to the Hough Space by applying an elliptic *HT*. We have chosen the *HT* over any RANSAC implementation as it promises a higher resistance to noise (Jacobs, Weiss, and Dolan, 2013). With multiple scan positions, the ground beneath the tripod is recorded by other scanners and exhibits varying densities.

After testing different approaches for ellipse detection, we decided to use the variant of Xie and Ji (2012) as it performed best in testing and was safe to implement. The chosen algorithm has a worst-case runtime behaviour of $O(n^3)$ and the discretization grid should be rather coarse. If a selected pair reaches the required votes, during calculation, all points belonging to this subset are removed from the global set, reducing the size of calculations for the next ellipse.

After all ellipses are identified, two things are verified: Are the recordings parallel to the XY-Plane and does the assumption hold that the Z-axis is aligned with the gravity vector. If both are correct, no further corrections are needed. If the XY-Plane is not parallel to the recording plane, the point cloud needs to be projected into the scanner's projected base. This base can be abstracted from the ellipse parameters. In contrast, if all recording planes are parallel to each other but not to the XY-Plane of the scan, we assume to have a non-aligned system. This system can be transformed into a common recording system using any scanners elliptic shape.

Ellipse Refinement. Good performing *TLS* work with trifling angles increments for θ and φ, resulting in small differences between the recorded vertical and horizontal lines. The centre of the ellipse is only as accurate as the discretization of the search space, and cannot be considered accurate enough. Hence refinement is needed. After identifying the *TLS* pose and the ellipse parameters, the original point cloud is transformed into the scanners system (only if needed) and projected to the XY-Plane (2D projection). For each scanner, a grid of 7x7 is placed around the identified centre (see Figure 5) and lines are identified with a secondary Hough Transform. This times the search is performed with a sufficient big sample size (we used 10 000 points) and has limited search space as the only unknown parameter is the position in the grid. This process of refinement is repeated multiple times with a bisected grid size and increasing minimal distance of the samples. This refinement is repeated until the voting will not determine a clear winner among the grid candidates. The grid cell selected from the previous iteration is considered the most probable TLS location.

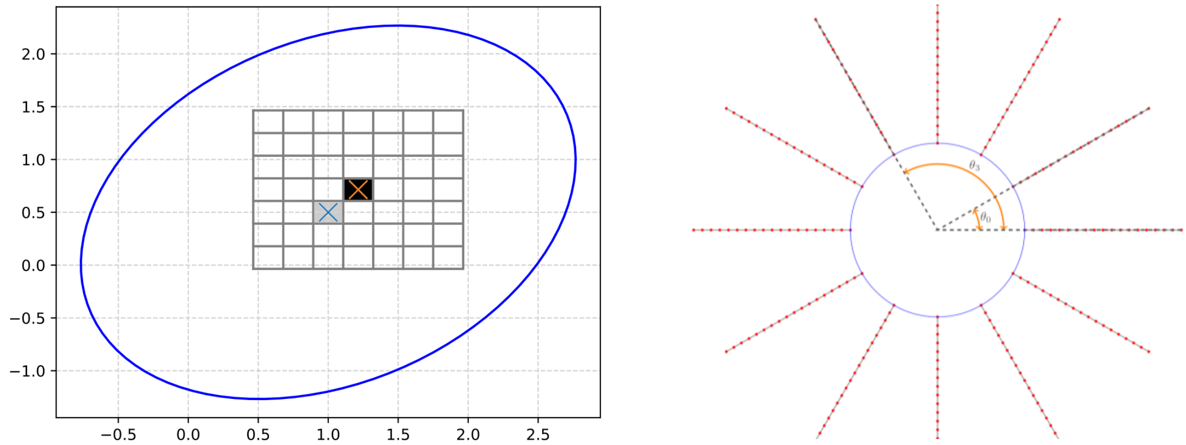

Figure 5: (**a**) **Refinement**: The initial location is selected based on the elliptic Hough Transform (orange & black). A grid is placed for further refinement. After refinement, the new centre is selected (blue & grey). This process is repeated on finer grid until no grid cell has the majority of votes. (**b**) **Point Association.** Each point is part of a vertical scan line. All angles are evaluated, and the greatest common divisor is selected.

3.2 Point Assignment

The assignment of points to a scanner is straight forward. The vector of the scan centre to the point is formed and vectors with similar angles φ are detected. If enough points are found, they are assigned to the current scanner. To speed up the process we use a polar grid. After all points have been assigned to a *TLS* position, the θ is used to identify singularities. For each point φ and θ are unique and representative. Furthermore, the greatest common divisor should be the scanners parameter $\Delta\varphi$.

The greatest common divisor is calculated in steps of .05 °. We calculate and collect φ for all points and analyse the separated sets (see Figure 5). Under the assumption that scanners increment with constant steps size, we check the value with a confidence interval. The line is constructed as:

$$\varphi = \Delta\varphi x - \min(\varphi) \tag{1}$$

where x is the array of steps taken.

If points exceed the confidence interval, they are removed from the current scanner. We end up with 3 classes of points: assigned, wrongly assigned, unclassified. Wrongly classified points can be retested to fit into other *TLS* poses. Unclassified points are recording glitches reflecting wrong positions. These points could be reclassified using intensity similarities between their nearest neighbours of different scanners. However, the measurement is not to be trusted.

3.3 Reflectivity Model

As a follow-up to the point assignment, we can calculate the reflectivity. We use the model described in Equation 2. We are creating normals by evaluating patches formed by the nearest neighbours. If the scanners use negative intensity values, the range is shifted to the positive range. Since we cannot estimate P_r from the point cloud data alone, we are left with two possible options: (1) Use the intensity values which will result in a corrected but non-normalized scan; (2) Use surface with known reflectivity values such as targets to calibrate.

4. Results

For verification we use artificial and real-world data: (1) The artificial data was created with Helios applied on an inner city 3D model (Bechtold and B. Höfle, 2016). The simulation resulted in two sets, featuring a one and a three *TLS* position survey. The materials were not defined, resulting in no useful intensity information. The resulting circles of the scanners were close to 5m in diameter. (2) The real-world test data is snipped of an ongoing construction site which was recorded with a Leica HDS6100 in 2018. The construction site featured overall 8 positions where 3 are in possible range of the selected area. The dataset consists of the properties *x, y, z, i* and was exported from Leica's Cyclone. During the recording, some equipment was moved and was only recorded by a single scan pose. The measured major axis was 1.3m.

4.1 TLS Detection

To benchmark our *TLS* detection, we measured the performance of each step individually. We were able to isolate the scanner ellipses in all data sets. For the artificial set, the contour search is visualized in the animation Figure 4). The filtering was concluded after 10 iterations for the single scanner, 12 for the three scanner and only 7 for the real dataset. However, the number of points was reduced to 2.5 % for the artificial data and <1% for the real-world data (see Figure 6. The difference is due the different density settings of the scanner, and the fixed number of nearest neighbours considered by the outlier filter.

Despite our effective isolation of the edge detection, the calculation is intensive. Both of our test datasets provide close to perfect circular shapes, which simplified the process as there was no need for further transformations. The results of the ellipse fit can be seen in Table 1. The centre

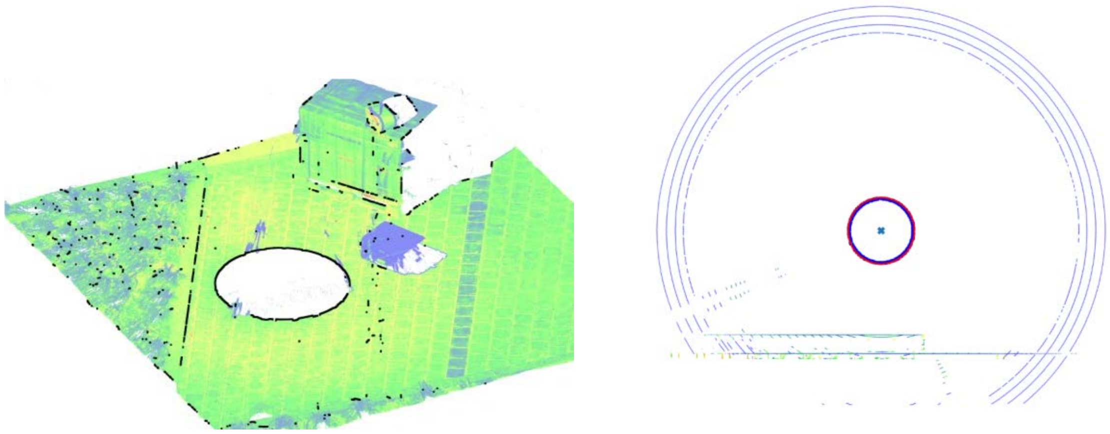

Figure 6: **(a) Contour Isolation.** The contours are overlaid (black) to the original real-world point cloud. Aside from the ellipse, only the edge to the cobbles is remaining. **(b) TLS Ellipse Fit**. The image shows the birds-eye view on the reduced point cloud in Figure 4. The ellipse was fitted, and the scanner position determined (green). The ellipse formed a perfect circle (red).

Table 1: **Initial Ellipse Fit.** For the real-world data, the points are measured with manual accuracy.

Scanner	**original [m]**		**detected [m]**		$\Delta x[mm]$	$\Delta y[mm]$	$\Delta rms[mm]$
1	14.17	-9.57	14.14	-9.57	26	4	26.3
2	8.95	23.14	8.93	23.12	20	16	25.6
3	42.22	-6.92	42.21	-6.93	6	5	7.8
real	51.09	48.06	50.11	48.08	23	19	29.8

of the scanner could be determined with very good accuracy for our artificial dataset as the initial ellipse fit provided an accuracy <27mm.

4.2 Point Assignment & Reflectivity model

As the noise levels in the artificial dataset are low compared to the real-world example, we were able to assign all points with high confidence. Due the order or processing and the real-world thresholds, few point were assigned to the wrong scanner. The reflectivity was calculated and within expected margins of the standard material. However, it showed outliers at the edges of the dataset. We assume this is due to the low-density settings of the dataset, introducing artefacts in the surface normals. For the real-world dataset, the calculations are still ongoing and will be presented at the conference.

5. Conclusion & Outlook

This paper combined specific Edge Filtering, Hough Transforms, Refinement Search and statistical methods to iteratively retrace the original recording positions. The *TLS* postilions were localized with good accuracy and further scan parameters, such as the line resolution and the recording angles, could be derived. With the reacquired meta-information, we assigned each point to the origin, which enabled further processing on secondary properties. As a showcase, we implemented a simple reflectivity model and were able to re-evaluate the intensity and resolve the dependency between the recording setup and the point cloud: The scan intensities were renormalized and transformed to position independent values. We further showed that the given approach is suited for the revaluation of legacy laser scans. The newly obtained information can be used to improve filtering, segmentation, and general point cloud processing.

Additionally, to our findings, the concept should be extended with an advanced reflectivity model and a smart classification scheme for materials and surfaces. Material estimations are desired to improve Scan2Bim applications, and filtering. Extending this topic further, the inclusion of colour into the material classifiers will merge another layer of information.

Considering the presented approach, we want to mention that further datasets should be evaluated and benchmarked. Additionally, the evaluation of shading angles and a stochastic surface segmentation model should be implemented. This model may be used to identify fine grained contours and could also be used to re-evaluate outliers. This would create a closed loop system for analysis and increase the robustness compared to the current isolated approach.

References

Allmen, Martin von (1987). "Laser-Beam Interactions with Materials". Springer Berlin Heidelberg. DOI:10.1007/978-3-642-97007-8. URL: https://doi.org/10.1007%2F978-3-642-97007-8.

Bechtold, S. and B. Höfle (2016). "HELIOS: A Multi-Purpose LiDAR Simulation Framework for Research, Planning and Training of Laser Scanning Operations with Airborne, Ground-Based Mobile and Stationary Platforms". In: *ISPRS Annals of Photogrammetry, Remote Sensing and Spatial Information Sciences* III-3, pp. 161–168. DOI: 10.5194/isprs-annals-III-3-161-2016.

Bolkas, D. (2019). "Terrestrial laser scanner intensity correction for the incidence angle effect on surfaces with different colours and sheens". In: *International Journal of Remote Sensing* 40.18, pp. 7169–7189. DOI:10.1080/01431161.2019.1601283.

Choi, Changhyun, Alexander J. B. Trevor, and Henrik I. Christensen (Nov. 2013). "RGB-D edge detection and edge-based registration". In: *2013 IEEE/RSJ International Conference on Intelligent Robots and Systems*. IEEE. DOI: 10.1109/iros.2013.6696558.

CloudCompare (2020). *GPL software*. Version 2.11 alpha. URL: https://www.cloudcompare.org.

Duda, Richard O. and Peter E. Hart (Jan. 1972). "Use of the Hough transformation to detect lines and curves in pictures". In: *Communications of the ACM* 15.1, pp. 11–15. DOI: 10.1145/361237.361242.

Eickeler, Felix and André Borrmann (2019). "Adaptive feature-conserving compression for large scale point clouds". In: *Proc. of the 26th EG-ICE Workshop on Intelligent Computing in Engineering*. Leuven, Belgium.

Hackel, Timo, Jan D. Wegner, and Konrad Schindler (June 2016). "Contour Detection in Unstructured 3D Point Clouds". In: *2016 IEEE Conference on Computer Vision and Pattern Recognition (CVPR)*. IEEE. DOI:10.1109/cvpr.2016.178.

Han, Xian-Feng et al. (Sept. 2017). "A review of algorithms for filtering the 3D point cloud". In: Signal Processing: *Image Communication* 57, pp. 103–112. DOI: 10.1016/j.image.2017.05.009.

Hassanein, Allam Shehata et al. (2015). "A survey on Hough transform, theory, techniques and applications". In: *arXiv preprint arXiv:1502.02160*.

Höfle, Bernhard and Norbert Pfeifer (2007). "Correction of laser scanning intensity data: Data and model-driven approaches". In: *ISPRS Journal of Photogrammetry and Remote Sensing* 62.6, pp. 415–433. DOI: 10.1016/j. isprsjprs.2007.05.008.

Hulik, Rostislav et al. (Jan. 2014). "Continuous plane detection in point-cloud data based on 3D Hough Transform". In: *Journal of Visual Communication and Image Representation* 25.1. DOI:10.1016/j.jvcir.2013.04.001.

Jacobs, Lucas, John Weiss, and Dan Dolan (May 2013). "Object tracking in noisy radar data: Comparison of Hough transform and RANSAC". In: *IEEE International Conference on Electro-Information Technology , EIT 2013*. IEEE. DOI: 10.1109/eit.2013.6632715.

Jelalian, A.V. (1992). Laser Radar Systems. Artech House radar library. Artech House. ISBN: 9780890065549.

Kaasalainen, Sanna et al. (2011). "Analysis of Incidence Angle and Distance Effects on Terrestrial Laser Scanner Intensity: Search for Correction Methods". In: *Remote Sensing* 3.10, pp. 2207–2221. DOI: 10.3390/rs3102207.

Khoshelham, K. (2007). “Extending generalized hough transform to detect 3D objects in laser range data”. In: *Proceedings of the ISPRS workshop Laser Scanning 2007 and Silvi Lasser 2007, Espoo, Finland, 12-14 September 2007*. International Society for Photogrammetry and Remote Sensing (ISPRS), pp. 206–210.

Lazebnik, Svetlana (2009). *Lecture notes in Computer Vision (COMP 776)*.

Leeuwen, Martin Van, Nicholas C. Coops, and Michael A. Wulder (2010). “Canopy surface reconstruction from a LiDAR point cloud using Hough transform”. In: *Remote Sensing Letters* 1.3, pp. 125–132. DOI:10.1080/01431161003649339.

Levashev, S. P. (2019). “Segmentation of a Point Cloud by Data on Laser Scanning Intensities”. In: *Pattern Recognition and Image Analysis* 29.1, pp. 144–155. DOI: 10.1134/s1054661819010152.

Li, Qinghua et al. (2019). “Towards Uniform Point Density: Evaluation of an Adaptive Terrestrial Laser Scanner”. In: *Remote Sensing* 11.7, p. 880. DOI: 10.3390/rs11070880.

Pawłowicz, Joanna A. (2018). “Impact of physical properties of different materials on the quality of data obtained by means of 3d laser scanning”. In: *Materials Today: Proceedings* 5.1, p. 1997. DOI 10.1016/j.matpr.2017.11.304.

Pfeifer, Norbert et al. (Jan. 2007). “Investigating terrestrial laser scanning intensity data: quality and functional relations”. In: *8th Conference on Optical 3-D Measurement Techniques*.

Rabbani, Tahir and Frank Heuvel (Jan. 2005). “Efficient Hough transform for automatic detection of cylinders in point clouds”. In: *Proceedings of the ISPRS workshop Laser Scanning 2005*. Vol. 36. International Society for Photogrammetry and Remote Sensing (ISPRS).

Schmitz, Berit et al. (2019). “How to Efficiently Determine the Range Precision of 3D Terrestrial Laser Scanners”. In: *Sensors* 19.6, p. 1466. DOI: 10.3390/s19061466.

Strutz, Tilo (2016). “Data Fitting and Uncertainty”. Springer Fachmedien Wiesbaden. DOI: 10.1007/978-3-658-11456.

Torrente, Maria-Laura, Silvia Biasotti, and Bianca Falcidieno (Jan. 2018). “Recognition of feature curves on 3D shapes using an algebraic approach to Hough transforms”. In: Pattern Recognition 73, pp. 111–130. DOI:10.1016/j.patcog.2017.08.008.

Trowbridge, T. S. and K. P. Reitz (May 1975). “Average irregularity representation of a rough surface for ray reflection”. In: *Journal of the Optical Society of America* 65.5, p. 531. DOI: 10.1364/josa.65.000531. Voegtle, T, I Schwab, and T Landes (2008). “Influences of different materials on the measurements of a terrestrial laser scanner (TLS)”. In: 37, pp. 1061–1066.

Weber, Christopher, Stefanie Hahmann, and Hans Hagen (2011). “Methods for feature detection in point clouds”. In: *Visualization of Large and Unstructured Data Sets-Applications in Geospatial Planning, Modeling and Engineering (IRTG 1131 Workshop)*. Schloss Dagstuhl-Leibniz-Zentrum fuer Informatik.

Xie, Yonghong and Qiang Ji (2012). “A new efficient ellipse detection method”. In: *Object recognition supported by user interaction for service robots*. IEEE Comput. Soc. DOI: 10.1109/icpr.2002.1048464.

Yuen, H. K., J. Illingworth, and J. Kittler (1988). “Ellipse Detection using the Hough Transform”. In: *Proceedings of the Alvey Vision Conference 1988*. Alvey Vision Club. DOI: 10.5244/c.2.41.

Yuen, H. K., J. Princen, et al. (1989). “A Comparative Study of Hough Transform Methods for Circle Finding”. In: *Proceedings of the Alvey Vision Conference 1989*. Alvey Vision Club. DOI: 10.5244/c.3.29.

Assessing Students’ Hazard Identification Ability in Virtual Reality using Eye Tracking Devices

Yewei Ouyang[1], Chi Kwong Wong[1], Xiaowei Luo[1]
City University of Hong Kong, Hong Kong
yewouyang2-c@my.cityu.edu.hk

Abstract. Researchers have applied eye-tracking to assess construction trainees' hazard-identification ability as eye movements can reveal people’s mental processes. However, existing studies asked the workers to identify hazards in static pictures, which fails to capture the dynamic characteristics in the real world or risky job site. To address this limitation, this paper integrates Virtual Reality (VR) with eye-tracking to assess students’ hazard-identification ability, because VR could represent the real world better than pictures. Compared to sending the trainees to the job site, it is safer and more flexible to assess the trainees' hazard identification ability in a VR environment. This study developed a VR construction site with 20 hazards, and 14 students were invited to walk around the virtual job site to identify the potential hazards. Their performance and eye-movement data were collected and analyzed to assess their hazard-identification ability. The results validated that the VR environment could provide a more comprehensive assessment of the students’ hazard identification ability using the eye-tracking data.

1. Introduction

The construction industry has been notorious for its poor safety performance. Among the existing practices for construction accident prevention, identifying hazards and taking follow-up actions is one of the most straightforward approaches. However, many workers fail to identify hazards, partially because they might not have sufficient safety knowledge or might not have the ability to apply the learned knowledge to practice. How to assess those hazard identification ability and provide enhanced personalized training becomes critical to improve job site safety performance.

Eye-tracker is a device for measuring the point of eye-gaze and eye movement, which has been widely used to investigate human cognition. Eye-tracking exhibits immense potentials of providing deeper insights into construction workers' hazard-identification patterns, which enables a more objective and reliable approach to reflect workers' reactions to hazards on construction sites. Therefore, researchers have recently begun to examine the applications of eye-tracking technology in studying construction workers' safety knowledge and hazard-identification skills (Dzeng et al., 2016, Hasanzadeh et al., 2017a, Hasanzadeh et al., 2017b, Hasanzadeh et al., 2017c, Jeelani et al., 2019, Xu et al., 2019). However, most existing studies used static pictures to present the site scenarios, and the static pictures might not capture all of the dynamic and real situations of the construction sites. For example, static pictures fail to sufficiently portray the construction operations' dynamic natures, while many hazards happen during construction operations. On the other hand, it is challenging to use an eye-tracking device for safety knowledge assessment on-site because there are many uncontrollable risks on-site, and it might put the trainees in danger, and the associated cost would also increase.

Therefore, a virtual environment is a better alternative as it is a sufficiently authentic simulation of a construction site, which fully mimics the dynamic characteristics of construction sites. The virtual environment is risk-free for the trainees and cost less than implementation on job sites. It is flexible and scalable to create a variety of hazards in the Virtual Reality (VR) environment, providing an opportunity to comprehensively assess the hazard identification ability. Besides, the VR learning environment has proved to be more effective in maintaining trainees’ attention and concentration (Sacks et al., 2013) and beneficial for the developing civil engineering students' hazard identification ability (Perlman et al., 2014).

At present, lightweight eye-tracking devices fitting VR headsets become available, making accurate real-time eye movements tracking and extensive scale data collection possible. The eye-tracking in VR provides researchers new possibilities for conducting research related to human perception and behavior (Clay et al., 2019). Ye and König (2019) developed an approach of applying eye tracking to gather eye-movement data (e.g., dwell time, fixation sequence, and 3D heat map) in the VR scenario for cognitive studies. On top of those studies, this paper intends to combine the VR application and eye-tracking device together to assess students' hazard-identification ability. In the proposed system, the eye-tracking device is used to track students' eye movements to assess their safety knowledge toward hazard-identification. We aim at detecting students' safety-knowledge deficiencies through the assessment, and the results could support the safety training personalization to enhance their safety knowledge.

2. Eye Tracking Studies in Construction Hazard Identification

As eye-movement data reflects the cognitive processes occurring in a particular task (Rayner, 1978), some researchers applied eye-tracking to study the hazard-identification skills of construction workers. In the study by Dzeng et al. (2016), experienced and novice workers identified hazards in four screenshots in Google SketchUp, which presents both obvious and unobvious hazards of workplaces. The differences in the workers' searching patterns for hazard identification were compared. The experienced workers were found to recognize hazards significantly faster than the novices, and their scanning paths are consistent. Habibnezhad et al. (2016) and Hasanzadeh et al. (2017a) developed a series of eye-tracking tests using 35 construction site images. They found that: 1) workers with different levels of risk perception do not show the same eye movement in hazard identification (Habibnezhad et al., 2016), and 2) workers' hazard-identification skills, work experience, and injury exposure have influences on their attentional distributions as well as visual search strategies by checking their eye movement metrics (e.g., run count, dwell percentage, and first fixation time), which can be used to predict workers' hazard-identification capabilities (Hasanzadeh et al., 2017a, Hasanzadeh et al., 2017b). Hasanzadeh et al. (2018) and Xu et al. (2019) conducted the eye-tracking experiment in a real environment. Hasanzadeh et al. (2018) used a mobile eye-tracker in a real job site with tripping hazards to observe how workers with low and high situation awareness levels would allocate their attention while walking. They found that workers with higher situation awareness periodically looked down and scanned ahead to remain fully aware of the environment and its associated hazards. Xu et al. (2019) invited participants to search for hazards in a structural laboratory which has a lot of common with a construction site. Their research focused on eye-tracking scan patterns which reveal strategies of construction safety inspections. Their results show that successful participants follow a logical and serial search pattern, and they concentrate on specific hazardous areas instead of unimportant distractors.

These studies chose proper eye-tracking metrics as the indicators of subjects' hazard-identification patterns. These studies demonstrate that eye-tracking can reveal the individual differences in hazard identification, although they are based on static images or a real site with the aforementioned shortcomings. It can be inferred that students with different abilities in hazard-identification might present diverse eye movement patterns in hazard searching. In addition, eye tracking has been proved to be a useful skill assessment tool in other fields. Tien et al. (2014) conducted a systematic literature review and found that eye-tracking provided reliable quantitative data and served as an objective assessment tool in different subject areas. Hermens et al. (2013) concluded recording of eye movements might be beneficial both for skill assessment and training purposes in surgical training. Therefore, the authors expect that eye trackers can also serve as an effective tool in assessing construction students' hazard-identification ability.

3. Research Methodology

3.1 VR Scenario Development

Construction scenes with different types of hazards are conceptualized for VR scenarios development. Unity 3D engine is chosen to develop VR scenarios representing 20 most common construction hazards (shown in table 1), covering falling from heights, struck by machines or objects, electric shock, collapse, and explosion. These hazards result from various roots, including unsafe postures, improper personal protective equipment, poor housekeeping, and regulation violation. In Table 1, four hazards (H_8, H_{10}, H_{14}, and H_{15}) are presented by animations. The safety knowledge related to those 20 hazards is considered as the essential ones in construction students' safety education. The students should be able to identify these hazards to protect themselves from injury when they go to job sites. Therefore, these hazards are supposed to achieve a comprehensive assessment of students' hazard-identification ability. The sample screenshots with hazards are shown in Figure 1.

Table 1: 20 Hazards Presented in the VR Scenario

Hazard index	Hazard Scenario	Hazard Type	Number of students correctly identified the hazard
H_1	No safety locks for the electricity box	Electric shock	1
H_2	Excavation near power lines		6
H_3	Guardrail missing at the open edges of a roof	Falling from height	1
H_4	Guardrail missing around a lift shaft		7
H_5	Workers sitting on the edge of a roof without the harness		7
H_6	Scaffold platform not being fully planked		0
H_7	A worker climbing the scaffold bracing		1
H_8	Lifting workers using a material hoist		0
H_9	Workers without wearing hardhat on site	Struck-by /Tripping	9
H_{10}	Two workers standing and talking with each other under a lifting machine		10
H_{11}	Bricks are loosely stacked with a height of 9 feet		7
H_{12}	Exposed nails protruding from lumber		3
H_{13}	Bricks stacking in racks and facing main walking paths for workers		14
H_{14}	Hoist operation of a tower crane but signalman is missing		1
H_{15}	Backing a truck while a worker is working in the blind spot behind the truck		1
H_{16}	Scaffold without a safety net		2
H_{17}	Timber formwork being scattered on the ground		10
H_{18}	Scaffold missing base plate	Collapse	1
H_{19}	Scaffold missing sweeping rod		1
H_{20}	Oxygen cylinder and acetylene cylinder are stored together	Explosion	0

Motion sickness of VR players must be considered when running a VR system. Motion sickness occurs due to the disparity between the users' visual and vestibular stimuli, and it is associated with the users' moving patterns in VR and the framerate of the VR scene (Clay et al., 2019). To tackle dizziness, subjects in this study move at a constant speed in the VR scenario, and the authors made a trade-off between the realistic levels of the experimental scene and smoothness of the VR system to keep a high running framerate. By using a trial and error method, a smooth and stable scenario was achieved in the development stage before the formal test.

Eliminating the influence of irrelevant variables in the experiment is another issue when designing the scenario. This research focuses on the relationship between students' eye-movement data and hazard-identification ability. However, students' walking path, visual angle, and uniformity of light intensity in the scene may significantly affect students’ visual choice because subjects tend to be attracted by things with brighter colors as a result of the bottom-up attention (Bojko, 2013). Therefore, the authors restrict a pre-defined path for all participants and ensure uniform lighting in the whole scene.

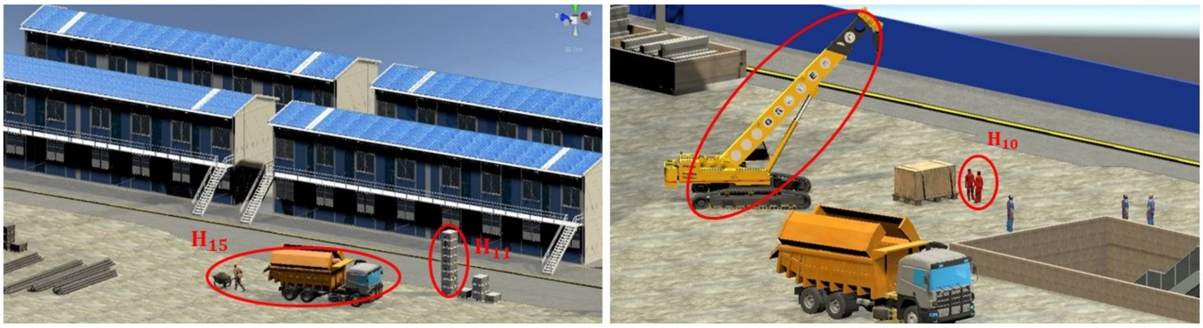

Figure 1: Screenshots with Hazards (H_{10}, H_{11}, H_{15}) in the VR Scenario

3.2 Eye-Tracking Experiment Design

Subjects. 14 undergraduate students in civil engineering were invited to participate in the study. These students completed the same class on construction safety, but they are not in the same academic cohort. Ten of them have less than two months of working experience on construction sites. All participants have uncorrected normal vision or corrected-to-normal vision.

Experiment Process. During the experiment, participants wore HTC VIVE head-mounted display (HMD) integrated with an eye-tracker from Pupil Labs, sitting on a chair and controlling movement in the VR scenario through a keyboard and a mouse, as shown in Figure 2. Before the formal experiment, the participants received a briefing of the experiments and practiced moving in a VR scenario to become familiar with VR hardware and operation, eliminating the impacts on hazard-identification performances caused by unskilled operation in VR.

Calibration is done first to ensure the accuracy of eye-tracking measurements. Participants were instructed to fixate on several target points at different locations in their VR view. The calibration process establishes a mapping from pupil to gaze coordinates (Kassner et al., 2014). Then, students walked around the job site in the VR environment following a pre-defined path and spoke out on the identified hazards while they are looking at the hazardous object once they discover any potential hazard. Their head is required to keep stable during the whole experiment to avoid accuracy loss of eye-tracking, which is caused by the VR headset sliding resulted from head movement.

Students' performance of hazard identification and eye movement are recorded. Their hazard discovery is regarded as correct only when they point out a hazard and describe it at the same time; otherwise, it is considered incorrect. They are expected to finish the hazard discovery process in ten minutes and complete a questionnaire after the experiment.

Figure 2: VR & Eye-Tracking Devices and Experimental Set-up

Analysis. Jacob and Karn (2003) defined Area of Interest (AOI) as an area in the display or visual environment that is of interest to the research. As this paper aims to study subjects' hazard-identification ability, the authors define hazardous objects and hazardous parts of objects as Areas of interest (AOIs). Four AOI examples (objects marked with red circles) are shown in Figure 1. In total, there are 27 AOIs defined in the virtual job site.

Students' gaze points and scanning paths were analyzed to see how they allocated attention and what their search patterns were when looking for hazards. As shown in Figure 3, the green dots represent the position of gaze, and the red line represents the scanning sequence. Pupil Capture is used to record eye-movement data, and Pupil Player is used to export eye-movement metrics into Microsoft Excel to calculate R_1 and R_2 to assess their ability of hazard identification using Eq.(1) and Eq.(2) respectively. The fixation time is a frequently used eye-movement metric, which refers to time spent on a particular object or location. Very often, people's attention is directed toward the point they are looking at, and fixations are important for information acquisition (Holmqvist et al., 2011). Researchers can infer which portions of a scene attract the participant's visual attention and which portions are ignored, based on the proportion of time spent looking at somewhere (i.e., fixation time) (Bhoir et al., 2015). How to allocate attention during hazards-searching indicates one's ability in hazard-identification, and thus the authors can perform the assessment by analyzing subjects' fixations.

R_1 is the ratio between fixation duration on all AOIs with total fixation duration. It indicates how frequently students allocate their attention to hazardous objects other than non-hazardous parts during the whole searching process. If students have a good understanding of the essence of safety inspection, they might know which portions in the VR scenario are potential dangerous-sources and thus choose to focus on those portions more often. Therefore, R_1 reflects students′ ability to concentrate on potential safety hazards and removing interferences from unimportant things.

$$R1 = \frac{Fixation\ time\ on\ AOIs}{Fixation\ time} \tag{1}$$

$$R2 = \frac{Fixation\ time\ contributing\ to\ accurate\ identification}{Fixation\ time\ on\ AOIs} \tag{2}$$

Figure 3: Visualization of Gaze Point and Scan Path

Even though students notice the hazardous objects, those without sufficient safety knowledge might still fail to recognize hazards correctly. R_2 is the ratio between the duration of fixations contributing to accurate identification and the time spent in fixations on all AOIs. R_2 indicates how frequently students achieve successful identification when scanning the hazardous objects, which reflects students' ability to identify hazards correctly. R_1 and R_2 together can be used to assess students' hazard-identification ability and discover their safety knowledge deficiencies. Moreover, the scanning path indicates students' searching patterns and shows the motion trail of eyes and the sequence of fixations. Therefore, the scanning path can also reflect students' hazard-identification ability. Meantime, the aforementioned eye-movement analysis is implemented with a combination of students' performance data, including the accuracy rate of hazard-identification and identification time.

4. Results and Analysis

Table 2 presents each participant's experimental results. The overall performance is not very good, with only 6 hazards being identified correctly on average, indicating that these hazards are effective in finding out students' safety-knowledge deficiencies. Furthermore, there are similarities among participants when looking at the times of each hazard being identified, as shown in the last column of Table 1. Hazards related to workers' personal protection (H_9 and H_{10}) and unsafe material storage (H_{13} and H_{17}) are correctly identified by most participants because these hazards are obvious and only require simple safety knowledge. In contrast, hazards related to the scaffold (H_6, H_7, and H_{16}), unobvious hazards (H_3, H_{12}, and H_{15}), and those requiring specific safety regulations (H_1, H_8, H_{14}, and H_{20}) tend to be ignored by a majority of students. Besides, these participants are found to be sensitive to safety protection and the tidy stack of materials that they always categorized non-hazardous objects as dangerous sources when there is no protection surrounding machines or materials or when there is messy storage of materials.

Table 2: Experiment Results of Each Participant

Students' index	Number of hazards correctly identified	Total identification time (min)	Fixation duration on all AOIs (ms)	Fixation duration contributing to correct identification (ms)	R_1	R_2
S_1	7	5.00	17,389.97	7,756.55	24.21%	44.60%
S_2	6	4.00	21,304.67	9,614.83	37.55%	45.13%

S_3	3	5.07	15,539.21	3,696.12	24.42%	23.79%
S_4	6	7.33	20,909.34	3,936.84	21.45%	18.83%
S_5	6	10.33	16,638.62	3,373.57	17.33%	20.28%
S_6	6	7.67	15,387.25	10,312.29	33.33%	67.02%
S_7	8	9.05	62,513.59	51,099.05	41.36%	81.74%
S_8	9	4.50	24,528.57	19,839.35	28.22%	80.88%
S_9	7	11.08	5,189.92	4,862.47	13.15%	93.69%
S_{10}	10	6.48	13,348.94	8,776.03	24.22%	65.74%
S_{11}	6	8.00	16,738.58	4,813.22	15.85%	28.76%
S_{12}	5	8.85	11,306.34	6,233.98	14.86%	55.14%
S_{13}	5	7.83	16,033.74	7,223.81	12.43%	45.05%
S_{14}	6	6.62	8,280.05	4,286.02	4.87%	51.76%
Mean Value	6	-	-	-	22.38%	51.6%

It can be inferred from Table 2 that there is no positive correlation between the accuracy rate and total time spent on hazard searching. The reason might be other factors (e.g., the operation proficiency of VR and personal searching patterns) in addition to the hazard-identification ability also influence the searching time. Similarly, both fixation time on AOIs and fixation time contributing to correct identification do no show strong relationships with the accuracy rate.

In terms of the portion of attention on AOIs (i.e., *R1*), the figure of this sample is relatively low, with a mean value of 22.38% and a maximum of 41.36% (less than 50%). This indicates that, to a great extent, participants are distracted by other irrelevant components in the VR scenario. On the one hand, it takes more time when participants are puzzled about what they see and when they look at the scenes closely and repeatedly. On the other hand, these participants are used to stop and look at all workers, machines, and materials whenever they meet those objects. This behavior is consistent with what they reflect in questionnaires that they are actually not sure about many hazards and always feel hesitant to make a judgment, which also demonstrates the eye-tracking exhibits their cognitive process. However, there are still some AOIs not being noticed, including the electricity box, the movable scaffolding, and the edge of a roof. All these are essentially caused by a lack of safety knowledge to guide students exactly to allocate their attention to hazardous objects.

When it comes to R_2, it can be seen that there are distinct individual differences in the frequency of identifying hazards correctly when noticing AOIs. Only three participants' figures exceed 80%, indicating that those three students can recognize hazards more often once noticing them. The low average value (51.6%) of R_2 reveals insufficient safety knowledge of these participants. To be specific, even relevant AOIs are highly noticed, H_9 and H_{20} are missed by all, and H_7, as well as H_{14}, are identified by merely one person. This is because the students do not know the following safety regulations: oxygen cylinder and acetylene cylinder should be kept at a safe distance; there should be a signalman for the hoist operation with a tower crane; climbing scaffold bracings is prohibited; material hoist is not allowed to lift people. In the same way, the authors can obtain each student's safety-knowledge deficiencies by analyzing their eye-movement data.

Four kinds of searching patterns are found when checking students' scanning path. Six students (S_2, S_4, S_7, S_8, S_{10}, and S_{13}) scan the scenario in a regular manner, from right to left, then from top to down, so they can capture details well. Their accuracy rates are above average except S_{13}. Four students (S_1, S_6, S_{11}, and S_{12}) only move their eyes from left to right without looking at the top parts, which results in missing H_3, H_5, and H_7. Two students (S_5 and S_9) glance at the whole scene quickly at first and then fixate on their interesting parts, which might result in the fact that they take the longest time among all participants, but they do not show superior performances. Merely S_3 searches hazards in a disorderly and unsystematic way, which may be responsible for his worst performance (only identified three hazards correctly). Besides, three students (S_4, S_5, and S_{12}) have regression, but they find nothing new. To conclude, the selection of search strategies has an impact on search performances and reflects students' ability to search for hazards logically and roundly.

The authors asked for students' thoughts and feelings as well as their feedbacks about the VR scenario and the experiment design through questionnaires. Five students felt a little dizzy, but there is no adverse effect on the test. Two students claimed that the headset is a little bit heavy for them. All students admit they detect their safety-knowledge deficiencies after the test, and they think the task is neither too difficult nor too easy for them. Nine of them suggested having a VR scenario with a higher resolution. Merely one student thinks the scenario's lighting is too bright, and one claimed the moving speed in VR is slightly too fast. The specific thoughts they wrote down demonstrates that eye-tracking indeed exhibits their mental process as analyzed before. Also, it is suggested to provide other types of stimulated construction sites and add more animations to the scene.

5. Discussion

Participants' poor performances in identifying hazards correctly and their subjective comments indicate their knowledge deficiencies are detected through the experiment, which is the contribution of VR, enabling realistic and sufficient hazards to conduct a more comprehensive assessment. It shows the superiority of VR over static images and the real site. A personalized training schema can be developed according to the identified individual's deficiencies in safety knowledge, but it might be better if a VR scene could be provided with higher resolution and diversified objects. Also, eye-movement data exhibits participants' cognitive process in searching for hazards that their attention allocation and search patterns are obtained by observing the fixations and scanning paths. To what extent students are distracted by unimportant objects and whether they identify hazards or not when having paid attention to, are quantified by the eye-movement data, allowing evaluating students' ability to concentrate on the hazardous area and applying knowledge to identify hazards. A further assessment might be achieved by analyzing more eye-movement metrics and making more specific analyses towards each AOI in the future study since the authors only focus on fixations and scanning paths in this paper. In the future study, construction workers should be invited for the experiment to validate the effectiveness of the assessment tool built on the integration of VR and eye-tracking. Participants of the experiment adopting a more logical searching pattern indeed have better performances, which is consistent with the findings of Xu et al. (2019), who found that successful participants were observing one sub-area fully before a systematic shift to another one. Xu et al. (2019) also pointed out that successful participants concentrate on specific hazardous areas rather than unimportant distractors. However, no positive relationship is found between the portion of attention on hazardous objects and the accuracy rate in the authors' study. One possible explanation is that safety knowledge (e.g., relevant safety regulations) is also required to achieve correct identification after noticing the hazardous areas. This is also why the authors consider the portion of fixations contributing to accurate identification.

Except for revealing individual differences as previous studies have examined, the eye-movement data also implies more by looking into the similarities among individuals. This experiment exposes what safety knowledge is not mastered by most students, informing teachers teaching deficiencies to help them enhance teaching and provide personalized training for each student.

6. Conclusion

Identifying safety hazards and taking actions in a construction site is one of the most straightforward approaches for construction workers to prevent injuries. Thus, it is essential to assess people's hazard identification ability and provide them with enhanced personalized training. Eye-tracking has been applied in related researches because it reveals people's cognitive processes when identifying hazards, but it is limited to static images or risky and uncontrollable real sites in previous studies. This paper implemented an eye-tracking experiment in a VR scenario that is superior to both images and real sites due to its authenticity, safety, flexibility, and low cost. A VR scenario simulating a construction site with 20 hazards of five types was developed in Unity 3D, and 14 students wearing VR headset and eye-tracker were invited to search for those hazards. Both their performance data (accuracy rate and identification time) and eye-movement data (fixation duration and scan path) were recorded and analyzed to evaluate their hazard-identification ability. These stimulated hazards in the VR scenario reveal each student's deficiencies in safety knowledge. The experimental result indicates that students allocate considerable attention to non-hazardous objects, and they failed to identify hazards even though having fixated on them due to lack of safety knowledge. Specifically, these students can identify obvious hazards but fail to recognize those related to specific safety regulations. Also, students adopting a more logical searching tend to have better performances.

The availability of dynamic and unlimited hazards in VR provides sufficient hazards to detect students' safety-knowledge deficiencies, which facilitates a more comprehensive assessment of students' hazard-identification ability. Eye-tracking provides quantitative data to reveal students' attention allocation and searching patterns, which can serve as assessment criteria.The proposed methodology of using eye-tracking in VR for hazard identification provides other researchers references for further exploration.

Acknowledgment

This work was supported by the Research Grant Council (PJ#11214518), the National Science Foundation of China (PJ#51778553), and the CityU Teaching Development Grant (PJ# 6000679). The conclusions herein are those of the authors and do not necessarily reflect the views of the sponsoring agency.

References

Bhoir, S. A., Hasanzadeh, S., Esmaeili, B., Dodd, M. D. & Fardhosseini, M. S., (2015) Measuring construction workers' attention using eye-tracking technology. Proc., ICSC15: The Canadian Society for Civil Engineering 5th Int./11th Construction Specialty Conf, 2015. Univ. of British Columbia, Vancouver, Canada.

Bojko, A., (2013). *Eye Tracking the User Experience: A Practical Guide to Research*, Rosenfeld Media.

Clay, V., König, P. & Koenig, S. (2019). Eye Tracking in Virtual Reality. *Journal of Eye Movement Research,* 12.

Dzeng, R.-J., Lin, C.-T. & Fang, Y.-C., (2016). Using eye-tracker to compare search patterns between experienced and novice workers for site hazard identification. *Safety Science,* 82**,** 56—67.

Habibnezhad, M., Fardhosseini, S., Vahed, A. M., Esmaeili, B. & Dodd, M. D., (2016). The relationship between construction workers' risk perception and eye movement in hazard identification. Construction Research Congress 2016. 2984—2994.

Hasanzadeh, S., Esmaeili, B. & Dodd, M. D., (2017a). Impact of construction workers' hazard identification skills on their visual attention. *Journal of Construction Engineering and Management,* 143**,** 04017070.

Hasanzadeh, S., Esmaeili, B. & Dodd, M. D., (2017b). Measuring the impacts of safety knowledge on construction workers' attentional allocation and hazard detection using remote eye-tracking technology. *Journal of Management in Engineering,* 33**,** 04017024.

Hasanzadeh, S., Esmaeili, B. & Dodd, M. D., (2018). Examining the Relationship between Construction Workers' Visual Attention and Situation Awareness under Fall and Tripping Hazard Conditions: Using Mobile Eye Tracking. *Journal of Construction Engineering and Management,* 144**,** 04018060.

Hasanzadeh, S., Esmaeili, B., Dodd, M. D. & Pellicer, E., (2017c). Using eye movements to identify hazards missed by at-risk workers.". *ISEC, Fargo, ND*.

Hermens, F., Flin, R. & Ahmed, I., (2013). Eye movements in surgery: A literature review.

Holmqvist, K., Nyström, M., Andersson, R., Dewhurst, R., Jarodzka, H. & Van de Weijer, J., (2011). *Eye tracking: A comprehensive guide to methods and measures*, OUP Oxford.

Jacob, R. J. & Karn, K. S., (2003). Eye tracking in human-computer interaction and usability research: Ready to deliver the promises. *The mind's eye.* Elsevier.

Jeelani, I., Albert, A., Han, K. & Azevedo, R., (2019). Are Visual Search Patterns Predictive of Hazard Recognition Performance? Empirical Investigation Using Eye-Tracking Technology. *Journal of Construction Engineering and Management,* 145.

Kassner, M., Patera, W. & Bulling, A., (2014). Pupil: an open source platform for pervasive eye tracking and mobile gaze-based interaction. *Proceedings of the 2014 ACM International Joint Conference on Pervasive and Ubiquitous Computing: Adjunct Publication.* Seattle, Washington: ACM.

Perlman, A., Sacks, R. & Barak, R., (2014). Hazard recognition and risk perception in construction. *Safety Science,* 64**,** 22—31.

Rayner, K., (1978). Eye movements in reading and information processing. *Psychological bulletin,* 85**,** 618.

Sacks, R., Perlman, A. & Barak, R., (2013). Construction safety training using immersive virtual reality. *Construction Management and Economics,* 31**,** 1005—1017.

Tien, T., Pucher, P. H., Sodergren, M. H., Sriskandarajah, K., Yang, G.-Z. & Darzi, A., (2014). Eye tracking for skills assessment and training: a systematic review. *journal of surgical research,* 191**,** 169—178.

Xu, Q., Chong, H.-Y. & Liao, P.-C., (2019). Exploring eye-tracking searching strategies for construction hazard recognition in a laboratory scene. *Safety Science,* 120**,** 824—832.

Ye, X. & König, M., (2019). Applying Eye Tracking in Virtual Construction Environments to Improve Cognitive Data Collection and Human-Computer Interaction of Site Hazard Identification. ISARC. Proceedings of the International Symposium on Automation and Robotics in Construction, 2019. IAARC Publications, 1073—1080.

Investigating Information Overload and Cognitive Correlation of Crane Operators

Jinjing Ke, Xiaowei Luo, Hainan Chen
City University of Hong Kong, Hong Kong
jingke4-c@my.cityu.edu.hk

Abstract. Information overload (IO) is a potential threat to safety decisions and work efficiency of practitioners during construction programs in such an era of information exploding. Nevertheless, research about the impact of IO at a construction site is scarce. This paper is a pre-experimental attempt about the effect of IO on performance based on three crane operators, using a cognitive perspective to explore the influencing mechanism. Crane operators are wired up with Electroencephalography (EEG) headset to finish the corresponding operational task within different levels of information load (IL) in a virtual environment. The preliminary outcomes indicate that information amount and presentation type indeed affect cognitive load via self-ratings and EEG measures. This paper provides insights into IO's adverse impact, recognizes primary contributors leading to IO. More importantly, later findings of cerebral activity can reveal the cognitive influence of IO.

1. Introduction

Information overload (IO) is an increasingly severe issue that almost everyone in daily work or life would suffer, such as E-mail overload. In 2010, losses arising from information overload were estimated at $997 billion by Basex (Rogers, 2011). People need to receive, filter, integrate, retrieve, analyze, and use the information to deal with each task and decision. Information delivery between the sender and receiver and information overload occurs when the receiver is given volumes of information than can absorb (Meyer, 1998), and when the information processing demand on an individual's time exceeds the time available (Schick, Gordon and Haka, 1990). Redundant information would mislead decision-making and behavior since a receiver's limited information processing capacity cannot fit excessive information.

IO is a potential threat to safety decisions, work efficiency, mental stress, the collaboration of practitioners during construction programs in such an era of information exploding. Information overload also has been confirmed as a barrier to effective safety communication because messages can be ignored or lost during transmission (Preece and Stocking, 1999). Information and communication technology (ICT) innovations committed to tackling the problem of information accessibility and sharing, yet accompanied by volumes of information. Although the decision support system and the acquisition of information developed rapidly, the decision-makers' cognitive capacity did not (Roetzel, 2018). The more prick issue is how to obtain valuable information timely rather than the access to information in such an information flooding era. Generally, unnecessary information brings about stress and fatigue and misleads judgment, especially for those positions that are highly associated with safety like crane operators.

Cranes are indispensable for projects, whatever their scale. Safe crane operation under regulations is the key to the success of the project. The prior study found that frequent crane accidents caused by comprehensive factors, such as human factors, routine safety checks, mechanical maintenance, professional training (Zhou *et al.*, 2018). Operators, signalmen, and slingers as front-line staff are the dominant part of human factors, and effective communication among them is essential for correct operation. Crane operators need to receive the command

and guidance of the signalman and understand the information conveyed from both signalman and environment to make the exact reaction. However, information overload will occur accordingly due to the complicated situation and the tight schedule, that crane drivers are always required to complete the operation task in limited time. Too much safety information means increased demands for employees at site who are likely to miss important information until overload decreases (Gibson, Ivancevich. and James H. Donnelly, 2001). Nevertheless, it is unclear whether information overload is a potential source that has threats to cognitive load and crane decisions. To fill the research gap, this paper studies the impact of information load on operators' response and mental load from a perspective of cognitive influence.

2. Literature Review

IO results in stress, anxiety, and tiredness, as well as influences performance and efficiency. This problem worth more concern in construction management, so the section reviewed IO related studies in the construction industry and summarized internal and external causes of IO.

2.1 Information Overload in Construction

In the construction industry, information overload, which often occurs in the communication process of different project participants, such as engineers of different professions in the design stage. Haksever et al. surveyed information overload about 140 project managers in the UK and used time as a measurement unit to set an information load matrix (ILM). He found information overload in construction and the design stages are higher than that in the stage of procurement and feasibility analysis, and interactions with consultants, clients and architects are the most overloaded (Haksever and Fisher, 1996). In this case, the cognitive difference between different disciplines is the main factor that leads to information overload during communication. In terms of the effect of information quantity and quality on IO, R. Zhang et al. conducted a study in the relationship between inter-metric information processing (amount & quality) and design coordination performance of design institutes (Zhang, Liu and Chan, 2018). The relationship between the amount and the performance follows a nonlinear exponential expression, and the effect of information quality on performance is stronger than that of the amount.

In engineering projects, communication includes many aspects. From the perspective of information categories, there are design information, safety information, schedule and progress information, cost information. Here we focus on the communication of safety information because smooth communication of safety information will directly affect safety attitudes, decisions, and behaviors. However, studies of safety information (SIN) reported accounting for 0.68% of all safety-related research in the construction industry (Zhou, Goh and Li, 2015). Almost only a few articles exclusively discussed how to identify information overload possible situations in construction management but not aimed at safety information. At the construction site, crane signals, as one of the forms of safety information, play an essential role in crane operation. Crane signals communication is critical that involve in the interaction among people, machinery, environment. Furthermore, operation decisions highly correlated with the safety of crane and employees around. Currently, manual operation cannot be entirely replaced by smart control through unmanned control is emerging; reducing the impact of human factors will raise the safety performance of operators. The ability of crane drivers to process information decreases with fatigue and physical discomfort caused by working for long hours in a narrow workspace. It is needed to investigate the effect of IO on safe operation.

2.2 Information Overload Causes

There are several stages from the sending of a message to its being understood: information expression, transmission, the interaction between information characteristics and task environment, and the understanding and judgment of the receiver (Roetzel, 2019). Different factors also cause the occurrence of information overload in these processes, which divide into five levels: information attributes, information expression, information technologies, receiver limited cognition, task properties, as shown in Figure1.

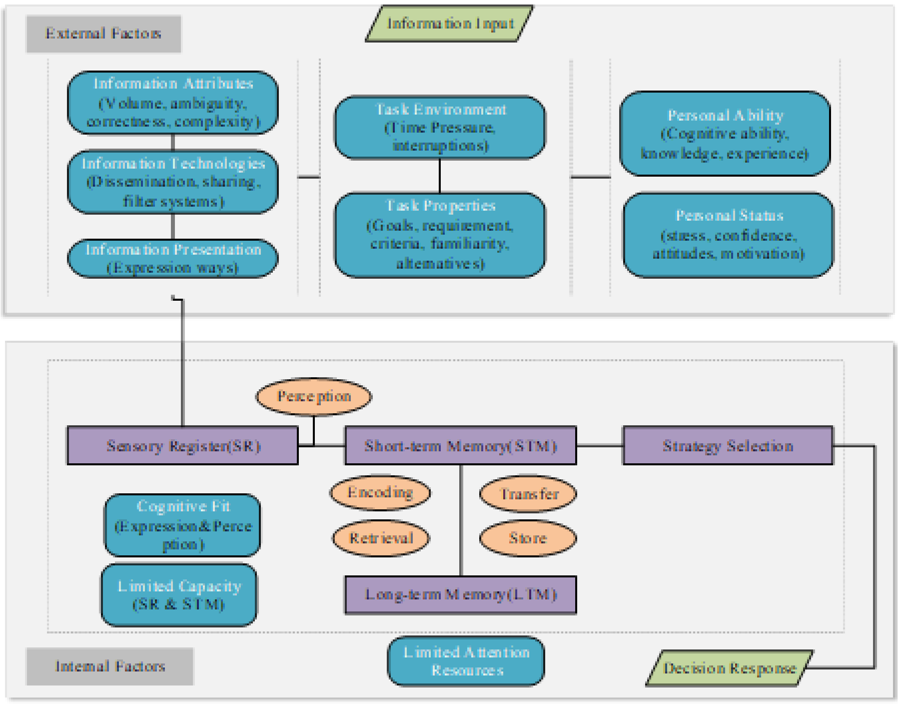

Figure 1: Comprehensive Factors of IO

Information features consist of information volume, quality, uncertainty, complexity, which directly act on information processing performance. Excessive, incorrect, or incomplete information would cause confusion and misjudgment. Traditionally, people have a subconscious that more information is better, but a study confirmed that too much information just increased confidence and satisfaction with decreased lower accuracy (O'Reilly, 1980). Information expression has a variety of presentation formats such as oral expression, gestures, and signals reports in written language, media form, visualization technologies. Conveying information in an exact format to different people needed can facilitate the understanding effectively; otherwise, it would hinder the expected effect. Information technologies achieved ease of dissemination and can provide the quantity of data for recipients. Though information technologies made information sharing possible, people have to filter and process massive information while searching to make a choice, which means information burden potentially. Personal reasons include limited cognitive ability and cognition difference between the sender and receiver. That's why interdisciplinary communication cost more time than that with colleagues in the same profession. Besides, personal attitudes, motivations, age, the experience would contribute to a temporary decline in the ability to process information. Task properties as environmental impact include time pressure and interruptions imposed on the receiver. Time pressure depends on the time required and self-judgment of information processing performance.

Whether information load acts on attention or emotion (acute stress, frustration level), SR or STM, thus influence cognitive load is unknown. Factors vary in different scenarios, but whether there is a common influence mechanism is unknown.

2.3 Cognitive Load and Measurement

Cognitive load is the total amount of mental effort that is being used by the working memory at a given time. If information overload is regarded as an external cause, cognitive load is the main internal one of the IO that affects decision-making.

Cognitive load cost attention and cognitive resources, namely, mental effort existing in main information-processing stages: sensory register (SR) to recognize input, short-term memory (STM) to operate and integrate, long-term memory (LTM) to encode and retrieve (Atkinson and Shiffrin, 1968). If the task presentation does not match with a problem, which means additional cognitive effort needed to transform presentation to mental representation. This type of mismatch disobeys the cognitive fit model (Kelton, Pennington and Tuttle, 2010), which is likely to cause IO. Furthermore, the capacity of SR and STM are confirmed limited, in contrast to infinite LTM. The range of SR and LTM is 3-7 units (0.5-3 seconds) and 7-9 (5-15 seconds) chunks (Miller, 1956), which is one of the bottlenecks of information load. Limited attention resources that are dominated by these stages is another inducement of IO (Wickens, 2002). During the information processing, more mental effort is allocated by information load, so less attention is for decision accuracy due to trade-offs between error and effort, time and accuracy (Vessey, 1994). That is exactly why IO has an impact on decision performance.

Different techniques to measure cognitive load are available, including subjective ratings, performance-based measures, and physiological methods. The EEG is sensitive and can detect not only cumulative load but also instantaneous load and average load. Many scholars proposed CL indices via EEG, such as band-based spectral power, function connectivity, entropy (Majdic *et al.*, 2017). Since many articles agreed that parietal alpha and theta of frontal regions are closely associated with task CL change, the paper adopted theta(1-4Hz) and alpha(8-14Hz) to assess CL level (Antonenko *et al.*, 2010). Besides, the indices related to wavelet coefficients are also adopted because the paper has common in that of experiment design with a set of subtle variables (Zarjam, Epps and Lovell, 2015).

Information load and cognitive load are closely related, but the relationship between the information load and cognitive load is unclear. Hence, the paper aimed to simulate a construction scenario to analyze the effect of information elements (amount, information accuracy, information expression) on crane operator performance, and cognitive load. By a quantitative analysis of IL and CL, the purpose is to discover the relationships and influencing mechanism.

3. Methodology

Quantification of IL and CL in the experiment is the key. IL is set by information dimensions and time constraints of the experiment, whilst CL is measured by brain activities and subjective rating scale. Figure 2 illustrates the framework of this research.

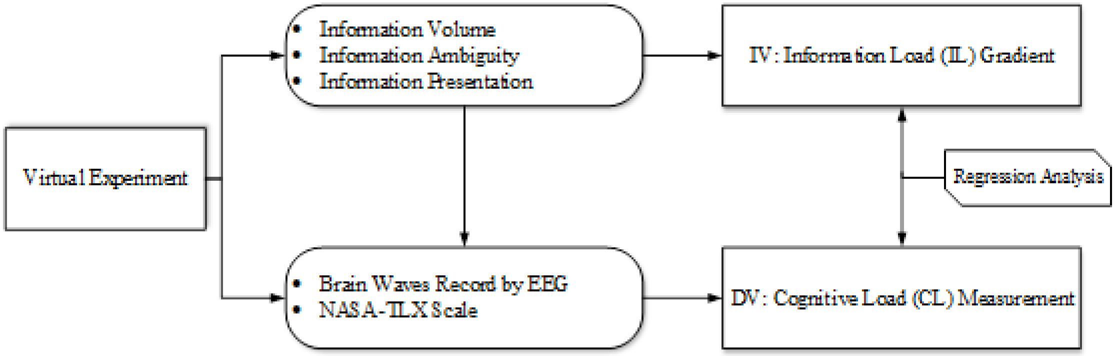

Figure 2: The Framework of the Experiment

3.1 Experiment

The authors designed a virtual construction site to simulate immerse crane operation shown in Figure 3, which set different levels of information dimension. VR was adopted because it is challenging to set variables and monitor data in a complex construction field. The task is to identify crane signals presented by preset signalman in the virtual environment and respond to the correct operation. The signals are most common and frequently used at the construction site: hoist and lower the hook, extend boom, retract the boom, turn left or right, and emergency stop as Figure 4 shows.

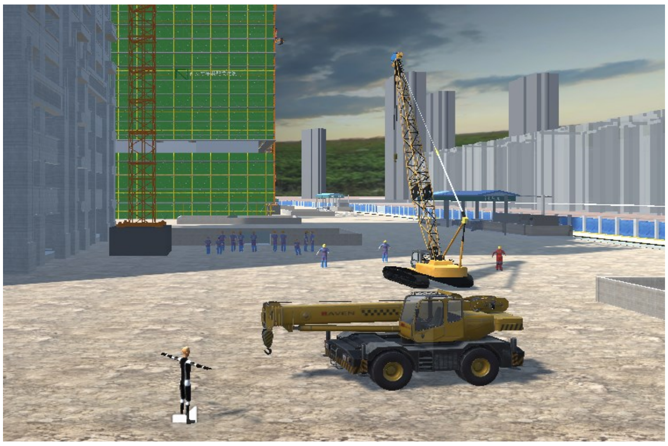

Figure 3: Virtual Scenario of the Experiment

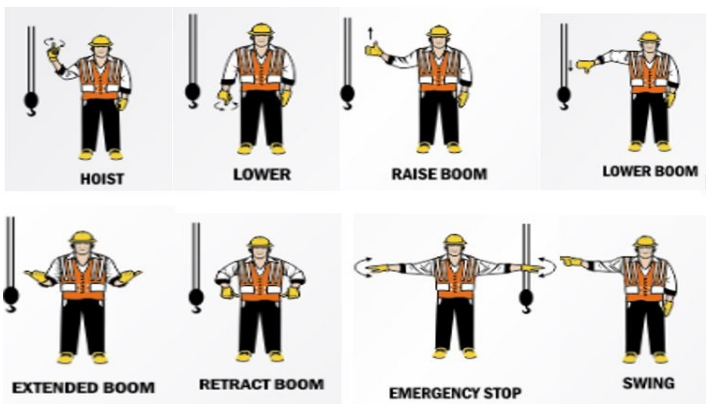

Figure 4: Signals Presented in the Experiment

Experiment Design. Information load (IL) is induced by three information attributes amount, ambiguity, presentation format (auditory, visual, mixed) reference to Appendix 1. The degree of information load was produced by the interactive effect of limited time and information attributes. Hence, the first module means participants need to identify the different amounts of crane hand signals (5,10,15) in one minute. Module B adds fuzzy gestures to simulate the condition that signalmen give non-standard signals when they are lax and exhausted, or when other objects occlude signalmen. Crane signals are conveyed in two ways at the actual workplace: hand signals and radio communication. Modules C&D have taken signals presentation into consideration, which provides participants with audio signals and mixed signals that alter between audio and gestures.

Participants. Three students participated in the preliminary experiment, who are all male and age ranged from 24-29 years. The ethical research committee approved the ethical application of the experiment. The author intends to invite ten crane operators, including novice and experienced operators in the formal experiment.

Experiment Procedure. Participants are informed about detailed procedures and requirements before the experiment, and they have 30 minutes to practice operating. Participants are required to complete each module in turn and record operation performance and synchronous EEG waves meanwhile. The EEG apparatus is Emotiv EPOC with 14 electrodes. At the end of every trial, operators need to fill out the NASA Task Load Index (NASA-TLX) scale (Carswell *et al.*, 2010) to record subjective ratings of cognitive load.

3.2 Hypotheses

Based on the literature review and designed experiment, the authors proposed the following hypotheses in the crane signals communication:

1. The number of crane signs would lead to a significant increase in information load than ambiguity;
2. Auditory crane signals have a positive effect of decreasing of information load than visual presence;
3. The mixed presentation of crane signals negatively influenced information load than a single format;
4. The relationship between information load and cognitive load follows a linear correlation.

4. Preliminary Results

For lack of space, this paper only includes response results and self-ratings of cognitive load, and preliminary EEG related results.

4.1 Response Accuracy

The average response accuracy of modules ABCD are 88.52%, 90.74%, 92.96%, and 93.33%, and the accuracy of signal number 5&10&15 are 96.67%, 88.33%, 89.17%. A two-way ANOVA with factors (presentation ways vs. signal number) shows the signal number is a significant factor ($F=3.65$, $df=2$, $p=0.04$) but presentation format not ($F=0.65$, $df=3$, $p=0.59$), and the interaction between them is not significant. The current statistical comparison is mostly affected by the small sample size. The specific response accuracy of each module shows in Figure 5. The accuracy between crane hand signals and signals with ambiguity does not show a significant difference among almost all signal numbers. Audio signals do improve operational accuracy than crane signals. Besides, the shift between presentation ways seems to improve accuracy overall. Besides, the increase in number almost reduces the accuracy, but modules of A&B do not show gradient descent. Instead, C&D modules show the trend, especially module D shows obvious gradient descent when participants are facing mixed signals.

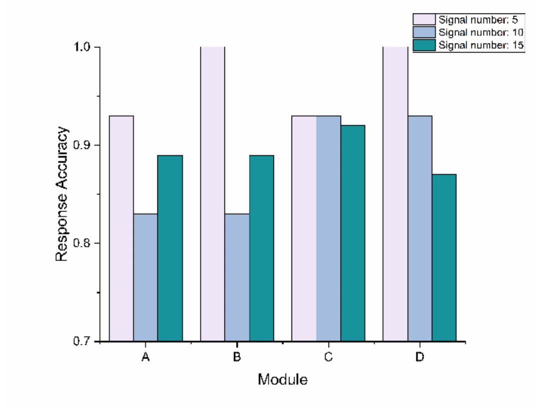

Figure 5: Average Response Accuracy of Each Module

4.2 NASA-TLX Results

NASA task load index scale is a technique that has been developed by NASA to assess the relative importance of six factors (mental demand, physical demand, temporal demand, performance, effort, frustration level) in determining how much cognitive load you experienced. Table 1 reports the descriptive results of the average workload of participants. The task load is higher when the amount of information is ten than when the amount of information is 5 in all modules. However, when the amount of information ranges from 10 to 15, the cognitive load does not increase significantly but tends to decrease. In terms of the effect of information attributes, audio signal significantly reduces cognitive load compared with gesture signals (48.93 and 54.22). Ambiguous and non-standard information mixed in the signals increased the cognitive load of the subjects (61.15 and 54.22). The shift in signal expression did not significantly lead to an increase in cognitive overload (57.89 and 54.22).

Table 1: Workload assessed by NASA-TLX scale

Type	**Number of Signals**			**Mean ± SD**
	5	**10**	**15**	
Hand Signals	49±13.75	54.78±6.68	58.89±12.85	54.22±10.87
Fuzzy Signals	59.78±8.77	62.22±8.00	61.44±17.22	61.15±10.51
Audio Signals	41.11±5.70	51.11±4.60	54.55±3.10	48.93±7.24
Shift signals	54.00±8.33	64.78±9.26	54.89±6.21	57.89±8.68

According to task-load feedback of participants in Figure 6, the operational task has much higher mental demand than physical demand. The main content of the operation task is real-time processing of information from the signaler or the outside environment, which is indeed a mental-consuming activity. The effort remains higher in all modules, especially fuzzy signals presented while signals are 5 or 10. Furthermore, signal switches of expression have higher requirements for effort and time. In terms of frustration level, fuzzy signals are likely to decrease the confidence level of participants. However, subjects always are confident with task accuracy and performance in the face of audio signals. When delivery more signals to subjects to process, there is a continuous upward trend in the temporal demand. Change in the amount of information can cause more time pressure on the information processor than vague expressions in the signal.

It can be seen that the audio signals can significantly reduce the mental load of the subjects. Moreover, in the process of processing the voice signal, the participants also have more confidence in their processing and judgment. Therefore, hypothesis 2 is preliminarily verified by self-ratings, and the audio expression mode can reduce the difficulty of judgment and understanding in the communication of crane signals. In other words, more hand signals are likely to result in information overload, but the increase in audio signals does not necessarily lead to information overload. Concerning information quality, the decrease in information quality would lead to a loss of confidence in information processing.

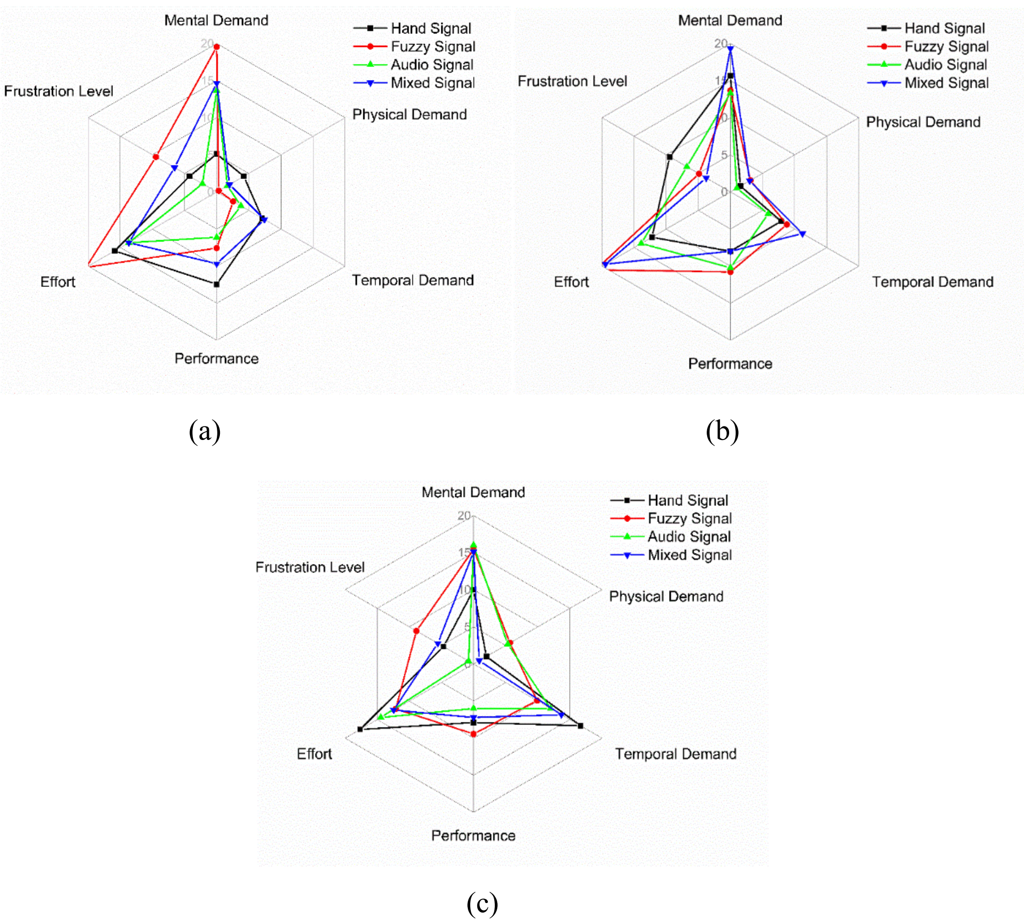

Figure 6: Assessment of Subjective Cognitive Load; (a)(b)(c) correspond to when 5, 10, 15 Signals Presented

4.3 EEG Preliminary Results

The collected EEG raw data firstly was preprocessed by EEGLAB to reject artifacts like spikes, electrooculography (EOG), electromyography (EMG). The filtered data was transformed into the energy of each frequency band through discrete wavelet transform (DWT). We currently obtained the average energy of parietal alpha (P7, P8) and frontal theta (F3, F4, F7, F8, FC5, FC6) of each trial, as Figure 7 shows. With the increase of cognitive load, the parietal alpha attenuation and the increase in frontal theta are validated (Antonenko et al., 2010). Herein, the reduced alpha and the enhanced theta are considered to represent the increase of CL level in this paper.

In terms of the impact of the signal number on CL, the alpha power tends to decrease as the number of signals increases. It is not apparent that the signal number changes from 5 to 10 but from 10 to 15. Theta energy does not show a distinct trend when the number of signals changes. For the impact of presentation type on CL, module A does not show a consistent trend in alpha and theta. Surprisingly, the alpha power of module B is more significant in S5 and S10, while theta energy is smaller in all modules. The outcome may be because the signal ambiguity is not enough from participants' feedback. The alpha energy in module C is more considerable in the three groups, and theta is smaller in S10 and S15, indicating that audio signals can reduce cognitive load. The energy of alpha in group D is relatively small among the three variables, and theta value is relatively high in S10 and S15. Constant switching of signal forms indeed consumes more cognitive resources.

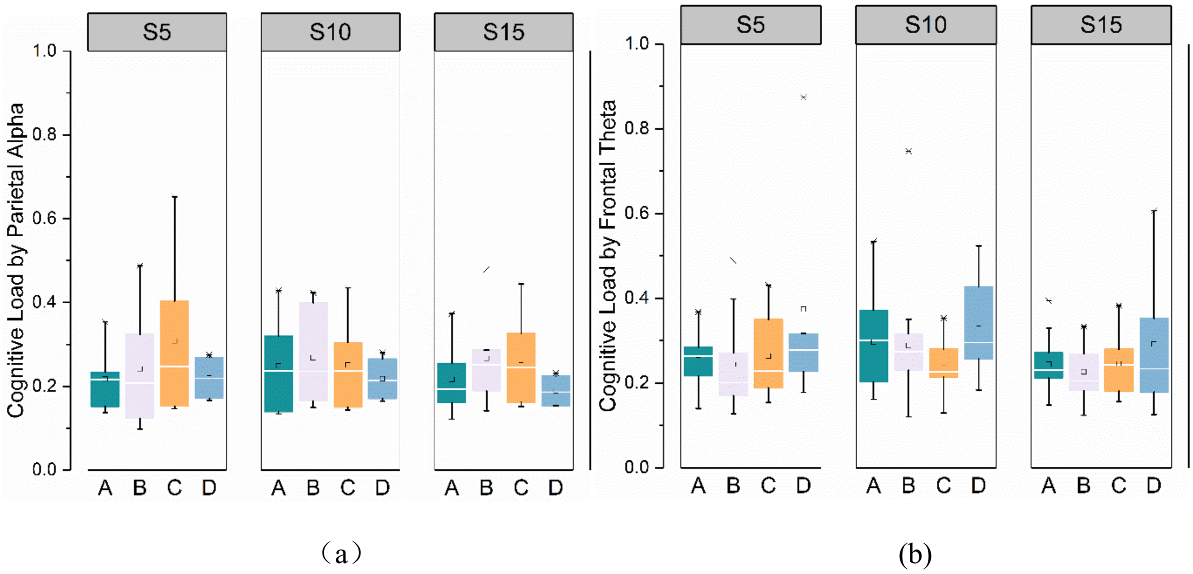

Figure 7. Assessment of Cognitive Load; (a) Parietal Alpha Power; (b) Frontal Theta Power

5. Discussion

To conclude, different information presentation ways indeed have an impact on cognitive load from the self-rating results and EEG preliminary results, and the signal number affects response accuracy. However, it is needed to combine further EEG indices to quantify cognitive load and explore cognitive areas undergoing information overload. The main limitations of the pre-experiment are the samples, which are too small, and the subjects are not professional operators. After all, students have no operational experience, and the training duration is limited, so their response to different signals will be affected by their nonproficiency. It is also noted that this experiment was conducted in a virtual environment, and the difference between VR and the real situation is unknown. More research needs to probe into the interaction between the decision maker's performance and information processing process, attention allocation, emotions reaction, and the environment.

References

Antonenko, P. *et al.,* (2010). 'Using Electroencephalography to Measure Cognitive Load', *Educational Psychology Review*, 22(4), pp. 425–438. doi: 10.1007/s10648-010-9130-y.

Atkinson, R. C. and Shiffrin, R. M., (1968). 'Human Memory: A proposed system and its control processes BT - The Psychology of Learning and Motivation', *The Psychology of Learning and Motivation*, 2(5), pp. 89–195. doi: 10.1111/j.2007.0030-1299.15674.x.

Carswell, C. M. *et al.,* (2010). 'Hands-free administration of subjective workload scales: Acceptability in a surgical training environment', *Applied Ergonomics*. Elsevier Ltd, 42(1), pp. 138–145. doi: 10.1016/j.apergo.2010.06.003.

Gibson, J. L., Ivancevich., J. M. and James H. Donnelly, J., (2001). *Organizations: behaviour, structure and processes*.

Haksever, A. M. and Fisher, N., (1996). 'A method of measuring information overload in construction project management', *Proceedings CIB W89 Beijing International Conference*, pp. 310–323.

Kelton, A. S., Pennington, R. R. and Tuttle, B. M., (2010). 'The Effects of Information Presentation Format on Judgment and Decision Making: A Review of the Information Systems Research', *Journal of Information Systems*, 24(2), pp. 79–105. doi: 10.2308/jis.2010.24.2.79.

Majdic, B. *et al.*, (2017). 'Monitoring brain waves in an effort to investigate student's cognitive load during a variety of problem solving scenarios', *2017 Systems and Information Engineering Design Symposium, SIEDS 2017*, pp. 186–191. doi: 10.1109/SIEDS.2017.7937713.

Meyer, J. A. (1998) 'Information overload in marketing management', *Marketing Intelligence & Planning*, 16(3), pp. 200–209. doi: 10.1108/02634509810217318.

Miller, G. A., (1956). 'The magical number seven, plus or minus two: some limits on our capacity for processing information', *Psychological Review*, 63(2), pp. 81–97. doi: 10.1037/h0043158.

O'Reilly, C. A., (1980). 'Individuals and Information Overload in Organizations: Is More Necessarily Better?', *Academy of Management Journal*, 23(4), pp. 684–696. doi: 10.2307/255556.

Preece, C. and Stocking, S., (1999). 'SAFETY COMMUNICATIONS MANAGEMENT IN CONSTRUCTION CONTRACTING', 2(September), pp. 15–17.

Roetzel, P. G., (2018). 'Information overload in the information age: a review of the literature from business administration, business psychology, and related disciplines with a bibliometric approach and framework development', *Business Research*. Springer International Publishing. doi: 10.1007/s40685-018-0069-z.

Roetzel, P. G., (2019). 'of the literature from business administration , business approach and framework development', *Business Research*. Springer International Publishing, 12(2), pp. 479–522. doi: 10.1007/s40685-018-0069-z.

Rogers, R. D., (2011). 'The cost of information overload', pp. 93–97.

Schick, A. G., Gordon, L. a. and Haka, S., (1990). 'Information Approach: A Temporal Approach', *Accounting, Organizations and Society*, 15(3), pp. 199–220. doi: 10.1016/0361-3682(90)90005-F.

Tam, V. W. Y. and Fung, I. W. H., (2011). 'Tower crane safety in the construction industry: A Hong Kong study', *Safety Science*. Elsevier Ltd, 49(2), pp. 208–215. doi: 10.1016/j.ssci.2010.08.001.

Vessey, I., (1994). 'The effect of information presentation on decision making: A cost-benefit analysis', *Information and Management*, 27(2), pp. 103–119. doi: 10.1016/0378-7206(94)90010-8.

Wickens, C. D., (2002). 'Multiple resources and performance prediction', *Theoretical Issues in Ergonomics Science*, 3(2), pp. 159–177. doi: 10.1080/14639220210123806.

Zarjam, P., Epps, J. and Lovell, N. H., (2015). 'Beyond Subjective Self-Rating: EEG Signal Classification of Cognitive Workload', *IEEE Transactions on Autonomous Mental Development*, 7(4), pp. 301–310. doi: 10.1109/TAMD.2015.2441960.

Zhang, R., Liu, A. M. M. and Chan, I. Y. S., (2018). 'Effects of Quality and Quantity of Information Processing on Design Coordination Performance', pp. 41–49. doi: 10.4236/wjet.2018.62B005.

Zhou, W. *et al.,* (2018). 'Tower crane safety on construction sites: A complex sociotechnical system perspective', *Safety Science*. Elsevier, 109(June), pp. 95–108. doi: 10.1016/j.ssci.2018.05.001.

Zhou, Z., Goh, Y. M. and Li, Q., (2015). 'Overview and analysis of safety management studies in the construction industry', *Safety Science*. Elsevier Ltd, 72, pp. 337–350. doi: 10.1016/j.ssci.2014.10.006.

Appendix

Appendix 1: Experiment Modules Design

Modules	Independent Types	Independent Variables	Trial	Duration(minute)
A	Amount	5 (hand signals)	1	1
		10 (hand signals)	2	1
		15 (hand signals)	3	1
B	Ambiguity	3* out of 5 (hand signals)	4	1
		6* out of 10 (hand signals)	5	1
		9* out of 15 (hand signals)	6	1
C	Presentation Ways	5 (auditory)	7	1
		10 (auditory)	8	1
		15 (auditory)	9	1
D	Presentation Ways	5 (mixed)	10	1
		10 (mixed)	11	1
		15 (mixed)	12	1

Note: * means non-standard crane hand signals.

Formal analysis and validation of Levels of Geometry (LOG) in building information models

Jimmy Abualdenien, André Borrmann
Chair of Computational Modelling and Simulation
Technical University of Munich, Germany
jimmy.abualdenien@tum.de

Abstract. Construction projects are multidisciplinary and contractual. The collaboration among the project participants and the quality of the exchanged building information throughout the project lifecycle are prescribed in legal agreements. The Level of Development (LOD) concept is widely used for describing the building elements' maturity. Detailing models to a certain LOD is crucial for integrating the partial models as well as consumes additional time and costs. Every LOD comprises requirements for both Level of Geometry (LOG) and Level of Information (LOI). Thus far, the validation of LOD is limited to the LOI, whereas, checking the quality of the LOG is a complex and unsolved task. This paper proposes a framework for validating the LOG of building elements. In more detail, a LOG dataset is modelled, and then a formal metric is defined based on an extracted set of geometric features. Finally, a random forest model is developed for predicting the LOG.

1. Introduction

Several countries worldwide are promoting the research and development of BIM-based methodologies to facilitate their integration in the projects' life cycle. As construction projects are multi-disciplinary, a fundamental pillar for integrating BIM is describing the building elements' maturity at a particular design phase. This is crucial for the overall collaboration among the project participants as it acts as an agreement of (what) information should be available at what time (when). Based on that information, it can be decided for what the model can be used for (purpose), which makes it possible to determine what model deliverables are expected from the involved actors (who) (Beetz, Borrmann and Weise, 2018). The exchange of complete BIM data within the Architecture, Engineering, and Construction (AEC) industry is crucial, as it is prescribed in legal agreements, where the information for each specific model is specified. Accordingly, a common legal framework for organizing this data is required.

Data quality is described by the compliance of its characteristics to requirements (ISO, 2015). More specifically, the quality of building information quality is expressed by the correctness and completeness of the topological relationships, geometric detailing, and semantics. Various guidelines were published to deliver a standard in which practitioners can use as a basis for a common language in their projects. A popular concept for defining the content of a model at a certain point during the design process is the Level of Development (LOD) (BIMForum, 2019). The LOD refers to the completeness and reliability of the building elements' information. A similar concept was introduced by the European Standardization Organization (CEN) (DIN, 2019), which defines the term Level of Information Needs (LOIN) comprising specifications for LOG and LOI for supporting a particular use-case.

Currently, practitioners rely on the LOD concept terminology to specify which information they need to deliver and/or to carry out their tasks (Leite *et al.*, 2011). However, as the different LOD specifications are loosely defined, each practitioner has a different interpretation of what a specific LOD means and which information should be present in the model (van Berlo and Bomhof, 2014). Such inconsistencies cause severe miscommunication and additional expenditure, which increases project risks (Leite *et al.*, 2011). For example, a structural engineer might model a highly detailed structural system in case it was understood that building elements are at high LOD, giving the impression that they are stable and less subject to change. However, the building model might be a sketch at the early design phase, which would drastically change in the subsequent phases (van Berlo and Bomhof, 2014).

Exchanging building models among the project participants requires checking the models' conformance with the defined LOD requirements, which includes semantics, a.k.a Level of Information (LOI), and geometric information, a.k.a. Level of Geometry (LOG). While checking the completeness of the semantic information is straightforward (Abualdenien and Borrmann, 2019) and several commercial software solutions exist for this purpose, confirming that the modelled geometry fulfils the expected LOG is a complex and still unsolved task.

This paper addresses the currently existing gap of determining the LOG of building elements by investigating the major characteristics representing the increase of detailing based on a formal metric. To this end, a set of BIM elements of different family types are modelled at multiple LOGs, and the geometric information of each level is investigated. In more detail, in each LOG, the geometrical features are extracted, and their complexity is measured using a combination of various advanced geometry processing algorithms. Finally, this paper contributes with a standard criterion that facilitates inferring the LOG of any given building element.

The paper is organized as follows: Section 2 discusses the background and related work. Section 3 provides an overview of the framework developed in this paper, explaining the approach followed to generate the LOG dataset and extracting geometric features. A model for predicting the LOG of building elements is developed and evaluated in Section 4. Finally, Section 5 summarizes our progress hitherto and presents an outlook for future research.

2. Background and Related Work

2.1 3D Shapes

The 3D representation of objects is a fundamental aspect for numerous domains, starting from computer graphics to building information modelling. A popular approach to represent shapes in various applications is the polygonal mesh representation, which explicitly captures a shape's surface characteristics and topology (Botsch *et al.*, 2010; Garland, 1999; Shikhare, 2001). Polygonal meshes require only a small number of polygons to represent simple shapes (regardless of their size). Additionally, it has the necessary capability to comprehensively represent complex shapes with high resolution, capturing the salient surface features. Accordingly, simple shapes are represented by few large polygons, while detailed and complex shapes are represented by many small polygons. The mesh polygons comprise a set of vertices, which are interpolated through a connectivity graph to approximate the desired surface.

2.2 Shape Complexity

As detailed below, there are strong indicators that there is a correlation between LOG and shape complexity. The meaning and measurement of a shape complexity can vary according to different aspects. Processing geometric models can be as simple as iterating over a mesh's vertices, faces, and edges, or as complex as performing different calculations to extract information about the curvature or shape topology. Numerous researchers have developed algorithms to retrieve the most dominant features (Botsch *et al.*, 2010), including detecting sharp edges, deducing surface patches, and decomposing the shape into smaller and meaningful shapes, a.k.a segmentation (Shapira, Shamir and Cohen-Or, 2008). Dominant features provide an essential description of the geometrical objects' resolution and detailing. In the same context, Hanocka *et al.* (2019) and Nikhila *et al.* (2020) have developed MeshCNN and PyTorch3D by employing deep-learning approaches to analyze, process, and extract features from 3D shapes.

A popular classification for shape complexity was firstly introduced by Forrest, where it defines three main types (Forrest, 1974): (1) geometric, describes the shapes' basic features, such as lines, curves, faces…etc., (2) combinatorial, refers to the topology of the shape, i.e. the number of components that comprise it, and (3) dimensional, which classifies the shape as 2D, 2.5D or 3D. Other researchers have interpreted shapes as a set of rules through shape grammars (Heisserman, 1994). Shape grammars describe the shape decomposition as a set of rules and series of transformations, including addition, subtraction, rotation, etc.

Accordingly, defining what a shape complexity means in the AEC industry requires the specification of which geometric features are essential for capturing the degree of maturity of building elements at the different LOGs.

2.3 Level of Development (LOD)

As a response to the need of having a consensus about what information should exist during the development of building elements, various guidelines were published to deliver a standard, which practitioners can use as a basis for a common language in their projects. Prior to the LOD concept, a relatively similar concept, a.k.a Level of Detail (LoD), was already common in computer graphics. The LoD is used to bridge the graphical complexity and rendering performance by regulating the amount of detail used to represent the virtual world. In computer graphics, the LoD concept is mainly concerned with the geometrical detailing (Luebke *et al.*, 2003). In Geographic Information System (GIS), the LoD represents different levels of geometric and semantic complexity of a city model (Kolbe, Gröger and Plümer, 2005).

In the AEC industry, the LOD represents the completeness and reliability of the geometrical and semantical information associated with building elements (BIMForum, 2019). The first initiative was by VicoSoftware® (Trimble, 2013; VicoSoftware, 2005), where the Level of Detail (LoD) was introduced. The LoD concept has then been adopted and refined by the American Institute of Architects (AIA) to become the Level of Development (LOD) (AIA, 2008). The AIA introduced a definition of the LOD that comprises five levels, starting from LOD 100 and reaching LOD 500. The BIMForum working group developed LOD 350 and published the Level of Development Specification based on the AIA definitions (BIMForum, 2019). At the same time, Trimble's Project Progression Planning (Trimble, 2013) was published and is widely used in practice.

2.4 LOG Analysis and Validation

The process of adopting a LOD specification in a particular country (or even internally in the individual firms) requires a comprehensive analysis and understanding of which geometric and semantic information should be present at each LOD. However, practitioners have an inconsistent understanding of the information necessary at each LOD (Abualdenien and Borrmann, 2019; van Berlo and Bomhof, 2014). This is because although the specification of semantics is usually simplified to a list of properties, defining the geometrical complexity is highly vague and systematically checking it is an unresolved task.

In this regard, Leite *et al.* (2011) evaluated the modelling effort associated with generating BIM models at different LODs. The authors have shown the need for an increased modelling time ranging from doubling the modelling effort to eleven folding it, to detail models further to reach a higher LOD. Additionally, van Berlo and Bomhof (2014) has analysed 35 building models (where each comprises multiple building elements) taking into account different ratios between volume, triangles, space areas, and the number of properties, in an attempt to find a standard or relationship between the different LODs. However, the authors did not find any standard or pattern of increasing the complexity across the LODs. The main reason for not detecting any standard for increasing the complexity is because of the inconsistencies and different interpretations of the LOD specifications (Gigante-Barrera *et al.*, 2018). More specifically, using the LOD concept for describing the maturity of the overall building model versus the individual elements. Van Berlo and Bomhof (2014) performed their experiments on the overall building models rather than the individual elements. In this regard, the LOD specifications provided by the AIA (AIA, 2008), BIMForum (BIMForum, 2019), and Trimble (Trimble, 2013) describe the geometric and semantic information of the individual elements rather than the overall building model. On a wider scale, Wong and Ellul (2016) analysed the geometry of 3D city models for fit-for-purpose by looking into the ratios between the number of buildings, geographic area, geometrical details, and disk size.

3. Methodology

The hypothesis in this paper is that the geometric complexity of the individual elements can be represented by multiple features, forming the basis for a metric allowing to formally assess the geometric complexity of a given model. Through analysing the changes of the extracted features across the LOGs, the detailing pattern can be recognised, which in turn provides the means for the LOG classification of building elements.

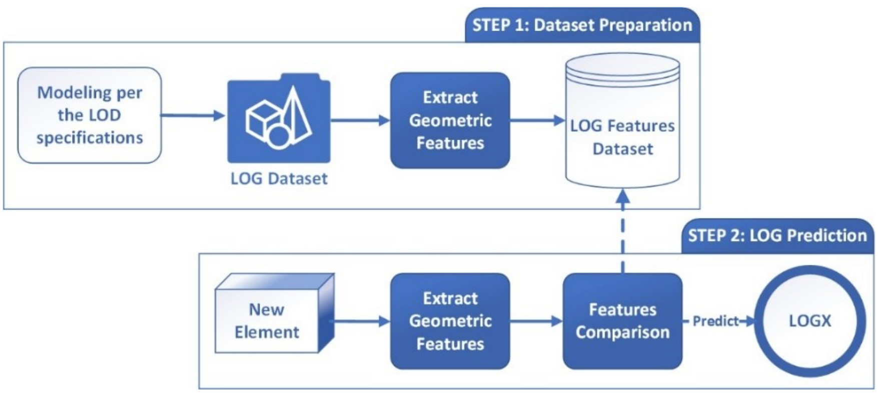

Figure 1: The proposed framework for LOG prediction

As depicted in Figure 1, the proposed approach consists of two steps. First, a LOG dataset is modelled according to the most common LOD specifications. The dataset generation took into account modelling the different kinds of building elements as well as additional cases for including openings and reinforcement. Afterwards, multiple geometry processing algorithms are performed to extract the most prominent features representing the shape complexity of each building element. The result is a dataset of geometric features for diverse building elements on the LOGs 200 - 400. The second step describes the process of predicting the LOG of a new element. The geometric features of the new element are extracted in a similar way to the dataset generation, and then the individual features are compared for similarity to the features available in the dataset to predict the new element's LOG. The complete framework is discussed in detail in the next subsections.

3.1 Modelling per the LOD Specifications

In this study, the BIMForum's LOD specification (BIMForum, 2019) and Trimble's Project Progression Planning (Trimble, 2013) were comprehensively reviewed and followed during modelling different families on multiple LODs. We followed the combination of multiple specifications because although the BIMForum's definitions are descriptive for many building elements, they are in many cases, vague in describing the progression of the geometric detailing. Despite the fact that the specification is prepared in a way that visualizes the newly added parts in every LOD, the graphical illustrations for many elements are inconsistent and ambiguous. For example, when modelling a stair, information regarding the riser count and height should be available starting from LOD 300 (per the text description). However, the graphical illustration at LOD 200 already includes them.

Based on the LOD specifications, LOG 100 (conceptual model), is limited to a generic representation of the building, meaning no shape information or geometric representation. At LOG 200 (approximate geometry), elements are represented by generic placeholders, depicting the overall area reserved by their volume. At LOG 300 (precise geometry), the elements' main shape is refined, showing the fundamental detailing required for describing the element type. Next, at LOG 350 (construction documentation), any parts that are necessary for depicting the connections with other elements, that are attached or nearby, are additionally modelled. Modelling these parts, like supports and connections, is crucial for the coordination with different domain experts. Finally, at LOG 400, elements are fully detailed, providing the accuracy required for fabrication, assembly, and installation. LOG 500 represents the field verified model state, which means in terms of design and detailing, it is the same as LOG 400.

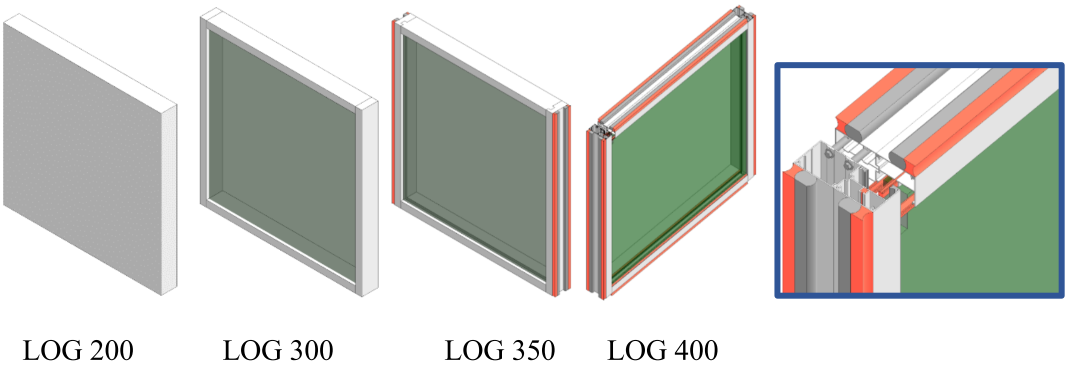

Figure 2: Dataset sample: window at LOGs 200 - 400

The modelling process followed to generate the dataset was focused on the LOGs 200 - 400. In order to have confidence in how to model the families, we have modelled first most of the families existing in the specifications, taking guidance from the text description as well as the visual illustrations. Afterwards, we have expanded the dataset size by making use of the available BIM objects libraries[1], where the families were downloaded and adjusted to match the different LOGs. Figure 2 shows a window on multiple LOGs from the modelled dataset. In

[1] https://www.bimobject.com/ | https://www.nationalbimlibrary.com/ | https://market.bimsmith.com/ | https://www.revitcity.com/ | http://www.familit.com/ | https://www.arcat.com/

total, the modelled dataset included 216 objects (54 families at four LODs). Figure 3 shows an example of an elevator, stairs, brick wall, and wall frame on multiple LODs.

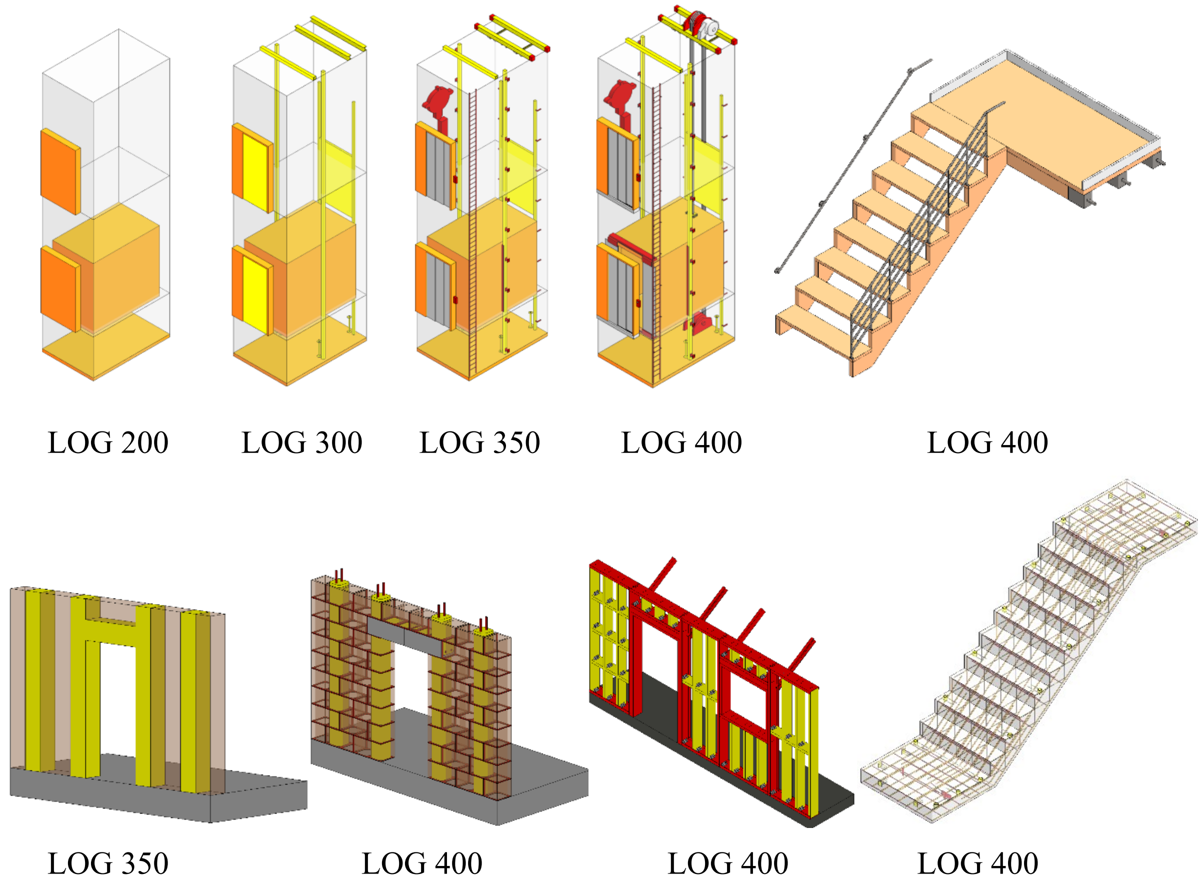

Figure 3: Dataset sample: selected models at different LOGs

3.2 Analysis and Extraction of LOG Features

Typically, shapes having more numerous or smaller features can be viewed as more detailed. The challenge in identifying the LOG through analysing geometric features lies in deducing a standard pattern that describes the individual LOGs. The simplest geometric metrics can be based on the total number of vertices, faces, and edges. However, an increased number of these features does not necessarily mean an increased detailing or higher LOG. For example, a window at LOG 200 (rectangular shape) consists of 30 vertices, 16 faces, and 78 edges, while a cylindrical column or heating tank at LOG 200 is formed by 2358 vertices, 4268 faces, and 13244 edges. Thus, the sole consideration of vertices, faces and edges does not provide a suitable metric. To measure the geometric detailing (i.e. LOG) of elements, the applicable features need to be capable of representing the geometric detailing of elements taking into account the overall shape.

In the proposed approach, we combine the extracted results of multiple geometric features to observe various aspects of the shape detailing. In total, we investigated the effect of detailing across the LOGs through four main aspects, resulting in 14 geometric features, as follows:

1. **Basic Geometric Features:** The increase of vertices, faces, and edges. Here, the ratio of vertices to faces provided an additional indicator for the shape complexity (this ratio indicates the required points for capturing the shape details). In more detail, a shape

with just rectangular parts always has a ratio of 2, adding more complex parts, like screws or reinforcement, substantially reduces the ratio.

2. **Edges Length:** Count and length of edges can provide a strong description of the shape complexity. Numerous short edges reflect more detailing and additional complex parts. In this regard, we measured the length of 50%, 62.5%, and 75% of edges, and compared it to the total edges' length. Similarly, the mean edge length is also calculated and compared.
3. **Sharp Edges:** Sharp edges represent the most prominent surface characteristics of a geometric shape. Therefore, sharp edges are extracted and counted by measuring the change in curvature as well as counting the number of surface patches bounded by those edges.
4. **Diameter-based Segmentation:** In this process, the shape is segmented into smaller meaningful pieces based on the change in diameter (Shapira, Shamir and Cohen-Or, 2008). This segmentation provides additional insights into the complexity of the parts comprising building elements on each LOG. Accordingly, we count the segments, measure their area, and evaluate their shape (flat surfaces, cubic, or cylindrical). In this aspect, the segments with similar shapes are grouped, and the ratio of the count and area of each shape to the overall segments can characterize the overall shape (differentiating a window from a tube system).

The discussed geometric features above were extracted for the complete dataset presented in Section 3.1. Additionally, multiple ratios were calculated to capture different positive or negative correlations among the features, including average area per surface patch and segment, as well as average vertices per face, patch, and segment. Finally, the extracted features were normalized to make the features correspond to the elements' geometric complexity regardless of their total area or total edges length.

After the extraction of features, their change across the LOGs was analysed. Figure 4 shows three features for three different elements, wall, column, and a stair. Those three different elements are selected to show the difference in their pattern throughout the LOGs. Interestingly, we have noticed relatively similar patterns among rectangular shapes (e.g. walls, doors, windows), cylindrical shapes (e.g. columns, heating tanks, tube systems), and complex shapes (e.g. stairs, escalators, elevators). In the same context, we observed that in case the count of the cylindrical segments is low and represents more than ~50% of the overall area, then the overall shape has a high probability of having a cylindrical overall shape (a pipe as an example).

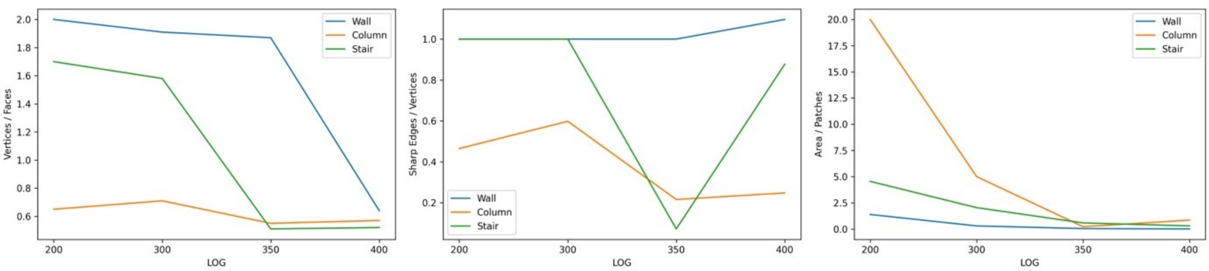

Figure 4: Three geometric features of three building elements on different LOGs

Additionally, rectangular and complex shapes at LOG 350 and 400, are composed of a high number of cylindrical segments while representing less than ~40% of the overall area. When reinforcement is modelled, then the number of cylindrical segments is relatively high (~50 – 80%), while their aggregated area is less than ~40% of the overall area.

4. Prediction of LOG

The analysis of the extracted features (presented in the previous section) showed multiple patterns that are present in the dataset. Predicting the LOG of a new building element is a classification problem, i.e. detecting which class (LOG) an observation (the set of extracted features) belongs to. The simplest way to classify new observations is to consecutively try to split the dataset observations (based on feature values) in a way that groups similar observations as much as possible. This is exactly what a decision tree (Breiman, 2001) performs while following a certain route yielding a specific result. However, as decision trees are based on a greedy model, meaning it tries to find the most optimal decision at each step and does not consider the global optimum, we decided to build a random forest model (Breiman, 2001). A random forest consists of numerous decision trees that operate as an ensemble; each decision tree selects features randomly and predicts a class; the class that receives the highest number of votes becomes the final prediction.

In order to develop the random forest model, the modelled elements presented in Section 3.1 were randomly split into training and test datasets with a ratio of 80% (172 elements) and 20% (44 elements) respectively. The resultant model is composed out of 22 trees, where the max depth of each is four. Figure 5 shows one decision tree of the developed random forest using the training dataset. In this tree, the average area of surface patches is the first metric splitting the dataset to LOG 200 and 400. The Gini Impurity represents the likelihood of classifying a new instance incorrectly (Raileanu and Stoffel, 2004). Then, the metrics of the average vertices per faces, as well as the average area of surface patches, are used to split the dataset further. Going deeper in the right branch, the tree is completely confident about predicting LOG 300 for two samples while 94% confident of LOG 200 of 32 samples. On the other hand, the left branch has lower confidence at the first level, but it increases in the next levels. It is important to emphasize here that this is one decision tree of the complete forest. The other trees randomly employ a different set of geometric metrices to reach a final decision.

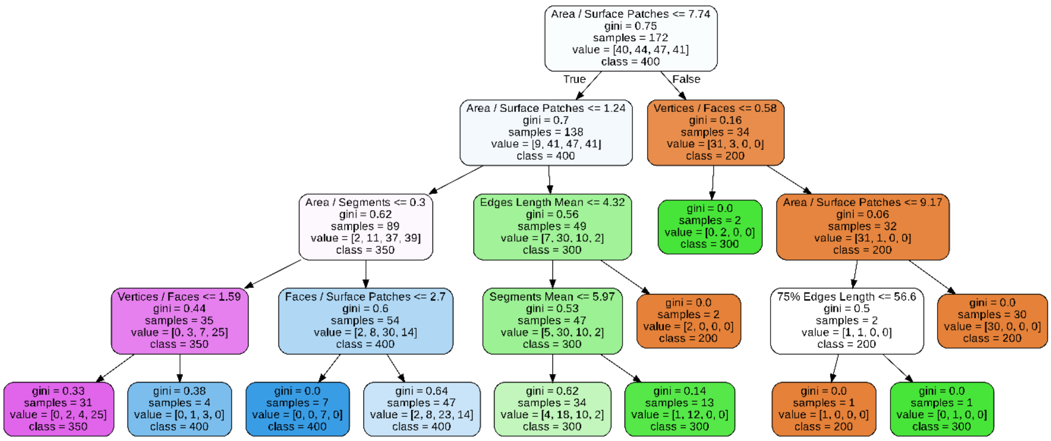

Figure 5: Random forest model: showing the selected features of one decision tree

The evaluation of the performance of the developed random forest model for predicting the LOG was conducted on a completely new set of elements (test dataset - 44 elements). The performance metrics is described as precision, recall, and F-Score, as presented in Table 1. Precision describes the model performance in positive predictions while considering false positives. Recall incorporates false negatives instead of false positives, and F1-score provides a balance between precision and recall. Table 1 shows the confusion metrics, depicting the difference between the actual and predicted LOG. In total, 35 out of 44 elements were predicted correctly. Additionally, investigating the incorrect predictions further, we can notice that the classes were confused with the its close neighbours, e.g. LOG 200 with 300. This is mainly because, in this specific case, the number of changes modelled to detail the model further from LOG 200 to 300 are not necessarily increasing the shape complexity enough to be differentiated. Moreover, this approach heavily relies on the dataset size (finding similar observations). Therefore, increasing the dataset size would substantially improve the model performance.

Table 1: Performance metrics, precision, recall, F1-score, and accuracy for each LOG. On the right side, the prediction confusion metrics depicts the ratio between the actual and predicted LOGs.

LOG	Precision	Recall	F1-score
200	0.90	0.82	0.86
300	0.80	0.86	0.83
350	0.67	0.80	0.73
400	0.86	0.67	0.75
Accuracy			
Macro Avg.	0.81	0.79	0.79
Weighted Avg.	0.81	0.80	0.80

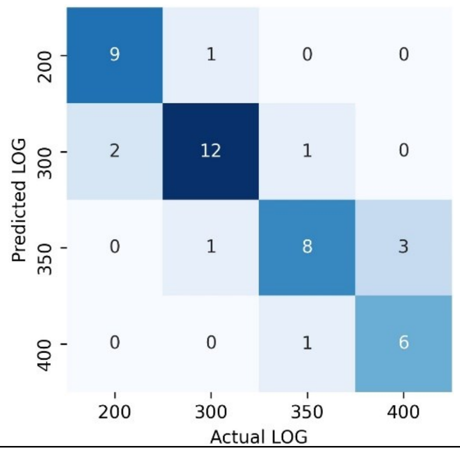

5. Conclusions and Future Research

Building models consist of numerous and diverse kinds of information to fulfil multiple use-cases, including fire-safety regulations, structural and energy analysis, as well as pedestrian simulations. Hence, practitioners need a common ground to communicate the content of their requirements and deliverables across the design phases. The LOD concept brings multiple benefits for describing and managing the expected information in the individual design phases. The geometric representation of building elements is crucial for the collaboration among domain experts as it forms the basis for integrating the partial models and carrying out the different kinds of simulations. However, the currently available tools are only capable of checking the completeness of semantic information; validating the conformance of the modelled geometry to the required LOG is currently manual and prone to multiple interpretations.

This paper has proposed a framework for predicting the LOG of building elements. The prediction is based on a formal metric of a LOG dataset that includes 216 elements. The elements were modelled according to the most common LOD specifications. The metric is formed out of four main aspects, basic geometric details, edges length, sharp edges, and diameter-based segmentation. Finally, a random forest model was developed and evaluated, showing the ability to predict the LOG of 44 new building elements. As a next step, additional building elements should be modelled to improve prediction accuracy. Additionally, the state-of-the-art acritical neural networks will be evaluated for extracting geometric features and predicting the LOG.

Acknowledgement

We gratefully acknowledge the support of the German Research Foundation (DFG) for funding the project under grant FOR 2363. We thank the student Patrick Nordmann for his contribution in modelling the LOG dataset.

References

Abualdenien, J. and Borrmann, A., (2019). 'A meta-model approach for formal specification and consistent management of multi-LOD building models', *Advanced Engineering Informatics*, 40, pp. 135–153.

AIA, (2008). 'Building Information Modeling Protocol Exhibit'. Available at: https://bit.ly/2NZBbTV (Accessed: 7 May 2019).

Beetz, J., Borrmann, A. and Weise, M., (2018). 'Process-based definition of model content', in *Building Information Modeling:* Springer, pp. 127–138.

BIMForum, (2019). 'Level of Development Specification Guide'. Available at: http://bimforum.org/lod/ (Accessed: 19 March 2020).

Botsch, M. *et al.*, (2010). *Polygon mesh processing*: CRC press.

Breiman, L., (2001). 'Random forests', *Machine learning*, 45(1), pp. 5–32.

DIN, (2019). 'DIN EN 17412:2019-07 Building Information Modelling - Level of Information Need - Concepts and principles'. Available at: https://www.beuth.de/en/draft-standard/din-en-17412/306353980 (Accessed: 1 April 2020).

Forrest, A.R., (1974). 'Computational geometry-achievements and problems', in *Computer aided geometric design:* Elsevier, pp. 17–44.

Garland, M., (1999). *Quadric-based polygonal surface simplification*.

Gigante-Barrera, A. *et al.,* (2018). 'A grounded theory based framework for level of development implementation within the information delivery manual', *International Journal of 3-D Information Modeling (IJ3DIM)*, 7(1), pp.30–48.

Hanocka, R. *et al.,* (2019). 'MeshCNN: a network with an edge', *ACM Transactions on Graphics (TOG)*, 38(4), pp.1–12.

Heisserman, L., (1994).'Generative geometric design', *IEEE Computer Graphics and Applications*, 14(2), pp.37–45.

ISO, (2015). 'ISO 9000:2015(en) Quality management systems — Fundamentals and vocabulary'. Available at: https://www.iso.org/obp/ui/es/ (Accessed: 1 April 2020).

Kolbe, T., Gröger, G. and Plümer, L., (2005). 'CityGML: Interoperable access to 3D city models', in *Geo-information for disaster management:* Springer, pp. 883–899.

Leite, F. *et al.,* (2011).'Analysis of modeling effort and impact of different levels of detail in building information models', *Automation in Construction*, 20(5), pp. 601–609. doi: 10.1016/j.autcon.2010.11.027

Luebke, D. *et al.,* (2003). *Level of Detail for 3D Graphics*: Morgan Kaufmann.

Nikhila, R. *et al.*, (2020). 'PyTorch3D'.

Shapira, L., Shamir, A. and Cohen-Or, D., (2008). 'Consistent mesh partitioning and skeletonisation using the shape diameter function', *The visual computer*, 24(4), p. 249.

Shikhare, D., (2001). 'Complexity of Geometric Models', *National Centre for Software Technology, Mumbai*.

Trimble, (2013). 'Project Progression Planning with MPS 3.0'. Available at: http://support.vicosoftware.com/FlareFiles/Content/KB/Trimble%20-%20Progression%20Planning%20V15.pdf (Accessed: 19 March 2020).

van Berlo, L. and Bomhof, F., (2014). 'Creating the Dutch national BIM levels of development', in *Computing in Civil and Building Engineering (2014)*, pp. 129–136.

VicoSoftware (2005) 'BIM Level of Detail'. Available at: http://www.vicosoftware.com/ (Accessed: 13 May 2019).

From Physical to Analytical Models: Automated Geometry Interpretations

Goran Sibenik, Iva Kovacic, Valentinas Petrinas
TU Wien, Austria
goran.sibenik@tuwien.ac.at

Abstract. Building information modelling promises model-based collaboration between stakeholders in the project design stage. However, physical and analytical building models used for architectural design and structural analysis respectively can rarely be interchanged between the stakeholders due to numerous differences in building element representation, especially the representation of geometry. This papers aims to overcome the geometry representation differences by proposing geometry interpretation methods. The interpretation methods, such as linearization, planarization, reconnecting elements and perimeter adjustment, were defined for a use-case building model and implemented using a novel open data exchange framework. The methods facilitate automated conversion between physical and analytical models and provide a base for lacking standardization of interpretations. This work fills the gaps in the existing model-based communication that could eventually help with facilitating a seamless data exchange between physical and analytical models.

1. Introduction

Construction industry, as one of the least digitized, aims to increase productivity by implementing building information modeling (BIM) and achieving digital collaboration (Agarwal et al. 2016). An obstacle still present in achieving a seamless data exchange for digital collaboration is the lack of software interoperability (Grilo and Jardim-Goncalves 2010). They state that the interoperability concept needs to be expanded beyond the information systems towards business processes, employees and culture, and management of external relationships. In our previous research we identified the need to focus on domain-specific data models instead of integrated building models, and interpretations between them as business processes for improving software interoperability and eventually automating the data exchange (Sibenik and Kovacic 2019).

The level of achievement of a seamless data exchange varies between professional domains. Numerous software tools belonging to different professional domains have also differing internal structures, which hinders the full interoperability across the software tools. However, the stakeholders belonging to various domains still aim to exchange the information of interest. One of the greatest challenges is a transfer of a building model between architectural design and structural analysis (Kepplin et al. 2017). The experts exchanging information of interest need to have mutual understanding of each other's domains in order to facilitate the communication (Luyten 2015). We find the collaboration during the developed design (*Einreichsplan* in Austria) stage particularly interesting since both the architectural design plans and structural analysis calculations are required for the building permit (Kovacic et al. 2015). Software tools in both domains allow for the use of building models, however, the model-based data exchange is still burdened with problems (Sibenik 2016).

As in Eastman et al (2018), models used for architectural design are referred to as physical (or architectural (Qin et al. 2011), or BIM models (Ramaji and Memari 2018)), while the structural analysis models are analytical (or structural (Qin et al. 2011)). Representations of building elements have significant differences, especially regarding the geometry representation. While physical models aim to render the elements similarly to their real-world 3d shape, analytical models tend to simplify the geometries and reduce dimensionality of building elements to points, lines and surfaces. We identified the need to further explore these complex geometry interpretations in order to improve the interoperability itself. The interpretations (or transformations (Ramaji and Memari 2018)) have been performed mostly intuitively based on the experience of structural engineers (Kepplin et al. 2017). Therefore, the existing intuitive interpretations represent the process of defining analytical models based on information available in physical models mainly based on the experience of structural engineers.

Several research papers considered model interpretations between physical and analytical models, however not focusing on the geometry interpretation rules. A paper which most thoroughly documents the geometry interpretations is Ramaji and Memari (2018), giving a list of required interpretations for a transformation of an industry foundation classes (IFC) physical model to an IFC analytical model. Their paper emphasizes the importance of interpretations, however it is limited to swept-solid geometry defined with IFC standard (naming physical and analytical representations as swept-solid and topological respectively). In order to further edit the interpretation rules for IFC geometry definitions and contribute to the framework, expert IFC knowledge is required. Authors such as Hu et al. (2016), Qin et al. (2011) or Liu et al. (2010) focus on developing new data exchange frameworks between architectural design and structural analysis. Although geometry interpretations are an unavoidable part of each framework, they are not described in detail, serve the examined case studies, but cannot be validated for the general use or other business processes. The existing intuitive interpretation practices are not documented, nor related to the proposed interpretation methods. The interpretations serve for an "end-to-end" model transformation automation without allowing a detailed insight for end users.

Structural engineers cannot rely on completely automated processes, which are not transparent or comprehensible ("black-box scenario") (Holzer et al. 2007); as they carry the responsibility for the calculation and need to have a completely reliable model as a starting point. Therefore, a framework in our work uses open interpretation rules, which could be tailored for additional workflows and practices. Due to the lack of documented cooperative knowledge of structural engineers and architects, in this paper we will try to map some common rules for establishing an analytical model from a physical model. The research question we aim to answer is: *how to automate existing intuitive interpretations of physical to analytical building model?*

The following Section 2 will present the methodology and explain how the interpretations were defined. Section 3 describes single interpretation methods including linearization, planarization, reconnecting elements and perimeter adjustment. The methods and resulting structural model are discussed in Section 4, and the conclusion belongs to Section 5.

2. Methodology

In our previous work (Sibenik and Kovacic 2019) a novel framework and the corresponding system architecture were developed that incorporate interpretation rules in an open data exchange. The framework consists of three procedures: i) classification, ii) interpretation and iii) automation. In the first procedure, classification, the terminology and domain-specific requirements are defined. Interpretation procedure defines the relations between domain-specific classification systems, predefined terminology and definitions. Finally, the automation procedure implies automatic communication between the domain-specific models on the central database with the proprietary software tools and the belonging proprietary models.

Interpretation procedure consists of several procedural steps such as: validation, filtering, non-geometrical interpretation, geometrical interpretation and enrichment and reasoning. For the exchange between architectural design and structural analysis models the geometrical interpretation is the most challenging procedural step. Possibilities to model analytical geometry are usually numerous and not standardized, and therefore the resulting model depends on the structural engineer's experience. However, numerous similarities between different approaches exist and documenting the existing intuitive interpretations could lead to standardization. Due to the lack of documented practices, in this paper we make a new proposal to interpret geometries based on the use-case building. Additionally, the newly defined interpretations are implemented within the previously described framework.

For the use-case building model, a model of Villa Savoye was chosen. It represents the modernist work of architecture, where concrete columns define the main support system with concrete slabs. Additionally, basement walls and staircase walls on the roof terrace were considered as part of the structural system. The use case building was modelled with Autodesk Revit 2019 and exported to IFC 2x3. The IFC building model is converted to the JSON format with a self-made converter *IFCtoJSON* (Sibenik and Petrinas 2020) in order to store it in the semi-structured database MongoDB.

Further on, a geometry kernel is used to define and edit geometry. Geometry kernels such as 3d ACIS Modeler (ACIS) were already used to overcome the differences between architectural design and structural analysis (Mora et al. 2006, Romberg et al. 2004) and to manage complex geometric interpretation. Xu et al. (2019) use an additional geometry kernel to generate meshes for finite element modeling, focusing on the boundary-representation (BRep) models. This research focuses on the early design stage, and therefore does not use the full potential of architectural BIM models in the developed design stage, where building elements are already defined. Also, in the aforementioned research, the resulting models are not analytical models with reduced dimensionality extracted from the existing architectural models, which is a standard workflow in the developed design stage.

Workflow implemented in this research is depicted in Figure 1. After exporting the IFC model from Revit, the IFC model is converted to JSON format, filtered and the geometry definitions are adapted to Open Cascade geometry classes. There are numerous geometry kernels for handling of geometry on the market, however we chose Open Cascade as a free open source geometry kernel. We created the methods by focusing on the IFC geometry definitions found in the IFC model (swept solid, mapped representation, clipping and BRep) and converting them to Open Cascade classes. All these steps (red dashed box in Figure 1) could be replaced with the direct export from Revit to the desired format, however the IFC approach was chosen in order to be more flexible and allow the use of multiple proprietary software tools.

The geometrical interpretation steps take place with the Open Cascade geometry definitions with the help of available Open Cascade methods. We created redDim (*red*uce *Dim*ensionality) program that contains all the methods implemented for the use-case building. Besides the geometry information, redDim uses information about the element type, load-bearing property, element id and material name for further import to structural analysis software tool. The interpretations depend on building element type and Open Cascade geometry, which will be tested for extensibility in our future work. The resulting geometries are also defined with the Open Cascade kernel. Methods are developed in such a way to overcome the differences between physical and analytical representations of all structural elements of the use case building, and a model as a whole, resulting in a useable structural analysis model. The resulting model is an open structural analysis model, and in the further steps it can be imported by mapping the information to the structural analysis software tool. In that way, the geometry interpretations are not anymore part of the problematic software import (Sibenik 2016).

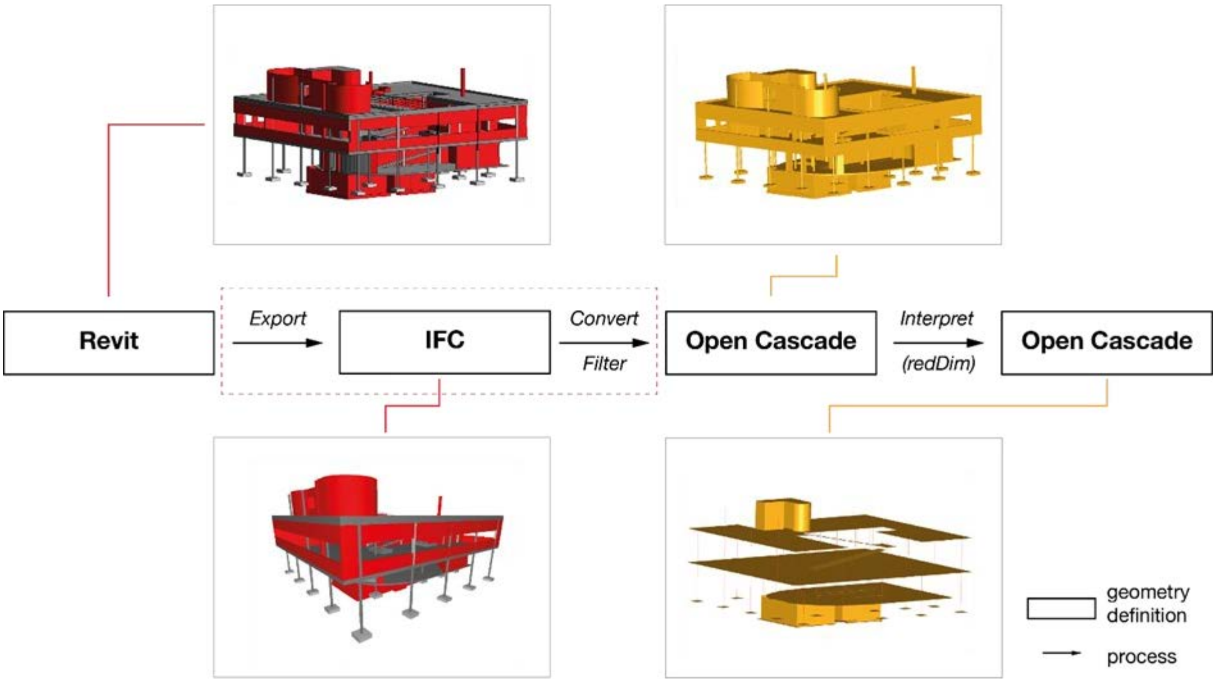

Figure 1: Workflow for the data exchange between native and central physical and analytical building models including geometry definitions and processes

3. Interpretation Methods

The geometry interpretation methods for the data exchange from physical into analytical model, developed and applied within the framework include linearization, planarization, reconnecting elements and perimeter adjustment. The methods are based on the thorough literature review (Ramaji and Memari 2018, Liu et al. 2010), and they were chosen in order to support specific geometries present in the use case building model, such as columns with round and rectangular cross section, straight and curved one-layered walls with uniform thickness, horizontal and tilted uniform-thickness slabs and single foundations.

3.1 Linearization

Linear elements in the use case building model were only columns with round and square cross-sections. The columns are represented as Open Cascade topological shapes: cylinders and boxes. For both topologies a single algorithm was used to convert the shape to edge, consisting of several methods (Figure 2): i) top and bottom faces are identified by analyzing and comparing all the faces constituting the shape; two parallel faces with smallest area could also be identified for linear elements, e.g. in the case of non-vertical linear elements (such as beams); ii) vertices defining the centers of mass of the faces is found; iii) edge is created between the vertices representing the linear element.

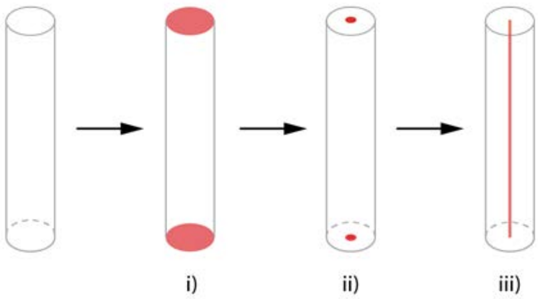

Figure 2: Linearization of building elements

3.2 Planarization

Planar elements of the use case building were walls and slabs (including flat roof), both represented as topological shapes of Open Cascade, some containing openings. As a starting point, a complex topological shape is created consisting of the wall or slab shape and the corresponding openings. The planarization method involved (Figure 3): i) locating the largest face of the shape; ii) finding the element thickness by analyzing distances from the central face vertex to its projection on the neighboring surfaces; iii) offsetting the largest face for half of the thickness to the inner part of the topological element. In that way a planar element axis is created and represented as Open Cascade face.

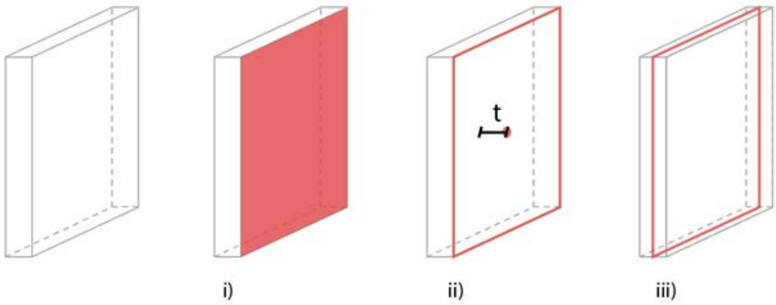

Figure 3: Planarization of building elements

3.3 Reconnecting Elements

Physical and analytical representations of elements are interrelated. Connected physical building elements need to be investigated for the neighboring elements. Based on the results, the analytical elements need to be reconnected. In order to make this, several methods were developed (Figure 4): i) finding neighboring elements in the physical model by checking the minimum distance between elements, and also considering the element type (e.g. columns cannot be reconnected to other columns or walls, but can to slabs) and inclination (tilted slabs); ii) addressing each element in their structural representation and their neighbors, also in the structural representation; further on, depending on whether an element is linear or planar: iii)a) linear elements or edges in Open Cascade are extended until the intersection point with the neighboring planar element; iii)b) the planar elements are extended or trimmed based on the geometry: rectangular geometries are recreated in such a way that the closest edges are projected, adjacent edges extended and the remaining edges unchanged. Vertical planar elements are connected both to horizontal and vertical neighboring planar elements.

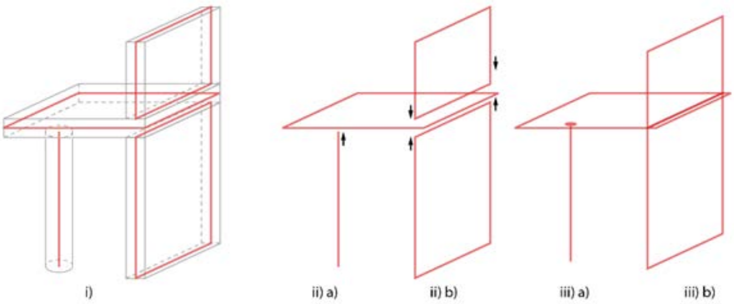

Figure 4: Reconnecting elements in structural representation

3.4 Perimeter Adjustment

Similar as in the previous method, the information about the neighboring building elements is used in order to adjust the perimeter of horizontal planar elements. In the use-case model, the edges of horizontal planar elements were adjusted to the vertical building elements supporting them. Firstly, the list of neighboring building elements is filtered and the elements near the perimeter edges are identified. Additionally, linear vertical elements are connected to two closest vertical load-bearing elements in the same neighbor list and in such way *load-bearing fronts* are created. These *fronts* were used to check if the slab edge should be adjusted to the underlying columns. As an overview, for perimeter adjustment the following method sequence was developed (Figure 5): i) underlying vertical elements close to the perimeter in the analytical model are found; ii) "load-bearing fronts" are created from the vertical linear elements; iii) projections of planar vertical elements and "fronts" are found on the horizontal planar element; iv) the intersection distance to the edge of the slab are checked, those further than tolerance eliminated; parallelism of the edges to the projections is checked; iv) face is extended or trimmed to the edges which fulfill the conditions from iii).

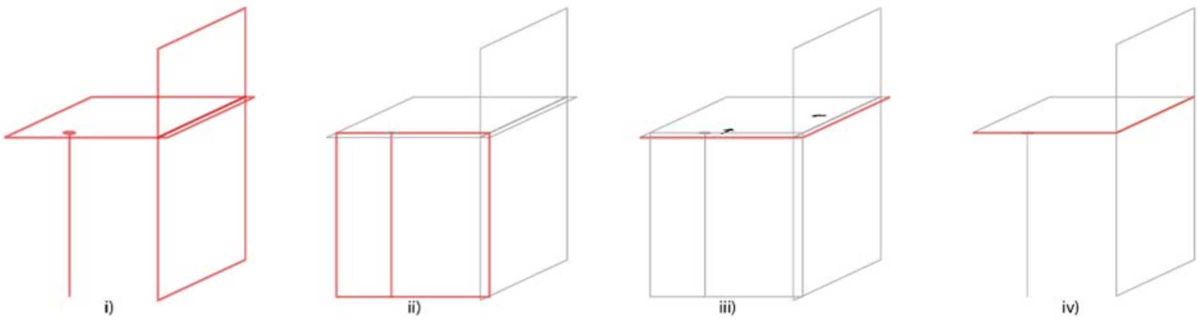

Figure 5: Perimeter adjustment of horizontal structural elements

4. Discussion

The research question "how to automate intuitive processes of interpreting physical to analytical building model?" is answered by proposing four interpretation methods based on the geometrical elements from the use-case building. The four methods cover some common building elements and relatively simple but commonly present geometries such as columns with constant cross-sections and walls and slabs with constant thickness through the use-case model. The interpretations take place during the definition of an analytical model from the physical model. They are not standardized nor documented for the existing workflows, which causes many inconsistencies and problems for the data exchange practices between architectural design and structural analysis domains. The interpretation methods are implemented with a novel framework, described in our previous work (Sibenik and Kovacic 2019).

The main advantage of the novel framework is that it moves the procedural steps for interpretation from single software tools (either architectural design or structural analysis) to the central database. Interpretation methods are facilitated with the open source geometry kernel on the central database. Therefore, the end users (or coordination/BIM managers) have the insight to the methods taking place, understand the model behavior and can adjust it to their workflows if needed. This is in the current practices mostly impossible since the import or export procedures work as "black-boxes" defined in the proprietary software tools.

The innovative aspects of this research lies primarily within documenting of the intuitive interpretations rules in such a way that they could be automated with other software tools or geometry kernels. Secondly, the innovation is the implementation of the interpretations in previously defined open exchange framework.

All building elements in the use-case building have been successfully interpreted, through application of above described methods of linearization, planarization, reconnecting elements and perimeter adjustment. Some interpretations were more elaborate to automate than the others, partly because of the complexity of the traditional intuitive process and partly because of the technical reasons such as geometry kernel suitability and predefined methods. The level of difficulty depended on several factors: a) difficulty to translate IFC to Open Cascade geometry; b) understanding the traditional intuitive process; c) difficulty in translating the traditional intuitive process to a method. Current focus of research was on the usability of technology, in the future research the impact of different factors will be investigated and evaluated more closely.

One of the current limitations of this approach is the lack of options for interpretations on single building elements. The use case is completely automated, which could pose a problem for other practices and building models. Structural engineers need more control over the interoperation process. The methods defined in this research are limited to the use-case model. For wider practical implementation it is necessary to extend them with additional ones and to cover more geometries. The interpretations are based on the IFC building models that depend on the export performance of native software tools and their IFC interface, which are different from the building models in the native software. Therefore, this step could be replaced with the direct connection of the software tool to the central database.

Next steps will include the optimization of the framework together with application of the interpretation steps in order to get the direct open exchange model from Revit. The framework, after being enhanced with additional methods, will be tested on the models from design offices. In that way the scalability of the current approach will be tested. The usefulness and usability of the novel software can be tested only after a user-friendly interface is provided, which is also one of the future steps, where the engineers can tackle a single element and better control the interpretations. Additionally, an exchange in the other direction will be tested, from analytical to physical model.

5. Conclusion

This paper aims to cover a knowledge gap in describing and documenting the intuitive procedural step of geometrical interpretations taking place between physical and analytical models. This knowledge is found to be a requirement in overcoming the discrepancies between architectural design and structural analysis building models and achieving a successful data exchange.

Methods described in the paper are linearization, planarization, reconnecting elements and perimeter adjustment. Although the described geometrical interpretations represent only a small part of numerous possibilities and undocumented knowledge taking place during the information exchange between physical and analytical models, the geometries present in the use case, namely vertical columns with constant cross section, and walls and slabs with constant thickness, can often be found in building models. Hence it is possible to predefine the majority of geometrical interoperations in such a way. Implementing the interpretations in this or other framework might significantly simplify the data exchange process, the most common and repetitive tasks could be automated, leaving a small portion of building elements, geometries and interpretations to structural engineers to manually deal with.

Acknowledgements

This work was conducted as part of the Doctoral College "Computational Design" on TU Wien (TUW) and the project DATAFILTER in cooperation with Strabag AG. The authors wish to express their appreciation to Dr. Wendelin Sprenger and Theodor Sansakrit Strohal for their support and contribution to the study on the side of Strabag SE.

References

Agarwal, R., Chandrasekaran, S., and Sridhar, M., (2016). Imagining construction's digital future, [Blog] McKinsey&Company, June. Available at: https://www.mckinsey.com/industries/capital-projects-and-infrastructure/our-insights/imagining-constructions-digital-future, accessed July 2018.

Eastman, C., Teicholz, P., Sacks, R. and Lee, G., (2018). BIM handbook: A guide to building information modeling for owners, managers, designers, engineers and contractors, 3rd Ed., John Wiley and Sons Inc., Hoboken, New Jersey, USA.

Grilo, A. and Jardim-Goncalves, R., (2010). Value proposition on interoperability of BIM and collaborative working environments. Automation in Construction, 19(5), pp.522–530. https://doi.org/10.1016/j.autcon.2009.11.003

Holzer, D., Tengono, Y., and Downing, S., (2007). Developing a Framework for Linking Design Intelligence from Multiple Professions in the AEC Industry. Dong, A., Moere, A.V., and Gero, J.S. (Eds.). Computer-Aided Architectural Design Futures (CAADFutures) 2007: Proceedings of the 12th International CAADFutures Conference, Dordrecht, Netherlands: Springer, pp.303–316.

Hu, Z. Z., Zhang, X. Y., Wang, H. W., and Kassem, M., (2016) Improving interoperability between architectural and structural design models: An industry foundation classes-based approach with web-based tools. Automation in Construction, 66, pp.29–42. https://doi.org/10.1016/j.autcon.2016.02.001

Kepplin, R., Schnellenbach-Held, M. and Held, M., (2017). Building Information Modeling – Umsetzung in der Tragwerksplanung. Bautechnik, 94, pp.220–226. doi:10.1002/bate.201700003

Kovacic, I., Vasilescu, D., Filzmoser, M., Suppin, R. and Oberwinter, L., (2015). BIM in teaching — lessons learned from exploratory study. Organization, technology & management in construction, 7 (3), pp.1358–1366. https://doi.org/10.5592/otmcj.2015.3.3

Liu, Z.-Q., Li, Y.-G., Zhang, H.-I., (2010). IFC-based integration tool for supporting information exchange from architectural model to structural model. Journal of Central South University of Technology, 17 (6), pp.1344–1350. https://doi.org/10.1007/s11771-010-0640-z

Luyten, L., (2015). CAAD and Conceptual Design Collaboration between Architects and Structural Engineers. Martens, B., Wurzer, G., Grasl T., Lorenz, W. E., and Schaffranek, R. (Eds.). Real Time - Proceedings of the 33rd eCAADe Conference - Volume 2, Vienna, Austria, pp.215–224. http://papers.cumincad.org/cgi-bin/works/Show?ecaade2015_206

Mora, R., Rivard, H., and Bédard, C., (2006). Computer Representation to Support Conceptual Structural Design within a Building Architectural Context. Journal of Computing in Civil Engineering, 20(2), pp.76–87. https://doi.org/10.1061/(asce)0887-3801(2006)20:2(76)

Qin, L., Deng, X.-Y. and Liu, X.-L., (2011). Industry foundation classes based integration of architectural design and structural analysis, Journal of Shanghai Jiaotong University (Science), 16(1), pp.83–90. https://doi.org/10.1007/s12204-011-1099-2 (Accessed 29 January 2019)

Ramaji, I. J. and Memari, A.M., (2018). Interpretation of structural analytical models from the coordination view in building information models, Automation in Construction, 90, pp.117–133. https://doi.org/10.1016/j.autcon.2018.02.025

Romberg, R., Niggl, A., van Treeck, C. and Rank, E., (2004). Structural Analysis based on the Product Model Standard IFC. Beucke, K., Firmenich, B., Donath, D., Fruchter, R., and Roddis, K. (Eds.). Proceedings of 10th International Conference on Computing in Civil and Building Engineering (ICCCBE), Weimar, Deutschland.

Sibenik, G., (2016). Building information modelling based interdisciplinary data exchange: a case study. Proceedings of 1st International UK BIM Academic Forum Conference. Glasgow, UK, 13-15 September, pp.379–90.

Sibenik, G. and Petrinas, V., (2020). IFCtoJSON. Doi: htts://zenodo.org/badge/latestdoi/246248514

Sibenik, G. and Kovacic, I., (2019). Automation of software independent data interpretation between architectural and structural analysis models. Proceedings of the 36th International Conference of CIB W78, Newcastle-upon-Tyne, UK, pp.810–820.

Wang, X., Cui, Z. P., Zhang Q. L. and Yang, H. Z., (2013). Creating Structural Analysis Model from IFC-Based Structural Model, Advanced Materials Research, 712-715, pp.901–904 https://doi.org/10.4028/www.scientific.net/AMR.712-715.901

Xu, Z., Rao, Z., Gan, V. J. L., Ding, Y., Wan, C., and Liu, X., (2019). Developing an Extended IFC Data Schema and Mesh Generation Framework for Finite Element Modeling. Advances in Civil Engineering, 2019. https://doi.org/10.1155/2019/1434093

Underground Engineering Orientated Data Mapping from Construction Information Models to Structural Analysis

Nan Zhu[1], Fangzheng Lin[2], Raimar J. Scherer[2], Philipp Dohmen[1]
[1]Amberg Engineering AG, Switzerland
[2]Institute of Construction Informatics, TU Dresden, Germany
nzhu@amberg.ch

Abstract. In this paper, we throw light on underground engineering, present a data mapping methodology from construction information models (Revit models) to structural analysis utilizing: first, an algorithm is developed for extracting all segments' coordinates from parameters of information models. Second, analytical models for structural analysis are reconstituted employing the data filter output from the proceeding step. For implementation, the software Autodesk Revit is adopted to establish information models, while SOFiSTiK and ABAQUS/CAE for corresponding structural analysis. In the case study for validation, we evaluated our method on cases of pile-group and tunnel structure, and demonstrated robust results readily useful for practical applications.

1. Introduction

Building information modelling (BIM) has shown its potential to bring the evaluation of the Architecture, Engineering and Construction (AEC) industry (Eastman et al., 2011). In building structures, information models are extensively applied during planning, designing, constructing operating and maintaining phase. The information models are not only able to be applied in buildings but also in other construction projects. Underground structures hold high complexity and have great demand on a shared knowledge resource for modelling information, which facilitates the decision making during the structure's life-cycle. Focusing on tunnel structure and pile-group foundation, which are two typical underground structures, this paper addresses the data mapping issue from the construction information models to structural analysis using commercial FEA software.

In the field of data mapping, the majority of articles are related to building structures, since the schema of building data modelling for practical application is earliest developed, and already relatively maturely supported by software. Taking advantage of an IFC building model, a web platform is developed to manage data exchange from a building information model to input models from several kinds of FEA software (Hu et al., 2016). Some theoretical research concentrates on establishing exchange-data models for enriched implementation of BIM standard (Eastman C. M. et al., 2010). It is noticed that many people do still not finger construction models, especially in infrastructure, yet. On the other hand, the conventional research in underground engineering is interested in developing analytical method to calculate the structural behaviors under soil pressure (Amann et al., 2011; Puzrin, 2012). Optimization of the modelling procedure in pre-processing is barely concerned by the experts from geotechnics.

In comparison with a building project in Revit, fewer specific elements of infrastructure can be semantically defined. It is chiefly because infrastructure elements such as bridges, tunnels and railways intuitively keep relatively simple and onefold form in comparison to buildings. Focusing on solving problems from complicated structures by using BIM tools, both academic and industrial circles do not pay sufficient attention to infrastructure elements. Nonetheless, the increasing demand of improving relevant pre-processing efficiency and reducing model data loss has brought the data mapping of infrastructure elements to the foreground. Therefore, it makes sense to analyze the data structure of a general construction information model, which captures all types of structure elements. This paper aims at underground structures, emphasizes tunnels and pile-group foundations, and is expected as well to take other related kinds of constructions into consideration.

This paper is dedicated to determine an approach to map the model data from parametric modelling software (Autodesk Revit) to FEA software (ABAQUS and SOFiSTiK). In this research work, the data structure of tunnel and pile-group information models built in software Revit are firstly studied. Then, the modeling philosophy of pre-processing in FEA software ABAQUS and SOFiSTiK is analyzed. Based on these two studies, a methodology is subsequently conceived to realize an automatic data exchange process. Within this paper, plug-ins associated with corresponding Software are developed for model parameter extraction from BIM software and preprocessing acceleration in FEA software. As consequence, a tunnel model and a pile-group model are utilized in the case study in order to validate the proposed methodology.

2. Information Modelling in Autodesk Revit

Our hierarchical data mapping method starts with modelling the construction information models in Software Revit. This step yields an understanding of the modelling philosophy and the sequence therein, which will play a central role in the formulation of the second step (see Section 3).

2.1 Parametric Modelling

Autodesk Revit, one of the most widely used commercial BIM software, is a practical parametrical modelling tool for architects, landscape architects, structural engineers, mechanical, electrical and plumping (MEP) engineers, designers and contractors. The graphical “family editor” in Revit, which captures all relationships between components, views, and annotations, ensures the model consistency. Modification of any element can be propagated to others automatically: the alleged context-driven parametrics. This bi-directional associativity (Raiz, 2020) between components, views, and annotations is the major reason of adopting Revit as parametric modelling software in our paper. One adjustment to any element in Autodesk Revit generates alteration of numerical model in FEA software, considering proliferation of changes to all affected elements in both Revit and FEA software. Moreover, its functionality of information modelling does not only cover building but also other kinds of structures.

Autodesk Revit already holds abundant system families in sub region of building structure, which are precisely mapped into numerical models in FEA software. This is shown in Figure 1 top (a) which depicts common building structure elements in Revit. Data from construction information models built by these pre-defined elements can be transferred into numerical models in FEA software, such as SOFiSTiK.

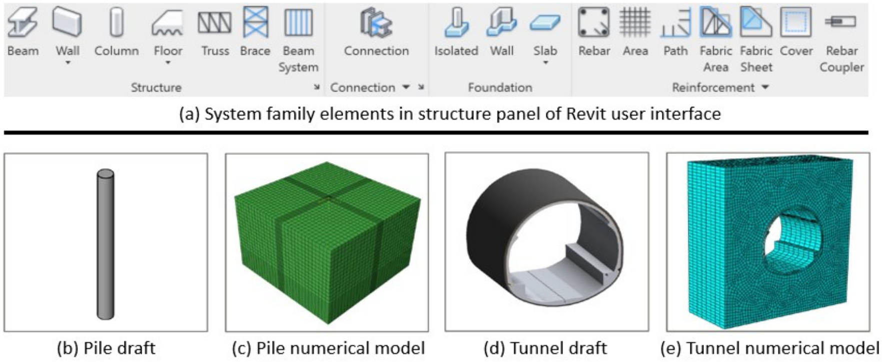

Figure 1: **Top:** (a) System family elements in Revit structure panel. These elements come from building structure and are mapped into numerical elements in FEA software. **Bottom:** (b) Generic pile element in Revit and (c) corresponding numerical pile model considering soils. (d) Generic tunnel element in Revit and (e) corresponding numerical tunnel model considering soils.

2.2 Modelling of Pile Foundation

Piles hold a relatively simple shape extruded by a circular section (Figure 1 bottom (b)). The modelling procedure starts with constructing pile cross sections in a two dimensional plane in Revit. It is highly recommended to model pile cross section in x-y plane, which coincides the modelling procedure in FEA software. This pretreatment ensures a convenient data transfer from construction information models towards structural analysis but is not the prerequisite. The coordinate systems of freely and optionally built model can be adjusted.

With the constructed cross sections in the preceding 2D plane, a pile model is thus established by extrusion along the normal direction of the 2D plane. Both geometric and mechanical parameters of cross sections and the starting/end points obtained from the extrusion are requested to be filtered out to situate the piles in the spatial coordinate system in FEA software.

2.3 Modelling of Tunnel Structure

Different from pile models, tunnel structures (Figure 1, bottom (d)) demonstrating more complex forms are employed to enrich the proposed data mapping in terms of robustness and feasibility. A typical tunnel section is composed of four components: shot-concrete calottes, a sealing layer, tunnel inner linings and in-situ concrete shoulders. Similar to pile elements, all these tunnel components from a tunnel structure are extruded sections. By means of that, cross sections are firstly constructed in a 2D plane, and then extruded to shape a three dimensional model.

Considering an actual circumstance that extrusion vector of tunnel elements can be non-perpendicular to the cross-section plane, all components from infrastructure construction in form of curve or oblique line (i.e. tunnels, railways, etc.) are included, as curves can be divided into finite oblique lines. This orthoselection of structure types ensures the universality of the data mapping method in this paper.

3. Modelling Philosophy in FEA Software

Each kind of FEA software has its own specific schema for building a model in the input files, these schemata are interpreted as modelling philosophy. Though there is something in common between their modelling philosophies according to the identical theory of Finite Element Method (FEM), however, the compatible possibility is difficult to realize. Hence, both modelling philosophies (SOFiSTiK and ABAQUS in this paper) are requested to be analyzed for extension of the data exchange conception.

3.1 Modelling in SOFiSTiK

SOFiSTiK offers two approaches to complete pre-processing: either users are able to use Graphic User Interface (GUI) to build a model through mouse's clicks, or in the TEDDY editor a model can be written through scripts using programming language CADINP and obeying the own schema of SOFiSTiK. For the automatic data mapping, the latter thus is chosen to be studied, whereby the written scripts are interpreted as the input models/files.

Composed of modules, the SOFiSTiK input file is normally written in the form of a batch program, including material and cross section definition, structural element construction, constraints definition, calculation, etc. The summarized typical work steps and modules of modelling in SOFiSTiK are elaborated:

Material and cross section definition. Material definition comes with title (KOPF), release scope (ECHO), norm (NORM) for calculation, and individual material definition.

Meshing. Module SOFIMSHC deals meshing the constructed models. A FE-net will be automatically generated, after the input of structure boundaries. Structure lines (SLN) in form of straight and curve (SLNB) are built with starting, middle and end points. Sealed structure areas (SAR, SARB) are then established with structure lines. Once the extrusion vector is determined, the volumetric model can be created by using extrusion and sweeping command EXTR. It should be mentioned that the global mesh density can be controlled with command STEU HMIN.

Load definition. SOFILOAD define the load for all SOFiSTiK module (SOFiSTiK 2018). The load can be added on nodes or elements with controlled direction in controlled stages.

Boundary condition definition. SOFiSTiK supports all types of boundary conditions like hinge, rigid or slide connection, etc. Spring connection with given stiffness is also available.

Calculation. Module ASE execute static and dynamic calculation of structure in arbitrary form. Linear, non-linear and dynamic calculation are involved in this module considering the loads defined in module SOFILOAD.

3.2 Modelling in ABAQUS

Analogous to SOFISTIK, software ABAQUS CAE (Computer-Aided Engineering) also has graphic user interface for modelling, pre-processing, visualizing and analysis of mechanical components. (Dassault Systèmes, 2013a). Depending on the complexity of model, two fundamental approaches are adopted for the pre-processing: manual modelling for simple model and input script for complicated. Model information and load cases of clean and simple model are intuitionistic, which facilitates post-processing and analysis of the model. The system-generated input file does not have to be checked and processed, because all details can be intuitively observed and processed from visualized user interface. However, complexity of visualized model and the corresponding system input file, develops with increasing details of FE-model. In this case, pure manual modelling from visualized user interface is not suitable for model with high complexity anymore. System-generated input script must be sorted and reorganized for further processing.

ABAQUS macro manager allows users to record a sequence of ABAQUS scripting interface commands into a macro file while the user interact with ABAQUS/CAE (Dassault Systèmes, 2013b). Each command corresponds to an interaction with ABAQUS/CAE, and replaying the macro reproduces the sequence of interactions (Dassault Systèmes, 2013b). This facilitates the whole modelling procedure: one precise manual modelling can be documented and then repeated many times automatically. In addition, the parameters of the model can be purposely adjusted, for other research cases. In this paper, ABAQUS macro manager adopted for recording modelling sequence generates system input files. Then model nodes and elements created in the system input file will be extracted for reconstitution of a well-structured and intuitive input file, and as preparation for succeeding simulation.

For realization of the aforementioned automatic modelling, an ABAQUS plug-in can be established as an extension the functionality of ABAQUS. In ABAQUS, there are two types of plug-ins: kernel and GUI. A kernel plug-in consists of a file containing functions written using the ABAQUS Scripting Interface (Dassault Systèmes, 2013c). In contrast to a kernel plug-in, a GUI plug-in is written using the ABAQUS GUI Toolkit and contains commands that create graphical user interfaces, which in turn send commands to the kernel (Dassault Systèmes, 2013c). An ABAQUS plug-in hereby is developed for importing model data from Revit and reconstructing FE model in ABAQUS automatically. Section 4 elaborates the details of the data mapping workflow from Revit to ABAQUS are explained. The procedures of modelling and reconstructing FE model are pictorial demonstrated in Figure 2. Before the step of meshing manipulation (Step 3 in Figure 2), parts of the model are created and partitioned initiatively. Then the mesh is generated for further element and node sets selection. After inputting materials, a system input file can be finally achieved. Eventually, useful information from system input file should be extracted for creating a new and well-structured input file.

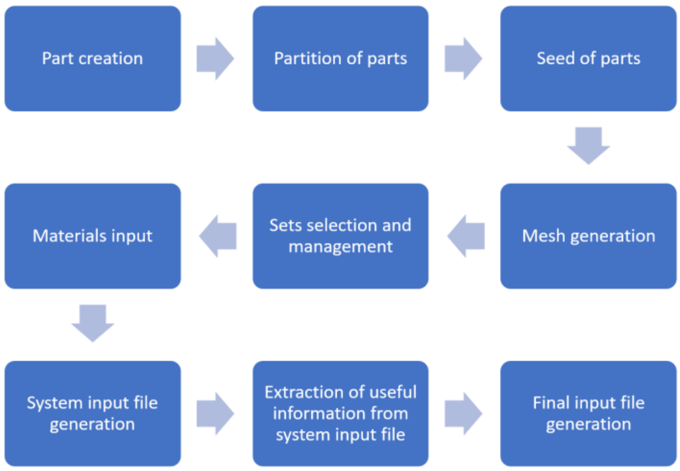

Figure 2: Modelling procedure in Abaqus

4. A Data Mapping Methodology

Section 3 and Section 4 elaborate a comprehensive data requirement analysis during mapping process. Based on the study results, a methodology is established to determine which data from information models in Revit can be converted to the corresponding input parameters in the input files of ABAQUS and SOFiSTiK. The major issues that need to be address lay in coordination transformation and meshing effects. Initially, the global and local coordinates of Revit models are exported accompanied by other essential information and then converted into the coordinates in input models from FEA software. Next in order, meshing is automatically executed by the given parameter, so that the analytical models can be advanced prepared for simulation. The subsections beneath expound the corresponding procedures.

4.1 Data Extraction from Revit Models

The Revit Application Programming Interface (API) is invoked for filtering out geometric and spatial information from Revit models namely coordinates of each component. Autodesk Revit API platform holds an abundant function library, compatible with Microsoft .NET framework for programming language C# and Visual Basic (VB). In this paper, coordinates of each component are extracted by accessing the Revit API functions with programming language C#.

In Revit API library, namespace "Autodesk.Revit.DB" contains all the information of Revit functions and Revit model. Model coordinates, materials, dimensions, etc. can be acquired from this namespace. Besides namespace "Autodesk.Revit.DB", "Autodesk.Revit.UI" executes functions about user interface. Namespace "Autodesk.Revit.UI.Selection" also belongs to "Autodesk.Revit.UI" for model selection. These namespaces are selected in this paper, for development of Revit plug-in and data extraction of BIM model (Figure 3a).

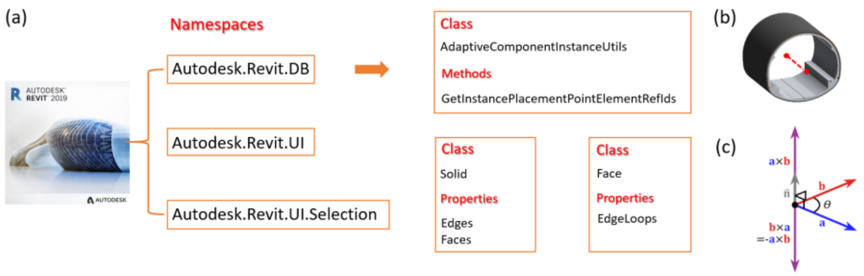

Figure 3: (a) Namespaces used in Revit API library and classes used for reading and extraction of model coordinates in namespace "Autodesk.Revit.DB" (b) Starting and end points of the extrusion vector for tunnel section (c) Vector cross product for selection of extrusion vector

Namespace "Autodesk.Revit.DB" contains class "AdaptiveComponentInstanceUtils" with method "GetInstancePlacementPointElementRefIds" (Figure 3a). This function enables access to extrusion vector in form of starting and end points of the extrusion model. This can be seen in Figure 3 (b), where model is built with extruded faces. After the successful extraction of extrusion vector, faces adopted for extrusion in the model should be found, for further reading of face coordinates.

To have access to faces in the model, class "solid" is used in namespace "Autodesk.Revit.DB". This class covers all solid elements in Revit and contains properties "Edges" and "Faces" of all solids (Figure 3 (a)). The normal vectors of selected faces are adopted to conduct cross product with the previous model extrusion vector. Once the cross-product value is nearly negligible, the face for extrusion is picked out. This is shown in Figure 3c, where the cross-angle θ is almost zero, which indicates the face normal vector is parallel to the extrusion vector. Edges of the extrusion face can then be accessed with property "EdgeLoops" from class "Face". The coordinates of all edges in the extrusion face are extracted afterwards. With the method described above, all useful coordinates of the construction information model are successfully picked up, for further model reconstitution in FEA software. This method is valid for all extrusion models such as piles and tunnel sections.

4.2 Data Mapping into SOFiSTiK

Section 3.1 has given a brief introduction of all the modules adopted in SOFiSTiK in this paper. Model coordinates are converted into the coordinate description in the input file of SOFiSTiK in form of CADINP language: structure line: "SLN + line number" and straight and arcs:

"SLNB + coordinates of start, end and middle points". Structure lines are then collected to constitute structure area "SAR" with outer boundary lines "SARB AUS" and inner "SARB IN". Moreover, extrusion vector imported from Revit model is also defined in form of structure line, for further extrusion of face into volume solids. It should be mentioned that Revit and SOFiSTiK hold the same coordinate system: cartesian coordinate system. However, the z directions of these two software are opposite: SOFiSTiK downward and Revit upward. Coordinates from Revit should be transformed to match those in SOFiSTiK. The mesh generation in SOFiSTiK is coarsely controlled by the global mesh control command "CTRL OPT HMIN", which defines the upper bound for the meshed element size. Accurate mesh control is purely conducted in Abaqus for further static analysis.

4.3 Data Mapping into ABAQUS

Model data input into ABAQUS starts with importing extracted coordinates of Revit model. The coordinates of construction information model in Revit are picked up and saved into a json file. An ABAQUS plug-in is then developed for reading the json file and automate the modelling procedure. In this step, ABAQUS macro manager is adopted for recording the modelling and pre-processing sequence, and generating the macro scripts, by using the imported coordinates from Revit. A system input file is then built, with nodes and elements of the model. This system input file is used for rebuilding a clean and understandable input file, by extracting model nodes and elements from it. In the new ABAQUS input file, material properties, connection properties and load cases are appended after the pre-defined model nodes and elements. The coordinate systems for Revit and Abaqus are the same, which facilitates the coordinate transfer procedure. The mesh control of pile structure can be seen in Figure 4a and Figure 4c, while the surrounding soil elements (Figure 5a) fits the mesh size of pile. The bottom part of pile is deliberately finer meshed for accurate stress analysis. Criterium for meshing control is trying to make the hexahedral elements as cubic as possible.

5. Case Study for Structural Analysis

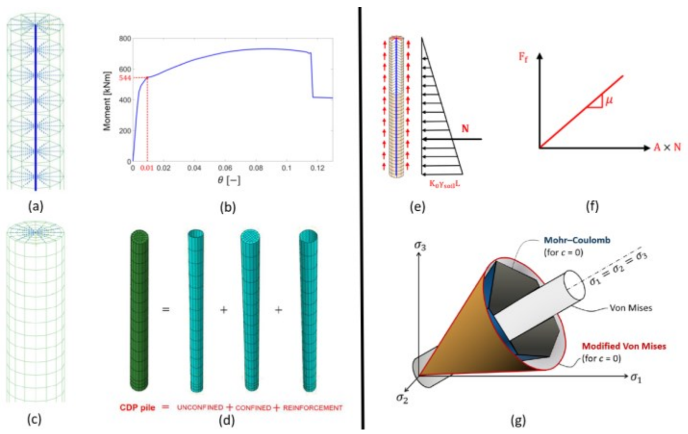

Figure 4: **Left:** (a) Moment curvature pile with centralized beam element which controls the surrounding nodes (b) Moment curvature relationship of the centralized beam element for MC pile (c) Concrete Damaged Plasticity (CDP) pile with multiple-points-constraints connections on the top CDP pile (d) Three components of CDP pile **Right:** (e) Soil pressure acted on the surface of the pile shaft (f) Linear relationship between friction force and normal force on the pile shaft surface (g) Adopted failure criteria in 3D principal stress space in comparison to von-Mises and Mohr-coulomb

The objective of this work is to accelerate the pre-processing, and meanwhile the mapped models ought to be feasible. In case study, a pile-group foundation and a tunnel section with a constant but irregular cross-section are built in Revit. While the pile-group foundation is transformed to ABAQUS to check its safety in the given environment, the tunnel model is mapped into SOFiSTiK and ABAQUS to investigate stress distribution under solid pressures for structural design.

Figure 4a and Figure 4c have shown two types of pile structure adopted in the case study: MC piles with pre-defined moment curvature relationship on centralized beam element, and CDP piles with pre-defined three-layers concrete material. In a MC pile, the centralized beam element controls the surrounding pseudo solid element and only the central beam needs to be accurately defined, which facilitates the simulation of pile structure. During modelling CDP piles, three layers, which compose a CDP pile and respectively confined concrete, reinforcement and unconfined concrete, are defined from inside to outside. Figure 4g has shown the modified soil failure criteria used for simulation of soil elements in ABAQUS. This modified Von-Mises failure criteria has not only the advantages of Mohr-coulomb failure criteria (good fit to experimental data in triaxle compression and extension but not convenient), but also makes the calibration of parameters more straight-forward. The interface between pile and soil consists of pile tips and pile shafts. Nodes on pile tips are coupled with soil elements. For friction force between pile shafts and soil, Figure 4e and Figure 4f indicates the determination of friction coefficient on pile shaft. The friction force can be simplified into modified undrained shear strength along pile shaft, while soil pressure acted on the pile surface can be simulated as a concentrated force acting at the 2/3 of the pile length (Figure 4e). With the normal force and friction force above, the friction coefficient can be found.

Figure 5 has shown the mapped FEA model for pile foundation, together with compression and tension test result diagram. Legend of the diagram is not discussed here, as the focus is on the data mapping, not on internal forces. Figure 6 have shown the mapped FEA model for tunnel section with component in-situ concrete shoulders, tunnel inner linings, sealing, shot-concrete calottes and soil elements from inside to outside. It should be mentioned that the original parametric construction information model for pile and tunnel section are listed in Figure 1b and Figure 1d.

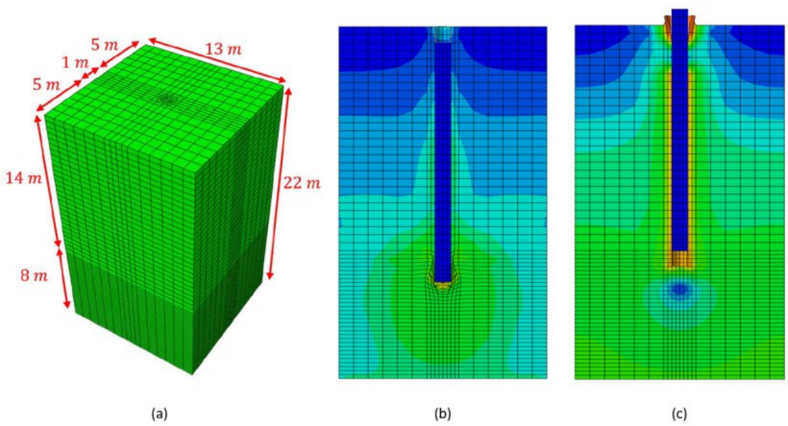

Figure 5: (a) Dimension of single pile foundation FEA model in ABAQUS (b) Single pile compression test (c) Single pile tension test

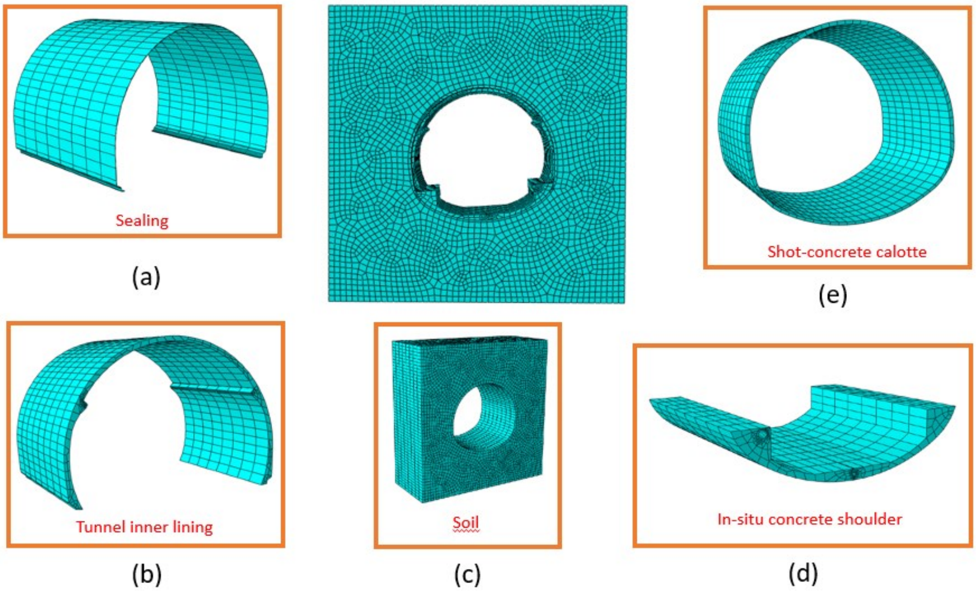

Figure 6: Components of meshed tunnel section model with soil element

6. Conclusion

Certainly, BIM is named after buildings, nevertheless, the development and application of information models can be extended into other categories of constructions in AEC industry. Thus, focusing on underground structure, this paper emphasizes pile group foundation and tunnel structure, and explores the data mapping from information models of underground structure towards structural analysis via FEA software. According to the data structure of model definition from Autodesk Revit, a Plug-in is developed based on the official APIs for the purposed of filtering out the required information from both above-mentioned kinds of underground structure. Meanwhile, the modelling philosophy in preprocessing of FEA software SOFiSTiK and ABAQUS are studied, so that the input models for both kinds of software could be (semi-) automatically generated.

As the case study demonstrates, the feasibility of developed prototype for methodology implementation and the rightness of exported analytical (input) models are validated. Due to the complexity of underground structure modelling, geometrical data exchange and meshing effect are merely concerned in this paper. Constrains including loads and boundary conditions are supposed to be taken into consideration in future work.

References

Amann, P., Lang, H.-J., Huder, J. and Puzrin, A., (2011). “Grundbegriffe”, in Lang, H.-J., Huder, J., Amann, P. and Puzrin, A.M. (Eds.), Bodenmechanik und Grundbau: Das Verhalten von Böden und Fels und die wichtigsten grundbaulichen Konzepte, Springer, Berlin, Heidelberg, pp. 1–12.

Dassault Systèmes, (2013a). “Abaqus/CAE User’s Guide (6.13)”, available at: http://dsk.ippt.pan.pl/docs/abaqus/v6.13/books/usi/default.htm (accessed 25 February 2020).

Dassault Systèmes, (2013b). “ABAQUS/CAE User’s Manual (v6.6)”, available at: https://classes.engineering.wustl.edu/2009/spring/mase5513/abaqus/docs/v6.6/books/usi/default.htm?startat=pt02ch09s05s05.html (accessed 25 February 2020).

Dassault Systèmes, (2013c). “ABAQUS/CAE User’s Manual (v6.6)”, available at: https://classes.engineering.wustl.edu/2009/spring/mase5513/abaqus/docs/v6.6/books/usi/default.htm?startat=pt08.html (accessed 25 February 2020).

Eastman C. M., Jeong Y.-S., Sacks R. and Kaner I., (2010). “Exchange Model and Exchange Object Concepts for Implementation of National BIM Standards”, Journal of Computing in Civil Engineering, American Society of Civil Engineers, Vol. 24 No. 1, pp. 25–34.

Eastman, C., Teicholz, P., Sacks, R. and Liston, K., (2011). BIM Handbook: A Guide to Building Information Modeling for Owners, Managers, Designers, Engineers and Contractors, John Wiley & Sons.

Hu, Z.-Z., Zhang, X.-Y., Wang, H.-W. and Kassem, M., (2016). “Improving interoperability between architectural and structural design models: An industry foundation classes-based approach with web-based tools”, Automation in Construction, Vol. 66, pp. 29–42.

Puzrin, A., (2012). Constitutive Modelling in Geomechanics: Introduction, Springer-Verlag, Berlin Heidelberg, available at:https://doi.org/10.1007/978-3-642-27395-7.

Raiz, L., (2020). “What Does Full Bi-Directional Associativity Mean?”, What Does Full Bi-Directional Associativity Mean, available at: https://www.augi.com/forums/showthread.php?12813-What-Does-Full-Bi-Directional-Associativity-Mean (accessed 25 February 2020).

Examining and Improving Accuracy in a Deep Learning-based Pipeline for the Prediction of Building Energy Demand

Manav Mahan Singh[1, *], Philipp Geyer[1, 2]
[1] KU Leuven, Belgium
[2] Technische Universität Berlin, Germany
[*] manavmahan.singh@kuleuven.be

Abstract. It requires energy prediction of several hundreds of building design combinations to explore the design space and evaluate the effect of design parameters which lead to the development of quick energy prediction tool. In the past, researchers have suggested the use of data-driven approaches such as machine learning (ML) to make quick energy prediction. However, the challenge is to develop an ML model which is generalisable enough to accommodate the variations of the early stage, such as different shapes. Component-based ML (CBML) is a solution which we are developing further in this research. This ML model uses several ML components composed in a system entering way to predict building energy demand. Hence, accuracy relies on the performance of each component. In this paper, we are using two ML technique to understand the accuracy of CBML model. First, ceiling analysis serves to examine the improvement in accuracy by examining and exchanging internal model structure. Second, the feature importance exercise delivers information on the importance of a feature in prediction accuracy. By these methods, we identify ML components which have a higher potential to improve the accuracy of overall predictions. The inclusion of new features is examined as one way of prediction improvement. The test case applies CBML on 300 random shapes. In the test case, infiltration, heating energy, and energy demand components have been identified to improve the accuracy more than other ML components. We introduced additional features to improve the accuracy of these models. The accuracy has increased from 0.971 to 0.981 after including new features.

1. Introduction

Machine learning (ML) models are suitable to make thousands of energy predictions in few seconds which is required to explore a multi-dimensional design space for an energy-efficient design (Tian *et al.*, 2018; Singaravel, Suykens and Geyer, 2019). However, the development of a generalisable ML model which predicts the energy demand of different shapes is challenging. We are using component-based machine learning (CBML) which is based on the concept of using several machine learning components arranged in a particular order to address a problem. CBML is based on the modular paradigm of systems engineering. In some ML applications such as text recognition, ML models are arranged in a linear order, commonly referred to ML pipelines (Brad Neuberg, 2017). In case of building energy predictions, we refer to CBML, in which the components (ML models) are arranged into levels following decomposition of a building in an engineering way. A building is composed of zones, and a zone is composed of building elements (Geyer and Singaravel, 2018). The components are reusable ML models, organised into three levels and used for different building shapes. In the CBML approach, it makes intermediate predictions of heat flows for each building element. Zone components aggregate heating and cooling energy demand. Finally, a building level component determines the energy demand for the whole building, as shown in Figure 1. This CBML forms a machine learning pipeline in which input from the lower-level model is utilised to make higher-level predictions. Hence, the inaccuracies in energy demand prediction are the result of errors in each component.

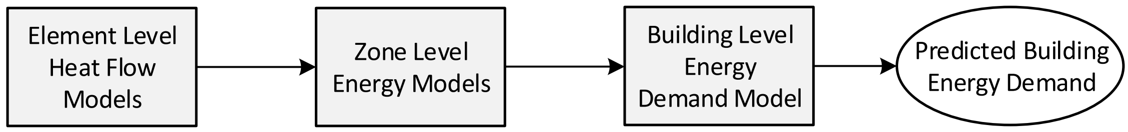

Figure 1: CBML based energy demand prediction approach

The objective of this paper is to explain the source of errors in overall predictions in the pipeline at the component level and improve its accuracy. Besides this component level error source, we are studying individual ML components to improve their performance. It is required to analyse which component has the biggest influence on the error and thus the best potential to improve the accuracy of energy demand predictions before focussing on component improvement. We are using a ceiling analysis tool for this purpose which allows identifying a component in ML pipeline with the highest potential to improve performance (Roncancio, Hernandes and Becker, 2013). It observes the improvement in accuracy of predictions dependent on replacement of model predictions by true values. Ceiling analysis measures the accuracy within the ML pipeline that can be achieved if the ML component makes exact predictions as true values. This provides evidence about the prediction improvement by component improvement.

Following the ceiling analysis, we have identified a few ML components in the pipeline, whose improvement increases the accuracy of predictions more than others. We worked on improving the performance of these ML components by introducing additional manually engineered features. The change in accuracy of ML components and overall accuracy of CBML is an important indicator to prove the relevance of feature engineering. The measurement of the importance of additional features allows for concluding that additional features are relevant. We are calculating the feature importance using an external model-independent technique known as permutation importance. In this technique, feature importance is measured by calculating a change in the model accuracy depending on the permutation of a feature supplied as noise.

In summary, the first step identifies important ML components and focusses on their individual need for improvement to increase accuracy. The second step introduces additional features to improve the performance and determines their impact using feature importance. Thus, it helps in identifying relevant features to improve the performance of individual ML components.

2. Background

It is important to focus on energy-efficient building design from an early stage as it has the potential to improve the performance with a lesser cost of change (Geyer and Schlüter, 2014). A generalisable ML model for different building shapes is necessary for its use at an early stage of design. Previous works related to this development do not assess their applicability of ML model on the building shapes which are not used for training. Such as Catalina et al., 2008 introduced features like time constant and shape factors to improve the generalisability of regression models for different building shapes, but the test data has very limited variability in terms of shape (Catalina, Virgone and Blanco, 2008). Asadi et al. developed regression-based models for variable building shapes (Asadi, Amiri and Mottahedi, 2014). Geyer and Singaravel introduced component-based ML model, but a decrease in accuracy is observed when tested on shapes which are independent of training data (Geyer and Singaravel, 2018). Thus, there is a small but growing set of ML methods to predict energy demand in design especially in early stages, in which important decisions are made.

In machine learning pipeline, such as the case of CBML, it is very important to understand the importance of individual components in the overall accuracy of predictions. Roncancio *et al.* have used it to determine the importance of individual components to detect human figures in an image (Roncancio, Hernandes and Becker, 2013). Other applications, such as character recognition in an image utilises three components arranged sequentially to identify characters. It has been found the first component which detects part of the image containing text will improve the accuracy of predictions much more than other components (Ng, 2019). Thus, it is useful to identify and work on the component, which improves the accuracy of predictions. In the case of CBML, there are many models arranged on three levels and working on all of them may not be useful and time-consuming. Since the concept of CBML or ML pipeline is rarely used in building energy prediction, ceiling analysis has not been used for detecting relevant components to improve accuracy.

We are using a technique of permutation importance to calculate the importance of features in individual ML components (Breiman, 2001). This technique is quite valuable in assessing the feature importance in model accuracy without retraining them. However, this technique has many limitations, such as it does not make a correct estimate of feature importance if features are correlated or the model features are changed (Hooker and Mentch, 2019).

3. Research Methodology

We are using component-based ML model for predicting building annual energy demand. CBML utilises the concept of decomposing a building into subordinate components in a system engineering way. The ML models for components are created and composed for prediction. A building is composed of zones which are composed of construction elements, such as walls, windows, roofs, floors, etc., as shown in Figure 3. The system flows in the composed structure serve for making energy predictions, as shown in Figure 2. The details of the initial features for each ML components are shown in Table 1. This composition allows the reusability of the ML model trained on one shape to the other shapes and thus the reuse of ML models in new design cases.

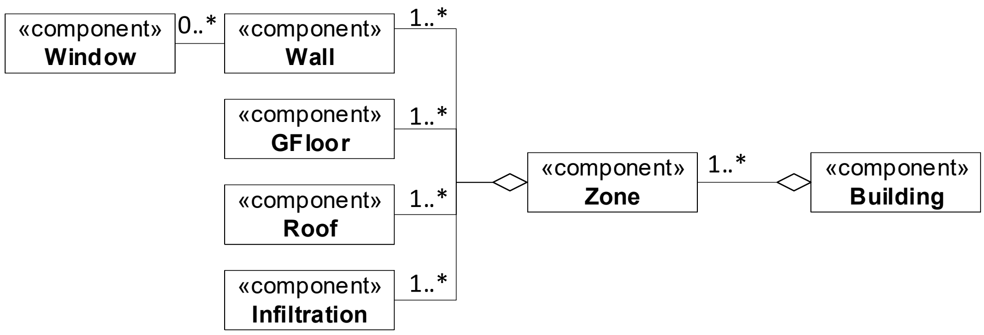

Figure 2: System based representation of BIM

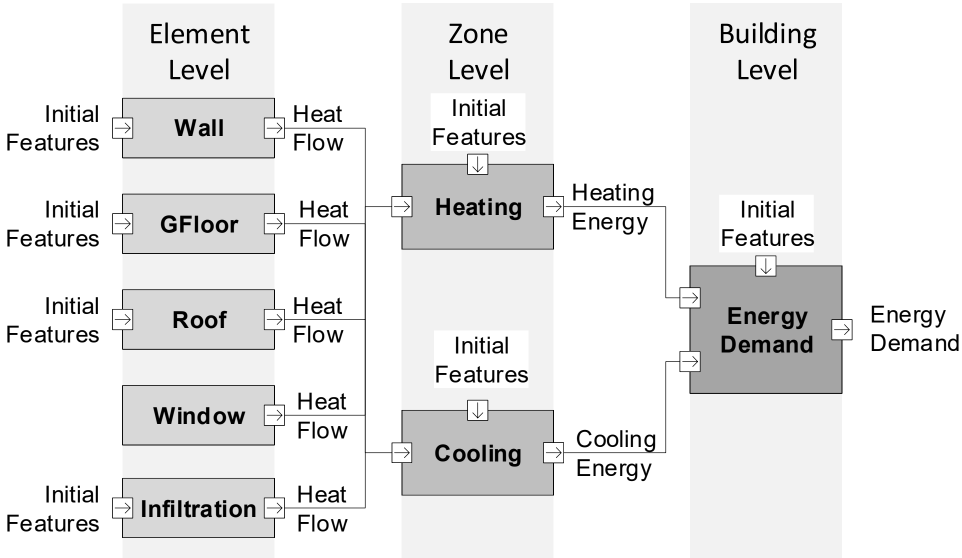

Figure 3: Structure of CBML

Table 1: Details of initial features for ML components

ML Component	Initial features
Wall	Area, Orientation, U Value
Ground Floor (GFloor) or Roof	Area, U Value
Window	Area, Orientation, U Value, g- Value
Infiltration	Zone Volume, Infiltration
Zone Heating and Cooling	Zone Area, Internal Heat Gain[1], Operating Hours, (All Heat Flows)
Building Energy Demand	Boiler Efficiency, Chiller COP, (Zone Heating and Cooling Energy)

[1] Internal heat gain refers to the sum of light and equipment heat gain.

3.1 Ceiling analysis

Ceiling analysis assesses the contribution of an individual model in an overall accuracy of machine learning pipeline by observing the change in accuracy when the model predictions are replaced by the true values (Ng, 2020). First, we calculate the baseline accuracy using the predictions from each component model, as shown in Figure 4. In the proposed CBML, there are three levels of models and a higher-level model utilises predictions from lower-level models. We carried out this exercise to identify the components which require focus to improve the performance of overall energy predictions. The baseline accuracy is calculated using the final predictions P. Then, we replace the predictions from a component model 1 by true values and make final predictions again P1. The accuracy which is possible to achieve by making component model 1 accurate is calculated using prediction P1. Similarly, for component model 2 is calculated using final predictions P2. If we replace prediction values by true values for all components, we will get true values T and accuracy will be 1. Thus, the change in accuracy when predicted values are replaced by true value shows a possible improvement in overall accuracy if the component makes perfect predictions and thus allows to determine the component's impact on accuracy.

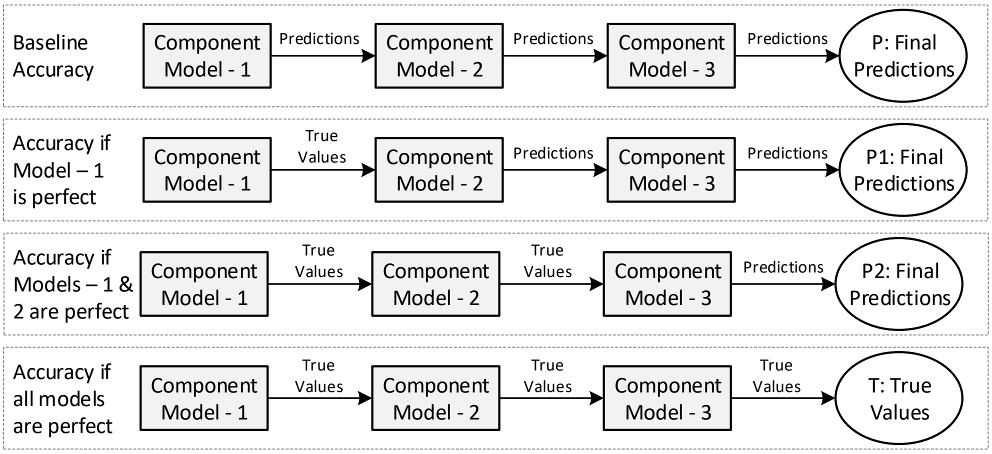

Figure 4: Explanation of ceiling analysis exercise

3.2 Feature importance

Feature importance for an ML model is estimated using a technique called permutation importance (Breiman, 2001; Altmann *et al.*, 2010). Information for one feature of the model is replaced by random noise, and a mean decrease in the accuracy of the model is recorded to calculate feature importance. The simplest way to introduce noise is to shuffle values for a feature, i.e. a feature is permuted. Since this technique requires randomisation, the task is repeated for 25 times to get reliable results. Feature importance (FI) is equal to a mean decrease in model accuracy when a feature is permuted. In this paper, we calculated this error on the test dataset. The algorithm to calculate feature importance based on the works of Fisher, Rudin and Dominici, 2018 is as follows:

1. Assume feature matrix is X, target prediction is y and trained ML component is f(X)
2. The model error e = R^2 (y, f(X))
3. For each feature i = 1, . . ., n
    a. Generate feature matrix X^i by permuting i^{th} feature in the matrix X.
    b. Estimate error $e^i = R^2$ (y, f(X^i))
    c. feature importance $FI^i = e^i - e$

3.3 Testcase and data generation

The implementation of an ML model pipeline for a medium-sized office building located in Munich demonstrates our approach. Building design parameters, mentioned in **Error! Not a valid bookmark self-reference.**, serve to generate the random combinations of building designs. Parametric energy simulations have been performed using the dynamic energy simulation tool EnergyPlus to get data for developing and testing the ML model. It is at this moment practically impossible to get energy consumption data for the building with varying shapes and required value of other design parameters; hence, we are relying on energy predictions from a well-established dynamic energy simulation tool (US Department of Energy, 2018). The tool is validated regularly against the performance of realized buildings, systems and components. The building shapes are generated randomly. Few of these shapes are shown in Figure 5. There are no internal zone divisions following one-zone-per-floor rule to create BEM (Sefaira, 2019). A total of 1000 samples are generated for training ML components, and 300 samples are generated for testing and reporting accuracy impact.

Accuracy - The accuracy of ML components and overall predictions is measured by the coefficient of determination R^2.

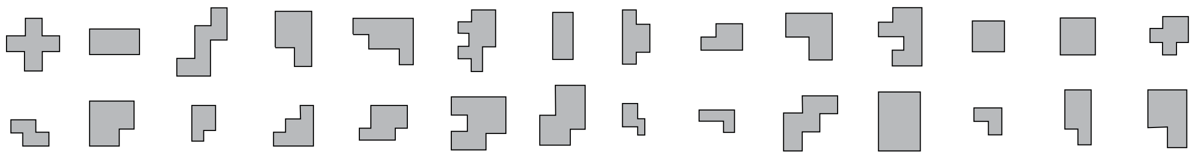

Figure 5: Randomly generated building shapes for testing energy prediction models

Table 2: Design parameters used in this study

Design Parameter	Min	Max	Design Parameter	Min	Max
Area	100	2000	u-value of Intermediate Floor	0.1	0.75
No. of Floors	1	5	Heat Capacity of Floor Slabs	800	1600
Floor Height	2.5	4.5	WWR_N/E/W/S	0.1	0.9
Orientation	0	180	Infiltration	0.2	0.8
u-value of Wall	0.1	0.6	Operating Hours	8	12
u-value of Ground Floor	0.1	0.6	Light Heat Gain	5	15
u-value of Roof	0.1	0.6	Equipment Heat Gain	5	15
u-value of Window	0.3	1.3	Chiller COP	3	5
g-value of Window	0.3	0.9	Boiler Efficiency	0.7	0.95

3.4 Training of ML components

Each ML component has a six-layer deep neural network architecture. It also utilises L2-regularisation and early stopping to restrict over-fitting. L2-regularisation prevent overfitting by adding a squared-term of model parameters to the cost function. Early stopping terminates the training process once there is no decrease in the cost. A total of five hyper-parameters are tuned for each ML component, i.e. the number of neurons in four hidden layers and the coefficient for L2 regularisation. We tuned these hyper-parameters for least validation-loss calculated on the validation data set (which is 20% of training data set). The values mentioned in Table 3 are used for different hyper-parameters.

Table 3: Values of different hyper-parameters

Parameter	Values
No. of neuron in hidden layer 1	500, 1000
No. of neuron in hidden layer 2	300, 500
No. of neuron in hidden layer 3	150, 300
No. of neuron in hidden layer 4	100, 150
Coefficient of L2-regularisation	0.0001, 0.00001

A total of 32 combinations of hyper-parameters has been tested to identify the least validation-loss has been selected for further use. ML models are developed using Keras library and TensorFlow backend (Chollet, 2015).

4. Results

The results section consists of two subsections. The first subsection describes the results of ceiling analysis exercise and identifies two components which improve the accuracy of predictions much more than other components. The section presents the results of feature importance analysis for the two models and introduces new features to improve the overall accuracy of models.

4.1 Ceiling analysis for CBML

The ceiling analysis measures a possible improvement in the accuracy of overall prediction if a component in the ML pipeline makes perfect predictions. Since, in the presented structure of CBML, there are models at three levels, the possible improvements are assessed at these three levels along with individual components. The accuracy of the baseline model is a coefficient of R^2 of 0.971. In brackets, it shows the difference from the best R^2 of 1, i.e. perfect prediction. There is a total improvement of 0.029, which is possible from the baseline model if all ML components make perfect predictions. If all the element level components make perfect predictions, the accuracy will improve to 0.984. If only the infiltration component perfectly predicts, the accuracy is 0.980. Thus, at the element level, infiltration is an important component and requires a focus for accuracy improvement.

Similarly, zone level components will improve the accuracy to 0.992. However, care must be taken to interpret this improvement. This value assumes that all the element level models are also making perfect predictions. Thus, the improvement which will be achieved after making zone level models perfect is only (0.992-0.984 = 0.008). The heating model contributes more than cooling model in this improvement. The remaining error of 0.008 is caused by building energy demand model.

As a result of this analysis, we will focus on three models to improve the performance, which are infiltration, zone heating and building energy demand model. These three models can improve the accuracy of overall prediction by 0.009, 0.006 and 0.008, respectively.

Table 4: Ceiling analysis for CBML components

	Model	**Accuracy (R2)**	
	Baseline	0.971 (0.029)	
Element Level Model	Wall Heat Flow	0.973	0.984 (0.016)
	Window Heat Flow	0.975	
	GFloor Heat Flow	0.974	
	Roof Heat Flow	0.974	
	Infiltration Heat Flow	0.980	
Zone Level Model	Zone Heating Energy	0.990	0.992 (0.008)
	Zone Cooling Energy	0.984	
Building Level Model	Building Energy Demand	1.000	

4.2 Feature Importance for ML components

The three identified relevant components identified in the previous section form the basis of the feature importance analysis. Improving these three models has the potential to increase the accuracy of the overall prediction more than others. We calculated the feature importance in these two models and then introduced additional features to improve the model performance.

Table 5: List of features in infiltration heat flow, zone heating energy and energy demand model

Model	Initial Features	Additional Features
Infiltration Heat Flow	Zone Volume, Infiltration	Zone Area, Internal Heat Gain, Operating Hours, Total Heat Capacity[1]
Zone Heating Energy	Zone Area, Internal Heat Gain, Operating Hours, Wall Heat Flow, Window Heat Flow, GFloor Heat Flow, Roof Heat Flow, Infiltration Heat Flow	Zone Volume, Total Heat Capacity[1]
Building Energy Demand	Boiler Efficiency, Chiller COP, Heating Energy, Cooling Energy	Total Floor Area

[1] Total heat capacity is the sum of heat capacities of all the elements of the zone including wall, roof, floors and internal mass.

It should be noted that in this section, we are reporting the accuracy of individual ML components in this section as opposed to the previous section, in which, the accuracy of overall prediction is reported. After introducing additional features, the performance of the infiltration model improves from 0.976 to 0.981. Similarly, zone heating energy model shows an improvement from 0.986 to 0.989 and building energy demand model improves from 0.992 to 0.996. Improvement in these models results in the improvement in building energy demand prediction from 0.971 to 0.981. We analysed the importance of additional features along with the initial feature, and the results are presented in Figure 6. We found that among additional features, zone area has the highest importance in infiltration heat flow model, zone volume is important feature in zone heating energy model, and total floor area improves the performance of building energy demand model.

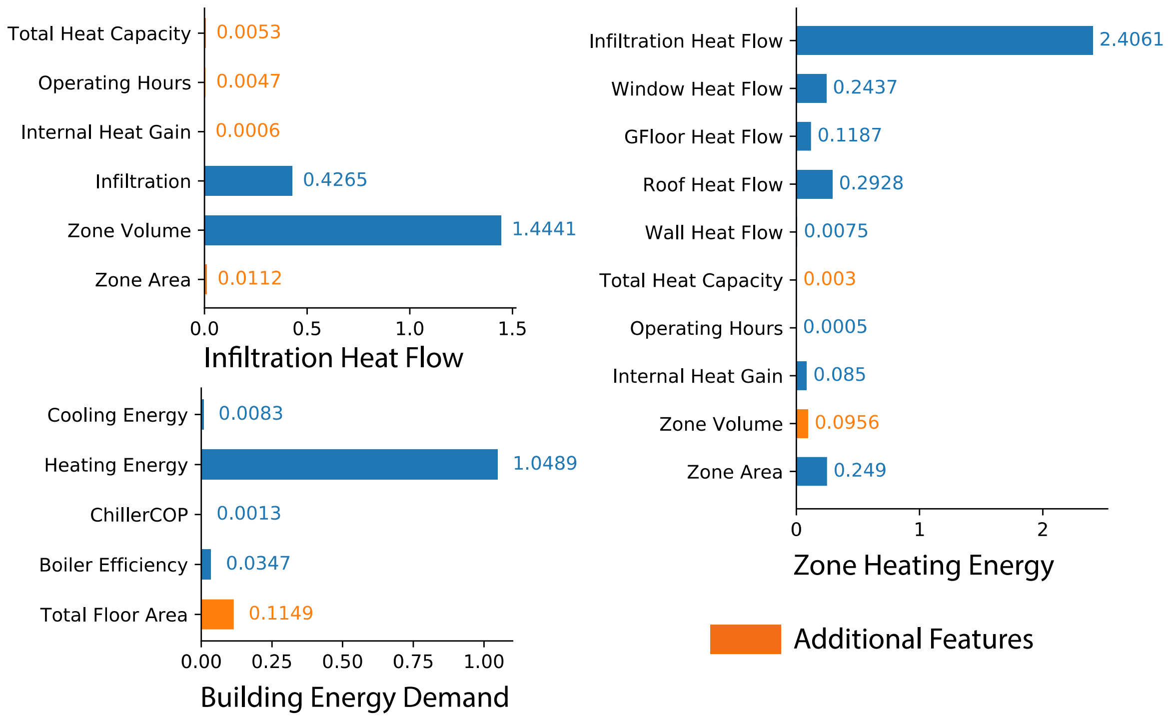

Figure 6: Feature importance for infiltration, zone heating, and building energy demand model

5. Discussion

The approach of ceiling analysis allows identifying the source of errors in the ML-based energy prediction pipeline. ML components are organised into three levels in CBML based energy prediction model. An improvement of 0.029 is possible in energy prediction if all ML components make perfect predictions (refer Figure 7). Improving all ML components to make perfect predictions will require significant computing resources, and it may not be useful to achieve such a small improvement at the cost of computing resources. However, it is useful to analyse the ML components which area causing a maximum part of this error and focus on a few components only and where to invest resources to improve accuracy. Out of this 0.029, 0.984-0.971 = 0.013 (45%) is caused by errors in element level models, 0.992-0.984 = 0.008 (28%) is caused by errors in zone level models, and the remaining, 1-0.992 = 0.008 (28%) is caused by errors building energy demand model. These values are a mere indication of possible improvement in CBML based predictions, but not be possible to achieve as it will require to develop ML components making perfect predictions. We improved a few of ML components, namely, infiltration heat flow, zone heating energy, building energy demand model. A few additional features are included to train these ML components again. These additional features result in an overall improvement of 0.981-0.971 = 0.01 (34%) against the possible improvement of 0.029. This example shows how to determine the components with the highest potential to improve the prediction accuracy by the implementation of additional features.

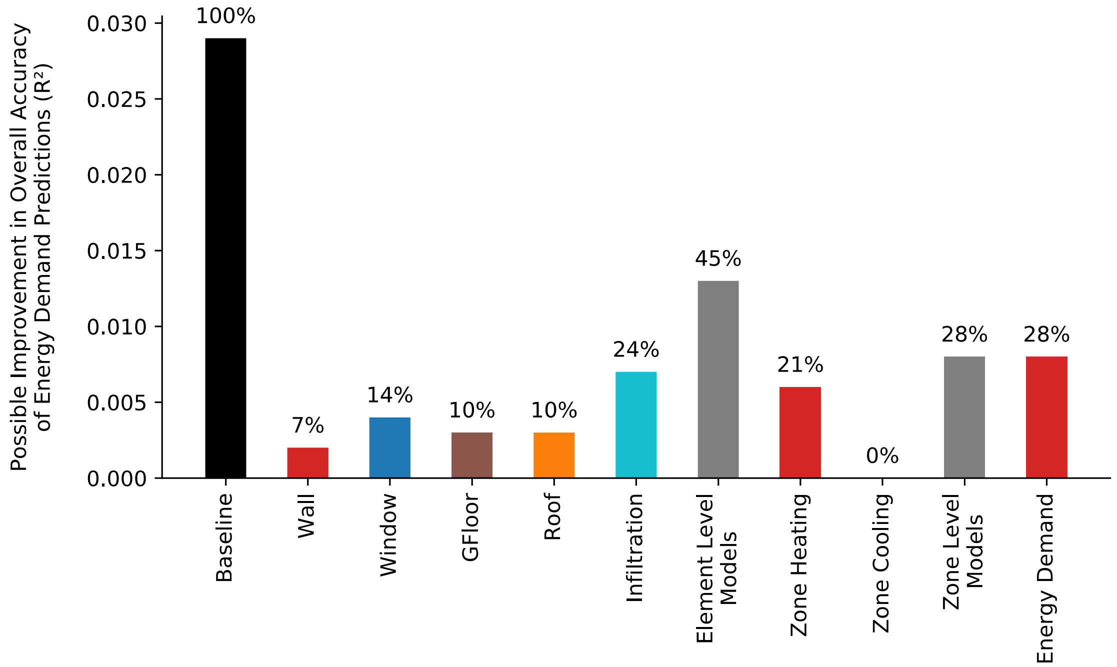

Figure 7: Improvement possible in overall accuracy corresponding to each ML component

Feature importance analysis for these components serves to assess the contribution of additional features in the accuracy of three ML components. The feature importance analysis suggests that additional features improve the prediction accuracy slightly. However, the results of feature importance must be interpreted with extreme care because of the following limitations of the technique. First, the feature importance is not equal to a decrease in the accuracy if the feature is removed. It is just equal to a decrease in accuracy when a feature is passed as random noise. Second, correlated features reduce the importance of each other. For example, in the infiltration heat flow model, zone volume and zone area are correlated. This model shows the accuracy of

0.981. After removing zone volume from the feature list, the accuracy reduces to 0.9136, but feature importance of zone area becomes 0.8146 from 0.0112. Thus, the value of feature importance is only indicative; it is a relative measure if there is no change in the model.

6. Conclusions

The approach of CBML allows the development of energy prediction models for a case where the building cannot be described by a set of parameters such as different building geometries or different zoning conditions etc. However, this approach presents a challenge of training several ML components and structuring them to make energy demand predictions. Since the accuracy of energy demand predictions in CBML based model depends on the prediction accuracies of individual ML components, this study has presented an approach to examining the source of error and reducing it. This gives valuable information for future development of future CBML models by providing information which are the crucial components.

The approach of ceiling analysis is useful to identify components of CBML that cause the highest share of the error. In the presented case, there is a total of 9 ML components, structured in three levels to make energy demand predictions. However, just improving three models improves the accuracy from 0.971 to 0.981. This increase is 34% of the possible improvement of 0.029. It should be noted that the full improvement, i.e. achieving the accuracy of $R^2 = 1$, is not possible. Hence, 34% of improvement possible, just by improving 3 out of 9 ML components, is significant. This method significantly reduces the efforts required for improving all ML components by feature engineering. An approach of feature engineering and importance analysis serves to improve individual ML components. In the test case, only three of the nine ML components required this process. Additional features have been introduced in these ML components, which results in the mentioned improvement of these components. Feature importance suggests that few additional features have quite significant importance, but few of them have relatively low importance. However, a technique of feature importance has limitations for related features which need to be considered. In sum, the methodology provides an efficient approach to improve the performance of CBML based energy prediction models using ceiling analysis and feature importance.

Acknowledgements

The authors want to acknowledge the support of Deutsche Forschungsgemeinschaft (DFG) for funding the research through research unit FOR 2363. The computational resources and services used in this work were provided by the VSC (Flemish Supercomputer Center), funded by the Research Foundation - Flanders (FWO) and the Flemish Government – department EWI.

References

Altmann, A. *et al.,* (2010). ‘Permutation importance: a corrected feature importance measure’, *Bioinformatics*, 26(10), pp. 1340–1347. doi: 10.1093/bioinformatics/btq134.

Asadi, S., Amiri, S. S. and Mottahedi, M., (2014). ‘On the development of multi-linear regression analysis to assess energy consumption in the early stages of building design’, *Energy and Buildings*, 85, pp. 246–255. doi: 10.1016/j.enbuild.2014.07.096.

Brad Neuberg, (2017). *Creating a Modern OCR Pipeline Using Computer Vision and Deep Learning*, *dropbox.tech*. Available at: https://dropbox.tech/machine-learning/creating-a-modern-ocr-pipeline-using-computer-vision-and-deep-learning (Accessed: 8 May 2020).

Breiman, L., (2001). ‘Random Forests’, *Machine Learning*, 45(1), pp. 5–32. doi: 10.1023/A:1010933404324.

Catalina, T., Virgone, J. and Blanco, E., (2008). 'Development and validation of regression models to predict monthly heating demand for residential buildings', *Energy and Buildings*, 40(10), pp. 1825–1832. doi: 10.1016/j.enbuild.2008.04.001.

Chollet, F., (2015). *Keras*. Available at: https://keras.io (Accessed: 6 May 2019).

Fisher, A., Rudin, C. and Dominici, F., (2018). 'All Models are Wrong but many are Useful: Variable Importance for Black-Box, Proprietary, or Misspecified Prediction Models, using Model Class Reliance'. Available at: http://arxiv.org/abs/1801.01489.

Geyer, P. and Schlüter, A., (2014). 'Automated metamodel generation for Design Space Exploration and decision-making – A novel method supporting performance-oriented building design and retrofitting', *Applied Energy*, 119, pp. 537–556. doi: 10.1016/j.apenergy.2013.12.064.

Geyer, P. and Singaravel, S., (2018). 'Component-based machine learning for performance prediction in building design', *Applied Energy*, 228, pp. 1439–1453. doi: 10.1016/j.apenergy.2018.07.011.

Hooker, G. and Mentch, L., (2019). 'Please Stop Permuting Features: An Explanation and Alternatives'. doi: arXiv:1905.03151.

Ng, A. Y., (2020). *Ceiling Analysis: What Part of the Pipeline to Work on Next*, *Coursera*. Available at: https://www.coursera.org/lecture/machine-learning/ceiling-analysis-what-part-of-the-pipeline-to-work-on-next-LrJbq (Accessed: 8 May 2020).

Ng, R., (2019). *https://www.ritchieng.com/machine-learning-photo-ocr/*. Available at: https://www.ritchieng.com/machine-learning-photo-ocr/ (Accessed: 2 March 2020).

Roncancio, H., Hernandes, A. C. and Becker, M., (2013). 'Ceiling analysis of pedestrian recognition pipeline for an autonomous car application', in *2013 IEEE Workshop on Robot Vision (WORV)*. IEEE, pp. 215–220. doi: 10.1109/WORV.2013.6521941.

Sefaira, (2019). *Zoning Strategy - Perimeter / Core*. Available at: https://support.sefaira.com/hc/en-us/articles/115000093632-Zoning-Strategy-Perimeter-Core (Accessed: 16 December 2019).

Singaravel, S., Suykens, J. and Geyer, P., (2019). 'Deep convolutional learning for general early design stage prediction models', *Advanced Engineering Informatics*, 42, p. 100982. doi: 10.1016/j.aei.2019.100982.

Tian, W. *et al.,* (2018). 'Uncertainty and sensitivity analysis of energy assessment for office buildings based on Dempster-Shafer theory', *Energy Conversion and Management*, 174, pp.705–718. doi: 10.1016/j.enconman.2018.08.086.

US Department of Energy, (2018). 'EnergyPlus 8.9.0'. Available at: https://energyplus.net/documentation.

BIM to BEM: an Investigation of Practical Interoperability Challenges When Working with Revit and DesignBuilder

Khaleel Odeh, Pieter de Wilde
University of Plymouth, United Kingdom
pieter.dewilde@plymouth.ac.uk

Abstract. This paper explores some of the practical issues that emerge when importing building information model (BIM) data into a building energy modelling (BEM) tool. Whilst in general the interoperability between BIM and BEM has made significant advances, barriers still remain. A case study augmented with expert interviews is used to capture some of the issues that emerge when transferring building geometry data from Revit to DesignBuilder via the intermediate industry format of gbXML. It is concluded that gbXML may not capture all essential data required for building energy analysis. Other issues may require that the BIM side raises its awareness of the data needs of the BEM tool, and are unlikely to be addressed simply by improved one-directional data transfer; however this may impinge of the idea of BIM being a flexible, neutral format.

1. Introduction

Building Information Modelling (BIM) is a group of processes, technologies and tools for the management of information for building planning, operation and performance, and it is one of the most important contemporary trends for improving information handling throughout a building projects lifecycle (Arayici *et al.,* 2018). A key driver for the uptake of BIM is digital exchange of building information that enables the collaboration between different stakeholders (Borrmann *et al.,* 2018) and prevents the need to re-enter information for different tasks. Building Energy Modelling (BEM) is the management of information required to apply physical and mathematical equations in order to quantify building energy performance (Underwood and Yik, 2004).

The importance of interoperability between BIM and BEM has been recognised since the 1990s and has been the subject of studies by many R&D projects, with significant progress demonstrated in the area. However, practical problems are still present for those working in the industry and wanting to transfer data from an BIM editing tool to a building performance analysis tool (Prada-Hernández *et al.*, 2015). Consultants working in industry report that they use various analysis tools and have to set up bespoke building models in each tool due to lack of proper interoperability in practice (Tillberg, 2020) or that they have to rework (‘trace’) models received from third parties (Bradbury, 2020). Similar issues are observed in academia when students on building simulation courses try to import data created during design studio sessions, leading to significant student frustrations and sometimes even rejection of the simulation model. Part of this challenge relates to the fact that BIM captures all data pertaining to a building, whereas analysis tools typically operate on one or at most only a small subset of building performance aspects such as thermal, lighting or acoustic performance. In such cases the analysis tool only requires a small subset of all data contained within the BIM (Augenbroe, 2019; de Wilde, 2018). Building geometry is required by most analysis tools, but the required level of resolution varies widely with the application; for instance a thermal tool may need information about zones, whereas a lighting tool will need information about surfaces. To facilitate the data transfer from BIM to BEM, many industrial applications use a specific industry-based middleware named gbXML (Green Building eXtensible Mark-up Language). The gbXML format has been defined by BEM vendors in order to leverage the information contained in BIM Models. Yet often the use of gbXML yields geometry errors in BEM models. Most geometry issues in BEM are associated to problems with thermal zones, wrong interpretations of non-planar geometry and varying boundaries of a room footprint, which will lead to missing or duplicated objects and incorrect or missing volumes of a space in energy models (Gourlis and Kovacic, 2017).

The aim of the paper is to explore some of the practical issues that emerge when importing building information model (BIM) geometry data into a building energy modelling (BEM) tool using the gbXML standard as intermediate format. It presents an in-depth case study and evaluates some of the geometry errors when exporting data from mainstream BIM software into a popular building energy simulation tool. The case study is augmented by input from experts in the field. The paper reflects on fundamental approaches to solve the observed problems.

2. BIM to BEM: a brief State-of-the-Art

The data exchange between BIM and BEM has long been the subject of R&D; for a good review of past work see van Treeck *et al.* (2018). However, there remain challenges. El Asmi *et al.* (2015) conclude that even the most extended and advanced data frameworks still fail to generate all reliable information required to be exported from BIM to BEM. Tillberg (2020) reports that consultants in industry still manually create building models for dedicated tools in the thermal, lighting and airflow domains. Bradbury (2020) mentions a need for energy consultants to rework the BIM models received by architects and other partners in order to allow a basic level of interoperability with the tool suite used inside his company. Gourlis and Kovacic (2017) observe that geometry being transferred from BIM to BEM has problems in terms of being associated to correct thermal zones, wrong interpretations of non-planar geometry such as curved walls, and handling varying boundaries of room outlines. This may lead to missing or duplicated objects and spaces, and incorrect attributes (Maile *et al.,* 2013). According to Kensek and Noble (2014), a fundamental cause is that architectural models are strongly focussed on floor space and thus emphasize the boundaries of interior walls, whereas most energy models are based on the definitions of boundary walls via the centre line of vertical or horizontal partitions regardless of their thicknesses. If not properly handled this may cause issues in the analytical representation of the design model, which will need manual transformation to be used for energy performance simulation (Steel *et al.*, 2012).

Data exchange between BIM and BEM often employs an intermediate data exchange format named gbXML. The gbXML is designed specifically to support communication between CAD systems and simulation tools. It captures geometry, user profiles, weather data and other information that is pertinent to simulation. Hijazi *et al.* (2015) state that no less of 88% of BEM tools support import through the gbXML schema, while only 12% of BEM tools support import through the Industry Foundation Classes (IFC) which are the defacto common BIM standard. The use of gbXML allows the use of middleware that operates between BIM and BEM. Such middleware may help to analyze and resolve any issues with the intermediate data. Examples are the work by Kamel and Memari (2019), Dimitriou *et al.* (2016) and Pinheiro *et al.* (2018). These middleware efforts often expand on the Model View Definition (MVD) and Information Delivery Manual (IDM) within the IFC as a starting point. They aim to remedy issues in terms of duplicate and missing data, and have the objective of ensuring that the data provided to the energy simulation tool are consistent and reliable. An alternative for the use of middleware like gbXML is the use of 'semantic enrichment that provides domain context to IFC files, so that data exchange can happen directly from the model view definition (Belsky *et al.*, 2016). However, BEM vendors do not currently support this approach.

Some of the work in gbXML and intermediate formats is as follows. Kumar (2008) investigated the gap in the interoperability between BIM and BEM whilst looking at three intermediate formats including gbXML. A data loss between BIM (Revit) and BEM (IES-VE) was reported in all cases. Rather than repair the intermediate files, Kumar suggested the use of a patch file in Revit that provides templates for a set of wall families that derive their structure from the IES model. However, this approach has been criticised for being limited to a specific analysis tool (Hijazi *et al*., 2015). Jalaei and Jrade (2014) employ the Ecotect Integrated Data Model structure in order to clean up data from the IFC and taken into gbXML in a way that includes zone and geometry in a way that it is understandable to simulation tools. Maile *et al.* (2013) developed BIM-geometry modelling guidelines and recommendations for building simulation tools. Their guidelines and the recommendations are based on the participation of the authors in the conversion of geometry in many projects such as (Nasa Ames Sustainability Base) and after conducting numerous case studies. They report that the most restricting requirement is the correct enclosure of spaces through space boundary surfaces. Ladenhauf *et al.* (2016) propose an algorithm that prepares data for BEM by simplifying geometry. This reduces the elements in the building geometry to a set of surfaces which only represent the internal boundaries and the thermal shell, and then associates the boundary parts with the data relevant to the materials of the layers and their thermal properties. Heffernan *et al.* (2017) use the Solibri model checker to identify the gaps and clashes of the surfaces before exporting geometry from BIM to BEM. Chen *et al.* (2018) investigated interoperability issues between BIM and BEM by conducting a case study which has two different building shapes (rectangular and irregular). Revit was used as the BIM tool and combined with four BEM tools (DesignBuilder, IES-VE, EQUEST, and Ecotect). In terms of building geometry, they started with simplifying the Revit model and defining the spaces and zones. They report deficiencies in data transfer to all BEM tools; for example, there were geometry issues associated to the irregular shaped building (round shaped) and issues related to window numbers. They concluded that misrepresentation of some elements imported from BIM was common; for example, windows on irregular shaped walls (curved) in BIM were not recognised by BEM tools.

Lobos and Wandersleben (2014) have conducted several case studies on data transfer from BIM to BEM. In two of these, they used Revit and DesignBuilder: they studied the Revit to DesignBuilder plug-in, and the route via gbXML. Both cases yielded the same results (advantages and disadvantages). They reported that geometry information was exported without any issues apart from zone use due to some issues in recognising some elements as interior walls as outer walls and vice versa in DesignBuilder. A similar case was explored by Douglass and Leake (2011), who imported gbXML data into DesignBuilder. They reported that all data exported looked correct and complete, but voids caused some of the thermal zones to be unenclosed. Deeper inspection of the model revealed many issues regarding geometry in the model including additional surfaces and gaps. As the first attempt was unsuccessful, they found that simplifying thermal zones in the Revit model might improve the results in the imported model. This simplified Revit model when imported to DesignBuilder has shown significant improvement, but was not completely free of errors.

More recently, Gourlis and Kovacic (2017) explored the potential of BIM to assess the energy performance of industrial buildings. They used Revit and exported the model to gbXML. Their case study is a new industrial facility which was designed in BIM but not specifically designed for assessing the performance. Thus, the level of detail in the model was very high, with every room and all objects like columns, walls, partitions explicitly modelled. They reported that all walls were designed layer-by-layer and all information about construction was available in the BIM, but directly exporting all of this to BEM was not possible.

Exporting it through gbXML led to a very complicated geometry in BEM with many errors related to boundary conditions of zones, gaps between the adjusted space (wall layering) and some openings. Consequently, the zones were simplified in the BIM model by changing and deleting some rooms and changing the boundary conditions of slabs by making the boundary at the same level. The results then yielded better interior surfaces however the quality of the exported geometry was very low, and it had to be deleted and created from scratch and some constructions had to be defined manually. One of the most important reasons behind these issues in the geometry was found to be the use of no compound elements to divide the space (walls) which led to wrong interpretations in the boundaries of thermal zones. Simplifying the architectural model and re-defining the boundaries were the greatest challenges faced to define thermal zones, so they used so-called air-walls to define the thermal zones because there were no physical boundaries dividing the thermal zones. No academic research papers or case studies were found that specifically describe and discuss the gbXML design viewer or that identify its limitations, strengths or shortcomings.

3. Methodology

In order investigate the challenges when importing building information model (BIM) geometry data into a building energy modelling (BEM) tool using the gbXML standard as intermediate, this paper presents an in-depth case study. This employs a mainstream BIM software tool, Revit, and a popular building energy simulation tool, Design Builder. Data handling issues have been augmented by input from experts in the field. The specific tool versions used in this paper are Revit Architecture 2018, gbXML Design viewer, release 9.11, and DesignBuilder, Version 5.0.3.007. Revit Architecture is one of the leading BIM tools used in architectural education as well as practice. DesignBuilder is a tool built around the EnergyPlus thermal simulation engine, which is a key software used in thermal consultancy work across the globe. DesignBuilder has invested significant efforts in enabling their tool to import gbXML data.

The case study is the Former Porter's Lodge at the Oceansgate site located in Plymouth. The building is considered a heritage centre; it consists of three floors. The Former Porter's Lodge was selected as the case study because of earlier use of the same building as a renovation design project in the undergraduate courses at the local university, ensuring high familiarity of the modellers with the building and its properties, including energy model validation and calibration. It also is a good case as it has a challenging geometry, with varying floor heights and indents between floors.

Figure 1: Porter's Lodge Building, Oceansgate, Plymouth, UK

The case study consisted of the following steps:

1. The building was modelled in Revit whilst following a specific guideline provided by DesignBuilder on how to design in Revit to prevent geometry issues in DesignBuilder (DesignBuilder, 2019). Amongst others, this guideline suggest manual rework in Revit before export of the data, reworking rooms, zones, separations, and conducting volume calculations and checks.
2. A gbXML file was extracted from the Revit model and imported into the gbXML design viewer to identify all geometrical issues.
3. Finally the gbXML file was imported into DesignBuilder, inspected in the DesignBuilder interface, and used to run an energy simulation.

The guidance of DesignBuilder used in step 1 has been developed in order to help users of Revit to transfer Revit (BIM) models into DesignBuilder (BEM). It starts with explanation of the transition process from Revit to DesignBuilder, it then shows how a Revit model should be prepared before the start of the transition process and how the final model can be checked once exported into DesignBuilder, and finally it provides detailed instructions on how to load a model from Revit into DesignBuilder. There is considerable intelligence embedded in the Revit (BIM) data provided. However, the BIM model will not contain any of the specific zonal or volumetric data required by DesignBuilder, this data has to be superimposed to the data inside the Revit model and thus more or less 'redesigned'. After this additional information is added the Revit 'architectural model' will be referred to as a separate 'analytical model'. The most important thing which was taken into account when redesigning the Revit model is to accurately identify the rooms, because the values that rooms store for different parameters will affect the subsequent building analysis such as the geometry and the volumes of spaces. For the case study seven rooms were created, two rooms in the basement floor, one room in the ground floor and four rooms in the first floor. Bounding elements such as floors, walls and roofs are used to identify rooms. Revit refers to these bounding elements when it computes the area, volume and parameter of rooms. The property 'room bounding' in Revit can be turned off/on to allow for flexibility in configuring the rooms. It was turned on when all elements such as walls, floor and roofs were created. When exporting the gbXML file from Revit, the data of the gbXML will be mainly based on rooms and their bounding elements, and the mechanism in DesignBuilder will be identifying and converting the rooms into zones and blocks. The 'Spaces' component is used for Revit MEP instead of 'Rooms' component in order to maintain space information, while the 'Rooms' component is used for Revit Architecture. Revit (MEP) 'Spaces' and Revit Architecture 'Rooms' are very similar; however, 'Rooms' are architectural components used to maintain information about any occupied areas, while 'Spaces' are MEP components used to analyse volumes.

The web-based tool gbXML design viewer used in step 2 allows checking the geometry of the BIM model before exporting it into DesignBuilder and helps to identify issues within the viewer itself (Ladybug tools, 2019). The two-stage approach enables checking for improvements in the analytical model, which will help to know whether the guidance have actually helped to improve the geometry of the model. The export to DesignBuilder allows using the error reporting facility within the BEM tool in order to find residual issues not picked up by the gbXML viewer.

Subsequently recommendations and suggestions were sought from experts in this domain, especially experts who are involved in the process of exporting data from BIM to BEM, regarding the issues identified and their causations. The interviewees included a technical director of DesignBuilder, a university lecturer teaching DesignBuilder at undergraduate level on a building/construction course, and a Revit expert working in the construction industry.

The interview process was open ended and tailored to the domain expertise of the interviewees.

4. Case Study Results

There were no major issues needing specific consideration whilst modelling on Revit following the energy model preparation guidance, as the guide points out all issues that need to be checked in the Revit architectural model and gbXML analytical model within Revit before exporting the gbXML analytical model to DesignBuilder. The only thing that could be considered as major point of contention while modelling on Revit in order to ensure the success of the transition process to DesignBuilder is the need to define the bounding elements correctly, and to ensure that the ceiling does not become a structurally bounding element to most spaces which will result in wrong computation of volumes.

The gbXML file was extracted from Revit then imported into the gbXML Design viewer. In general, all rooms created on Revit are exported and correctly recognised by the gbXML viewer and all main bounding elements are recognised as they are supposed to be recognised. See figure 2. In gbXML viewer the model in general looks fine with no gaps identified, and all elements seem to be correctly recognised.

The ability to identify errors that are invisible errors in the Revit analytical model and the energy model on DesignBuilder by using the gbXML viewer is a strength point and should be general practice, as it will reduce the time a modeller needs to go back to a Revit architectural model and correct errors shown on a Revit analytical model. This will also reduce the time of exporting from Revit and importing into DesignBuilder since errors are identified on the energy model before passing this on to DesignBuilder, as otherwise invisible issues might keep occurring because they will not be identified.

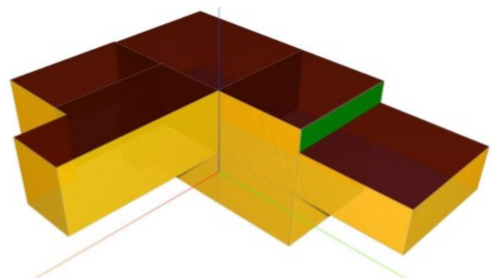

Figure 2: The final analytical model on the gbXML Design Viewer

The gbXML file was then imported into DesignBuilder. All rooms created in Revit are found to have transferred and correctly been recognised in DesignBuilder. Running thermal simulations of the model in DesignBuilder model is possible and does not flag up any errors.

Further issues in the transition process have been identified using the gbXML viewer. A total of 55 problems have been identified and seem to persist in spite of following the modelling guidance. Out of these 55 issues only one issue is visible on all three tools (Revit Analytical Model, gbXML Viewer and DesignBuilder), while the 54 remaining problems are not visible in the Revit model or the DesignBuilder model; these have only been identified in the gbXML report. Detailed inspection of the gbXML report shows that there are 46 duplicated CAD objects. Duplicated CAD objects mean that multiple gbXML elements were created from a single CAD element. Out of these 46 errors, 23 are related to exterior walls, 10 errors to interior floors, 8 to interior walls and 5 errors related to roofs. Furthermore, there are 8 duplicated adjacencies. Duplicated adjacencies mean that there is an error as some interior surfaces with both adjacencies are pointing to same ID (Room). Out of the 8 issues, 6 issues are linked to some problems in interior floors and 2 issues to interior walls.

It was expected the report would show that there are three storeys, however only two storeys are recognised. The gbXML viewer refers to the storeys as level 0 (ground and first floor) and level -3 (basement). When the Revit model was developed only two storeys were created but with three floor levels, each floor having a different height: first floor (1000mm from the ground level), ground level, and basement (-3000mm). When the Revit analytical model was prepared and exported into the gbXML viewer and DesignBuilder, the first floor and the ground floor appeared on the same level (first floor level). The one-meter offset in height between the two floor levels was ignored and they were assumed to be at the same floor level. As a follow-up error this reduced the height of room 1 to 2 metres instead of 3m. See figure 3, here the floor of the room should be 1 meter below its current position while the roof position is correct.

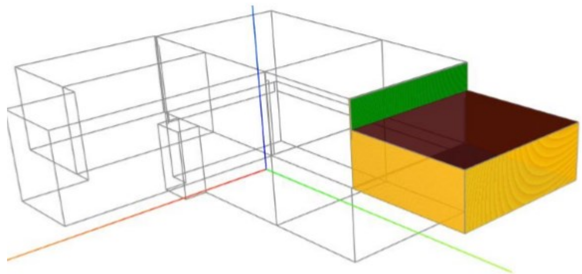

Figure 3: The floor surface of the toggled room must be one meter below its current position

Another 46 errors are related to multiple gbXML elements created from a single CAD element. Errors from 0-4 are shown in figure 4 below which are linked to the same external wall.

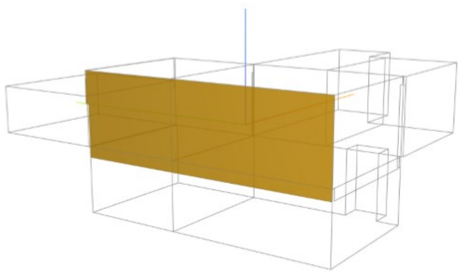

Figure 4: Five gbXML elements created from an external wall

Finally, eight errors relate to duplicate adjacencies. Duplicated adjacencies mean that; there is an error where interior surfaces with both adjacencies pointing to same ID (Room or space). These eight errors are shown in figure 5.

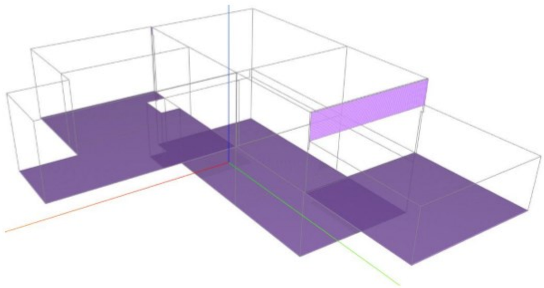

Figure 5: Eight duplicate adjacencies

5. Expert Feedback

Discussion of the case study with the experts gives the following insights:

- Running a thermal analysis of a model with some geometry issues in DesignBuilder is technically possible and is not prevented by any code. The typical test by academic tutors and industrials is to make sure that no gaps can be identified when looking at the DesignBuilder model. However, models with open manifold blocks cannot be used for CFD or Daylighting simulations in DesignBuilder as these require fully closed manifold block geometry, and in those cases the tool prevents simulations that do not meet this criterion. It is not clear why this is not imposed on thermal models.
- We were told that in industry a rough guideline is used that assumes that if approximately 90% of the energy model is correct, the model can be used to run a thermal simulation. However a 10% error acceptance seems a rather high level.
- Technically, DesignBuilder attempts to identify connected gbXML spaces that have the same floor and ceiling heights and, if they can be combined and represented using extruded geometry, DesignBuilder creates a single block from the various zones. It should be possible to import models with split floor levels provided these models have been set up correctly in Revit.
- The duplicate elements and adjacencies may relate to the fact that walls are made of multiple elements, so it might be pointing at the different layers within the same wall. It was suggested that different versions of the gbXML viewer might handle this slightly differently.
- It is known that there may be issues related to room enclosures and wall extents/breaks; these should be set to enclose rooms within the extents of a wall, then other spaces enclosed in separate wall enclosures. People who know about this aim can avoid conflicts in the computation of room boundaries when modelling the building in Revit. Engineering consultancies often employ a dedicated BIM manager to retrace all drawings received from collaborators in order to ensure there are no issues when transferring data into gbXML and onto other tools like IES-VE and Daysim.

6. Discussion and Conclusions

As demonstrated in this case study, the interoperability approach for parsing data from BIM to BEM still has some issues. As observed by many working in industry, it has not yet reached the point where sending BIM data to BEM can be performed by simply clicking a button. But actors in industry see it as an important objective to ensure that the processes are seamless, and ask for further improvements and automation of the process.

In general, errors in data exchange between BIM and BEM can stem from three root causes: user modelling skills, differences in object definition within the BIM and BEM environment, and errors in the export/import functions.

The general potential of interoperability between BIM (Revit) and BEM (DesignBuilder) is demonstrated by the case study, but it also is clear that the transition process from BIM to BEM gets harder as models get more complex. It is concluded that a focus in the work should be the full enclosure of spaces, as this is a main source of errors. Improving the modelling procedure in BIM editing tools like Revit and simplifying a model will result in far less errors and better geometry quality when transferring models into BEM tools like DesignBuilder. Overall the correct computation of space volumes will depend on the bounding elements selected while modelling. The use of a model checker to inspect the intermediate file before importing a gbXML file into BEM can play a significant role to save time and identify unseen errors that could not be identified on the BIM and BEM tool themselves, as it helps to identify detailed errors in the model. On many occasions, issues in energy models are mentally linked to requirements of the BEM tools; in fact however errors may also stem from the way a model was designed on a BIM tool and the capability of any middleware used.

To move forwards, it is important that the developers of BEM software like DesignBuilder make it clear what the root cause of import errors is. In that way it will become clearer to users what the restrictions of any middleware is, and what issues stem from the BIM tool used to generate the model. The gbXML schema might be expanded to include a capability for recognising and handling more complicated building shapes. Furthermore, it should be capable to transfer all necessary building data that is required for energy analysis tools such as DesignBuilder. Energy tools should support the attributes provided by a BIM file. The spaces enclosed between center planes, which is the difference between analytical and inner volume must be considered. In order to avoid data loss when exchanging data, more middleware inspection and augmentation tools should be developed. BIM tools might include new warnings or errors alerts if a BIM model does not include some of the required information for BEM tools. As some of data required by the energy tools might not be defined by users of the BIM tools, BEM tools might use default values that are set by different standards like those offered by CIBSE or ASHARE, and this will need to be carefully inspected particularly when multiple BEM tools are used in projects that adopt BEM.

In general, the authors believe that expanding the middleware handling software and thus strengthening model view definitions is the best way forward to maintain full flexibility in the BIM model, whilst easing the transition of data to a BEM tool.

References

Augenbroe, G., (2019). The role of simulation in performance-based building. In: Hensen J. and Lamberts R. (eds). Building Performance Simulation for Design and Operation. London: Routledge, pp.341–373

Arayici, Y., Fernando, T., Munoz, V., & Bassanino, M. (2018). 'Interoperability specification development for integrated BIM use in performance based design'. Automation in Construction, 85 167–181.

Belsky, M., Sacks, R. and Brilakis, I. (2016). Semantic enrichment of building information modelling. Computer-aided Civil and Infrastructure Engineering. 31: 261–274.

Borrmann, A., König, M., Koch, C. and Beetz, J. (2018). Building Information Modeling : Technology Foundations and Industry Practice. Cham, Switzerland: Springer, pp.337–345.

Bradbury, J (2020). Private communication.

DesignBuilder. (2019). DesignBuilder Revit – gbXML Tutorial. [online] Available at: https://forums.autodesk.com/autodesk/attachments/.../133/.../db_revit_tutorial_v1.pdf [Accessed 9 Jan. 2019].

De Wilde, P. (2018). Building Performance Analysis. Chichester: Wiley Blackwell, pp 367–368

Dimitriou V., S.K. Firth, T.M. Hassan, F. Fouchal, (2016) 'BIM enabled building energy modelling: development and verification of a GBXML to IDF conversion method', Proceedings of the 3rd IBPSA-England Conference BSO 2016, Newcastle, 12th–14th September 2016.

Douglass, C & Leake, J (2011). 'Instructional Modules Demonstrating Building Energy Analysis Using a Building Information Model'. American Society for Engineering Education.

El Asmi E, Robert S, Haas B, Zreik K. (2015). 'A standardized approach to BIM and energy simulation connection'. SciTechnol; 21(1):59–82.

Gourlis G, Kovacic I. (2017). 'Building Information Modelling for analysis of energy efficient industrial buildings – A case study'. Renewable and Sustainable Energy. 68: 953–963.

Heffernan, E., Sohel, M. I., Beazley, S. & McCarthy, T. J. (2017). 'From BIM (Building Information Modelling) to BEM (Building Energy Modelling): a collaborative approach.' Australasian Building Simulation 2017 Conference Proceedings (pp.1–11).

Hijazi, M. Kensek, K. Konis, K. (2015). 'Bridging the gap: supporting data transparency of BIM to BEM.' Architecture Research Center Consortium (ARCC) Conference,Chicago, IL.

Kamel. E & Memari. (2019), 'A Review of BIM's application in energy simulation: Tools, issues, and solutions', Automation in Construction, 97:164–180.

Kumar, S. 2008. Interoperability Between Building Information Models (BIM) and Energy analysis Programs, University of Southern California.

Ladenhauf D, Battisti K, Berndt, R, Eggeling, E, Fellner, D, Gratzl-Michlmair, M & Ullrich, T, (2016) 'Computational geometry in the context of building information Modeling', Energ. Buildings 115: 78–84.

Ladybug.tools. (2019). [online] Available at: http://www.ladybug.tools/spider/readgbxml/polyloop/r1/read-gbxml-polyloop.html [Accessed 9 Jan. 2019].

Lobos, D., Wandersleben, G., and Castillo, L. (2014). 'Interoperability Map between BIM and BPS Software.' Computing in Civil and Building Engineering (2014): pp. 601–608.

Maile T, O'Donnell J, Bazjanac V, Rose C. (2013) 'BIM-geometry modelling guidelines for building energy performance simulation'. Building Simulation Conference; 2013.p.3244–3249.

Pinheiro S, Wimmer R, O'Donnel J, Muhi. S (2018). 'MVD based Information Exchange Between BIM and Building Energy Performance Simulation' Automation in Construction. 90: 91–103.

Prada-Hernández, A. V., Rojas-Quintero, J. S., Vallejo-Borda, J. A. & Ponz-Tienda, J. L., 2015. 'Interoperability of Building Energy Modeling (BEM) with Building Information Modeling (BIM)'. Proceedings of the VI Elagec, pp. 519–526.

Steel J, Drogemuller R, Toth B. (2012). 'Model interoperability in building information modelling. Software System Model'. 11(1):99–109.

Tillberg M (2020). Design of low-energy buildings & building systems: software and tools. Proceedings of HVAC & Energy Management Systems of Commercial Buildings, Berlin, Germany

Underwood C, Yik F (2004). Modelling Methods for Energy in Buildings. Oxford: Blackwell

Van Treek, C, Wimmer R. and Maile, T. (2018). BIM for energy analysis. In:Borrmann, A., König, M., Koch, C. and Beetz, J. (Eds). Building Information Modelling: technology foundations and industry practice, Cham: Springer, pp. 337–347

Reno-Inst: An Ontology for Installation of Components in Building Renovation Projects

Jerson Alexis Pinzon Amorocho, Timo Hartmann
Technische Universität Berlin, Germany
j.pinzonamorocho@tu-berlin.de

Abstract. Buildings play an important role in implementing energy efficiency at the urban level. Since new buildings account just for 1% of the stock, the largest opportunity comes from the renovation of existing buildings. While installation and commissioning procedures for energy efficiency elements in new buildings may be well established, renovation projects address specific challenges. Main particularities are related to unknowns in pre-existing conditions, presence of occupants, and space/time limitations. This paper presents an ontology mapping the knowledge regarding the installation procedures of renovation elements and their constraints. The Reno-Inst ontology may contribute to developing a shared understanding of this domain and enable easier information processing, reuse and retrieval in renovation projects. The ontology development relies on literature review, catalogues, guidelines, and input from experts, focusing on windows, thermal insulation panels, and heat radiators, three common elements of renovation projects.

1. Introduction

Buildings account for 40% of the EU's energy consumption, 36% of its CO2 emissions and 55% of its electricity consumption Artola et al. (2016), thus playing an important role in implementing energy efficiency at the urban level. Since new buildings account just for 1% of the stock, the largest opportunity comes from the renovation of existing buildings. Nevertheless, the current renovation rate of existing buildings is low, even as renovation accounts for 57% of all construction activity, only about 1-2% of the building stock is renovated each year Artola et al. (2016). Some of the renovation activities currently taking place are mainly about the replacement of windows, heating, cooling, lighting systems or roof insulation Saheb (2016).

While installation and commissioning procedures for energy efficiency elements in new buildings may be well established, renovation projects address specific challenges that call for specialized supporting tools and procedures. Renovation projects in residential buildings deal with particularities such as the construction process being performed, in most of the cases, while the building is occupied. In these cases, the execution of renovation activities should consider potential impacts on occupants and implement measures to mitigate them. For instance, traditional approaches for envelope refurbishment need scaffolding on the outer façade for very long times (12 to 24 months), requiring occupants to seal the windows and introduce safety issues Salvalai et al. (2017). A representation of these and other particular conditions for the installation of different elements in the context of building renovation may support stakeholders to plan better the construction activities in renovation projects.

Many industries have developed ontologies for efficient knowledge management. In the construction industry, ontologies are introduced and studied widely because building projects involve many collaborative works from multiple professionals, stakeholders and phases Zhong et al. (2019). The adoption of ontologies in the architectural design and construction industry relies often on the inference potential offered by the logical foundations of the semantic web technologies Pauwels et al. (2017). In the context of building-related knowledge, the development of ontologies has been focused on energy efficiency Díaz et al. (2013), building environment Zhong et al. (2018), materials Bilal et al. (2017), cost estimation Lee et al. (2014), and certification labels Kamsu-Foguem et al. (2019). Most of these efforts are developed around the construction process of new buildings or the operational phase of existing buildings. However, ontologies may also contribute to building renovation projects.

Therefore, this paper presents an ontology that focuses on the installation procedure of renovation elements in residential buildings. The purpose of the Reno-Inst ontology is to support stakeholders such as project managers and site-directors during the planning and construction coordination phases. Structuring a representation of the installation procedure and constraints for common elements of renovation projects such as windows, thermal insulation panels, and HVAC components can facilitate the activity planning and material, tools and workforce estimation process. We specify the scope of the ontology and present its structure and potential uses. The paper is structured as follows: Section 2 presents the background and research motivation. Section 3 summarizes the methodology implemented for ontology specification and knowledge capture. Section 4 presents the Reno-Inst ontology. Finally, the discussion and conclusions are synthesized in Sections 5 and 6, respectively. In this paper *renovation* will be used as a general term comprising building improvements in the form of rebuilding, refurbishing or retrofitting.

2. Background and Research Motivation

Building renovation projects are treated most of the times as special cases of conventional new building projects. However, one of the major renovation constraints is the uncertainty of unforeseen and varying conditions related to unknowns in preexisting conditions, which can impact the performance of construction activities Singh et al. (2014). Renovation projects encounter deteriorate existing conditions of materials and structural elements and additional decommissioning activities of previous elements, which could affect construction and installation activities. Moreover, if the building is occupied, the presence of occupants may modify conventional practices. Ward et al. (2017) analyze the challenges to maintain a balance between building operations and completing a renovation project. Changes in the conventional construction practices comprise including the occupants' schedule in the activity planning, changes on the definition of egress pathways and other routes in the construction site, and modifications of material storage and waste management plans. In addition, special measures should be implemented to guarantee occupants' safety and control aspects such as noise, dust and debris production.

According to Singh et al. (2014), by studying the constraints of renovation projects, it is possible to better plan for these constraints and to minimize their impacts on construction activities and overall performance of the project. The authors identify a set of critical activities that may have an impact on the final performance of renovation projects:

- Preparation of plans and specifications,
- site investigation by contractor,
- preparation of site logistics plan,
- mobilization and demobilization,
- temporary construction,
- selective demolition,
- material and equipment procurement,
- demolition waste management,
- mechanical, electrical, and plumbing (MEP) rough-ins.

It is important to notice that most of these critical activities are related to the installation tasks of renovation elements. For instance, the installation of a window includes performing a survey of the openings in the building (site investigation by contractor), coordinating with the occupants to install the new window (preparation of site logistics plan), removing the previous window (selective demolition), and disposing the old window (demolition waste management).

To the best of our knowledge, there is not a common representation or understanding of the particularities and critical aspects of the installation procedure of different elements in the renovation of residential buildings. In general, the lack of a shared understanding can lead to difficulties in identifying requirements from a system, an approach to solving this problem is to develop formalized knowledge representations Uschold and Gruninger (1996). An ontology is a representation which provides an explicit specification of concepts, terminologies and relationships that are known in a particular domain Gruber (1995). It includes a set of concepts/classes, relations/properties, instances/individuals, and axioms. These elements can be described based on the semantic web, using the Web Ontology Language (OWL) and the Resource Description Framework (RDF), which allow representing knowledge in an understandable form to computers and humans. The use of the semantic web technologies in the AEC industries has been focused on supporting: a) interoperability, b) linking information across domains such as BIM-GIS, manufacturer data-building data, and building performance analysis; and c) logical inference to check model consistency and completeness, compliance, construction safety, and perform cost estimation and home automation Pauwels et al. (2017).

Some previous research works have focused on domains related to the building construction process. Bilal et al. (2017) propose a building materials database based on an ontology which captures semantically diverse data of building materials, in order to establish the core of a building waste analysis tool. Niknam and Karshenas (2017) presents a shared ontology approach for semantic representation of building information, which is used to integrate information from different sources such as design, cost estimating and scheduling concepts. Díaz et al. (2013) introduce an ontology that describes the structure of the building, the distribution and connectivity of its systems, objects, and spaces, the functionality and characteristics of the energy-consuming devices, and energy efficiency metrics corresponding to the building and its components. On the other hand, Zhong et al. (2015) present an ontological approach to support the definition and verification process of a construction plan. The authors model the construction plan domain including tasks, methods, resources and constraints and present a particular case focused on a deep foundation pit excavation.

Nevertheless, building renovation seems to be a neglected area in the field of ontological representations. An ontology covering the domain of renovation projects may contribute to developing a shared understanding of this domain. A review of existing literature demonstrates that renovation projects face different challenges, especially during the construction stage and the installation of new elements, when multiple limitations and constraints appear. These particularities are mainly related to existing conditions of the building, the presence of occupants, and space limitations. A shared understanding and a representation of these concepts and their relationships may contribute to supporting stakeholders during the activity planning and construction process in the context of renovation projects. Therefore, the specific objective underlying this study is to develop an ontology to represent the installation of windows, external thermal insulation composite systems-ETICS panels, and radiators in the renovation of residential buildings, considering different requirements and constraints. The proposed Reno-Inst ontology may support stakeholders in tasks such as identifying the activities with the greatest number of constraints, particular requirements to guarantee occupants' safety during the performance of a specific task and checking activities coordination, materials and tools. Moreover, according to Lenat and Feigenbaum (1991), a great deal of real-world knowledge is a prerequisite for an intelligent program to perform complex analytical tasks accurately, therefore, a representation with machine-readable data for the installation of renovation elements may also contribute to developing tools to support and make easier information processing, reuse and retrieval in the context of renovation projects.

3. Research Approach

This section presents the methodology we implemented to develop an ontology modelling the knowledge from the domain of the installation of renovation elements. The development of the ontology is based on the guidelines presented in Noy and Mcguinness (2001) and the Methontology approach Fernández-López et al. (1997). These methodologies enable documenting the motivation for the development of the ontology, its use and purpose in natural language. The research approach describes the ontology specification, including competency questions and the knowledge acquisition and conceptualization process.

3.1 Ontology Specification

The goal of the specification phase is to produce a general description of the ontology comprising minimum information regarding the purpose, use, users and domain covered by the ontology Fernández-López et al. (1997). This section presents the specification of the Reno-Inst ontology using natural language and a set of competency questions.

What is the purpose? The Reno-Inst ontology was developed to represent concepts related to the installation of renovation elements in order to support planning tasks in residential building renovation projects.

What is the scope? The ontology will cover concepts and relations regarding the installation of windows, ETICS panels, and radiators, which are common renovation elements. The ontology includes information on physical features, general installation procedures, constraints that should be considered, and additional elements such as workforce, time, and tools requirements.

What are the intended end-users? The final intended users are project managers, site-directors and other stakeholders which may be involved in the planning and scheduling of construction activities in residential building renovation projects.

What is the intended use? The intended use of the ontology is to facilitate reasoning over the installation information for different purposes. The set of competency questions presented in Table 1 was developed to identify some of the concepts that users may be interested on. For instance, a user may list the tools and materials required to install a window, this information can be used to schedule the procurement of the specific supplies. A user may also verify whether a specific construction task can be performed in presence of occupants, this kind of information can help the stakeholders to identify which installation activities require special measures and coordinate them accordingly. Hence, the ontology will support the end-users to plan the installation activities of renovation elements considering time schedules, required tools, materials and workforce, and constraints related to the existing conditions in the building and occupants.

Table 1: Competency questions and answer examples.

Competency questions	Example answers
What are the *tools* required to install an ETICS panel?	Drill, cutting tool, mixing and delivery machine, scaffolding
What *regulation* should be considered when installing ETICS panels?	ETAG 004, EN 13162, EN 13163
What *activity* should be finished before driving rain-proof connection of a window?	To Install air-thigh joint closure
What kind of *pollution* should be controlled when *anchoring* an ETIC panel?	Noise, dust, and vibration
What is the material of the wall where a specific radiator will be installed?	Clay brick
Which activities require a *high* level of *safety* to avoid potential impacts on the occupants?	Lifting of a window from indoor, materials transportation through the staircase

3.2 Knowledge Capture and Conceptualization

The knowledge acquisition includes identifying the relevant concepts in the ontology, developing a class hierarchy, and establishing class properties. The main goal is to identify what is the information required for the installation of each renovation element and how these diverse concepts can be gathered in a knowledge network including different classes, relationships and properties. The specification and competency questions presented in the previous section are used to guide the identification of relevant terms. The capture of knowledge relies on literature review, catalogues from manufacturers, guidelines from regional associations, and input from experts on the field as summarized in Table 2. The input from experts was collected through a brief workshop and a semi-structured interview. The experts involved in the study comprise an architect, a BIM coordinator and a R&D director from three different construction companies. Special attention was given to information related to physical features of the renovation element and the building interface where it will be installed, and constraints imposed by the presence of occupants and other aspects.

Table 2: Sources for ontology knowledge.

Main Concepts	Terms Examples	Source
Renovation elements	Functional component, interface component, material	Darup et al. (2015), ift (2016), Joint Research Centre (2012)
Installation procedure	Main installation activity, tools, construction material, activity description	EAE (2011), ift (2016), and experts' input
Existing conditions and Constraints	Building interface, opening, pollution constraint, activities coordination	Singh et al. (2014), Ward et al. (2017) and experts' input

4. Ontology for Renovation Elements Installation

Reno-Inst covers the installation of windows, ETICS panels, and radiators in the context of renovation projects. These three elements have diverse concepts associated to them and different installation procedures. Developing an ontology to represent each of these procedures separately could derive in a complex, large and probably unpractical approach. In order to address this challenge, the main classes of Reno-Inst comprise the general concepts which are common for the installation of diverse renovation elements. As shown in Fig. 1, each *RenovationElement* has *Component*, *Documentation* and *InstallationActivity*, and it is linked to a *BuildingInterface*. The *InstallationActivity* of each renovation element requires *WorkforceToolsAndMaterials* and have *Constraint* regarding to existing conditions, coordination and safety. Moreover, the *BuildingInterface* where a *RenovationElement* will be installed has *PhysicalAttribute* and is located at a *BuildingElement*.

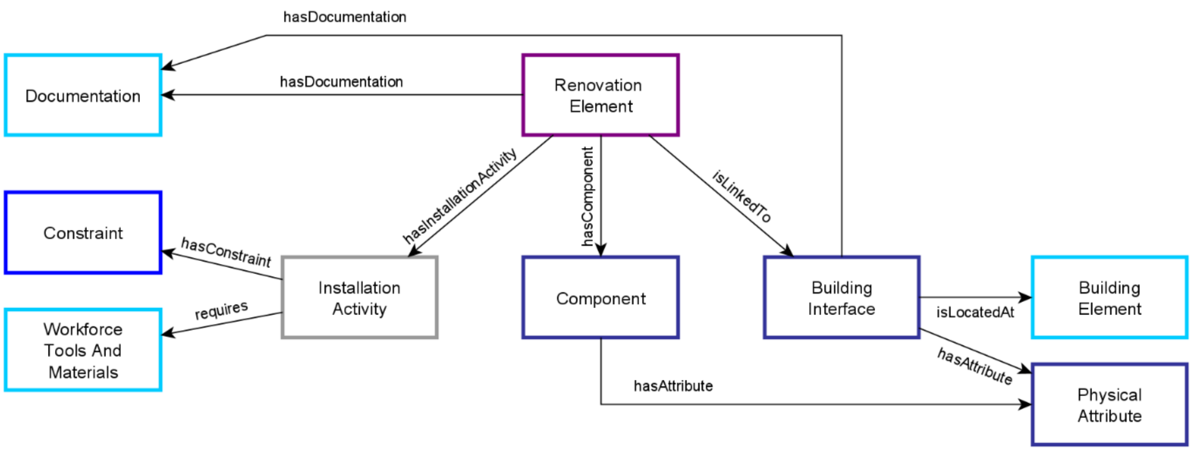

Figure 1: Ontological model Reno-Inst

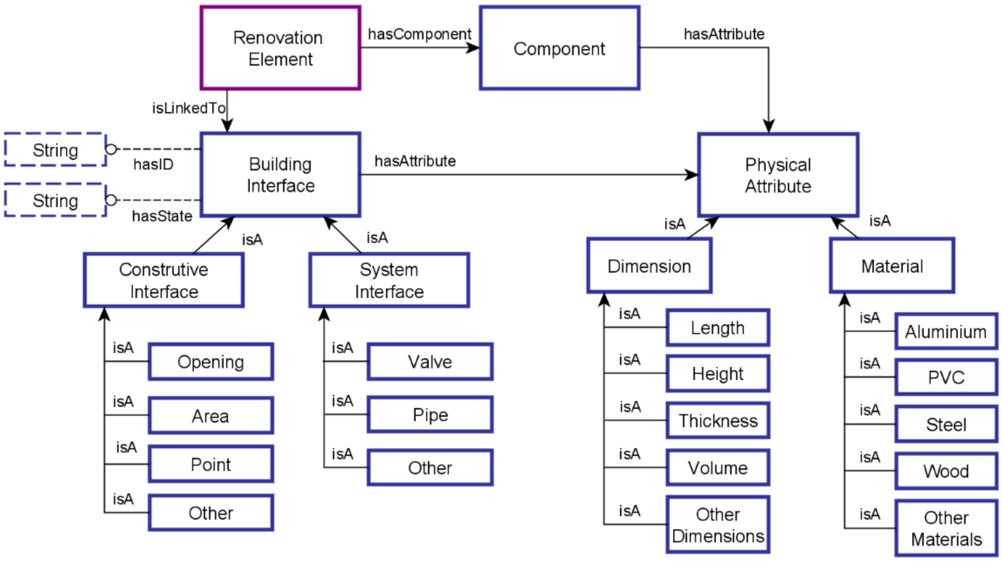

Figure 2: Major classes *BuildingInterface*, *Component*, and *PhysicalAttribute*

As presented in Fig. 2 each *RenovationElement* will be linked to a *BuildingInterface*, which may be a *ConstructiveInterface* or a *SystemInterface*. Architectural elements where a *RenovationElement* may be installed such a specific point in a wall, an opening, or an area in a floor correspond to *ConstructiveInterface*. In contrast, *SystemInterface* gathers building elements that link one of the building systems to a *RenovationElement*, e.g. an existing hot water pipeline that will be connected to a new radiator. On the other hand, the concept *PhysicalAttribute* gathers the features that can be used to describe a Component of a *RenovationElement* or a *BuildingInterface*. For instance, the frame of a window can be described by *Length*, *Height*, *Thickness* and *Material Wood*. Moreover, an *Opening* where a window will be installed, can be described by *Length*, *Height* and *Material ClayBrick*.

In a deeper level of abstraction, specific knowledge related to different renovation elements can be added as blocks of concepts. A *Window*, a *Radiator* and other elements can be represented under the concept *RenovationElement* as presented in Fig. 3. The *Component* of a *RenovationElement* may be a *FunctionalComponent* or *InterfaceComponent*. The concept *FunctionalComponent* represents the main components of a *RenovationElement*, which perform the main function of it, e.g. the core of a radiator. In contrast, *InterfaceComponent* represents the specific components that will be directly linked to the *BuildingInterface*, e.g. a radiator has a fixing mechanism that will be linked to a point in a wall. Individual blocks with the components for each renovation element can be added. In a similar fashion, consider the *InstallationActivity* class in Fig. 4, it includes *RemovalActivity*, *WorkAreaPreparationActivity*, and *InstallationVerificationPhase* which are concepts shared by different renovation elements. A block with a concept *WindowMainInstallationActivity* and activities *FixingActivity*, *AirtightClosureActivity*, *RainProofConnectionActivity*, and *ThermalInsulationActivity* can be added to represent specific tasks for the installation of windows. Equivalent blocks can be built for ETICS panels and other elements. This proposed ontology structure may facilitate the integration of new renovation elements, contributing to extend Reno-Inst in future applications.

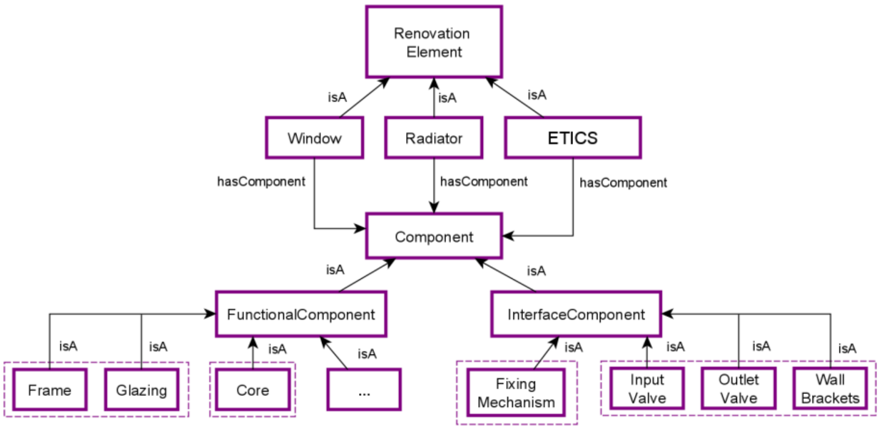

Figure 3: *RenovationElement* class and knowledge blocks for different renovation elements

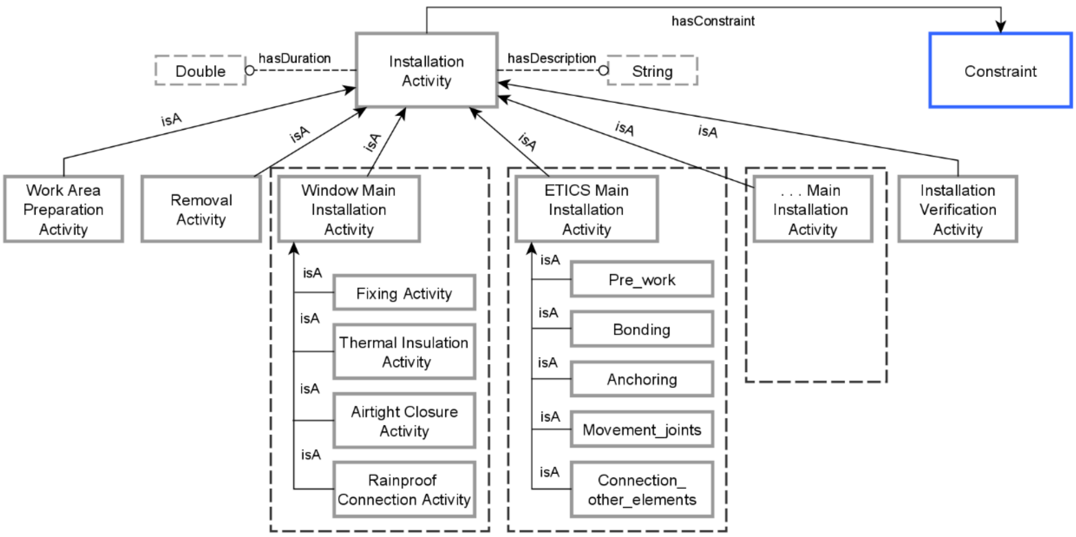

Figure 4: *InstallationActivity* class and knowledge blocks for different renovation elements

As shown in Fig. 5, the *Constraint* class includes five main concepts named *PhysicalConstraint*, *UncertaintyConstraint*, *CoordinationConstraint*, *PollutionConstraint*, and *SafetyConstraint*. Including these diverse constraints contributes to getting a better understanding of the particularities of the construction process in renovation projects. The sub-classes *PhysicalConstraint* and *UncertaintyConstraint* represent restrictions due to physical limitations and lack of information from the existing building. The sub-class *CoordinationConstraint* is related to temporal constraints on the installation tasks, it allows considering special restrictions imposed by the building operational schedule and the sequence of the activities during the installation procedure. For instance, consider the *ThermalInsulationActivity* for the installation of a window, this activity has a *PreviousActivity* (*FixingActivity*) that should be performed before the thermal insulation starts. Moreover, the *ThermalInsulationActivity* has also a *FollowingActivity* (*AirthightClosureActivity*) that should be executed after the thermal insulation finishes. On the other hand, *PollutionConstraint* is related to situations such us large dust production during the activity, the handling of building materials containing contaminants, or high noise production during long periods, which may affect occupants. The last sub-class *SafetyConstraint* represents the level of impact of each activity on occupants' safety. A *High SafetyConstraint* means that the activity cannot be performed with the presence of occupants and special considerations should be taken to execute this task.

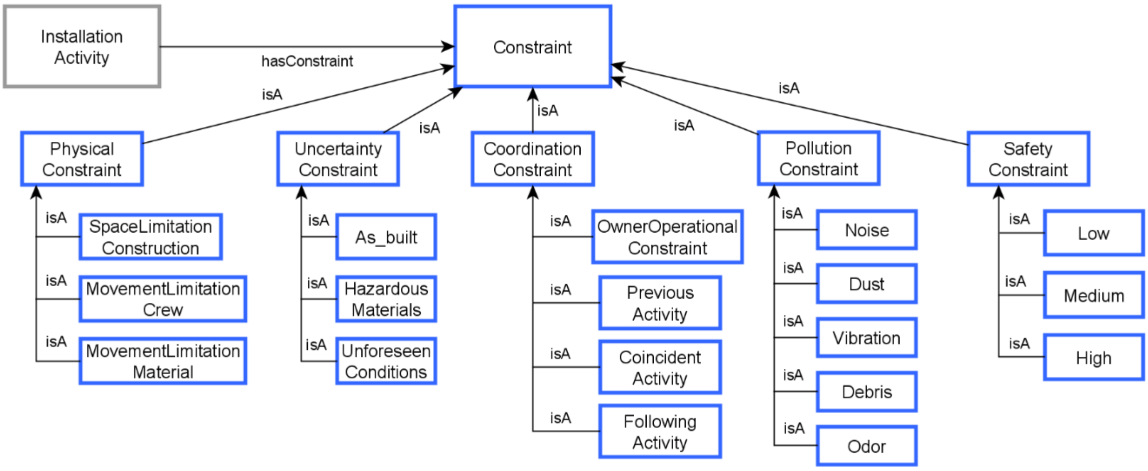

Figure 5: *Constraint* class representation

Finally, the major classes *Documentation*, *WorkforceToolsAndMaterials* and *BuildingElement* are depicted in detail in Fig. 6.

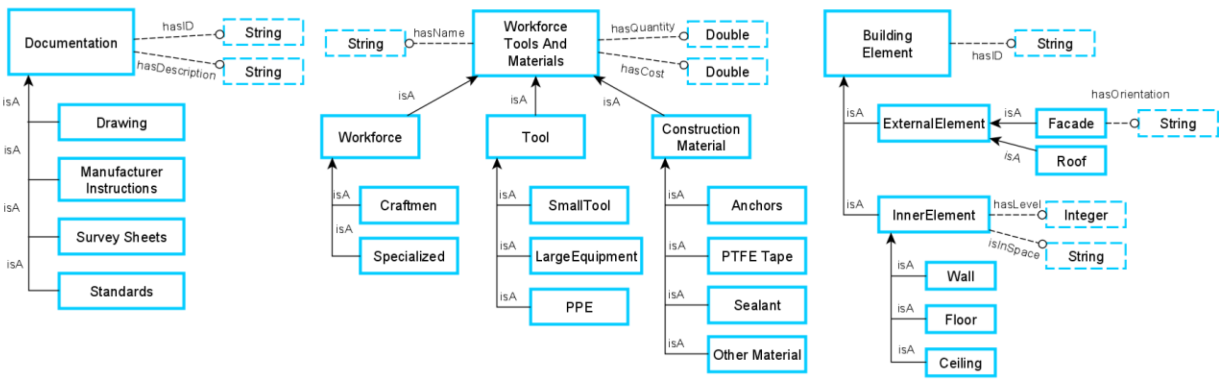

Figure 6: Major classes *Documentation*, *WorkforceToolsAndMaterials* and *BuildingElement*

5. Discussion

The proposed Reno-Inst ontology contributes to the body of knowledge by providing a representation of the installation of different elements in the renovation of residential buildings, considering different requirements and constraints. This ontological representation comprises the description of renovation elements and the building interface where they may be installed; it also covers the installation activities and the constraints related to them. The representation of these concepts can support stakeholders to check critical aspects of the existing building, external constraints or limitations that can affect the construction process in the context of renovation projects. This information is relevant during the activity planning; disregarding some of these aspects may impact the performance of the renovation project and lead to cost and schedule overruns.

One of the limitations of the proposed ontology is related to the renovation elements covered during the knowledge acquisition. The structure of the Reno-Inst ontology was defined based on the information captured for three common renovation elements, however, there are multiple components, activities and constraints that can be considered during a renovation, and some of them may not fit into the proposed representation. An additional knowledge capturing process should be conducted to map information about other renovation elements such as roof insulation, heating pipes and lighting appliances, with the aim of checking opportunities to extent the ontology. A more detailed representation of the building interface will be also pursued. Furthermore, it was not possible to identify existing ontologies in the renovation domain, nevertheless, the integration with models from related domains such as the ontological approach for plan definition developed in Zhong et al. (2015) will be studied. Future activities include to implement the Reno-Inst ontology using OWL/RDF to develop a machine-readable model. A dataset from a specific case may be used to evaluate the capability of the ontology to retrieve and infer relevant information for the intended users, through SPARQL queries.

6. Conclusion

While installation and commissioning procedures for energy efficiency elements in new buildings may be well established, renovation projects address specific challenges that call for specialized supporting tools and procedures. These particularities are mainly related to existing conditions of the building, the presence of occupants, and space/time limitations. This paper introduced the Reno-Inst ontology, which represents the main concepts and relationships covering the installation of windows, thermal insulation panels, and heat radiators, which are common renovation elements, considering different requirements and constraints. This ontology provides an integrated view of the information that can support the activity planning and construction process in the context of renovation projects. The developing of the Reno-Inst ontology relied on catalogues, guidelines, and input from experts.

Acknowledgements

This research project is funded under the European Union’s program H2020-NMBP-EEB-2018, under Grant Agreement no 820553.

References

Artola, I., Rademaekers, K., Williams, R. and Yearwood, J. (2016), Boosting building renovation: What potential and value for europe?, Technical report, Policy Department A: Economic And Scientific Policy. Available at: http://www.europarl.europa.eu/committees/en/supporting-analyses-search.html.

Bilal, M., Oyedele, L. O., Munir, K., Ajayi, S. O., Akinade, O. O., Owolabi, H. A. and Alaka, H. A. (2017), 'The application of web of data technologies in building materials information modelling for construction waste analytics', Sustainable Materials and Technologies 11, pp. 28–37.

Darup, B. S., Zwiauer, K. and Burghardt, M. (2015), Thermal building renovation – thermal renovation of building components, Technical report, Verein e-genius. Available at: https://www.e-genius.at/en/.

Díaz, J. J. V., Wilby, M. R., González, A. B. R. and Muñoz, J. G. (2013), 'Eeont: An ontological model for a unified representation of energy efficiency in buildings', Energy and Buildings 60, pp. 20–27.

EAE (2011), European application guideline for etics, Technical report, EAE European Association for External Thermal Insulation Composite Systems. Available at: https://www.ea-etics.eu/publications-events/brochures/.

Fernández-López, M., Gómez-Pérez, A. and Juristo, N. (1997), Methontology: From ontological art towards ontological engineering, in 'AAAI 1997'.

Gruber, T. R. (1995), 'Toward principles for the design of ontologies used for knowledge sharing?', International Journal of Human-Computer Studies 43(5), pp. 907–928.

ift (2016), Guideline for the installation of windows and external doors, Technical report, ift - Institut für Fenstertechnik.

Joint Research Centre (2012), Green public procurement windows and external doors technical background report, draft, Technical report, European Commission. Available at: https://susproc.jrc.ec.europa.eu/windoors/docs/Technical%20background.pdf.

Kamsu-Foguem, B., Abanda, F., Doumbouya, M. and Tchouanguem, J. (2019), 'Graph-based ontology reasoning for formal verification of breeam rules', Cognitive Systems Research 55, pp. 14–33.

Lee, S.-K., Kim, K.-R. and Yu, J.-H. (2014), 'Bim and ontology-based approach for building cost estimation', Automation in Construction 41, pp. 96–105.

Lenat, D. B. and Feigenbaum, E. A. (1991), 'On the thresholds of knowledge', Artificial Intelligence 47(1), pp. 185–250.

Niknam, M. and Karshenas, S. (2017), 'A shared ontology approach to semantic representation of bim data', Automation in Construction 80, pp. 22–36.

Noy, N. and Mcguinness, D. (2001), 'Ontologydevelopment101: A guide to creating your first ontology', Knowledge Systems Laboratory 32.

Pauwels, P., Zhang, S. and Lee, Y. C. (2017), 'Semantic web technologies in aec industry: A literature overview', Automation in Construction 73, pp. 145–165.

Saheb, Y. (2016), Energy transition of the eu building stock — unleashing the 4th industrial revolution in europe, Technical report, Build up. Available at: https://www.buildup.eu/en/practices/publications/ energy-transition-eu-building-stock-unleashing-4th-industrial-revolution-0.

Salvalai, G., Sesana, M. M. and Iannaccone, G. (2017), 'Deep renovation of multi-storey multi-owner existing residential buildings: A pilot case study in italy', Energy and Buildings 148, pp. 23–36.

Singh, Y., Abdelhamid, T., Mrozowski, T. and El-Gafy, M. (2014), 'Investigation of contemporary performance measurement systems for production management of renovation projects', Journal of Construction Engineering 2014.

Uschold, M. and Gruninger, M. (1996), 'Ontologies: principles, methods and applications', The Knowledge Engineering Review 11(2), pp. 93–136.

Ward, A. E., Azhar, S. and Khalfan, M. (2017), 'Construction in occupied spaces', Slovak Journal of Civil Engineering 25(2), 15–23.

Zhong, B., Ding, L., Love, P. E. and Luo, H. (2015), 'An ontological approach for technical plan definition and verification in construction', Automation in Construction 55, pp. 47–57.

Zhong, B., Gan, C., Luo, H. and Xing, X. (2018), 'Ontology-based framework for building environmental monitoring and compliance checking under bim environment', Building and Environment 141.

Zhong, B., Wu, H., Li, H., Sepasgozar, S., Luo, H. and He, L. (2019), 'A scientometric analysis and critical review of construction related ontology research', Automation in Construction 101, pp. 17–31.

Applying Deep Incremental Learning-based Posture Recognition Model for Injury Prevention in Construction

Junqi Zhao, Esther Obonyo
Pennsylvania State University, U.S.
eao4@psu.edu

Abstract. This research investigated the feasibility of applying a Deep Incremental Learning model to achieve a high posture recognition performance with Wearable Sensors (WS). The authors use the recognition of Musculoskeletal Disorder (MSDs) related postures among construction workers as the testbed. This research proposed the Convolutional Long Short-Term Memory (CLN) model under Incremental Learning (IL), where a trained model adapts to new subject' postures to maintain high recognition performance. The model was evaluated on datasets from nine construction workers. Results show: i) CLN model with shallow convolutional layers achieved high recognition accuracy (Macro F1 score) under personalized (0.87) and generalized (0.84) modelling; ii) Generalized CLN model under "Many-to-One" IL strategy can adapt to a new subject and balance the forgetting of learnt subjects; iii) incremental CLN model gave close detection of posture proportion and holding time to ground-truth, which facilitates reliable MSDs risk assessment and further prevention through monitoring injury-related postures.

1. Introduction

This research is part of a project directed at developing a Machine Learning (ML)-enabled Decision Support System for mitigating the risk of developing awkward posture-related Musculoskeletal Disorders (MSDs) such as sprains, strains, and other soft tissue injuries. Manually intensive construction trades have been used at the initial use case. Construction-related MSDs account for 30% of all workplace injuries (BLS 2016). These injuries resulted in compensation costs of over $50 billion in the U.S. in 2009 alone (Mutual 2011). Awkward posture detection contributes to both MSDs risk assessment and proactive injury prevention in construction.

In previous efforts, the authors investigated the potential of a Deep Neural Networks (DNN)-based approach in awkward posture recognition from Wearable Sensors (WS) (Zhao and Obonyo 2019). These efforts built on other successful deployments of data-driven ML-based models (Alwasel et al. 2017, Chen et al. 2017, Nath et al. 2018, Ryu et al. 2018, Zhen Yang et al. 2019, Zhao and Obonyo 2018). It has the potential to address limitations of conventional ML-based approaches – reliance on heuristic manual feature engineering, ignoring sequential motion patterns, and fragmented model development processes (Plötz and Guan 2018) through integrating multi-layer Convolutional Long Short-Term Memory (LSTM) DNN architecture. The Convolutional LSTM (CLN) model outperformed the benchmarking ML models when being applied to posture data collected from four construction workers. This suggests that the deployed DNN-based automated feature and sequential pattern learning can enhance conventional ML-based recognition models.

There is a need to enhance and validate the use of CLN models in posture recognition for MSDs assessment. The current recognition models were developed from full motion datasets given prior to model training – this was based on an assumption that the data and underlying structure are static (Gepperth and Hammer 2016, Wang et al. 2012). However, such an assumption may not hold in practice because of the variation of postures among people over time. The motion data from low-cost WS may suffer from noise and drift over time. Highly dynamic WS-based posture recognition warrants an adaptive model to learn new data patterns and classes without naively model re-training from scratch (Wang et al. 2012). An Incremental Learning (IL) approach can yield better outcomes (Fallahzadeh and Ghasemzadeh 2017). Moreover, the influence of posture recognition performance on MSDs risk assessment results should also be evaluated (Nath et al. 2018), particularly when using posture-based rules under recognized postures with errors.

This objective of this study is two-fold: developing an incremental CLN-based recognition model and evaluating the use of recognized posture for MSDs risk assessment. The remainder of the paper is organized as follows. Section 2 reviews the research background. Section 3 describes the development and implementation of proposed incremental CLN model. Section 4 presents the evaluation of developed models. The test result and discussion are reported in Section 5, followed by the conclusion and further work summarized in Section 6.

2. Theoretical Background

2.1 Deep Incremental Neural Networks Model for Posture Recognition

Posture recognition models trained once using short-term datasets may not be reliable for long-term applications under dynamic conditions. Firstly, small-scale motion data are insufficient to cover varying posture characteristics. More training data are usually required to develop models for different people and even the same person in different conditions. The classification models should be updated with the new training dataset to maintain their high-performance. Secondly, the classification model should be capable of freely learning new classes from incoming data. Additionally, low-cost wearable sensors may suffer from noise and drift over time. The classifiers need to adapt to the variation in the sensor output or even sensors. These requirements make the native solution – repetitive model re-training time-consuming and impractical. Therefore, the recognition models are expected to: i) easily learn additional information from incoming training data; ii) add new classes for classification freely; iii) update models without previously used training data (Wang et al. 2012). As a result, the Transfer Learning (TL) approach is warranted (Fallahzadeh and Ghasemzadeh 2017).

TL is the ability to extend what has been learned from one source domain to another non-identical but similar target domain that shares the common features (Pan and Yang 2009). The domain variation in WS-based posture recognition can be attributed to users, sensors (e.g., placement and output quality), and posture classes (Fallahzadeh and Ghasemzadeh 2017). The TL is typically realized through IL, which refers to the situation of continuous model adaptation based on a constantly arriving data stream (Gepperth and Hammer 2016). The incremental adaptation can eliminate the model re-training from scratch and user-interruption (Siirtola et al. 2019).

Conventional ML-based models typically need to be trained from scratch when new training data are available. Using ML-based models under IL needs sophisticated adaptions, such as incremental ensemble training (Polikar et al. 2001) or Prototype-based methods (Gepperth and Hammer 2016). DNN-based models can work in the regime of TL and multi-task settings, where they are generalized to new classes and tasks (Bengio 2012). Training DNN models often include a supervised model fine-tuning stage. The weights in DNN models are typically optimized using the Stochastic Gradient Descent (SDG) algorithm. Such an optimization algorithm estimates the error gradient for the current state of the model using examples from the training dataset. Then it updates the weights using the backpropagation of errors. The amount of weight update is referred to as "Learning Rate (LR)". The DNN models randomly initialize the weights when training from scratch, followed by the weight optimization for learning salient and discriminative features of postures. When applying a pre-trained DNN model with learned weights, the newly collected (labeled) data are used for updating saved weights via backpropagation. The incremental training with new data is a straightforward implementation of the IL approach (Yang Yang et al. 2019). The DNN models trained under IL have the potential to adapt to a new classification task while preserving the ability to undertake the previous tasks.

Incremental training provides an easy-to-use IL approach for DNN models. It is important to note the straightforward backpropagation approach may lead to the "stability-plasticity" dilemma, if incremental DNN models are trained in the same way as models trained from scratch (Yang Yang et al. 2019). The quick model update allows rapid adaptation to new tasks, while the memory of old tasks may be forgotten equality quickly. The memory of old tasks will be preserved longer but model reactivity decreases in the case of slow model adaption. This is a well-known constraint for artificial as well as biological learning systems (Mermillod et al. 2013). The failure to address such a dilemma can result in the "Catastrophic Forgetting" behavior of the learning model (McCloskey and Cohen 1989). The pre-trained DNN models can forget to perform previous tasks after adapting to new tasks, given the DNN models' high adaptability (Goodfellow et al. 2013).

The forgetting effect in this research reveals as the pre-trained DNN models forget the learned subjects' postures after learning a new subject's posture. Both model complexity and LR can affect the adaptability of DNN-based models. The model performance converges slowly under an overly complex model (deep model), while the learning capacity can be restricted if the model is simple (Yang Yang et al. 2019). LR may be the most important hyperparameter for fine-tuning the DNN models (Goodfellow et al. 2016). Choosing the LR is challenging as a value too small may result in a long training process that could get stuck; whereas a value too large may result in learning a sub-optimal set of weights too fast or an unstable training process. It is, therefore, necessary to evaluate the feasibility of implementing the developed CLN model under IL. It also warrants the investigation on how the model architecture and training strategy can influence the recognition performance under IL. These can help with model performance optimization under different objectives, such as improving the model adaptability for new tasks, controlling catastrophic forgetting of old tasks, or balancing the contradicting goals of IL.

2.2 Posture-based Ergonomics Assessment for Proactive MSDs Prevention

Human posture recognition is often the initial step in real-world applications (Wang et al. 2019). Awkward working postures pose high risks for MSDs (Nunes and Bush 2012). These posture-based ergonomics rules can serve as the criteria for evaluating the workers' injury risk levels based on the captured awkward postures. The assessment results can provide preventive feedback to workers. In particular, the Ovako Working Posture Analyzing System (OWAS) (Karhu et al. 1977) has provided actionable recommendations for correcting awkward postures at varying levels of urgency regarding the posture usage proportion in unit working time. The Maximum Holding Time (MHT) (Miedema et al. 1997) thresholds are provided for different awkward postures, which allows identifying postures held for too long, thus triggering alarms in real-time (Yan et al. 2017). Moreover, both OWAS and MHT provide guidance for defining human postures in a rough manner. These have enabled using recognized postures with OWAS and MHT rules. The posture recognition result is not perfect. The posture misclassification may result in false alarm or misdetection of MSDs risks when using the posture-based rules. It is, therefore, important to evaluate the validity of using recognized postures for MSDs risk assessment. This helps with understanding how the recognition errors can influence the risk assessment results.

3. Development and Implementation of Incremental Convolutional LSTM Model

3.1 Convolutional LSTM Model Architecture

A CLN model example using one-layer CNN and one-layer LSTM is shown in Figure 1.

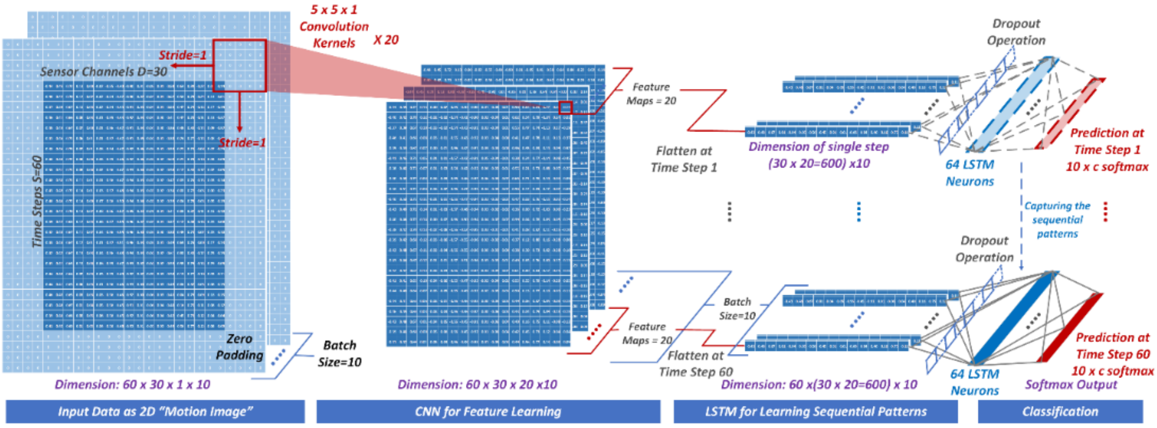

Figure 1: Simple CLN Model Example CLN Conceptual Architecture integrating one-layer CNN and one-layer LSTM. The numbers used are exemplary model setup for illustration.

The CLN model architecture developed in our initial study (Zhao and Obonyo 2019) was applied in this paper. The convolutional layer depth is reported as a key hyperparameter influencing DNN-based model recognition performance (Ordóñez and Roggen 2016, Zhao and Obonyo 2019). This research investigated the optimal CLN model architecture by varying convolutional layer depth from one to five as suggested by Ordóñez and Roggen (2016). For each CNN layer, we adopted the parameter set up in the initial study, which has shown promising results (Zhao and Obonyo 2019). Specifically, each CNN layer had 64 kernels with a size of 5 by the number of sensor channels, 1×1 stride, and zero-padding. The recommend 2-layer architecture with 128 neurons in each LSTM layer (Karpathy et al. 2015, Ordóñez and Roggen 2016) was applied. A dropout operation (50%) was used before fully-connected layers to control model overfitting. Such a model can be expressed as $C(64) \times N \ - RL(128) \times 2 - Sm$, where C, RL, and Sm represent convolutional, LSTM, and softmax classification layers, respectively. The hyperbolic tangent function (tanh) was used as activation function for CNN and LSTM layers. CLN models were trained under Supervised Learning. The model weights were optimized by minimizing the Categorical Cross Entropy as loss function. To implement IL, this research adopted the Adam algorithm (Kingma and Ba 2014) for optimization. Adam is an extension of classical SGD. It leverages i) a per-parameter LR that improves the performance on problems with sparse gradients; ii) an adaptive LR (approximately bounded by the initial LR) based on the average of recent magnitudes of gradients for the weight (e.g. how quickly the rate changes), which empowers the model's capability in IL. Empirical results support the Adam is recommended for models with convolutional layers (Kingma and Ba 2014).

3.2 Incremental Model Development Strategies

One challenge in human posture recognition is balancing the personalized and generalized modeling. The personalized model focuses on learning subject-specific features for high recognition performance, while it requires repetitive model re-training for each subject. The generalized model, learning subject-invariant features, aims at recognizing multiple subjects' postures using one generic model. However, the generalized model may not achieve reliable performance when being used on a new subject. One ideal situation is “adaptive personalization” (Plötz and Guan 2018), which adapts the trained model to a new subject as a personalized model. The adaptive personalization modeling is aligned with the goal for IL. This research evaluated the proposed CLN model’s performance under both personalized and generalized modeling. Then, the CLN model was further evaluated under different IL strategies described below.

Personalized and Generalized Modeling. The personalized modelling was implemented by training and testing a recognition on one subject’s dataset (Figure 2-a). The motion dataset was a combination of multiple subjects under generalized modelling (Figure 2-b).

Incremental Modeling. The major domain variation for modeling workers’ postures was the subject difference in this paper. This brought the variation in posture distribution among subjects. The authors investigated the CLN model’s i) adaptability to a new subject’s postures after being trained for other subjects; ii) forgetting effect on previous recognition tasks after adapting to the new subject. Two IL strategies investigated are described as below.

One-to-One (OtO). The trained personalized model M_c developed from the current subject S_c continuously adapts to an incoming new subject S_N (Figure 2-c). Personalized modelling is used for training S_N’s recognition model M_N. However, the difference is that M_C is re-loaded as a starting point for training M_N, instead of re-training from scratch. After learning S_N’s postures, the updated model M_N is tested on the posture data of $S_C$via the same dataset used for validating M_C. This evaluates the model’s forgetting effect after adaptation to a new subject.

Many-to-One (MtO). MtO investigates the trained generalized model’s adaptability for a new subject. S_C becomes a group of subjects while S_N is still one new subject (see Figure 2-d). The “leave-one-out” is applied to evaluate the MtO-based IL performance on one subject, where the rest multiple subjects are used for developing the generalized model. Similarly, M_C and M_N are tested on the same multi-subject dataset S_C to evaluate the forgetting effect.

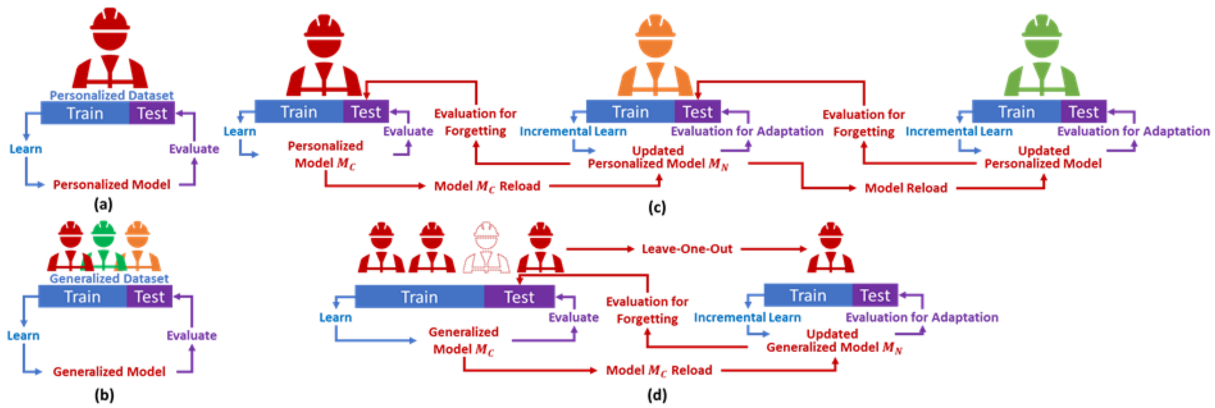

Figure 2: DNN Model Development Strategies. (a) Personalized Modelling; (b) Generalized Modelling; (c) OtO Incremental Learning; (d) MtO Incremental Learning

4. Evaluation of Posture Recognition Models

4.1 Data Collection and Preparation

Nine subjects were recruited from nearby construction projects. Five IMUs sensors (Mbinet Lab Meta Motion C) were deployed at the hardhat, upper arm, chest center, right thigh, and right calf (Appendix 1) by sticking on cloth. Each subject was asked to perform their routine tasks for 20-30 minutes. Their activities were recorded for cross-referencing. A total of nine commonly used postures were identified, including: Bending (BT), Kneeling (KN), Literal Bending (LB), and Climbing Movement (MO), Squatting (SQ), Standing (ST), Walking (WK), Transitional Movement (TR), and Work Overhead (WO). (See Appendix 2). The output was down-sampled to 40 Hz from all the sensors' channels for S2-S9. The data for S1 was collected at 25 Hz and downsampled to 20 Hz. Each record was labelled with video reference. This research used a 1-second window with 50% overlap for segmentation. Windows were labelled using majority label.

4.2 Training and Testing for the CLN Model

Stratified Random Shuffle (SRS) splitting approach used in this study randomly splits the train-test datasets while preserving the percentage of samples for each posture class. The five-round SRS using split ratio in Figure 3 and different random state was applied to minimize the splitting bias and improve the reliability of the model evaluation. The Macro F1 (Eq. 1) evaluation metric was adopted to account for the imbalance of posture dataset, where both majority and minority postures were given equal weights when training the recognition model for all postures. The model training checkpoint was set to save the trained model with improved performance in an "overwritten" way. It saved the CLN model with highest Macro F1 after all model training epochs.

4.3 Posture Recognition Model Implementation

Personalized and Generalized Modeling. Each pre-processed dataset of S1 to S9 was used for personalized modelling. The generalized dataset was constructed by combining the personalized datasets of S3 to S9. Two subjects were excluded due to the low frequency of motion data (S1) and lack of arm sensor output (S2). The TR posture was deleted from S3 when combing the datasets. The recognition performance of the proposed CLN model, baseline DNN models, and benchmark ML-based models were compared under both personalized and generalized modelling. The SRS was used in dataset splitting. The test results are discussed in Section 5.1.

Incremental Modeling. The OtO IL strategy was iteratively conducted from S3 to S9. The "leave-one-out" was repeated for each subject in the generalized dataset (combining S3 to S9) to evaluate the performance of MtO IL strategy. The models MC and MN are tested on the same combined dataset SC to evaluate the forgetting effect. Three levels of LR (LR1-10^{-2}, LR2-10^{-3}, and LR3-10^{-4} in Adam optimizer) for CLN model with varying (convolutional layer depth) were tested under both OtO and MtO strategies. Test results were presented and discussed in Section 5.2.

4.4 Posture-based Ergonomics Risk Assessment

Section 2.2 shows both the posture proportion continuous holding time are key input for MSDs risk assessment. This study compared the detection results of proportion and holding time by using postures from ground-truth, incremental CLN model, and personalized CLN model. Specifically, personalized model was the C2L2[1] developed using a new subject's dataset from scratch, incremental model was the C1L2 under MtO, simulating the situation when one uses the trained generalized CLN model to adept to a new subject. These models were selected given their higher recognition performance achieved in Sections 5.1 and Section 5.2, respectively.

[1] C*N*L*M* denotes a $\mathrm{C}(64) \times \mathrm{N} - \mathrm{RL}(128) \times \mathrm{M} - \mathrm{Sm}$ model, where N and M represents number of layers.

Notably, motion data of every continuous posture was stratified split as two parts (Figure 4). The first 90% was used as train dataset, which was further randomly split into training and validation subsets using ratios of 4:1 as shown in Figure 3. The last 10% was used as a test dataset. Both the train and test datasets have the same postures distribution and sequential pattern as the original dataset. Such splitting imitated an "experiment" where one subject firstly conducts prescribed postures in a longer period for training recognition model. Then the subject conducts the prescribed postures again in a shorter period for testing the trained recognition model. The evaluation was repetitively conducted by using each of S3 to S9 as the new subject, while the motion data of the rest six subjects were used for developing generalized CLN models.

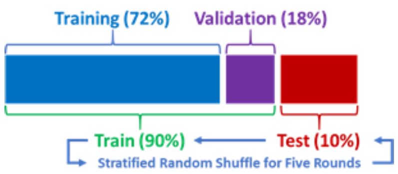

Figure 3: Data Distribution under SRS

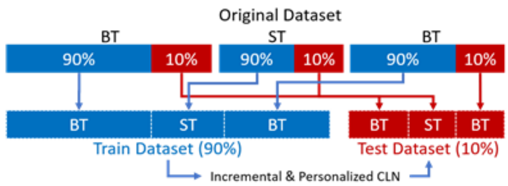

Figure 4: Dataset Splitting for Evaluating Posture-based Ergonomics Assessment Rules

$$\text{Macro F1} = \frac{1}{N}\sum_i 2\,\frac{\text{Precision}_i \times \text{Recall}_i}{\text{Precision}_i + \text{Recall}_i} \qquad \text{Eq. 1}$$

5. Result and Discussion

5.1 Investigation of Optimal CLN Architecture

The CLN models were trained and tested under personalized and generalized modelling. Figure 5 depicts the evaluation results. Increasing the convolutional layer from zero to two tended to improve the personalized CLN model's performance. There was a plateau when convolutional layer depth reaches three to four layers before the model performance started to decrease with five convolutional layers. The generalized CLN model's performance increased significantly when convolutional layer depth increased to one. The model performance fluctuated between two to four convolutional layers until it depredated with five convolutional layers.

These results suggest that a relatively "shallow" CLN architecture (C2L2) can effectively recognize postures under personalized modelling. The optimal CLN architecture under generalized modelling was "shallower" with one-layer CNN (C1L2). The overly deep architecture (C5L2) gave the lowest model performance under both personalized and generalized CLN models. Greater model depth increases the number of parameters significantly. In addition to the greater depth with limited training data being overfitting, the "gradient vanishing" problem can also emerge. The greater convolutional layer depth decreased training time per epoch (Figure 5-b), which, in turn, impedes real-time onboard deployment of recognition models (Nweke et al. 2018). Based on these results, the recommended CLN architectures were identified for personalized ($C(64)\times 2 - RL(128)\times 2 - Sm$) and generalized ($C(64)\times 1 - RL(128)\times 2 - Sm$) models.

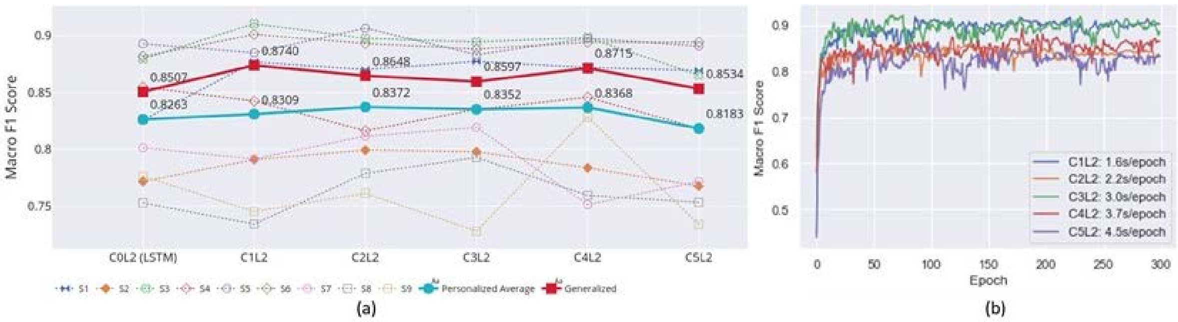

Figure 5: Analysis of Convolutional Layer Depth-Influence on Model Performance. (a) Analysis of CLN model performance. The dots for S1-S9 represent the average performance over five-round SRS. (b) CLN Model Training Process. In the legend, "C*N*L2: Xs/epoch" means one training epoch requires X seconds.

5.2 Evaluation of Incremental CLN Model

Figure 5 shows the C4L2 model can give a close performance to optimal "shallow" CLN architectures under both personalized and generalized modelling. The authors, therefore, evaluated the CLN models' incremental and forget performance with varying LR levels and model depth. The incremental performance represents the CLN model's performance on the current subject after updating from the precedent subject (or subjects). The forget performance denotes the CLN model's performance on the precedent subject (or subjects) after the model adapts to the new subject. Figure 6 and Figure 7 describe test results for each subject. The average IL performance over subjects is described in Table 1..

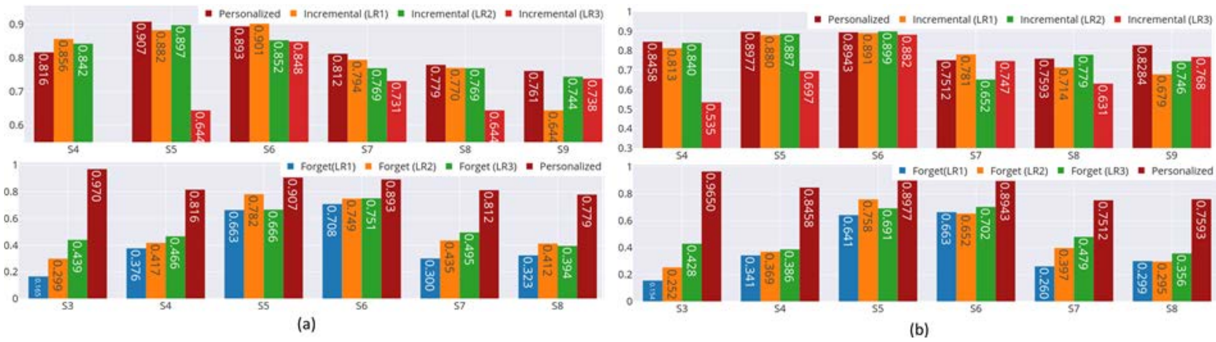

Figure 6: OtO IL Results. (a) C2L2 Model; (b) C4L2 Model

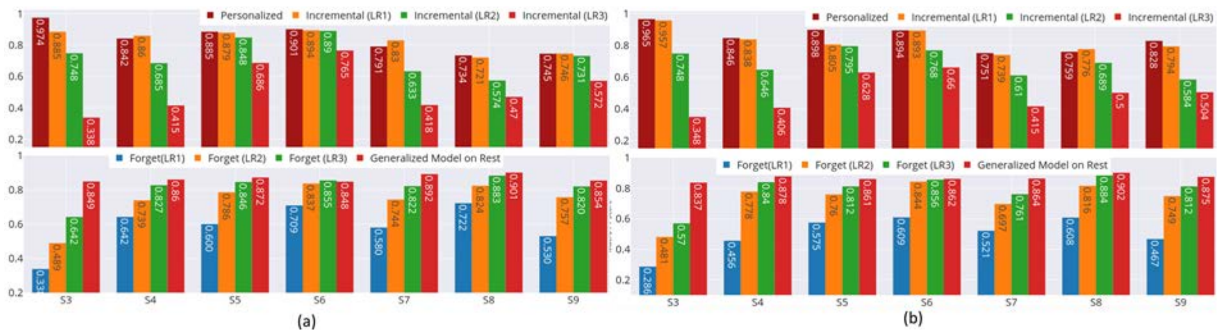

Figure 7: MtO IL Results. (a) C1L2 Model; (b) C4L2 Model

Table 1: Evaluation of Incremental Learning. Average Macro F1 Score across subjects was used as a metric.

Incremental Training Strategies		LR	Incremental Performance		Forget Performance		Personalized on Target Subject	Generalized on Rest Subjects
			F1 Score	Change	F1 Score	Change		
OtO	C2L2	LR1	0.808	-2.4%	0.422	-49.0%	0.828	N/A
		LR2	0.812	-1.9%	0.516	-37.7%		
		LR3	0.682	-17.6%	0.535	-35.4%		
	C4L2	LR1	0.793	-4.5%	0.393	-52.7%	0.830	N/A
		LR2	0.801	-3.6%	0.454	-45.3%		
		LR3	0.710	-14.4%	0.507	-38.9%		
MtO	C1L2	LR1	0.831	-1.0%	0.589	-32.2%	0.839	0.868
		LR2	0.730	-13.0%	0.739	-14.8%		
		LR3	0.523	-37.6%	0.814	-6.3%		
	C4L2	LR1	0.829	-2.4%	0.503	-42.1%	0.849	0.868
		LR2	0.691	-18.5%	0.732	-15.7%		
		LR3	0.494	-41.8%	0.791	-8.9%		

Incremental Performance. Table 1 shows the small LR (LR3) tended to impede effective incremental learning. The MtO strategy requires a larger LR (LR1) to achieve optimal incremental performance than the OtO regardless of model complexity. This can be explained by that the generalized CLN model used in MtO needs a larger extent of model weight updating for adapting to a new subject. The results also show the "shallow" CLN architecture tended to achieve higher incremental performance regardless of training strategies and LR. This might be explained by that the shallow architecture with reduced model complexity can regularize the deep model, which in turn improves the model generality. Additionally, it is important to note the deeper model architecture typically shows a higher learning capacity for processing large-scale image data (Yang Yang et al. 2019). In this paper, one subject's dataset for IL typically contains around 1,000 "Motion Images" with less than six classes of postures to be recognized. The simplicity in a dataset may also eliminate the need for an overly complex model.

The incremental performance under MtO was higher than that achieved under OtO. Table 1 shows, the optimal MtO incremental model (C1LN+LR1) performance was 1.0% lower than the personalized model, outperforming that achieved under the optimal OtO incremental model (C2LN+LR2). The higher incremental performance can be attributed to the generalized model used in MtO IL. Section 5.1 discussed that the generalized CLN architecture can learn subject-invariant features. This allows the generalized CLN model to capture generic features from new subject' motion data and adapt to recognize the targeted subject's postures. The generalized CLN model was trained with more posture datasets than a personalized model. The greater dataset for training helps to reduce both bias and variance for a recognition model, which improves the model's performance. These may explain the observation that the MtO incremental model can even occasionally outperform personalized models (e.g., S4, S7, S9 in Figure 7-a.). The CLN architecture with MtO has the potential for "adaptive personalization" (Plötz and Guan 2018).

Forgetting Performance. Controlling catastrophic forgetting is needed when using the adapted model for previous tasks (Wang et al. 2012).

Table 1 shows LR can effectively control the forgetting effect. IL models showed a lower forget effect with decreasing LR regardless of model complexity and IL strategies. CLN models slowly adapt to the new subject under low LR, thus controlling the forgetting effect on previously learnt subjects. Results also show shallow CLN architectures outperformed the deep models with respect to forgetting, regardless of IL strategies and LR. One possible explanation is that the IL test was conducted on a single new subject with limited data. A deeper architecture tends to overfit the small-size training data from a new subject during adaptation; resulting in a high forgetting effect on learnt subjects. In comparison, the shallow CLN model can regularize the CLN architecture and control the catastrophic forgetting.

Table 1 shows the MtO can have better control of forgetting effect than the OtO approach under different LR and model complexity. It may reduce the extent of posture distribution difference, when the posture dataset is constructed from a larger number of workers. The incremental and forgetting performances show contradiction under the proposed CLN architecture. It might be able to achieve a balanced performance by tuning the LR. Particularly, Table 1 shows C1L2+LR2 under MtO strategy gave relatively high performance for both incremental and forget performances.

5.3 Evaluation of Posture-based MSDs Risk Assessment

Table 2 describes the MSDs risk assessment result based on the use of postures from Ground Truth (G), Incremental (I) model, and Personalized (P) model. Specifically, "I" was the C1L2 under MtO; "P" was the C2L2. These models were applied as they achieved higher recognition performance as discussed in Sections 5.1 and Section 5.2.

Table 2: Comparison of Postures Assessment. All postures from S3-S9 were synthesized.

Posture		Count of MHT Breach			Posture Proportion (Percentage)			Notes
		G	I*	P*	G	I	P	
Awkward Postures	BT	5	5	5	11.1	12.3	12.0	The MHT threshold was set as 30 seconds and scaled-down by 10%, as test dataset was the 10% subsample motion dataset.
	KN	6	5	6	8.8	8.9	8.9	
	SQ	0	0	0	0.4	0.2	0.3	
	WO	18	15	15	33.0	29.4	29.4	

* Model I: Macro F1-0.708, Accuracy-0.812. Model P: Macro F1-0.758, Accuracy-0.812.

The incremental model had misdetections for KN and WO breaching the MHT thresholds. The misdetection was caused by the recognition errors occurred in the middle of the continuous postures. Figure 8 shows there were misclassifications around 78s and 86s when recognizing continuous KN from S3. Multiple misclassifications also occur between 70s and 84s when detecting continuous WO from S7. Additionally, the recognition models were prone to errors when detecting the beginning (24s in Figure 8-a) and ending (2s and 36s in Figure 8-a) of the continuous posture. These errors resulted from misclassification between KN and ST can be explained by the inter-class similarity between transitional postures.

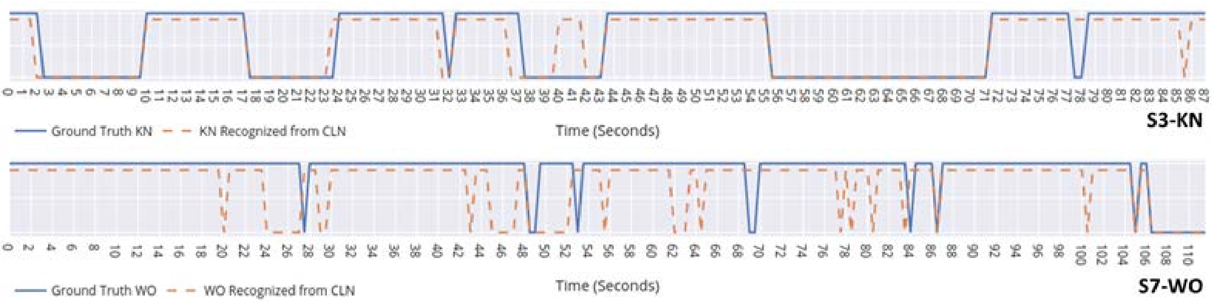

Figure 8: Distribution of Posture Recognition Errors. Using KN from S3 and WO from S7 as examples.

6. Conclusions and Further Work

The authors' previous work observed that the increased convolutional layer depth (over 4) can reduce the recognition performance of baseline CNN model (Zhao and Obonyo 2019). The results in this paper further identified the "shallow" CLN model with one or two convolutional layers as recommended architecture, which can achieve high recognition performance and reduced model complexity. It is feasible to implement the proposed CLN model for IL under direct incremental training. The generalized CLN model ($C(64) \times 1 - RL(128) \times 2 - Sm$) using LR1 under MtO strategy can give high performance when adapting to a new subject, even comparable to personalized models. By tuning down the LR, such IL implementation can balance the performance in adaptation and forgetting. The proposed CLN architecture can be used as a generalized recognition model for "adaptive personalization" among different subjects.

Awkward posture proportion and holding time are key inputs for MSDs assessment rules. The assessment results using recognized and ground truth postures yield comparable results in our test. The findings indicate the recognized postures have a high potential in providing reliable results under the posture-based MSDs risk assessment. The proposed incremental CLN-based recognition model is a promising approach for proactively detecting MSDs risks and thus enabling further interventions for injury prevention among workers.

The learning capacity is limited when the CLN model architecture is fixed, resulting in the difficulty in achieving high performance for old and new tasks simultaneously. Further work will be done to investigate an ensembled CLN architecture to enlarge learning capacity. Additionally, the attention mechanism can be adopted in our further work, which allows the CLN model to focus more on targeted awkward postures during model training. This can potentially reduce the misdetection of awkward postures.

References

Alwasel, A., Sabet, A., Nahangi, M., Haas, C. T. and Abdel-Rahman, E., (2017). Identifying poses of safe and productive masons using machine learning. Automation in Construction, 84, pp.345–355.

Bengio, Y., (2012). Practical recommendations for gradient-based training of deep architectures. in Neural networks: Tricks of the trade: Springer. pp.437–478.

BLS, (2016). Injuries, Illnesses, and Fatalities, Available: https://www.bls.gov/iif/ [Accessed 04/22 2019].

Chen, J., Qiu, J. and Ahn, C., (2017). Construction worker's awkward posture recognition through supervised motion tensor decomposition. Automation in Construction, 77, pp.67–81.

Fallahzadeh, R. and Ghasemzadeh, H., (2017). Personalization without user interruption: Boosting activity recognition in new subjects using unlabeled data. in Proceedings of the 8th International Conference on Cyber-Physical Systems: ACM. pp.293–302.

Gepperth, A. and Hammer, B., (2016). Incremental learning algorithms and applications. in.

Gers, F. A., Schmidhuber, J. and Cummins, F., (1999). Learning to forget: Continual prediction with LSTM.

Goodfellow, I., Bengio, Y. and Courville, A., (2016). Deep learning, MIT press.

Goodfellow, I. J., Mirza, M., Xiao, D., Courville, A. and Bengio, Y., (2013). An empirical investigation of catastrophic forgetting in gradient-based neural networks. arXiv preprint arXiv:1312.6211.

Karhu, O., Kansi, P. and Kuorinka, I., (1977). Correcting working postures in industry: a practical method for analysis. Applied Ergonomics, 8(4), pp.199–201.

Karpathy, A., Johnson, J. and Fei-Fei, L., (2015). Visualizing and understanding recurrent networks. arXiv preprint arXiv:1506.02078.

Kingma, D. P. and Ba, J., (2014). Adam: A method for stochastic optimization. arXiv preprint arXiv:1412.6980.

LeCun, Y., Bengio, Y. and Hinton, G., (2015). Deep learning. Nature, 521(7553), pp. 436.

McCloskey, M. and Cohen, N. J., (1989). Catastrophic interference in connectionist networks: The sequential learning problem. in Psychology of learning and motivation: Elsevier. pp. 109–165.

Mermillod, M., Bugaiska, A. and Bonin, P., (2013). The stability-plasticity dilemma: Investigating the continuum from catastrophic forgetting to age-limited learning effects. Frontiers in psychology, 4, pp. 504.

Miedema, M. C., Douwes, M. and Dul, J., (1997). Recommended maximum holding times for prevention of discomfort of static standing postures. International Journal of Industrial Ergonomics, 19(1), pp. 9–18.

Mutual, L., (2011). Liberty Mutual Workplace Safety Index (pp. 1–2). Hopkinton, MA: Liberty Mutual Research Institute for Safety.

Nath, N. D., Chaspari, T. and Behzadan, A. H., (2018). Automated ergonomic risk monitoring using body-mounted sensors and machine learning. Advanced Engineering Informatics, 38, pp. 514–526.

Nunes, I. L. and Bush, P. M., (2012). Work-related musculoskeletal disorders assessment and prevention. in Ergonomics-A Systems Approach: InTech.

Nweke, H. F., Teh, Y. W., Al-Garadi, M. A. and Alo, U. R., (2018). Deep learning algorithms for human activity recognition using mobile and wearable sensor networks: State of the art and research challenges. Expert Systems with Applications, 105, pp. 233–261.

Ordóñez, F. J. and Roggen, D. (2016) Deep convolutional and lstm recurrent neural networks for multimodal wearable activity recognition. Sensors, 16(1), pp. 115.

Pan, S. J. and Yang, Q., (2009). A survey on transfer learning. IEEE Transactions on knowledge and data engineering, 22(10), pp. 1345–1359.

Plötz, T. and Guan, Y., (2018). Deep Learning for Human Activity Recognition in Mobile Computing. Computer, 51(5), pp. 50–59.

Polikar, R., Upda, L., Upda, S. S. and Honavar, V., (2001). Learn++: An incremental learning algorithm for supervised neural networks. IEEE Transactions on Systems, Man, and Cybernetics, Part C (Applications and Reviews), 31(4), pp. 497–508.

Ryu, J., Seo, J., Jebelli, H. and Lee, S., (2018). Automated Action Recognition Using an Accelerometer-Embedded Wristband-Type Activity Tracker. Journal of construction engineering and management, 145(1), pp. 04018114.

Siirtola, P., Koskimäki, H. and Röning, J., (2019). Personalizing human activity recognition models using incremental learning. arXiv preprint arXiv:1905.12628.

Wang, J., Chen, Y., Hao, S., Peng, X. and Hu, L., (2019). Deep learning for sensor-based activity recognition: A survey. Pattern recognition letters, 119, pp. 3–11.

Wang, Z., Jiang, M., Hu, Y. and Li, H., (2012). An incremental learning method based on probabilistic neural networks and adjustable fuzzy clustering for human activity recognition by using wearable sensors. IEEE Transactions on Information Technology in Biomedicine, 16(4), pp. 691–699.

Yan, X., Li, H., Li, A. R. and Zhang, H., (2017). Wearable IMU-based real-time motion warning system for construction workers' musculoskeletal disorders prevention. Automation in Construction, 74, pp. 2–11.

Yang, Y., Zhou, D.-W., Zhan, D.-C., Xiong, H. and Jiang, Y., (2019). Adaptive Deep Models for Incremental Learning: Considering Capacity Scalability and Sustainability. in Proceedings of the 25th ACM SIGKDD International Conference on Knowledge Discovery & Data Mining: ACM. pp. 74–82.

Yang, Z., Yuan, Y., Zhang, M., Zhao, X. and Tian, B., (2019). Assessment of Construction Workers' Labor Intensity Based on Wearable Smartphone System. Journal of construction engineering and management, 145(7), pp. 04019039.

Zhao, J. and Obonyo, E., (2018). Towards a Data-Driven Approach to Injury Prevention in Construction. in Advanced Computing Strategies for Engineering. EG-ICE 2018,Cham: Springer International Publishing. pp.385–411.

Zhao, J. and Obonyo, E., (2019). Convolutional Long Short-Term Memory Model for Recognizing Postures from Wearable Sensor. in CEUR Workshop Proceedings.

Appendix

Appendix 1: Subjects Working with Sensors (the sensors blocked are not circled)

Appendix 2 Description of Collect Motion Dataset

Subjects (Time-min)	Working Postures (Proportion %)									Posture Label Explanation
	BT	KN	LB	MO	TR	SQ	ST	WK	WO	
S1 Masonry (30.3)	14.7	2.0	12.3	0.0	0.0	0.0	52.4	3.4	7.2	BT-Bending, minor movement with bending, literal bending, and pick up.
S2 Labour (30.3)	72.9	0.0	0.0	0.0	4.3	0.0	12.5	9.1	0.0	KN-Kneel on one leg and both legs. LB-Literal bend
S3 Electrician (18.5)	13.6	46.7	0.0	0.0	15.0	3.0	22.0	0.0	0.0	MO-climbing ladders. SQ- Squatting.
S4 Electrician (18.5)	12.3	0.0	0.0	0.0	0.0	0.0	71.5	12.3	0.0	ST- Standing with minor movement. WK-Walk.
S5 Labour (19.4)	18.7	0.0	0.0	1.8	0.0	0.0	23.6	19.9	32.6	TR-Transition between postures. WO- Overhead work with at least one arm.
S6 Painter (19.6)	10.5	0.0	0.0	0.0	0.0	0.0	17.0	14.1	54.4	
S7 Painter (20.5)	1.7	0.0	0.0	0.0	0.0	0.0	5.9	2.1	83.6	
S8 Carpenter (12.5)	7.1	0.0	0.0	1.8	0.0	0.0	27.3	8.0	23.1	
S9 Labour (18.5)	10.0	0.0	0.0	0.0	0.0	0.0	26.5	56.4	0.5	

Automatic Clustering of Proper Working Posture

JuHyeong Ryu, Tasha McFarland, Carl T. Haas, Eihab Abdel-Rahman
University of Waterloo, Canada
j4ryu@uwaterloo.ca

Abstract. Construction workers regularly perform physically strenuous and demanding tasks involving heavy lifting, awkward postures, and forceful exertion. These activities can diminish productivity and threaten worker safety by increasing the risk of work-related musculoskeletal disorders (WMSDs). With advanced sensing technologies and analytical tools, significant efforts have attempted to address WMSDs by identifying and monitoring risk factors in construction. However, an objective definition of proper work techniques has yet to be determined. Previous studies found that more experienced workers adopt safer and more productive work techniques. This study aims to identify the proper working postures that experienced workers develop to increase their safety as well as productivity. Specifically, this study reports on an automated posture clustering technique based on applying a learning algorithm to whole-body kinematic data.

1. Introduction

Construction workers frequently perform physically demanding tasks which, combined with awkward postures and repetitive motions, can contribute to work-related musculoskeletal disorders (WMSDs) (Wang et al., 2015). WMSDs adversely impacts workers' health and wellbeing as well as their productivity and income. In particular, for over a decade, the back has been the primary body segment affected by WMSDs among construction workers. Between 2003 and 2015, the proportion of WMSDs caused by back injuries (e.g., low back disorders) has consistently accounted for more than 40% of WMSD cases in the United States (CPWR, 2013; 2018). Other body parts (e.g., the upper and lower extremities), however, made up about 10% of WMSD cases (CPWR, 2013; 2018).

Among construction trades, masonry requires repetitive heavy manual lifts and frequently involves awkward postures. According to Hess et al. (2010), block masons manually lift at least 200 concrete blocks per day. Considering that a standard concrete masonry unit (CMU) weighs 16.6 kg (CCMPA, 2013), masons manually lift over 3,300 kg daily. Overexertion while lifting is the most commonly cited cause of construction WMSDs resulting in days away from work (CPWR, 2013; 2018). In the U.S., the masonry sector had the highest rate of overexertion injuries resulting in days away from work at 66.5 per 10,000 full-time equivalent workers, more than double the average overall rate for the construction industry at 28.5 per 10,000 full-time equivalent workers (CPWR, 2013).

To prevent occupational disorders in these industries, various ergonomic practices have been promoted. These practices include regulatory procedures (e.g., the National Institute for Occupational Safety and Health's lifting equation (NIOSH, 2014)), rule-based postural assessments (e.g., Rapid Upper Limb Assessment (McAtamney and Nigel Corlett, 1993), and the Rapid Entire Body Assessment (Hignett and McAtamney, 2000)).

Recent advancements in sensing technologies have enabled the identification and assessment of WMSD risk factors from automatically collected data. Analyzing various data sources including heart rate (Gatti et al., 2010, Lee et al., 2017), muscle engagement (Trask et al., 2010), and body kinematics (i.e., postures and motions), researchers have investigated the physical demands of construction activities. Among these data types, body kinematics have been most commonly used to evaluate ergonomic risk due to their association with joint loads (joint force and moment), which are directly related to vulnerability to WMSDs (NIOSH, 2014). Wearable inertial measurement units (IMUs) have been widely utilized to acquire a broad range of accurate body kinematic data, thereby allowing researchers to analyze workers' ergonomic risks (Ryu et al., 2018; 2019b, Valero et al., 2017, Zhang et al., 2018; 2019) and monitor their activities (Joshua and Varghese, 2014, Ryu et al., 2016; 2019a) in construction context. These studies have successfully identified and monitored risk factors of WMSDs within a job. However, insufficient research has objectively described or suggested proper work techniques or motion patterns.

When workers execute manual tasks (e.g., lift materials), they exhibit qualitatively different movement techniques (e.g., stoop vs. squat lift) (Park et al., 2005, Zhang et al., 2000). Previous studies revealed that expert journey-level masons, those with more than 20 years of work experience, adopt ergonomically safer and more productive work methods than novice masons (Alwasel et al., 2017a, Ryu et al., In press). They specifically compared CMU lifting motions and found that journey-level masons adopt lifting techniques that lower biomechanical loads (joint forces and moments). Later studies revealed the existence of differences between the working postures (i.e., represented as body joint locations) of expert masons (journeymen) and those of non-expert masons (novices with no experience, 1-year and 3-year apprentices) that enabled their automatic classification using a Support Vector Machine algorithm (Alwasel et al., 2017b).

These findings indicate that distinctive working postures and motion patterns identified from expert's work techniques can be deployed proactively to improve the ergonomics and productivity of workers. Furthermore, it is essential that construction workers learn proper working postures and techniques during safety training in their apprenticeship programs. Adequate instruction will prevent potential health and safety hazards. Therefore, this study aims to identify proper working postures that experienced workers develop to increase their safety and productivity. We report on automated posture clustering by applying a learning algorithm, k-means clustering, to whole-body motion data. The dataset in this study is expanded from a previous study (Alwasel et al., 2017b), by increasing the number of participants from twenty-one to forty-five masons.

2. Research Methods

Figure 1 shows the overall analytical frame which consists of (1) data collection and processing; (2) *k*-means clustering; (3) posture comparison; and (4) recommendation. In this study, wearable IMU-based motion capture systems were used to collect whole-body motion data. The systems do not interfere with the subject's natural movements, thus enabling automated information-rich motion data collection. They were used to collect motion data from masonry workers with different levels of working experience. To achieve automated posture clustering, we applied a *k*-means clustering algorithm to the whole-body motion data. The clustered postures were then grouped into expert and apprentice postures. Finally, preliminary training material was created to illustrate safe and efficient postures frequently adopted by experts and not by apprentices.

2.1 Data collection and processing

Forty-five masons with varying levels of work experience were recruited at two Ontario Masonry Training Centres: Conestoga College (Waterloo, Ontario) and Canada Masonry Design Centre (Mississauga, Ontario). The cohort was divided into two groups, expert (journeymen with more than 20 years of experience) and apprentice (novices with no experience, 1-year and 3-year apprentices). Their mean height and weight were 181.1 (SD 6.57) cm and 87.88 (SD 15.38) kg, respectively. Data collection received ethics approval from the Office of Research Ethics at the University of Waterloo and the Research Ethics Board at Conestoga College, Ontario, Canada.

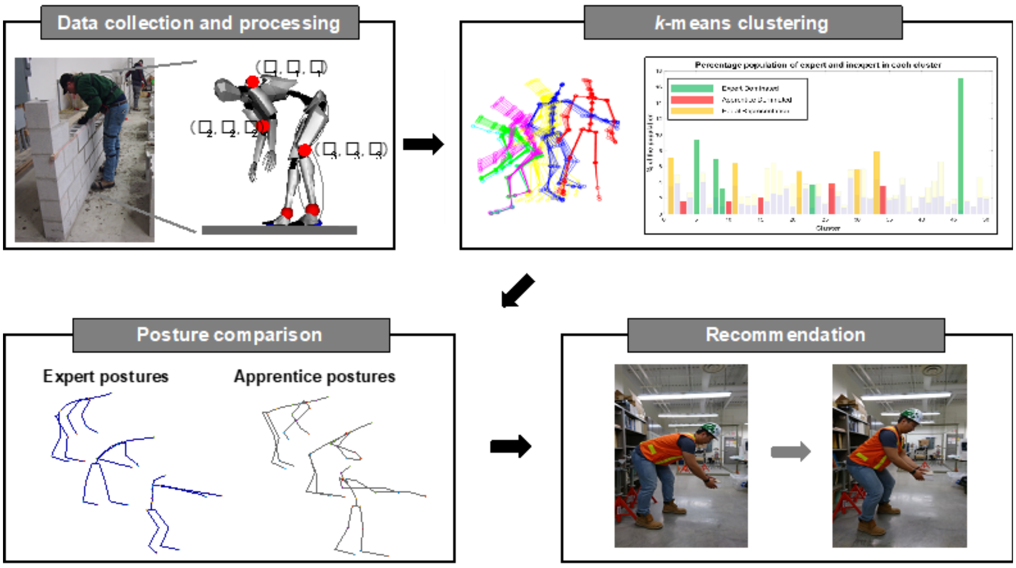

Figure 1: Analytical Framework

Each participant completed a pre-built standard wall, Figure 2, using 45 concrete masonry units (CMUs), CSA – Type “A” unit weighing 16.6 kg with dimensions of 0.19 × 0.19 × 0.38 m (W × H × L) (CCMPA, 2013). Two sets of commercial wearable IMU-based motion capture systems (Xsens MVN (Xsens, 2016) and Noitm Perception Neuron (Noitom Ltd, 2017)) were employed to collect whole-body motion data. Both motion capture systems accurately estimate joint kinematics when compared to the gold standard (optical motion capture), with root mean square errors under 5° (Robert-Lachaine et al., 2017, Robert-Lachaine et al., 2020). The systems have also been applied to fields including sports, ergonomics, and gaming (Xsens, 2016, Noitom Ltd, 2017). The motion capture system consists of 17 IMUs, each composed of a three-axis accelerometer, a three-axis gyroscope, and a magnetometer. Using elastic straps, the IMUs were attached to the head, back, shoulders, upper and lower arms, hands, upper and lower legs, and feet.

Figure 2: Experimental Setup

Each system pairs and communicates with its in-house software, MVN studio (Xsens, 2016) and Axis Neuron (Noitom Ltd, 2017), which manages and calibrates the data obtained from the suits. At the beginning of each experiment, a calibration session (T-pose, A-pose, and S-pose) was conducted following the software prompts to determine the sensor-to-body alignment and body dimensions. Then, the motion data was sampled at a frequency of 125Hz and reconstructed as the 3D human skeleton model. The systems implement Kalman filters within proprietary algorithms to counteract sensor drift.

The collected motion data was extracted as a Biovision Hierarchy (BVH) file that defines hierarchical body segment locations and orientations as local rotations and translations with respect to a root coordinate system between the hip joints (Meredith et al., 2001). Using a "BVHViewer" software, we exported the 3D joint center coordinates for 26 body joints in an inertial frame as a .txt file, as shown in Figure 3.

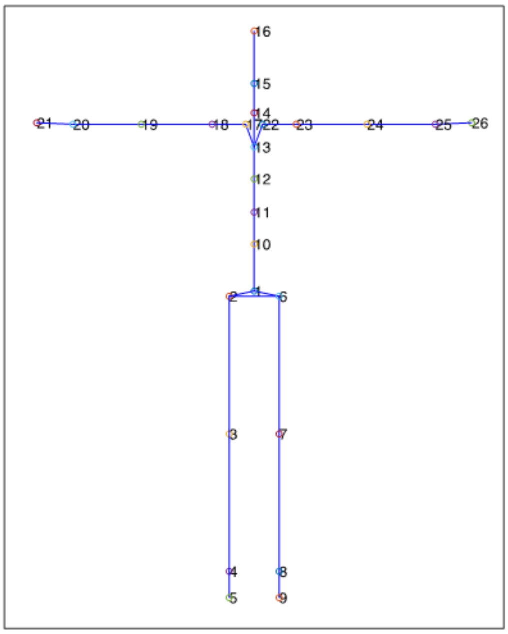

Joint No.	Joint Name
1	Hip
2	Right Hip
3	Right Knee
4	Right Ankle
5	Right Ball of Foot
6	Left Hip
7	Left Knee
8	Left Ankle
9	Left Ball of Foot
10	Spine
11	Spine
12	Spine
13	Sternoclavicular Joint
14	C7/T1
15	Head Origin
16	Head End
17	Right Pre-shoulder
18	Right Shoulder
19	Right Elbow
20	Right Wrist
21	Right Grip Center
22	Left Pre-shoulder
23	Left Shoulder
24	Left Elbow
25	Left Wrist
26	Left Grip Center

Figure 3: The Joint Locations for a T-Pose

Manual block lifting is an integral part of masonry, frequently requiring back-bending postures to lift heavy blocks. As a result, masons are exposed to a greater risk of WMSDs (Alwasel et al., 2017a). This study investigated various lifting postures adopted by apprentices and experts. Therefore, the processed joint-location data was segmented into 45 individual CMU lift motion files for each participant. A CMU "lift" was comprised of a sequence of three motions: picking up the CMU from a pallet, moving the CMU to the wall and laying the CMU within the wall. Other masonry activities, such as spreading mortar on the CMU, were not included in this analysis. Data segmentation was done manually with reference to simultaneously recorded videos of the experiments.

2.2 k-means clustering

The *k*-means clustering algorithm was introduced by MacQueen (MacQueen, 1967). It is one of the most commonly used clustering algorithms for many practical applications (Aggarwal and Aggarwal, 2012, Jain et al., 1999, Johnson and Wichern, 2002). The algorithm partitions a given set of data into *k* disjointed clusters around the nearest *k* means, where the value of *k* is fixed in advance (MacQueen, 1967).

In this study, each CMU lift motion was composed of a sequence of postures. As the sampling rate was held constant, the number of postures was only dependent on the duration of the motion. For example, a CMU lift of 4 seconds consists of a sequence of 500 postures or frames. Each posture was then represented by a 78-component vector consisting of the coordinates of 26 body joints. The processed posture dataset was categorized into *k* clusters by minimizing the sum of the squared Euclidian distance between the individual postures. Each cluster has one centroid posture (i.e., vector) and contains the postures most similar to it. Initial center points were defined for the clusters and iteratively updated to obtain the final cluster locations (Singh et al., 2013).

The previous study by Alwasel et al. (2017b) used *k*-means clustering to identify a set of dominant poses based on a simplified feature set (posture representation) made of six key-joint locations, namely C7/T1 disc, hip center, right and left wrists, and right and left knees. Different *k* values, the number of clusters (i.e., bins), were tested to investigate classification accuracy. They achieved a 92.04% accuracy in classifying expert and novice poses using 50 clusters (i.e., $k = 50$). Expanding the data set from the twenty-one participants in the study by Alwasel et al. (2017) to forty-five participants, and considering the previously identified optimal classification result, we adopt 50 clusters.

Furthermore, the main goal of this study is to determine the objective differences between postures of experts and apprentices rather to classify them. One limitation of the current approach is that a cluster may include postures adopted by both expert and apprentice masons. Concurrent adoption by these two population types indicate postures common to human locomotion and trade, rather than those related to experience. Therefore, we identified postures distinctive to each group by assessing the frequency expert and apprentice populations in each bin. This study annotates bins more than 65% populated by journey-level masons as 'Expert-dominated' and bins more than 65% populated by apprentice masons as 'Apprentice-dominated'. In the case of other proportions, the bins were annotated as 'Equally represented'.

3. Results

We used the *k*-means clustering algorithm to identify proper working postures frequently adopted by experienced workers during CMU lifts. Figure 4 shows the resulting clusters ($k = 50$). The proportion of the two experience groups in each cluster are marked in blue and yellow.

One interesting finding is that few clusters out of the overall 50 were dominated by experts. In contrast, the apprentices participated in most posture bins. This finding indicates that expert masons adopt a limited set of motions when performing a repetitive lift task while apprentices may utilize more varied lift techniques.

Furthermore, certain clusters were mainly populated by experts but rarely seen in apprentices. For example, experts primarily adopted the postures in clusters #5 and #46, but rarely took the postures in clusters #3, #39, and #48. This result is in accord with the previous study indicating that expert masons adopt distinctive work postures and motion patterns different from that of apprentice masons (Alwasel et al., 2017b; Ryu et al., 2019). Specifically, Alwasel et al. (2017a) and Ryu et al., (In press) found that the expert masons adopt safer (i.e., lower joint loads) and more efficient (i.e., higher production rate) working methods that are distinct from those of less experienced masons.

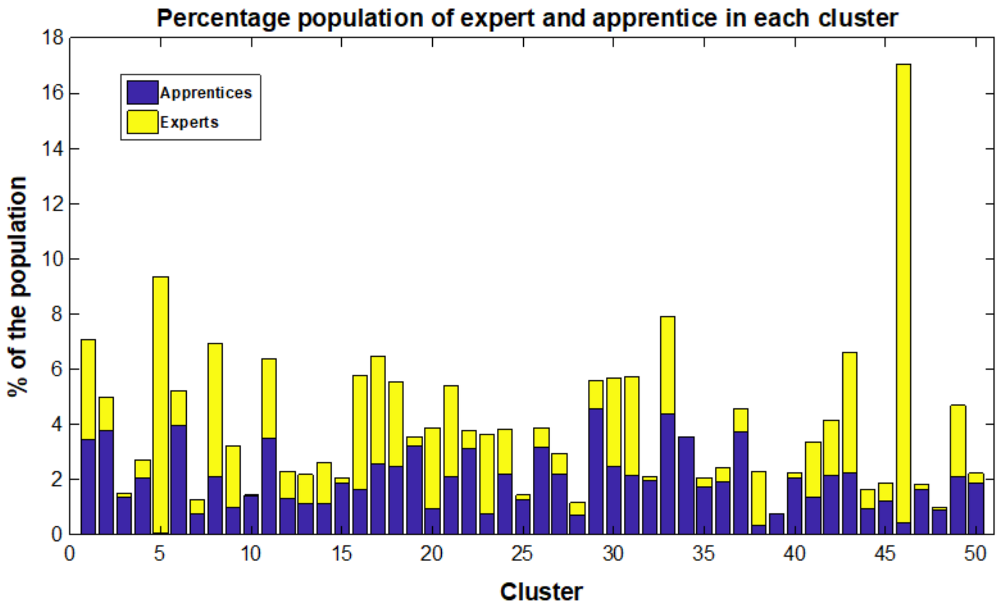

Figure 4: Posture Clusters Obtained from *k*-means Clustering

As noted in the Research Methods section, some of the cluster histograms were ambiguously populated with similar proportions of experts and apprentices, such as cluster #11 (48% experts and 52% of apprentices). Accordingly, the 50 clusters were categorized into one of three annotations: expert-dominated (10 clusters), apprentice-dominated (24 clusters), and equal representation (16 clusters). Representative postures of each annotation are shown in Figure 5.

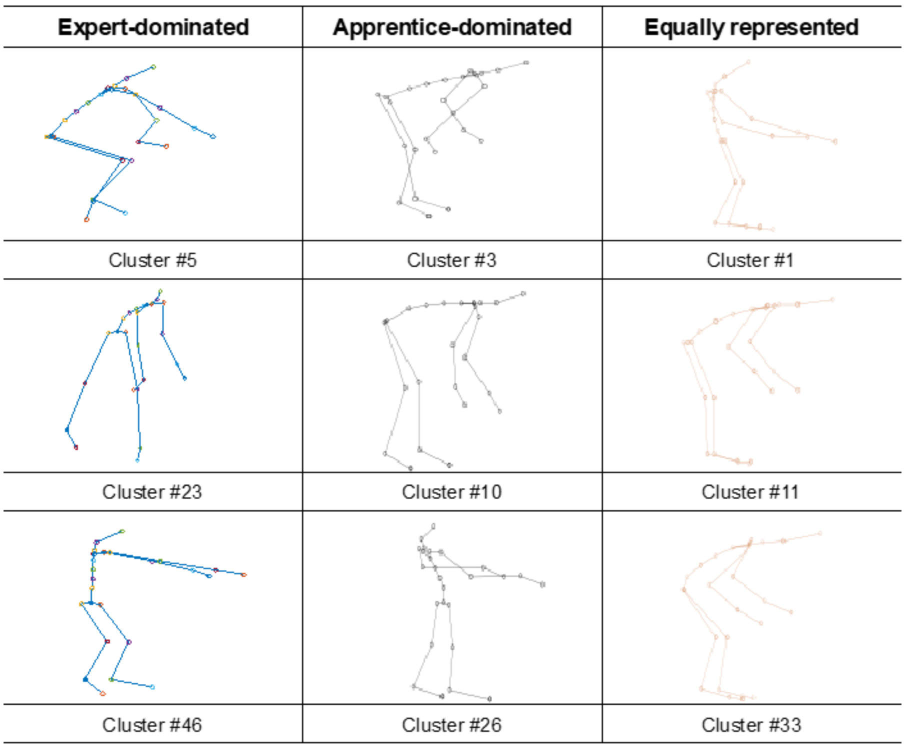

Figure 5: Examples of Postures for Each of the Three Annotations

For objective comparison between expert- and apprentice-dominated postures, each posture was assigned to one of the three CMU lift phases (i.e., picking up, moving, and laying down).

These demarcations were then used to identify and compare how different masons perform similar functions. Considering most lifts were completed within 3 to 5 seconds, equivalent to 360 to 600 frames, the first and last 150 frames were defined as CMU pick up and lay down phases, and the frames in between were defined as CMU moving phase. Figure 6 shows a comparison between an expert-dominated posture and a corresponding apprentice-dominated posture during the CMU moving phase. The figure shows two projections of each posture in the sagittal and frontal planes. Comparing the two postures in the sagittal plane, the expert positioned the CMU closer to the center of body mass and had significantly lower back and knees flexion angles. In the frontal plane, the expert posture maintains better body symmetry than the apprentice.

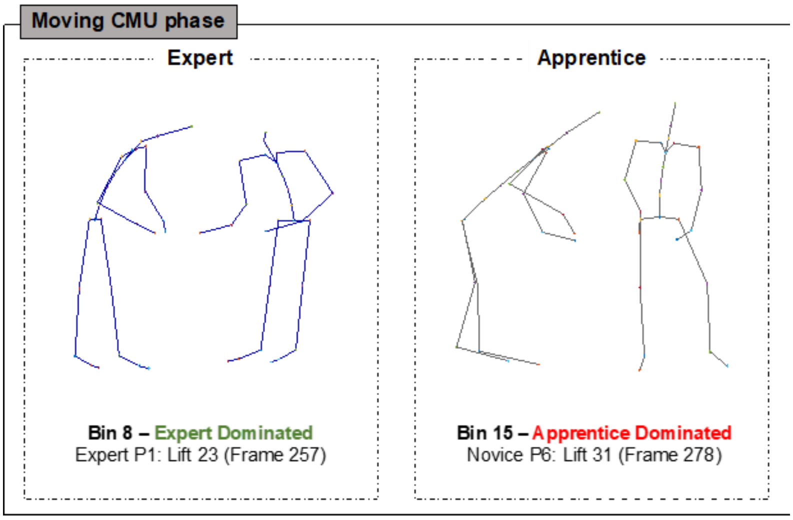

Figure 6: Comparison of Expert-dominated and Apprentice-dominated Postures During the CMU Moving Phase

4. Conclusion

In the current study, an automated posture clustering method was proposed to identify proper working postures developed as workers gain experience. It utilizes whole-body motion data and the *k*-means clustering algorithm. The motion data was collected from forty-five masons with varied work experience while they carried out an indoor masonry task, namely completing a lead wall using standard CMUs.

The results indicate that the proposed method can automatically cluster the most frequent working postures among two experience groups: expert and apprentice. Furthermore, by analyzing the proportion of each group's participation in each cluster, expert-dominated and apprentice-dominated postures were determined. Finally, frame-based annotated postures enabled objective (quantitative) comparison of the different postures adopted by experts versus apprentices in each of the three CMU lift phases. This is a significant finding when compared to manual observation-based work assessment, commonly used in worksites, where it is almost impossible to accurately obtain and compare target postures that occur during continuous body motion. Furthermore, the visualized clustered postures allow an intuitive understanding of differences between ‘good’ and ‘bad’ postures.

The scope of the present study is to identify proper working postures by investigating the expert postures which are distinguishable from those of less experienced masons. Previous studies using a partial (Alwasel et al., 2017a) or an extended (Ryu et al., in press) dataset compared to the current study have reported that working methods adopted by expert masons can help reduce occupational injuries and improve productivity. Therefore, our approaches and findings may play important roles in 1) providing insights for an objective comparison of working postures of experts and apprentices; and 2) conveying these experts' work methods to apprentices and trainers with highly detailed visual information that can be used as training material.

Future work will attempt to cluster expert and apprentice motion patterns based on kinematic features (e.g., joint angles, acceleration, and velocity) and biomechanical loads. The quantitative comparison will be used to determine the degree of postural differences between the two groups.

Acknowledgement

We acknowledge the excellent support from the Ontario Masonry Training Centre (OMTC) at Conestoga College in Waterloo, Ontario, Canada and the Canada Masonry Design Centre (CMDC) in Mississauga, Ontario, Canada for their considerable help in collecting data. The work presented in this paper was supported financially by the Canadian Concrete Masonry Producers Association (CCMPA), CMDC, and the Natural Sciences and Engineering Research Council of Canada (NSERC) (CRDPJ 494786-16).

References

Aggarwal, N. & Aggarwal, K., (2012). A mid-point based k-mean clustering algorithm for data mining. *International Journal on Computer Science and Engineering,* 4**,** pp.1174–1180.

Alwasel, A., Abdel-Rahman, E. M., Haas, C. T. & Lee, S., (2017a). Experience, Productivity, and Musculoskeletal Injury among Masonry Workers. *Journal of Construction Engineering and Management,* 143**,** 05017003.

Alwasel, A., Sabet, A., Nahangi, M., Haas, C. T. & Abdel-Rahman, E., (2017b). Identifying poses of safe and productive masons using machine learning. *Automation in Construction,* 84**,** pp.345–355.

CCMPA, (2013). *Metric Technical Manual (Section 4. Physical Properties)* [Online]. Available: http://ccmpa.ca/wp-content/uploads/2012/02/Final2013Sec4.pdf [Accessed Dec. 14, 2019].

CPWR, (2013). *The Construction Chart Book: The U.S. Construction Industry and Its Workers.* [Online]. Available: https://www.cpwr.com/sites/default/files/publications/5th-Edition-Chart-Book-Final.pdf [Accessed Nov. 13, 2019].

CPWR, (2018). *The Construction Chart Book: The U.S. Construction Industry and Its Workers.*

Gatti, U. C., Migliaccio, G. C., Schneider, S. & Fierro, R., (2010). Assessing physical strain in construction workforce: A first step for improving safety and productivity management. Proceedings, 27th international symposium on automation and robotics in construction (ISARC), international association for automation and robotics in construction (IAARC), 2010. pp.255–264.

Hess, J., Weinstein, M. & Welch, L., (2010). Ergonomic best practices in masonry: regional differences, benefits, barriers, and recommendations for dissemination. *J Occup Environ Hyg,* 7**,** pp.446–55.

Hignett, S. & McAtamney, L., (2000). Rapid entire body assessment (REBA). *Appl Ergon,* 31**,** 201-5.

Jain, A. K., Murty, M. N. & Flynn, P. J., (1999). Data clustering: A review. *Acm Computing Surveys,* 31**,** pp.264–323.

Johnson, R. A. & Wichern, D. W., (2002). *Applied multivariate statistical analysis*, Prentice hall Upper Saddle River, NJ.

Joshua, L. & Varghese, K., (2014). Automated recognition of construction labour activity using accelerometers in field situations. *International Journal of Productivity and Performance Management,* 63**,** pp.841–862.

Lee, W., Lin, K.-Y., Seto, E. & Migliaccio, G. C., (2017). Wearable sensors for monitoring on-duty and off-duty worker physiological status and activities in construction. *Automation in Construction,* 83**,** pp.341–353.

MacQueen, J., (1967). Some methods for classification and analysis of multivariate observations. Proceedings of the fifth Berkeley symposium on mathematical statistics and probability. Oakland, CA, USA, pp.281–297.

McAtamney, L. & Nigel Corlett, E., (1993). RULA: a survey method for the investigation of work-related upper limb disorders. *Appl Ergon,* 24**,** pp.91–9.

Meredith, M., Maddock, S. & Road, P., (2001). Motion Capture File Formats Explained. *Motion Capture Stuff***,** pp.1–36.

NIOSH, (2014). Observation-based posture assessment: review of current practice and recommendations for improvement. Cin-cinnati, OH: U.S. Department of Health and Human Services, Centers for Disease Control and Prevention, National Institute for Occupational Safety and Health, DHHS (NIOSH): By Lowe BD, Weir PL, Andrews DM.

Noitom Ltd., (2017). *"Perception Neuron"* [Online]. Available: https://neuronmocap.com/ [Accessed Dec. 12, 2019].

Park, W., Martin, B. J., Choe, S., Chaffin, D. B. & Reed, M. P., (2005). Representing and identifying alternative movement techniques for goal-directed manual tasks. *J Biomech,* 38**,** pp.519–527.

Robert-Lachaine, X., Mecheri, H., Larue, C. & Plamondon, A., (2017). Validation of inertial measurement units with an optoelectronic system for whole-body motion analysis. *Med Biol Eng Comput,* 55**,** pp.609–619.

Robert-Lachaine, X., Mecheri, H., Muller, A., Larue, C. & Plamondon, A., (2020). Validation of a low-cost inertial motion capture system for whole-body motion analysis. *J Biomech,* 99**,** 109520.

Ryu, J., Alwasel, A., Haas, C. T. & Abdel-Rahman, E. In press. Analysis of Relationships Between Body Load and Training, Work Methods, and Work Rate: Overcoming the Novice Mason's Risk Hump. *Journal of Construction Engineering and Management (ASCE)*.

Ryu, J., Seo, J., Jebelli, H. & Lee, S., (2019a). Automated Action Recognition Using an Accelerometer-Embedded Wristband-Type Activity Tracker. *Journal of Construction Engineering and Management,* 145.

Ryu, J., Seo, J., Liu, M. Y., Lee, S. & Haas, C. T., (2016). Action Recognition Using a Wristband-Type Activity Tracker: Case Study of Masonry Work. *Construction Research Congress 2016: Old and New Construction Technologies Converge in Historic San Juan***,** pp.790–799.

Ryu, J., Zhang, L., Diraneyya, M., Haas, C. T., Abdel-Rahman, E. & Banting, B., (2019b). Ergonomic Assessment of Standard vs. Heavy-Weight CMU Lifts. *13th North American Masonry Conference (NAMC).* Salt Lake City, UT, USA: The Masonry Society (TMS).

Ryu, J., Zhang, L., Haas, C. T. & Abdel-Rahman, E., (2018). Motion Data Based Construction Worker Training Support Tool: Case Study of Masonry Work. ISARC. Proceedings of the International Symposium on Automation and Robotics in Construction, 2018. IAARC Publications, pp.1–6.

Singh, A., Yadav, A. & Rana, A., (2013). K-means with Three different Distance Metrics. *International Journal of Computer Applications,* 67.

Trask, C., Teschke, K., Morrison, J., Johnson, P., Village, J. & Koehoorn, M., (2010). EMG estimated mean, peak, and cumulative spinal compression of workers in five heavy industries. *International Journal of Industrial Ergonomics,* 40**,** pp.448–454.

Valero, E., Sivanathan, A., Bosche, F. & Abdel-Wahab, M., (2017). Analysis of construction trade worker body motions using a wearable and wireless motion sensor network. *Automation in Construction,* 83**,** pp.48–55.

Xsens 2016. *"Xsens"*.

Zhang, L., Diraneyya, M. M., Ryu, J., Haas, C. T. & Abdel-Rahman, E., (2018). Assessment of Jerk As a Method of Physical Fatigue Detection. ASME 2018 International Design Engineering Technical Conferences and Computers and Information in Engineering Conference, 2018. American Society of Mechanical Engineers, V01BT02A010-V01BT02A010.

Zhang, L. C., Diraneyya, M. M., Ryu, J., Haas, C. T. & Abdel-Rahman, E. M., (2019). Jerk as an indicator of physical exertion and fatigue. *Automation in Construction,* 104**,** pp.120–128.

Zhang, X., Nussbaum, M. A. & Chaffin, D. B., (2000). Back lift versus leg lift: an index and visualization of dynamic lifting strategies. *J Biomech,* 33**,** pp.777–782.

Augmented Virtuality in Construction Safety Education and Training

Samed Bükrü[1], Mario Wolf[1], Bianca Böhm[1], Markus König[1], Jochen Teizer[2]
[1] Ruhr-University Bochum, Germany
[2] Aarhus University, Denmark
teizer@eng.au.dk

Abstract. Accidents resulting from poorly planned or set up work environments are a major concern within the construction industry. While traditional education and training of personnel offer well known approaches for establishing safe work practices, Serious Games in Virtual Reality (VR) are increasingly being used as a complementary approach for learning experiences. Their designs yet have to take full advantage of how players can manipulate and interact with virtual imagery generated by the computer. In addition, little of construction safety research has focused on generating and analyzing the inherent data that can be collected about the players. This research presents a novel framework for the generation and assessment of the player's data in Augmented Virtuality (AV). The proposed approach is tested in a virtual work environment consisting of, next to a player carrying out a realistic work task, multiple hazards that are consistent within today's construction sites. Sensors on construction tools augment the immersion of the player in the virtual scene in real-time and analysis of the collected data allow for rapid personalized feedback. Results on the experience of players are presented and discussed. An outlook presents future avenues towards enhancing existing education and learning methods and automating the proposed assessment method.

1. Introduction

Several safety best practices exist today to mitigate dangerous work environments in construction projects early, starting with a good organizational safety culture and tight safety processes (Rajendran and Gambatese 2009). Multiple means have been used for safety education training in construction. These include standard approaches like verbal explanation and paper-based documentation and testing. Such practices can also range from autodidactic learning to more advanced techniques like microlearning offers (Emerson 2018). While each of these approaches have their place in education and training, they do lack in regards of the user's actual actions to facilitate in-situ, active learning. In addition, modern learning styles using serious games tend to prefer instant personalized feedback (Bükrü et al. 2020, Teizer et al. 2020). The layers in the hierarchy of controls, therefore still have to take full advantage of a human's emotional states in risk assessment and decision making (Bhandari et al. 2019) and of data that can be provided by technology during education and training sessions (Albert et al. 2014, Teizer 2016, Hassan et al. 2019), such as in serious games in virtual reality (VR).

Safety training often correlates with hazard detection. Standard techniques are lacking in terms of training risk identification. This is important, because in industries like construction where potentially dangerous tools or materials are used, it is crucial for workers to have experience in their safe operation. According to the Occupational Safety and Health Administration (OSHA 2019) 20.7% of all fatalities in 2017 were in construction, totaling 971 fatalities. Up to 50% of construction hazards remain unrecognized despite training and certification (Sacks et al. 2013, Carter et al. 2006). Like these statistics on construction accidents show, their probability caused by incorrect handling of tools through insufficient training rise. These numbers also show that safety training is still needed and might be enhanced by the help of new approaches.

2. Background

For years VR has been used for training purposes. A high number of VR applications exist in the fields of military, aviation, and medicine. For example, a serious game (defined 'serious' because of a primary purpose other than pure entertainment) helped to increase the awareness of airplane passengers in case of an emergency situation (Chittaro and Buttussi 2015). Like many studies, it evaluated two user groups (one group using the standard approach with safety cards, the other using a serious game) based on questionnaires and pre- and exit-interviews. Studies related to construction (Sacks et al. 2013, Hilfert et al. 2016, Kassem et al. 2017, Wang et al. 2018, Li et al. 2018, Zaker and Coloma 2018, Burke et al. 2011, Hassan et al. 2019) concluded that VR-based safety awareness training offers more engaging learning environments. Study participants also reported to favor personalized feedback over no feedback as is common in lectures, videos, or demonstrations (Sacks et al. 2013). Some of the observed benefits VR-based safety training are:

- Presents trainees with hazards directly and realistically without compromising their own physical safety;
- Holds the attention of trainees better than conventional classroom teaching does;
- Gives trainees a measure of control in the environment, thus reinforcing learning; and
- Allows trainers to repeat learning content for many participants under the same training conditions.

VR learning scenarios were criticized by some for being unsophisticated and unrealistic compared to the real world experience (Zhao and Jason 2015). A reason is that creating VR scenarios is a very time-consuming task, requiring a lot of attention to fine details (Sacks et al. 2013) such as programming logic, whereas (Golovina et al. 2016, Bailenson et al. 2008, Teizer et al. 2018) proposed using BIM to increase the realism level of VR scenes. Reducing motion sickness for some players, teaching users unaccustomed to computerized environment, creating multi-user environments (incl. training larger groups), and providing options to instantly record and analyze the players' behaviors seem to be challenges for realistic VR-implementations. Known limitations are:

- Despite that hard- and software technology are rapidly evolving and decreasing in monetary cost, the investment of developing training materials and virtual construction scenarios is still high (i.e., several rounds of iterations are required involving early user experience feedback).
- Several studies (Sacks et al. 2013, Burke et al. 2011, Hilfert et al. 2016, Zhao and Jason 2015) claim that the gained safety knowledge of some trainees may remain at similar levels compared to standard learning approaches.

This section further explains noteworthy details to learning platforms related to the Reality-Virtuality-Continuum (Teizer et al. 2018). As illustrated in Figure 1, the developed virtual safety learning platform consists of a user (e.g., trainee), a trainer for supervised feedback, a virtual construction site environment (e.g., 3D content generated from building information models or open source libraries), scene- or object-related content (e.g., typical sounds), and soft- and hardware technology (e.g., authoring tools and head mounted displays, respectively).

In summary, whereas *Augmented Reality (AR)* is a specialization of Mixed Reality, where the virtual objects are superimposed upon the real world, in *Virtual Reality (VR)* the user is completely immersed in a computer-generated virtual environment (Azuma 1997). While there are AR concepts regarding safety training (Le et al. 2015, Behzadan et al. 2011, Izkara et al. 2007) the approach at hand focusses on the augmented nature of VR called *Augmented Virtuality (AV)*. AV is a hybrid form of VR with real-world elements (Teizer 2018). Usually a real object is used as an input device (e.g., a tool) and tracked and modeled in the virtual environment. While AV serves multiple purposes, it is also used for hazard recognition (Chen 2013) and strengthen data collection to increase safety awareness (Cheng et al. 2010, Bhandari et al. 2019). Few of these studies though have addressed realism of control in AV.

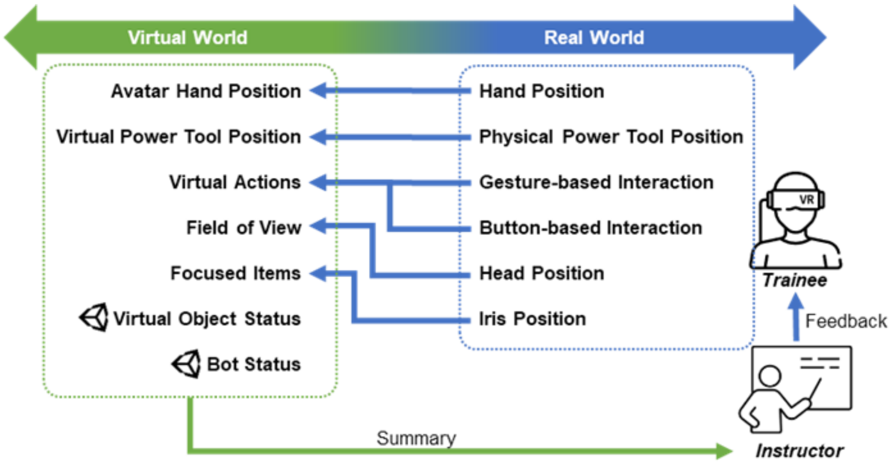

Figure 1: Augmented Virtuality (AV) safety learning platform

3. Methodology

As stated earlier, this paper aims to offer insights into mechanisms for the rapid generation of valid, helpful, and constructive feedback for construction trainees after a training session in AV. With respect to the developed methods, the authors aim at answering the following research questions:

- Which metrics can an AV training application gather to aid the instructor’s feedback to a trainee?
- How can one generate instant feedback to the trainee?
- How big is the difference between self-assessment and measured values concerning the success of the training?
- Can AV be a valid tool in vocational training?

For that purpose, two separate types of data will be gathered. First, the direct inputs from the trainees in form of self-assessment and answers given to specific questions or multiple-choice decisions. Second, further data that can be collected “on the go” while using a AV application, like training session duration, reaction or view times, movement, gaze direction, etc. To be able to gather and evaluate this data, the following 7-step plan was implemented.

Phase 0: The AV scenario aims at construction trainees (equipment operators) in training. The authors’ previous work encompassed the creation of similar safety trainings (using VR only) for a feasibility study (Golovina et al. 2016), so that the creation of the AV application can be reduced to an extension for the requirements of the newly arisen research questions. For that matter, the existing VR training (Bükrü et al. 2020) needs rework regarding usability, data logging, and variety of displayed hazards. The accompanying questionnaire must cover relevant base data about the trainees as well as motivational and strain-related aspects.

Phase 1: The first step of the actual study process is to offer the trainees insights into the motivation and goals of the study, the expected test duration and actions they must take.

Phase 2: The next step is to introduce each trainee individually to the kind of interactions in the AV scenario. As of today, VR and specifically AV are still a very young medium and as such, most users have yet to experience the immersion and behavior of controls in such applications. Not only is it crucial to familiarize the unexperienced with the new visualization method, but also introduce every participant to the specific controls of the AV scenario, just like the instructor would introduce the controls of a new construction site vehicle.

Phase 3: Phase 1 and 2 are the necessary preparation for testing the trainees' knowledge and awareness for hazards in the (virtual) working environment. After the introduction, the application should guide the trainee through the training, giving and repeating instructions on request, as well as tracking the progress and taken steps.

Phase 4: Directly after the VR training, the trainees are asked to fill out the prepared questionnaire. The goal is to gather the trainees' self-assessment of their success and their general opinion on the AV training experience. It is essential to have an (anonymous) unique identifier between the training run in the AV application and the questionnaire to later correlate the findings.

Phase 5: After filling out the questionnaire, the trainees are offered a direct feedback over the AV training's success via a prepared overview with hits and misses regarding the hazards. The feedback is given individually and not in relation to the whole group.

Phase 6: Further analysis of all the gathered data is necessary to accumulate the findings, correlate self-assessments with the application's log data, and deduct future adjustments. As the log data will be extensive and may require further post-processing, while the questionnaire data must be transferred to a digital format to be analyzed, both need to be merged to be analyzed statistically against the entire training group or benchmarks. This can add further value in personalizing feedback.

4. Implementation and Setup

The requirements were implemented in a VR scene, modeled in the Unity 3D engine, which is inspired by a gas pipeline maintenance or pumping station. The scene contains many 3D objects related to construction and maintenance tasks, such as ladders, gas bottles, personal protective equipment (PPE), fencing, face shields, pipelines, and various sorts of hand-powered or electrical tools. The various objects are placed in the scene to make it feel more life-like and as a (realistic) diversion for the participants. Just like in the real world, the working space should be searched for hazards, the appropriate personal safety equipment should be worn, while ensuring that one's work will not harm others.

The space in the scene is divided between a tutorial area (Figure 2, No. 1), an outdoor area (No. 2) and an indoor area (No. 3, view through the roof). The participant's progress through the areas is controlled by an instructor via hotkeys available on the PC running the VR application. Through this, human interaction is still part of the VR experience, as the instructor can either reset a specific area and the participant's position to default or advance the participant to the next area, depending on the participant's success or wishes. The instructor does however not give singular tasks within the applications, as this is part of the application's logic.

Figure 2: Plan view of the developed scenario in Augmented Virtuality (AV)

Figure 3: Modified angle grinder (left) in use by a participant in the indoor area of the AV scenario (right)

The functionalities for interaction in the VR training are practiced in the tutorial area. The four main types of *interaction methods* are:

1. The object is highlighted when looking at an object. The interaction is otherwise finished. This is only used for the tutorial session.
2. Looking at an object, the object is not highlighted, but can be interacted with when pressing the action button on the AV controller (see marker in Figure 3). A menu with three predefined answers pops up and a selection can be made. Selecting an option is final and finishes the interaction. All other interactions are blocked while no selection is made.
3. Looking at an object, the object is not highlighted, but can be interacted with when pressing the action button on the AV controller. The action button triggers a certain action (e.g., opening/closing a valve). The interaction ends upon finishing the action.
4. Interaction between the AV angle grinder and destructible material. Although force feedback is missing, the behavior is near-identical to the real world. Touching destructible objects (e.g., predefined marker on pipe) with the spinning disc of the angle grinder slowly cuts through them. During cutting the interaction of the spinning disc and destructible objects cause flying sparks and some dust. Typical sounds and noise levels of an angle grinder appear, unless the participant starts wearing virtual ear muffs to block out noise and protect their hearing.

The outdoor area is the first “serious” part of the training, meaning that there are hazards in the work environment, which need to be identified using the second interaction method. The main task for the user is to identify the hazards common in outdoor construction work environments and then to cross over a trench.

The hidden hazards are:

- An unsecured excavated trench (not secured against collapse)
- An unsecured spoil pile (too near to the trench)

- An unsafe footbridge (particle board)

The user has the choice detecting any of these or none. For example, replacing the footbridge (made out of particle board) replaces it with a safe overpass (prefabricated steel). The spoil pile of earth material, if detected, is moved further away from the excavated trench and/or trench boxes are placed inside the trench. However, the user can cross the trench at any time by walking to the teleportation marker, which brings the participant into the indoor area. The task in the indoor area is to ensure everyone's safety (including the co-workers), prepare your own working space and then cut one of the pipes where it has been marked.

The indoor area contains a mixture of objects that need to be interacted with. Static items are personal protective equipment (PPE) items, which need to be worn to safely cut the pipe (i.e., helmet, face shield, hearing protection). Then there are the static hazards, such as a missing fire extinguisher, a fuse box that emits electric sparks, two unsecured gas bottles and an axe nearby. All these static objects can be interacted with using second interaction method. Then there are two relevant (out of six) valves that need to be closed using the third interaction method.

Dynamic hazards are represented by: an animated co-worker that stands by too closely where the activity needs to be performed; another co-worker without the proper PPE; an additional co-worker using the wrong kind of ladder. These hazards can be solved using the second interaction method.

The last interaction is the cutting process using the fourth interaction method. If all hazards have been identified (and thereby fixed) and all relevant valves are closed, the cut can be made safely. Otherwise gas leaks from the cut in the pipe, the work scene explodes, and the indoor area is reset to default.

The SteamVR SDK (Unity3D 2019) was used in conjunction with the HTC Vive VR Headset and the HTC Vive Trackers to integrate the AV angle grinder. A text-to-speech plugin provides audio instructions additionally to the written ones in the VR scene. To calculate gaze times, a central ray cast from the VR Headset is used instead of actual eye/iris tracking. As experienced, third party eye tracking solutions for the HTC Vive did not work well. They often de-calibrated with head movement over time and are costly in processing power. As the sharpness of the VR headset's displays is greatest in the center, participants tend to directly look at their focus point instead of having the focus point in the corner of their eye.

5. Study and Data Analysis

As described in the methodology section, the authors propose a two-part evaluation to correlate the VR training metrics with the self-assessment questionnaire. The questionnaire contains the following criteria categories: personal data, general usage of 3D applications, self-assessment of training success, evaluation of operation and functions in the VR application, learning achievements and motivational aspects. The VR application logged answers given by the participants, session time and gaze times for every (relevant) object in the VR scene where the focus point rests longer than 30ms on that object.

Table 1 lists the safety hazards/items and how well the participants (n=15) spotted them. Most often the users recognized the face shield (73.3%) and hearing protection (66.6%) as well as the first/closest gas bottle (53.3%), followed by the helmet (33.3%). Roughly a quarter (26.7%) of the participants spotted a missing fire extinguisher, the co-worker too close to the own activity, the unsafe bridge and the second gas bottle as possible hazards. Those participants who were able to spot hazards most often also said that they:

- Found the simulations’ handling intuitive.
- Quickly were able to understand the handling and put the simulation to use.
- Found the information given in the simulation was sufficient to work on the given task.
- Found the information given in the simulation helpful to solve the given task.

Those participants able to locate and remove possible safety hazards also said that they could work well with the application and that its built-in instructions helped them to solve the given tasks. Two of the participants listed to the instructions for an extended time before continuing.

Out of the 14 hazards/items to be corrected or used, the 15 participants achieved an average score of 27%. The best three participants reached 64%, 57% and 50%, while the worst three did not recognize (or did not interact with) any of the objects.

Table 1: Participant’s recognition rates (in %) for hazards by type (n=15)

Category	Hazard / Item	Not recognized	Wrongly Recognized	Correctly recognized
Outdoor area	Missing trench boxes	86.7	6.7	6.7
	Distance of spoil pile to trench	100	0	0
	Unsafe footbridge	73.3	0	26.7
Indoor area	Helmet	60	6.7	33.3
	Face shield	26.7	0	73.3
	Hearing protection	33.3	0	66.7
	Missing fire extinguisher	73.3	0	26.7
	Sparks coming out of fuse box	93.3	0	6.7
	Gas bottle 1 (partially obstructed)	46.7	0	53.3
	Gas bottle 2 (nearest)	73.3	0	26.7
	Unsecured axe	80	0	20
	Co-worker without proper PSA	86.7	0	13.3
	Co-worker on wrong kind of ladder	73.3	20	6.7
	Co-worker within own workspace	66.7	6.7	26.7

However, still 40% of all participants were able to successfully finish the simulation with the actual work task of cutting the pipe. 60% of all participants lost their Avatar’s life(s) because they were unable to detect and remove possible hazards and provoked an explosion. Even if they were given the possibility to retry, they were still unable to solve the given task and the learning curve was quite poor. Two participants required four times to complete the activity, although hardly detecting and resolving any hazards. Those participants whose Avatars did not die used significantly more time to solve the task than those participants whose Avatars died. This outcome was unrelated to age or prior work experience within the group of participants. These results overall are comparative to other studies (Albert et al. 2014, Hilfert et al. 2016, Hassan et al. 2019). Since the participants in this study were in their first year of a formal apprenticeship program, they had not been sensitized to detecting and resolving risks in the work environment yet.

Table 2 shows a phenomenon that is consistent throughout all the 14 hazards/items. The average gaze time on objects that were recognized lies between 1.5 to 2.5 seconds, while the average gaze time for unrecognized hazards/items varies with the sheer visibility or obviousness. A good example for that is the unsecure footbridge. While it was looked at for over 800ms on average without reaction, the reason for that may as well be the crossing of the bridge to reach the other side of the trench. On the other end of the spectrum are the unsecured axe with a sharp blade, leaning next to a table with minimal gaze time, and the seldomly looked at co-worker without proper PPE, working on the opposite side of the indoor area.

Table 2: Excerpt from the application's gaze time data logs

Hazard type	Avg. Gaze-Time without reaction [ms]	Avg. Gaze-Time with reaction [ms]
Co-worker without proper PSA	63.6	1424
Unsecured Axe	137	2244.3
Co-worker crossing your Working Space	474	1912.6
Co-worker wrong kind of Ladder	418.2	1987.3
Unsecure Footbridge	871	2545.8

Concerning the usability of the simulation, users were asked to make comments on their experience using the application. Theirs answers as well as the collected personal data, like their work experience and self-assessments concerning technical understanding, were then searched for significant correlations. This study showed that users, who assessed their own technical understanding as high or relatively high, also thought the used simulation was a very realistic depiction of a real building site and its possible hazards. Users, who assessed their own technical understanding as high or relatively high, also felt that their knowledge was enough to spot possible hazards and to warn others in case of them facing possible hazards. Those who felt like the given information was enough to successfully use the simulation also felt well-prepared for the work with angle grinders in the real world. This self-assessed proficiency was, however, not related to how well or poorly they did during the simulation.

Concerning the NASA Task Force Test (Colligan 2015), the study showed that those participants that found the simulation to be physically challenging also said that working with it was mentally challenging as well.

Concerning the overall use of VR, participants who used VR overall in their free time and those who play 3D games often also used professional applications for learning purposes. Not surprisingly, if participants used 3D applications more often, they also found the elements used in the application easy to use and they found the information given in the application easy to understand. This shows that prior experience with 3D applications, even if it was only for gaming purposes, had a positive effect on the ease of use for the learning application used in this experiment.

It could be concluded that some participants did not take enough time to properly scan their work environment for safety hazards while those who did take the time were able to solve the task successfully. Maybe the simulation was not able to foster every participants' motivation or seriousness and some participants did not take enough time to thoroughly work through it.

Motivational factors, however, were high: All participants stated that they would welcome the use of more applications and simulations for trainings like this in their education and training in the future. The younger they were, the more they would like to see and use them.

6. Conclusions and Future Work

Like other studies have shown, current learning methods do not engage the trainees in effective ways of self-experiencing high risk work activities. These often cannot be implemented, especially in field-based safety training where they would endanger one's life. The novelty of the proposed augmented virtuality approach is to provide both a safe learning environment where mistakes can be made without suffering the normal consequences and feedback on training success and personal hazard awareness.

This research first designed a safe learning process, then a learning platform using serious games in VR) and AV. The implementation and testing of a realistic AV environment was supported by standard commercially-existing head-mounted display (HMD) units and actual three-dimensional (3D) work environment models. New content of the developed outdoor and indoor scenario was created for purposes of realism (e.g., a body motion suite was used to generate realistic worker movements, texture and geometry of objects in the scene were altered for a characteristic work scene). As such, several hazards related to a work activity were added to the virtual training scenario. Consequentially, personal safety performance data on the participants experiencing the scenario individually were collected and analyzed. Quantitative analysis and visual safety performance information became available for behavioral reasoning, suggesting that VR- and AV-based training can provide previously unobserved data objectively. As a results, many participants performed poorly in hazard recognition and overestimated their safety performance. Based on the feedback collected among the participants and trainers, VR and AV can become a viable tool in safety training and assessment.

Future work would benefit from additional and follow-up studies with more participants and varying degrees of assistance in findings hazards. Future research could shift the focus from "testing hazard recognition" to "training hazard recognition". Further investigation regarding gaze time vs. recognition time could be conducted to achieve objective vs. subjective feedback in active personalized learning environments using Virtual or Augmented Virtualities. Additional work could finally concentrate on hazard awareness training vs. behavioral change.

References

Albert, A., M. R. Hallowell, B. Kleiner, A. Chen, and M. Golparvar-Fard (2014). Enhancing construction hazard recognition with high-fidelity augmented virtuality. Journal of Construction Engineering and Management, 140(7): 04014024, https://doi.org/10.1061/(ASCE)CO.1943–7862.0000860.

Azuma R.T. (1997). A Survey of Augmented Reality. *Presence: Teleporters and Virtual Environments,* 355–385.

Bhandari, S., Hallowell, M.R., Boven, L, Welker, K.M., Golparvar-Fard, M., Gruber, J. (2019). Using Augmented Virtuality to Examine How Emotions Influence Construction-Hazard Identification, Risk Assessment, and Safety Decisions, Journal of Construction Engineering and Management, DOI:10.1061/(ASCE)CO.1943–7862.0001755.

Bailenson J., Yee, N., Blascovih J., Beall A.C., Lundblad N., Jin M. (2008). The Use of Immersive Virtual Reality in the Learning Sciences: Digital Transformations of Teachers, Students, and Social Context, J. Learning Practices, 17:102–141.

Behzadan A.H., Iqbal A, Kamat V.R. (2011). A collaborative augmented reality based modeling environment for construction engineering and management education. *Winter Simulation Conference (WSC)*, pp.3568–3576.

Bükrü, S. Wolf, M., Golovina, O., Teizer, J. (2020), "Using Field of View and Eye Tracking for Feedback Generation in an Augmented Virtuality Safety Training", Construction Research Congress, Tempe, Arizona, USA, March 8–10, 2020.

Burke et al.'s., (2011). The Dread Factor: How Hazards and Safety Training Influence Learning and Performance, Applied Psychology, 96: pp.46–70, 201.

Carter G., Smith S.D. (2006). Safety Hazard Identification on Construction Projects, *Construction Engineering and Management*, 132: pp.197–205.

Chen A., Golparvar-Fard M., Kleiner B. (2013). Saves: A Safety Training Augmented Virtuality for Construction Hazard Recognition and Severity Identification, 13th Intl. Conf. Constr. Applications of Virtual Reality: pp.373–383.

Cheng, T., Teizer, J. (2010). Real-time Data Collection and Visualization Technology in Construction, Construction Research Congress, Banff, Canada, pp. 339–348, https://doi.org/10.1061/41109(373)34.

Chittaro L., Buttussi F. (2015). Assessing Knowledge Retention of an Immersive Serious Game vs. Traditional Education Method in Aviation Safety. IEEE Trans. on Visualization and Computer Graphics, 21(4), pp.529–538.

Colligan, L, Potts, H.W.W., Finn, C.T., Sinkin, R.A. (2015). Cognitive workload changes for nurses transitioning from a legacy system with paper documentation to a commercial electronic health record, *International Journal of Medical Informatics*, 84(7), pp.469–476. doi:10.1016/j.ijmedinf.2015.03.003.

Emerson, L. C., & Berge, Z. L. (2018). Microlearning: Knowledge management applications and competency-based training in the workplace. *Knowledge Management & E-Learning: An Intl. Journal*, 10(2), pp. 125–132.

Golovina O., Teizer J., Pradhananga N. (2016). Heat map generation for predictive safety planning: preventing Struck-by and near miss interactions between workers-on-foot and construction equipment, *Automation in Construction*, 71, pp. 99–115, http://dx.doi.org/10.1016/j.autcon.2016.03.008.

Hassan, M., Carozza, L., Bosché, F., Abdel-Wahab, M. (2019). Effectiveness of a Novel Untethered Augmented Virtuality System for Immersive Industrial Training. 36th International Conference of CIB W78, Newcastle-upon-Tyne, UK, 18-20 September, pp. 986–998 (ISSN: 2706-6568), http://itc.scix.net/paper/w78-2019-paper-093

Hilfert T., Teizer J., König M. First Person Virtual Reality for Evaluation and Learning of Construction Site Safety, 33rd ISARC, 2016, https://doi.org/10.22260/ISARC2016/0025.

Izkara J.L., Pérez J., Basogain X., Borro D. (2007). Mobile Augmented Reality, an Advanced Tool for the Construction Sector. CIB W078 Intl. Conference on Information Technology, pp. 453–460.

Kassem M., Benomran L., Teizer J. (2017). Virtual environments for safety learning in construction and engineering: seeking evidence and identifying gaps for future research, *Visualization in Engineering*, Springer, 5:16, 2017, http://doi.org/10.1186/s40327-017-0054-1.

Le Q.T., Pedro A., Lim C.R., Park H.T., Park C.S., Kim H.K. (2015). A Framework for Using Mobile Based Virtual Reality and Augmented Reality for Experiental Construction Safety Education. *Intl. Journal of Engineering Education,* 31(3), pp. 713–725, 2015.

Li X., Yi W., Chi H., Wang X., Chan A. (2018). A critical review of virtual and augmented reality (VR/AR) applications in construction safety. *Automation in Construction*, 86, pp.150–62.

Rajendran S., Gambatese, J.A. (2009). Development and Initial Validation of Sustainable Construction Safety and Health Rating System, *Construction Engineering and Management*, 135, pp.1067–1075.

Sacks R., Perlman A., Barak R. (2013). Construction safety training using immersive virtual reality, *Construction Management and Economics*, pp.1005–1017.

OSHA (2019). Commonly Used Statistics, https://www.osha.gov/oshstats/commonstats.html (Accessed 1-1-19).

Teizer J. (2016). Right-time vs. real-time pro-active construction safety and health system architecture, *Construction Innovation: Information, Process, Management*, Taylor and Francis, 16(3), pp. 253–280, http://dx.doi.org/10.1108/CI-10-2015-0049.

Teizer J., Wolf M., König M. (2018). Mixed Reality Anwendungen und ihr Einsatz in der Aus- und Weiterbildung kapitalintensiver Industrien, *Bauingenieur*, Springer, pp. 73–82, ISSN 0005-6650.

Teizer, J., Embers, S., Golovina, O., Wolf, M. (2020). A serious gaming approach to integrate BIM, IoT and Lean Construction in Construction Education", Construction Research Congress, March 8–10, 2020.

Unity3D. https://assetstore.unity.com, 2019.

Wang P. Wu P., Wang J., Chi H., Wang X. (2018). A Critical Review of the Use of VR in Construction Engineering Education and Training, *Environment Research and Public Health*, 15(6):1204.

Zaker R., Coloma E. (2018). Virtual reality-integrated workflow in BIM-enabled projects collaboration and design review: a case study, *Visualization in Engineering*, 6:4.

Zhao D., Jason L. (2015). Virtual reality simulation for construction safety. *Injury Control and Safety Promotion*, 22:1, pp. 57–67.

Unsupervised Crack Segmentation from Disaster Site Point Clouds using Point Feature Clustering

Jingdao Chen, Yong K. Cho
Georgia Institute of Technology, United States of America
jchen490@gatech.edu

Abstract. 3D as-damaged models of a disaster site can be reconstructed from LiDAR scans by analyzing the point cloud data for indicators of damage such as cracks. Conventional methods for crack detection have limitations in terms of robustness or requiring a large training database. To achieve the goal of structural damage detection that can be used to reconstruct the 3D as-damaged geometry of a disaster site, this research proposes an unsupervised learning method to perform crack segmentation directly from LiDAR-scanned point cloud data. First, column segments are extracted from the building façade by region growing and rule-based filtering. Next, five different types of point features are extracted, namely RGB color, intensity, normal vector, curvature, and neural network-based features. Then, K-means clustering is used to isolate the cluster of points belonging to the cracked region. The effectiveness of the proposed method is measured quantitatively using the precision and recall metrics and qualitatively by visualizing the segmentation results compared to the ground truth. Experimental results show that the neural network-based features achieved the best performance in terms of precision and recall.

1. Introduction

LiDAR technology plays an important role in disaster relief operations in scanning affected infrastructure and identifying the hazard level of different buildings on the disaster site. LiDAR technology is able to capture the 3D geometry of a building at mm-level accuracy, thus various deformations such as cracking and spalling on a building structure can be detected and analyzed from point cloud data. Once damaged regions have been identified, infrastructure damage information can then be compiled and categorized according to typical damage modes and compiled into an as-damaged Building Information Model (Ma, Sacks and Zeibak-shini, 2015; Sacks *et al.*, 2016). These models contain detailed and semantically rich information about the location and shape of infrastructure damage present in a building that can be useful to civil engineers and reconstruction and recovery (R&R) personnel. In order to generate these models, it is important to have automated methods that can detect damaged structures accurately and efficiently.

In contrast to LiDAR-based damage modeling, conventional methods for structural damage analysis rely on a long sequence of steps including field observations (Noh, Lallemant and Kiremidjian, 2015) and vibration analysis (Noh, Rajagopal and Kiremidjian, 2013) that is very labor-intensive. In addition, these methods depend on having physical access to the disaster site which may not be practical for hazardous areas that can only be accessed remotely (e.g. by mobile scanning robots). Other methods can perform damage detection from live sensor data such as RGB images (Feng *et al.*, 2017; Zhang *et al.*, 2018). However, these methods rely on having a large amount of labeled training data which is difficult to obtain when there are many different types of structural damages.

To achieve the goal of structural damage detection that can be used to reconstruct the 3D as-damaged geometry of a disaster site, this research proposes an unsupervised learning method to perform crack segmentation directly from LiDAR-scanned point cloud data without explicit training on the task of crack segmentation. The advantage of an unsupervised detection method is that it does not require training data of annotated cracks but can still adapt to different distributions of test data. The proposed method is evaluated based on laser-scanned point clouds from the 2015 Nepal earthquake.

2. Literature Review

Conventional methods for structural damage analysis rely on data from quantitative measurements such as vibration analysis (Noh, Rajagopal and Kiremidjian, 2013) and qualitative measurements from field observations (Noh, Lallemant and Kiremidjian, 2015). However, without direct access to the physical site, the alternative is to measure structural damage indirectly from sensor data collected from the field. A simple method to identify cracks and spalling is to estimate the surface normal and measure the deviation from a nominal value (Bose *et al.*, 2016) or finding outliers using a combination of the surface normal and color information (Erkal and Hajjar, 2017). Other methods for detecting damage include measuring the distance change from a reference plane (Liu, Chen and Hauser, 2011) or measuring the laser intensity contrast (Tsai and Li, 2012). The limitation of these methods is that they require tuned parameter thresholds or carefully constructed scoring algorithms to work well.

Alternatively, deep neural networks can also be trained to label points that correspond to cracks (Feng *et al.*, 2017; Zhang *et al.*, 2018) in a data-driven manner. The challenge with these approaches is that they require a large database of annotated cracks in order to train the neural network. In addition, they work mainly in the 2D domain and do not have the full 3D geometric information of the damaged region.

In the case of damage detection from 3D point clouds, a prior method has been developed for the classification of synthetically deformed building elements (Chen, Cho and Ueda, 2018). The method was only applied for pre-segmented, single object point clouds and may not work with point clouds with a large number of objects and clutter where the segmentation results are much noisier. In addition, the method only considered synthetically deformed objects and was not evaluated in actual disaster scenarios. An alternative method to perform damage analysis is to detect the deviation between the as-damaged point cloud and the as-designed model (Chen and Cho, 2018, 2019). However, this requires a detailed as-designed model that closely matches the damaged building which may not be available for all buildings.

3. Methodology

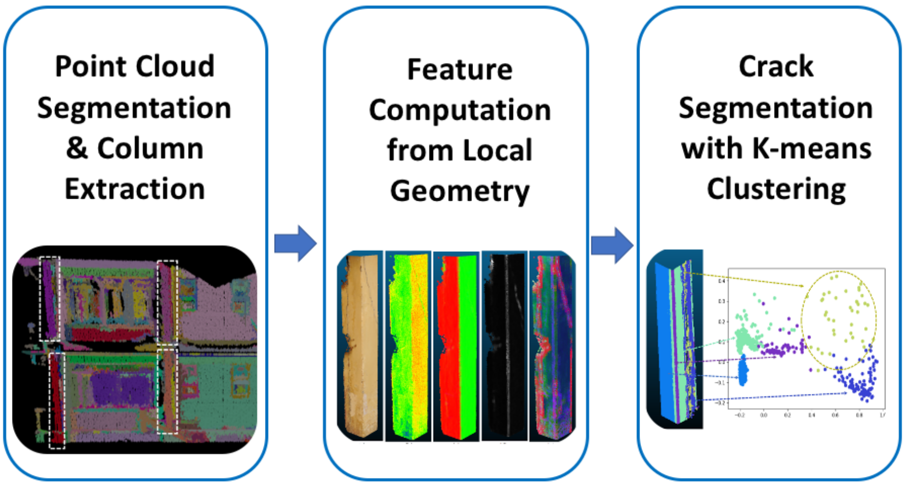

Figure 1: Workflow of point cloud processing steps to perform crack segmentation

The dataset used in this study is taken from LiDAR scans in Nepal after the 2015 earthquake (also known as the Gorkha earthquake). The earthquake, at Mw=7.8 intensity, caused significant structural damage and ground failure across several districts in Nepal. The earthquake resulted in structural damage such as shear cracking, deformation, and spalling in various school buildings, apartments, and hospital buildings. To closely analyze the structural damage, researchers have collected ground-based LiDAR scans at mm-level accuracy from multiple sites across Nepal to form a complete dataset (Brando *et al.*, 2017).

This study will focus on a point cloud scan of the maternity hospital in the Nepal dataset, which contains many instances of cracked columns. Figure 1 shows the workflow of how the point cloud data is used in terms of pre-processing, feature computation, and crack segmentation. The following subsections will describe each step in detail.

3.1 Building Façade Segmentation

The raw point cloud data consists of 5.6 million points that have been mapped with RGB color from the built-in camera as well as intensity values from the LiDAR scan. This study will focus on columns since the structural damage in this dataset occurs mostly on the columns. The first step is to automatically extract the column points from the point cloud of the entire building façade. A region growing procedure is used to merge similar neighboring points together into object-level segments. Then a rule-based filter is applied to identify columns by selecting point cloud segments with height greater than 2.5m and aspect ratio greater than 2. Figure 2(a) shows the layout of seven columns extracted from the building façade. Whereas, Figure 2(b) shows the point cloud segmentation results (each point cloud segment is visualized in a different color) and the detected columns. Each column consists of roughly 50,000 points, spanning a volume of 0.4m x 0.4m x 2.6m.

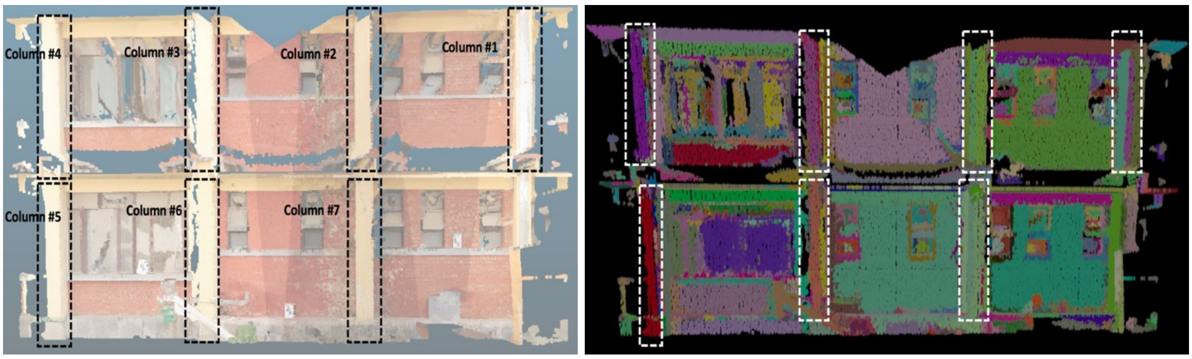

(a) (b)

Figure 2: Point cloud of a building façade and the corresponding segmentation results

3.2 Feature Computation

The next step is to extract relevant features from the point cloud data that can help distinguish between undamaged points and damaged points, such as that from a crack. The features are computed at the point level such that each point in the point cloud has an associated feature vector. This study considers five different types of features that can be extracted from the point cloud data for comparison (Figure 3). The first two features, RGB color and intensity can be extracted directly from the raw data. Whereas, the next two features, normal vector and curvature, can be computed by performing eigenvalue analysis of the local neighborhood around each point (Rusu and Cousins, 2011). The normal vector indicates the orientation of the local surface around each point and can be interpreted as the direction of least change in the distribution of points in the local neighborhood. This can be visualized as shown in Figure 3c, where front-facing points are colored red whereas side-facing points are colored green. Whereas the curvature indicates whether the local surface around each point is mostly flat or curved. For example, in Figure 3d, points on flat surfaces are mostly darker while points on curved surfaces are mostly lighter.

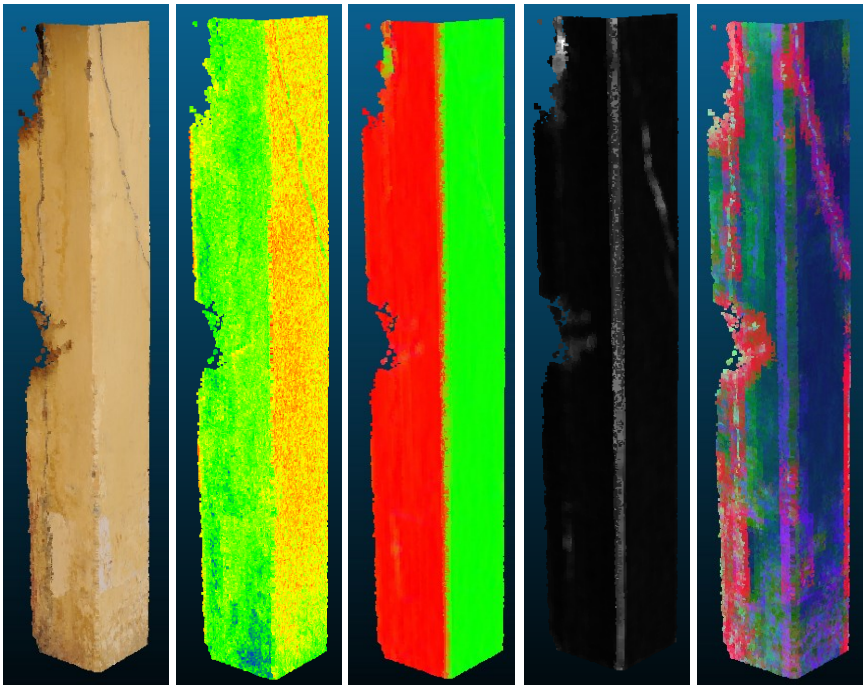

(a) (b) (c) (d) (e)

Figure 3: Visualization of different features derived from point cloud data of a single column (from left to right: RGB color, intensity, normal vector, curvature, neural network)

This study also considers the use of a neural network to extract discriminative features from point cloud data. Recent research in point cloud data processing (Qi *et al.*, 2017; Chen, Cho and Ueda, 2018) has shown that neural networks are effective in converting raw point cloud data into useful semantic representations. This study uses MCPNet (Chen, Cho and Kira, 2019) to extract a 10-dimensional feature embedding for each point. The network is pre-trained on a separate dataset of indoor building elements for the task of semantic instance segmentation. The network takes in as input the set of 50 randomly sampled points in the local neighborhood and performs various convolution and pooling operations to compute an output feature vector. The advantage of using features derived from a neural network is that it incorporates many latent features such as color and curvature without having to explicitly perform any feature engineering or parameter tuning. Figure 3e shows a false-color representation of the features computed by the neural network. The false-color is obtained by projecting the feature vector into three color dimensions using Principal Component Analysis (Locantore *et al.*, 1999). As shown in Figure 3e, the neural network-based features effectively delineate the point cloud data into different regions based on the differences in their local surface properties. Note that using the neural network to compute features is still considered unsupervised learning since the network is pre-trained on a different task and does not require supervision in terms of training data annotated with cracks.

3.3 Crack segmentation

This study approaches the problem of crack segmentation using unsupervised machine learning. The benefit of unsupervised methods is that they do not require training data of annotated cracks but can still adapt to different distributions of test data. This approach takes advantage of the fact that in a point cloud of a damaged structure, damaged points usually have irregular features whereas undamaged points usually have regular features. Thus, an unsupervised clustering algorithm can be used to separate out the points in cracked or damaged regions from points in undamaged regions based on their corresponding features. The advantage of using a clustering algorithm is that it does not depend on a fixed threshold to classify damaged points, since damaged points may have a different appearance in different scenarios. Instead it adapts to different scenarios by considering the distribution of features instead of the feature values themselves.

This study implements the K-means clustering algorithm (Chehata, David and Bretar, 2008) due to its speed and interpretability. K-means clustering works by dividing the input data into K number of clusters such that each cluster contains data points which have roughly similar features. The intuition behind this step is that points with regular features will be grouped into large clusters whereas points with irregular features will be grouped into smaller clusters or appear as outliers. To perform crack segmentation, K-means clustering is applied to the features computed in the previous step (Section 3.2) and the resulting cluster with the fewest number of points is assigned as the cracked or damaged region. In this study, the K-parameter is set to 2 for the curvature-based method, 5 for the neural network-based method, and 3 for all other methods (depending on which setting results in the best clustering).

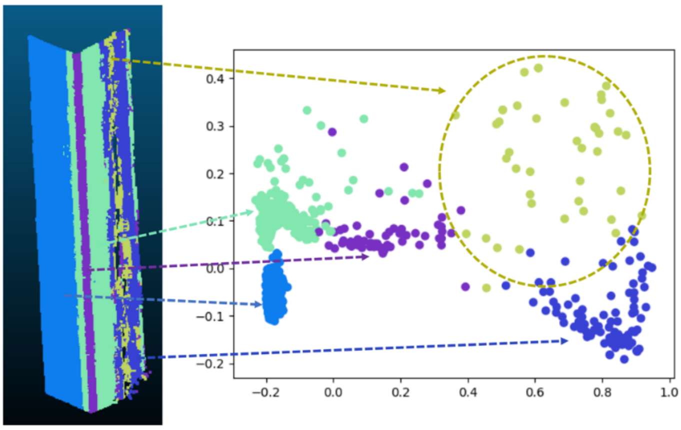

Figure 4: Visualization of K-means clustering used to isolate the points belonging to the cracked region

Figure 4 shows a visualization of the K-means clustering results when applied on the neural network-based features. The left subfigure shows how the column point cloud has been subdivided into 5 different regions (each region is visualized in a different color), since the K-parameter is set to 5. The visualization shows that cluster assignment mostly follows the boundary of different regions in the point cloud (i.e. points on the front face are mostly blue, points on the side face are mostly dark blue, edge points are mostly purple, points close to the edge are mostly green, while the remaining points near the crack are mostly yellow). Whereas, the right subfigure shows the distribution of different types of points in feature space. Note that the features have been projected to 2 dimensions from the original 10 dimensions using the Principal Component Analysis (Locantore *et al.*, 1999) technique so that it is easy to visualize. The visualization shows the undamaged points (blue, dark blue, green, and purple) show up as dense clusters in the feature space whereas the damaged points (yellow) show up as a sparse region since the points appear as outliers to other regions in the feature space. Thus, the cracked area in the original point cloud can be identified by selecting this cluster as representing the damaged area.

4. Results

The effectiveness of the proposed point feature clustering approach for crack segmentation is evaluated on the Nepal dataset based on the point-level (i) precision and (ii) recall metrics. The predicted points are compared against the ground truth points in the cracked region that are manually annotated. Precision is defined as the ratio between the number of points correctly identified and the total number of points predicted to be in the cracked region. Whereas, recall is defined as the ratio between the number of points correctly identified and the total number of points that are actually in the cracked region.

Table 1 below shows a comparison of the precision metric whereas Table 2 below shows a comparison of the recall metric. The results show that the neural network-based feature showed the best performance overall in terms of both precision and recall scores. This is because the neural network is able to learn a set of robust features instead of relying on any single feature. Whereas, the intensity-based and normal vector-based features showed the worst performance overall. This is because the intensity and normal vector are noisier and less discriminative when it comes to differentiating between damaged and undamaged points. From Tables 1 and 2, it can also be observed that the crack segmentation works well for some columns (e.g. #1, #3) but not for other columns (e.g. #4, #6). This is because those columns have thinner and less visible cracks so the features extracted for those cracks are less distinctive.

Table 1: Point-level precision for crack segmentation with different point features

	RGB Color	Intensity	Normal Vector	Curvature	Neural Network
Column #1	0.88	0.24	0.11	0.31	0.75
Column #2	0.51	0.43	0.14	0.51	0.57
Column #3	0.93	0.16	0.59	0.51	0.90
Column #4	0.25	0.00	0.00	0.02	0.34
Column #5	0.36	0.00	0.27	0.22	0.73
Column #6	0.26	0.01	0.00	0.02	0.36
Column #7	0.53	0.24	0.07	0.17	0.44
Average	0.53	0.15	0.17	0.25	0.58

Table 2: Point-level recall for crack segmentation with different point features

	RGB Color	Intensity	Normal Vector	Curvature	Neural Network
Column #1	0.23	0.29	0.04	0.20	0.56
Column #2	0.29	0.64	0.03	0.34	0.29
Column #3	0.52	0.35	0.40	0.46	0.37
Column #4	0.44	0.00	0.00	0.01	0.05
Column #5	0.35	0.00	0.10	0.12	0.48

Column #6	0.24	0.07	0.00	0.02	0.36
Column #7	0.32	0.40	0.02	0.09	0.40
Average	0.34	0.25	0.08	0.18	0.36

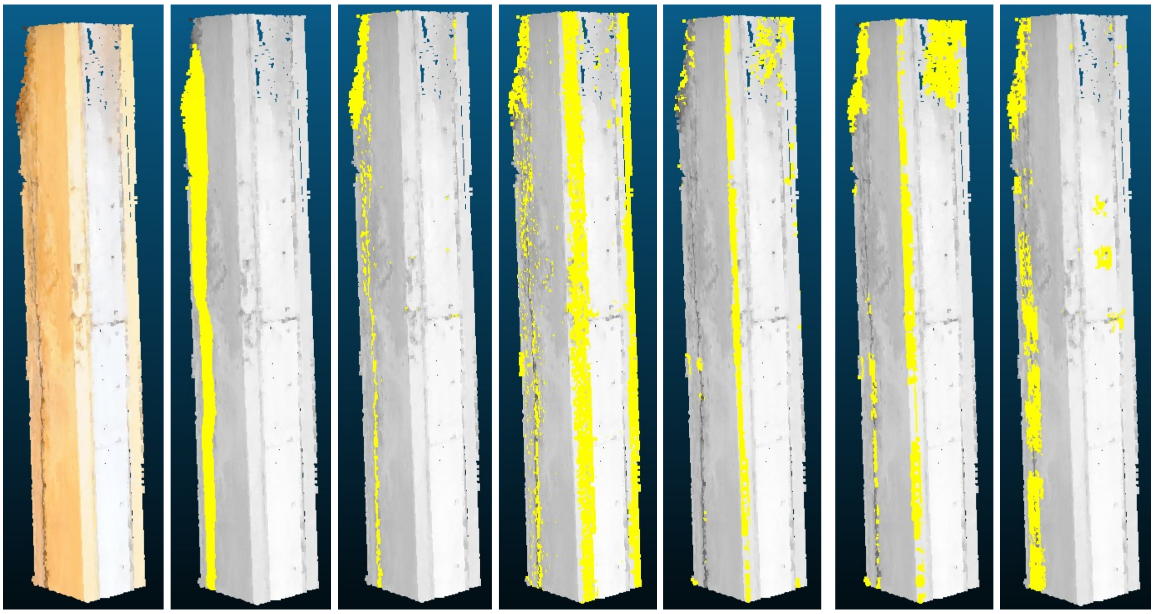

(i) (ii) (iii) (iv) (v) (vi) (vii)

Figure 5: Crack segmentation results for Column #1 with different point features (yellow points indicate crack location). The subfigures are: (i) original point cloud, (ii) ground truth, results from (iii) RGB color (iv) intensity (v) normal vector (vi) curvature (vii) neural network

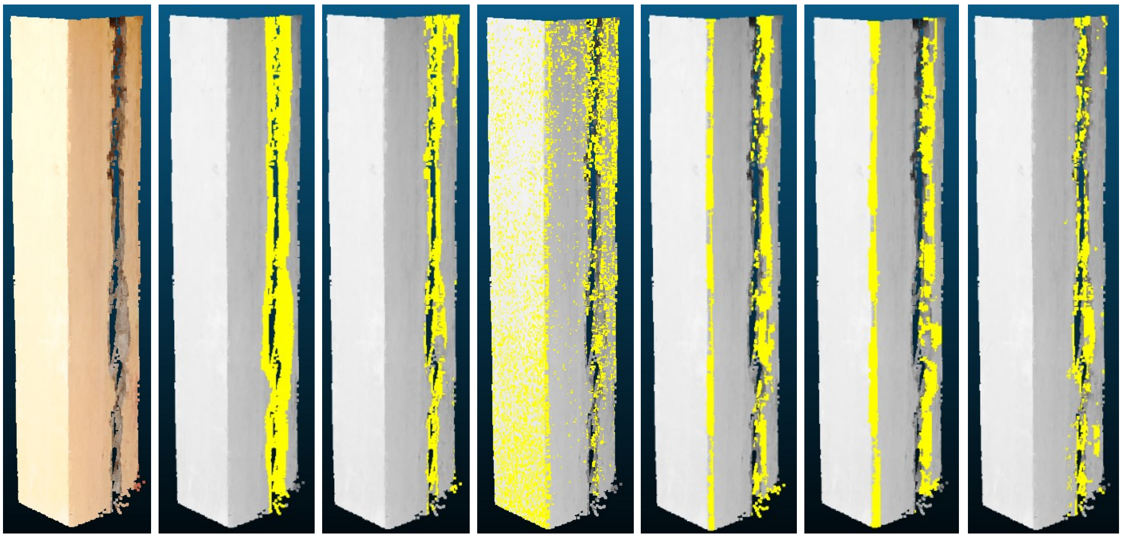

(i) (ii) (iii) (iv) (v) (vi) (vii)

Figure 6: Crack segmentation results for Column #3 with different point features (yellow points indicate crack location). The subfigures are: (i) original point cloud, (ii) ground truth, results from (iii) RGB color (iv) intensity (v) normal vector (vi) curvature (vii) neural network

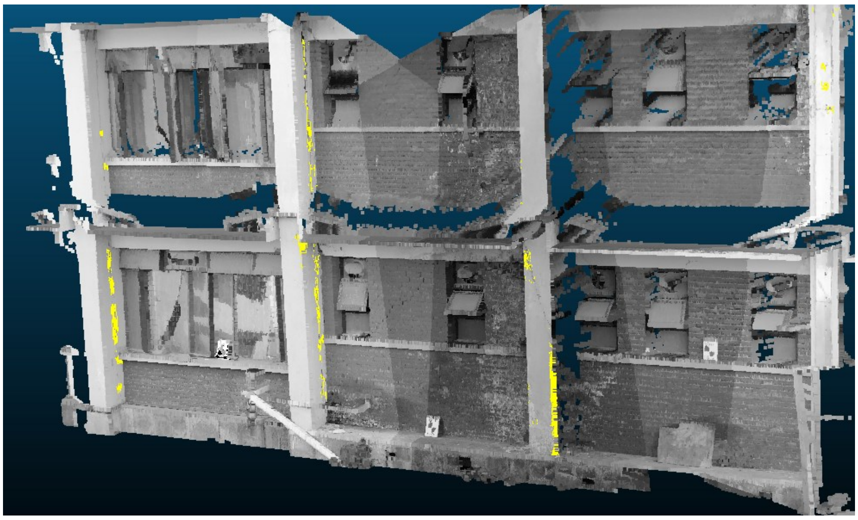

Figure 7: Crack segmentation results mapped back to the original scene

5. Conclusion

In conclusion, this research proposes an unsupervised method for crack segmentation from disaster site point clouds based on point feature clustering. The proposed method is evaluated on point cloud data from the 2015 Nepal earthquake using five different types of point features. Quantitative results using the point-level precision and recall metrics show that the neural network-based feature obtained the best performance overall. For future work, the detection of other types of structural damages such as debris and concrete spalling and will also be explored.

Acknowledgment

This work is supported by the United States Air Force Office of Scientific Research (Award No. FA2386-17-1-4655), and by a grant (18CTAP-C144787-01) funded by the Ministry of Land, Infrastructure, and Transport (MOLIT) of Korea Agency for Infrastructure Technology Advancement (KAIA). Any opinions, findings, and conclusions or recommendations expressed in this material are those of the authors and do not necessarily reflect the views of the United States Air Force, MOLIT, or KAIA.

References

Bose, S. *et al.,* (2016). 'Structural Assessment of a School Building in Sankhu, Nepal Damaged Due to Torsional Response During the 2015 Gorkha Earthquake', in Pakzad, S. and Juan, C. (eds) *Dynamics of Civil Structures, Volume 2*. Cham: Springer International Publishing, pp. 31–41.

Brando, G. *et al.,* (2017). 'Damage Reconnaissance of Unreinforced Masonry Bearing Wall Buildings After the 2015 Gorkha, Nepal, Earthquake', *Earthquake Spectra*, 33(S1), pp. S243–S273. doi: 10.1193/010817EQS009M.

Chehata, N., David, N. and Bretar, F., (2008). 'LIDAR data classification using hierarchical K-means cluster', in *The International Archives of the Photogrammetry, Remote Sensing and Spatial Information Sciences.*

Chen, J. and Cho, Y. K., (2018). 'Point-to-point Comparison Method for Automated Scan-vs-BIM Deviation Detection', in *Proceedings - 17th International Conference on Computing in Civil and Building Engineering*. Available at: http://programme.exordo.com/icccbe2018/delegates/presentation/303/.

Chen, J. and Cho, Y. K., (2019). 'Detection of Damaged Infrastructure on Disaster Sites using Mobile Robots', in *2019 16th International Conference on Ubiquitous Robots (UR)*, pp. 648–653. doi: 10.1109/URAI.2019.8768770.

Chen, J., Cho, Y. K. and Kira, Z., (2019). ‘Multi-view Incremental Segmentation of 3D Point Clouds for Mobile Robots’, *IEEE Robotics and Automation Letters*, 4, pp. 1240–1246. doi: https://doi.org/10.1109/LRA.2019.2894915.

Chen, J., Cho, Y. K. and Ueda, J., (2018). ‘Sampled-Point Network for Classification of Deformed Building Element Point Clouds’, in *Proceedings of the 2018 IEEE Conference on Robotics and Automation (ICRA)*.

Erkal, B. G. and Hajjar, J. F., (2017). ‘Laser-based surface damage detection and quantification using predicted surface properties’, *Automation in Construction*, 83, pp. 285–302. doi: https://doi.org/10.1016/j.autcon.2017.08.004.

Feng, C. *et al.,* (2017). ‘Deep Active Learning for Civil Infrastructure Defect Detection and Classification’, in *International Workshop on Computing in Civil Engineering*. Seattle.

Liu, W., Chen, S. and Hauser, E., (2011). ‘LiDAR-based Bridge Structure Defect Detection’, *Experimental Techniques*, pp. 27–34. doi: 10.1111/j.1747-1567.2010.00644.x.

Locantore, N. *et al.,* (1999). ‘Robust principal component analysis for functional data’, *Test*, 8(1), pp. 1–73. doi: 10.1007/BF02595862.

Ma, L., Sacks, R. and Zeibak-shini, R., (2015). ‘Information modeling of earthquake-damaged reinforced concrete structures’, *Advanced Engineering Informatics*. Elsevier Ltd, 29(3), pp. 396–407. doi: 10.1016/j.aei.2015.01.007.

Noh, H., Rajagopal, R. and Kiremidjian, A. S., (2013). ‘Sequential structural damage diagnosis algorithm using a change point detection method’, *Journal of Sound and Vibration*. Elsevier, 332(24), pp. 6419–6433. doi: 10.1016/j.jsv.2013.07.005.

Noh, H. Y., Lallemant, D. and Kiremidjian, A. S., (2015). ‘Development of empirical and analytical fragility functions using kernel smoothing methods’, *Earthquake Engineering & Structural Dynamics*, (October 2014), pp. 1163–1180. doi: 10.1002/eqe.

Qi, C. *et al.,* (2017). ‘PointNet: Deep Learning on Point Sets for 3D Classification and Segmentation’, *Proc. Computer Vision and Pattern Recognition (CVPR), IEEE*. doi: 10.1109/3DV.2016.68.

Rusu, R. B. and Cousins, S., (2011). ‘3D is here : Point Cloud Library (PCL)’, in *IEEE International Conference on Robotics and Automation (ICRA)*.

Sacks, R. *et al.,* (2016). ‘Preparation of Synthetic As-Damaged Models for Post-Earthquake BIM Reconstruction Research’, *Journal of Computing in Civil Engineering*, 30(3), pp. 1–12. doi: 10.1061/(ASCE)CP.1943-5487.0000500.

Tsai, Y.-C. J. and Li, F., (2012). ‘Critical Assessment of Detecting Asphalt Pavement Cracks under Different Lighting and Low Intensity Contrast Conditions Using Emerging 3D Laser Technology’, *Journal of Transportation Engineering*, 138(5), pp. 649–656. doi: 10.1061/(ASCE)TE.1943-5436.0000353.

Zhang, A. *et al.,* (2018). ‘Deep Learning Based Fully Automated Pavement Crack Detection on 3D Asphalt Surfaces with an Improved CrackNet’, *Journal of Computing in Civil Engineering*, 32(5), p. 4018041. doi: 10.1061/(ASCE)CP.1943-5487.0000775.

Disaster Impact Information Retrieval Using Deep Learning Object Detection in Crowdsourced Drone Footage

Yalong Pi, Nipun D. Nath, Amir H. Behzadan
Texas A&M University, USA
abehzadan@tamu.edu

Abstract. Collecting and sharing timely and reliable post-disaster data is of utmost importance in disaster mitigation. Current methods of aerial search for post-disaster reconnaissance rely on human involvement, making them expensive, subjective, and slow. We propose to equip ordinary drones with convolutional neural networks (CNN) for fast object detection and viewpoint projection to assist in evacuation, wayfinding, resource allocation, and damage assessment. In this research, an in-house hurricane video dataset and the YOLO object detection algorithm are used. Testing the trained CNN model on unseen drone footage yields an overall accuracy of 74.48%. Next, GPS-free geometrical projection is used to autonomously transform the pixel coordinates of detected objects from the drone's perspective view to the world coordinates in an orthogonal map. When tested on classes undamaged roof and car, a high accuracy (~5% error) is achieved, demonstrating the robustness of this method for real-time mapping of disaster footage.

1. Introduction

Natural disasters impact societies, economies, and the built infrastructure. According to U.N. Office for Disaster Risk Reduction (2019), between 2004 and 2014, 1.7 billion people were affected by natural disasters globally, resulting in 700,000 deaths and $1.4 trillion in damages. Disaster management (a process that involves preparedness, mitigation, response, and recovery) requires timely access to accurate information describing disaster impact (Guha-Sapir and Lechat, 1986). Aerial reconnaissance is commonly used for locating victims and assessing damage, particularly in large-scale events such as hurricanes, tsunamis, and wildfires. While traditionally, helicopters and low-altitude flying aircrafts are deployed for data collection, the rapidly growing drone technology provides a more flexible, scalable, safer, and lower-cost alternative (Adams and Friedland, 2011). It is estimated that by the year 2022, there will be more than 2.4 million UAVs in the U.S. (Federal Aviation Administration, 2018), which can lead to opportunities for crowdsourced data collection and exchange in disaster events. In addition to collecting large and diverse disaster data, engaging people and communities in sharing volunteered geographic information (VGI) (Haworth and Bruce, 2015) can also lead to more transparency and trust in technology. The current practice of processing disaster footage, however, requires intensive manual data curation (data cleaning, formatting, analyzing, synthesizing, and delivering). Considering the lack of skilled personnel, and limited support and computing resources in the disaster's aftermath, this can hinder the full utilization of data by users, e.g., response teams, aid agencies, volunteer groups, and the general public.

This research aims to investigate whether aerial footage captured by drone-mounted red green blue (RGB) cameras can be processed using deep learning (DL) methods to automatically extract critical disaster-related information. Particularly, a convolutional neural network (CNN) algorithm, namely you-only-look-once (YOLO v2) (Redmon and Farhadi, 2017), is employed to detect and localize key ground objects in drone footage, at fast speed, and with high accuracy. In computer vision, the task of identifying the class labels and pixel positions of objects in an image is termed object detection. The pixel coordinate of each detected object (herein referred to as target of interest or ToI) is then transformed into real-world positions to create geocoded maps of disaster impact. The designed methodology is validated using a video dataset.

2. Literature Review

Previous research has mined disaster-related VGI. For example, Craglia et al. (2012) used Facebook and Twitter text data to map disaster impact. Kim and Hastak (2018) used social media data to map the damage after the 2016 Louisiana flood. Faxi et al. (2017) utilized machine learning to extract infrastructure damage from tweets in Fort McMurray during a wildfire. Drones have been also adopted for ground inspection and information extraction. For example, Radovic et al. (2017) used YOLO (Redmon and Farhadi, 2017) to identify airplanes, buses, and cars on the ground. Han et al. (2012) integrated region-based CNN (R-CNN) and kernelized correlation filter (KCF) (Henriques et al., 2014) to track humans on the ground. Baker et al. (2016) implemented a decentralized Monte Carlo tree search algorithm to find survivors in a simulated drone path planning scenario. They conducted tests on data from the 2010 Haiti earthquake and reported consistent performance gains of up to 18% over a discretized algorithm in the number of located survivors. However, there is a dearth of work in the area of large-scale, multi-class disaster object detection and mapping from drone footage.

Object detection has evolved rapidly in recent years along with advancement of graphic processing unit (GPU), which in part led Girshick et al. (2014) to design R-CNN and Fast R-CNN (Girshick, 2015) that replaced traditional sliding box methods with region of interest (RoI) to improve processing speed. Later, Girshick (2015) proposed Faster R-CNN with region proposal network (RPN) that achieved 73.2% mean average precision (mAP) on VOC dataset (Everingham et al., 2015). Redmon et al. (2016) introduced YOLO which takes input image grids and outputs classification and position at once. Later, YOLO v2 (Redmon and Farhadi, 2017) was introduced with a better performance. Also, single shot detector (SSD) algorithm, presented by Liu et al. (2016), predefines anchor boxes and feature maps, and achieves 76.8% mAP on VOC dataset (Everingham et al., 2015). RetinaNet, proposed by Lin et al. (2017b), uses a focal loss function that puts more weight on rare training samples and yields 37.8% average precision (AP) on COCO dataset (Lin et al., 2014). As listed in Table 1, there is a tradeoff between detection accuracy and speed. For example, YOLO v2 can achieve a speed of 40 frames per second (FPS) which is faster than typical video frame rate (i.e., 30 PFS). In comparison, RetinaNet processes images at 5.81 FPS, but achieves 16.2% higher accuracy.

Table 1: Speed and accuracy comparison among CNN models (Lin et al., 2017b).

CNN architecture	COCO-AP (%)	FPS
YOLOv2 (Redmon and Farhadi, 2017)	21.6	40.00
SSD321 (Liu et al., 2016)	28.0	16.39
R-FCN (Dai et al., 2016)	29.9	11.76
DSSD513 (Liu et al., 2016)	33.2	13.70
FPN FRCN (Lin et al., 2017a)	36.2	6.41
RetinaNet-101-800 (Lin et al., 2017b)	37.8	5.81

3. Methodology

3.1 Problem Statement

The 2017 U.S. hurricane season caused a staggering $125 billion in damages (Benfield, 2018) from hurricanes Harvey, Maria, Irma, and other named storms. With sea temperatures on the rise, it is expected that more water-related disasters will strike coastal communities around the world every year (Trenberth et al., 2018). In this research, crowdsourced drone videos (from YouTube) capturing the aftermath of hurricanes are annotated with multiple class labels (i.e., flooded area, building roofs, car, debris, vegetation) to enable the detection of ToIs, listed in Table 2). These class labels are chosen for their value to disaster response. For instance, mapping flooded areas helps first responders in wayfinding, search and rescue, and evacuation planning. Over time, these fine-grained flood maps will be instrumental for flood map assessment by showing how floodwaters move and which downstream neighborhoods are more prone to flood damage. In this paper, two experiments are conducted to test the performance of trained CNN models and mapping technique.

Table 2: Disaster-related ToIs and applications

ToI	Potential application
Flooded area	Rescue planning, resource deployment, wayfinding, storm surge mapping, aid delivery, flood plan improvement, public education
Undamaged roof	Damage information map, insurance claims, mapping reference points
Damaged roof	Rescue, damage information map, insurance claims, construction repair, debris removal
Car	Rescue, insurance claims
Debris	Clean-up, damage information map, construction repair, rescue
Vegetation	Clean-up, public education

3.2 Model Architecture, Training, and Deployment

For ToI detection from drone footage, a CNN architecture trained on an in-house experimental dataset is used. Given speed and accuracy tradeoff (Table 1), and considering that the ultimate goal of this work is to equip drone with onboard capability for real-time image processing and situational awareness, YOLO v2 (Redmon and Farhadi, 2017) is selected as an ideal CNN candidate. Similar to other CNN models, YOLO v2 takes the RGB values of an image (in form of a matrix) and outputs the class labels of ToIs and their pixel coordinates. As shown in Figure 1, there are 23 linked layers in this architecture including convolutional and max-pooling layers. Each layer computes its input and feeds into the next layer. A max-pooling layer selects the maximum value from boxes that scan the entire input with a stride, and then combines the maximum values to form the output. As a result, max-pooling downsizes the input while preserving the representative features. On the other hand, convolutional layer applies a kernel i.e., matrix with weights ($w_1, w_2, \ldots, w_n$), on the input to extract features (e.g., color and shape). With multiple kernels, a convolutional layer outputs a denser layer. Altogether, YOLO v2 takes an image divided into a 13×13 grid (each grid predicts 5 anchor boxes), and outputs a multidimensional matrix that describes the predictions. For each prediction, the output contains X- and Y- pixel coordinates, width, height, confidence (likelihood that the box contains a ToI), and probability for each class. The key to achieving accurate predictions is the weights of the kernels in convolutional layers, i.e., models with optimum weights yielding precise predictions. The process of obtaining the optimum weights is referred to as model training (LeCun et al., 1998). During training, randomly initialized weights are updated by feeding the model with the input (images) and annotated output (class labels and pixel coordinates). Weights that lead to wrong predictions are penalized while those leading to correct predictions are rewarded. Eventually, optimized weights are used in the trained model. The trained model is then tested on unseen images and predictions (class labels and pixel coordinates) are recorded.

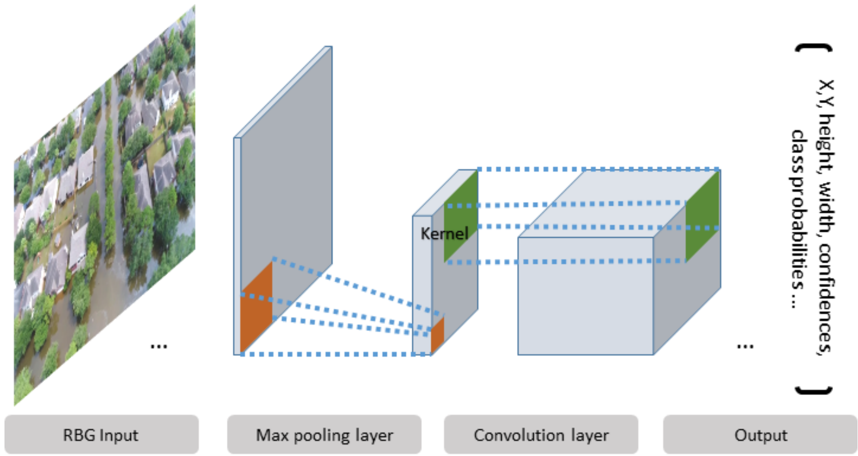

Figure 1: Schematic Representation of YOLO v2 Architecture

As shown in Figure 2, in this work, the CNN model is trained using transfer learning, i.e., pre-trained on COCO dataset followed by retraining on Volan2018, an in-house dataset of annotated hurricane footage. Transfer learning takes advantage of pre-trained weight on datasets such as COCO and VOC, which are later updated using an in-domain dataset (Oquab et al., 2014), thus leading to better predictions. The trained model is tested on unseen hurricane footage to retrieve disaster impact information.

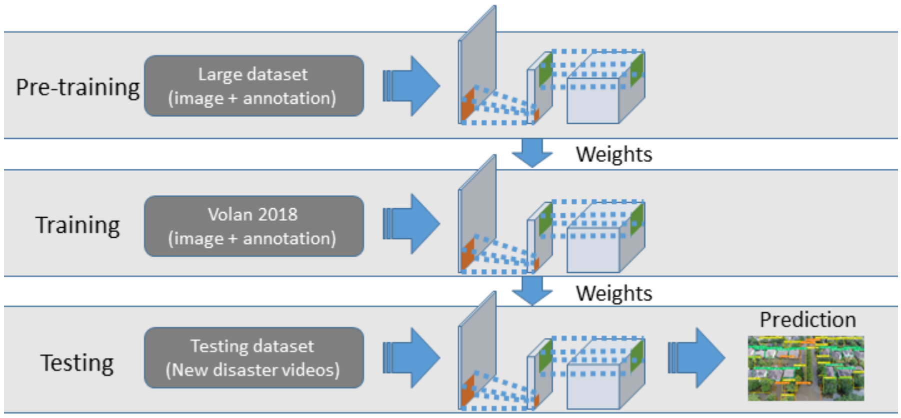

Figure 2: CNN Model Training and Deployment

3.3 Projection from the Drone's Perspective View to an Orthogonal Map

The fully trained CNN model can detect ToI classes and coordinates of pixel boxes in hurricane footages. However, detected bounding boxes cannot be readily used in mapping applications that utilize grid systems such as the universal transverse Mercator (UTM) coordinate system or the United States national grid (USNG). Since these mapping systems are widely used in disaster response and coordination, projecting the output of CNN detection from the perspective view into an orthogonal grid system is desired. This mathematical transformation can be done knowing the pixel positions (in drone's local view) of four reference points (with any three not being collinear) and their corresponding real-world positions. For pixel coordinates, with the uppermost left pixel of the image serving as the origin, rows parallel to the X-axis, and columns parallel to the Y-axis, the pixel coordinates of the centroid of the detected bounding box is determined. The real-world position of the object, on the other hand, refers to the location in the Cartesian grid system (global coordinates on Earth). Using these conventions, the goal of projection is to transform detected pixel coordinates of any ToI with class and size information onto the grid system that is independent of video properties such as camera position, viewpoint, or zoom factor in any particular frame. Figure 3 shows an example in which (x_1, y_1), (x_2, y_2), (x_3, y_3), and (x_4, y_4) are four reference points in drone view, with their corresponding real-world positions marked as (x'_1, y'_1), (x'_2, y'_2), (x'_3, y'_3), and (x'_4, y'_4) in an orthogonal map.

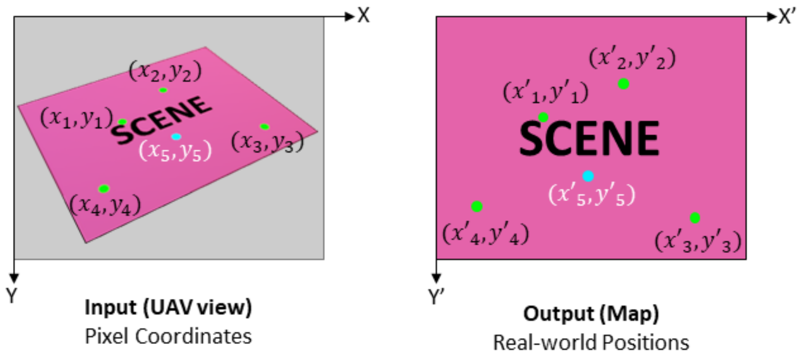

Figure 3: Perspective to Orthogonal Projection of drone's Viewpoint

From these reference points, transformation matrix $M = B.A^{-1}$ is calculated using Equations 1 through 4. Next, for any new point in the drone's perspective view, denoted by pixel coordinates (x_5, y_5), the corresponding real-world position (x'_5, y'_5) can be obtained using Equation 5, in which (x''_5, y''_5, w) is the homogenous coordinates of the ToI, i.e., $w = 0$ means that the point is at infinite distance from the camera. For reference point selection, different types of visible ground objects (e.g., landmarks, buildings, parking lots, road intersections) can be used as long as their real-world positions are known or can be extracted.

$$\begin{bmatrix} a_1 \\ a_2 \\ a_3 \end{bmatrix} = \begin{bmatrix} x_1 & x_2 & x_3 \\ y_1 & y_2 & y_3 \\ 1 & 1 & 1 \end{bmatrix}^{-1} . \begin{bmatrix} x_4 \\ y_4 \\ 1 \end{bmatrix} \tag{1}$$

$$A = \begin{bmatrix} a_1.x_1 & a_2.x_2 & a_3.x_3 \\ a_1.y_1 & a_2.y_2 & a_3.y_3 \\ a_1 & a_2 & a_3 \end{bmatrix} \tag{2}$$

$$\begin{bmatrix} b_1 \\ b_2 \\ b_3 \end{bmatrix} = \begin{bmatrix} x'_1 & x'_2 & x'_3 \\ y'_1 & y'_2 & y'_3 \\ 1 & 1 & 1 \end{bmatrix}^{-1} . \begin{bmatrix} x'_4 \\ y'_4 \\ 1 \end{bmatrix} \tag{3}$$

$$B = \begin{bmatrix} b_1.x'_1 & b_2.x'_2 & b_3.x'_3 \\ b_1.y'_1 & b_2.y'_2 & b_3.y'_3 \\ b_1 & b_2 & b_3 \end{bmatrix} \tag{4}$$

$$\begin{bmatrix} x''_5 \\ y''_5 \\ w \end{bmatrix} = M. \begin{bmatrix} x_5 \\ y_5 \\ 1 \end{bmatrix} \Rightarrow x'_5 = \frac{x''_5}{w}, y'_5 = \frac{y''_5}{w} \tag{5}$$

4. Experiment and Results

4.1 Data Collection and Description

The dataset used in this research, Volan2018, is created using web-mined videos from YouTube, and contains eight videos from four different hurricanes striking 8 different U.S. coastal regions during the 2018-2019 hurricane season (including hurricanes Harvey, Maria, Irma, and Michael), captured by drones and helicopters. These videos are extracted frame by frame, and ToIs in each frame are annotated with the classes and pixel coordinates using DarkLabel (2017). In this paper, only three of these videos (Volan1, 2, and 3) are used since they are captured by drone camera. All three videos are captured from the aftermath of hurricane Harvey in 2017, in and around Houston, Texas. The duration of these videos is 84, 72, and 1,333 seconds, for Volan1, 2, and 3 respectively. The total number of instances per ToI for each video is summarized in Table 3. Annotation is done frame by frame by drawing one bounding box covering each ToI (e.g., one car or one damaged roof). For example, the video frame presented in Figure 4 contains 4 instances of undamaged roof, and 1 instance of damaged roof, 4 instances of debris, and 3 instances of flooded area.

Table 3: Statistics of Volan2018 videos used in this study

TOI class/Video number	Volan1	Volan2	Volan3
Flooded area	1,015	1,572	38,480
Undamaged roof	1,814	1,174	37,661
Damaged roof	1,457	871	296
Car	1,046	612	24,710
Debris	2,678	1,653	0
Vegetation	123	0	38,976

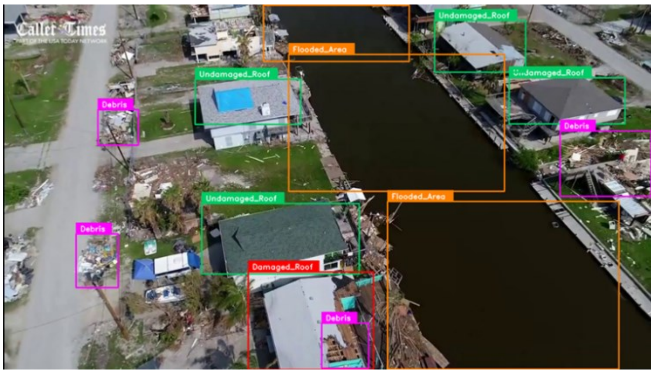

Figure 4: Annotation Example from Volan2018 Dataset

4.2 CNN Model Training and Testing

All frames in Volan1, 2 and 3 videos are combined and then split into three portions: training (60%; 34,791 frames), validation (20%; 8,258 frames), and testing (20%; 8,264 frames). At the start of training, the first 22 layers of the model are frozen, and only the last layer is trained (for 25 epochs at learning rate 10^{-3}). After unfreezing the first 22 layers, all layers are trained simultaneously (at learning rate 10^{-4}), and if loss does not drop after 3 epochs, the learning rate is reduced by half, and the process iterates. Training is terminated if the validation loss does not decrease in 10 consecutive epochs. In the example shown in Figure 5(a), several instances of vegetation, flooded area, and undamaged roof are detected, but no debris or damaged roofs are found. Each detection box is labeled with the predicted class and a confidence index. The trained CNN model is further tested to measure detection performance for each class, as well as the overall mAP. As shown in Figure 5(b), classes debris and flooded area have the highest precision of 90.27% and 86.16%, respectively, while class car achieves the lowest precision of only 45.67%. The overall mAP (for detecting all ToIs) is 74.48%.

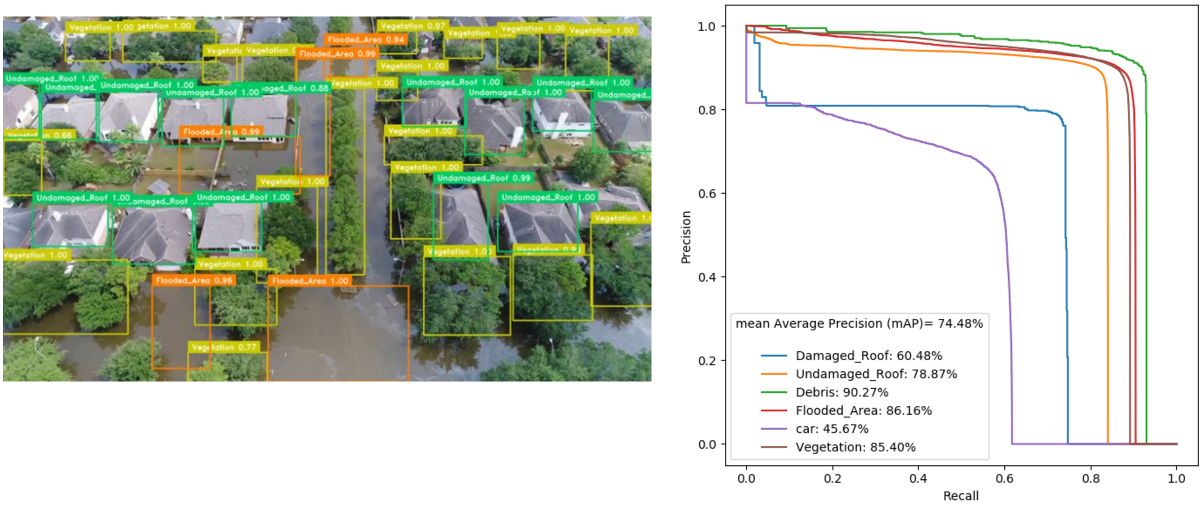

Figure 5: (a) Detection Example from Volan2018 Dataset; (b) Model Performance for All Classes

4.3 Projection Error Measurement and Results

Two example classes are used to demonstrate the technique for projecting detected ToIs on a 2D orthogonal map without reliance on drone's position information, as described in Section 3.3. Four building roofs are marked as reference points with their real-world positions obtained from Google Earth, and all other detected building roofs and two cars are projected from drone's perspective view to a 2D map following the UTM coordinate system. The input drone video (Volan3) is from Houston, TX, and covers zone 15R of the UTM system. Two example frames of this video in which detected undamaged roofs (including reference points), flooded areas, and cars are marked is shown in Figure 6. For example, for frame #12210 shown in Figure 6(a), the pixel positions of all detections and the real-world positions of reference points 1-4 are used to project all other detections in the real-word coordinate system.

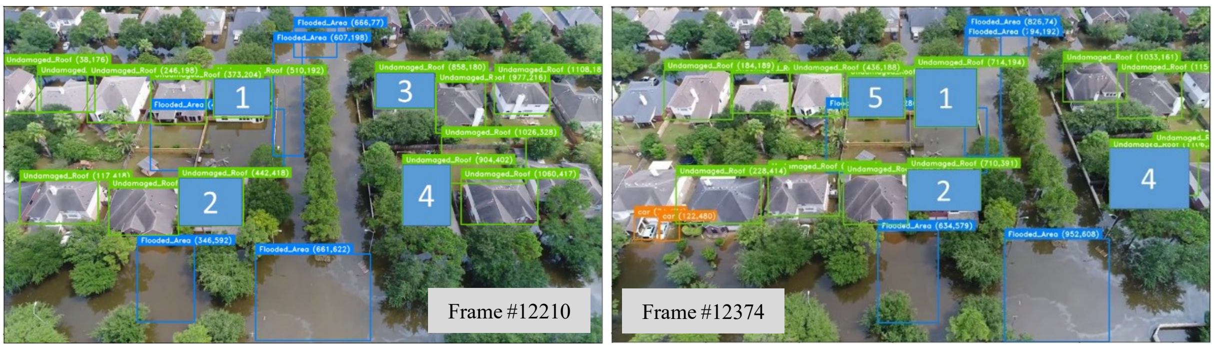

(a) (b)

Figure 6: Pixel Coordinates (Box Centroids) of Reference Points and Detected ToIs in Two Frames

In Figure 7(a), these four points are marked with numbered circles, and all other detected undamaged roofs are marked with rectangles numbered 5-14. Real-world positions of these undamaged roofs serve as ground truth to measure the projection error. Figure 7(b) shows the frame projection on UTM system. For each instance of undamaged roof, the Euclidean distance between the ground truth and projected positions is defined as error. The frame-level projection error is calculated by Equation 7, in which n is the total number of detected ToIs in that frame.

$$frame\ error = \frac{1}{n} \cdot \sum_{i=1}^{n} error_i \tag{7}$$

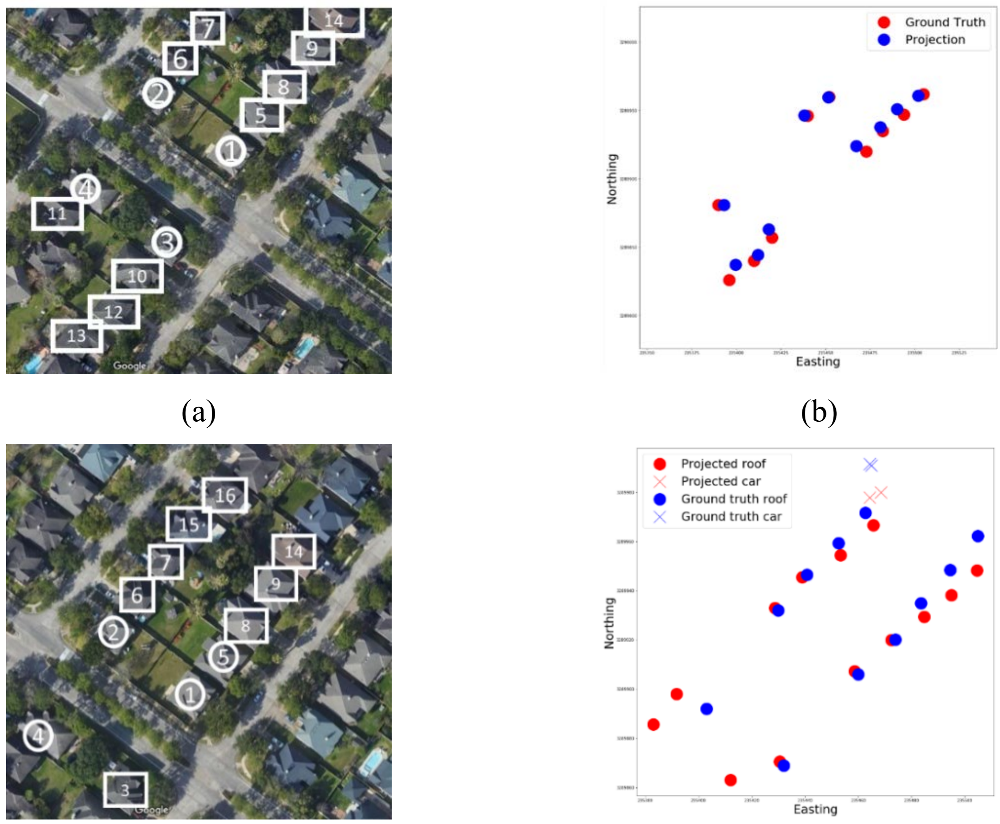

(a) (b)

(c) (d)

Figure 7: Real-World Positions of ToIs on Google Earth (left), and Projection Errors (right)

Projecting undamaged roofs in a 1-second long segment between frames #12210 and #12240 (drone moving to the left in 30 consecutive frames) of Volan3 video yields a frame error of 7.18 meters. Considering the size of the visible area by the drone in the frame (173.95×130.53 m^2), this projection error translates to approximately 5%, indicating the high accuracy of the designed technique for transforming perspective drone views to orthogonal maps. As shown in Figure 6(b), two car instances are additionally detected in frame #12374 of Volan3 video, which are also projected along with building roofs, as shown in Figures 7(c) and 7(d). In this projection, detected roofs 1, 2, 4, and 5 are selected as reference points, yielding a 7.79-meter (or 5%) frame error considering both classes. It must be noted that the change of viewpoint (as a result of drone moving in the scene) may cause any or all of reference points (i.e., building roofs) in one frame to fall out of sight, in which case, new reference points are needed to have an uninterrupted projection. For instance, comparing Figures 7(a) and 7(c), reference point 3 is replaced with a new reference point 5, using an ad-hoc reference point tracking and selection. A description of this process, however, is outside the scope of this paper.

5. Conclusion and Discussion

This research demonstrated the capability of using CNN models (trained on disaster footage) and viewpoint transformation to detect ToIs in drone-captured perspective views and project them onto orthogonal maps. The need for this operation was justified through describing practical examples of how timely and reliable collection and delivery of disaster impact information could add value to disaster management. Experiments were conducted to demonstrate the process of disaster-related ToI detection and projection, and measure performance. Results indicated that the model trained on an in-house dataset, Volan2018, could successfully detect several ToI classes (flooded areas, damaged and undamaged roofs, cars, debris, vegetation) from drone-mounted RGB cameras with an mAP of %74.48. Furthermore, as a proof-of-concept experiment for viewpoint transformation based on the real-world positions of four reference points on the ground was conducted on two classes, and an average error of ~5% was achieved, demonstrating the robustness of the method in processing drone videos for geocoded mapping of disaster footage with limited reliance on GPS information. Beyond the immediate application domain described in this paper, the developed GPS-free projection technique can be extended to other applications that require simultaneous localization and mapping (SLAM) using existing (natural or manmade) landmarks and reference points. Examples include construction robotics, traffic management, agriculture and forestry, and marine research. Future research will also enable the ad-hoc selection of projection reference points with less reliance on prior knowledge. Another direction of future work will be to perform ToI detection and mapping beyond hurricane footage, by training and testing CNN models on other types of natural disasters such as earthquakes and wildfires.

Acknowledgments

Model training was performed on Texas A&M University's High Performance Research Computing (HPRC) clusters. Any opinions, findings, conclusions, and recommendations expressed in this paper are those of the authors and do not represent those of the HPRC.

References

Adams, S.M., Friedland, C.J. (2011). A survey of unmanned aerial vehicle (UAV) usage for imagery collection in disaster research and management. In: 9th International Workshop on Remote Sensing for Disaster Response, 2011, Stanford, CA, pp. 15–16.

Baker, C.A.B., Ramchurn, S., Teacy, W.T., Jennings, N.R. (2016). Planning search and rescue missions for UAV teams. In: Twenty-second European Conference on Artificial Intelligence, 2016, Netherlands.

Benfield, A. (2018). Weather, Climate and Catastrophe Insight: 2017 Annual Report. Aon Rep. GDM05083, p. 56.

Craglia, M., Ostermann, F., Spinsanti, L. (2012). Digital Earth from vision to practice: making sense of citizen-generated content, International Journal of Digital Earth 5(5), pp. 398–416.

Dai, J., Li, Y., He, K., Sun, J. (2016). R-FCN: object detection via region-based fully convolutional networks. In: Advances in Neural Information Processing Systems, 2016, Barcelona, Spain, pp. 379–387.

DarkLabel (2017). Image Labeling and Annotation Tool, https://darkpgmr.tistory.com/16, accessed January 2020.

Everingham, M., Van Gool, L., Williams, C.K.I., Winn, J., Zisserman, A. (2015). The pascal visual object classes challenge: a retrospective., International Journal of Computer Vision 111(1), pp. 98–136.

Faxi, Y., Rui, L., Ouejdane, M. (2017). An information system for real-time critical infrastructure damage assessment based on crowdsourcing method: a case study in Fort McMurray. In: International Conference on Sustainable Infrastructure, 2017, New York City, NY.

Federal Aviation Administration (2018). Fact Sheet – Federal Aviation Administration (FAA) Forecast Fiscal Years (FY) 2017-2038, https://www.faa.gov/news/fact_sheets/news_story.cfm?newsId=22594, accessed January 2020.

Federal Emergency Management Agency (2016). Damage Assessment Operations Manual, https://www.fema.gov/media-library-data/1459972926996-a31eb90a2741e86699ef34ce2069663a/PDAManualFinal6.pdf, accessed January 2020.

Girshick, R. (2015). Fast R-CNN. In: IEEE International Conference on Computer Vision, 2015, Boston, MA, pp. 1440-1448.

Girshick, R., Donahue, J., Darrell, T., Malik, J. (2014). Rich feature hierarchies for accurate object detection and semantic segmentation. In: IEEE Conference on Computer Vision and Pattern Recognition, 2014, Columbus, OH, pp. 580–587.

Guha-Sapir, D., Lechat, M.F. (1986). Information systems and needs assessment in natural disasters: an approach for better disaster relief management, Disasters 10(3), pp. 232–237.

Han, S., Shen, W., Liu, Z. (2012). Deep Drone: object detection and tracking for smart drones on embedded system, Stanford University.

Haworth, B., Bruce, E. (2015). A review of volunteered geographic information for disaster management, Geography Compass 9(5), pp. 237–250.

Henriques, J.F., Caseiro, R., Martins, P., Batista, J. (2014). High-speed tracking with kernelized correlation filters, IEEE Transactions on Pattern Analysis and Machine Intelligence 37(3), pp. 583–596.

Kim, J., Hastak, M. (2018). Social network analysis: characteristics of online social networks after a disaster, International Journal of Information Management 38(1), pp. 86–96.

LeCun, Y., Bottou, L., Bengio, Y., Haffner, P. (1998). Gradient-based learning applied to document recognition, Proceedings of the IEEE 86(11), pp. 2278–2324.

Lin, T.Y., Dollár, P., Girshick, R., He, K., Hariharan, B., Belongie, S. (2017). Feature pyramid networks for object detection. In: IEEE Conference on Computer Vision and Pattern Recognition, 2017, Honolulu, HI.

Lin, T.Y., Goyal, P., Girshick, R., He, K., Dollár, P. (2017). Focal loss for dense object detection. In: IEEE International Conference on Computer Vision, 2017, Venice, Italy, pp. 2980–2988.

Lin, T.Y., Maire, M., Belongie, S., Hays, J., Perona, P., Ramanan, D., Dollár, P., Zitnick, C.L. (2014). Microsoft COCO: common objects in context. In: European Conference on Computer Vision, 2014, Zurich, Switzerland.

Liu, W., Anguelov, D., Erhan, D., Szegedy, C., Reed, S., Fu, C.Y., Berg, A.C. (2016). SSD: single shot multibox detector. In: European Conference on Computer Vision, 2016, Amsterdam, Netherlands.

Oquab, M., Bottou, L., Laptev, I., Sivic, J. (2014). Learning and transferring mid-level image representations using convolutional neural networks. In: IEEE Conference on Computer Vision and Pattern Recognition, 2014, Columbus, OH.

Radovic, M., Adarkwa, O., Wang, Q. (2017). Object recognition in aerial images using convolutional neural networks, Journal of Imaging 3(2), p. 21.

Redmon, J., Divvala, S., Girshick, R., Farhadi, A. (2016). You only look once: unified, real-time object detection. In: IEEE Conference on Computer Vision and Pattern Recognition, 2016, Las Vegas, NV.

Redmon, J., Farhadi, A. (2017). YOLO9000: better, faster, stronger. In: IEEE Conference on Computer Vision and Pattern Recognition, 2017, Columbus, OH.

Trenberth, K.E., Cheng, L., Jacobs, P., Zhang, Y., Fasullo, J. (2018). Hurricane Harvey links to ocean heat content and climate change adaptation, Earth's Future 6(5), pp. 730–744.

United Nations Office for Disaster Risk Reduction (2019). Economic and Human Impacts of Disasters, https://www.unisdr.org/we/inform/disaster-statistics, accessed January 2020.

Modeling Geometry and Semantics of Physical Damages using IFC

Mathias Artus, Christian Koch
Bauhaus-Universität Weimar, Germany
mathias.artus@uni-weimar.de

Abstract. Germany invests more than 12 billion Euros in the rail infrastructure in 2020. Beside others, bridges and stations have to be rehabilitated. Several inspections and maintenance actions take place within these processes during which different actors collect, digitize and exchange bridge and damage information. Currently, inspection and maintenance practice relies on paper based data collection and exchange, which is time consuming and error prone. A way of storing and exchanging damage data in a digital format would lower the costs as well as support future needs, e.g. automated maintenance planning, structural integrity analysis and mixed reality inspections. A majority of damages are physical damages, like cracks and spalling. This paper presents two different approaches to model physical damages using the Industry Foundation Classes (IFC). Finally, the modelling concepts are tested with multiple BIM applications. Although the tests show that IFC is capable of modeling physical damages, current software tools do not support IFC up to its full potential.

An Experimental Study of Wearable Technology and Immersive Virtual Reality for Drone Operator Training

Md Nazmus Sakib, Theodora Chaspari, Changbum R. Ahn, Amir H. Behzadan
Texas A&M University, USA
abehzadan@tamu.edu

Abstract. Unmanned aerial vehicles (UAVs) are increasingly being used in construction and heavy civil projects in tasks such as surveying and mapping, safety and progress monitoring, and site surveillance. Flying a drone, however, requires the operator to maintain his or her body posture for an extended time while holding the controller and looking up to monitor drone movements, causing awkward body postures, stress, and fatigue. When coupled with the mental workload as a result of delegated tasks, this could potentially put the drone mission, people, and property in jeopardy. In this study, an analysis of drone operator's physiological data collected by wearable devices at the time of virtual reality (VR) training and during real-world deployment is performed. The goal of this research is to provide a basis for understanding the effectiveness of VR training by verifying if similar task complexity in VR and real-world experiments results in similar patterns in drone operator's performance, mental workload, and stress.

1. Introduction

The use of unmanned aerial vehicles (UAVs) to support tasks such as surveying and mapping, safety and progress monitoring, traffic management, and site surveillance is on the rise, and by some estimates, there will be more than 3 million drones in the U.S. by 2020 (Federal Aviation Administration, 2018). Drone data collection has also become a standard component in defense, agriculture, archaeology, entertainment, and sports applications. Current laws and regulations mandate a clear line of sight between the drone and the operator at all times, and prohibit flying drones over people, to ensure safety and eliminate potential injuries or damages. Drone pilots must always be cognizant of their surroundings and constantly maintain full situational awareness. Flying a drone, however, requires the operator to maintain his or her body posture for an extended time while looking up to monitor drone movements, causing awkward body postures, stress, and fatigue. When coupled with the mental load as a result of delegated tasks, this could potentially put the drone mission, people, and property in jeopardy. Proper training in virtual reality (VR) simulation could eliminate some of these problems by exposing drone operators to situations and tasks they may encounter in the real-world. Past research suggests that a trainee's performance in a VR environment is correlated with how immersive or realistic the experience feels. However, in the area of drone pilot training, there has been few studies investigating the influence of VR environments on the effectiveness of the training experiment. Existing work mainly uses retrospective self-reports or observational coding to assess the effectiveness of VR training. In this research, the goal is to analyze drone operator's physiological data collected by wearable devices at the time of VR training and during real-world deployment. This analysis enables a more objective comparison of how VR training resembles real-world situations. We present a methodology for collecting, annotating, and assessing drone operator's physiological data using wearable devices to determine and compare physiological states that can potentially lead to operator's errors. Different levels of task complexity are simulated in VR and replicated in an outdoor (OD) environment to analyze variations in physiological readings. Machine learning models for predicting mental workload, performance, and stress are also trained and tested on extracted physiological features and self-report data.

2. Literature Review

With the increase in the use of drones, it is expected that the number of drone-related incidents will be on the rise. Operating a drone is a demanding and stressful task, and may cause muscular fatigue by inducing mental fatigue, thus negatively affecting performance. To date, the majority of drone accidents are attributed to human error (Israel and Nesbit, 2004). Previous work has shown that proper training can be a good way to understand and improve drone operator's performance in certain tasks (Khuwaja et al., 2018). Training drone operators in the real-world, however, may pose certain logistical and safety challenges. In recent years, immersive VR or augmented reality (AR) environments have been designed for different professional training and exercise (Eller et al., 2018; Li et al., 2018; Pereira et al., 2018; Postal et al., 2016; De Winter et al., 2012). A drone operator's physiological and mental state is a very important factor in understanding his or her flight performance. To our best knowledge, existing methods of quantifying operator's skill and performance are mostly based on self-reports or third-party observations (Zhang et al., 2002). There is also a limited body of work on qualitative (thematic) analysis for evaluating human performance in drone operations based on self-reports and task completion (Kim and Irizarry, 2019).

New wearable devices and smart technologies have facilitated the collection of human vital signs such as heart rate (HR), heart rate variability (HRV), breathing rate, inter-beat interval (IBI), and electrodermal activity (EDA) in a host of applications (Acharya et al., 2004; Dawson et al., 2000; Hjortskov et al., 2004; Kantor et al., 2001; Thayer et al., 2010). HRV and HR are good physiological indices for multidimensional analysis of human body (Kantor et al., 2001). HR can be affected by ambient factors such as noise, increase in physical activity, and stress (Taelman et al., 2009). Electrodermal activity (EDA) and skin temperature have been also found to be related with emotional state (Kim et al., 2004; Yadav et al., 2019). EDA has been closely linked with emotional arousal (Dawson et al., 2000). Past work has cited skin conductance level (SCL) and skin conductance response (SCR) readings as distinctive EDA features for detecting stress and cognitive load resulting from a stimuli (Fowles et al., 1981).

In this study, we utilize non-intrusive means of collecting physiological data to understand and predict drone operator's mental workload (related to physical effort), stress (related to emotional arousal) and performance (related to task completion). We have previously used physiological data to understand mental stress in a public speaking task (Sakib et al., 2019; Yadav et al., 2019), and explored the effectiveness of VR drone training by comparing participant's physiological indices and self-reported feedback (Sakib, 2019). Through comparing drone operator's performance in VR and OD environments, it is possible to determine whether results obtained in VR training are representative of the expected outcome in the real-world. High levels of immersion can cause an increased sense of presence, or a more realistic experience, which can make VR training more effective (Bowman and McMahan, 2007). To our best knowledge, there has been no systematic study on the use of participants' physiological data to evaluate the effectiveness of VR training for drone operators and predict their real-world drone flying performance.

3. Study Design and Data Description

As shown in Figure 1, a VR drone flying environment was developed in Unity (Unity, 2019) which resembles an outdoor courtyard where real-world drone flights took place. A total of 25 participants (19 males, 6 females) of 25-30 years of age participated in data collection, which was divided into two sessions: outdoor (OD) and virtual reality (VR). Each session consisted of two tasks, tagged as easy and complex. The order of sessions was randomly selected for each participant; 10 performed the VR session first and 15 performed the OD session first. At the conclusion of the study, a post-experiment survey was distributed to collect feedback from participants on how the two sessions compared.

Figure 1: Flying a Drone in easy (top) and complex (bottom) tasks in OD (left) and VR (right).

The data collection protocol is summarized in Figure 2. Three types of data were collected in each session, including physiological data, self-reports, and observer feedback.

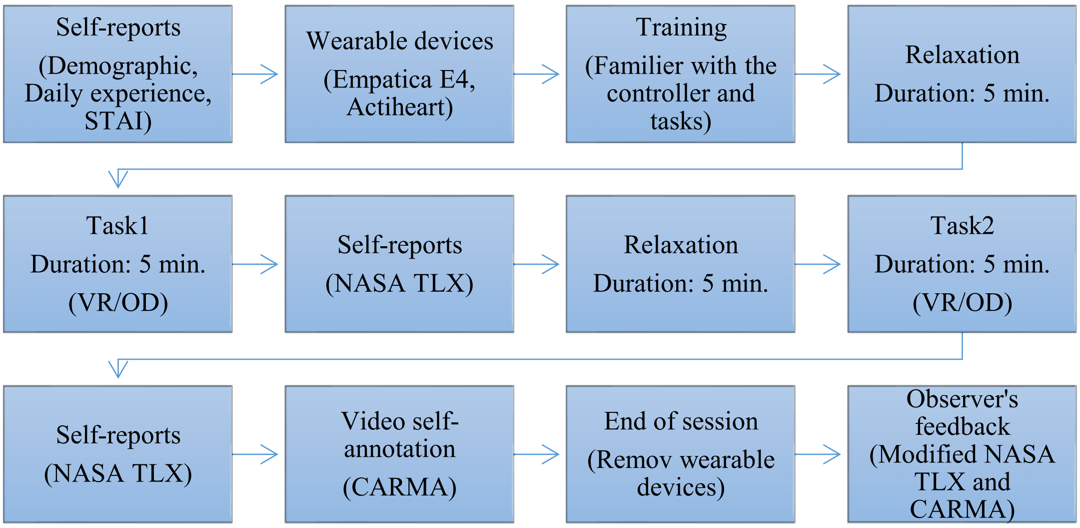

Figure 2: Data collection protocol.

Several self-reports were used to collect responses from each participant. At the start of the first session (VR or OD), each participant filled out daily experience and demographic data forms. At the start of the second session (OD or VR), each participant filled out only the daily experience form. In addition, the State-Trait Anxiety Inventory (STAI) form was filled out in both sessions to report participant's trait and state anxiety (Spielberger, 2010). Sessions started with a brief training during which instructions were provided about the tasks and basics of drone navigation, and the participant flew the drone for 5 minutes. This was followed by a 5-minute relaxation period (during which, a calm video was played to the participant while s/he was sitting in a natural position) to capture participant's baseline physiological data. Next, the participant was asked to fly a drone along a path and perform certain flight actions (e.g., maneuvering between obstacles, turning in various directions). These actions were designed considering basic cognitive skills and abilities required for drone flight and navigation, as well as take-off and landing (Howse, 2011). At the conclusion of each task (easy or complex), participants filled out a NASA task load index (NASA TLX) to report their mental, physical, and temporal demands, as well as effort and performance in each task (Hart, 2006). To understand the mental/physical state of the participants more precisely, an open-source self-feedback software called CARMA is used (Girard, 2014). In addition, observer feedback is obtained by displaying the recorded video of each session to a third-party observer who then filled out a modified version of NASA TLX and logged perceived stress scores in the CARMA system for each participant.

4. Methodology

In order to investigate whether operator's state (performance, stress, mental workload) can be quantified using physiological markers, and if the state obtained in VR can help predict the state in OD, a process established in our previous work is followed. Physiological data segmentation is performed in MATLAB and Python (Sakib, 2019; Yadav et al., 2019).

4.1 Feature Extraction from Physiological data

In this study, Emaptica E4 (Empatica Inc., 2019), and Actiheart 5 (CamNtech Ltd, 2019) wearable devices are used to collect physiological data. Empatica E4 records EDA, HR, Skin temperature, and BVP. Actiheart 5 captures ECG, IBI, HR, Tri-axial acceleration, and HRV.

From Empatica E4, four physiological data, namely EDA, BVP, HR, and skin temperature are used, and significant features are extracted. Collected data is first segmented into four sections (i.e., Relax 1, Task 1, Relax 2, and Task 2). Each data block is about 5 minutes long, which is subsequently converted to 20-second segments. Features extracted from EDA data are mean SCL, and SCR amplitude and frequency (Sakib, 2019; Yadav et al., 2018). Raw data is checked for missing values. Since data missing rate of 15%-20% is common in physiological data collection (Enders, 2003), participants with more than 20% missing values are removed from further analysis. For participants with less than 20% missing values, all missing, and outlier values are replaced using linear interpolation. For outliers, median and quartile range (10~90 percentile) are used because these statistics are less sensitive to outlier values than standard deviation (Kwak and Kim, 2017). Figure 3 shows the results of EDA data interpolation. SCR amplitude and frequency are calculated by first smoothing the raw skin conductance data using a window size 4 and a threshold value of 0.002 μS. The choice of a lower threshold value is due in part to the fact that the controlled environment in VR session reduced the effect of sweat-based EDA. Also, window size and threshold were selected to yield the fewest NaN (Not a Number) extracted features and avoid peaks due to noise (Benedek and Kaernbach, 2010).

From Actiheart, HR and ECG data are collected, and a total of 30 features are extracted by R-peak detection (Papakonstantinou et al., 1986; Papakonstantinou and Gritzali, 1981; Trahanias and Skordalakis, 1990) in BioSPPy toolbox (Carreiras et al., 2015). Examples of these features are root mean square of successive differences (RMSSD) of R-R intervals, low-frequency (LF) and high-frequency (HF) energy of the ECG, and low-to-high frequency (LF:HF) ratio. To calculate mean HR, raw data is segmented, and missing or outlier values are linearly interpolated. For participants with >20% missing HR values, these values are either replaced with mean HR readings obtained from the Empatica E4, or removed from analysis if it is determined that a loose connection may have affected other physiological signals as well.

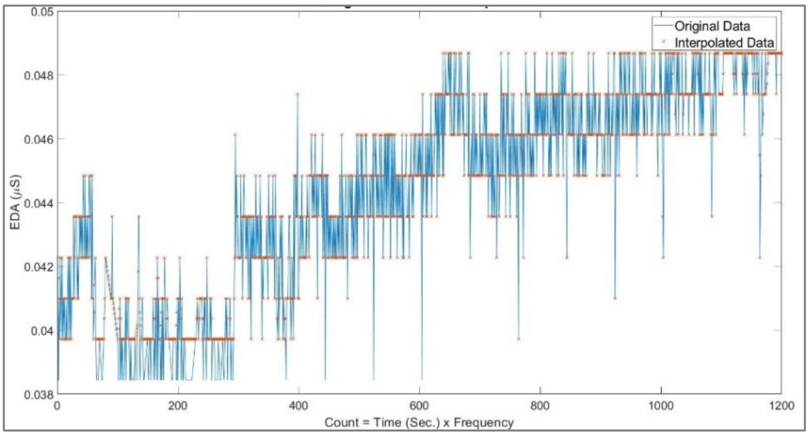

Figure 3: Sample interpolation of missing and outlier values

4.2 Feature Extraction from Self-Reports

Mental workload (MWL), stress level, trait and state anxiety, and demographic and daily experience data are reported by each participant. NASA TLX, which is a multidimensional scale of six metrics that together describe one's workload after a task, is used to estimate MWL. Participants filled out a NASA TLX form after each task. Results were converted to MWL by multiplying the raw score of each scale with the number of times the associated workload factor was chosen in a paired-choice task, and dividing by the sum of all weights (Hart, 2006). The CARMA software (Girard, 2014) is used to log the instantaneous stress experienced by participants in each task, at a 30Hz sampling rate. Stress level is measured from 1 (no stress) to 5 (high stress), and the overall stress is defined as the mean of all stress values recorded in each task. STAI is administered at the start of each session to capture participant's trait and state anxiety (Spielberger, 2010), and the sum of all scores is taken as a feature. From demographic data, only the first session type (either VR or OD) and participant's gender is used as features, since other demographic factors do not appear to be distinctive given the outcome of interest. From daily experience data, sleep time and caffeine intake are selected as features for analysis.

4.3 Performance Measurement

Time of completion and number of collisions are used to measure task performance, calculated as the average time to complete one loop, including the time lost due to collision (i.e., penalty). Therefore, a longer completion time corresponds to a lower performance, and vice versa.

5. Results

5.1 Features from Empatica E4

Box plots of mean SCL, SCR Amplitude and Frequency, and mean Skin temperature are plotted in Figure 4, which shows that for all four features, values obtained in OD have larger range than those obtained in VR. This can be explained considering that the VR session was performed in a controlled (ventilated) setting, resulting in less variations in Empatica E4 readings. Table 1 shows the results of a paired two sample for means t-test performed between VR and OD sessions. As shown in this Table, comparing OD and VR sessions, only mean SCL and mean skin temperature show significant differences ($p<\alpha=0.05$). However, the difference in skin temperature is mainly due to the controlled VR environment, and mean SCL correlates with sweating, which also depends on the surrounding environment.

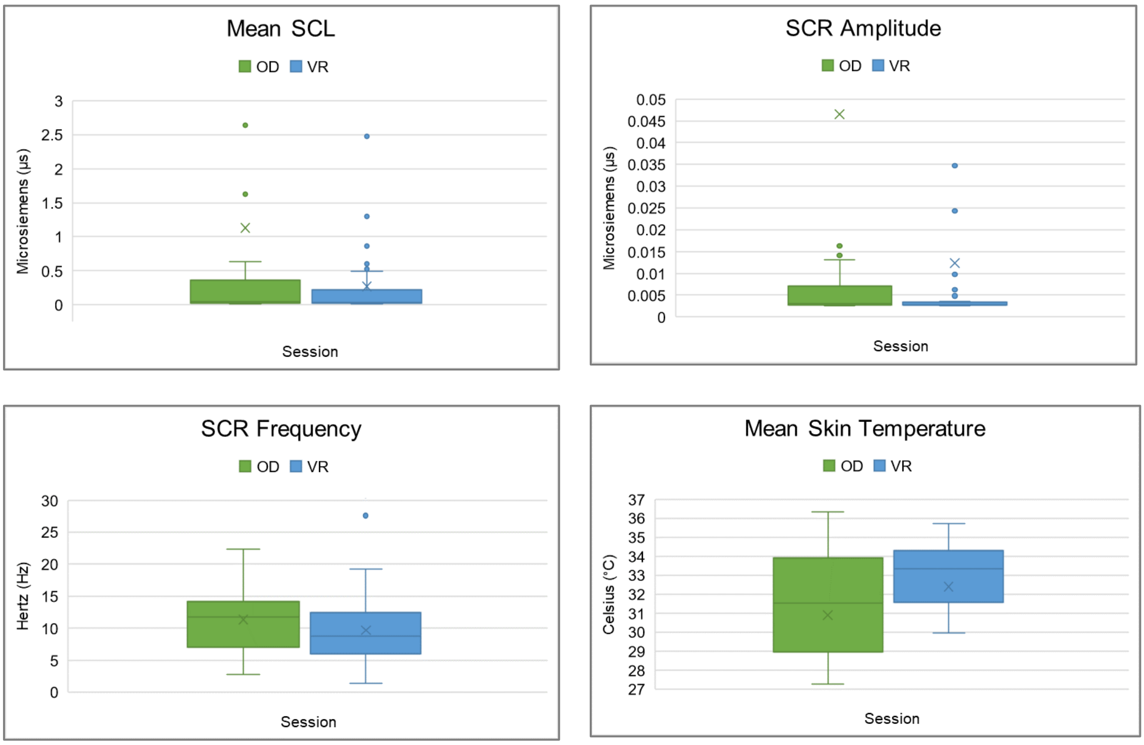

Figure 4: Box plot of extracted features from Empatica E4.

Table 1: T-test: paired two sample for means for Empatica E4 features.

Features	OD (Mean, SD)	VR (Mean, SD)	*t*(df)	*P*(*T*<=*t*)
Mean SCL	(1.103, 2.638)	(0.265, 0.529)	*t*(49)=2.01	0.036*
SCR Amplitude	(0.045, 0.134)	(0.012, 0.035)	*t*(49)=2.01	0.106
SCR Frequency	(11.491, 4.413)	(9.782, 5.757)	*t*(49)=2.01	0.137
Mean Skin Temperature	(31.467, 2.709)	(33.014, 1.604)	*t*(49)=2.01	0.001*
				*: p<0.05, significant

5.2 Features from Actiheart

A box plot of mean HR is plotted in Figure 5, where both VR and OD sessions seem to create a similar range of values. Results of a paired two sample for means t-test performed between VR and OD sessions show no significance difference ($t(49)$=2.01, p=0.43) in mean HR between OD (M=78.99, SD=11.78) and VR (M=78.01, SD=10.31) sessions. Although RMSSD shows some significant differences ($t(49)$=2.01, p=0.001) between OD (M=214.19, SD=135) and VR (M=63.94, SD=126.54), which could be attributed to environmental (e.g., wind, temperature) effect on the participants, which is also confirmed by post-experiment survey.

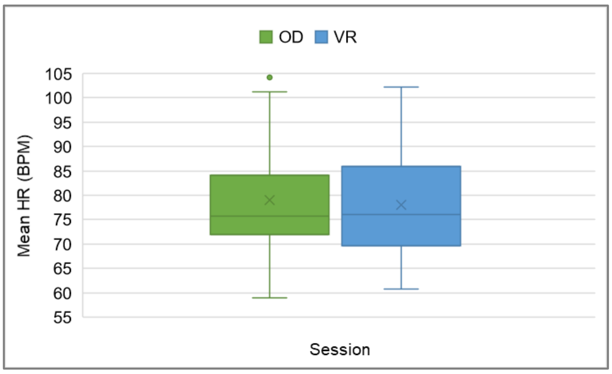

Figure 5: Box plot of mean HR

5.3 Features from Self-Reports and Observations

Figure 6 show that participants who performed the VR session first experienced a lower mean MWL in outdoor than those directly participating in the outdoor session (without VR training). Also, Table 2 shows the results of a paired two sample for means t-test performed between VR and OD sessions for STAI, stress level, MWL, and Performance. As evidenced by these results, comparing OD and VR sessions, only MWL shows a significant difference ($p<\alpha=0.05$).

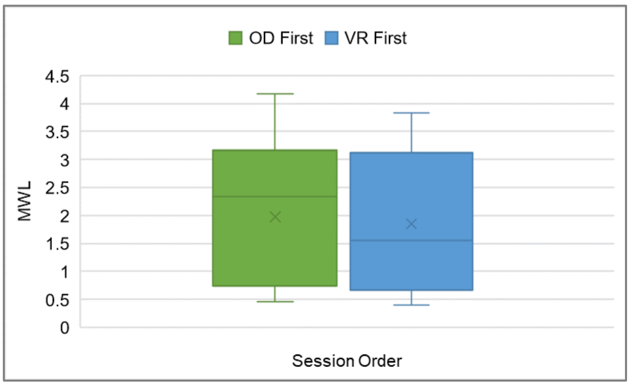

Figure 6: Box plot of MWL as per session order

Table 2: T-test: paired two sample for means for STAI, stress level, MWL and, performance.

Features	OD (Mean, SD)	VR (Mean, SD)	*t*(df)	*P*(*T*<=*t*)
STAI	(49.42, 5.51)	(50.67, 5.49)	$t(49)=2.01$	0.06
Stress Level	(1.70, 0.98)	(1.64, 1.07)	$t(49)=2.01$	0.69
MWL	(1.89, 1.22)	(2.39, 0.86)	$t(49)=2.01$	0.002*
Performance	(1.79, 1.35)	(1.84, 2.01)	$t(49)=2.01$	0.86
				*: $p<0.05$, significant

6. Predicting Real-World Outcomes from VR Data

Further analysis is performed to predict performance, stress, and MWL from physiological and self-reported features. A machine learning model is developed using all 44 (physiological and self-reported) features obtained from all participants in both VR and OD sessions. Participants with missing data are removed from both training and testing datasets. Taking all data from the VR session only, a regression analysis is performed with 5-fold cross-validation to find the best model type using principal component analysis (PCA) with 95% explained variance (Ballabio, 2015). Results show that decision tree (DT) has the lowest root mean square error (RMSE) of 0.88005 in predicting performance, while support vector machine (SVM) has the lowest RMSE of 1.1109 and 0.87984 in predicting stress and MWL, respectively. The models are then trained with VR data and tested on OD data to predict performance, stress, and MWL. Prediction values are converted from the continuous scale to a 5-class scale, as listed in Table 3. According to the summary of results in Table 4, when tested on the OD data, an accurate prediction of performance, stress, and MWL class is made in 21, 24, and 9 cases, respectively.

Table 3: Range of values for performance, stress, and MWL.

Level	Performance	Stress	MWL
Low	4-5	0-1	1.0-1.8
Medium Low	3-4	1-2	1.8-2.6
Medium	2-3	2-3	2.6-3.4
Medium High	1-2	3-4	3.4-4.2
High	0-1	4-5	4.2-5.0

Table 4: Class prediction error.

Prediction Type	Prediction Model	Class Prediction Error				Total Cases
		±0 Class	±1 Class	±2 Class	±3 Class	
Performance	DT	21	20	6	0	47
Stress	SVM	24	19	2	2	47
MWL	SVM	9	18	20	0	47

7. Conclusion and Future Work

This study provided quantifiable evidence, based upon physiological data collected by wearable devices, that immersive VR training can be a viable proxy for training drone operators in the real-world. Results of the statistical analysis conducted on different physiological data and self-repots reveals that in most cases, no significant differences are found between VR and OD sessions. For instance, at 95% (α=0.05) confidence, no significant difference was found in stress levels between OD and VR sessions. Also, statistical analysis proves that immersiveness in VR creates a physiological footprint on participants similar to that of OD. At 95% (α=0.05) confidence, no difference was found in mean HR and in performance between OD and VR sessions. The significant difference found in mean SCL and mean skin temperature is mainly due to the controlled environment of the VR experiment. Furthermore, machine learning models developed using all physiological features and self-reported data from VR sessions and tested on OD data can predict the correct performance, stress, and MWL level ±1 class in 87%, 91%, and 57% of cases, respectively. It is thus fair to conclude that immersive VR can be a suitable alternative for training and reskilling drone operators, and predicting human outcomes in real-world flying conditions. This important finding paves the way for future research on VR training systems where access to real-world sites is expensive or impossible (e.g., remote locations), the cost of making mistakes during training is high (e.g., drone breakdown), or mistakes could lead to life-threatening situations (e.g., flying drones over crowds). Future work will explore an improved sense of presence by incorporating a performance reward and penalty system, and investigating the effect of wind, temperature, humidity, luminance, and background noise in the VR environment. Simulating these environmental factors can help assess operator's readiness (i.e., availability, serviceability, sustainability) to fly (Verhoeff et al., 2015).

Acknowledgments

We would like to acknowledge the support of Nipun Nath, Xin Liu, and Henry Ruiz, Ph.D. students at Texas A&M University. Some of the experiments described in this paper are conducted using an ANAFI drone that was generously provided by Parrot, Inc. We are thankful to Mr. Jerome Bouvard, Director of Strategic Partnerships at Parrot Inc. Any opinions, findings, conclusions, and recommendations expressed in this paper are those of the authors and do not necessarily represent the views of Parrot Inc., or the individuals named above.

References

Acharya, R., Kannathal, N. and Krishnan, S.M. (2004). Comprehensive analysis of cardiac health using heart rate signals. Physiological Measurement, IOP Publishing, Vol. 25 No. 5, p. 1139.

Ballabio, D. (2015). A MATLAB toolbox for Principal Component Analysis and unsupervised exploration of data structure. Chemometrics and Intelligent Laboratory Systems, Elsevier B.V., Vol. 149, pp. 1–9.

Benedek, M. and Kaernbach, C. (2010). A continuous measure of phasic electrodermal activity. Journal of Neuroscience Methods, Elsevier B.V., Vol. 190 No. 1, pp. 80–91.

Bowman, D.A. and McMahan, R.P. (2007). Virtual reality: how much immersion is enough? Computer, IEEE, Vol. 40 No. 7, pp. 36–43.

CamNtech Ltd. (2019). "CamNtech", available at: https://www.camntech.com/products/actiheart/actiheart5-overview (accessed 24 August 2019).

Carreiras, C., Alves, A.P., Lourenço, A., Canento, F., Silva, H. and Fred, A. (2018). BioSPPy: Biosignal processing in Python (2015–). BioSPPy.

Dawson, M., Shell, A. and Fillion, D. (2000). The electrodermal system. Handbook of Psychophysiology, pp. 200–223.

Eller, C., Bittner, T., Dombois, M. and Rüppel, U. (2018). Collaborative immersive planning and training scenarios in VR. In: The Workshop of the European Group for Intelligent Computing in Engineering, Springer, pp.164–185.

Empatica Inc. (2019). Real-time physiological signals: E4 EDA/GSR sensor. available at: https://www.empatica.com/research/e4/ (accessed 24 August 2019).

Enders, C.K. (2003). Using the expectation maximization algorithm to estimate coefficient alpha for scales with item-level missing data. Psychological Methods, American Psychological Association, Vol. 8 No. 3, p. 322.

Federal Aviation Administration (2018). FAA Aerospace Forecast, FY2018-38, available at:https://doi.org/10.1017/CBO9781107415324.004.

Fowles, D.C., Christie, M.J., Edelberg, R., Grings, W.W., Lykken, D.T. and Venables, P.H. (1981). Publication recommendations for electrodermal measurements. Psychophysiology, Wiley Online Library, Vol. 18 No. 3, pp.232–239.

Girard, J.M. (2014). CARMA: Software for continuous affect rating and media annotation. Journal of Open Research Software, NIH Public Access, Vol. 2 No. 1.

Hart, S.G. (2006). NASA-task load index (NASA-TLX); 20 years later. In: The Human Factors and Ergonomics Society Annual Meeting, Vol. 50, Sage publications Sage CA: Los Angeles, CA, pp.904–908.

Hjortskov, N., Rissén, D., Blangsted, A.K., Fallentin, N., Lundberg, U. and Søgaard, K. (2004). The effect of mental stress on heart rate variability and blood pressure during computer work. European Journal of Applied Physiology, Springer-Verlag, Vol. 92 No. 1–2, pp. 84–9.

Howse, W.R. (2011). Knowledge, Skills, Abilities, and Other Characteristics for Remotely Piloted Aircraft Pilots and Operators. Damos Aviation Services Inc, Gurnee IL.

Israel, K. and Nesbit, R. (2004). Defense Science Board Study on Unmanned Aerial Vehicles and Uninhabited Combat Aerial Vehicles. Defense Science Board, Washington, DC.

Kantor, L., Endler, N.S., Heslegrave, R.J. and Kocovski, N.L. (2001). Validating self-report measures of state and trait anxiety against a physiological measure. Current Psychology, Springer, Vol. 20 No. 3, pp. 207–215.

Khuwaja, K.S.A., Chowdhry, B.S., Khuwaja, K.F., Mihalca, V.O. and Ţarcă, R.C. (2018). Virtual reality based visualization and training of a quadcopter by using RC remote control transmitter. In: IOP Conference Series: Materials Science and Engineering, Vol. 444, IOP Publishing, p. 52008.

Kim, K.H., Bang, S.W. and Kim, S.R. (2004). Emotion recognition system using short-term monitoring of physiological signals. Medical and Biological Engineering and Computing, Springer-Verlag, Vol. 42 No. 3, pp.419–427.

Kim, S. and Irizarry, J. (2019). Human Performance in UAS Operations in Construction and Infrastructure Environments. Journal of Management in Engineering, Vol. 35 No. 6, p. 04019026.

Kwak, S.K. and Kim, J.H. (2017). Statistical data preparation: Management of missing values and outliers. Korean Journal of Anesthesiology, Vol. 70 No. 4, pp. 407–411.

Li, X., Yi, W., Chi, H.-L., Wang, X. and Chan, A.P.C. (2018). A critical review of virtual and augmented reality (VR/AR) applications in construction safety. Automation in Construction, Elsevier, Vol. 86, pp. 150–162.

Papakonstantinou, G. and Gritzali, F. (1981). Syntactic filtering of ECG waveforms. Computers and Biomedical Research, Elsevier, Vol. 14 No. 2, pp. 158–167.

Papakonstantinou, G., Skordalakis, E. and Gritzali, F. (1986). An attribute grammar for QRS detection. Pattern Recognition, Vol. 19 No. 4, pp. 297–303.

Pereira, R.E., Gheisari, M. and Esmaeili, B. (2018). Using panoramic augmented reality to develop a virtual safety training environment. In: Construction Research Congress 2018, pp. 29–39.

Postal, G.R., Pavan, W. and Rieder, R. (2016). A virtual environment for drone pilot training using VR devices. In: XVIII Symposium on Virtual and Augmented Reality (SVR), IEEE, pp. 183–187.

Sakib, M.N. (2019), Wearable Technology to Assess the Effectiveness of Virtual Reality Training for Drone Operators, Texas A&M University.

Sakib, M.N., Yadav, M., Chaspari, T. and Behzadan, A.H. (2019). Coupling virtual reality and physiological markers to improve public speaking performance. In: 19th International Conference on Construction Applications of Virtual Reality (CONVR2019), Bangkok, Thailand, pp. 171–180.

Spielberger, C.D. (2010). State-Trait anxiety inventory. The Corsini Encyclopedia of Psychology, Wiley Online Library, p. 1.

Taelman, J., Vandeput, S., Spaepen, A. and Van Huffel, S. (2009). Influence of mental stress on heart rate and heart rate variability. In: 4th European Conference of the International Federation for Medical and Biological Engineering, Vol. 22, Springer, Berlin, Heidelberg, pp. 1366–1369.

Thayer, J.F., Yamamoto, S.S. and Brosschot, J.F. (2010). The relationship of autonomic imbalance, heart rate variability and cardiovascular disease risk factors. International Journal of Cardiology, Elsevier, Vol. 141 No. 2, pp. 122–131.

Trahanias, P. and Skordalakis, E. (1990). Syntactic pattern recognition of the ECG. IEEE Transactions on Pattern Analysis and Machine Intelligence, Vol. 12 No. 7, pp. 648–657.

Unity. (2019). Unity Real-Time Development Platform. available at: https://unity.com/ (accessed 21 February 2020).

Verhoeff, M., Verhagen, W.J.C. and Curran, R. (2015). Maximizing operational readiness in military aviation by optimizing flight and maintenance planning. Transportation Research Procedia, Elsevier, Vol. 10, pp. 941–950.

De Winter, J., Van Leeuwen, P.M. and Happee, R. (2012). Advantages and disadvantages of driving simulators: A discussion. In: Measuring Behavior, Vol. 2012, Citeseer, p. 8th.

Yadav, M., Chaspari, T., Kim, J. and Ahn, C.R. (2018). Capturing and quantifying emotional distress in the built environment. In: The Workshop on Human-Habitat for Health (H3): Human-Habitat Multimodal Interaction for Promoting Health and Well-Being in the Internet of Things Era, ACM, p. 9.

Yadav, M., Sakib, M.N., Feng, K., Chaspari, T. and Behzadan, A. (2019). Virtual reality interfaces and population-specific models to mitigate public speaking anxiety. In: 8th International Conference on Affective Computing and Intelligent Interaction (ACII), IEEE, Cambridge, United Kingdom, pp. 1–7.

Zhang, X., Ye, Z., Zhu, J.-H. and LI, S. (2002). Unmanned aerial vehicle flight simulation and training system based on virtual reality. Acta Ssmulata Systematica Sinica, Vol. 8.

An Integrated Approach to Capture Construction Workers' Response towards Safety Alarms using Wearable Sensors and Virtual Reality

Zhengbo Zou, Suzana Duran Bernardes, Abdullah Kurkcu, Semiha Ergan, Kaan Ozbay
New York University, USA
zz1658@nyu.edu

Abstract. Despite the continuous efforts from federal and state agencies to improve safety at traffic work zones, incidents continue to occur, resulting in 675 fatalities in the U.S. during the last decade. Current safety measures at work zones, such as visual and audible alarms are ineffective due to the lack of calibration studies to evaluate the attention span of workers towards alarms, given variances in the alarm modality, frequency and duration. This study proposes an integrated approach combining virtual reality (VR) and wearable sensors to capture data regarding workers' behaviors towards safety alarms when workers are exposed to simulated dangerous situations in VR. This dataset is needed to understand the relationships between workers' responses (i.e., react or dismiss) and the characteristics of the received alarms (i.e., modality, frequency, and duration). The proposed approach was implemented on an urban intersection from a real-world work zone in New York City for user studies.

1. Introduction

According to Occupational Safety and Health Administration (OSHA), an average of three construction workers died every day in the U.S. during 2013-2018 (OSHA 2018). A recent study that comprehensively reviewed the current safety measures in roadway work zones shows that a significant amount of the fatalities and injuries occur at traffic work zones, when workers come into contact with construction equipment or passing by vehicles (Yang et al. 2014). The Federal Highway Administration (FHWA) revealed that 50% of crashes occur within or adjacent to work zones during construction, putting workers in danger together with drivers (FHWA 2010). The majority of literature on work zone safety focused on driver behavior (Yang et al. 2013; Debnath et al. 2015; Ravani et al. 2015), where speed, aggressive behavior towards workers, distraction, and substance use were identified as factors contributing to work zone incidents. However, work zone safety studies have yet to be coupled with the behavior analysis of construction workers.

Currently, proactive warning approaches implemented at work zones include blinking lights with audible alarms, detection of vehicles crossing a predetermined perimeter, drone radars, and traffic cones with sound alerts (Theiss et al. 2017; TxDOT 2002). One of the major impediments in wide real-world deployment of such technologies is the false and frequent alarms that cause workers to disregard them. Another limitation is the lack of knowledge on the systematic assessment of different modalities of pushing alarms (e.g., vibration, audio, visual) along with the alarm frequency and duration to understand their effectiveness on workers. Hence, this study aims to improve the work zone safety in horizontal construction projects by examining the issues from workers' perspective and assessing workers' behaviors towards alarms with the aim to calibrate the duration and frequency of alarms as well as determining an effective medium to push these alarms.

With the development of wearable technologies, an increasing number of research studies have been exploring the feasibility of using wearable sensors to push alarms to construction workers (Awolusi et al. 2018; Choi et al. 2017). The advancement of VR enabled researchers to simulate potentially dangerous situations (e.g., speeding vehicles) in work zones without putting workers in harm. Therefore, the combination of VR and wearable sensors provides an opportunity for researchers to study the optimal alarm delivery system. This paper proposes an integrated approach utilizing VR and wearable sensors to determine when, how, and at what frequency to push alarms to workers at work zones based on the physiological states of workers collected from the wearable sensors and workers' behavior towards the alarms when they are in dangerous situations in VR. The approach is composed of four steps as: (1) recreating real-world work zones in VR, (2) enabling interactions in VR for construction activities, (3) conducting traffic simulation to obtain realistic traffic patterns near work zones and embedding vehicle movements in VR, and (4) developing a smartwatch application to send safety alarms and monitoring workers' responses as well as their physiological states using wearable sensors. The user studies will be conducted in VR, with the valid assumption that user behaviors in VR are reflective of real settings (Du et al. 2019, Ergan et al. 2019, Shi et al. 2019). The platform developed and introduced in this paper is aimed at studying human behavior towards alarms with the aim to calibrate the frequency and duration of alarms without putting people in real dangerous situations.

The sensors used in this study include a smartwatch to receive safety alarms, and a photoplethysmogram (PPG) sensor to monitor workers' heart-rate variability when encountering a dangerous situation in VR and when alarms arrive. Three scenarios based on real incidents were identified as more likely to lead to work zone incidents, including (1) setting up barriers to define a work zone perimeter that is close to an urban intersection (McIntosh 2019); (2) striping/marking a road on an urban highway (Fox and Cook 2018); and (3) installation of traffic sensors on the side of an urban highway (Yang et al. 2014). In this paper, the approach was implemented on an urban intersection VR environment based on a real-world work zone in New York City (i.e., based on scenario one). The proposed approach fills the gap of quantitative and systematic assessment of the characteristics of alarms (i.e., modality, frequency, and duration) with the goal to improve work zone safety.

2. Background

This study builds on the previous research in (1) the current safety measures implemented at work zones to prevent incidents, (2) the feasibility of monitoring human behaviors in VR using wearable sensors, and (3) methods for conducting microscopic traffic simulations.

2.1 Current safety measures at work zones

Safety measures adopted at work zones vary according to the work zone complexity, which depends on the duration of the construction activity. Long-term (i.e., more than 3 consecutives days) and intermediate-term (i.e., more than a daylight period and no more than 3 consecutive days, or more than an hour during night-time) work zones are usually well planned and structured, while short-term (i.e., more than an hour but not more than a daylight period) and mobile (i.e., up to an hour and moves intermittently) work zones have fewer safety guidelines. Hence, short-term and mobile work zones are more prone to incidents, given that workers conducting tasks out of a secure perimeter are exposed to a higher risk of being struck by upcoming traffic (Wong et al. 2011).

Prevalent work zone safety measures aim to raise drivers' attention around work zones. Such measures include but are not limited to, (1) speed control measures, such as fixed and variable message signs, police enforcement, speed display trailer, and (2) channelizing devices, such as cones, drums, and barricades, flashing arrow panels, Portable Concrete Safety Shape Barrier (PCBs), and high-visibility worker's apparel (Zhang and Gambatese 2017). A noteworthy emerging safety measure is the use of wireless warning systems using sound to either alert drivers to reduce speed due to the presence of a work zone or workers on-foot ahead and/or to alert workers of construction equipment (Park et al. 2016) or vehicle intrusion (Yang et al. 2014). In addition to measures taken to raise drivers' attentions, new technologies have been in development to address the common safety hazards (e.g., slips and trips, struck by objects, electrocution) observed at work zone construction projects. Strides have been made in the areas of (1) proximity detection e.g., object detection, distance measurement using Bluetooth low energy tags (Park et al. 2016) and (2) location tracking e.g., worker location tracking and material tracking using Global Positioning Systems (GPS) (Zhang et al. 2015) and Radio Frequency Identification (RFID) (Andoh et al. 2012).

However, few of the technologies developed for vertical projects were adopted by transportation work zones. Furthermore, contradictory findings exist in the literature regarding the impact of traffic control devices on the frequency and severity of crashes in work zones, with studies supporting the use of traffic control devices to reduce the frequency of crashes (e.g., Koilada et al. 2019) and studies that indicate the opposite (e.g., Meng and Weng 2011). Such contradictory findings reveal the need for investigating the existing and emerging safety measures further.

2.2 Feasibility of monitoring human behaviors and bodily states in VR using wearable sensors

With the advances in ubiquitous sensing and computing, it became easier to collect various types of physiological data on workers' bodily responses, health status, fatigue levels, and active/idle status. Wearable sensors such as smartwatches, wristbands, smart glasses are easy to deploy even in harsh construction environments (Hwang and Lee 2017). Various metrics have been proposed to understand the implications of human emotional and physiological states. Commonly used metrics include heart rate, muscle movement, and blood pressure to measure human experiences such as stress, pain, and anxiety (Parsons et al. 1998). Wearable sensing devices enabled researchers to measure and monitor such metrics and to relate those metrics to the events and stimuli presented to the subjects. Wrist worn PPG sensors were especially sought after in previous studies in the area of worker safety due to their ability to monitor elevated/reduced worker stress through heart-rate variability (HRV) (Jebelli et al. 2018). HRV is an indicator of the bodily response triggered by a stimulus (e.g., an alarm received on the wrist), which can be used to capture construction workers' physiological states in dangerous situations (Hwang and Lee, 2017; Jebelli et al. 2018). Previous research showed wrist worn PPG sensors can achieve accurate measurements when worn correctly and when the subjects are not under heavy physical load, as compared to the gold standard of medical grade chest worn electrocardiography (ECG) sensor (Menghini et al. 2019).

Due to the impracticality of creating job site hazards in real-world conditions, VR has been selected as a platform to evaluate worker safety on job sites. VR environments provide the flexibility to rapidly replicate and alter real-world conditions under controlled experiments. Previous studies confirmed that VR provides a high degree of realism for users (Du et al. 2018) and can be used to study user behaviors as in real-world experiences (Heydarian et al. 2015). The combination of VR and wearable sensors has also been validated from multiple previous studies focusing on design evaluation (Ergan et al. 2019), worker stress evaluation (Jebelli et al. 2018), and worker cognitive load under stressful environments (Shi et al. 2019).

2.3 Traffic simulation in work zone studies

The complexity of transportation systems and the difficulties in conducting real-world experiments make computer simulation an efficient tool for evaluating various traffic conditions. Microscopic traffic simulators are essential tools for describing traffic since they can model the interactions and dynamics between individual vehicles. These simulators have been commonly used for over 60 years now to analyze, evaluate, or test traffic management strategies, design changes or emerging smart transportation technologies representing traffic conditions in various locations from a couple of intersections to large city-wide networks. Microscopic traffic simulators describe the behavior of every "driver-vehicle" unit that compose the traffic flow. The inputs for these simulators are dynamic variables such as aggregated traffic volume, turning movement counts, and travel time. The simulation output such as vehicle trajectories (position and speeds), traffic data collected from modelled detectors, travel time are used to analyze target scenarios quantitatively. In this paper, the open-source traffic simulator Simulation of Urban Mobility (SUMO) was used to get the traffic pattern of the roads scanned for each scenario.

Microscopic traffic simulation models have been thoroughly used in work zone studies for traffic risk assessment (Liu et al. 2019), effects of speed control devices and speed limit reduction on the traffic in work zones (Ye et al. 2018), and impact of the work zone presence in the traffic conditions (Bharadwaj et al. 2018). However, these studies have mainly focused on the effects of work zone on traffic but not on the interaction between traffic and workers. There is still a gap in the literature on the use of traffic simulation models to help understand the behavior of workers exposed to traffic in work zones.

This paper identified the potential for improving work zone safety by integrating studies of construction worker behavior using VR technology and wearable sensors with traffic simulation models. From the microscopic traffic model built with SUMO, information such as vehicle, speeds and traffic volume were integrated to the VR application to be used in different scenarios. The integration of the microscopic traffic model with VR guarantees that the application is as close to reality as possible, since the simulation model is calibrated using real field data. Therefore, the reactions and behavior of the participants of the experiments would be closer to those when they are exposed to real-world traffic.

3. An Integrated Platform for Evaluating Workers' Behaviors and their Physiological States towards Safety Alarms

An integrated approach using VR and wearable sensors is proposed to study workers' behavior towards safety alarms they receive in variant modality, frequency and duration. The approach is composed of four steps as: (1) recreating real-world work zones in VR, (2) enabling interactions in VR for construction activities, (3) conducting a calibrated microscopic traffic simulation to obtain realistic traffic patterns near work zones and embedding vehicle movements with potential dangerous situations in VR, and (4) developing a smartwatch application to send safety alarms to monitor workers' responses as well as their physiological states using wearable sensors. In this study, dangerous situations are simulated to be caused by vehicles passing a virtual work zone. A dangerous situation can be caused by either a vehicle speeding or a vehicle invading the perimeter of a work zone, which corresponds to either speeding or collision alarms.

3.1 Reconstruct work zones in VR

This step includes using a laser scanner to capture 3D point clouds of real-world work zones and then recreate 3D models of the work zone in VR. The process of "scan to VR" has been an active research topic in the Architecture, Engineering and Construction (AEC) domain due to the increasing availability of high-resolution scanners and VR headsets. Furthermore, laser scanners provide a fast and accurate way of creating a digital representation of the real-world work zones, hence eliminating the need of a surveyor physically taking measurements of work zones repeatedly. However, there has not been a standard "best-practice" of "scan to VR" that is widely accepted. Two types of methods have been proposed, with the first being "scan-mesh-VR" and the second being "scan-measurements-VR" (Yang et al. 2011), as shown in Figure 1.

"Scan-mesh-VR" takes the scanned point cloud as an input to generate 3D mesh objects. Next, the mesh objects can be exported as common geometrical representation file formats such as .obj or .fbx files and later be imported to game engines where the objects can be modeled from the mesh or used as is. This method promises an automated approach, where no intervention from the modeler is needed. However, in practice, even with the state-of-the-art mesh generating algorithms, the process of scan to mesh cannot produce realistic results when the point cloud is not dense enough to form a consistent surface (Chen et al. 2017). On the other hand, "scan-measurements-VR" requires manual efforts. First, measurements of the object of interest (OOI) should be taken (e.g., the width of a street). Given enough measurements of the OOI, a modeler can use the measurements to recreate 3D objects in a modeling tool. This method suffers from long implementation time due to the extensive manual efforts from the modeler to take measurements, but it can be more accurate as compared to "scan-mesh-VR" because the measuring points are cherry-picked by the modeler. However, depending on the application domain and its needs, either method could be used.

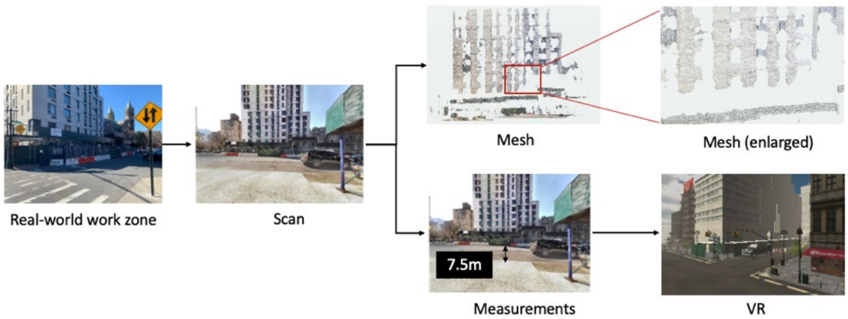

Figure 1: Scan-mesh and scan-measurement-VR process.

In this study, we used the "scan-measurements-VR" approach, where we relied on manual measurements of OOI to recreate the objects in a game engine. The OOI in this implementation is the road where the work zone is located. The width of the road and the length of the block were measured and used as references to recreate the work zone in a game engine. Models of general objects such as buildings, fences, and traffic signals can be found online with open licenses, hence do not need to be remodeled. We also ignored the exact locations of the smaller objects in the scene such as garbage bin and trees and added them at sensible locations.

3.2 Enable user interactions for construction tasks in VR

VR is widely adopted in the AEC domain for the purpose of design visualization (Ergan et al. 2019), coordination (Du et al. 2018), education (Sampaio et al. 2010), and safety training (Shi et al. 2019). User interactions in these VR studies (i.e., how users control the avatar in VR and get feedbacks from the VR environment) vary based on the specific VR application. However, a consensus exists that natural and realistic VR interactions are more desired because higher level of realism of interaction has been associated with improved user experience and performance in VR (McMahan et al. 2016). The level of realism for interactions in VR can be measured by *interaction fidelity*, which describes the degree of exactness with which real world actions are reproduced in VR (MaMahan et al. 2016). Interaction fidelity (Figure 2) checks if the user interactions include accurate kinematic and kinetic representations relayed to the VR environments. Kinematic representation describes how well a body motion in the real-world is reproduced in VR. On the other hand, kinetic representation describes how well force implemented by the user in real-world is reproduced in VR.

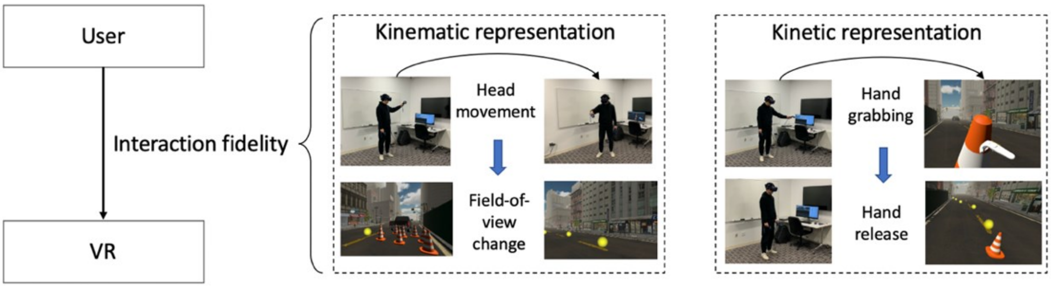

Figure 2: User interactions in VR measured by interaction fidelity.

In this study, worker head and hand movements are tracked and translated in the VR environment to enable worker position tracking and field-of-view change. Additionally, workers can grab the controller using either hand to trigger a grabbing motion in VR. The construction task in this study is setting up a perimeter for a mobile work zone at an urban intersection (Figure 3). Workers are expected to put six orange traffic cones unloaded from a truck (in a red circle in Figure 3) in pre-determined designated locations to finish setting up the perimeter of the work zone. This task was chosen based on previous studies' findings of mobile work zones without a structured perimeter having one of the highest incident rates (Wong et al. 2011). Furthermore, the selection of this task also eliminates the possibility of test subjects performing heavy physical workload to ensure the accuracy of the PPG sensor data. In VR, designated locations of the traffic cones are marked using blinking yellow spheres. Once a worker finished putting one traffic cone, the corresponding location will have a steady green sphere to signal the worker that the cone is in place. When all traffic cones are put in place, the worker will be notified for the completion of the assigned task. This task was customized to ensure that users can finish within an hour according to the institutional review board (IRB) requirements.

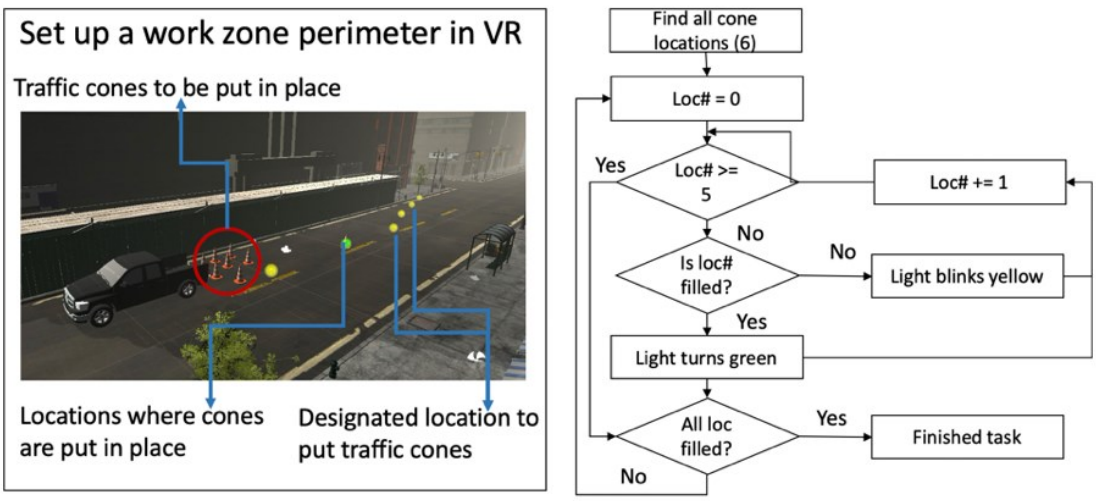

Figure 3: Enabling construction tasks as setting up work zone perimeters in VR.

3.3 Conduct traffic simulation to obtain realistic traffic patterns and embed vehicle movements in VR

Varying traffic patterns, such as increased demand during peak hours and vehicle trajectories containing vehicle positions and speeds in the vicinity of the real-world work zone, were simulated in the open-source micro simulator SUMO. The inputs of the simulation include (1) the network with its roads and intersections, (2) traffic demand, (3) vehicle types and their characteristics, and (4) vehicle routes. Traffic volume and turning movement counts during peak hours (6-10 a.m.) were manually collected at the study intersection and the simulation model was calibrated to represent these observed traffic parameters. The simulation network (an urban segment between two intersections) used in this study was calibrated to represent the observed volumes at the study location. The output of the traffic simulation includes vehicle ID, speed, acceleration, trajectory, and traffic volume.

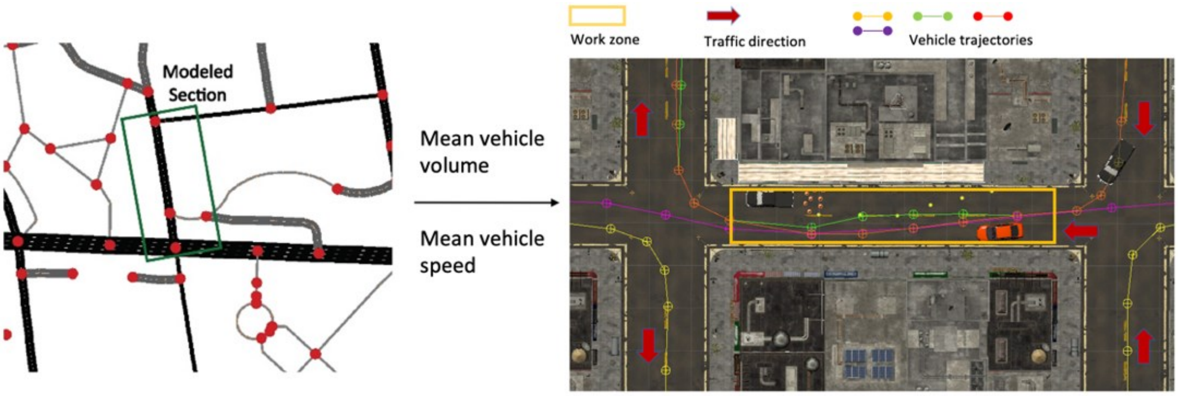

Figure 4: Traffic simulation outputs embedded in VR.

To realistically simulate traffic in the VR environment, the average vehicle speed and volume at the work zone location were calculated using the simulation outputs. By default, the VR work zone is a safe environment, where cars travel at the average speed in an average volume (Figure 4). The simulated dangerous situations were added purposefully, which can be divided into two categories: speeding and invasion of work zone perimeter. Work zones have a strict speed limit usually lower than the regular speed limit of the same road to protect workers. Speeding while passing by a work zone is especially dangerous due to lane changes and narrowed lanes. In this study, when a vehicle is traveling 20% faster than the average speed, it is categorized as a dangerous speeding situation. On the other hand, invasion of work zone perimeter leads to crashes in work zones and causes damages to the work zone structure as well as workers on site. Vehicle trajectories were defined using sets of invisible nodes in VR. Vehicles travel from one node to the next to follow a trajectory. The locations of the nodes were hand-picked by the authors to reflect both safe and dangerous situations. When a vehicle travels on a trajectory that leads to invasion of the work zone perimeter, it is categorized as a dangerous situation.

3.4 Monitor worker behavior towards safety alarms using wearable sensors

This part of the integrated platform has two major components, including a cloud server which handles alarms originated from the VR application, and wearable sensors to receive alarms from the server and monitor workers' physiological states. To elaborate, the occurrence of a dangerous situation in VR triggers an alarm sent to a cloud server through an HTTP request (Figure 5a). The request contains information about the alarm, including alarm ID, type (e.g., speeding, collision), alarm sent time, and the vehicle ID that triggered the alarm.

On the cloud server (Figure 5b), a queue of safety alarms is maintained containing the alarm information from the VR application. The newly arrived alarm will be added to the alarm queue while the oldest alarm currently in the queue being checked for time-out (i.e., exceeds the maximum time to respond to an alarm). If the alarm is not timed-out, the cloud server then sends the alarm to the smart watch equipped on the worker. The smart watch (Figure 5c) then uniformly draws from a pre-defined set of modalities (e.g., vibration, sound), frequencies (e.g., 3/20 seconds, 6/20 seconds), and durations (e.g., 3 seconds, 5 seconds). Next, the alarm will be delivered to the worker on the smart watch, and the worker can decide to read or dismiss the alarm by tapping the smart watch display or simply ignoring the alarm. In the meantime, the workers' response (i.e., dismiss or read) towards the alarms are being monitored. Currently, the test subjects can acknowledge receipt of the alarm by touching the screen of the smartwatch once and dismiss the alarm by touching the screen twice. In the version that will be deployed, the smartwatch will also be modeled in the VR environment, and alarms will be replicated in VR as subjects receive them. Additionally, while the workers are performing the assigned tasks in VR, their HRVs are constantly monitored by a PPG sensor. HRV is used to infer the level of vigilance and stress of workers when they receive safety alarms of potentially dangerous situations.

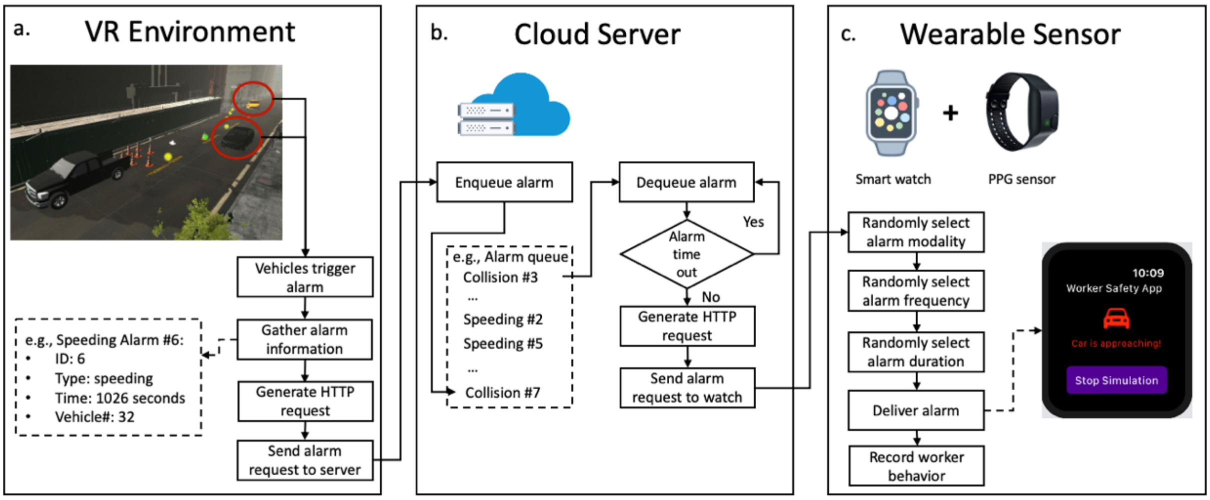

Figure 5: Alarm delivery mechanism from VR to wearable sensors on workers.

4. Conclusion and Future Work

This paper proposed an integrated approach to create a VR plus wearable sensor platform to study when and how to push safety alarms to construction workers at work zones based on their behaviors towards previous alarms. The data collected from the wearable sensors will be used to calibrate an alarm system to optimally deliver safety alarms for maximum worker attention. Towards this goal, within the context of this paper, we introduced the technical details of the system components and how they were integrated over a specific scenario implemented in VR. The content of this paper will extend the current line of research by providing the technical guidance on integrating biometric sensors, traffic simulations, and interaction gadgets (e.g., smart watch) in VR platforms for interactive user studies.

The research team had secured an approval from the institution's IRB with the application number IRB-FY2020-3946 and had started initial alpha tests within the research group with four participants. The participants' response towards the alarms delivered in various modalities, frequencies and duration were monitored and analyzed. During initial testing, the alarms were delivered in two modalities, as vibration and visual alarm. Alarm frequency was set as either 3/20 seconds or 6/20 seconds, and the alarm duration was set as either 1 second or 3 seconds. The hypothesis of the initial testing is that the behaviors of the workers (i.e., read or dismiss) will be statistically significantly different when the alarms are sent in different modalities, frequencies, and durations with a significance level of 0.05. The hypothesis was tested using a paired t-test. From the t-test results, it is apparent that the participants were sensitive to (i.e., the participants' behavior towards the alarm being statistically significant) the alarm modality and frequency but not the duration. Further user tests will be conducted to validate the initial results with a larger subject pool.

The research team is continuing to recruit more participants with transportation work zone construction experience to test the proposed platform. The outcome of this study will (a) inform us whether data from wearables are meaningful to correlate with human responses to alarms and (b) provide a guidance to effectively integrate wearables to work practices at job sites and define a sequence of steps to follow to analyze the collected data. In the long run, as shown in (Xie et al. 2017), it is also possible to use other rich sources of real-world data in addition to the simulated data that is being collected in this study to further analyze safety impacts of different traffic work zones at the network level.

References

Andoh, A. R., Su, X., & Cai, H. (2012). A framework of RFID and GPS for tracking construction site dynamics. In Construction Research Congress 2012: Construction Challenges in a Flat World (pp. 818–827). https://doi.org/10.1061/9780784412329.083

Awolusi, I., Marks, E., & Hallowell, M. (2018). Wearable technology for personalized construction safety monitoring and trending: Review of applicable devices. Automation in Construction, 85, pp. 96–106 . https://doi.org/10.1016/j.autcon.2017.10.010

Bar, M., & Aminoff, E. (2003). Cortical analysis of visual context. Neuron, 38(2), pp. 347–358. https://doi.org/10.1016/S0896-6273(03)00167-3

Bharadwaj, N., Edara, P., Sun, C., Brown, H., & Chang, Y. (2018). Traffic flow modeling of diverse work zone activities. Transportation research record, 2672(16), pp. 23–34. https://doi.org/10.1177/0361198118758056

Chen, S., Tian, D., Feng, C., Vetro, A., & Kovačević, J. (2017). Fast resampling of three-dimensional point clouds via graphs. IEEE Transactions on Signal Processing, 66(3), pp. 666–681. https://doi.org/10.1109/TSP.2017.2771730

Choi, B., Hwang, S., & Lee, S. (2017). What drives construction workers' acceptance of wearable technologies in the workplace? Indoor localization and wearable health devices for occupational safety and health. Automation in Construction, 84, pp. 31–41. https://doi.org/10.1016/j.autcon.2017.08.005

Debnath, A. K., Blackman, R., & Haworth, N. (2015). Common hazards and their mitigating measures in work zones: A qualitative study of worker perceptions. Safety Science, 72, pp. 293–301. https://doi.org/10.1016/j.ssci.2014.09.022

Du, J., Zou, Z., Shi, Y., & Zhao, D. (2018). Zero latency: Real-time synchronization of BIM data in virtual reality for collaborative decision-making. Automation in Construction, 85, pp. 51–64. https://doi.org/10.1016/j.autcon.2017.10.009

Ergan, S., Radwan, A., Zou, Z., Tseng, H. A., & Han, X. (2019). Quantifying human experience in architectural spaces with integrated virtual reality and body sensor networks. Journal of Computing in Civil Engineering, 33(2), 04018062. https://doi.org/10.1061/(ASCE)CP.1943-5487.0000812

FHWA – Federal Highway Administration (2010). What We Know about Work Zone Fatalities, http://sites.google.com/site/trbcommitteeahb55/Welcome/discussionsthreads/2010annualmeeting/WZSafetyData-WhatWeKnowandDoNotKnow(ver2).ppt, access date: 11/27/2018.

Fox, A., Cook, L. (2018). DOT Worker Struck and Killed on Hutchinson River Parkway, Cops Say. amNY. Retrieved from https://www.amny.com/news/dot-worker-killed-hutchinson-river-parkway-1-17859975/, access date 01/11/2019.

Heydarian, A., Carneiro, J. P., Gerber, D., Becerik-Gerber, B., Hayes, T., & Wood, W. (2015). Immersive virtual environments versus physical built environments: A benchmarking study for building design and user-built environment explorations. Automation in Construction, 54, pp. 116–126. https://doi.org/10.1016/j.autcon.2015.03.020

Hwang, S., & Lee, S. (2017). Wristband-type wearable health devices to measure construction workers' physical demands. Automation in Construction, 83, pp. 330–340. https://doi.org/10.1016/j.autcon.2017.06.003

Jebelli, H., Choi, B., Kim, H., & Lee, S. (2018, April). Feasibility study of a wristband-type wearable sensor to understand construction workers' physical and mental status. In Construction Research Congress (pp. 367–377). https://doi.org/10.1061/9780784481264.036

Koilada, K., Mane, A. S., & Pulugurtha, S. S. (2019). Odds of work zone crash occurrence and getting involved in advance warning, transition, and activity areas by injury severity. IATSS Research. https://doi.org/10.1016/j.iatssr.2019.07.003

Liu, B., Yan, H., & Zhao, W. (2019). Traffic Risk Assessment Model for Expressway Maintenance Work Zones Based on Risk Index. In CICTP 2019 (pp. 787–798). https://doi.org/10.1061/9780784482292.071

McIntosh, D. (2019). Fatality Investigation: Traffic Control Worker Struck and Killed. EHSToday, retrieved from https://www.ehstoday.com/construction/article/21920280/fatality-investigation-traffic-control-worker-struck-and-killed, access date 08/11/2019.

McMahan, R. P., Lai, C., & Pal, S. K. (2016, July). Interaction fidelity: the uncanny valley of virtual reality interactions. In International Conference on Virtual, Augmented and Mixed Reality (pp. 59–70). Springer, Cham. https://www.springerprofessional.de/en/interaction-fidelity-the-uncanny-valley-of-virtual-reality-inter/10335622

Meng, Q., & Weng, J. (2011). A Genetic algorithm approach to assessing work zone casualty risk. Safety science, 49(8-9), pp. 1283–1288. https://doi.org/10.1016/j.ssci.2011.05.001

Menghini, L., Gianfranchi, E., Cellini, N., Patron, E., Tagliabue, M., & Sarlo, M. (2019). Stressing the accuracy: Wrist-worn wearable sensor validation over different conditions. Psychophysiology, 56(11), e13441. https://doi.org/10.1111/psyp.13441

OSHA - Occupational Safety and Health Administration. (2018). Injuries, Illnesses, and Fatalities: TABLE A-3, retrieved from https://www.bls.gov/iif/oshwc/cfoi/cftb0324.htm, access date: 02/20/2020

Park, J., Cho, Y. K., & Timalsina, S. K. (2016). Direction aware bluetooth low energy based proximity detection system for construction work zone safety. In ISARC. Proceedings of the International Symposium on Automation and Robotics in Construction (Vol. 33, p. 1). IAARC Publications. http://rical.ce.gatech.edu/Papers/ISARC_2016_proximity.pdf

Parsons, R., Tassinary, L. G., Ulrich, R. S., Hebl, M. R., & Grossman-Alexander, M. (1998). The view from the road: Implications for stress recovery and immunization. Journal of environmental psychology, 18(2), pp.113–140. https://doi.org/10.1006/jevp.1998.0086

Ravani, B., Fyhrie, P., Wehage, K., Gobal, A., & Hong, H. Y. (2015). Work Zone Injury Data Collection and Analysis (No. CA16-2257). http://www.dot.ca.gov/research/researchreports/reports/2015/CA16-2257_FinalReport.pdf

Sampaio, A. Z., Ferreira, M. M., Rosário, D. P., & Martins, O. P. (2010). 3D and VR models in Civil Engineering education: Construction, rehabilitation and maintenance. Automation in Construction, 19(7), pp.819–828. https://doi.org/10.1016/j.autcon.2010.05.006

Shi, Y., Du, J., Ahn, C. R., & Ragan, E. (2019). Impact assessment of reinforced learning methods on construction workers' fall risk behavior using virtual reality. Automation in Construction, 104, pp. 197–214. https://doi.org/10.1016/j.autcon.2019.04.015

Theiss, LuAnn; Ullman, Gerald L.; Lindheimer, Tomas (2017), Closed Course Performance Testing of the AWARE Intrusion Alarm System, retrieved from "https://www.workzonesafety.org/publication/closed-course-performance-testing-aware-intrusion-alarm-system/", access date: 11/27/2018.

TxDOT (2002), Use of drone radar, safety intrusion alarms, CB Wizard, and automated flaggers in work zones, retrieved from "https://www.workzonesafety.org/practice/use-of-drone-radar-safety-intrusion-alarms-cb-wizard-and-automated-flaggers-in-work-zones/", access date: 11/27/2018.

Wong, J. M., Arico, M. C., & Ravani, B. (2011). Factors influencing injury severity to highway workers in work zone intrusion accidents. Traffic injury prevention, 12(1), pp. 31–38. https://www.ncbi.nlm.nih.gov/pubmed/21259171

Xie, K., Ozbay, K., Kurkcu, A. and Yang, H., (2017) Analysis of Traffic Crashes Involving Pedestrians Using Big Data: Investigation of Contributing Factors and Identification of Hotspots. Risk Analysis 37(8), pp. 1459–1476. https://doi.org/10.1111/risa.12785

Yang, H., Bartin, B., Ozbay, K., Chien, S. Investigating Motorists' Behaviors in Response to Supplementary Traffic Control Devices at Land Surveying Work Sites, Journal of Traffic Injury Prevention, Volume 15, Issue 4, 2014. https://doi.org/10.1080/15389588.2013.823165

Yang, H., Ozbay, K., Ozturk, O., Yildirimoglu, M. Modeling Work Zone Crash Frequency by Quantifying Measurement Errors in Work Zone Length. Journal of Accident Analysis & Prevention, Volume 55, pp. 192–203, June 2013. https://doi.org/10.1016/j.aap.2013.02.031

Yang, H., Ozbay, K., K. Xie (2014). Work Zone Safety Analysis and Modeling: A State-of-the-Art Review. Traffic Injury Prevention, Vol. 16, Issue4, pp. 387–396. https://doi.org/10.1080/15389588.2014.948615

Yang, W. B., Chen, M. B., & Yen, Y. N. (2011). An application of digital point cloud to historic architecture in digital archives. Advances in Engineering Software, 42(9), pp. 690–699. https://doi.org/10.1016/j.advengsoft.2011.05.005

Ye, H., Tu, L., & Fang, J. (2018). Predicting Traffic Dynamics with Driver Response Model for Proactive Variable Speed Limit Control Algorithm. Mathematical Problems in Engineering, 2018. https://doi.org/10.1155/2018/6181756

Zhang, F., & Gambatese, J. A. (2017). Highway construction work-zone safety: Effectiveness of traffic-control devices. Practice Periodical on Structural Design and Construction, 22(4), 04017010. https://doi.org/10.1061/(ASCE)SC.1943-5576.0000327

Zhang, S., Teizer, J., Pradhananga, N., & Eastman, C. M. (2015). Workforce location tracking to model, visualize and analyze workspace requirements in building information models for construction safety planning. Automation in Construction, 60, 74–86. https://doi.org/10.1016/j.autcon.2015.09.009

Exploring Thermally-Driven Occupant Behavioral Intention in Immersive Virtual Environment

Sanaz Saeidi, Yimin Zhu
Louisiana State University, USA
yiminzhu@lsu.edu

Abstract. The authors explored the feasibility of using immersive virtual environments (IVEs) as an apparatus for replicating real-life experiences of an indoor environment and studying the thermally-driven behavioural intention of participants. A series of experiments was conducted in an augmented virtual reality environment, i.e., virtual reality combined with a climate chamber. A total of 27 participants completed all sessions of experiments in IVE and *in-situ* settings, including a cooling sequence and a heating sequence at two different times with two to three months in between. Participants' behavioural intention choices and their thermal state votes (i.e., thermal sensation, thermal acceptability, and thermal comfort) were collected at the end of the heating and cooling sequences. The heating sequence data was analysed using the Fisher's exact test to determine if the thermal state difference of participants was associated with their behavioural intention difference between IVE and *in-situ*. The results revealed that the association was random. The results suggested factors other than thermal state difference had influenced their behavioural intention choices.

1. Introduction

During the design and engineering stage of a building project, energy performance simulation is critical because it is one of the major methods that designers and engineers employ to understand and analyze the performance of buildings under design. Recent studies suggested that occupants played an important role in building energy consumption (Hong and Lin, 2012) and the lack of good understanding about occupant behavior had caused many high performance buildings to fail in meeting their design expectations (Janda, 2014). Therefore, incorporating occupant behavior analysis into building performance simulation is important.

So far data related to occupant behavior is mainly collected through field (*in-situ*) observations, lab experiments, or surveys. Although these approaches are important for understanding occupant behaviors in existing buildings, there are various weaknesses associated with them to be used for performance simulation during design. For instance, data collected by observing or surveying occupants in a specific building might be less relevant to the context of a new building under design. Similarly, while collecting data in laboratory is common, the significance of the contextual factors of an actual building is normally ignored by this approach. Therefore, it is often difficult to effectively apply those results to other buildings or new designs (Mahdavi and Pröglhöf, 2008). During the design stage when the actual building is not in existence, a new approach to better address this issue is desirable.

As a proxy to reality, immersive virtual environments (IVEs) have shown great potential in building design. For instance, validating IVEs for occupant behavior studies and understanding behaviors in IVEs are two types of applications to building design (Zhu et al., 2018). In particular, many studies have been reported using IVEs for studying artificial lighting use behavior (Heydarian et al., 2015)(Chokwitthaya et al., 2017) due to the maturity of IVE technologies for lighting simulation. However, the simulation of thermal conditions using IVEs is different because such simulation is beyond what traditional IVE technologies can offer. We have explored the potential of using an external heating/cooling source, such as a climate chamber, in addition to an IVE to elicit thermal sensation and thermal comfort (Saeidi et al., 2016)(Saeidi et al., 2017). However, these studies have not examined if IVEs can be used to reliably observe occupant behaviors related to thermal comfort.

Therefore, the main objective of this study is to study occupant behavioral responses to thermal stimuli across *in-situ* and IVE settings. We are interested in the relationship between the thermal state (i.e., thermal sensation, thermal acceptability, and thermal comfort) difference and the difference of thermally-driven behavioral intentions across *in-situ* and IVE settings.

2. Related Work

2.1 Thermal Comfort

According to the American Society of Heating, Refrigerating and Air-Conditioning Engineers (ASHRAE), thermal comfort is "(the) condition of mind which expresses satisfaction with the thermal environment". Thermal comfort is one of the most important physical needs of occupants, as well as one of the factors of occupant satisfaction and well-being (Vischer, 2007). Studies showed that thermal comfort was among the most important conditions for building occupants to derive overall satisfaction from the indoor environment, because occupants were particularly sensitive to the environment temperature (Frontczak and Wargocki, 2011).

Thermal comfort in indoor environments is a complex topic, since many factors are involved in how the indoor thermal environment may be perceived. Fanger (1970) categorized these factors into environmental (e.g., radiant temperature, humidity, air velocity) and personal (e.g., clothing and metabolic rate) factors. Besides these, there are many indirect factors such as the access to thermostat control that can have impact on occupants' satisfaction with the indoor environment (Rupp *et al.*, 2015). Conventionally, thermal comfort in indoor environments is normally assessed through the static or classic steady-state method (i.e., Predicted Mean Vote) (Fanger, 1970). This model was the basis of many national and international comfort standards, e.g., ISO 7730 (ISO Standard 1994) and ASHRAE Standard 55 (ASHRAE 1992). In addition to thermal comfort, thermal sensation and thermal acceptability are two commonly applied measurements. For example, Table 1 shows the ASHARE 7-point Likert scale for measuring thermal sensation. Table 2 shows a thermal comfort scale similar to that in (Zhang *et al.*, 2010) and a customized thermal acceptability scale based on (Zhang and Zhao, 2008). These scales were used to collected data in IVE and *in-situ* experiments. In this study, we use the term thermal state to describe thermal sensation, thermal comfort, and thermal acceptability collectively.

Table 1: ASHRAE Thermal Sensation Scale

Value	Thermal Sensation
+3	Hot
+2	Warm
+1	Slightly Warm
0	Neutral
-1	Slightly Cool
-2	Cool
-3	Cold

Table 2: Thermal Comfort and Thermal Acceptability Scales

Scale	Thermal Acceptability	Thermal Comfort
+3	Perfectly Acceptable	Very Comfortable
+2	Acceptable	Comfortable
+1	Slightly Acceptable	Slightly Comfortable
-1	Slightly Unacceptable	Slightly Uncomfortable
-2	Unacceptable	Uncomfortable
-3	Totally Unacceptable	Very Uncomfortable

It needs to be noted that this is not a thermal comfort study. Rather, it is to understand the potential of IVEs to reliably replicate the thermal state of participants as *in-situ*. Therefore, the design of the experiments is limited to measuring basic thermal state responses in a controlled environment. Its capability to simulate advanced thermal comfort modelling such as adaptive thermal comfort modelling (de Dear and Brager, 1998) is not yet the focus of this study.

2.2 Thermally-Driven Behavioural Intention

Changes in the thermal condition of a person, whether due to environmental or personal changes, may lead to the need of behavioral adjustments such as adjusting the thermostat or opening a window, which are examples of energy-related occupant behavior in buildings (Hong *et al.*, 2015). Behaviors that are taken to restore occupants' thermal comfort are called thermally-driven behavior in this study such as adjusting the temperature of a space or using a fan. Previous studies have shown that occupant behavior is context-dependent (O'Brien and Gunay, 2014). It is still an open question whether thermally-driven behavior remains the same for similar conditions between IVE and *in-situ* settings. Therefore, instead of directly observing behavior, we explore the use of a different measurement in this study based on the theory of planned behavior (TPB).

TPB, developed based on the Theory of Reasoned Action (Fishbein and Ajzen, 1977), is a well-known theory that predicts an individual's intention to engage in a behavior. "(I)ntentions are indicators of how hard people are willing to try, of how much of an effort they are planning to exert, in order to perform the behavior (Ajzen *et al*. 1991)." The major elements of this theory are the attitude, the perceived individual and social pressure, and the belief in one's ability to perform the behavior. A combination of these elements determines the behavioral intention. Intention and actual behavior control together determine the final action (Figure 1). Considering the actual behavior control is difficult to simulate in IVEs, intention is chosen as a proximal predictor of actual behavior.

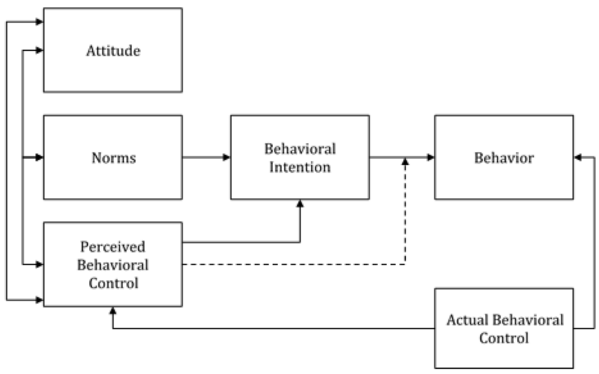

Figure 1: Theory of Planned Behavior (Ajzen *et al.*, 1991)

Different disciplines have extended TPB and adapted this model for specific purposes. In the domain of sustainable building design, engineering, and operations, TPB has shown a considerable potential in predicting occupants' actions by exploring their attitudes, normative beliefs, and perceived control beliefs (Abrahamse and Steg, 2009)(Menezes *et al.*, 2012)(Claudy *et al.*, 2013).

2.3 IVE Applications and Thermal-Related Experiments

IVE applications have shown great potential in creating experimental constructs in a wide range of research contexts including social science, health care, education, and built environment design, engineering, construction, and operation (Zhu *et al.*, 2018). For behavioral studies related to the built environment, many of them were focused on applying the visual-spatial capability of IVE technologies because it provides participants with the opportunity to vividly experience specific environments under controlled laboratory circumstances. Examples include building design and analysis such as home design (Mackie *et al.*, 2004), artificial lighting use behavior (Heydarian *et al.*, 2015), architectural daylighting design (Hong and Michalatos, 2016), emergency situations such as evacuation from tunnel fire (Kinateder and Warren, 2016), construction safety (Lu and Davis, 2016), and human movement and spatial behavior in urban environments (Natapov and Fisher-Gewirtzman, 2016).

So far there is only a limited number of studies related to the thermal state of participants, or thermally-driven intention or behavior. Since conventional virtual reality technologies don't directly provide thermal stimuli, external sources need to be integrated with virtual realty for such applications. Although attempts to elicit human thermal sensations by combining virtual reality with external heating/cooling sources existed in computing [12], these efforts were not mature enough for conducting occupant energy behavior experiments due to the lack of control over the external heating/cooling sources. On the other hand, pilot studies were reported studying the impact of IVE on human thermoception by comparing IVE and *in-situ* settings (Saeidi *et al.*, 2016)(Saeidi *et al.*, 2017). Nevertheless, these studies have not investigated the impact of IVE on thermally-driven behaviors or behavioral intentions.

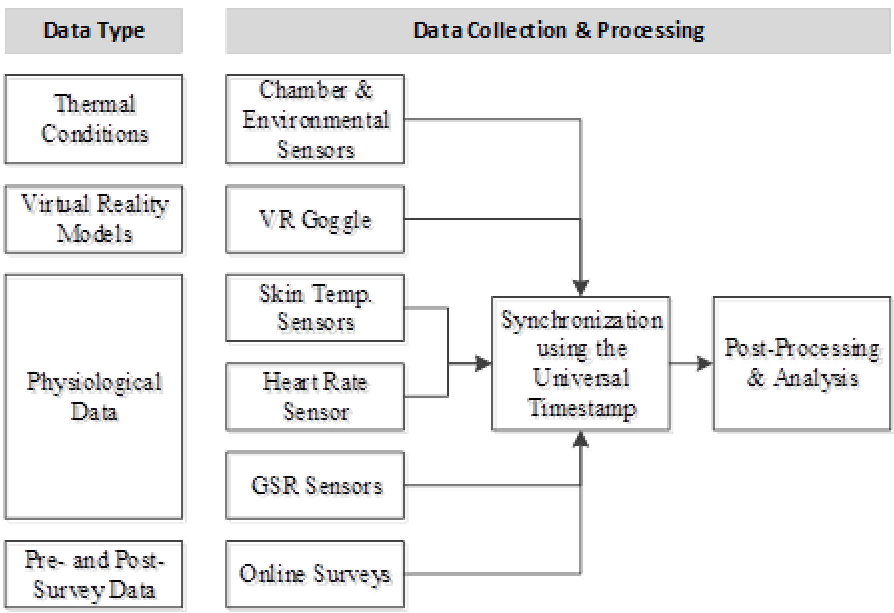

Figure 2: Data Collection and Processing

3. Computing Environment

Figure 2 is a conceptual diagram showing the type of data and data collection and processing in the computing environment. The climate chamber includes a test area and a control/rest area with a Metasys system to control the temperature, humidity, and air flow (Figure 3).

(a) Test Area

(b) Control/Rest Area

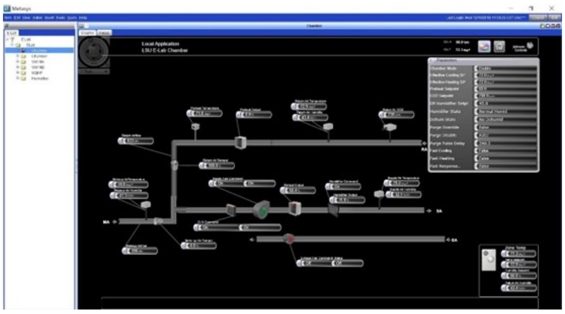

(c) Metasys System

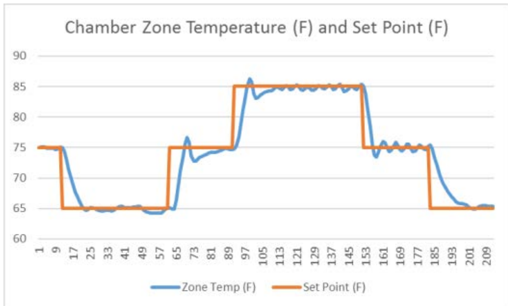

(d) Sample Zone Temperature and Set Point

Figure 3: Climate Chamber

A head mounted display (HMD), the HTC Vive, was using to render the interior space of the chamber. Figure 4 shows the display of the chamber interior.

Figure 4: Chamber Virtual Environment

Table 3 is a list of sensors applied to collect physiological data.

Table 3: Sensors for Collecting Physiological Data

Type	Sensor
Heart Rate (HR)/ Heart Rate Variability (HRV)	Polar Ft 7
Skin Temperature	Vernier Surface Temperature Sensors
Galvanic Skin Response	Qubit GSR Sensors

Participants' social and background information was collected using online surveys before experiment; their psychological data including immersive tendency, presence, simulator sickness, and thermal state was collected during experiment using a portable device.

Particularly, a questionnaire was designed and used to discover participants' thermally-driven behavioral intentions at the end of the experiment when the temperature was beyond normal individuals' thermal comfort zone (65ºF/18.3ºC or 85ºF/29.4ºC). Typically, thermally-driven behaviour includes: adjusting clothing; changing posture; changing activity; eating hot/cold foods; drinking hot/cold beverages; moving to a different location; opening/closing windows; opening/closing window blinds; using handheld fan; turning on/off fans or heating; blocking air diffusers; and operating other HVAC controls (e.g., adjusting thermostat) (Langevin *et al*., 2015).

4. Research Objective and Experiment Procedure

4.1 Research Objective and Hypothesis

The objective of this study is to acquire initial understanding about the impact of IVE on thermally-driven behavioral intentions. To achieve the objective, the first question to answer is what contributes to the difference of behavioral intentions between experiment settings, i.e., IVE vs. *in-situ*. Since thermal discomfort is the main potential trigger of thermally-driven behavioral intentions, we need to determine if participants' thermal state differences between IVE and *in-situ* significantly affect their differences in behavioral intentions. Therefore, we hypothesize that there is no significant assocaition between participants' thermal state difference and their thermally-driven behavioural intention difference:

H0: Δstate is not significantly associated with Δintention

H1: Δstate is significantly associated with Δintention

where Δstate (i.e., thermal state difference) is the difference in the general thermal sensation, general thermal acceptability and general thermal comfort between the IVE and *in-situ* experimental settings (e.g., Δstate (thermal sensation) at 85ºF/29.4ºC, heating sequence = |thermal sensation choice at 85ºF/29.4ºC, heating sequence, IVE - thermal sensation choice at 85ºF/29.4ºC, heating sequence, *in-situ*|). To support statistical analysis, Δstate was presented with two levels (Different vs. Not different). If the Δstate was 0, it was referred to as "Not different" and any Δstate that was greater or equal to 1 was presented as "Different."

Δintention (i.e., thermally-driven behavioural intention difference) is the number of common adaptive behavioural intentions between IVE and *in-situ*. Since each participant has three most preferred choices from the same list in *in-situ* and IVE experiments, there are four possible outcomes, i.e., 0 – no match between IVE and *in-situ*, 1 – one match, 2 – two matches, and 3 – three matches.

4.2 Participants and Procedure

Undergraduate and graduate students, and a few staff members at a major state university in the central south region of the US were invited to partake in this research. Data of 27 participants are complete and used in the analysis of this study. The 27 participants had two visits when the outdoor temperature difference was at least 20ºF/11ºC. Upon meeting the inclusion criteria, a consent form was given to and signed by the experiment volunteers.

Participants were instructed to come to the lab with a predefined set of clothing requirements in all the sessions; shoes, socks, underwear, light pants, and a light long-sleeved shirt/T-shirt. There was always an ~20 minutes resting period in the rest area, after a participant arrived at the lab. This ensures that the participant is acclimatized to the indoor condition. Afterwards, they were asked to get into the chamber and sit down on a chair so that the experimenter could start attaching the sensors (i.e., HR, Tsk, GSR) to their body. Participants' tasks in this study was limited to sedentary or near sedentary physical activity levels—seated at rest. An experiment included a heating exposure (i.e., from 65ºF/18.3ºC to 85ºF/29.4ºC) and a cooling exposure (i.e., from 85ºF/29.4ºC to 65ºF/18.3ºC) in both IVE and *in-situ* settings. The heating exposure test used a heating sequence with three heating steps from 65°F/19.3°C to 75°F/23.9°C and to 85°F/29.4°C; and the cooling exposure test used a cooling sequence with three cooling steps from 85°F/29.4°C to 75°F/23.9°C to 65°F/19.3°C. After each temperature step change, the experimenter waits for ~5 minutes before collecting thermal state data. Also, at the end of each sequence, the behavioural intention data was collected.

5. Data Processing, Results and Discussions

5.1 Data Processing

This step is to remove the extreme values of the data, or the outliers. The actual indoor temperature around the participants was compared with the target temperature (e.g., temperature set point) to ensure the temperatures around the participants were not significantly different. This process was to ensure that participants' thermal state votes were representative of the aimed experimental condition. Individuals detect the changes of their surrounding temperature based on mostly the rate of the temperature change. If the temperature changes at a rate of less than 0.5°C/0.9°F per min, an individual can be unaware of a 4-5°C (7.2-9°F) temperature increment (Darian-Smith and Johnson, 1977). In the climate chamber used in this study, changing 0.6°/C 1°F temperature (anywhere between 65°F/19.3°C - 85°F/29.4°C) often takes 1 min. With this rate, we assumed that the participants had not been aware of changes of 3°F/1.7°C in ~10 min (10 min is the approximate duration to rise/drop 10°F/5.6°C). With this assumption, the data points, which were ±3°F/1.7°C far from the target temperature, were removed from the analyses.

5.2 Results and Discussions

To perform the hypothesis test, the thermal state votes at the end of the session, e.g., heating exposure at 85 ºF/29.5ºC were taken into account. This data was collected right before providing the participants with adaptive behavioural choices. Yet, because of the limited numbers of the datapoints in the cooling exposure at 65 ºF/19.3ºC, the hypothesis test was limited to examining the Δstate of the heating exposure.

The Fisher's exact test was used to investigate the possible association between the participants' reported thermal state difference (Δstate) and their thermally-driven behavioural intention difference (Δintention). Fisher's exact test is to determine the possible association between two categorical variables, in this case Δstate and Δintention. Tables 4, 5 and 6 are the data and the test results related to thermal sensation, thermal comfort and thermal acceptability respectively.

Table 4: Thermal Sensation vs. Behavioural Intention

Thermal Sensation		**Δintention**				**Total**	***p*-value**
		0	**1**	**2**	**3**		
Δstate	**Different**	5	5	1	8	19	0.5402
	Not different	8	13	5	9	35	
Total		13	18	6	17	54	

Table 5: Thermal Comfort vs. Behavioural Intention

Thermal Comfort		**Δintention**				**Total**	***p*-value**
		0	**1**	**2**	**3**		
Δstate	**Different**	7	5	4	7	23	0.2990
	Not different	6	13	2	10	31	
Total		13	18	6	17	54	

Table 6: Thermal Acceptability vs. Behavioural Intention

Thermal Acceptability		**Δintention**				**Total**	***p*-value**
		0	**1**	**2**	**3**		
Δstate	**Different**	6	8	2	6	22	0.9190
	Not different	7	10	4	11	32	
Total		13	18	6	17	54	

The *p*-values associated with the tests (all greater than 0.05) indicate that there is no significant association between the two variables, the thermal state difference (Δstate) and the thermally-driven behavioural intention difference (Δintention). In other words, the difference in thermally-driven behavioural intention choices cannot be explained by the difference in thermal state difference. If participants sensed or perceived the thermal environment differently between IVE and *in-situ* settings, their corresponding behavioural intention differences did not necessarily follow a consistent pattern. There may be other factors that influence the Δintention across the *in-situ* and IVE experimental settings. Such factors can be individual-related such as experience with virtual reality technologies, immersive tendency, or simulation sickness, or experiment protocol related such as how behavioural intention data is collected. In addition, the sample size in this study is relative small, the results need to be tested when a larger sample is available. It also needs to be noted that the 54 data points include the same individual participated in both contrasting outdoor conditions.

6. Conclusions and Future Directions

In this study, we reported an initial attempt of using a new computing method to elicit thermally-driven occupant behavioural intentions. The new method is an augmented immersive virtual environment using a climate chamber as an external source to provide and control thermal conditions. At about 85ºF/29.4ºC, there are variances in terms of thermally-driven behaviour intention votes. The differences cannot be explained solely by the corresponding thermal state differences. Therefore, varying the thermal conditions in IVEs alone may not be able to reliably produce expected behavior intentions as *in-situ*. To use IVEs to elicit such intentions, other factors in combination with thermal condition changes need to be identified, applied in experiments, and included in analysis. Further studies are needed to identify such factors.

Acknowledgement

This research was supported by the NSF grant CBET-1805914. Any opinions, findings, and conclusions or recommendations expressed in this material are those of the author(s) and do not necessarily reflect the views of the National Science Foundation.

References

Abrahamse, W. and Steg, L. (2009) 'How do socio-demographic and psychological factors relate to households' direct and indirect energy use and savings?', *Journal of Economic Psychology*, 30(5), pp. 711–720. doi: 10.1016/j.joep.2009.05.006.

Ajzen, I., Netemeyer, R. and Ryn, M. Van (1991) 'The theory of planned behavior', *Organizational Behavior and Human Decision Processes*, 50(2), pp. 179–211. doi: 10.1016/j.drugalcdep.2011.10.011.

Chokwitthaya, C. *et al.* (2017) 'The Impact of Lighting Simulation Discrepancies on Human Visual Perception and Energy Behavior Simulations in Immersive Virtual Environment', in *International Workshop of Computing in Civil Engineering*. Seattle, WA: ASCE.

Claudy, M. C., Peterson, M. and O'Driscoll, a. (2013) *Understanding the Attitude-Behavior Gap for Renewable Energy Systems Using Behavioral Reasoning Theory*, *Journal of Macromarketing*. doi: 10.1177/0276146713481605.

Darian-Smith, I. and Johnson, K. O. (1977) 'Thermal sensibility and thermoreceptors.', *Journal of Investigative Dermatology*, 69(1).

de Dear, R. J. and Brager, G. S. (1998) 'Developing an adaptive model of thermal comfort and preference', *ASHRAE Transactions*, 104(1), pp. 1–18.

Fanger, P. O. (1970) *Thermal comfort: Analysis and applications in environmental engineering*. Copenhagen, Denmark: Danish Technical Press.

Fishbein, M. and Ajzen, I. (1977) 'Belief, Attitude, Intention, and Behavior: An Introduction to Theory and Research', *Philosophy and Rhetoric*, 10(2), pp. 130–132. Available at: https://philarchive.org/rec/FISBAI?all_versions=1 (Accessed: 6 February 2020).

Frontczak, M. and Wargocki, P. (2011) 'Literature survey on how different factors influence human comfort in indoor environments', *Building and Environment*. Elsevier Ltd, 46(4), pp. 922–937. doi: 10.1016/j.buildenv.2010.10.021.

Heydarian, A. *et al.* (2015) 'Immersive virtual environments, understanding the impact of design features and occupant choice upon lighting for building performance', *Building and Environment*, 89, pp. 217–228.

Heydarian, Arsalan *et al.* (2015) 'Use of immersive virtual environments to understand human-building interactions and improve building design', in *Communications in Computer and Information Science*, pp. 180–184. doi: 10.1007/978-3-319-21380-4_32.

Hong, T. *et al.* (2015) 'An ontology to represent energy-related occupant behavior in buildings. Part II: Implementation of the DNAS framework using an XML schema', *Building and Environment*, 94(P1), pp. 196–205. doi: 10.1016/j.buildenv.2015.08.006.

Hong, T. and Lin, H. (2012) 'Occupant behavior : impact on energy use of private offices', *Asim IBSPA Asia Conference*, (January).

Hong, Y. and Michalatos, P. (2016) 'LumiSpace: A VR Architectural Daylighting Design System', *SIGGRAPH ASIA 2016 Virtual Reality Meets Physical Reality: Modelling and Simulating Virtual Humans and Environments*, pp. 10:1--10:2. doi: 10.1145/2992138.2992140.

Janda, K. B. (2014) 'Building communities and social potential: Between and beyond organizations and individuals in commercial properties', *Energy Policy*. Elsevier, 67, pp. 48–55. doi: 10.1016/j.enpol.2013.08.058.

Kinateder, M. and Warren, W. H. (2016) 'Social Influence on Evacuation Behavior in Real and Virtual

Environments', *Frontiers in Robotics and AI*, 3(July), p. 43. doi: 10.3389/frobt.2016.00043.

Langevin, J., Gurian, P. L. and Wen, J. (2015) 'Tracking the human-building interaction: A longitudinal field study of occupant behavior in air-conditioned offices', *Journal of Environmental Psychology*, 42, pp. 94–115. doi: 10.1016/j.jenvp.2015.01.007.

Lu, X. and Davis, S. (2016) 'How sounds influence user safety decisions in a virtual construction simulator', *Safety Science*. Elsevier Ltd, 86, pp. 184–194. doi: 10.1016/j.ssci.2016.02.018.

Mackie, C. *et al.* (2004) 'Desktop and immersive tools for residential home design', in *Proceedings of CONVR Conference on Construction Applications of Virtual Reality*, pp. 63–70.

Mahdavi, A. and Pröglhöf, C. (2008) 'Observation-based models of user control actions in buildings', in *25th Conference on Passive and Low Energy Architecgture*. Dublin, Ireland. Available at: http://plea-arch.org/ARCHIVE/2008/content/papers/oral/PLEA_FinalPaper_ref_169.pdf.

McDonald, J. H. (2014) *Handbook of Biological Statistics*. 3rd Editio. Baltimore, MD: Sparky House Publishing.

Menezes, A. C. *et al.* (2012) 'Predicted vs. actual energy performance of non-domestic buildings: Using post-occupancy evaluation data to reduce the performance gap', *Applied Energy*. Elsevier Ltd, 97, pp. 355–364. doi: 10.1016/j.apenergy.2011.11.075.

Natapov, A. and Fisher-Gewirtzman, D. (2016) 'Visibility of urban activities and pedestrian routes: An experiment in a virtual environment', *Computers, Environment and Urban Systems*. Elsevier Ltd, 58, pp. 60–70. doi: 10.1016/j.compenvurbsys.2016.03.007.

O'Brien, W. and Gunay, H. B. (2014) 'The contextual factors contributing to occupants' adaptive comfort behaviors in offices - A review and proposed modeling framework', *Building and Environment*. Elsevier Ltd, 77, pp. 77–88. doi: 10.1016/j.buildenv.2014.03.024.

Rupp, R. F., Vásquez, N. G. and Lamberts, R. (2015) 'A review of human thermal comfort in the built environment', *Energy and Buildings*. Elsevier B.V., 105, pp. 178–205. doi: 10.1016/j.enbuild.2015.07.047.

Saeidi, S. *et al.* (2016) 'Immersive Virtual Environment as an Apparatus for Occupant Behavior Studies', in *ConVR 2016*. Hong Kong.

Saeidi, S. *et al.* (2017) 'Application of Immersive Virtual Environment (IVE) in Occupant Energy-use Behavior Studies Using Physiological Responses', in *Application of Immersive Virtual Environment (IVE) in Occupant Energy-use Behavior Studies Using Physiological Responses*. Seattle, WA: ASCE.

Vischer, J. C. (2007) 'The effects of the physical environment on job performance: Towards a theoretical model of workspace stress', *Stress and Health*. doi: 10.1002/smi.1134.

Zhang, H. *et al.* (2010) 'Thermal sensation and comfort models for non-uniform and transient environments, part II: Local comfort of individual body parts', *Building and Environment*. Elsevier Ltd, 45(2), pp. 389–398. doi: 10.1016/j.buildenv.2009.06.015.

Zhang, Y. and Zhao, R. (2008) 'Overall thermal sensation, acceptability and comfort', *Building and Environment*, 43(1), pp. 44–50. doi: 10.1016/j.buildenv.2006.11.036.

Zhu, Y. *et al.* (2018) 'Potential and challenges of immersive virtual environments for occupant energy behavior modeling and validation: A literature review', *Journal of Building Engineering*, 19. doi: 10.1016/j.jobe.2018.05.017.

Zhu, Y. *et al.* (2018) 'Potential and challenges of immersive virtual environments for occupant energy behavior modeling and validation: A literature review', *Journal of Building Engineering*. Elsevier Ltd, 19(January), pp. 302–319. doi: 10.1016/j.jobe.2018.05.017.

A Design Evaluation Framework for Building Lifts Based on BIM and Pedestrian Simulation

Hui-Hsin Cheng, Shang-Hsien Hsieh
Department of Civil Engineering, National Taiwan University, Taipei, Taiwan
r06521606@ntu.edu.tw; shhsieh@ntu.edu.tw

Abstract. This paper presents a framework for evaluating the lift design of a building by integrating BIM (Building Information Modeling) technology and pedestrian flow simulation. The pedestrian waiting time for lifts in the building can also be estimated by taking pedestrian behavior into consideration in this framework. Besides, social force simulation is utilized to implement agent-based simulation and to imitate pedestrian behavior of taking lifts under various conditions. After that, a design evaluation can give feedback to the initial building design. The proposed framework is examined by a case study in the Civil Engineering Research Building at National Taiwan University.

1. Introduction

In the past decades, high-rise buildings have been constructed in many cities around the world as a part of the competitive efforts among nations to boast of skyscrapers with landmark height (Gipps & Marksjö 1985). Within these buildings, besides the horizontal movement in a single building floor, the vertical transportation between floors is important in human society for people to connect to each other. Consequently, lift design is regarded as a significant role to enable a favorable operation of the building. However, it is quite difficult for designers to understand the relation between spatial distribution and pedestrian behaviors by only their senses and experiences (Okazaki & Matsushita 1993).

Currently the minimum requirements specified by lift design regulations do not explicitly consider pedestrian behaviors in a building. For example, the regulations may only require that the distance between lift entrance and exit of the building in the ground floor should be less than 30 meters. However, complex interaction between various pedestrian flows in the building may lead to unexpected situations for lift design and the "rules of thumb" derived from designer’s experiences is usually employed in design. To address this issue in lift design, this study proposes a pedestrian simulation model with multiple simulation methods. Furthermore, for the last few years, there has been an increasing emphasis on BIM research and pedestrian simulation systems. However, few has used BIM and human behavior simulation tool to evaluate the lift design in a building.

Hence, this study aims to enhance the lift design iteration of the building by providing a lift design evaluation framework based on BIM and pedestrian simulation. It is hoped that a descriptive minimum service level requirement (e.g. waiting time) for lift design may be implemented into design specifications to ensure lift performance. In the following we briefly reviews related literature on BIM and pedestrian flow simulation.

Rüppel and Schatz (2011) explored effect of building condition on human behavior during the evacuation process by transforming data from BIM model to a virtual game engine through an interactive simulation. Mayer et al. (2014) developed a pedestrian simulation model and used information of the BIM model during the operation phase of a building to analyze pedestrian streams under various hazardous conditions (e.g. emergency evacuation, fire and smoke). Marzouk and Daour (2018) managed labor safety based on BIM technology and computer simulation of laborer behavior in construction sites. The model integrated human behavior simulation with BIM tools for planning labor evacuation in the construction sites.

Pedestrian simulation is an essential tool to identify the design issues at the initial design stage and can be applied to the whole lift cycle. A significant number of studies have been conducted in pedestrian flow simulation so as to visualize the pedestrian behavior and predict the potential problems at the building operation stage. Depending on the spatial discretization of the simulation area, we can distinguish two different types of pedestrian simulation models: macroscopic and microscopic models (Schadschneider 2009). They are discussed in the following.

Macroscopic models evaluate pedestrian flows using fundamental fluid flow theory and partial differential equations governing flows of a single type (Hughes 2002). However, a pedestrian flow is multidirectional and they cannot be explained by a single flow-density relationship. The experimental data analyses imply that a pedestrian flow cannot be expressed by a unique fundamental diagram because of the complicated characteristics of a multidirectional flow (Lam et al. 1995). Also, general fundamental diagrams for pedestrian flows have not yet been completed in previous studies. Alternatively, microscopic simulations have advantages when we evaluate pedestrian flows in more general situations by modeling individual pedestrian behavior (Asano et al. 2010). Besides microscopic simulation models, social force model was proposed by Helbing and Molnar (1995), and is a simulation model that can represent pedestrian behavior by a combination of physical and psychological effects. In particular, it represents the interaction among pedestrian and the environment, which can truly simulate the behavior of individual pedestrians taking lifts. Therefore, in this research the concept of social force model is adopted for simulating lift taking scenarios in the building. For example, a pedestrian tends to keep a distance from others, walk in a comfortable speed, and walk along the shortest path to the destination. With these pedestrian behaviors, the lift operation issues like congestion can be identified through pedestrian flow simulations and can also be addressed or even eliminated early in the design stage.

Therefore, this study proposes a framework based on pedestrian simulation methods and Building Information Modeling (BIM) to help evaluate building lift design.

2. The Proposed BIM-based pedestrian flow simulation framework for lift design

This paper proposes a framework to enhance lift design iteration of a building by combining BIM technology and pedestrian flow simulation. The proposed framework of BIM-based pedestrian flow simulation for lift design can be divided into three modules: (A) BIM data extraction module, (B) Simulation module and (C) Redesign interface Module (as shown in Figure 1). More details for the proposed lift design evaluation framework can be found in Cheng (2020).

A system which integrated BIM software and pedestrian simulation software has been developed on the basis of the proposed framework for the feasibility study of the proposed framework. A social force model has been conducted in this study to simulate the pedestrian behaviors. The accuracy of the pedestrian simulation is verified by real world pedestrian flow data collected in the Civil Engineering Research Building (CERB) at National Taiwan University Campus. In addition, flexible adjustment of design parameters, for instance, lift capacity and lift velocity, has been applied to the simulation. Based on this, pedestrian behaviors and lift cost can be analysed for evaluation of lift design.

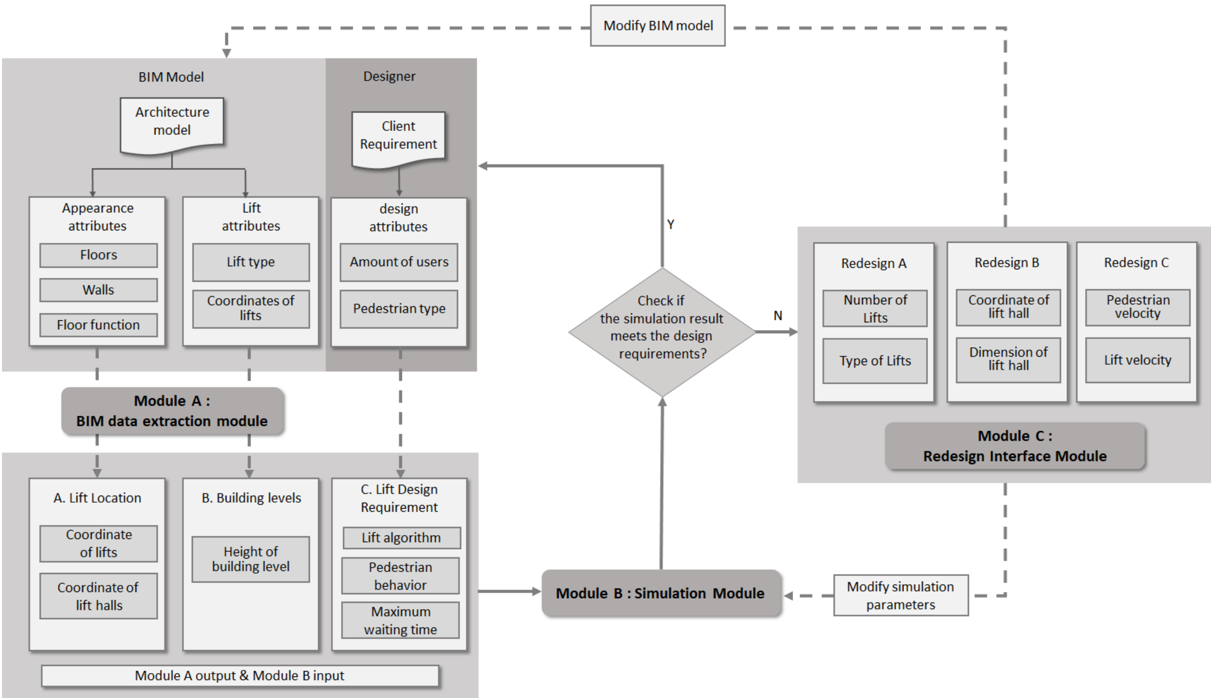

Figure 1: The Proposed BIM-based Pedestrian Flow Simulation Framework for Lift Design

2.1 BIM Data Extraction Module

The purpose of Module A: BIM Data Extraction Module is to extract information from BIM models for a building designer to create a 3D pedestrian simulation environment. Although BIM models can provide representation and visualization of each building component in detail, they cannot be directly used to simulate the pedestrian flow for revealing potential issues in lift design and operations. Because the computational load for simulation can be very high when all the detailed geometry features of the building are considered, necessary geometry simplification is required. In this study, a whole building is simplified into an environment in which only pedestrians waiting and taking lifts and their needed spaces are modeled. There are three main objects extracted from BIM models: lift halls, walls and lifts. The geometric parameters including all coordinates and dimensions of waiting halls and lifts, and the height of each floor level are exported to a text file, which is later used as the input for simulation (see Figure 2).

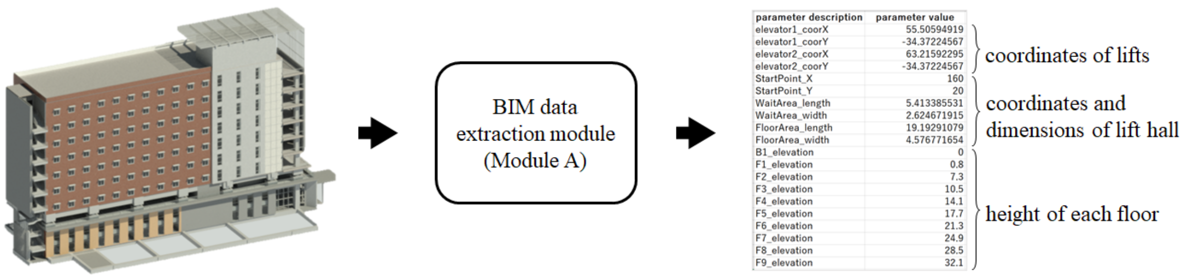

Figure 2: BIM Data Extraction Module Example (Cheng 2020)

2.2 Pedestrian Simulation Module

The purpose of Module B: Pedestrian Simulation Module is to set up a 3D pedestrian simulation environment and allow for visualization of the interaction between pedestrians and lifts in a building. By means of pedestrian simulations, potential problems exist in lift operations can be identified early and the lift design can be evaluated at the initial design stage (Eastman 2011). In addition to the 3D environment created based on the output from the BIM data extraction module, both the lift and pedestrian behaviors should be modeled in the pedestrian simulation Furthermore, the properties can be changed flexibly in the simulation, for instance, the lift type, lift speed and the entry rate of pedestrians into the building. After the pedestrian simulation, an outcome report is exported and analysed. There are three core steps in the pedestrian simulation module: (1) Simplified 3D model creation, (2) Multiple simulation approach and (3) Simulation outcome and data visualization. They are introduced in the following subsections.

2.2.1 Simplified 3D model creation

Since a simplified 3D environment is required for pedestrian simulation, the information about the dimension, location and design requirement are imported to the pedestrian simulation module and used to create a new simplified model for simulation. As shown in Figure 3, after both the dimension and location information are extracted, all the values are used as the input to create the 3D model with simplified geometry for pedestrian simulations. For example, the information of a floor object can be obtained from the output of the BIM data extraction module. Based on the starting point coordinates and the length, width and height values of floors, the geometry of the floor objects can be created. Since the height of a floor can also be specified by the elevation value in the BIM model extraction data, floor objects can be created in the 3D space.

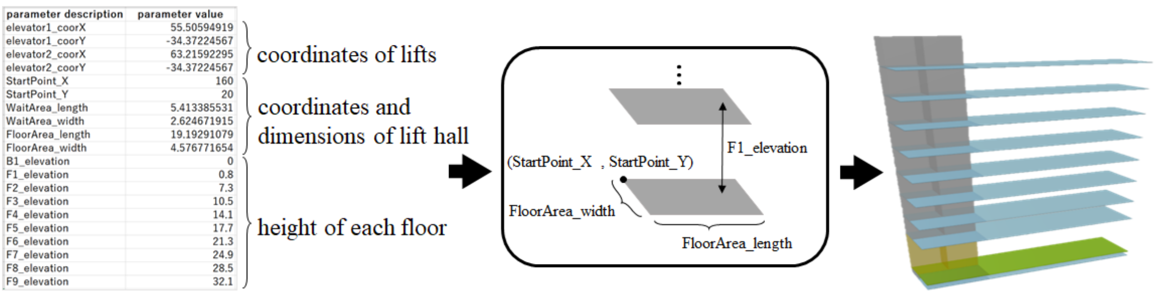

Figure 3: Illustration of the Simplified 3D Model Based on the Data Extracted from a BIM Model (Cheng 2020)

2.2.2 Multiple Simulation Approach

Once the required data for pedestrian simulation are extracted from the BIM model, a simplified spatial model can be created for the simulation software, called Anylogic (Anylogic.com 2020), which is a commercial simulation software, providing a multi-method simulation that supports system dynamics, agent-based and discrete event methodologies. Through simulations, how the pedestrians interact with each other and with their environments can be visually observed.

The mechanism of the multiple simulation approach is briefly introduced here. Because state variables in the pedestrian simulation change only at discrete time instants, a discrete-event model is usually implemented in the approach. Upon discrete event modeling method, simulators operate on a fixed spatial environment and objects are guided within scenarios in a fixed time step. However, the objects in the model should be self-contained and identifiable; for example, the forces acting on agents to interact with each other should be considered on top of scenarios in the simulation. Agent-based model can explicitly model the complexity arising from individual actions and interactions in the real world. In the system dynamics model, the real-world processes are represented in terms of stocks (e.g. of material, knowledge, people, money), flows between these stocks, and information that determines the values of the flows.

Among these, we have implemented the system dynamics model to simulate the lift behavior in the simulation model (Asano et al. 2010).

Internal Mechanism of Pedestrians

Flow of people through a building depends on different characteristics, such as building use (office, classroom, laboratory, etc.), time of the day, existence of "attractions" (e.g. Trash rooms) and other factors (Mayer et al. 2014). In particular, there are three main fundamental modes of traffic: up-peak, heavy two-way, and down-peak (Cho et al. 1999). In this study we focus on the up-peak and down-peak traffic. In Anylogic, the pedestrian flow simulation model generates a series of forces based on the pedestrian's target, the adjacent distance between pedestrians, and the location of obstacles. These forces are summed and used to form the acceleration of movement as shown in Table 1.

Table 1: Force Component Between Pedestrians (Marzouk & Daour 2018)

Force	Description
Destination	Force required to nudge agent so that it walks in comfort speed toward its target
Neighbor	Repulsive force from each neighbor within range
Cohesion	Force pushing towards centroid of neighbors with similar targets
Collision	Force pushing agent away from collisions with oncoming neighbors
Drift	Force pushing agent in bias direction when faced with oncoming agents in narrow spaces
Approach target	Force pushing agents towards the middle of a target when approaching

Lift Dispatching Logic

The lift dispatching logic adopted is a common and simple one. While taking a lift, the passenger makes a request by pressing a button on the current floor. The button triggers a direction signal that calls a lift to come and the system of lifts will select the most suitable lift to answer the call immediately. The lift that is going in the same direction as the call signal will be asked to pick up the passenger. After passengers enter the lifts, they will press the target floor buttons which trigger requests to the lift dispatching system, and the target floors will be arranged in an ascending or descending order.

2.2.3 Data Visualization of Simulation

The outputs of the Pedestrian Simulation Module (Module B) are simulation results with data visualization. Upon the simulation, the interaction between pedestrians and lifts in a building can be observed. Meanwhile, a lift service level in a building can be materialized based on the data visualization and data analysis of the simulation. For example, the average waiting time in the lift hall of each floor can be obtained to assess if the lift distribution in the building is appropriate. If pedestrians often spend long time waiting a lift, the lift design of the building may need to be re-examined and improved.

In the simulation, several parameters related to lift design, e.g. criterion of maximum waiting time for pedestrians, the type and speed of lift, etc., can be flexibly set by the designer to explore different design scenarios. Based on the criterion set in the simulation and the data analysis after the simulation, possible directions on redesign related to lifts in the building are suggested to the designer. Then, the output of the Pedestrian Simulation Module is exported as the input of the Redesign Interface Module in which the designer is guided to make desired design revisions in the BIM model.

2.3 Redesign Interface Module

The purpose of Module C: Redesign Interface Module is to assist the designer to carry out desired redesign for the lifts in the BIM model based on the evaluation output of the Pedestrian Simulation Module. Possible redesign options are suggested to the designer for improving lift design in the building. Once the desired redesign option is selected, the module brings the designer to the corresponding objects in BIM model for redesign.

Three redesign options are currently provided in the system as shown in Figure 1. They are corresponding to the redesign of the volume of lifts (type and quantity), lift halls (position and dimensions), and the speed of lifts and assumed pedestrian entry rate into the building. For example, when congestion issue is observed in the simulation, the designer can choose one of the three options in the Redesign Interface Module for design revision and the target objects for redesign will be automatically brought to the designer in the BIM model.

3. Case Study

A prototyped system is developed on the basis of the proposed framework for a feasibility study. The Civil Engineering Research Building (CERB) at National Taiwan University Campus is chosen for the study.

3.1 Data Extraction from BIM Model

The framework outlined in Section 2 and in Figure 1 was employed to simulate the lift design iteration of a building project. CERB is located in the Taipei City, Taiwan, consisting of 9-stories and 1-story basement with a site area of 990 m^2 and a total floor area of 8250 m^2. The building is mainly used for hosting some laboratories, classroom, and offices for faculty and graduate students. The BIM model of CERB was created using Autodesk Revit. The Autodesk Revit API (Application Programming Interface) was used to develop custom tools for extracting BIM data from the BIM model in this study.

3.2 Pedestrian Flow Simulation

As mentioned earlier, pedestrian behaviors change with the environment (Gipps & Marksjö 1985). Understanding how the lift design changes pedestrian behaviors is important for the building designer to envision if a potential problem may happen at the operation stage. A microscopic simulation is able to generate movement of each pedestrian. Therefore, a minor change of the pedestrian movement pattern or change in the simulation environment layout can cause a very different simulation outcome. The simulation is particularly helpful for us to check specific phenomena like congestion or long waiting time when people are taking lifts at rush hours.

3.3 Redesign

According to the parameters set in the simulation model, the simulation is used to estimate the pedestrian waiting time for lifts and check if the allocation of lifts in the building is appropriate. Based on the simulation results, the prototype system provides the designer with redesign options for modifying the current lift design in the building. Figure 4 illustrates the three redesign options currently supported by the prototype system.

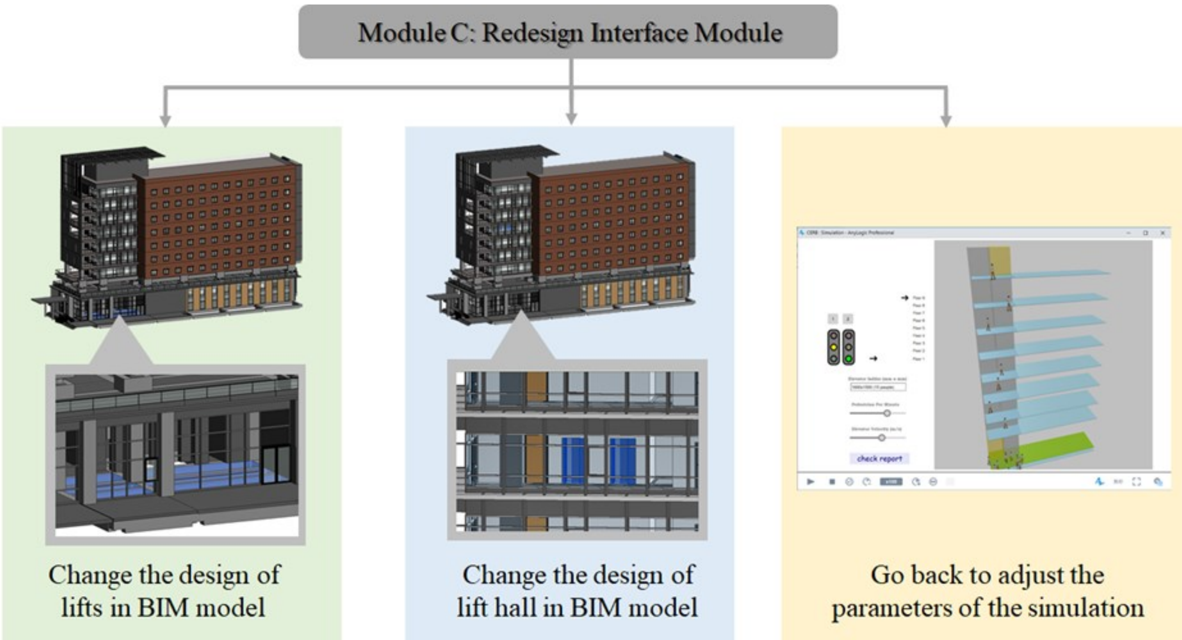

Figure 4: Three Redesign Options Supported by the Prototype System (Cheng 2020)

4. Discussion on the Simulation Results

This research takes advantage of the research conducted by Hsu (2019) to obtain real pedestrian flow data in CERB through multi-target, multi-camera tracking. The data of pedestrian flow in CERB from 7 a.m. to 12 p.m. on May 15th, 2019 are used as control data in this study. As can be seen in Figure 5, the simulation results are compared with the real world data captured in CERB.

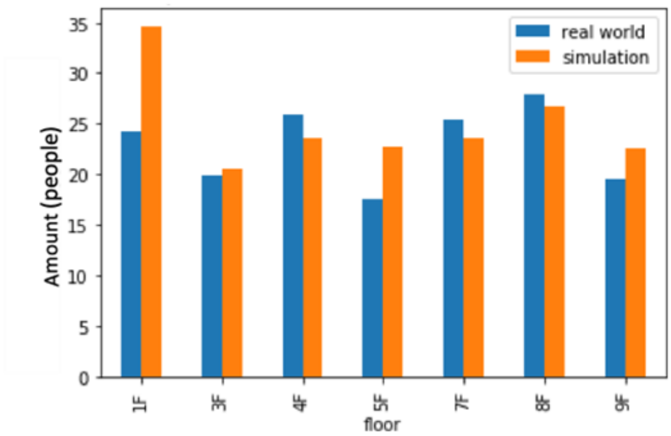

Figure 5: The waiting time for lifts on variation of levels (Cheng 2020)

4.1 Pedestrian Waiting Time Versus Lift Capacity

Figure 6 shows the average pedestrians waiting time versus lift capacity from the pedestrian simulation. It can be seen that if the crowd has only 355 people, the increase of lift capacity helps little on reducing the waiting time. However, when the number of people goes up to 900, the increase of lift capacity does help on reducing the waiting time.

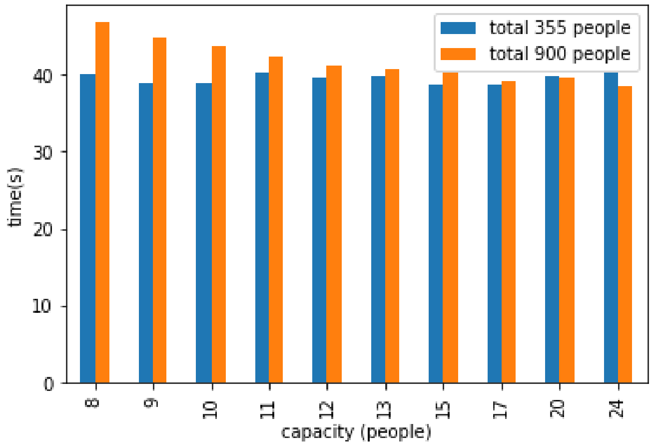

Figure 6: The Average Pedestrian Waiting Time Versus Lift Capacity (Cheng 2020)

4.2 Pedestrian Waiting Time Versus Lift Velocity

Figure 7 shows the average waiting time of pedestrians versus lift velocity at different pedestrian entry rates. It can be seen that, under the condition of high average pedestrian entry rate (e.g. 3.54 people/min – 5.9 people/min), the average waiting time decreases when the lift velocity increases. However, this effect becomes less obvious when the average pedestrian entry rate is low (e.g. 2.36 people/min).

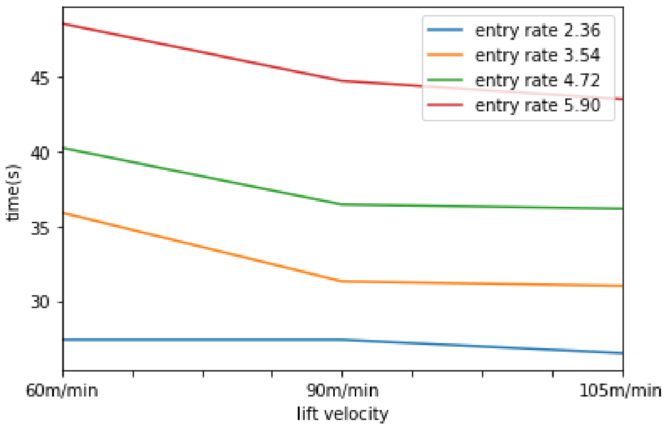

Figure 7: Average Waiting Time of Pedestrians Versus Lift Velocity at Different Pedestrian Entry Rates (Cheng 2020)

5. Conclusion

In this paper, a design evaluation framework considering pedestrian behavior at the conceptual design stage of building lift design has been proposed to avoid potential problems at the lift operation stage. A prototype system based on the framework has also been developed to demonstrate how the design iteration can be accelerated with the simulation and evaluation approach that integrates BIM and pedestrian simulation techniques. There are three main highlights for our integrated application of BIM and pedestrian simulation:

1. Building information can be automatically extracted from a BIM model and a simplified 3D model can be subsequently created to support pedestrian flow simulations.

2. Parameters like lift type, lift velocity and the pedestrian entry rate in the simulation model can be flexibly adjusted to explore different design scenarios and visualize their different design outcomes.
3. The redesign interface prototyped demonstrates the feasibility of automatically bringing the designer to the target BIM objects related to the selected redesign options in the BIM model.

Based on the above, the lift design can be evaluated earlier at the initial design stage and issues at operation stage can be resolved in advance in the iterative design process.

Acknowledgement

The authors would like to thank Prof. I-Chen Wu of National Kaohsiung University of Science and Technology for her support of the Anylogic software.

References

Anylogic.com (2020). AnyLogic: Simulation modeling software tools & solutions for business. Available at: https://www.anylogic.com.

Asano, M., Iryo, T. and Kuwahara, M. (2010). Microscopic pedestrian simulation model combined with a tactical model for route choice behavior. Transportation Research Part C: Emerging Technologies, Volume 18, Issue 6: pp. 842–855.

Casey, M.J. (2008). Work in progress: How building informational modeling may unify IT in the civil engineering curriculum. In: 38th Annual Frontiers in Education Conference, 2008, Saratoga Springs, NY, USA.

Cheng, H.H. (2020). A framework for building lift design evaluation based on BIM and pedestrian simulation. Master Thesis, Department of Civil Engineering, National Taiwan University, Taipei, Taiwan, 2020.

Cho, Y.C., Gagov, Z. and Kwon, W.H. (1999). Elevator group control with accurate estimation of Hall call waiting times. Proceedings 1999 IEEE International Conference on Robotics and Automation, 1999, Detroit, MI, USA.

Eastman, C., Teicholz, P., Sacks, R. and Liston, K. (2011). BIM handbook: A guide to building information modeling for owners, managers, designers, engineers and contractors, 2011: John Wiley & Sons Inc.

Gipps, P.G. and Marksjö, B. (1985). A micro-simulation model for pedestrian flows, Mathematics and Computers in Simulation (MATCOM), Elsevier, Volume 27, Issue 2: pp. 95–105.

Helbing, D. and Molnar, P. (1995). Social force model for pedestrian dynamics. Physical Review E, 1995. Volume 51, Issue 5: pp. 4282-4286.

Hughes, R.H. (2002). A continuum theory for the flow of pedestrians. Transportation Research Part B: Methodological, 2002. Volume 36, Issue 6: pp. 507–535.

Hsu, S.H. (2019). Indoor occupant behavior analysis with multi-target, multi-camera tracking. Master Thesis, Department of Civil Engineering, National Taiwan University, Taipei, Taiwan, 2019.

Lam, W.H.K., Morrall, J.F. and Ho, H. (1995). Pedestrian flow characteristics in Hong Kong. Transportation Research Record: Journal of the Transportation Research Board, 1995: pp. 56–62.

Marzouk, M., and Daour, I. (2018). Planning labor evacuation for construction sites using BIM and agent-based simulation. Safety Science, Volume 109, pp. 174–185.

Mayer, M., Klein, W., Frey, C. Simon, D., Kielar, P. and Borrmann, A. (2014). Pedestrian simulation based on BIM data. In: ASHRAE/IBPSA-USA Bldg Simulation Conference, 2014, Atlanta GA, USA.

Okazaki, S. and Matsushita, S. (1993). A study of simulation model for pedestrian movement with evacuation and queuing, in Proceedings of the International Conference on Engineering for Crowd Safety, 1993.

Rüppel, U. and Schatz, K. (2011). Designing a BIM-based serious game for fire safety evacuation simulations. Advanced engineering informatics, 2011. Volume 25: pp. 600–611.

Schadschneider, A., Klüpfel, H., Kretz, T., Rogsch, C. and Seyfried, A. (2009). Fundamentals of pedestrian and evacuation dynamics. Multi-Agent Systems for Traffic and Transportation Engineering, 2009, IGI Global. pp.124–154.

BIM-Based Bill of Quantities Generator following POMI and NRM2 Methods of Measurement

Tarek Zaki, Abdelrahman Magdy, Khaled Nassar
The American University in Cairo, Egypt
tarekzaki@aucegypt.edu

Abstract. Quantification tools in BIM software do not abide by a specific method of measurement; instead a set of rules are used to query parameters and properties from the geometric elements of the model and generate a tabular form of quantities. Different types of Methods of Measurement (MOM) set standardized rules for estimation and Bill of Quantities (BOQ) preparation by organizing works based on systematic structures, layouts, content and phrasing schemes. This paper presents rule-based quantity takeoff algorithms in BIM following takeoff schemes from different standard MOMs and accordingly generate descriptive BOQs ready for pricing. The algorithms were tested on a number of building elements then an industry case was used to validate the model followed by a discussion of the results. This study aims to contribute to the improvement of the industry practice by providing methods for integration between the standard methods of measurement in line with the ongoing BIM developments.

1. Introduction

Throughout the past years, BIM has been emerging in the field of construction and its presence is demonstrated in the different phases that vary among design, construction simulation, cost estimation, risk estimation, facilities management, etc. BIM technology is currently one of the most important tools used by the construction industry which is in continuous development to take over the traditional manual processes used projects throughout the project lifecycle. A Bill of Quantities (BOQ) is a project-specific document that provides an itemized quantification for all the project elements as defined in the drawings (or the BIM project) and specifications. BOQs are used for cost estimation to identify the price for carrying out the works. The amount of information within the BOQ is highly dependent on the design stage in which the BOQ was prepared. According to Zaki, et al. (2017), each design stage is controlled by a Level of Development (LOD) criteria, which provides a threshold for the extent to which details and information should be included or excluded within each design stage. As the project design progresses, more project information and details are identified. Thus, the reliability of quantification and cost estimating from BOQs prepared during the conceptual design stage (LOD100) would not be as reliable as BOQs prepared during the tender design stage (LOD300).

There are no specific ways or methods to write or classify items within a project's BOQ. However, using guidance from a standard format helps to avoid any ambiguities, misplacement, misinterpretation or misunderstanding when identifying work items to evade pricing errors. Some guidance formats are provided to overcome the downfalls of not using standards for drafting BOQs. The Construction Specification Institute (CSI) developed the "MasterFormat" standard which is originally used to draft project specifications. Prior to the year 2004, the MasterFormat was structured upon 16 divisions of work items defining information pertaining the construction requirements, products and activities of each item. After 2004 an update was released to further define works upon 50 divisions. As a common practice and in order to facilitate the communication among the different project stakeholders, BOQs are prepared following the MasterFormat for easier cross-referencing with the various project documents. Still, the MasterFormat does not provide specific rules for the measurement, item description or quantification of works. It is widely recognized that the presentation of a BOQ is subject to many factors including the project type, contract type, contract value, client requirements, project location, contractor scale, etc. For instance, BOQs prepared under lumpsum contract types are drafted with high abstraction levels compared to re-measured contracts types which require a clear level of detail for each item defined.

There are different standard Methods of Measurement (MOM) provided by international institutions all over the world that provide guiding rules on how define, describe and quantify items for a BOQ preparation. Commonly used international MOMs for building construction works include the Principles of Measurement Internationals (POMI), the Standard Method of Measurement 7th Edition (SMM7) which was superseded by the New Rules of Measurements (NRM2) starting January 2013. Other MOMs are used for Civil Engineering types of projects such as the Civil Engineering Method of Measurement 4th Edition (CEMM4). Each MOM has its advantages and disadvantages that governs its applicability on a project's BOQ (Magdy & Ezeldin, 2016). These MOMs do not necessarily provide a standard form of the BOQ; instead, it provides instructions on how to quantify items with what to include and what to exclude. Thus, the difference between BOQs prepared following a certain MOM would be demonstrated in the form of the content of the BOQ such as the level of details by which the items are broken down and the items description.

The BIM technology has gained its popularity over the years as it facilitates intelligent building design allowing the industry to shift to BIM-based quantity takeoff and estimation. BIM models are designed to be data-rich, intelligent and with the ability to incorporate material properties of different elements within the model to facilitate quantities extraction compared to the tradition human-based quantification and measurement methods. The extraction of quantities from a BIM project using any commercial BIM software is simply a matter of tabulation for elements with their drawn quantities (either itemized or grouped) without following a specific or standard MOM. This means that a BOQ preparation from a BIM project would first require the extraction of quantities from the BIM model - which would generate an intermediate table/schedule of items first – followed by the quantity surveyor's input in regrouping items from the extracted tables and manually drafting a BOQ from scratch. There are numerous commercial BIM software in the market, some of which incorporate the use of the standard MOMs within their quantity tabulation methods; however, non generate BOQs which is still a human-based task. Moreover, any changes or updates to the BIM project would require rebuilding the BOQ again.

This paper presents the application of automatically generating descriptive BOQs based on standard MOMs using rule-based quantity takeoff algorithms in BIM. The scope of this paper is limited to the use of POMI and NRM2 as rules for measurement. However, the ultimate objective is to contribute to the improvement of the industry practice by providing methods for integration between the standard MOMs in line with the ongoing BIM developments.

2. Literature Review

2.1 Methods of Measurement

Principles of Measurement International (POMI) was published by the Royal Institute of Chartered Surveyors (RICS) Business Limited in 1979 with the purpose of providing guidance towards preparing the BOQs for most types of projects. According to POMI (1979), a project can be divided into 15 work items with general rules on how to breakdown and define items. POMI is well known as an oversimplified method of measurement due to its generic measurement rules for items. Williams (2016) suggested that due to its generic and oversimplified methodology, POMI was naturally developed to serve different types of construction projects such as buildings, infrastructure or civil. POMI (1979) also suggests that this method could be used were no method of measurement was defined for a project. However, this method of measurement has some drawbacks. The oversimplification and abstraction of items may cause disputes when evaluating or pricing items in the BOQ; moreover, the fact the POMI was released in 1979 makes it ignore some of the new construction techniques (RICS, 2012).

The New Rules of Measurement (NRM2) were published by the Royal Institute of Chartered Surveyors (RICS) in 2012 with the aim of identifying how items should be measured in the building works (NRM2, 2012). The NRM are divided into three volumes; NRM1, NRM2 and NRM3 which were developed to facilitate the cost management process throughout the different project stages (Matipa et al., 2010). NRM2 is the volume that provides the set of guiding rules to prepare BOQs by defining how items should be measured and broken down. NRM2 divides the building works on to 41 sections. Each section provides a detailed breakdown of its measurement rules in a tabulated form; starting with mandatory information to be provided, works and materials deemed included followed by how items are described and measured on to tree levels of detail (NRM2, 2012). The advantages of NRM2 over other methods of measurement are highlighted from the fact that this method provides a thorough description of items within the BOQ. However, this has method has some drawbacks due to its detailed descriptive nature which can sometimes be time consuming for projects besides the fact that extensive item breakdown could cause an increase in the tender price with each broken down items being priced separately (Campbell, 2013).

POMI and NRM2 differ mainly in the level of details of the BOQ produced from each one. NRM2 is for building works only while POMI is flexible to be used in various project types. NRM2 divides the scope of the project into 41 work sections, unlike POMI that involves only 15 work sections. POMI is an old method of measurement that is familiar to construction firms and produces somehow abstract BOQs; unlike NRM2 that is a recent method of measurement used to produce very detailed BOQs. POMI might be suitable for projects that have traditional scope, local clients and contractors familiar with the project location, lower value projects and lump sum contracts. On the other hand, NRM2 can be useful in large scale projects with international clients and contractors and re-measured contract types (Magdy & Ezeldin, 2016).

2.2 BIM and Quantity Take-off

Despite the fact that BIM seems to be an effective tool in the cost control process of any project, the process of automating the quantity takeoff in a project faces some challenges. Montero et al. (2013) studied the use of BIM for quantity takeoff compared to the conventional CAD-based methods. The study reported that BIM quantity takeoff is not a straightforward process. It is essential to use a structured system of IDs and layers inside the model to ensure consistence of the takeoff process. Lee et al. (2013) proposed a methodology that automatically infers the most appropriate work items suitable for building elements in BIM on the work conditions using semantic technology. A query engine retrieves relevant information related to the inference of the work item using expert knowledge. The idea was to restructure BIM data which could then be used for accurate quantity takeoff. Zaki et al. (2017) developed a set of algorithms that could generate virtual mockups for block walls using parametric modeling in BIM. The idea was to provide a method for the auto generation of shopdrawings for block walls by detailing of wall assemblies. The algorithms were also developed for quantification of assemblies, which could work in concurrent with detailed method of measurements such as NRM2 quantifying blockwork elements in a BIM project. Abanda et al. (2017) explored the uses of cost estimating software with BIM. Such software might have a certain standard MOM defined on it which reduces its flexibility of being used for many projects. Also, most cost estimating BIM tools just provide a breakdown of the items with less capabilities of providing a spreadsheet BOQ (Eastman et al., 2011).

3. Model Design

A model was developed onto three modules; inputs module, engine module and outputs module as shown in Figure 1.

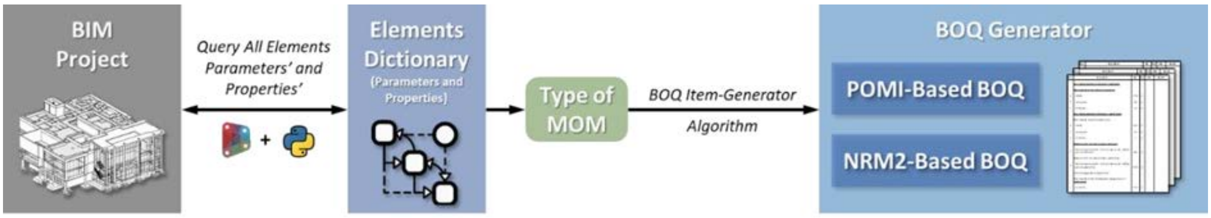

Figure 1: Model Design

Using a BIM project designed with LOD300 or higher, the project quantity surveyor would first select the type of MOM to be used when preparing the quantity extraction from the model. A set of developed rule-based takeoff algorithms are executed on a BIM project to generate descriptive quantification for each of the model elements and materials. The extracted information is restructured in the form of a data dictionary within the code, grouped by the category of elements and sub-grouped by functions and types of materials. Then, a developed sentence-generator algorithm (either rule-based or generic-based, depending on the type of MOM required) queries information from the coded data dictionary and restructures phrases to generate the required item descriptions along with the quantification and unit of measurement for each. The list of generated sentence structures is intelligently grouped by work type such as Concrete, Masonry, Finishes, etc. then placed and alphabetically numbered inside a BOQ template file under the required headers and in the required work divisions. A sample of the developed algorithm for the quantification of Walls is shown in Figure 2.

In this study, Autodesk® Revit® 2017 was used as the BIM environment while DesignScript® and Python® were used as the programming languages to access and query information from the Revit API. The codes were compiled in Dynamo v2.0.1 for Revit.

3.1 Inputs Module

Three inputs are required by the project quantity surveyor prior to the execution of the model; (1) BIM project, (2) the type of MOM to be used, and (3) the path of the BOQ template fire to use.

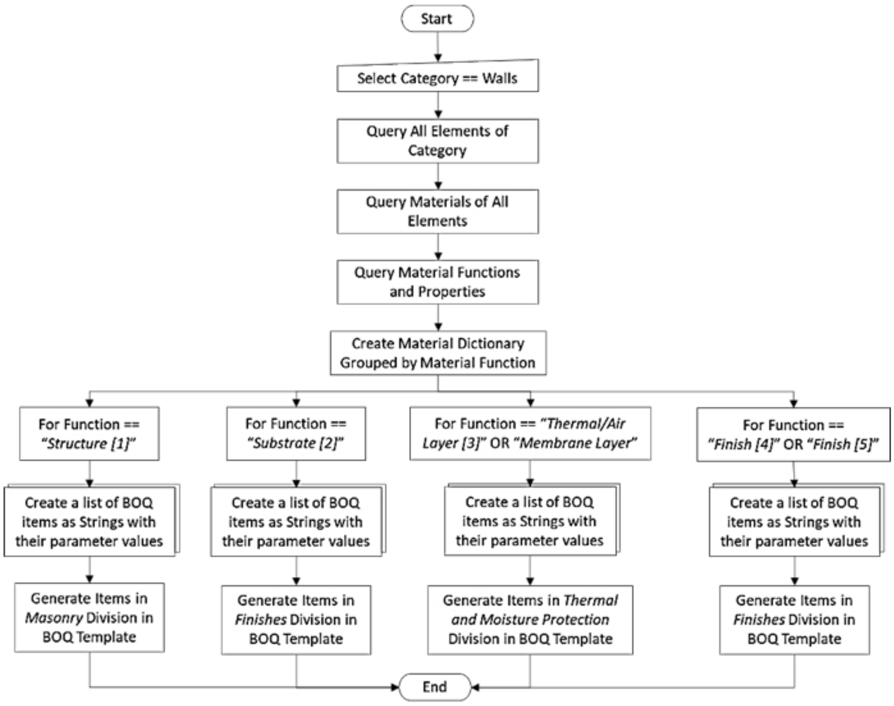

Figure 2: A sample algorithm for the quantification and items generator for Walls

3.1.1 BIM Project.

The first input would be a BIM project, designed with LOD300 or higher to ensure that all elements were drawn with the required level of information for accurate quantities extraction. Typically, LOD300 are tender models where all elements are defined with specific families, types and materials as per the project requirements and specifications.

3.1.2 The Type of MOM.

The second input would be which type of MOM to use in the measurement. This is a crucial part in the execution of the model since the type of measurement would specify the type of algorithm to use for information extraction and quantification from the model as well as the item description generation. To facilitate the selection of the MOM type, the model was designed with a user interface, starts by the executing the developed takeoff definition using Dynamo Player for Revit. Using the radio buttons on the interface, the user would select which type of MOM to use for preparing the BOQ.

3.1.3 Empty BOQ templates.

The third input would be empty BOQ templates files that shall be drafted based on the project's required MOM. For the purpose of this study, two empty BOQ templates were used, one was structured based on POMI and another based on NRM2. Both templates were drafted as MS Excel spreadsheets. Each BOQ was designed with a number of divisions including summary, preliminaries, measured works, provisional sums, dayworks, etc. Each division was designed with A4 paper sizes, having six columns of different widths with the following headers: No., Item Description, Quantity, Unit, Rate and Amount respectively. The main difference between either template files were the level of abstraction. POMI based BOQs are often generic since the MOM itself does not provide specific rules for measurement or describing items. On the contrary, NRM2 based BOQs are very detailed to the elemental level and provide specific rules of measurement.

3.2 Engine Module

The engine module was designed with two nested algorithms. The first would be the execution of a data-structuring takeoff algorithm that queries all the attached information to elements within the model based on their Category. For Example, for the category Walls, the algorithm would create a material dictionary grouped by material function then by material name while mapping geometric parameters to each material name. Materials in Revit are generally defined based on the Function of each and are classified according to the Table 1.

Table 1: Functions of Material Finishes.

Layer Function	Function Description
Structure [1]	The layer that supports the Element (Wall, Floor, Roof, …)
Substrate [2]	Material acting as foundation to another material (Plaster, …)
Thermal/Air Layer [3]	Insulation layer
Membrane Layer	Insulation membrane layers
Finish 1 [4]	The exterior finish layer
Finish 2 [5]	The interior finish layer

Thus, the algorithm would create a data tree classifying all elements in the selected category or in the model by Function then by Material Name, each with all attached parameters and properties such as Thickness, Area, Volume, etc. The objective of the restructured data tree is to facilitate the querying of information for the rule-based item description required by each MOM algorithm. For instance, one of the entries of the dictionary would be Masonry; Concrete Block; Hollow Core; Thickness 250mm; Type W2 in addition to all its attached parameters.

The BOQ generator-algorithm can be simply described as a fill-in-the-blanks routine. A set of blank areas are defined within the BOQ template file to work concurrently with the algorithm. The execution starts by user defining the category/categories required for takeoff. A query algorithm is executed which generates a dictionary of all elements within the category; grouped by material functions and properties with all parameter embedded within each element. A set of logic operators divert the type of element to a match the element functions and divert the elements each to the specific BOQ division.

3.2.1 POMI-Based Algorithm.

POMI does not provide specific rules when describing items in the BOQ; instead it provides some measurement rules when attempting to quantify elements. Therefore, it is the task of the quantity surveyor to describe items to suit best what is in the drawings, BIM model and specifications. The following Figure 3 represents the model output for the Masonry division from a pilot BIM project that was used for testing the POMI-based algorithm. Since POMI does not provide a specific BOQ structure, the template file was designed to follow the MasterFormat (16 Divisions). The Masonry works were grouped under Division 04 followed by cross-referencing items related to Walls under section 042000 Unit Masonry. Within the Unit Masonry section, items are grouped by a header with no specific grouping rules; thus, a suggestion would be by the "Fire Rating" parameter for walls. Since the purpose of the BOQ is to price elements, the sentence structure of the header should define what should be included and excluded from the upcoming items to be priced correctly. Thus, the sentence-generator algorithm would add up a set of parameters from the model's data-tree to form a header sentence with parameters separated being a semi-colon in the format: "*materialName; materialType; fireRatingParameter; genericPricingText*". Next, takeoff items having the same parameters within the header sentence are grouped under such header using an alphabetic counter routine.

Items are described to follow the string structure "*categoryName*; *thicknessParameter &&* "*thick*"; *familyTypeName*;" with each item description its respective quantity queried from the *areaParameter* and the *areaUnitParameter* from the model's developed data-tree.

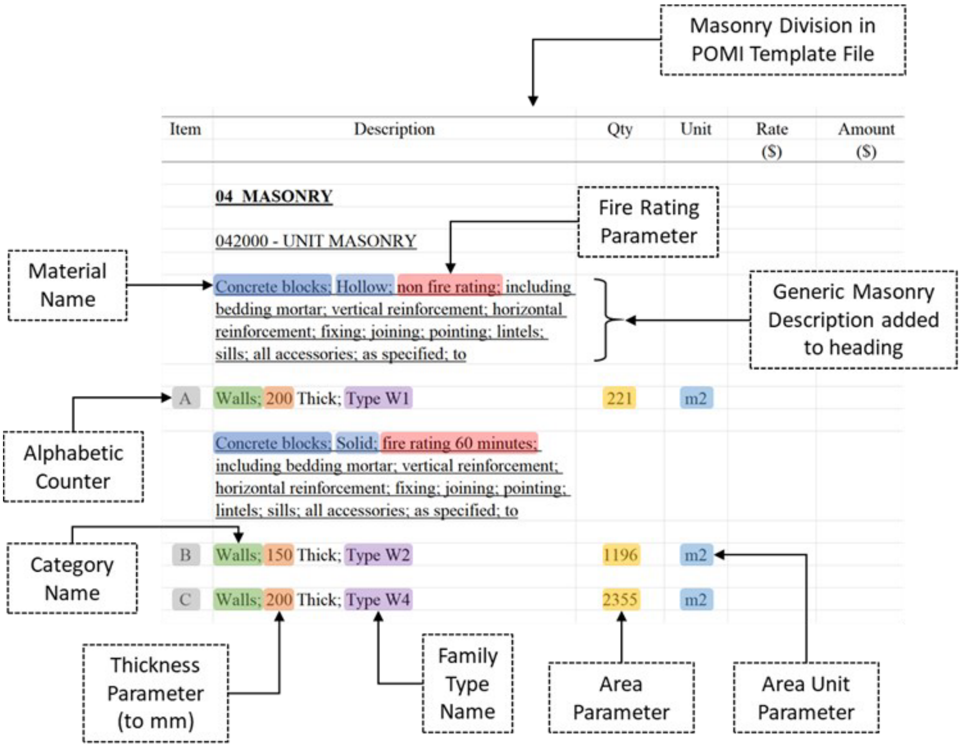

Figure 3: Sample Output for the POMI-Based Algorithm in the BOQ template

3.2.2 NRM2-Based Algorithm

Compared to POMI, NRM2 does provide specific rules to be followed when describing items in the BOQ, as well as some specific measurement rules when attempting to quantify elements. However, for each division a section preamble needs to be defined first. This section should include all referenced documents related to the section in hand as well as pricing requirements for all items on what should be included and excluded. Thus, the task of the quantity surveyor in this case is to manually define items under the preamble section for each division and review (and adjust as needed) the generated item descriptions from the model. The following Figure 4 represents a sample output for the Masonry division from a pilot BIM project that was used for testing the NRM2-based algorithm.

The header level defines what type of work is being measured with the over thickness stated; thus, the text generator would query and structure the following information: "*categoryName; thicknessParameter && "overall thickness"*. The takeoff items having the same parameters within the header sentence are grouped under such header using an alphabetic counter routine. items are described to follow the string structure "*materialName; wallFunction; fireRatingParameter; familyTypeName;*" with each item description its respective quantity queried from the *areaParameter* and the *areaUnitParameter* from the model's developed data-tree. An item is added to the end of the blockwalling section which is allowance for openings, defined as generic text to include all extra items for wall openings, since these items have different method of forming, a generic text that says "*method of forming to Contractor's discretion*" would suffice. As required by the NRM2 this type of quantity should be measured as lengths, thus the queried parameter in this case is the summation of the length parameters for doors and window families in the BIM model.

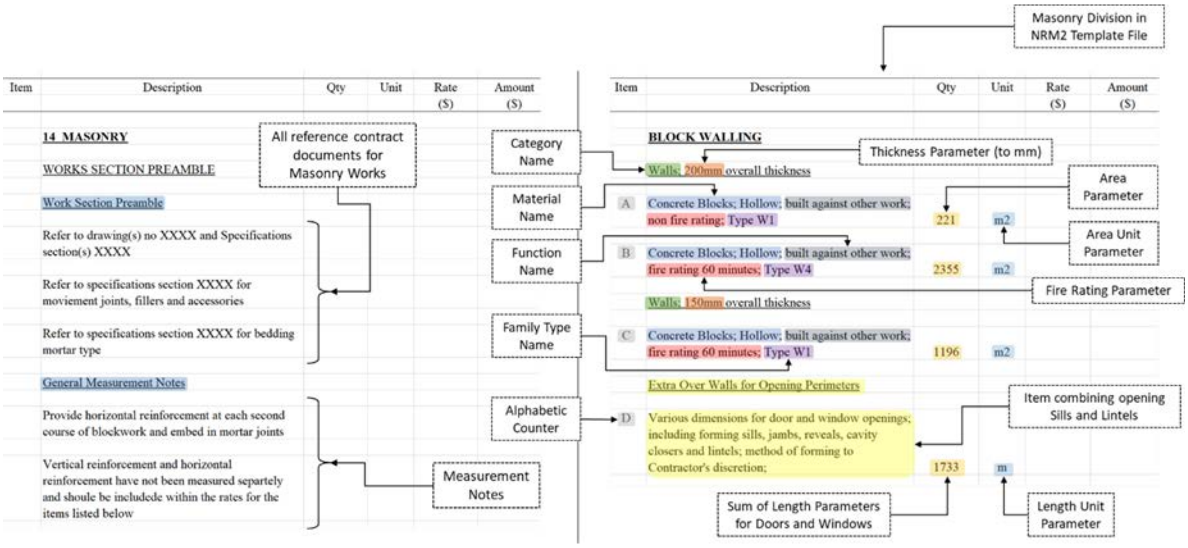

Figure 4: Sample Output for the NRM2-Based Algorithm in the BOQ template

4. Case Study

In order to validate the model, a tender BIM project for a university building designed to LOD300 using Autodesk® Revit® was used and along with its tender BOQ which was based on NRM2. The model was used to generate a BOQ for the Walls category of the building followed by comparing the results with the existing BOQ of the project. Executing the model starts by accessing the Dynamo Player within Revit's toolbar then running the NRM2-POMI Takeoff definition which pops up the model's interface, the Quantity Surveyor would tick the category Walls, followed by the selection of the MOM to follow and the location of the NRM2 BOQ template file to be used as shown in Figure 5.

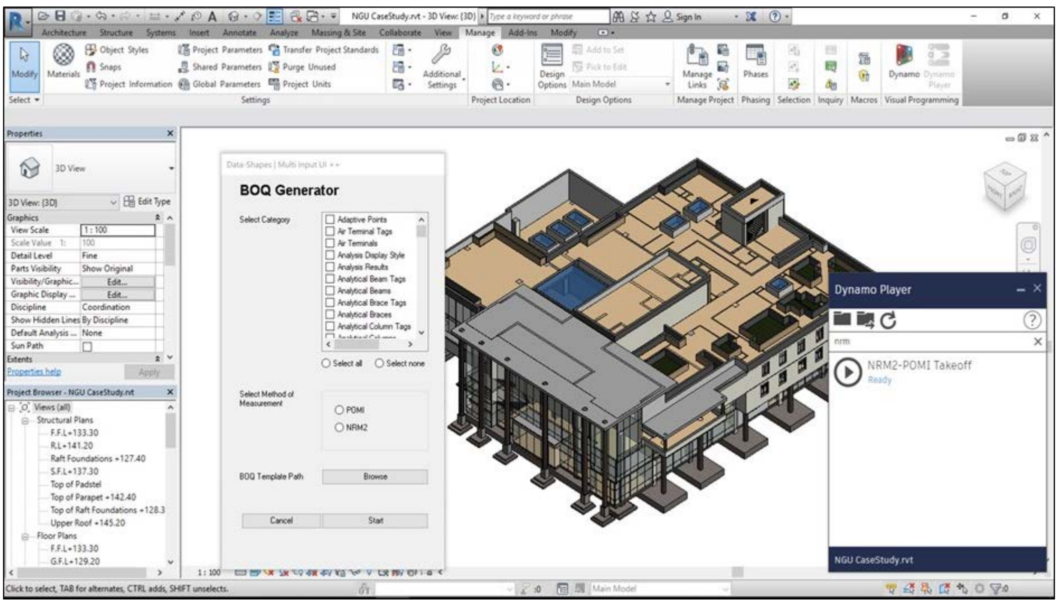

Figure 5 : Case Study with model designed user-interface

5. Results and Findings

A side by side comparison between the tender BOQ and the generated BOQ is shown in Figure 6. The first observation is that the model has produced a BOQ with exact similar structure and quantities compared to the tender BOQ. However, some differences were also noticed. The sentence structure for the tender BOQ was found to be slightly different in terms missed parameter which was the acoustic rating for the wall types. The sentence structure of the extra over walls was also found to be a bit different from that of the generated BOQ. The model generates a generic preamble work section which requires the quantity surveyor to specify the referenced contract documents such as drawings and specifications sections as a manual operation. this concludes that the BOQ generation process cannot be fully automated, there will always remain a part were the quantity surveyor amends or adjusts information as needed. However, the developed model could assist in significantly reducing the BOQ drafting time and provide a dynamic generation of BOQs when model adjustments are made.

Nr	Descriptions	Qty	Unit	Rate	Amount
	WORKS TO BASEMENT				
	Blockwork walling				
	Internal Walls: 150mm overall thickness				
A	Concrete Blocks; Hollow; built against other work; Type W2A; non fire rating; 55 acoustic rating	4,470	m2		
B	Concrete Blocks; Hollow; built against other work; Type W2B; fire rating 60 minutes; 55 acoustic rating	3,640	m2		
	Internal Walls: 200mm overall thickness				
C	Concrete Blocks; Hollow; built against other work; Type W3; non fire rating; 55 acoustic rating	3,365	m2		
	Extra over walls for opening perimeters				
D	Various difference dimensions for door and window openings; method of forming to contractors discretion; closing cavities, additional ties and all other additional work	4,181	m		

Item	Description	Qty	Unit	Rate ($)	Amount ($)
	BLOCK WALLING				
	Walls: 150mm overall thickness				
A	Concrete Blocks; Hollow; built against other work; non fire rating; Type W2A	4470	m2		
B	Concrete Blocks; Hollow; built against other work; fire rating 60 minutes; Type W2B	3640	m2		
	Walls: 200mm overall thickness				
C	Concrete Blocks; Hollow; built against other work; non fire rating; Type W3	3365	m2		
	Extra Over Walls for Opening Perimeters				
D	Various dimensions for door and window openings; including forming sills, jambs, reveals, cavity closers and lintels; method of forming to Contractor's discretion;	4181	m		

Figure 6: Case Study with model designed user-interface

6. Conclusions

BIM has been widely used for cost estimation with studies showing the useful contributions of using BIM over the traditional manual methods with potential cost reductions for a project. Quantifying items from BIM is simply a matter of quantities extraction and tabulation with no specific guidance to the method of measurement followed by regrouping extracted quantities in new items to be manually drafted in a BOQ. Any update in the BIM model would require re-doing the BOQ again. To tackle this issue a model was developed with rule-based quantity takeoff algorithms in BIM that follow the takeoff schemes from different method of measurements and accordingly generate BOQs ready for pricing. The model was designed to follow POMI and NRM2 methods of measurement. A sample algorithm for Walls was discussed in this study. The algorithms were validated with a case study for a project designed with a BIM software, and with a BOQ drafted with a NRM2 method of measurement. A side-by-side comparison between the case's BOQ and the model's generated BOQ shows the accuracy of the model meeting its required objectives. However, the BOQ generation process would still require human input and modifications; since some work sections such as preliminaries need to be defined manually and cannot be provided using a model. It can be concluded that it is essential to use a structured scheme inside the model to ensure consistence of the takeoff process. Such methodology could be incorporated within the BIM execution plan document for the project. This study aimed to contribute to the improvement of the industry practice by providing methods for integration between the standard methods of measurement in line with the ongoing BIM developments. Moreover, recommendations for future work could include the modeling of the different types of elements and the inclusion of more methods of measurement.

Acknowledgements

The authors would like to acknowledge the support by Mr. Kareem Mostafa, Lead Cost Manager, MSc., MRICS for his contribution in providing information related to the different method of measurements as well as the structure of each.

References

Abanda, F.H., Kamsu-Foguem, B. and Tah, J.H.M. (2017). BIM–New rules of measurement ontology for construction cost estimation. Engineering Science and Technology, an International Journal, 20(2), pp.443–459.

Campbell, C. R. (2013). The impact of the RICS New Rules of Measurement on the credibility of the cost advice supplied by Quantity Surveyors working within Small Enterprises, Edinburgh: Heriot-Watt University.

Eastman, C., Teicholz, P., Sacks, R. and Liston, K. (2011). BIM handbook: A guide to building information modeling for owners, managers, designers, engineers and contractors. John Wiley & Sons.

Lee, S.K., Kim, K.R. and Yu, J.H. (2014). BIM and ontology-based approach for building cost estimation. Automation in construction, 41, pp.96–105.

Magdy, A. & Ezeldin, S. (2016). A Decision Support System For Methods Of Measurement In Construction Projects. Kuching, ISEC.

Matipa, W.M., Cunningham, P. and Naik, B. (2013). Assessing the impact of new rules of cost planning on building information model (BIM) schema pertinent to quantity surveying practice. In 26th Annual ARCOM Conference, viewed (Vol. 16).

Monteiro, A. and Martins, J.P. (2013). A survey on modeling guidelines for quantity takeoff-oriented BIM-based design. Automation in Construction, 35, pp.238–253.

NRM2, (2012). NRM2: Detailed Measurement for Building Works. 1 ed. Reading: Royal Institute of Chartered Surveyors (RICS).

POMI, (1979). POMI - Principles of Measurement International. 6 ed. London: RICS Business Services Limited.

Williams, P. (2015). Managing Measurement Risk in Building and Civil Engineering. John Wiley & Sons.

Zaki, T., Nassar, K. and Hosny, O., (2017). Parametric Blockwall-Assembly Algorithms for the Automated Generation of Virtual Wall Mockups Using BIM. In AEI 2017 (pp. 844–854).

Digital Design Workflow for an Algorithm Aided BIM Approach in Research Led Teaching

Sophia S. Pibal, Iva Kovačić
Institute for Interdisciplinary Building Process Management,
Department of Integrated Planning and Industrial Building, TU Wien, Austria
sophia.pibal@tuwien.ac.at

Abstract. Despite the meanwhile extensive use of Building Information Modelling (BIM) in the Architecture, Engineering and Construction (AEC) Industry numerous problems with BIM-based digital design workflows cannot be neglected. This paper will address challenges of interdisciplinary teamwork in educational programs throughout a BIM-based workflow and data exchange issues between discipline specific software. A comparative study of two interdisciplinary design studios illustrates these challenges and presents a novel workflow approach, introducing Algorithm Aided BIM as a support for BIM-based digital design workflows to enhance interdisciplinary teamwork throughout the entire design process and to diminish software bound issues.

1. Introduction

The promises of Building Information Modelling-based (BIM-based) interdisciplinary collaboration are numerous, from enhanced stakeholder integration, collaborative processes, to large cost and time reduction (Succar, 2009). Despite the meanwhile extensive utilization of Building Information Modelling (BIM) in the Architecture, Engineering and Construction Industry (AEC) interdisciplinary teamwork throughout the BIM-process and seamless interdisciplinary data exchange within the collaborative digital design workflow must be addressed as main challenges in the adoption of BIM-based processes. Not only the AEC Industry but also educational programs that focus on teaching interdisciplinary design are facing these problems (Filzmoser et al., 2017, 2016). This is confirmed through our research led teaching within our Integrated Design Studios at the TU Wien, held since 2012. This paper will address the above-mentioned challenges through a comparative study of former Integrated Design Studio iterations and a newly established BIM Design Lab course based on a novel Algorithm Aided BIM approach in order to support and enhance the interdisciplinary teamwork and data exchange.

1.1 Research Led Teaching

Since 2012 the Department of Integrated Planning and Industrial Building at TU Wien focuses on teaching and researching interdisciplinary methods implementing BIM into the integrated design process. Insights from previous Integrated Design Studio iterations (Kovacic and Filzmoser, 2014) and ongoing research that includes an extensive literature review on BIM in education and design studios are the foundation of this paper (Filzmoser et al., 2016). The literature review on BIM in education showed that: a) most interdisciplinary BIM related student experiments were based on the optimization of given pre-designed architectural models and implemented BIM in later stages of the design process (Hyatt, 2011; Peterson et al., 2011; Poerschke et al., 2010), b) if BIM is used in early predesign stages the design studios were held in an mono-disciplinary manner (Haliburton et al., 2011; Woo, 2007) and c) if Parametric or Algorithm Aided Design were utilized, the design studios are either mono-disciplinary and do utilize BIM (Haliburton et al., 2011; Holzer, 2015; Radziszewski and Cudzik, 2019) or mono-disciplinary and do not utilize BIM (Alalouch, 2018; Rhodes, 2017; Schnabel, 2006). It can be stated that the Integrated Design Studio is a unique iterative studio that addresses the current challenges the AEC industry is faced with, such as BIM in early design stages and interdisciplinary data exchange; thus, pointing out the urgency for novel educational methods that would support development of new skills and digital competences. In previous research within the Integrated Design Studio iterations since 2012 (Filzmoser et al., 2017) we identified following challenges: a) the student experiments showed that the sole use of BIM software does not fully correspond to the needs of the predesign that is still in explorative stage, b) lack of contribution and integration of civil engineering students in preliminary design decisions (Kovacic and Filzmoser, 2015), as well as c) data exchange issues. In order to further address these problems a novel Algorithm Aided BIM (AAB) approach has been proposed for the newly established design course BIM Design Lab in 2019/20. This paper focuses on the comparison of Integrated Design Studio 2018/19 and BIM Design Lab in 2019/20.

2. Literature Review: Digital Design Workflow

Since our previous research led teaching (Filzmoser et al., 2017) has shown that the sole use of BIM software does not fully correspond to the needs of preliminary explorative stage of design (lack of discipline involvement and high remodelling effort), we integrated Algorithm Aided Design (AAD) into BIM within the BIM Design Lab. Thereby we use an Algorithm Aided BIM (AAB) approach for a) design exploration and b) data exchange based on Algorithm Aided Design supporting the BIM-based design workflow. The concepts of Algorithm Aided Design and Algorithm Aided BIM and related terminology will be closer explained in following section. Algorithm Aided Design (Österlund, 2013; Tedeschi and Lombardi, 2017) describes a specific field of Parametric Design in which the generation of geometry is controlled with an algorithm-based software and a specific set of parameters. The algorithm is defined as a set of finite steps leading to the solution of a problem, it contains unambiguous instructions, well defined input and thus creates well defined output. In Algorithm Aided Design, in order to get the best solution, you design the process not the final outcome. Feist (2016) describes it as a programming-based method of design where the designer develops a program that then later on generates the model. This enables the designer to explore various design variants by changing values of parameters. In the case of a cuboid, value parameters such as height, width and length can be changed and it will generate variants of a cuboid without manual modelling, Figure 1. These Algorithms can be either scripted in textual programming languages or visual programming languages (Ferreira and Leitão, 2015; Leitão et al., 2012). Principally, end-users of the AEC Industry are not meant to perform as programmers but as future competences architectural programming knowledge may be required. Visual programming languages allow the user to manipulate geometry without textual programming knowledge but by using graphical commands (Máder et al., 2018) as displayed in Figure 1. Graphical algorithm editors that embed visual programming languages, like *Grasshopper* (Rutten, 2014) or *Dynamo* (Autodesk, 2016) are tools offering the possibility of connecting Algorithm Aided Design, that defines geometry via algorithms, with BIM and Structural Design Modelling (Finite Element Method - FEM) software, that utilize object oriented modelling to generate geometry and metadata (Humppi and Österlund, 2016). Both, Algorithm Aided Design and BIM are seen as a part of parametric modelling (Haymaker et al., 2018), where parameters can either be defined within an algorithm or within an object itself. Algorithm Aided BIM (Humppi and Österlund, 2016) is the combination of Algorithm Aided Design and BIM; here algorithms are used to generate parametric object models, which contain embedded metadata that can be further utilized in the design and construction process. Other terms such as Algorithmic-based BIM or A-BIM (Caetano and Leitão, 2019; Feist et al., 2017, 2016), Generative BIM (Mirtschin, 2011) and Parametric BIM (Aish, 2013) refer to the same methodology. Hence there is no settled term for this approach yet, in this paper it will be referred to as Algorithm Aided BIM.

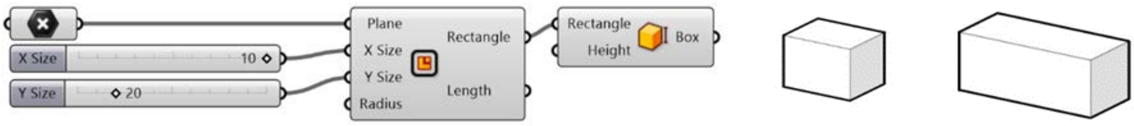

Figure 1: Grasshopper Visual Programming with Input, Instructions and Output Parameters and two resulting Variants of a Cuboid

The *Grasshopper-ARCHICAD Live Connection* (Graphisoft, 2016), *Grevit* (2016), *Hummingbird* (Guttmann and Meador, 2012) and the *Data Interface RFEM to Grasshopper* (Dlubal, 2019) combine Algorithm Aided and Object-Oriented Design and are as such main examples of Algorithm Aided BIM *plug-ins*. It has to be stated that Algorithm Aided BIM is referred to as an *approach* to support the explorative design stage in BIM-based workflows (variant exploration and optimization) via plug-ins that offer a *direct data interface* and *live connection* (diminishing the need of exchanging files) between Algorithm Aided Design tools (Grasshopper and Dynamo) and BIM software (*ARCHICAD* (Graphisoft, 1993) and *Revit* (Autodesk, 2000)) as well as Finite Element Method (FEM) software (*RFEM* (Dlubal, 1987)). In this paper we refer to Algorithm Aided BIM not only as a *design exploration tool* but also a *data interface*, since it is capable of both.

3. Methodology

This paper compares the workflows of the Integrated Design Studio 2018/19 and the BIM Design Lab in 2019/20. The student projects addressed the development of specific design tasks utilizing a *tested BIM- workflow* in 2018/19 and the *novel Algorithm Aided BIM - workflow* in 2019/20. Eight teams from both studio iterations consisting of two architecture and one or two civil engineering students delivered the data for this comparative study, Table 1. The design process has been conducted in an interdisciplinary manner, traditionally architecture students have been mainly involved in the design task and civil engineering students in structural planning. In the Integrated Design Studio, students were admonished to proactively work in teams, give peer on peer feedback and be involved in decision-making throughout the digital workflow phases, Figure 2. Different design tasks have been assigned to the iterations of 2018/19 and 2019/20: 1. Iteration BIM_port: Research and development centre and 2. Iteration BIM_home: Modular multi-storey affordable housing. In both courses students were provided with a functional program, site-plan, background information and supporting software trainings. Weekly meetings of student teams and course instructors, as well as two intermediate and one final presentation were held. Firstly, to evaluate the design quality and feedback students on their progress. Secondly, to assess and document the involvement of disciplines in each phase of the design process and thirdly, to document data exchange issues. Students not only delivered their design and structure submissions (Table 1) via project posters and models but also generated interdisciplinary workflow diagrams, this data was also used as empirical material to analyze and determine the involvement of disciplines and data exchange issues.

Table 1: Teams of Integrated Design Studio and BIM Design Lab, Submitted Data

Teams	**Integrated Design Studio 2018/19**		**BIM Design Lab 2019/20**	
	Architects	Civil Engineers	Architects	Civil Engineers
1	2	1	2	2
2	2	1	2	2
3	2	1	2	2
4	2	1	2	2
5	2	-	2	2
6	2	1	2	1
7	2	-	2	-
8	2	2	2	2

Data
Project Posters
BIM + FEM Model
IFC file
Workflow Diagram
AAB Algorithm*
*in 2019/20

3.1 Integrated Design Studio 2018/19 and BIM Design Lab 2019/20

In our previous research based on student experiments within the Integrated Design Studios, that simulate a BIM-based collaborative design process, we were able to identify challenges regarding interdisciplinary teamwork as well as software-bound and data exchange issues. It was shown that BIM software, when utilized solely, is not optimal for the *predesign* that is still in explorative stage. Furthermore, challenges related to *interdisciplinary teamwork*, more precisely a lacking contribution and integration of civil engineering students throughout the whole digital design workflow arose. *Data exchange issues* such as misinterpretation of geometry and metadata as well as data loss, resulting in significant remodelling efforts of already existing data led to introducing a novel approach within the BIM Design Lab 2019/2020.

Table 2: Software used and taught in 2018/19 and 2019/20

Software		**Integrated Design Studio 2018/19**		**BIM Design Lab 2019/20**	
		used	taught	used	taught
ARCHICAD	BIM	x	x	x	x
Revit	BIM	x	x	x	x
RFEM	FEM	x	x	x	x
Grasshopper	AAD			x	x
Karamba3D	AAD/FEM			x	x
Tekla	FEM	x			
AxisVM	FEM	x	x		
Grasshopper ARCHICAD Live Connection	AAB			x	x
Data Interface RFEM to Grasshopper	AAB			x	x
Hummingbird	AAB			x	x
Grevit	AAB			x	

For the BIM Design Lab, we proposed to address above mentioned challenges of the former Integrated Design Studio iterations by testing an Algorithm Aided BIM approach. Utilization of Algorithm Aided Design tools, such as Grasshopper together with BIM and FEM software, like ARCHICAD, Revit and RFEM; combined with Algorithm Aided BIM plug-ins, such as Grasshopper-ARCHICAD Live Connection or Data Interface RFEM to Grasshopper, characterizes this digital design workflow and has to be mentioned as the significant difference to the previous Integrated Design Studio. Algorithm Aided BIM adds an approach for design exploration in the preliminary design phase with the intention of pushing the process of collaborative decision making - generation of variants and optimizations - to the beginning of the digital design process - prior to detailed BIM and FEM modelling. The Integrated Design Studio focuses on the utilization of BIM and structural analysis based on Finite Element Method (FEM) software directly after the analogue concept phase; whereas in the BIM Design Lab, the analogue concept phase and the detailed modelling process in BIM and FEM are bridged by the Algorithm Aided BIM phase. Software trainings have been provided for each individual phase, which can be seen in Table 3. Both courses were organized into workflow phases, which will be described in the following section.

3.2 Digital Design Workflow Phases and Interdisciplinary Data Exchange

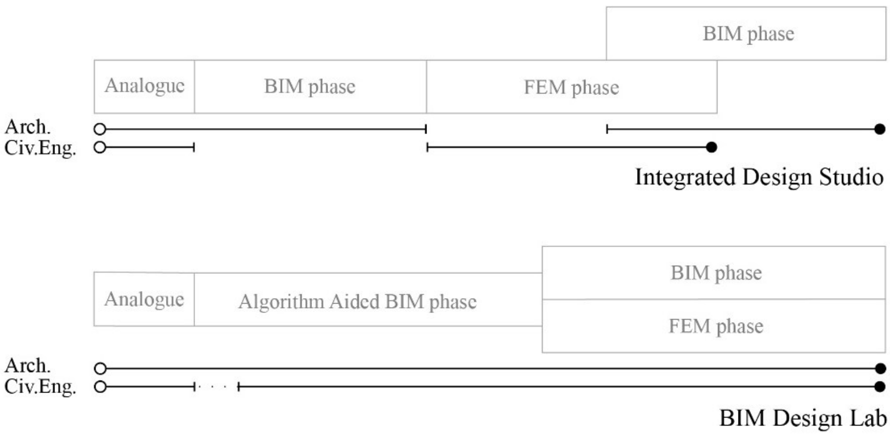

Figure 2: Digital Design Workflow Phases and Interdisciplinarity

The first phase can be described as the analogue concept phase, which started with team building, analyzation process of the presented task and the development of an interdisciplinary design concept during a supervised one-week workshop at the beginning of the semester. Concept of design and concept of structure were generated non-digital. Although the Integrated Design Studio and BIM Design Lab both start the design process in an analogue manner, the shift to the digital design workflow differs. The design exploration within the Integrated Design Studio is rather limited and mainly proceeds without digital support in the analogue concept phase. After developing an integrated concept, architecture students enter the BIM phase.

Table 3: Methods of Data Exchange

Teams	Manual Data Exchange		IFC		Data Interface	
	2018/19	2019/20	2018/19	2019/20	2018/19	2019/20
1	x			x		x
2	x	x				x
3	x			x		x
4	x			x		x
5			x		x	x
6		x			x	x
7						
8	x		x	x		x

After the generation of a BIM model, civil engineering students enter the FEM phase. Software utilized within the Integrated Design Studio are presented in Table 2 and data exchange mainly proceeded manually, Table 3. *Manual Data Exchange* is understood as the remodelling of an already existing discipline-specific model without any digital data transfer. *IFC* (Industry Foundation Classes) data exchange describes data transfer between discipline specific software via IFC format files. *Data Interface* refers to the data exchange between discipline specific software without export and import of data files, but either direct data transfer via software supported interfaces or live connections between software. Due to the novel approach introduced in 2019/20, the design exploration phase has been greatly extended and integrated into the Algorithm Aided BIM phase. The interdisciplinary teams utilized Grasshopper (Table 2) to conduct design exploration of variants and predesign evaluations and optimizations of structure. After the development of the collaborative algorithm and interdisciplinary design concept, architecture and civil engineering student simultaneously enter the BIM and FEM phase which proceeds parallel. Data exchange mainly proceeded via data interface and IFC; see Table 3. Figure 3 illustrates the digital design workflows of the Integrated Design Studio and BIM Design Lab. The BIM Design Lab workflow shows a direct shift from the analogue concept phase to the modelling process with BIM software, conducted by the architecture students to generate the first digital draft of the design. Data exchange from BIM to FEM software has been performed via manual data exchange, via data interface between Revit and RFEM or via IFC between ARCHICAD and RFEM.

Figure 3: Digital Design Workflows

Civil engineering students further performed the first performance evaluations and structural changes inside FEM software. Changes of the FEM model afterwards were re-implemented into the BIM model by architecture students, either via data interface or manual data exchange. This process has to be described as non-linear but iterative. Although the analogue concept phase of the BIM Design Lab can be described as similar to the analogue concept phase of the Integrated Design Studio, the shift from analogue to digital methods must be addressed as different. Entering the Algorithm Aided BIM phase the interdisciplinary teams collaboratively determine parameters, perimeters and constraints as well as an explicit statement of design intention and the steps to achieve it when utilizing Algorithm Aided Design tools. The aim of the novel approach is to enhance the interdisciplinary teamwork by generating a collaboratively used algorithm. This method ought to support the preliminary design exploration by offering a tool to create and test design variants and diminish data exchange issues by offering the same tool to conduct seamless data exchange via data interface. After determining rule sets regarding parameters and design intention, the architecture students initiated developing the algorithm via visual programming inside the Algorithm Aided Design tool Grasshopper. The algorithm was generated to be suitable for data exchange via Algorithm Aided BIM data interfaces (Table 2) to BIM and FEM software. The reference geometry does not have surfaces, volumes or extrusions; and is solely generated by points, 2D-lines, polylines or splines. The algorithm represents the reference geometry of the subsequently generated design object elements inside BIM and references for elements inside FEM. During this phase both disciplines utilize the same algorithm and collaboratively define the preliminary design and structure. As mentioned before, this graphical algorithm editors uses a visual programming language (Figure 5). Grasshopper also provides a wide range of plug-ins versatile for performance evaluations and analysis. Karamba3D, is a parametric structural engineering plug-in embedded in the Grasshopper environment that provides accurate analysis of spatial trusses, frames and shells and was used for the first of a double iterative performance evaluation of structure. Further plug-ins embedded in Grasshopper like the algorithm optimizer Galapagos, daylight optimization with Honeybee as well as zone and layout optimizations were utilized by the architecture students. Simultaneously the civil engineering students develop an object catalogue - which contains information regarding structural elements, gained from the evaluation and optimization with Karamba3D, and input data regarding building energy performance.

Figure 4: Segment of an Algorithm inside Grasshopper, BIM Model and FEM Model

On foundation of the object catalogue the architecture students generated BIM object elements inside ARCHICAD or Revit. The elements represent slabs, columns, walls, beams, façade elements and objects, these elements were embedded into the algorithm and bi-directionally linked between Grasshopper and ARCHICAD, Revit and RFEM (Figure 4 and 5). This offers the possibility to directly translate the algorithm into a full BIM model while still being able to conduct changes of geometry and parameters. The model updates as an immediate response to changes in the algorithm.

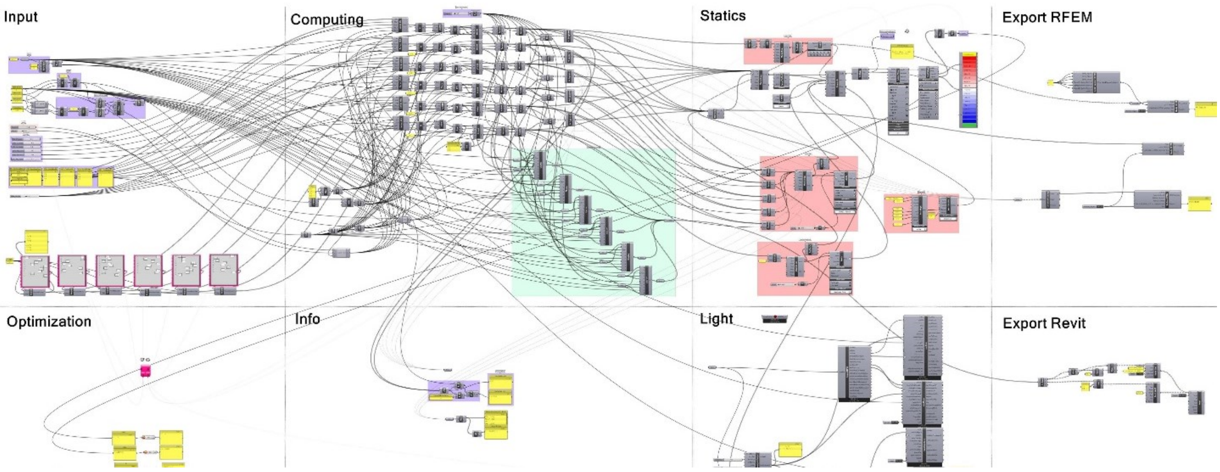

Figure 5: Algorithm inside Grasshopper

Not only is the algorithm source of information for BIM but also FEM. The Data Interface RFEM to Grasshopper, newly introduced at the end of 2019, has been the interface of choice for the data exchange regarding structure. Like the Grasshopper-ARCHICAD Live Connection, this data interface also is a live connection but mono-directional from Grasshopper to RFEM. The same reference geometries connected to the BIM object elements in Grasshopper are used as references for the FEM elements. Students conducted the data exchange to BIM and FEM via data interface and entered the next phase. Although students of both disciplines shifted their shared working environment from a collaboratively utilized algorithm to discipline specific software, data exchange was still performed. In the BIM and FEM phase students were given the opportunity to further develop the detail of design and structure. In the second double iterative performance evaluation detailed evaluations in RFEM could be performed. Due to the first evaluation with Karamba3D the preliminary evaluations already determined the structural system, grid and material; thus, evaluations in RFEM mainly concerned profiles, cross sections and dimensions. Data exchange between BIM and FEM has primarily been performed manually or via data interface. At this point the interdisciplinary teams had generated *one interdisciplinary algorithm* and *two corresponding BIM and FEM models*.

4. Results and Discussion

Our previous research within Integrated Design Studios has shown that firstly, BIM software when used solely does not fully satisfy the needs of predesign that is still in explorative stage, secondly, lack of interdisciplinary teamwork and thirdly, data exchange issues. All of the stated issues result in manual data exchange and significant manual remodelling efforts throughout the digital design workflow. Figure 2 illustrates the digital design phases of 2018/19 and 2019/20 and the involvement of disciplines throughout these phases. The previous Integrated Design Studios were subdivided into sequences of discipline specific modelling phases resulting in a rather sequenced involvement of disciplines and an intermitted interdisciplinary development of the project. Due to the fact that iterate structural performance evaluations are being conducted *after* the BIM model has already been generated, resulting changes regarding structure and design have to be performed under significant remodelling efforts. Furthermore, the data exchange via IFC or data interface were often unsuccessful due to *data loss* or *misinterpretation of geometry and metadata*. This resulted in either no digital data exchange and fully manual remodelling (manual data exchange) of existing discipline models (Case D, Figure 6) or partially successful data exchange resulting in partially manual remodelling in either BIM or FEM discipline models (Case B+C, Figure 6). Compared to the previous Design Studio the BIM Design Lab addresses these problems by implementing the novel approach. Here, the increased involvement of civil engineering students - as the interdisciplinary teamwork proceeds throughout almost the entire digital design process - can be confirmed (Figure 1).

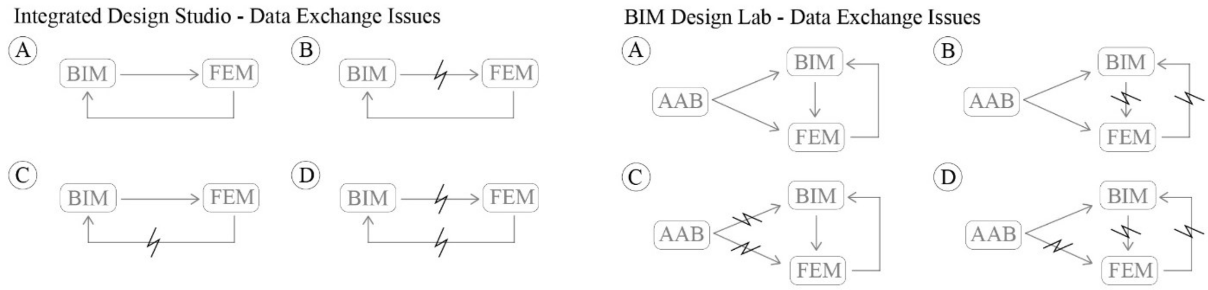

Figure 6: Integrated Design Studio and BIM Design Lab Data Exchange Issues

Particularly intensive teamwork occurred during the Algorithm Aided BIM phase in which optimizations regarding design decisions and performance evaluations regarding structure have been executed collaboratively. Both disciplines developed and worked on the same file utilizing and modifying the via visual programming scripted algorithm inside Grasshopper. Based on the extended preliminary design exploration during this phase, a majority of decisions regarding design and structure could be made *before* the more detailed BIM and FEM phase.

Table 4: Data Exchange Issues of Teams

2018/19	1	2	3	4	5	6	7	8
Data Exchange	D	D	B	B	A	A	D	B

2019/20	1	2	3	4	5	6	7	8
Data Exchange	A	C	A	A	B	B	-	D

The data exchange mainly has been taking place via Algorithm Aided BIM data interfaces (Table 2) from Grasshopper *to* either BIM or FEM and via data interface or IFC *between* BIM and FEM. Although this method reduced data exchange issues, *misinterpretation* or *data loss* still occurred and resulted in the problem of remodelling and manual data exchange. Figure 6 shows the most frequent intermitted data exchanges. Table 6 displays the data exchange issues of teams during the Integrated Design Studio 2018/19 and BIM Design Lab 2019/20. Furthermore, people bound problems such as lack of skills and competencies and communication (Filzmoser et al., 2017; Rekola et al., 2010) occurred, which were documented in the workflow diagram and during meetings. Ill-defined BIM-based processes and a lack of modelling conventions within the interdisciplinary team have been additional challenges not only in the Integrated Design Studio but also the BIM Design Lab and thus impaired a fluent digital design workflow.

5. Conclusion

In this paper we have shown the potentials of a novel Algorithm Aided BIM approach for earliest design stages through a comparative study of two design courses. The comparative study of the digital design workflows illustrates that the novel approach can be advantageous when addressing challenges the AEC Industry and educational programs face. Within the BIM Design Lab, the not sequenced but continuous involvement of both disciplines, architecture and civil engineering, along the entire digital design workflow has to be stated as highly beneficial for the interdisciplinary design process. Due to the collaborative interdisciplinary decision making and optimization processes in the preliminary design phase, significant remodelling efforts, which have been problematic during the previous Design Studios, could be diminished. Moreover, the data exchange method shifting from IFC or manual data exchange to an increased use of data interfaces must be mentioned as highly beneficial in terms of diminished data loss and misinterpretation. Although the novel method is valuable in engaging these challenges, it still faces challenges in itself. Due to the fact that this approach is based on a novel and complex method of combining the design strategies and tools of Algorithm Aided Design and BIM, the end-user is highly challenged in implementing this method. If the end-user is not familiar with neither Algorithm Aided Design nor BIM, utilizing this method is highly resource consuming. However, innovations in BIM teaching are necessary for the advancement of both education and planning practice. For further Research Led Teaching that integrates this method we propose the course to be held not over the course of one but two semesters. Firstly, introducing students of both disciplines to the concept of Algorithm Aided Design and *Algorithm Aided BIM* and secondly, implementing these methods into the *BIM-based digital design workflow*.

References

Aish, R., (2013). First build your tools. Inside Smartgeometry: Expanding Architectural Possibilities of Computational Design. 9781118522, pp.36–49. https://doi.org/10.1002/9781118653074.ch2

Alalouch, C., (2018). A pedagogical approach to integrate parametric thinking in early design studios. International Journal of Architectural Research. 12, pp.162–181. https://doi.org/10.26687/archnet-ijar.v12i2.1584

Caetano, I., Leitão, A., (2019). Integration of an algorithmic BIM approach in a traditional architecture studio. Journal of Computational Design and Enginering. 6,pp. 327–336. https://doi.org/10.1016/j.jcde.2018.11.004

Feist, S., Barreto, G., Ferreira, B., Leitão, A., (2016). Portable generative design for building information modelling. CAADRIA 2016, 21st International Conference on Computer aided Architectural Design Research in Asia: Living Systems and Micro-Utopias: Towards Continuous Designing, pp.147–156.

Feist, S., Ferreira, B., Leitão, A., (2017). Collaborative algorithmic-based building information modelling. CAADRIA 2017, 22nd International Conference on Computer aided Architectural Design Research in Asia: Protocols, Flows and Glitches.

Ferreira, B., Leitão, A., (2015). Generative design for Building Information Modeling. Proceedings of the 33rd International Conference on Education and Research in Computer Aided Architectural Design in Europe: Real Time.

Filzmoser, M., Kovacic, I., Vasilescu, D.-C., (2017). Integrated design studios: Education to overcome silo-thinking and enable full BIM-exploitation in AEC. The Engineering Project Organization Journal. 7. https://doi.org/10.25219/epoj.2017.00104

Filzmoser, M., Kovacic, I., Vasilescu, D.-C., (2016). Development of BIM-supported integrated design processes for teaching and practice. The Engineering Project Organization Journal. 6, pp. 129–141. https://doi.org/10.1080/21573727.2016.1267005

Haliburton, J., Ap, a I. a L., Ozener, O., Farias, F., Jeong, W., (2011). Parametric modeling and BIM : Innovative design education for integrated building practices. ACADIA 2011, Regional Conferences in U.S.A.: Parametricism: SPC.

Haymaker, J., Bernal, M., Tyrone, M. T. M., Okhoya, V., Szilasi, A., Rezaee, R., Chen, C., Salveson, A., Brechtel, J., Deckinga, L., Hasan, H., Ewing, P., Welle, B., (2018). Design space construction: a framework to support collaborative, parametric decision making. Journal of Information Technology in Construction (ITcon). 23, pp.157–178.

Holzer, D., (2015). BIM and Parametric Design in Academia and Practice: The changing context of knowledge acquisition and application in the digital age. International Journal of Architectural Computing. 13, pp.65–82. https://doi.org/10.1260/1478-0771.13.1.65

Humppi, H., Österlund, T., (2016). Algorithm-Aided BIM. Complex & Simplicity. eCAADe 2016, Conference in Finland. 2, pp.601–609.

Hyatt, B.A., (2011). A case study in integrating lean, green, BIM into an undergraduate construction management scheduling course. 47th ASC Annu. Int. Conf. Proc. 2007, pp. 1–8.

Kovacic, I., Filzmoser, M., (2015). Designing and evaluation procedures for interdisciplinary building information modelling use—an explorative study. The Engineering Project Organization Journal. 5, pp.14–21. https://doi.org/10.1080/21573727.2014.989426

Kovacic, I., Filzmoser, M., (2014). Key success factors of collaborative planning processes. The Engineering Project Organization Journal. 4, pp.154–164. https://doi.org/10.1080/21573727.2014.963056

Leitão, A., Santos, L., Lopes, J., (2012). Programming languages for generative design: A comparative study. International Journal of Architectural Computing. 10, pp.139–162. https://doi.org/10.1260/1478-0771.10.1.139

Máder, P.M., Rák, O., Háber, I.E., (2018). Contemporary architecture based on algorithms. Pollack Periodica. 13, pp.53–60. https://doi.org/10.1556/606.2018.13.3.6

Mirtschin, J., (2011). Engaging generative BIM workflows, LSAA 2011, Collaborative Design of Lightweight Structures

Österlund, T., (2013). Design possibilities of emergent algorithms for adaptive lighting system. Nordic Journal of Architectural Research. 25, pp.159–184.

Peterson, F., Hartmann, T., Fruchter, R., Fischer, M., (2011). Teaching construction project management with BIM support: Experience and lessons learned. Automation in Construction. 20, pp.115–125. https://doi.org/10.1016/j.autcon.2010.09.009

Poerschke, U., Holland, R.J., Messner, J.I., Pihlak, M., (2010). BIM collaboration across six disciplines The need for collaborative studios The organization of the collaborative BIM studio. EG-ICE 2010, 17th International

Workshop of Intelligent Computing in Engineering in United Kingdom, pp.1–6.

Radziszewski, K., Cudzik, J., (2019). Parametric design in architectural education. World Transactions on Engineering and Technology Education. 17, pp.448–453.

Rekola, M., Kojima, J., Mäkeläinen, T., (2010). Towards integrated design and delivery solutions: Pinpointed challenges of process change. Architectural Engineering and Design Management. 6, pp.264–278. https://doi.org/10.3763/aedm.2010.IDDS4

Rhodes, P.S., (2017). Algorithmic futures. The analog beginnings of advanced parametric design in first year studios. The Design Journal. 20, pp.822–S834. https://doi.org/10.1080/14606925.2017.1353029

Schnabel, M.A., 2006. Architectural parametric designing. 24th eCAADe, pp.216–221. https://doi.org/10.13140/RG.2.1.1952.7841

Succar, B., (2009). Building information modelling framework: A research and delivery foundation for industry stakeholders. Automation in Construction. 18, pp.357–375. https://doi.org/10.1016/j.autcon.2008.10.003

Tedeschi, A., Lombardi, D., (2017). The Algorithms-Aided Design (AAD), Informed Architecture: Computational Strategies in Architectural Design. Springer International Publishing, pp.33–38. https://doi.org/10.1007/978-3-319-53135-9_4

Woo, J.H., (2007). BIM (Building Information Modeling) and pedagogical challenges.

Modelling Co-presence in the Built Environment - a Spatio-temporal Approach to Human Perception and Movement

Beidi Li[1], John Fitzgerald[2], Carl Schultz[1]
[1]Aarhus University, Denmark; [2]Newcastle University, UK
beidi.li@eng.au.dk

Abstract. A building occupant's experiences are not passive responses to environmental stimuli, but are the results of multifaceted, prolonged interactions between *people* and *space*. We present a framework and prototype software tool for analysing occupant perception and behaviour in the context of dynamic aspects of buildings in operation. In particular, we focus on co-presence of different user groups and the resulting impact on perceptual and functional affordances of spatial layouts by utilising the concept of *spatial artefacts*. We have implemented our prototype architectural design reasoning tool in Answer Set Programming extended to support spatial reasoning, ASPMT(QS), and demonstrate initial results, through case scenarios in the Urban Sciences Building, Newcastle University, a large, state-of-the-art living laboratory and multi-purpose academic building that includes lectures, labs, a café, work offices, and exhibition/event areas.

1. Introduction

In the context of architectural design analysis, consider the scenario that a person has just entered a large spacious foyer of a university building, identifies some wayfinding signage and begins to approach it. Simultaneously, a lecture has just finished and a stream of students quickly emerges, cutting in between our building occupant and the sign. The presence of the crowd has an impact on the experience and behaviour of the occupant in relation to the sign [1]: people in the crowd intermittently occlude the occupant's line of sight; the crowd inhibits the occupant's ability to physically approach the sign; the occupant may feel some slight social discomfort if they cannot easily avoid being too close to the crowd (proxemics where the occupant is waiting in a wheelchair or standing), or need to stare past the faces in the crowd when trying to maintain a line of sight with the sign [2]. The crowd may have numerous positive effects on the occupant's sense of orientation as it may lead them to guess where the lecture hall is thus helping them to construct their cognitive map of the building [3, 4], it may evoke a sense of liveliness and stimulating bustle, and reassure the occupant that they are "allowed" to be in that space at that time (compare with a pin-drop silent, deserted building).

As this example demonstrates, a building occupant's experiences are not passive responses to environmental stimuli, but are the results of multifaceted, prolonged interactions between *people* and *space*. While prominent architectural design analysis tools such as space syntax couple human behaviour with space configuration parameters [5], the properties of *dynamism* and *change* can have a significant impact on an occupant's experience, particularly in situations where the presence of other agents intensifies or masks certain aspects of space. We argue that:

perceptual and functional affordances of spatial layouts are to be evaluated in the context of occupants, tasks, schedules, events and activities, and the co-presence of different user groups.

One approach for modelling such scenarios of co-presence is via agent-based simulation: model the crowd as particles flowing through the building, and gather statistics on (e.g.) the number of occlusions per second that the occupant experiences, etc. However, such empirical methods cannot address *existential* questions about a building, e.g. *"Does there exist a situation in which a wheelchair user will have significant difficulty in locating and engaging with any of the* *primary wayfinding signs?"* in a comprehensive and elegant way. We may attempt to address such a question by running hundreds of simulations with various combinations of parameters. However, the results of a simulation, while giving valuable empirical information, are always only an *instance* generated from an infinite set of possible simulation runs.[1] We cannot *reason* about the user experience of a building, in a logic-based sense, if our only tool for analysis is simulation.

To complement empirical analysis tools, we propose a novel approach to modelling dynamic aspects of the built environment, specifically crowds, that is amenable to static analysis, logic-based reasoning, and formal verification: we model crowds as *spatial artefacts* [8,15,25], regions of empty space that are rich with perceptual-locomotive semantics. We define axiomatic "rules" for how crowd artefacts interact with occupant's perceptual artefacts (visibility spaces, movement spaces, etc.) as a way of formally modelling research results from behavioural psychology, ergonomics, and cognitive science. We specify the appearance, geometry and properties of spatial artefact crowds based on context-specific events that take place in the environment. We have implemented our approach within logic programming language Answer Set Programming, with our extensions for supporting spatial reasoning, ASPMT(QS) [6, 7].

In the following sections, we define inferential rules of crowds' impact on an occupant's visual-locomotive experiences, propose a formal method to enhance a building's physical representation with crowd-related spatial artefacts, and demonstrate the logical verifiability and answerability of our model with typical scenarios in the USB.

2. Background and Basic Concepts

Spatial artefacts: the shape of empty space. Consider the region of empty space around an object such as an information kiosk; this region is meaningful because a person must be located in that region to perform a particular act (e.g. engage with the kiosk). The geometry of this *functional space* region depends on properties of the person (consider wheelchair users, children, etc.), the task, and the object. People have a *movement space* which are the regions in which they can move (travel) within. People and sensors have *range spaces* (which can be further refined: visibility space, hearing space, …), and so on. These are examples of *spatial artefacts*, a concept that was pioneered by Bhatt et al. in the context of architectural analysis: regions of empty space that are rich with perceptual-locomotive semantics [8,15,25]. Spatial artefacts "elevate" these semantically meaningful regions of empty space to become first-class objects, on the same ontological level as doors, walls, slabs, etc. within Building Information Models (BIM). For example, in the Industry Foundation Classes (IFC) data model, spatial artefacts form an abstract class that is a subclass of `IfcSpace`.

Crowd spaces: a new dynamic spatial artefact. Extensive studies on crowd dynamics proposed robust mathematical models for simulating and predicting crowd behaviours (merging, splitting, collision-avoidance, leader-following, etc. [9, 10, 11]). While such models provide deterministic and precise metrics for crowd characteristics such ad velocity, density, trajectories, etc., they often adopt a perspective view and thus, reflect poorly on an occupant's egocentric perception of crowds [12]. Moreover, such physical models are inevitably subject to computational regularization and numerical discretisation that hinder the accessibility to

[1] To use an analogy from software engineering, a suite of tests cannot *prove* that a software program has certain properties. At best, testing can reveal the presence of a defect, but can never tell us that no defects exist. On the other hand, formal software verification *can* prove properties about a software program, e.g. that the program in conjunction with preconditions logically implies a given postcondition.

underlying assumptions (fluid dynamics, mass conservation, minimum entropy, etc.) [11, 13, 14]. As human-environment interactions are conditioned by sociological, physiological, and psychological stimuli, factors such as flow condition, pedestrian type, cognitive heuristics, purpose of movement, and length of stay reject the hypothesis of an *average person* and require a rather qualitative description than a detailed parametrisation [1, 13, 16, 17, 18].

The aforementioned limitations of a (purely) statistical model prompted us to turn to a static, analytical representation of crowds, as humans have a natural propension to mentally abstract crowds into *blobs* corresponding to visually salient groups [20]. In fact, reconstruction of pedestrian flow in a virtual environment showcases high group-sensitivity in an individual's behaviour, e.g. individuals are likely to be absorbed in a group and align with the group's speed, position, orientation, etc [20]. Studies also highlighted other macroscopic descriptors of crowds such as collectiveness, uniformity, personal space, movement type, etc. [2, 12, 21] In this paper, we define the concept of a *crowd* as:

An artefactual object induced by occupants of the built space, positioned within a physcial region (in a loosely organised fashion), constrained by local configurations and time limits.

Similar to spatial artefacts, we model crowds as first-class objects having a certain geometric extent and if applicable, qualitative directedness and density, that persists in the space for an extended period of time.

3. Crowds as a visual and locomotive obstruction for other occupants

Crowds, as pervasive existences in the space, not only create visual obstruction, but also interfere with personal spaces, modify soundscape characters, and introduce movement obstacles. As a result, crowds enhance or inhibit people's perception, and entail changes in the cognitive and functional affordances of the space.

In this study, we propose a qualitative model to formalise the properties of a stationary object as perceived by an observer through crowds. We encode the impact of a particular situation as open-ended inference rules, so that the model takes input from occupant types, crowd conditions, local configurations, events, etc. More concretely, we identify typical itineraries triggered by routine activities (poster session, class dismissal, lunch queue, staff meeting, etc.), and derive crowd artefacts as a series of bounding boxes, taken into account the crowd's movement type (free flowing, congested, panic, stress, etc. [12, 13]), preferred interpersonal distances, pedestrian height, etc.

In this section, we exemplify the impact of crowds on an occupant (the *subject*) who is looking at or is interested in a *target*, the approachability, detectability, and visibility of which are affected by the crowd emerging *between* the target and the occupant. We base our examples on space in the Urban Sciences Building (USB)[2] at Newcastle University. This 12500 sqm academic building combines teaching and research laboratories with public spaces for exhibitions, events and a café, and thus provides a wide variety of usages, with crowd movements between. Our example space is the "forum" or foyer space at ground level. This roughly triangular space has the main building entrance at the mid-point of the base, with an event/teaching space at the left vertex, the main elevators at the top vertex, and the café at the right vertex. Signage is located to the left of the building reception. Table 1 at the end of this section showcases visibility and mobility aspects of three crowds in the foyer space of the USB.

[2] See https://www.ncl.ac.uk/computing/about/usb/. The USB is designed as a living laboratory and provides a public stream of data about its usage and performance via the Newcastle Urban Observatory project (https://www.urbanobservatory.ac.uk/).

Visibility Space: In the absence of crowds, the *isovist* of a target (e.g. a sign) denotes the region from which an unobstructed line of sight connects the observer and the target. We intersect the *isovist* with the observer's maximum visual field to obtain the *Visibility Space* of the target, from which the target is visible to the observer with specific eye-level, visual acuity, peripheral vision range, etc.

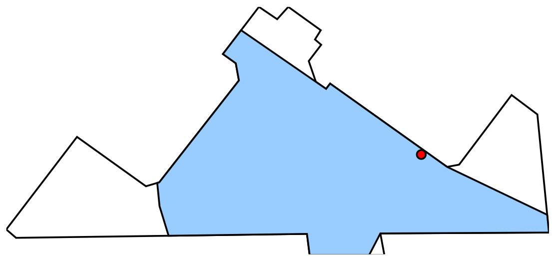

Figure 1: Visibility space of the information sign (the red dot) in the USB foyer. Roughly, north is at the top

Crowds and Visibility: In the presence of a single crowd, the target's visibility is unaffected to an observer that is located *between* the crowd and the target and thus, the target is *permanently visible* to such observers. On the contrary, the target has reduced visibility to observers *behind* the crowd, due to the intermittent visual occlusion of the crowd. In case of a perfectly aligned, homogeneous crowd moving at constant velocity, the line of sight of a motionless observer is interrupted at equal intervals, determined by average body measurements w and s, spacing d, speed v, and angle of incidence θ between the direction vector p and the surface normal n leaving the crowd.

Such a simplification of crowd movement is only a crude (qualitative) approximation of what often actually happens in crowds, as people tend to position themselves behind the shoulders of other pedestrians for a better overview of the situation. Moreover, this simplified representation abstracts from other phenomena such as *adaptive route choices* and complex collisional behaviours (step-and-slide, separation, cohesion, glancing, etc. [22]).

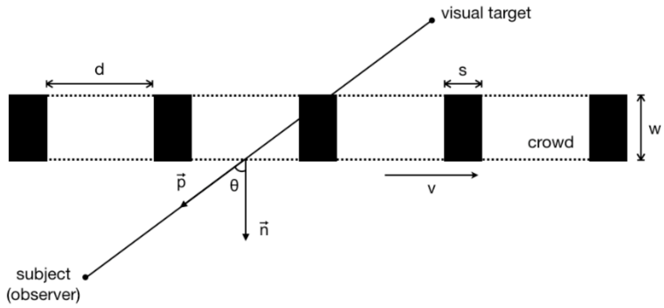

Figure 2: Intermittent visual disruption of a regularly spaced line of people crowd.

Nevertheless, this simple model is sufficient to capture the relationship that the severity of visibility loss is proportional to the projected crowd density, e.g. if the line of sight from subject to target is perpendicularly intercepted by a *directional* crowd, the visual disruption can be mitigated mentally (*continually visible*), whereas an angular visual occlusion by the crowd can lead to extended loss of sight (*occasionally visible*), even the sign's unintelligibility [1]. In case of *diffuse* crowds, the visual contact can be re-established with minimal head displacement, thus present yet distinctive qualities (*intermittently visible*) from directional crowds.

In this paper, we therefore represent *Perpendicular View Space*, *Acute View Space*, and *Head Adjustment Space* as subsets of the *Visibility Space* by subcategorising *visibility* in terms of the (qualitative) duration and the frequency of the crowd's visual occlusion. *Head Adjustment* refers to the situation where the subject only needs to move their head slightly to regain sight of the target through a diffuse crowd, rather than needing to move to a new location. For example, consider a small (sparse, diffuse) crowd standing in front of a painting in an art gallery; a subject standing behind the crowd will only occasionally need to adjust their head to the side to maintain sight of the painting as people in the crowd slowly amble around. In this paper, we choose *45°* as the threshold angle for θ above which the crowd's visual obstruction becomes adverse.

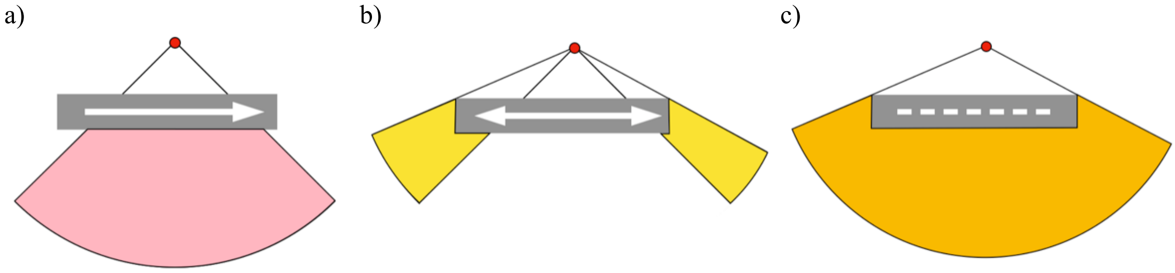

Figure 3: a) Perpendicular view space of a directional crowd; b) Acute view space of a bidirectional crowd; c) Head adjustment space of a diffused crowd.

Movement Spaces: Movement spaces are the regions in which a subject can move. We define the *Direct Movement Space* of a target as a circle centred on the target intersected with the complete (original) movement space. The radius of the circle specifies the distance within which a subject is near enough to the target that they would aim to take the (geometrically) shortest path that the environment affords. When a crowd is introduced, we distinguish sub-regions of the direct movement space within which a subject is forced to make a decision: either pass through the crowd to persist with their shortest path, or find a different (longer) path to the target. This region is geometrically computed as the intersection between (a) the direct movement space and (b) the "shadow" region that the crowd casts if the target is treated as a light source, denoted as *Disrupted Movement Space*.

Social discomfort from Viewing Angle: A subject may feel social discomfort if they must look into the faces of people within a *directed* crowd in order to try to see the target. Thus, we distinguish the region in which the angle of incidence between the subject's line of sight and the crowd region is less than *30º of an on-coming* crowd, i.e. the crowd is directed towards the subject, denoted as *Facing View Space*.

Social discomfort from Proximity: An occupant that is located within a threshold distance of the crowd, and located behind the crowd (with respect to the target) may experience some social discomfort, and thus we distinguish this region in our model as *Near Crowd Space*.

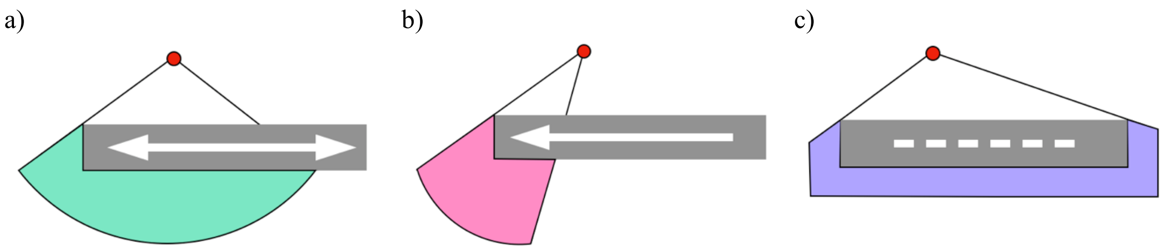

Figure 4: a) Disrupted direct movement space of a bidirectional crowd; b) Facing view space of a directional crowd; c) Near crowd space of a diffused crowd.

Crowd Superposition: In the presence of multiple crowds, the sign visibility cannot be improved by injecting more crowds into the environment. In principle, the sign visibility will always be qualitatively comparable to the visibility nullifying all other crowds except the one having the most drastic effects on visibility, e.g. superposition of two distinctive visual qualities equals the lower one.

Table 1: Visibility spaces and movement spaces induced by the target (red dot) in the presence of three distinct crowd artefacts

	Crowd, diffused	Crowd, bidirectional	Crowd, directional
Representation	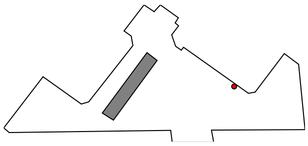	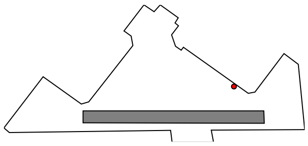	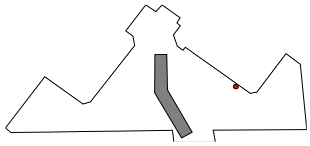
Perpendicular View Space	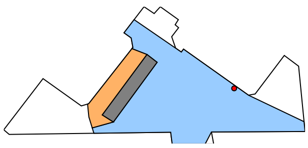	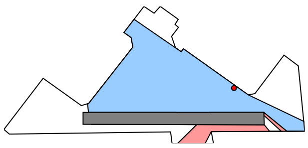	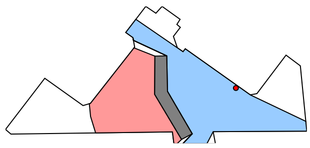
Acute View Space	(Head Adjustment Space)	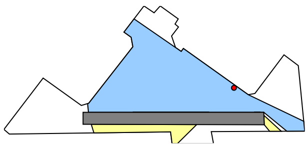	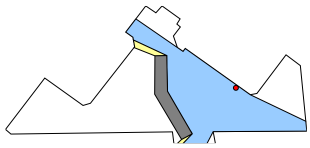
Facing View Space	/	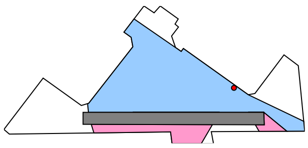	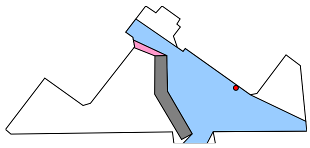
Disrupted Movement Space	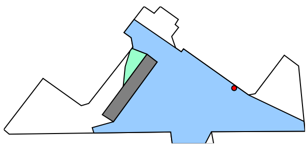	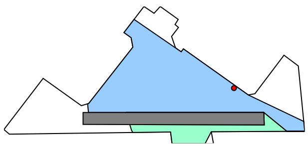	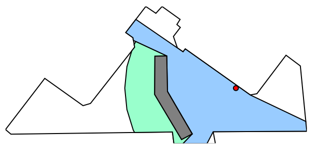
Near Crowd Space	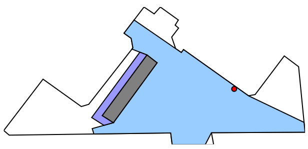	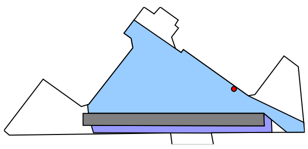	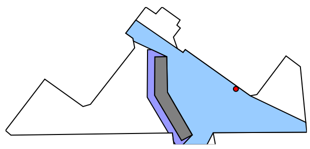

4. A gentle introduction to Answer Set Programming

As *visibility spaces* are semantically rich, complex geometries, we choose Answer Set Programming extended to natively support spatial reasoning, ASPMT(QS) [6,7,26]. ASP is a declarative logic programming language that is used to represent and reason about semantic information in a given application domain (such as BIM and crowds) in the form of *facts* and *rules*, and has an in-built search engine for finding *models* (combinations of deduced facts) that follow from the given premises. We use ASP to implement a range of novel *query services* that enable a user to analyse a BIM with respect to occupant experience in the presence (and absence) of crowds, where a BIM is encoded as ASP facts, rules capturing the interaction between crowds, subjects, and targets are encoded as ASP rules, and valid query solutions are encoded as ASP models discovered by the ASP search engine. The extension of ASP to support spatial reasoning (e.g. topological intersection between polygons) is ASPMT(QS) [6,7,26].

The kinds of queries we seek to support have the character of being *highly combinatorial*: find *combinations* of particular BIM objects, crowds and spatial artefacts that satisfy given semantic and geometric conditions. The ASP search engine has been specifically designed to rapidly find solutions to highly combinatorial problems, i.e. for NP-hard problems [23].

In logic programs, a *clause* is a formula of the form: $H \leftarrow B_1 \wedge \ldots \wedge B_m \wedge \text{not } B_{m+1} \wedge \ldots \wedge \text{not } B_n$ where H is an *atom*, and each B_i is either an *atom* or a *tautology*. H is called the *head*, and $B_1 \wedge \ldots \wedge B_m \wedge \text{not } B_{m+1} \wedge \ldots \wedge \text{not } B_n$ the *body*. In ASP syntax, a *rule* is a formula of the form: A_0 :- L_1 ,..., L_n where A_0 is an atom (constant or function), and each L_i is a literal of the form A (positive) or not A (negative), where A is an *atom*. A *rule* is read as an implication stating that if all positive literals in the rule body are true, and all negative literals are satisfied, then the rule head must be true. A *fact* is a rule that is unconditionally true, e.g. the body of the rule is always true, denoted as: A_0. An *integrity constraint* is a rule that prohibits solutions where the literals in the rule body are jointly satisfied, denoted as: :- L_1 ,…, L_n.

ASP deduces *minimal stable models* M_i to the logic program, such that all atoms in M_i are true with respect to M_i and all atoms not in M_i are false with respect to M_i. Unlike Prolog, a solution (or model) in ASP can distinguish between a proposition being True, False, or neither (in Prolog, negation is defined as *failure to prove*). The (classic) negation of a literal L in ASP is denoted -L, meaning as "L is False", and is semantically distinct from *not L*, which means "L is not True" (i.e. L is either False or neither True nor False). A choice rule in ASP enables one to express that a head may *optionally* be deduced, denoted: *{Head} :- Body.* In this paper, we use *clingo*, a complete ASP system composed of a grounder (*gringo*) and a solver (*clasp*), to find all viable solutions that do not contradict any program clauses, e.g. facts, rules, and integrity constraints.

5. Domain Model of Co-presence in ASP

In our domain model we define *events*, *crowds*, *targets*, and the (physical) *environment* that comes from a BIM. The environment induces *movement spaces*. Targets induce *visibility spaces* and *direct movement spaces*. Crowds together with targets induce the seven new spatial artefacts presented in Table 1. Crowds are related to specific events in which they occur, represented in our model via a *during* relation. For example, the following ASP program represents three events e_1, e_2, e_3 and three crowds c_1, c_2, c_3 such that crowd c_1 occurs during events e_1, e_2, crowd c_2 occurs during event e_2, and crowd c_3 occurs during event e_3:

```
event(e1;e2;e3). crowd(c1;c2;c3).
during(c1, e1). during(c1,e2). during(c2,e2). during(c3,e3).
```

A scenario is defined by the combination of events that currently *hold*, which in turn determines the crowds and subsequent crowd-based artefacts that *hold*. This is captured by the ASP rule:

```
holds(X) :- event(E), holds(E), during(X,E).
```

Geometric regions are modelled using the *representation*/2 predicate and point locations are modelled using *location*/2 predicate. In this first prototype regions are 2D polygons. Users can specify one or more *targets* each with a point location, and may optionally also specify one or more *subjects* each with a point location. We model the concept that certain spatial artefacts dominate another using a transitive *dominates* relation. E.g. for a given target, if a subject is standing is an *acute view space* (induced by one crowd) and a *perpendicular view space* (induced by a different crowd) then the dominating experience will the more restrictive *acute view*. This is captured by the following ASP facts and rules:

```
dominates(continually_visibl, permanently_visible e).
```

```
dominates(intermittently_visible, continually_visible).
dominates(occasionally_visible, intermittently_visible).
dominates(out_of_visual_field, occasionally_visible).

dominates(X,Z) :- dominates(X,Y), dominates(Y,Z).  %% transitivity
```

The experience of a *Subject* at a given location with respect to a *Target* is defined by the dominant spatial artefacts that the observer is located in:

```
experience(Exp, Observer, Target) :-
       subject(Observer), target(Target), location(Observer, ObsPoint),
       spatial_artefact(Exp, ArtefactId), induced_by(ArtefactId, Target),
       holds(ArtefactId),
       representation(ArtefactId, ArtefactRegion),
       incidence(interior, ObsPoint,  ArtefactRegion),
       not -experience(Exp, Observer, Target).

%% Having experience DomE for observer O and target T negates all
%% weaker experiences (i.e. that are dominated by DomE)
-experience(E,O,T) :- experience(DomE,O,T), dominates(DomE, E).
```

6. Empirical Evaluation on the Urban Sciences Building

We have implemented a prototype crowd analysis software tool, and in this section we evaluate our tool on the USB. The main purpose of this preliminary empirical evaluation is to demonstrate the rich range of novel query-answering features that our tool provides, and to also show that our approach provides query answers within a practical amount of runtime on large, real-world BIMs.

Figure 5: The USB forum space viewed from the middle of the western side, looking towards the main entrance (right), and reception desk (centre). Hawkins\Brown, used with permission.

Consider the scenario where a static, diffused crowd of lab staff is gathered on left side of the foyer, and a moving, bidirectional crowd of students is walking between the lecture theatre and the café, a building operation manager might want to know whether a person standing at the entrance is still able to visually engage with the information sign (see Figure 6(a)). In the context of ASP, we specify the combination of contingent facts with *integrity constraints*. Knowing the subject's location, ASP then deduces that the target is *continually visible* to the subject.

```
holds(e1; e2).    :- holds(e3).
target(s1). subject(p1). location(p1, point(1200, -931)).
```

In the meantime, perhaps a directed crowd of visitors is walking towards the elevator (see Figure 6(b)). We might wonder if this newly emerged crowd creates visual interruptions that are too long to recover from. We then allow ASP to freely choose from potential events with the constraint that the sign is at least *continually visible* to the subject. ASP concludes that *e3* would have induced *intermittent visibility* and thus, is excluded from the model.

```
{holds(e3)}.
:- experience(ViewQuality, p1, s1), dominates(ViewQuality, continually_visible).
```

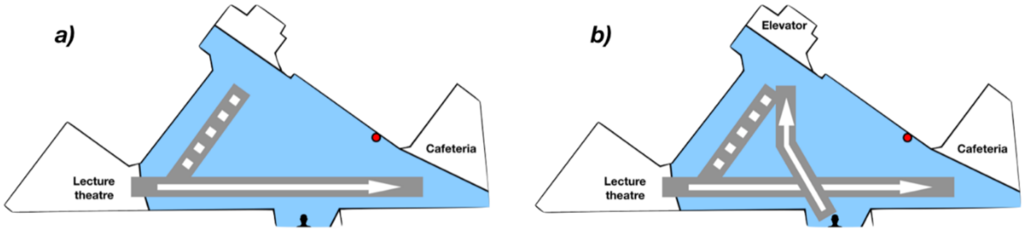

Figure 6: (a) A diffuse crowd of lab staff and a directional crowd of students; (b) An additional directional crowd of visitors.

Now suppose any event might occur, and we want to know if a region exists where a subject has exactly *continual* visual access to the signage. This would require that the worst visual attribute associated with each individual crowd is *continually visible*, e.g. the *continually visible* region of a crowd should not overlap with the visibility region of a different crowd with lower view quality.

```
:-  induced_by(ArtefactId1, Target), induced_by(ArtefactId2, Target),
    holds(ArtefactId1), holds(ArtefactId2),
    spatial_artefact(continually_visible, ArtefactId1),
    spatial_artefact(ViewQuality, ArtefactId2),
    dominates(ViewQuality, continually_visible).
    topology(overlap, ArtefactId1, ArtefactId2).
```

Mixed queries about visibility and mobility can also be interesting as to identify regions where a subject can see the sign but has disrupted movement access to the sign.

```
exists_space(R) :-
  induced_by(ArtefactId1, Target), induced_by(ArtefactId2, Target),
  holds(ArtefactId1), holds(ArtefactId2),
  ViewQuality = (permanently_visible; continually_visible; intermittently_visible),
  spatial_artefact(ViewQuality, ArtefactId1),
  spatial_artefact(disrupted_movement, ArtefactId2),
  topology(overlap, ArtefactId1, ArtefactId2),
  R = intersection(Artefact1, Artefact2).
```

Table 2 presents a summary of the queries we ran on the USB. Each query is asking about the relationship between a subject (observer), a combination of events that correspond with crowds, and the observer's visual and mobility access experience with one or more target signs. In general, any combination of these three aspects can be given as *input* ("given"), or left unspecified ("?"). Each valid way of solving for the unspecified aspects represents a solution to the query, i.e. informally "?" represents aspects that should be the *output* of the query. Thus, our tool provides a diverse range of query support features through a uniform, flexible interface: simply changing whether a parameter is input data or a variable changes the kind of query being asked. Moreover, the runtime of each query we executed was less than 1 second, showing that our approach is highly practical when applied to real-world scale BIMs.

Table 2. Summary of our sample queries and runtimes on the USB with the ASP system *clingo*.

Query Number	**Observer location**	**Events**	**Experience**	**Runtime on USB (seconds)**
1	Given	Given	?	0.55
2	Given	? (partially given)	Given	0.54
3	Given	?	Given	0.53
4	?	Given	Given	0.54
5	Given	Given	?	0.56
6	?	?	Given (visual and movement)	0.53

7. Conclusions and Future Work

As Gibson's ecological theory suggests, human's proprioception is primarily vision-based, e.g. occupants' action and movement are conscious responses to what they see [24]. Studies have highlighted the changes in an occupant's behavioural pattern under particular environmental situations, such as smoke, light, fire, debris, etc. [16].

In this study, we have proposed an analytical approach to describe human's embodied spatial experiences in terms of visibility, mobility, and proxemics in the presence of crowds. We further demonstrated the robustness and query-answering capabilities of such approach with ASPMT(QS), a declarative, logically verifiable, and extensible programming framework.

Our results provide a formal, systematic, and operational system to interpret crowds' impact on occupants, that can be used in a wide range of applications such as visibility of wayfinding signs, occupant flow control, contingency planning, automated orchestration of activities, etc. In the future, we intend to empirically validate our proof-of-concept formalisation with human-registered atmospheric changes, and to propose a sound, comprehensive set of rules to characterise crowds in the landscape and the soundscape of the building space.

This paper belongs to a series of research efforts of exploring the concept of spatial artefacts in the context of occupant's experiences in the built environment.

Acknowledgements

We are grateful to the Estates Service of Newcastle University for access to the BIM model of the USB. There have been many fruitful discussions with Ewan Graham and Louisa Bowles of Hawkins\Brown, and Becky Hayward of BuroHappold Engineering, Richard Watson and Kay Rogage of Northumbria University and BIM Academy.

References

1. Motamedi, Ali & Wang, Zhe & Yabuki, Nobuyoshi & Fukuda, Tomohiro & Michikawa, Takashi. (2017). Signage visibility analysis and optimization system using BIM-enabled virtual reality (VR) environments. Advanced Engineering Informatics. 32. pp.248–262.

2. Park, J.H., Rojas, F.A. and Yang, H.S. (2013), A collision avoidance behavior model for crowd simulation based on psychological findings. Comp. Anim. Virtual Worlds, 24: pp.173–183.

3. Gust, H., Krumnack, U., Kühnberger, K. U., & Schwering, A. (2008). Analogical Reasoning: A Core of Cognition. KI, 22(1), pp.8–12.

4. Freksa, C., Klippel, A., & Winter, S. (2007). A cognitive perspective on spatial context. In Dagstuhl Seminar Proceedings. Schloss Dagstuhl-Leibniz-Zentrum fr Informatik.

5. Penn, A. (2003). Space Syntax And Spatial Cognition: Or Why the Axial Line? Environment and Behavior, 35(1), pp.30–65.

6. Wałęga, P. A., Schultz, C., & Bhatt, M. Non-monotonic spatial reasoning with answer set programming modulo theories. Theory and Practice of Logic Programming, 17(2), pp.205–225. (2017).

7. Wałęga, P. A., Bhatt, M., & Schultz, C. ASPMT (QS): non-monotonic spatial reasoning with answer set programming modulo theories. In LPNMR (pp. 488–501). Springer, Cham.

8. Bhatt, M. & Schultz, C. & Huang, M. (2012). The Shape of Empty Space: Human-centred cognitive foundations in computing for spatial design. IEEE Symposium on Visual Languages and Human-Centric Computing, VL/HCC.

9. Shiwakoti, Nirajan & Gong, Yanshan & Shi, Xiaomeng & Zhirui, Ye. (2015). Examining influence of merging architectural features on pedestrian crowd movement. Safety Science. 75.

10. Robin, Th & Antonini, Giovanni & Bierlaire, M. & Cruz, J.. (2009). Specification, estimation and validation of a pedestrian walking behavior model. Transportation Research Part B: Methodological. 43, pp36–56.

11. Duives, Dorine & Daamen, Winnie & Hoogendoorn, Serge. (2013). State-of-the-art crowd motion simulation models. Transportation Research Part C: Emerging Technologies. 37, 193–209.

12. Yang, Fangkai & Shabo, Jack & Qureshi, Adam & Peters, Christopher. (2018). Do you see groups?: The impact of crowd density and viewpoint on the perception of groups, 313–318.

13. Bellomo, Nicola & Piccoli, Benedetto & Tosin, Andrea. (2012). Modeling crowd dynamics from a complex system viewpoint. Mathematical Models and Methods in Applied Sciences. 22.

14. Milan, Anton & Roth, Stefan. (2011). An analytical formulation of global occlusion reasoning for multi-target tracking. Proceedings of the IEEE International Conference on Computer Vision, pp.1839–1846.

15. Bhatt, M., & Freksa, C. (2015). Spatial computing for design—an artificial intelligence perspective. In Studying visual and spatial reasoning for design creativity (pp. 109–127). Springer, Dordrecht.

16. S. Gwynne, E.R. Galea, M. Owen, P.J. Lawrence, L. Filippidis. A review of the methodologies used in the computer simulation of evacuation from the built environment. Building and Environment. Volume 34, Issue 6, 1999, pp.741–749.

17. Moussaïd, Mehdi & Helbing, Dirk & Theraulaz, Guy. (2011). How simple rules determine pedestrian behavior and crowd disasters. Proceedings of the National Academy of Sciences of the United States of America. 108.

18. Meng, Qi & Kang, Jian. (2014). The influence of crowd density on the sound environment of commercial pedestrian streets. The Science of the total environment. 511C, pp.249–258.

19. I. Chatterjee and A. Steinfeld, "Performance of a low-cost, human-inspired perception approach for dense moving crowd navigation," 2016 25th IEEE International Symposium on Robot and Human Interactive Communication (RO-MAN), New York, NY, 2016, pp. 578–585.

20. Ennis, Cathy & Peters, Christopher & O'Sullivan, Carol. (2011). Perceptual Effects of Scene Context and Viewpoint for Virtual Pedestrian Crowds. ACM Transactions on Applied Perception. 8.

21. Shao, Jing & Loy, Chen Change & Wang, Xiaogang. (2016). Learning Scene-Independent Group Descriptors for Crowd Understanding. IEEE Transactions on Circuits and Systems for Video Technology. 27.

22. Rymill, Stephen & Dodgson, Neil. (2005). A Psychologically-Based Simulation of Human Behaviour. Theory and Practice of Computer Graphics 2005, TPCG 2005 - Eurographics UK Chapter Proceedings.

23. Ramli, C.D. (2015). Modelling and Analysing Access Control Policies in XACML 3.0.

24. Gibson, J. J. The visual perception of objective motion and subjective movement. (1954).

25. Bhatt, M., Hois, J., & Kutz, O. (2012). Ontological modelling of form and function for architectural design. Applied Ontology, 7(3), pp.233–267.

26. Bhatt, M., Lee, J. H., & Schultz, C. (2011, September). CLP (QS): a declarative spatial reasoning framework. In International Conference on Spatial Information Theory (pp. 210–230). Springer, Berlin, Heidelberg.

Model-based multiple-occupant tracking through floor vibrations

Slah Drira[1,2*], Sai G.S. Pai[1,2], Ian F.C. Smith[1,2]
[1] Swiss Federal Institute of Technology (EPFL) Lausanne, Switzerland
[2] Future Cities Laboratory, ETH Zurich Singapore
* slah.drira@epfl.ch

Abstract. Smart building applications such as security, energy management and caregiving require information on occupant movements. Unlike cameras and mobile devices, sensing approaches for occupant localization that are based on footstep-induced floor vibrations preserve the privacy of indoor occupants. Current occupant-localization methodologies that rely on vibration measurements are intended for single-occupant scenarios. In reality, multiple people walk regularly at the same time. Resulting floor vibrations include a superposition of the structural responses from all occupants walking simultaneously. Prior research into occupant localization using data-driven techniques typically involves triangulation, and this requires densely instrumented floor slabs to determine the difference between times of arrival of vibrations at sensor locations. Overlapping signals from multiple occupants limit the applicability of such strategies. Furthermore, these techniques do not account for the structural behavior of floor slabs, leading to ambiguous interpretations of vibration measurements in the presence of obstructions and varying floor rigidities. In this paper, a model-based data interpretation approach using error-domain model falsification (EDMF) is used to localize multiple occupants. EDMF incorporates information related to physics-based models in the interpretation of vibration measurements to identify a population of possible occupant locations. EDMF has the potential to identify accurately two occupant locations by explicitly accommodating systematic errors and model bias to reject models that contradict measurement data. Localization results of each detected footstep are used to identify occupant trajectories. A full-scale case study, instrumented with sparse sensor configuration (approximately one sensor per 75 m^2), is used to evaluate the utility of this methodology for multiple-occupant tracking. This data interpretation approach is able to identify accurately and precisely two-occupant locations in a full-scale structure.

1. Introduction

Identifying occupant movements inside buildings can potentially improve important functions such as security systems (Song, Choi and Lee, 2008) and caregiving (Cully, Cotton and Scanlon, 2012) as well as space and energy management (Diraco, Leone and Siciliano, 2015). Several sensing technologies have been proposed to achieve these goals, most commonly optical sensors (Erickson, Achleitner and Cerpa, 2013) and radio-frequency devices (Wang, Chen and Hong, 2018). However, optical sensors require clear lines of sight and large angles of coverage to achieve accurate identification of occupants (Narayana *et al.*, 2015). Also, the presence of structural and non-structural obstructions such as walls and furniture (Lam *et al.*, 2016) has limited the applicability of radio-frequency devices. These sensing techniques mostly rely on cameras and wearable devices. Such systems thereby compromise occupants' privacy and inevitably affect their behavior. Therefore, alternative sensing approaches such as vibration sensors proved necessary to preserve the privacy of occupants and avoid influencing their behavior.

Most of the data-driven techniques (triangulation-based approaches) for localization using floor vibrations have been conducted only for single occupants (Mirshekari *et al.*, 2018) walking on small-floor areas. In full-scale applications, multiple people walk regularly at the same time on the same floor-slab. Resulting floor-vibration measurements at a sensor location include a superposition of the structural responses from multiple occupants walking at their various speeds on their respective trajectories (i.e. overlapping signals).

Floor responses are influenced by the inherent variability in walking gaits (Hausdorff, 2007) of occupants due to their various walking speeds, shoe types, mood and health (Öberg, Karsznia and Öberg, 1993). Moreover, wave propagations induced by footstep impacts are dictated by the physical characteristics of the floor medium (such as obstructions and material properties) (Hall and Michaels, 2011). These uncertainties have led traditional techniques such as blind source separation (BSS) methods (Makino *et al.*, 2004) to be inapplicable for separating overlapping signals (Shi *et al.*, 2019), thereby limiting the applicability of model-free approaches for multiple-occupant localization.

Localizing multiple people using footstep-induced floor vibrations was first proposed by Pan et al. (2016a) (for two people) and more recently by Shi et al. (2019) (for three people). Vibration measurements from two people walking simultaneously, as shown by Pan et al. (2016a), were conducted at fixed impact locations. Extracted footstep-event signals were filtered at the natural frequency band of the floor to enhance their signal-to-noise ratio (SNR). Localization of the two occupants was then carried out using the time difference of arrival (TDoA) technique (i.e. a multilateration approach) (Mirshekari *et al.*, 2018). However, the localization of two occupants was carried out on a small space (~ a sensor per 2 m^2) using controlled measurements. This concentration of sensors resulted in insignificantly overlapping signals making event-signal separation possible and the estimation of TDoA values achievable.

Multiple-occupant localization as proposed by Shi et al. (2019) involved measurements from two people walking side by side, along the same line, and in opposite directions. Also, measurements from three occupants were conducted while walking side by side and in opposite directions. These measurements resulted in partially overlapping signals with varying offsets. The proposed strategy was based on decomposing the footstep-induced floor vibrations using the continuous wavelet transform (CWT) at frequency ranges above the fundamental frequencies of the floor slab. This made the floor response induced by the heel strikes from each occupant differentiable between sensor locations. Subsequently, an adaptive multidimensional scaling approach (Dokmanić, 2015) was applied to evaluated TDoA values at various wavelet scales to estimate the location of each occupant. Although the localization of three occupants was accurate, the proposed strategy was only tested on a small floor area (less than 10 m^2). Also, footstep events with low SNR signals might limit the applicability of TDoA techniques, leading to inaccurate localization (Bahroun *et al.*, 2014). Scenarios of synchronized footstep impacts might limit the applicability of the proposed model-free approach since signal contributions from multiple occupants were assumed to be partially overlapped.

In this paper, a model-based data interpretation approach using error-domain model falsification (EDMF) (Goulet and Smith, 2013) is evaluated for multiple-occupant tracking. This approach overcomes limitations of existing data-driven techniques, such as varying floor rigidities and overlapping signals. Including physics-based models in the interpretation of measured vibration, EDMF provides accurate localization of a single occupant (Drira, Reuland and Smith, 2019b, 2019a; Drira *et al.*, 2019). Model falsification is a population-based approach that explicitly accommodates systematic errors and model bias. Sequential analysis and a trajectory-determination operation are included using information about consecutive footstep events to track multiple occupants. An application to a full-scale floor (~600 m^2) involving real scenarios of two occupants walking simultaneously is assessed.

2. Multiple-occupant tracking methodology

The model-based tracking strategy is intended to identify possible locations of multiple occupants walking simultaneously on a floor slab. These locations are then used to determine possible trajectories of occupants. Steps that are involved in the multiple-occupant tracking methodology are shown in Figure 1. The proposed strategy accounts for information on structural behavior and uncertainties from multiple sources to achieve accurate and precise tracking of occupants.

To start, a model-free occupant detection operation is carried out to extract event signals resulting from multiple occupants walking together, and this is described in detail in Drira et al. (2019). This operation involves combining vibration components that are filtered at various frequency ranges to provide accurate signal extraction. Subsequently, a model-based approach using error-domain model falsification (EDMF) is carried out to identify possible locations of occupants. Occupant localization follows occupant detection. EDMF involves comparisons of footstep-impact simulations with measurements from multiple-occupant events, which are the focus of this paper.

Unlike military marching, the footstep impacts of multiple people walking simultaneously are mostly off-synchronized (Pan *et al.*, 2016b). This results in overlapping signals with varying time-offsets in floor responses. To a lesser extent, footstep impacts from multiple occupants can also be staggered, leading to separated floor responses from each individual.

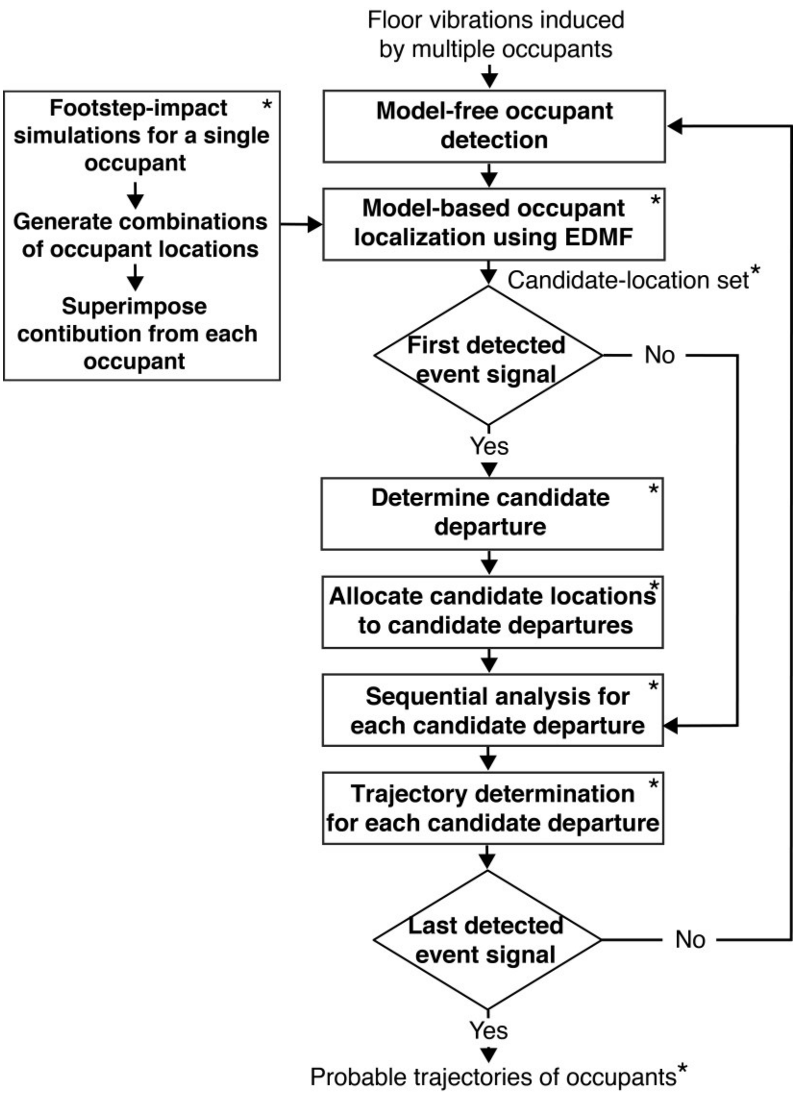

Figure 1: Multiple-occupant tracking methodology. The asterisks (*) indicate the focus of this paper.

Floor vibrations resulting from multiple occupants walking together include a superposition of the structural responses induced by each individual. The footstep impacts of a single occupant are first simulated at potential locations using a finite-element model. A moderate walking speed of 1.6 Hz is used for simulations (i.e. impact duration of 0.625 s). Then, two time-offsets: one-third (0.2 s) and two-thirds (0.4 s) of a footstep-impact duration are involved in superimposing contributions from each occupant at each possible location. These time offsets are chosen based on prior observations of measured vibrations from two occupants walking together on the floor of the tested case study (see Section 3). A fixed duration of 0.625 s of the superimposed signals is investigated for localization. Moreover, simulations from a single occupant are included in the initial model instances to account for staggered footstep events.

Simulated and measured vibrations are then decomposed, using continuous wavelet transform (CWT) (Ford, 2003), and reconstructed, using inverse wavelet transform (IWT), at the first few bending modes of the structure to increase their SNR. Maximum difference in amplitudes (Δ_{amp}) and standard deviation (σ) of processed event signals are used as metrics for the model-based occupant localization. Using EDMF, location instances are falsified when residuals between measured and simulated responses lie outside predefined localization thresholds. These thresholds are ascertained based on combined uncertainties and a target reliability for localization of 95 %. Location instances that do not contradict measured vibrations define the candidate-location set (CLS).

Subsequently, CLSs of detected event signals are used to determine candidate trajectories of each individual as shown by Drira et al. (2019a). Possible departure/arrival points are defined prior to the trajectory-determination operation. Candidate locations (CLs) resulting from the first detected event help determine candidate departures. Departure points that do not contain CLs within a radius of twice the distance between two footsteps (approximately 75 cm) are rejected. Departure points that are not rejected are taken as candidate departures. Then, CLs within a radius of twice the distance between two footsteps from the departure point are allocated to each candidate departure. CLs that correspond to each candidate departure point are subsequently used to investigate possible paths based on information from succeeding detected events. CLs that do not correspond to a possible departure are rejected.

The CLS related to each succeeding detected event is then subjected to a sequential analysis based on information from the previously detected event. This operation is repeated separately for each candidate departure. Sequential analysis, as explained by Drira et al. (2019a), assumes that the distance between two successive impact events cannot exceed the step-length. For a candidate departure, a CL of a current event is rejected when its distances to all CLs of a preceding event exceed the predefined step-length.

Finally, CLSs of each detected event, resulting from the sequential analysis, are investigated to determine possible trajectories. The trajectory-determination operation, as explained by Drira et al. (2019a), assumes that occupants walk until reaching their destinations without backtracking. Hence, a CL that corresponds to a possible departure is rejected when its distance to at least one possible arrival point is not reduced. When CLs that correspond to a candidate departure are falsified, related trajectories are rejected. Once CLSs of all detected event signals are investigated, paths connecting remaining candidate departures with possible arrivals that define CLs are taken as candidate trajectories.

3. Application to Full-Scale Floor Slab

The multiple-occupant tracking methodology is tested on a full-scale floor slab of a building located in Singapore (Drira, Reuland and Smith, 2019a), as shown in Figure 2. The tested area is approximately 600 m^2, as shown by the accessible area in Figure 2. The floor is a continuous reinforced-concrete slab, 25 cm thick. The floor slab is supported by ten concrete columns (see squares in Figure 2) and several reinforced-concrete walls. Apart from the high stiffness of the slab, unidirectional reinforced-concrete beams connecting the floor with the concrete columns as shown by section A-A in Figure 2a result in relatively short spans of the slab. The floor-slab supports several plasterboard and masonry walls. Use of a sparse sensor configuration for occupant tracking on a varying-rigidity floor slab is complex and little research is available regarding such cases. Therefore, this case-study investigates a possible bound for useful application of the occupant-localization strategy using a model-based approach.

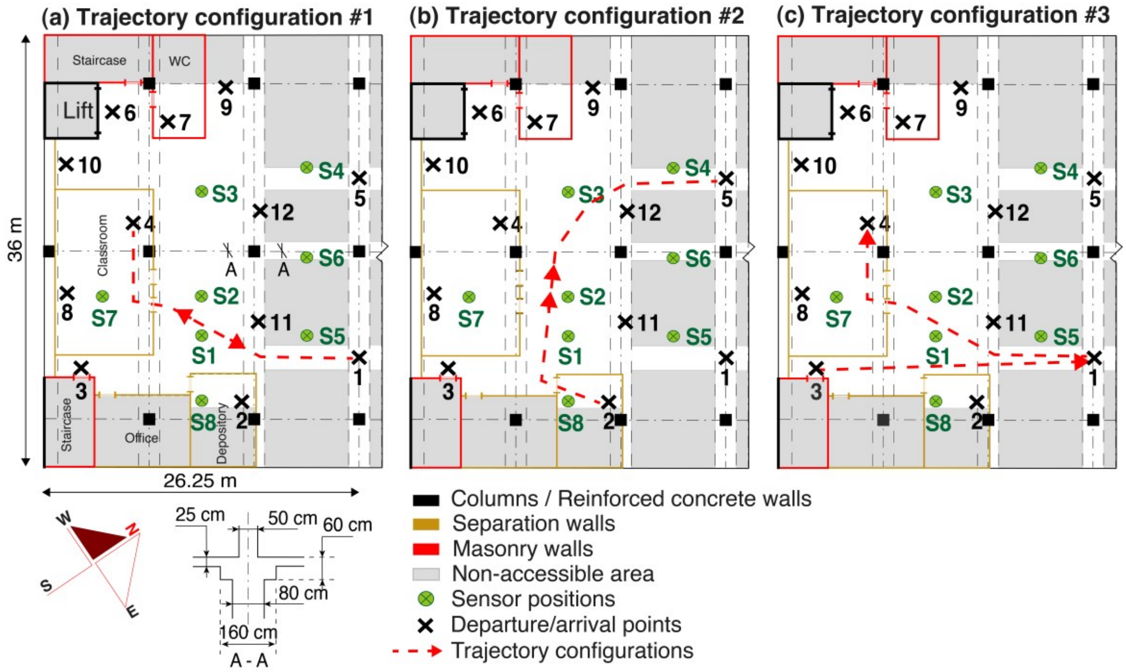

Figure 2: Two-occupant tracking is tested on a full-scale concrete slab. The slab contains twelve departure/arrival points (X1 to X12) for trajectories. (a to c) Three trajectory configurations of two occupants are used for testing the presented methodology (see Figure 1).

The floor slab is instrumented with eight unidirectional vibration sensors (Geophones SM-24 by I/O Sensor Nederland). These sensors are used to record the vertical velocity response of the floor. Sensor placements, as shown by circles in Figure 2, correspond to the locations of the dominant vertical bending modes of the floor slab. Floor vibrations are recorded with a sampling rate of 1000 Hz using an acquisition unit (NI USB-6003).

Regarding the access spots of this case study, twelve departure/arrival points are assumed, as shown by crosses (X1 to X12) in Figure 2. These predefined points lead to 132 possible trajectories. Three people (O1 to O3) weigh 93 Kg for O1, 87 Kg for O2 and 75 Kg for O3, wearing various types of shoes (hard, soft and intermediate soles) are involved in two-occupants walking tests. Floor vibrations from two occupants walking simultaneously following three trajectory configurations are recorded. For all measurement tests, occupants do not walk at fixed impact locations and their walking speed is moderate at approximately 1.6 Hz.

The first configuration, as shown in Figure 2a, involves two occupants (O1 and O3), walking towards each other along the same trajectory (X1 to X4/ X4 to X1). The second configuration, as shown in Figure 2b, involves two occupants (O1 and O3) walking along the same trajectory (X2 to X5) while one follows the other by four footsteps, only at the beginning. The third configuration, as shown in Figure 2c, involves one occupant (O2) walking from X3 to X1 while the other (O1) walks from X1 to X4. Three walking tests are carried out for each trajectory configuration.

3.1 Model Predictions

Modal analysis based on prior ambient vibration measurements has revealed that the first bending mode of the floor slab lies within the frequency range of 9-11 Hz. This allows characterizing the full-scale slab as a low-frequency floor (Pavic and Willford, 2005). For low-frequency floors, a deterministic vertical-load function for a single footstep impact is expressed in the time domain by the summation of harmonic components (Bachmann, Pretlove and Rainer, 1995) (i.e. Fourier series) as described in the following equation:

$$F(t) = G + \sum_{i=1}^{n} G\alpha_i \sin(2\pi i f_p t - \phi_i) \tag{1}$$

where $F(t)$ is presented by a static part expressed as G, which is the person's static weight, and a fluctuating part expressed by the harmonics. f_p is the walking frequency. t is time. ϕ_i is the phase shift of the i^{th} harmonic. α_i is the Fourier coefficient, also known as the dynamic load factor (DLF) of the i^{th} harmonic. n is the number of contributing harmonics. For this application, f_p is fixed at 1.6 Hz, and ϕ_i is assumed equal to zeros. Also, G is assumed equal to 85 Kg. DLFs proposed by Young (2001) as shown in Eq. 2, are involved for footstep-impact simulations (see Section 2).

$$\begin{aligned} \alpha_1 &= 0.41(f_p - 0.95) & f_p &= 1 - 2.8\, Hz \\ \alpha_2 &= 0.069 + 0.056 f_p & f_p &= 2 - 5.6\, Hz \\ \alpha_3 &= 0.033 + 0.0064 f_p & f_p &= 3 - 8.4\, Hz \\ \alpha_4 &= 0.013 + 0.0065 f_p & f_p &= 4 - 11.2\, Hz \end{aligned} \tag{2}$$

Footstep-impact simulations are generated using a finite-element model of the slab. The dynamic responses of the slab are generated based on linear-modal-superposition analysis in ANSYS (APDL, 2010). The floor slab is modeled using solid elements (SOLID185). The elastic modulus for the concrete slab is taken to be 35 GPa. The viscous damping ratio is taken to be 5% according to engineering heuristics (Willford, Field and Young, 2006). Columns and reinforced-concrete walls are modeled as simple supports (see Figure 2).

Two-thirds of the floor slab is divided into a grid of possible locations (see the accessible area in Figure 2). The distance between two possible locations is assumed to be 75 cm, leading to 796 possible footstep locations. These initial simulations are used to generate possible model predictions that correspond to two occupants walking simultaneously on the floor slab. Contributions from each occupant at each possible location are superimposed based on two time-offsets (0.2 s and 0.4 s, as explained in Section 2). Including contributions from a single occupant, simulated responses for two occupants result in 1,268,028 model instances (796x796x2 + 796).

3.2 Uncertainty estimation

Model simulations and measurements are prone to uncertainty from several sources. Common modeling uncertainties are related to model imperfections such as idealized boundary conditions and omissions. For example, the finite element model contains omissions including separation walls, room furniture, and connections between the floor slab and the reinforced concrete walls. Also, unknown model parameters and an idealized footstep-impact load function (see Eq.1) increase the modeling uncertainty. Uncertainty from model simplifications and omissions are estimated to be uniformly distributed between −20 % to +30 % on simulated amplitudes. These bounds are estimated based on engineering judgement and heuristics (Drira, Reuland and Smith, 2019a; Drira *et al.*, 2019).

Regarding measurement uncertainties, recorded vibrations are subject to the inherent variability in walking gaits of the same person and between individuals (Drira, Reuland and Smith, 2019a). These variations are influenced by occupant anatomy, walking speed, shoe type, health and mood (Pan *et al.*, 2015). Based on prior measurements, variability in walking gaits has been evaluated for an occupant walking on the same footstep impact locations multiple times and wearing hard- and soft-soled shoes. This evaluation results in a measurement uncertainty bounded by the interval of ± 45 %, which defines the 99th percentile of the resulting distribution.

3.3 Multiple-occupant tracking results

Tracking of two occupants, walking simultaneously on a full-scale floor slab, is achieved using a model-based approach. An example of CLSs of a few events (intermediate and last events) resulting from two occupants walking along three trajectory configurations (see Figure 2) are shown in Figure 3. In Figure 3, small green squares represent the CLSs, and dots represent the falsified location sets. Dashed lines represent the separation walls, and large black squares represent the concrete columns. Diamonds represent sensor locations, and real footstep locations of each occupant are represented with crosses.

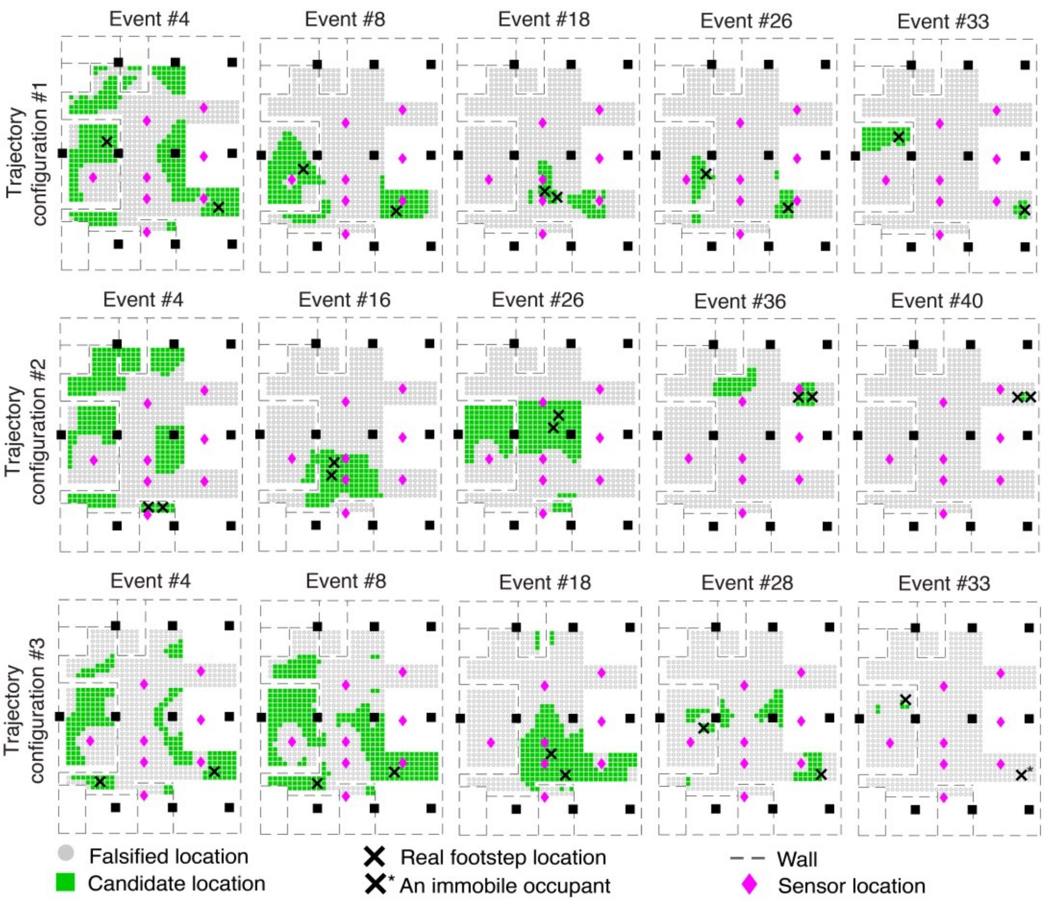

Figure 3: CLSs that are obtained using EDMF, sequential analysis and trajectory determination.

Regarding real footstep locations in Figure 3, incorporating physics-based models in the interpretation of event signals from two occupants using EDMF has led to accurate localization results for all detected events. Moreover, a sequential analysis that accounts for information from previous events, and trajectory determination, which assumes that occupants walk without backtracking until reaching their destinations, have proved to increase localization precision. It can be observed in Figure 3 that the size of the falsified location sets of the last few events are significant compared with the first few events and this is achieved without compromising accuracy.

Model-based occupant tracking has led to accurate determination of correct arrival points for all tested trajectories (see Figure 3). During measurement tests, occupants have remained immobile upon reaching their destinations. For the trajectory configuration #3 (see Figure 2), the first occupant requires 33 footstep events to attain the arrival point X4 from X1, while the second occupant requires 28 footstep events to attain the arrival point X1 from X3. Thus, starting from the 29th event, model instances related to the arrival point X1 are entirely falsified, since contributions to floor responses are only from the first occupant, as illustrated in Figure 3.

Assuming that all departure/arrival points are predefined, the model-based occupant-tracking operation provides precise candidate trajectories for two occupants walking simultaneously, as presented in Table 1. Tracking precision refers to the percentage of falsified trajectories from all possible paths (132 possible trajectories). If only one possible trajectory per occupant remains unfalsified once all detected events are investigated, then occupant tracking is taken to be 100 % precise.

Table 1: Model-based occupant-tracking precision.

	Path	Walking test	Number of footstep events	Tracking precision (%)	Average precision (%)
Trajectory configuration #1	X1 to X4	1	33	100	98
		2	33	100	
		3	33	100	
	X4 to X1	1	32	88.2	
		2	33	100	
		3	33	100	
Trajectory configuration #2	X2 to X5	1	40	100	100
		2	40	100	
		3	40	100	
Trajectory configuration #3	X3 to X1	1	28	80.6	90.3
		2	28	81.2	
		3	28	81.2	
	X1 to X4	1	33	100	
		2	33	100	
		3	33	98.6	

An average tracking precision of 96 % is observed for all tested measurements. For trajectory configurations #1 and #2, both occupants carried out approximately the same number of footstep events to reach their destinations (33 and 40 detected events). Model-based occupant tracking results in accurate and precise trajectory determination for each occupant. For trajectory configuration #3 the walking path, X3 to X1, of one occupant is achieved after 28 (out of 33) detected events with an average precision of 81 %, while the walking path X1 to X4 is determined precisely after exploring all detected events. This is due to the different number of events required to achieve both paths (see Figure 3).

EDMF, by including structural information and taking into account systematic errors and model bias, has the potential to accurately track occupant locations in a full-scale structure as shown in Figure 3. However, several ambiguities in the interpretation of measured floor response remain in the resulting CLSs, as shown in Figure 3. This may be due to the omission of the separation walls in the finite element model and to the employment of an idealized footstep-impact load function. A sensitivity analysis to evaluate the influence of the separation walls on the simulated responses, and a better design for the footstep-impact load function are under study.

Moreover, the number of model instances increases exponentially when defining multiple occupants walking simultaneously, which may limit the applicability of model-based approaches. Prior model-free classification to determine the number of occupants on the floor is needed for near-real-time applications. Also, signal processing techniques to separate emission sources may be useful to localize more than two occupants walking together.

Occupant tracking using sequential analysis and trajectory determination provided precise tracking of two occupants, as shown in Table 1. However, for more realistic scenarios, tracking multiple occupants without assuming predefined departure/arrival points is future work.

4. Conclusions

Model-based tracking has been applied successfully for two occupants walking simultaneously on a full-scale slab, and this leads to the following conclusions:

- Model-based identification (using EDMF) that includes structural information and takes into account systematic errors and model bias is able to accurately track occupants in a full-scale structure.
- Occupant tracking using sequential analysis and trajectory determination provides precise trajectories for two occupants.

Current work involves examining the potential of these strategies for application in more full-scale situations.

Acknowledgments

The authors acknowledge Tectus Dreamlab Pte Ltd and BBR Holdings Singapore for providing access to the full-scale structure to validate the model-based occupant-tracking strategy. This work was funded by the Applied Computing and Mechanics Laboratory (IMAC) EPFL, the Singapore-ETH centre (SEC) under contract no. FI 370074011-370074016 and the Swiss National Science Foundation (SNSF) under contract no. 200020-169026.

References

APDL, A. M. (2010) *Mechanical applications Theory reference*, *ANSYS Release*.

Bachmann, H., Pretlove, A. J. and Rainer, J. H. (1995) 'Vibrations induced by people', in *Vibration Problems in Structures*. Springer, pp. 1–28.

Bahroun, R. *et al.* (2014) 'New algorithm for footstep localization using seismic sensors in an indoor environment', *Journal of Sound and Vibration*. Elsevier, 333(3), pp. 1046–1066.

Cully, W. P. L., Cotton, S. L. and Scanlon, W. G. (2012) 'Empirical performance of RSSI-based Monte Carlo localisation for active RFID patient tracking systems', *International journal of wireless information networks*. Springer, 19(3), pp. 173–184.

Diraco, G., Leone, A. and Siciliano, P. (2015) 'People occupancy detection and profiling with 3D depth sensors for building energy management', *Energy and Buildings*. Elsevier, 92, pp. 246–266.

Dokmanić, I. (2015) 'Listening to Distances and Hearing Shapes: Inverse Problems in Room Acoustics and Beyond', *PhD Thesis: EPFL*, 6623. doi: 10.5075/epfl-thesis-6623.

Drira, S., Reuland, Y., Pai, S. G. S., *et al.* (2019) 'Model-Based Occupant Tracking Using Slab-Vibration Measurements', *Frontiers in Built Environment*, 5, p. 63. doi: 10.3389/fbuil.2019.00063.

Drira, S., Reuland, Y., Olsen, N. F. H., *et al.* (2019) 'Occupant-detection strategy using footstep-induced floor vibrations', in *The 1st ACM International Workshop on Device-Free Human Sensing (DFHS)*. New York, USA.

Drira, S., Reuland, Y. and Smith, I. F. C. (2019a) 'Model-based interpretation of floor vibrations for indoor occupant tracking', in *26th International Workshop On Intelligent Computing In Engineering*. Leuven Belgium.

Drira, S., Reuland, Y. and Smith, I. F. C. (2019b) 'Occupant tracking using model-based data interpretation of structural vibrations', in *9th International conference on structural health monitoring of intelligent infrastructure (SHMII-9)*. St. Louis, MO, USA.

Erickson, V. L., Achleitner, S. and Cerpa, A. E. (2013) 'POEM: Power-efficient occupancy-based energy management system', in *Proceedings of the 12th international conference on Information processing in sensor networks*. Philadelphia, Pennsylvania, USA, pp. 203–216.

Ford, M. S. (2003) 'The Illustrated Wavelet Transform Handbook: Introductory Theory and Applications in Science', *Health Physics*. LWW, 84(5), pp. 667–668.

Goulet, J.-A. and Smith, I. F. C. (2013) 'Structural identification with systematic errors and unknown uncertainty dependencies', *Computers & structures*. Elsevier, 128, pp. 251–258.

Hall, J. S. and Michaels, J. E. (2011) 'Model-based parameter estimation for characterizing wave propagation in a homogeneous medium', *Inverse problems*. IOP Publishing, 27(3), p. 35002.

Hausdorff, J. M. (2007) 'Gait dynamics, fractals and falls: finding meaning in the stride-to-stride fluctuations of human walking', *Human movement science*. Elsevier, 26(4), pp. 555–589.

Lam, M. *et al.* (2016) 'Robust occupant detection through step-induced floor vibration by incorporating structural characteristics', in *Dynamics of Coupled Structures, Volume 4*. Springer, pp. 357–367.

Makino, S. *et al.* (2004) 'Audio source separation based on independent component analysis', in *2004 IEEE International Symposium on Circuits and Systems (IEEE Cat. No. 04CH37512)*, pp. V--V.

Mirshekari, M. *et al.* (2018) 'Occupant localization using footstep-induced structural vibration', *Mechanical Systems and Signal Processing*. Elsevier, 112, pp. 77–97.

Narayana, S. *et al.* (2015) 'PIR sensors: Characterization and novel localization technique', in *Proceedings of the 14th international conference on information processing in sensor networks*. Seattle, Washington, pp. 142–153.

Öberg, T., Karsznia, A. and Öberg, K. (1993) 'Basic gait parameters: reference data for normal subjects, 10-79 years of age', *Journal of rehabilitation research and development*. Citeseer, 30, p. 210.

Pan, S. *et al.* (2015) 'Indoor person identification through footstep induced structural vibration', in *Proceedings of the 16th International Workshop on Mobile Computing Systems and Applications*. Santa Fe, New Mexico, USA, pp. 81–86.

Pan, S., Lyons, K., *et al.* (2016a) 'Multiple pedestrian tracking through ambient structural vibration sensing', in *Proceedings of the 14th ACM Conference on Embedded Network Sensor Systems CD-ROM*, pp. 366–367.

Pan, S., Mirshekari, M., *et al.* (2016b) 'Occupant traffic estimation through structural vibration sensing', in *Sensors and Smart Structures Technologies for Civil, Mechanical, and Aerospace Systems 2016*. Las Vegas, Nevada, USA, p. 980306.

Pavic, A. and Willford, M. R. (2005) 'Appendix G: Vibration serviceability of post-tensioned concrete floors', *Post-tensioned concrete floors design handbook*. Concrete Society Slough, pp. 99–107.

Shi, L. *et al.* (2019) ‘Device-free Multiple People Localization through Floor Vibration’, in *Proceedings of the 1st ACM International Workshop on Device-Free Human Sensing*, pp. 57–61.

Song, B., Choi, H. and Lee, H. S. (2008) ‘Surveillance tracking system using passive infrared motion sensors in wireless sensor network’, in *2008 International Conference on Information Networking*, pp. 1–5.

Wang, W., Chen, J. and Hong, T. (2018) ‘Occupancy prediction through machine learning and data fusion of environmental sensing and Wi-Fi sensing in buildings’, *Automation in Construction*. Elsevier, 94, pp. 233–243.

Willford, M., Field, C. and Young, P. (2006) ‘Improved methodologies for the prediction of footfall-induced vibration’, in *Building Integration Solutions*, pp. 1–15.

Young, P. (2001) ‘Improved floor vibration prediction methodologies’, in *ARUP vibration seminar*.

Parameterized IFC-based Graph Generation for User-oriented Path Search

Barbara Strug, Grażyna Ślusarczyk, Jakub Jas
Jagiellonian University, Poland
barbara.strug@uj.edu.pl

Abstract. This paper deals with the problem of transforming the data obtained from the IFC file of a given building into a weighted graph, which is used for searching shortest routes accessible for different types of users including people and mobile objects. This graph contains information about the topology and accessibility between building spaces. It is created using the parameter specifying the permissible distance from the center of a moving object to a wall. Edge weights are calculated based on the Euclidean distance between nodes representing doors or internal points of rooms with concave shapes. On the basis of information encoded in the graph the application calculates the shortest path between designated rooms and creates its visualization. The presented approach is illustrated on examples of searching shortest routs between spaces of the building extracted from the IFC file belonging to the free IFC model database.

1. Introduction

Nowadays, BIM (Building Information Modelling) technology is intensively developed, i.e. modelling and management of building information throughout its entire life cycle. However, this information is difficult to access for people who are not professionally involved in design. Access to design data contained in the BIM database is possible using the IFC (Industry Foundation Classes) format (buildingSMART, 2013). However, although the IFC is an open standard, its complex nature makes finding useful information difficult. Therefore it is important to create algorithms that allow for an easy access to building elements essential for solving user-defined tasks, to relations between these elements and their attributes (Langenhan et al., 2013; Jin et al., 2018). There is also a lot of research related to shortest path finding problem inside buildings (Lee et al., 2010; Llanos et al., 2014), but most of them do not take into account the preferences of different types of users in respect to their mobility.

This paper introduces a method of transforming the data obtained from the IFC of a given building into a weighted graph, which is used for searching shortest routes accessible for different types of users including people and mobile objects. This graph contains building-related knowledge, like information about the topology of spatial layouts of buildings and characteristics of elements ensuring access between spaces.

The application extracts from the IFC format file objects representing rooms (IfcSpace), doors (IfcDoor) and stairs (IfcStair) along with related geometric data, as well as relationships between these objects using IfcOpenShell tool (IfcOpenShell Academy). In the next step the so called *space of movement* is calculated for each room. The area of each polygon representing a space is decreased by a value of a parameter *distance* specifying the permissible distance from the center of a moving object to a wall. This value is determined on the basis of the profile of persons or mobile objects, which specifies their sizes, preferences and ability to move. The *distance* parameter allows us to create a representation of the area on which a person or an object can move and to adapt searched routes to their capabilities, and therefore becomes a parameter for the created graph of a building.

During a graph creation process also shapes of spaces are taken into account. In case of spaces with shapes described by concave polygons, their vertexes lying inside convex envelopes, called concavity points, are determined (Preparata & Shamos, 1985). Then a weighted graph is created, whose nodes represent points corresponding to doors and concavity points computed for concave polygons (Jas, 2019). Edges are created between nodes representing different doors of a space, if the straight line connecting them does not go beyond the outline of this space, or between nodes representing doors and concavity points. Edge weights are calculated based on the Euclidean distance between nodes. On the basis of the information encoded in the created graph the application calculates the shortest path between specified rooms and creates its visualization. If these rooms are located on different floors, then the path found consists of two fragments: the path from the start room to the stairs on one floor, and the path from the stairs to the destination room on another floor.

The presented research is motivated by the desire to find shortest routes in a building, which would be accessible for different types of users including pedestrians, disabled people with possible restrictions in mobility and various types of mobile objects (i.e., stand-alone vacuum cleaners). Moreover, while searching for the optimal routes it is important to take into account spaces with shapes described by concave polygons, through which sometimes the shortest path can not lead directly (i.e., in a straight line) from one door to the other.

The presented approach is illustrated on examples of searching shortest routs between rooms located on the same floor and different floors. The floor plans of the building are created on the basis of the IFC file belonging to the free IFC model database (Open IFC model repository, 2010).

2. Extraction of IFC Data

The proposed application extracts from the IFC format file, objects representing rooms (IfcSpace), doors (IfcDoor) and stairs (IfcStair) along with related geometric data, as well as relationships between these objects using IfcOpenShell tool (IfcOpenShell Academy). IfcOpenShell has a module enabling using the tool in Python. A method, which obtains all IfcStair elements on a given floor, written in IfcOpenShell-python is shown in the listing in Fig. 1. In Fig. 2 the listing of a method for obtaining all IfcSpace objects on a given floor is presented.

```
def getIFCStairsOnSpecifiedFloor(self, floor_name):
ifc_stairs = []
ifc_building_storeys = self.ifc_file.by_type('IfcBuildingStorey')
for ifc_building_storey in ifc_building_storeys:
if ifc_building_storey.Name == floor_name:
for related_element in ifc_building_storey.ContainsElements[0]
.RelatedElements:
if related_element.is_a('IfcStair'):
ifc_stairs.append(related_element)
return ifc_stairs
```

Figure 1: A method for obtaining all IfcStair elements on a given floor

```
def getIFCSpacesOnSpecifiedFloor(self, floor_name):
ifc_spaces = []
ifc_building_storeys = self.ifc_file.by_type('IfcBuildingStorey')
for ifc_building_storey in ifc_building_storeys:
if ifc_building_storey.Name == floor_name:
for ifc_object_definition in
ifc_building_storey.IsDecomposedBy[0].RelatedObjects:
ifc_spaces.append(ifc_object_definition)
return ifc_spaces
```

Figure 2: A method for obtaining all IfcSpace objects on a given floor

On the basis of the information from the IFC file the floor plans of the building are created. In Fig. 3 a model of the building, the IFC file of which is processed by our application, is shown. The layout of the building first floor is presented in Fig. 4. The spaces of the floor are labelled and the doors between them are denoted by circles.

Figure 3: An example of a building model

Figure 4: The layout of the building first floor

3. Graph Representation of the Extracted Data

In order to create a graph representing building topology and such that an algorithm calculating the shortest path between specified rooms will work efficiently on it, the position of graph nodes should be specified. We decided to calculate the path distance between points determining the position of doors instead of room centers. At first, so called *space of movement* is calculated for each room. The area of each polygon representing a space is decreased by a value of a parameter *distance* specifying the permissible distance from the center of a moving object to a wall (marked with a dotted line in Fig. 5a). This value is determined on the basis of profiles of different types of users, including pedestrians, people with disabilities (incorporating wheelchair users) and mobile objects. These profiles specify sizes, preferences and ability to move of persons and objects. The *distance* parameter allows us to create a representation of the area on which a person or an object can move and to adapt searched routes to their capabilities, and therefore the specified value becomes a parameter for the created graph of a building. During a graph creation process also shapes of spaces are taken into account. In case of spaces with shapes described by concave polygons, their vertexes lying inside convex envelopes, called concavity points, are determined (Preparata & Shamos, 1985) (Fig. 5b).

Then, a weighted graph is created, whose nodes represent points being orthogonal projections of the centers of doors (denoted by red points in Fig. 5a) onto the nearest edges of the spaces of movement (denoted by black points in Fig. 5a), and concavity points computed for concave polygons (Jas, 2019). Edges are created between nodes representing different doors of a space, if the straight line connecting them does not go beyond the outline of this space, or between nodes representing doors and concavity points. Edge weights are calculated based on the Euclidean distance between nodes.

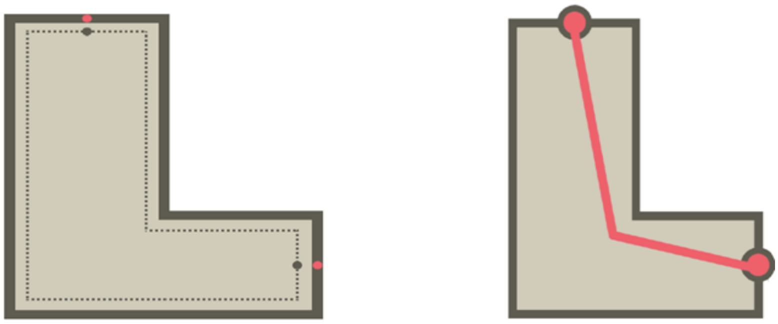

(a) (b)

Figure 5: Example of a concave space in a building (Jas, 2019); a) a space of movement, b) a path going through a concavity point

A graph created according to the algorithm described above and representing topology of the first floor of the building shown in Fig. 4 is presented in Fig. 6. There are 49 nodes, denoted by green circles, where edges are drawn in red. The same graph marked on the first floor plan is shown in Fig. 7.

Figure 6: A graph representing topology of the first floor of the building shown in Fig. 4

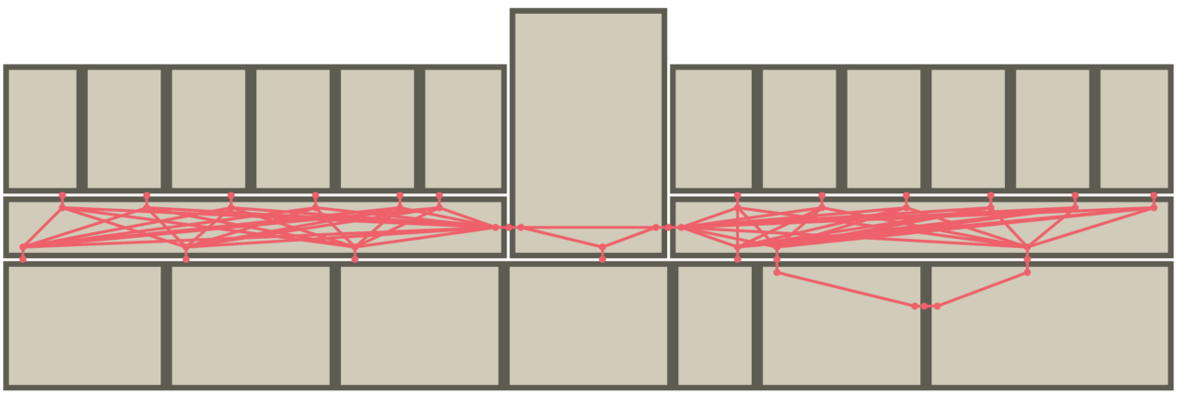

Figure 7: A graph from Fig. 6 marked on the first floor plan

4. Results of Path Finding

The method presented here has been implemented as a modular python application. The two main modules of the application are responsible for importing IFC file and generating a graph based on the obtained data. The third module calculates the shortest path on the derived graph and returns results and produces an image file with the path visualisation. Such a structure of the application makes it easy to change the way the shortest path is calculated as well as adding different graph-based algorithms that could perform other operations on the floor plan graph.

On the basis of information encoded in the created graph the application calculates the shortest path between specified rooms and creates its visualization. The shortest path is determined based on room names, for which thee corresponding doors are determined. If the connected rooms have more than one door, then it is necessary to calculate the shortest path between each pair in the form (door_room1, door_room2). The algorithm selects the pair of doors between which the distance is minimal.

If the selected rooms are located on different floors, then the found path consists of two fragments: the path from the start room to the stairs on one floor, and the path from the stairs to the destination room on another floor. The algorithm searches for the shortest path taking into account all possible staircases.

The shortest path from the west corridor on the building first floor to the office labelled *Buero_IL* on the same floor found by our application is shown in Fig. 8. The first part of the shortest path from the laboratory *K5* in the basement to the office *Buero Obermueller* on the first floor, leading from the laboratory to the stairs is presented in Fig. 9. The second part of this path leading through the first floor is shown in Fig. 10.

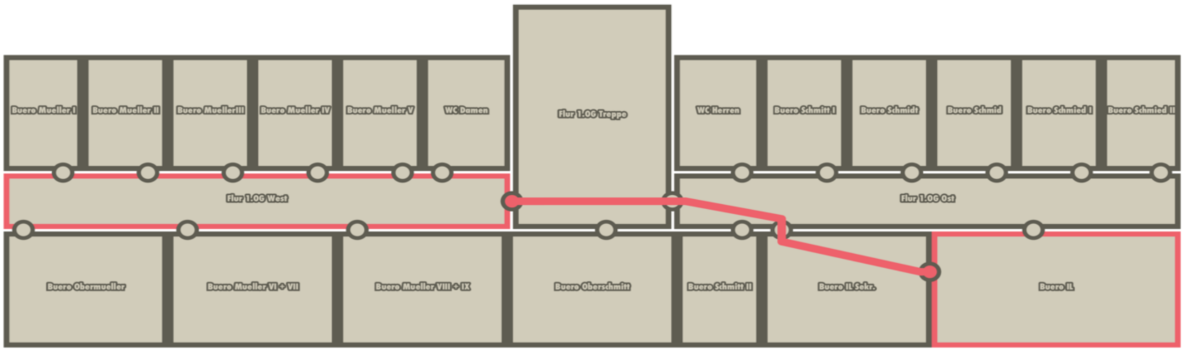

Figure 8: The shortest path between specified rooms on the same floor

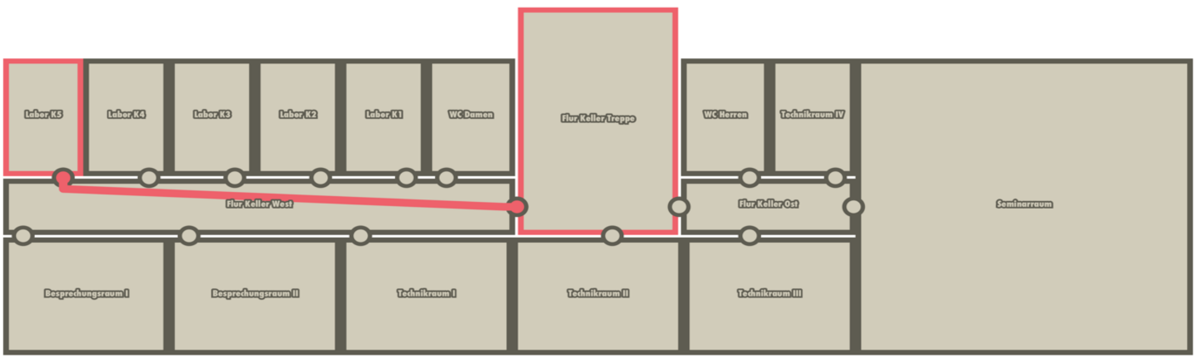

Figure 9: The first part of the shortest path from the laboratory *K5* to the office *Buero_IL*

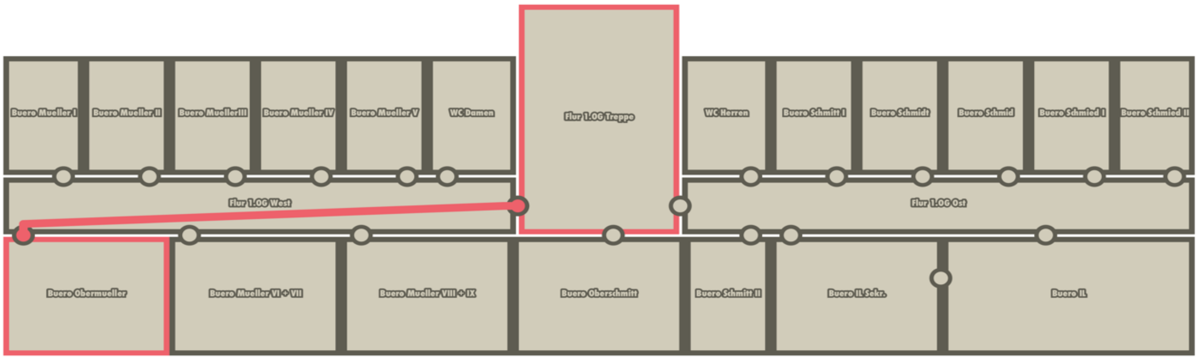

Figure 10: The second part of the shortest path from the laboratory *K5* to the office *Buero_IL*

5. Conclusions

In this paper a method of transforming the data obtained from the IFC file of a given building into a weighted graph, which is used for searching shortest routes accessible for different types of users including people and mobile objects is presented. The created graph contains information about the topology and accessibility between building spaces. It is created using the parameter specifying the permissible distance from the center of a moving object to a wall. This value of this parameter is determined on the basis of the profile of persons or mobile objects, which specifies their sizes, preferences and ability to move. Graph nodes represent points corresponding to doors and internal points of rooms with concave shapes. Edge weights are calculated based on the Euclidean distance between these points. On the basis of information encoded in the graph the application calculates the shortest path between designated rooms and creates its visualization.

In future work, while computing the space of movement for a given person or object, the additional obstacles, such as columns, furniture or unsafe places, which reduce this space, will be taken into account. Also adding other modules to the application, such as finding routes through several locations, is planned.

References

buildingSMART (2013). IFC2x3, http://www.buildingsmart-tech.org/ifc/IFC2x3/TC1/html/index.htm

IfcOpenShell Academy, http://academy.ifcopenshell.org

Jas, J. (2019). IFC-based path planning, Master thesis, Jagiellonian University, (in Polish).

Jin, C., Xu, M., Lin, L., Zhou, X. (2018). Exploring BIM Data by Graph-based Unsupervised Learning, Proceedings of the 7th International Conference on Pattern Recognition Applications and Methods – ICPRAM, 2018.

Langenhan, C., Weber, M., Liwicki, M., Petzold, F., Dengel, A. (2013). Graph-based retrieval of building information models for supporting the early design stages, Advanced Engineering Informatics, 27, pp. 413–426.

Lee, J., Eastman, C.M., Lee, J., Kannala, M., Jeong, Y. (2010). Computing walking distances within building using the universal circulation network, Environment and Planning B: Planning and Design, 37, pp.628–645.

Open IFC model repository (2010). http://openifcmodel.cs.auckland.ac.nz/Model/Details/110

Llanos, D.R., Gonzalez-Escribano, A., Ortega-Arranz, H. (2014). The Shortest-Path Problem: Analysis and Comparison of Methods (Synthesis Lectures on Theoretical Computer Science), Morgan & Claypool.

Preparata, F.P., Shamos, M.I. (1985). Computational Geometry – An Introduction, Springer-Verlag.

Developing a multi-criteria method to evaluate deep renovation options for buildings considering ecological, economic and socio-cultural factors over its lifecycle

Manuel Jungmann[1], Christoph Bindal-Gutsche[2], Timo Hartmann[2]
[1]Department of Industrial Building and Interdisciplinary Planning, TU Wien, Austria
[2]Chair for Systems Engineering, TU Berlin, Germany
manuel.jungmann@tuwien.ac.at

Abstract. The purpose of this paper is to develop a reliable multi-criteria method for the evaluation of deep renovation options. Currently there is a lack of simple to use and precise evaluation tools which consider a diversity of factors. Therefore, a set of ecological, economical as well as socio-cultural key performance indicators (KPIs) are investigated over the building's lifecycle taking the respective project aims due to a customised weighting into account. The different options are compared to the current condition as well as among each other. Additionally, the investment cost-efficiency is investigated. By presenting the results through radar charts the method is a helpful tool for decision-makers to estimate the impacts a priori measures are executed by using the state-of-the-art technology building energy performance simulation (BEPS). The method is applied to three investigation buildings and demonstrates its function.

1. Introduction

The construction sector is responsible for more than one third of the greenhouse gas emissions worldwide and with around 40 % of the European end energy demand buildings are the field with the greatest end energy consumption. The whole building stock within the territory of the European Union (EU) has a floor area of around 25 billion m² (European Commission 2013). Around 94 % of today's building stock in the EU has been built before 2000 (European Commission 2014), when EU-regulations on sustainable construction were non-existent. The first Europe-wide approach with regard to an energy performance of buildings took place in 2002. Thus, the older buildings are characterised by an insufficient insulation and thence by a high energy demand. A 2014 study of Germany's Federal Ministry for Economic Affairs and Energy (BMWi) found that German buildings constructed before 1995 have energy saving potentials of more than 50 % and the figure climbs even higher the older the buildings are. Hence, there are tremendous opportunities for the construction sector in the years ahead as the renovation field provides the second largest not yet used and cost-efficient potential regarding energy savings (Eichhammer et al. 2009). However, in 2016 the renovation rate was low with around 1 to 2 % (European Parliament 2016). Therefore, the EU supports refurbishment activities increasingly as it aspires to become climate-neutral by 2050. As renovation measures are comprehensive construction works entailing long-lasting effects on various criteria the whole lifecycle has to be considered and therefore a suitable evaluation method is expedient in order to find the right renovation option for each project.

This research seeks to develop a multi-criteria method which provides a holistic overview of the impacts and delivers realistic results by using a building energy model. The detailed results delivered through the multi-criteria approach make it possible to evaluate and compare the impacts of renovation options considering ecological, economic and social-cultural key performance indicators (KPIs). This paper firstly defines the necessary terms embedded within the academic state-of-the-art. Subsequently, the method is explained and several KPIs are set up. In the following the tool is applied on three buildings. Some retrofitting measures of an EU project are conducted by using input data files (IDFs) in EnergyPlus and comparing the as-is building status with the different modification measures. Finally, the results are presented. As a concluding element the method is discussed, taking into account the results of the research.

2. Theoretical Framework

Buildings have a durable lifecycle of roughly 50 up to 100 years. In contrast, it has been discovered that the building envelope ages after 20 to 30 years already (Chandler 1992). However, studies have shown that the negative environmental impacts are lower if the life period of existing buildings is expanded (Thomsen and van der Flier 2008). Moreover, it is proven that renovation options lead to economic (Balaban and Puppim de Oliveira 2017) and socio-cultural (Broderick et al. 2017) benefits as well. Scholars have indicated that a systematic approach is currently not performed, although a holistic review of the impacts of renovation measures is much more useful as this implies even higher savings regarding a variety of criteria (D'Agostino et al. 2017). Due to the comprehensive impacts of renovation measures evaluation methods facilitate the decision-making process for stakeholders immensely.

Overall the interaction of components within buildings and the fulfilment of renovation measures are highly complex engineering systems operating under many uncertainties, such as climate change, user behaviour and technical developments (Ma et al. 2012). Without a suitable evaluation method, it is not possible to precast the exact extents in advance so that it is difficile to find the appropriate renovation option for each project (Jones et al. 2013). Another missing feature is the cost-efficiency as stated by Ma et al. (2012). Hence, there is a clear demand for a reliable method that takes ecological, economic, social as well as technical aspects into account (D'Oca et al. 2018). Therefore, the research issue arises on how the impacts of different deep renovation options can be evaluated over a building's lifecycle. The following chapter develops a new method that mitigates the described shortcomings of the latest research. The results of the evaluation incorporate a multitude of KPIs, the efficiency of each option is investigated and the tool is easily feasible by using the state-of-the-art technology BEPS.

During the 1990s an assessment of buildings with regard to sustainable aspects began (Politi and Antonini 2017). A critical review of 16 different present building environmental evaluation tools has been conducted. Only five tools have been considered suitable for renovation measures. Among them were the famous certification programmes Leadership in Energy and Environmental Design (LEED) as well as the Building Research Establishment Environmental Assessment Methodology (BREEAM) (Haapio and Viitaniemi 2008). These are comprehensive complex tools, which have the disadvantages that they are time-consuming and costly especially for smaller projects (Politi and Antonini 2017). Apart from those measures, current research lacks in techniques for simpler and especially holistic tools. There are approaches but the focus is usually on ecological effects (Jensen and Maslesa 2015). Yet, a restricted variety of criteria limits the scope of impacts that are to be investigated. In different data-driven approaches disturbances arose, which are not predictable (Wong et al. 2010, Mejri et al. 2011). But obviously the reliability of precise estimations is substantial for a decision support tool. Hence, nowadays it is standard practice to use simulation programs and conduct BEPS upfront in order to assess the performance of buildings. These models are so called white box models as the systems are described by equations while each parameter has a physical meaning (Henze and Neumann 2011). Thus, white box models are the most realistic design possibility (Martin Tarr). Nevertheless, one has to note that models in general display a simplification of a real building and performance gaps occur (Augenbroe 2011). Nowadays there are several simulation programmes for the modelling like the widespread EnergyPlus engine, which is continuously enhanced (Zhu 2013).

3. Method

3.1 Illustration of the Method

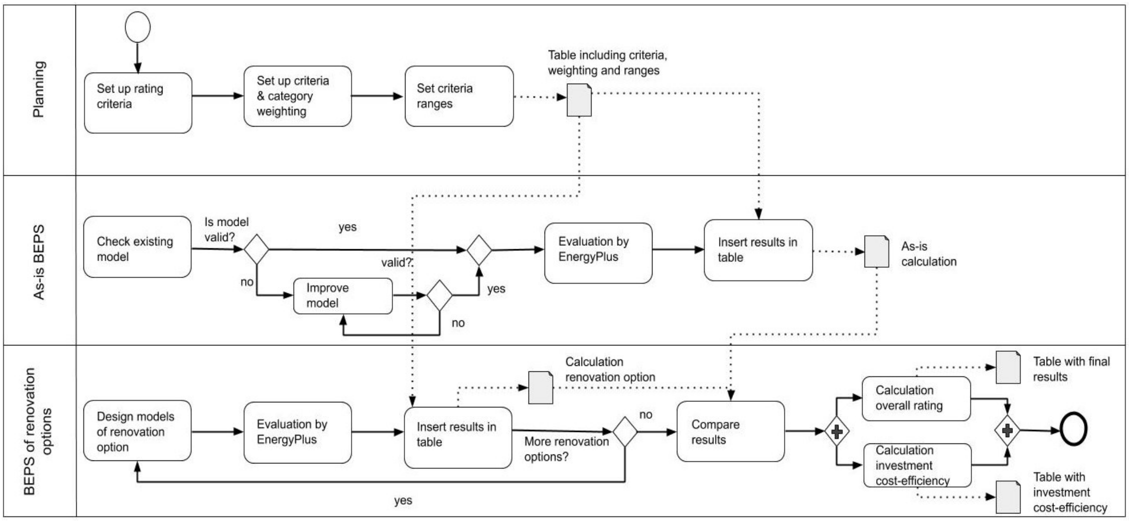

Figure 1: BPM

The developed method can be retraced in the Business Process Model (BPM) Figure 1. To successfully compare impacts, it is necessary to define various KPIs. For this study seven KPIs were developed. These seven criteria can be grouped into three categories. The ecological category consists of the KPIs primary energy, end energy as well as emitted global warming potential (GWP). The demanded energy is computed by EnergyPlus and the GWP is calculated as the respective CO2 equivalent factors were researched and multiplied with the related used primary energy source. The economic category includes the net present value over a certain lifecycle, in this study 40 years, and is calculated by equation 1 considering current factors:

$$NPV = IV + EC * \frac{1}{s} * (d^n - 1)/(d^n * (d - 1)) \tag{1}$$

NPV = Net Present Value	IV = Investment costs	EC = Energy costs
s = Price increase in % + 1	d = q/s	n = Lifecycle in years
q = Discounting rate in % + 1		

Moreover, the investment costs and the energy costs in the first year, the multiplication of the end energy demand with a current energy price for the respective country, are considered. The social-cultural category compromises the time not comfortable, which is based on Simple ASHRAE 55-2004 and calculated by EnergyPlus. The categories as well as the KPIs can be weighted so that every option receives an overall rating. Therefore, it is necessary to determine a weighting according to the agreed aims of the project, although it is not possible to create an ultimate weighting for all stakeholders. The summed up percentage of the categories is 100 % as well as the summed up percentage of the KPIs of each category. For the application on this study an example weighting is proposed (Table 1). For the most precise results, it is necessary to create an IDF that appreciates a building's current condition. If an IDF of the as-is condition is available, like for this study, it has to be tested for validity and reworked if it is not running reasonably. The valid IDF is subsequently evaluated by EnergyPlus with the respective International Weather for Energy Calculations (IWEC) files for the appropriate location of the building for one typical year. The results of EnergyPlus are inserted into a table in which the remaining KPIs are calculated automatically by the mentioned methods. Afterwards, for every possible modification option IDFs are designed and the impacts of the measures with regard to the KPIs are compared to the current status in absolute numbers as well as in percentages. In the end, an overall rating is calculated for each renovation option (Equation 2).

Table 1: Proposed weighting for categories and KPIs

Category	Ecological ①		Economic ⑧		Social-cultural ⑮		
	50 %		40 %		10 %		∑ 100 %
KPI	Primary energy ②	40 %	Net present value ⑨	60 %	Time not comfortable ⑯	100 %	
	End energy ④	20 %	Investment costs ⑪	30 %	-	-	
	GWP ⑥	40 %	Energy costs ⑬	10 %	-	-	
		∑ 100 %		∑ 100 %		∑ 100 %	

$$
\begin{aligned}
Rating = \Big(\Big(&Ecological\ category\ factor\ \textcircled{1} \\
&* \big(KPI\ factor\ \textcircled{2} * End\ energy\ improvement\ (\%)\ \textcircled{3} + KPI\ factor\ \textcircled{4} \\
&* Primary\ energy\ improvement\ (\%)\ \textcircled{5} + KPI\ factor\ \textcircled{6} \\
&* GWP\ improvement\ (\%)\ \textcircled{7}\big)\Big) \\
&+ \Big(Economical\ category\ factor\ \textcircled{8} \\
&* \big(KPI\ factor\ \textcircled{9} * Net\ present\ valueimprovement\ (\%)\ \textcircled{10} + KPI\ factor\ \textcircled{11} \\
&* Investment\ costs\ (\%)\ \textcircled{12} + KPI\ factor\ \textcircled{13} \\
&* Energy\ costs\ improvement\ (\%)\ \textcircled{14}\big)\Big) + (Socio - cultural\ category\ factor\ \textcircled{15} \\
&* \big(KPI\ factor\ \textcircled{16} * \ Time\ not\ comfortable\ improvment (\%)\ \textcircled{17})\big)\Big)
\end{aligned}
\tag{2}
$$

Each category factor is multiplied with the corresponding KPI factor and the percentage improvement in comparison to the as-is condition and the product values are summed-up. There is one exception as the investment costs of the most expensive option are the comparative amount. Finally, the summed up value is multiplied by 100 so that the results range between 0 and 100. Another noteworthy benefit of the method is that it is easily extendable as it can be tailored to the demands of any given decision-maker by adapting the equation accordingly. In addition, the method allows for taking the cost-efficiency into account. Therefore, the cost-efficiency is presented by relating the investment costs for every option to the absolute improvement of the remaining KPIs of each possibility. A further useful option of the method is to set ranges with minimum and maximum thresholds with regard to the KPIs, if required. All options that do not meet the requirements, are marked red. If certain goals need to be reached indispensably or specific constraints exist, this depiction is especially useful.

3.2 Investigation Buildings

The investigation buildings are three nursery schools that were constructed during different time periods and can be seen as representative for the European building stock in various climatic locations. The investigation case I in Genoa, Italy, is located on the second floor of a two storey building (Figure 2). The building was constructed in the 1930s and is in a poor condition. The windows are old single glazing ones with a U value of 5.906 W/(m²K) and a solar heat gain coefficient (SHGC) of 0.861. The U value of the different types of external walls is altering between 1.092 W/(m²K) and 3.072 W/(m²K). It is heated by a gas heating system.

The second case in Gdansk, Poland, was built in 1965 (Figure 3). According to EnergyPlus, the building is conditioned by district heating designed by an Ideal Loads Air System, a perfect, not realistic system. The different external walls have a U value of 2.389 W/(m²K) or 2.846 W/(m²K) and the windows U value is 5.0 W/(m²K) with a SHGC of 0.8. The third case is located in Warsaw, Poland, and consists of two storeys and a basement (Figure 4). The building was constructed in 1983. Again an Ideal Loads Air System was designed. The various above ground external walls are characterised by a U value of 2.221 W/(m²K) as well as 2.402 W/(m²K). The windows have a U value of 2.4 W/(m²K) and a SHGC of 0.6.

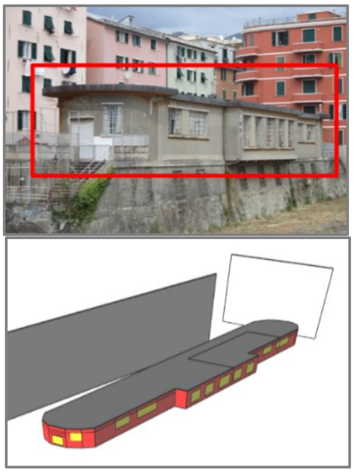

Figure 2: Case I Genoa

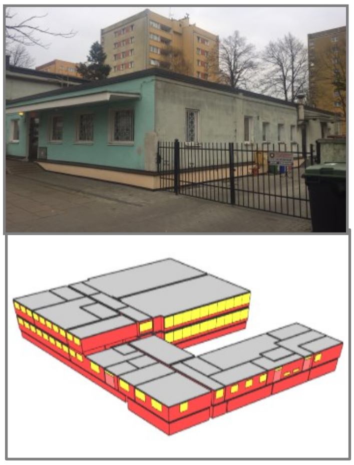

Figure 3: Case II Gdansk

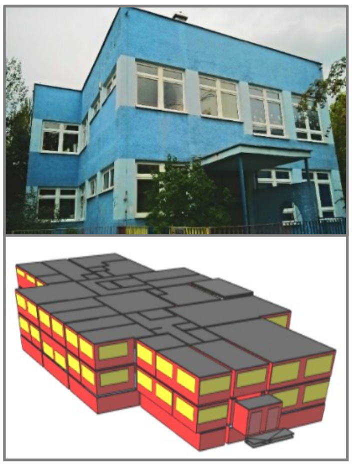

Figure 4: Case III Warsaw

3.3 Deep Renovation Measures

Within this study two different re-insulation options are investigated. The panel 1 (=P1) with a U value of 0.13 W/(m²K) that cost around 115 €/m². The alternative is the panel 2 (=P2) with a U value of 0.32 W/(m²K) and costs of 150 €/m². Additionally, two different smart windows with a low emissivity coating are tested. The glazing can be rotated by 180° in order to position the coating on the inside or the outside to minimise or maximise the solar heat gain. Namely a triple glazing window, with a U value of 1.0 W/(m²K) and a SHGC of 0.24 in summer mode and 0.44 in winter mode is examined and a double glazing, which has a U value of 1.3 W/(m²K) and a SHGC of 0.45 or 0.51 depending on the mode. 10 % higher costs incur for the triple glazing windows. For the heating system in Genoa an improvement of the efficiency from 80 % to 92 % was proposed. Costs of 8,000 € were provided for this measure. As the IDFs from Poland use an unrealistic system the change of the heating system was not investigated. Overall, there are 17 possible retrofitting options for the building in Genoa and eight for the Polish cases.

3.4 Modelling

For each renovation option a separate IDF was designed. This means that for the facade improvement within EnergyPlus the extra cladding was added in front of the existing external wall. Regarding the smart windows, it was necessary to find the optimal point in time to switch the window modes. Therefore, the monthly change was tested for each option and the case with the lowest energy demand was chosen for further investigation. As the improvement of the heating system does not change anything of a building's insulation the same months can be assumed as for the cases without an enhanced heating system.

4. Results

In the following analysis only the five best rated options are compared in more detail in order to maintain clarity. Due to low extents regarding the KPI time not comfortable, its cost-efficiency is not investigated.

4.1 Case I Genoa

The best ranked possibilities for the Genoa case are options 6, 7, 14, 15 as well as 16 according to the proposed weighting. Figure 5 presents the results of the different options in a radar chart.

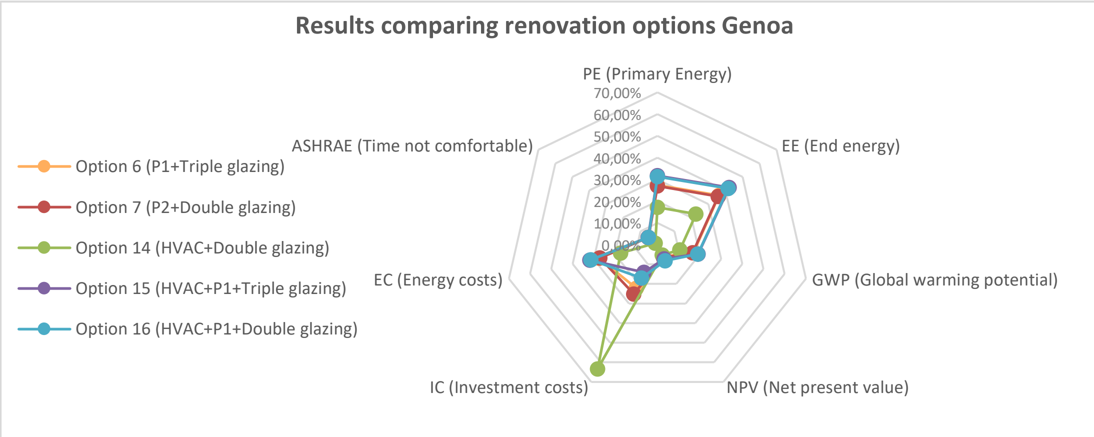

Figure 5: Radar chart results Genoa

According to EnergyPlus there is a current end energy demand of around 44,753 kWh and a primary energy demand of 66,648 kWh per year. Therefore, 24.5 tons of GWP are emitted. Option 15 shows the highest improvements with savings of 42 % end energy as the heating demand can be halved. As electricity has a higher multiplier in comparison to gas with regard to the primary energy and the GWP the end energy savings have the highest percentage change of the ecological category. 32 % less primary energy is necessary and 19 % less GWP are emitted every year. This means that over the whole lifecycle around 844,100 kWh primary energy and around 189 tons GWP can be saved. The usage of the summer mode from May or June until August is the optimal time period and it is detectable that for the double glazing windows a month more usage time is beneficial due to higher solar heat gains. Option 14 shows the lowest extents as the facade is not changed.

The lowest net present value results for option 16 with 329,117 €, an improvement of 9 % over the lifecycle of 40 years. Option 15 has a similar net present value, but the highest investment costs with 85,015 € and the lowest energy costs, 32 % less than in the as-is condition. On the contrary, option 14 has by far the lowest investment costs with 36,600 € as no new facade is installed. Option 6 has the weakest net present value improvement with 6 % due to high investment costs. Certainly the expenses of options 15 and 16 are slightly higher, however, the heating system leads to significant energy and thus also financial savings.

Due to insufficiently indicated set points the current time not comfortable by ASHRAE is high with 1,506 hours per year. For the heating set point, a schedule with a lower temperature limit of -20 degrees and an upper limit of 100 degrees was chosen, and 30 degrees for the cooling set point. Options 6 and 15 may lead to an annual improvement of 83 hours, i.e. 5.5 %. Options 7 and 16 show similar results, while option 14 lies far behind as the facade stays the same. The results show that the combination of a facade and the replacement of the windows are beneficial.

Table 2: Investment-cost efficiency Genoa

Option	Improvement PE/IC (kWh/€)	Improvement EE/IC (kWh/€)	Improvement GWP/IC (kg/€)	Improvement NPV/IC(€/€)
6	0.24	0.21	0.05	0.28
7	0.24	0.22	0.05	0.31
14	0.32	0.28	0.07	0.71
15	0.25	0.22	0.06	0.35
16	0.25	0.23	0.06	0.38

The most efficient possibility is option 14 (Table 2). For each Euro spent 0.32 kWh primary energy, 0.28 kWh end energy as well as 0.07 kg GWP are saved annually and monetary savings of the factor 0.71 are detectable over the whole lifecycle. A low efficiency regarding the GWP can be recognised for all options. The remaining options show similar result regarding all KPIs.

4.2 Case II: Gdansk

For the investigation case in Gdansk a threshold of 150,000 € investment costs was provided. Therefore, option 8 is not investigated further as it is outside the desired range. Hence, by using the chosen weighting the options with the highest rating are 2, 3, 6, 7 as well as 9 (Figure 6).

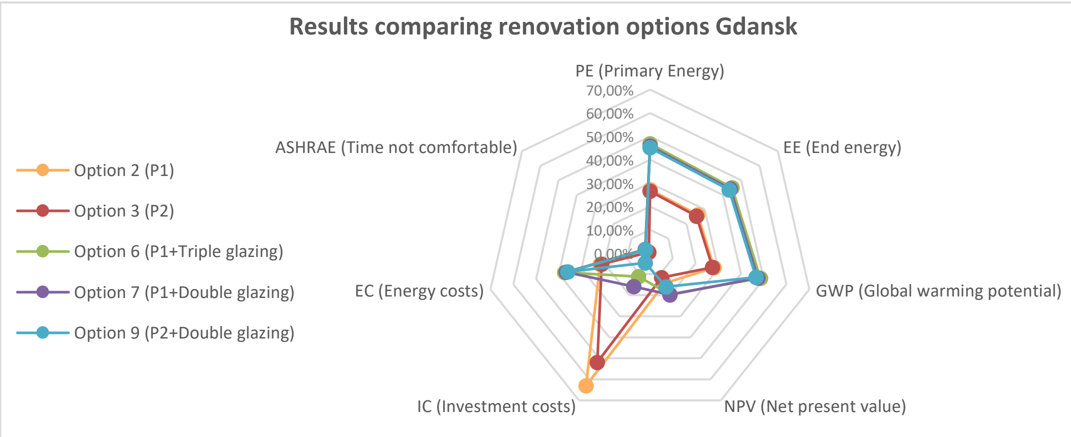

Figure 6: Radar chart results Gdansk

The existing building model of Gdansk uses 140,206 kWh end energy per year, which means around 487,632 kWh primary energy are necessary to provide this amount. About 377 tons of GWP will be emitted yearly. The options 6, 7 and 9 are leading to similar improvements in terms of ecological factors. Around 46 % primary energy, 45 % end energy and more than 47 % GWP can be saved in comparison to the current condition. The optimal usage time of the smart windows is during July and August. By option 6 improvements of 7,320 tons of GWP savings are possible as around 9,127 MWh less primary energy is used over the whole lifecycle. The reasons are the cold weather and the poor insulation. Especially the walls are not in a good condition. Therefore, option 2 and option 3 are leading to significant improvements of below 30 % regarding all ecological KPIs.

The investment costs are quite high for all measures but nevertheless all options are leading to an improvement of the net present value. Option 7 leads to the best improvements of almost 20 % in comparison to the pre renovation condition. The highest investment costs arise for option 9 with 145,800 € and therefore the net present value is slightly lower. Option 2 has the lowest investment costs with around almost one third of the most expensive one.

The time not comfortable according to ASHRAE is high with 1,749.75 hours per year. The reasons for this are the doubtful set points and the moderate insulation. The cooling set point is lying at around -60 degrees, while for the heating set point a lower limit of -60 degrees and an upper limit of 200 degrees are provided. All measures are improving the time not comfortable slightly. The range goes from 11.25 hours for option 3 up to 46.25 hours for option 6. The better insulation of the P1 and of the triple glazing can be recognized compared to their counterparts.

Due to a high primary energy multiplier of the district heating the primary energy shows the highest efficiency (Table 3). It is noticeable that option 2 is the most efficient measure in ratio to the investment costs. For every euro spent, 2.35 kWh primary and 0.65 kWh end energy are saved annually. Furthermore, 1.88 kg less GWP are produced and the net present value is reduced by the factor of 1.94. The efficiency of the remaining options is rather similar.

Table 3: Investment-cost efficiency Gdansk

Option	Improvement PE/IC (kWh/€)	Improvement EE/IC (kWh/€)	Improvement GWP/IC (kg/€)	Improvement NPV/IC(€/€)
2	2.35	0.65	1.88	1.94
3	1.76	0.49	1.40	1.20
6	1.68	0.46	1.34	1.10
7	1.74	0.48	1.39	1.17
9	1.51	0.42	1.21	0.84

4.3 Case III: Warsaw

The options 2, 3, 6, 7 as well as 8 are the possibilities with the highest rating (Figure 7).

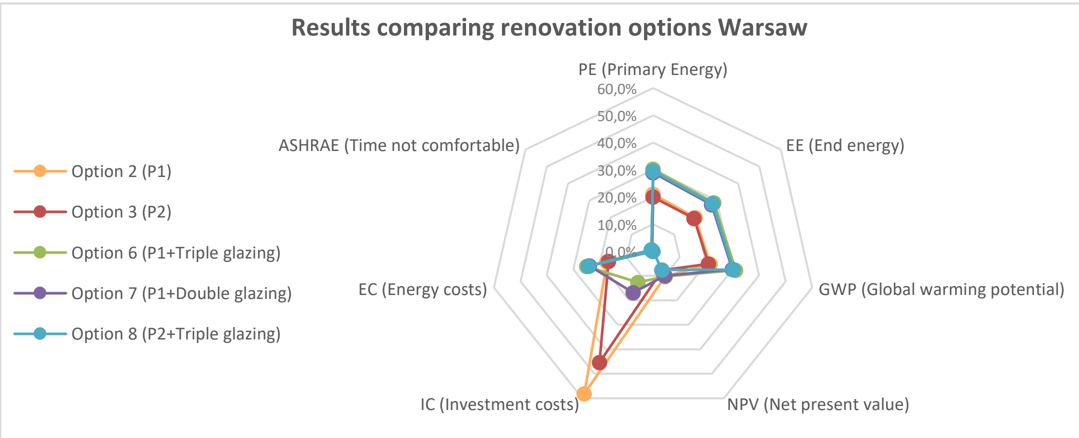

Figure 7: Radar chart results Warsaw

In the as-is condition the demonstration building in Warsaw has an end energy consumption of 229,395 kWh and a primary energy demand of 786,744 kWh by which 610 tons of GWP are emitted annually. The combination of measures within the options 6, 7 and 8 lead to similar results with savings of 30 % primary energy, 28 % end energy as well as a reduction of the GWP of around 31 %. This assumes the usage of the winter mode during the whole year. The reasons for the moderate savings are the Ideal Loads Air system and the good condition of the windows. The heating demand can be reduced by one third. The maximum reduction can be achieved by option 6 with savings of around 9,499 MWh primary energy and 7,608 tons of GWP over the lifecycle. Since the walls are in poorly condition, upgrading the outer wall is much more efficient in comparison to the windows. Therefore, a 20 % reduction with regard to the ecological criteria can be achieved by both singular options.

The net present value over 40 years can be decreased by around 10 % using options 2, 6 and 7. The remaining two options result in savings below 8 %. The combination of measures, options 6, 7 and 8 results in the lowest energy costs of around 25 % less than in the current condition. The investment costs are high with a maximum of almost 200,000 € for option 8. With almost 60 % less than the most expensive possible renovation option, option 2 is significantly cheaper.

The time not comfortable with an amount of 1,745.25 hours per year is high because the same set points as in the Gdansk model were used. The improvements are also minor. The highest reduction of 14 hours can be achieved by option 6. The different combinations of measures are in a similar range while the singular options achieving only the half improvements of it. Regarding the efficiency option 2 performs best by far as it has the lowest investment costs (Table 4). For each euro spent, 1.98 kWh primary energy and 0.55 kWh end energy are saved annually. Furthermore, this measure leads to savings of 1.58 kg GWP each year and 1.47 € for every euro over the lifecycle. Options 3, 6, and 7 are in a similar range. Option 8 has the lowest efficiency as significant investment costs are needed

Table 4: Investment-cost efficiency Warsaw

Option	Improvement PE/IC (kWh/€)	Improvement EE/IC (kWh/€)	Improvement GWP/IC (kg/€)	Improvement NPV/IC(€/€)
2	1.98	0.55	1.58	1.47
3	1.44	0.41	1.17	0.84
6	1.36	0.38	1.09	0.71
7	1.37	0.38	1.10	0.72
8	1.16	0.32	0.93	0.45

5. Discussion

The method was applied to three demonstration buildings in different climatic locations considering several deep renovation options. With the help of BEPS, extensive outcomes are generated with regard to several KPIs considering the whole lifecycle. Some approaches of the method were used in previous research, where an in-depth theoretical foundation has been formulated, but reproducibility in different settings strengthen the credibility of these. Due to the developed method it is possible to test and compare a magnitude of options while using the BPM as a guideline. Furthermore, the method allows adaptations as the weighting is configurable and further KPIs can be added. In general, the method depicts the advantages and disadvantages of different measures and options. Thus, the method helps to find the building's biggest weakness as the improved facades perform significantly better in the Polish models. Regarding the windows, the method reveals that smart windows of this kind are not useful in cold climatic conditions. Hence, the method detects limitations of smart windows as the expenses for such kind of glazing could be saved by using improved conventional windows for lower costs. It is shown that double glazing can be more cost-efficient than the triple glazing, although the triple glazing leads to higher ecological savings. The finding that the option with the highest energy savings is not the most efficient and economic one is consistent with the latest research (Ferreira et al. 2016). Moreover, the combination of insulation measures increases the thermal comfort significantly more than individual action. This accentuates the need for a holistic consideration further more in order to understand a building as a whole system due to its complex connections rather than individual approaches.

To conclude, the multi-criteria method has proven to be a helpful tool for stakeholders seeking to determine the best possible renovation strategy for their respective purposes. The validation of the results did not take place as the construction works are not executed yet. This is a limitation but it offers possibilities for prospective studies to investigate the performance gap. Additionally, future research regarding a sensitive analysis of the KPIs and the weighting can be done as these are complex issues during the decision-making process. Furthermore, the consideration of a dynamic LCA with time-dependent indicators in-depth is expediently for the future in order to receive more precise results, but one has to take into account the fact that the results are estimations and the real performance will take place somewhere in the range of these forecasts. Yet, determining the exact energy performance and consumption levels a priori renovation measures are applied, will still remain elusive.

Acknowledgements

The P2ENDURE project is funded under the EU programme H2020-EE-2016-PPP (supporting accelerated and cost-effective deep renovation of buildings through public private partnership (EEB PPP) under grant agreement number 723391. The information in this publication does not necessarily represent the view of the European commission.

References

European Commission (2014). EU project largest study of European building stock. https://cordis.europa.eu/news/rcn/36619/en, accessed April 2019.

Bundesministerium für Wirtschaft und Energie (BMWi) (2014). Endenergiebedarf für Wärme, Sanierungsbedarf im Gebäudebestand, pp. 11–12.

Eichhammer, W., Fleiter, T., Schlomann, B., Faberi, S., Fioretto, M. Piccioni, N., Lechtenböhmer, S., Schüring, A. and Resch, G. (2009). Study on the Energy Savings Potentials in EU Member States, Candidate Countries and EEA Countries Final Report. http://publica.fraunhofer.de/documents/N-167983.html

European Parliament (2016). Executive Summary, Boosting Building Renovation: What Potential and Value for Europe?, pp. 11–13.

Chandler, I. (1992). Repair and renovation of modern buildings. New York: McGraw-Hill.

Thomsen, A. F. and van der Flier, C. L. (2008). Replacement or reuse? The choice between demolition and life cycle extension from a sustainable viewpoint, Shrinking Cities, Sprawling Suburbs, Changing Countrysides, pp.1–13. http://resolver.tudelft.nl/uuid:a670a506-74e6-4c4e-b7b6-71107fb9778d

Balaban, O. and Puppim de Oliveira, J. A. (2017). Sustainable buildings for healthier cities: assessing the co-benefits of green buildings in Japan, Journal of Cleaner Production 162, pp. 68–78. https://doi.org/10.1016/j.jclepro.2016.01.086

Broderick, Á., Byrne, M., Armstrong, S., Sheahan, J. and Coggins, A. M. (2017). A pre and post evaluation of indoor air quality, ventilation, and thermal comfort in retrofitted co-operative social housing, Building and Environment 122, pp. 126–133. https://doi.org/10.1016/j.buildenv.2017.05.020

D'Agostino, D., Zangheri, P. and Castellazzi, L. (2017). Towards nearly zero energy buildings in Europe: A focus on retrofit in non-residential buildings, Energies 10, 117. https://doi.org/10.3390/en10010117

Politi, S. and Antonini, E. (2017). An expeditious method for comparing sustainable rating systems for residential buildings, Energy Procedia 111, pp. 41–50. https://doi.org/10.1016/j.eiar.2008.01.002

Haapio, A. and Viitaniemi, P. (2008). A critical review of building environmental assessment tools, Environmental Impact Assessment, Review 28, pp. 469–482.

Jensen, P. A. and Maslesa, E. (2015). Value based building renovation – A tool for decision-making and evaluation, Building and Environment 92, pp. 1–9. https://doi.org/10.1016/j.buildenv.2015.04.008

D'Oca, S., Ferrante, A., Ferrer, C., Pernetti, R., Gralka, A., Sebastian, R. and op't Veld, P. (2018). Technical, Financial, and Social Barriers and Challenges in Deep Building Renovation: Integration of Lessons Learned from the H2020 Cluster Projects, Buildings 8, 174. https://doi.org/10.3390/buildings8120174

Wong, S. L., Wan, K. K. W. and Lam, T. N. T. (2010). Artificial neural networks for energy analysis of office building with daylighting, Applied Energy 87 (2), pp. 551–557. https://doi.org/10.1016/j.apenergy.2009.06.028

Mejri, O., Del Barrio, E. P. and N. Ghrab- Morcos, N. (2011). Energy performance assessment of occupied buildings using model identification techniques, Energy and Buildings 43, pp. 285–299. https://doi.org/10.1016/j.enbuild.2010.09.010

Henze, G. P. and Neumann, C. (2011). Building simulation in building automation systems. In: J. L. M. Hensen, R. Lamberts (Eds.). Building Performance Simulation For Design And Operation, Abingdon: Spon Press, pp.402–441.

Martin Tarr. IDC. Modelling-Choosing a model. http://www.idc-online.com/technical_references/pdfs/electronic_engineering/Modelling_Choosing_a_Model.pdf, accessed June 2019.

Augenbroe, G. (2011). The role of simulation in performance based building. In: J. L. M. Hensen, R. Lamberts (Eds.). Building Performance Simulation For Design And Operation, Abingdon: Spon Press, pp. 15–36.

Zhu, D., Hong, T., Yan, D. et al. (2013). A detailed loads comparison of three building energy modelling programs: EnergyPlus, DeST and DOE-2.1E, Building Simulation 6 (3), pp. 323–335. 10.1007/s12273-013-0126-7

Ma, Z., Cooper, P., Daly, D. and Ledo, L. (2012). Existing Building Retrofits: Methodology and State-of-the-Art, Energy and Buildings 55, pp. 889–902. https://doi.org/10.1016/j.enbuild.2012.08.018

Jones, P., Lannon, S., and Patterson, J. (2013). Retrofitting existing housing: how far, how much?, Building Research & Information 41(5), pp. 532–550. https://doi.org/10.1080/09613218.2013.807064

Ferreira, M. Almeida, M. and Rodrigues, A. (2016). Cost-optimal energy efficiency levels are the first step in achieving cost effective renovation in residential buildings with a nearly-zero energy target, Energy and Buildings 133, pp. 724–737. https://doi.org/10.1016/j.enbuild.2016.10.017

BIM-based life cycle assessment framework for infrastructure design

Maarten Albert van Eldik, João Santos, Faridaddin Vahdatikhaki, Maarten Visser, Andre Dorée
University of Twente, The Netherlands
f.vahdatikhaki@utwente.nl

Abstract. This paper presents the development of a framework for performing real-time BIM-based life cycles assessment (LCA) analysis during the design process. The framework allows designers to perform an automated LCA analysis at any moment of the design stage and immediately assess the Environmental Impact Score (EIS) of their design choices. A prototype is developed and tested on a case study to indicate the feasibility of the proposed framework. The framework is assessed in terms of functionality, ease of use, scalability and contribution to raising sustainability consciousness through a workshop with experts. It is shown that the framework is able to quickly provide designers with accurate information about the potential environmental impact of all objects in infrastructure design projects. The workshop with experts showed that the tool clearly makes it easier to perform the EIS calculations compared to the existing, highly fragmented, process. This allows the design team to use this assessment on the same level as other design parameters in the decision-making process.

1. Introduction

The Architecture, Engineering, and Construction (AEC) industry is responsible for 40% of the total energy use, 32% of CO_2 emissions, and 25% of the generated waste in Europe annually (Carvalho et al., 2019). Given its high negative impact on the environment and the growing awareness on environmental protection, it is of upmost importance for the construction industry to adopt state-of-the-art methodologies and technologies that enable it to become more sustainable in their practices (Abidin, 2010).

The environmental performance of infrastructure designs is often done through the Life cycle Assessment (LCA) methodology. The LCA, as described in the standards ISO 14040 and ISO 14044, evaluates the potential environmental impact of a product, process or system throughout its complete lifecycle (ISO, 2006a; ISO, 2006b). However, this analysis is time-consuming, complex and requires a large amount of data (Bribián et al., 2009). Therefore, the LCA analysis is often performed at the end of the design phase when all required information is available. This means that design choices with the highest potential environmental impacts are already taken and therefore, it is too late to incorporate the environmental impact results in the decision-making process (Basbagill et al., 2013; Bueno et al., 2018; Bueno and Fabricio, 2018). This fragmented process creates a disconnection between the assessment of the environmental impact and other aspects of design evaluation which renders the improvement from the environmental sustainability perspective cumbersome and challenging. Also, the current workflow necessitates a feedback loop between sustainability experts and other members of the design team. This is not favorable to raise the global sustainability consciousness in the entire design team, especially among the designers.

In recent years, Building information modelling (BIM) has emerged as a potential solution to decrease the effort needed to perform a LCA analysis (Hollberg et al., 2020). There have been numerous studies on BIM-based LCA applications (Soust-Verdaguer et al., 2020; Hollberg et al., 2020; Cavalliere et al., 2019; Doan et al., 2017; Bryde et al., 2013). However, despite the existing interest for BIM-based LCA in infrastructure design, there is still a clear gap in the use of BIM for an integrated LCA analysis in the current design process of infrastructure. For instance, the LCA analysis is often conducted at the end of the infrastructure design phase due to the large information requirements and the need for an LCA expert. This means that it is difficult to use the results in the decision-making process because decisions with the highest potential environmental impact are made early in the design. Also, studies towards BIM-based LCA applications showed that interoperability between BIM- and LCA-software remains an issue. While there are export standards like Industry Foundation Classes (IFC), there is still a chance of errors because of the numerous manual steps and the need for a sustainability expert. Due to these reasons, several studies described the need for a simplified and integrated approach where the BIM environment is used as the basis for LCA calculations and visualizations, without the need for additional experts and numerous manual steps (Santos et al., 2020; Sust-Verdaguer et al., 2017, 2016). This approach allows the potential environmental impact to be calculated in every phase of the design and therefore included in the decision-making process of designers. Finally, there have been numerous studies that investigated the use of BIM for the integration of LCA in building design, which resulted in the development of frameworks and BIM-based LCA applications. However, studies on BIM-based LCA for infrastructure are scarce.

The research work presented in this paper aims to address the gaps identified above by proposing a framework for integrating the LCA analysis in the BIM-based design of infrastructure projects.

2. A framework for BIM-based Life Cycle Assessment (LCA) analysis

The proposed framework intends to automate and integrate the LCA analysis in the BIM environment. As illustrated by Figure 1, it consists of four main steps: (1) Data Collection, (2) Data Integration, (3) LCA analysis and, (4) Visualization. Shortly, the required information for the Life Cycle Inventory (LCI) stage of the LCA is firstly gathered from the BIM model. Next, the data is structured in a systematic way that allows bidirectional data exchange between the LCA database and BIM. Then, the potential environmental impact of each element in the project is assessed by finding the corresponding characterization factors values in the LCA database and proportioning it based on the quantities of different materials used in each element. Finally, the relative score for the potential environmental impact of each element is calculated and visualized in the BIM model using a heat map scheme.

2.1 Data Collection

In this step the required data to perform the BIM-based LCA analysis is collected. First, a comprehensive quantity take-off is carried out to identify different materials used in different elements of the project. Next, the supplier of each material is determined. This information can be obtained from project planning documents and allows the transportation distance of the materials to the construction site to be known. Posteriorly, it is used to determine the potential environmental impacts associated with the transportation phase. Finally, the required environmental properties to calculate the Environmental Impact Score (EIS) of each material in different infrastructure's life cycle phases (i.e., construction, operation and maintenance, and end-of-life (EOL)) are retrieved from the LCA database. This database contains for each infrastructure's life cycle phase the shadow price characterization factors for eleven environmental impact categories (Van Harmelen et al., 2004). Table 1 shows an example of a material with its different EISs.

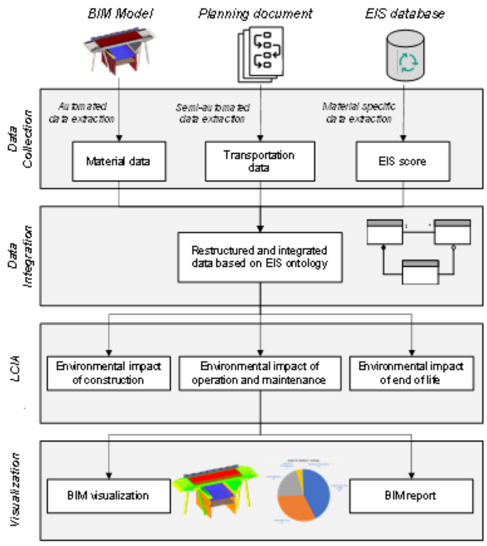

Figure 1: Proposed framework BIM-based LCA analysis for Infrastructure

Table 1: Example of a construction material with its different EIS

Material	Unit	Lifetime (years)	EIS$_{CON}$ (€/Unit)	EIS$_{O\&M}$ (€/Unit)	EIS$_{EOL}$ (€/Unit)	EIS$_{Total}$ (€/Unit)
Concrete mortar C20/25 (CEMIII)	m^3	100	29,48	0,00	3,21	32,69

2.2 Data Integration

This step aims to integrate and map in a structured manner the data collected in the previous step, so that it can be used to assess the potential environmental impact of the project. Figure 2 represents the structure for the data integration and mapping. As shown in this figure, each project is decomposed into its constituent elements (e.g., columns, decks, etc.) which are identified by a unique code (GUID). This GUID is used later to map the EIS data back into the BIM model. Other relevant environmental attributes are added to the BIM elements to accommodate the results of the EIS calculation in the BIM model, as will be explained in Section 2.4.

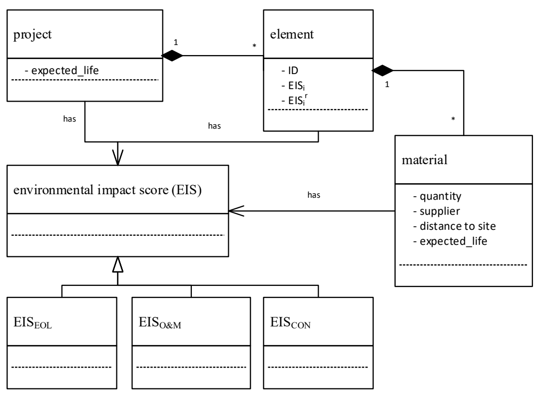

(a)

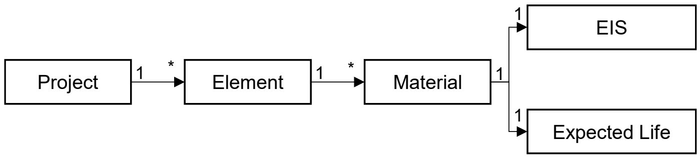

(b)

Figure 2: (a) Data structure needed for BIM-LCA integration, and (b) mapping of the data for EIS calculation

2.3 LCA analysis

The LCA analysis is performed by following the four-step methodology preconized by the ISO 14040-14044 standards (ISO 2006a; 2006b): (1) definition of the goal and scope; (2) LCI analysis; (3) life cycle impact assessment (LCIA); and (4) interpretation. More specifically, it adopts the methodology implemented by DuboCalc, which is a LCA-type software developed by the Dutch Directorate-General for Public Works and Water Management (Rijkswaterstaat, 2018) based on the European norm EN15804 (EN 15804, 2012). It calculates the environmental impact of an infrastructure by means of an environmental cost indicator (MKI) according to the Dutch National Environmental Database (NMD) (Stichting Bouwkwaliteit, 2019).

In the LCIA stage, after the data related to each infrastructure material j is gathered and properly structured as shown in Figure 2, its EIS can be determined according to Equation 1. The phases included in the system boundaries are the construction, use and maintenance, and EOL. Given that the LCA database present EIS of different materials in terms of unit costs per volume of the material, EIS needs to be multiplied by the quantity of the material. Additionally, the EIS_{CON} parameter includes the transportation distance to the construction site. The base value of EIS_{CON} is multiplied by the distance in kilometres. It should also be mentioned that $EIS_{O\&M}$ depends on the expected life of the material. When the expected life of the material (LT_m) is lower than the expected life of the project (LT_p), the $EIS_{O\&M}$ needs to be multiplied by a factor representing the ratio of LT_p to LT_m to account for the replacement of the material, as shown in Equation 2. The EIS of an element (EIS_i), in turn, is the summation of EIS_j of different materials used in the element, as shown in Equation 3. Likewise, the EIS of the entire project (EIS_{total}) is the summation of all the EIS_i of different elements in the project, as shown in Equation 4. Equation 5 describes the relative EIS of each element. Finally, Equation 6 describes the cumulative relative EIS of an element. This is the combined relative EIS of a group of elements which have identical object types (e.g., the combined EIS of all steel sheet piles).

$$EIS_j = Q_j \times (D_j \times EIS_{j,CON} + f_j \times EIS_{j,O\&M} + EIS_{j,EOL}) \tag{1}$$

$$f_j = \begin{cases} 1 & LT_j \geq LT_p \\ \dfrac{LT_p}{LT_j} & LT_j < LT_p \end{cases} \tag{2}$$

$$EIS_i = \sum_{j=1}^{J} EIS_j \tag{3}$$

$$EIS_{total} = \sum_{i=1}^{I} EIS_i \tag{4}$$

$$\mathrm{EIS}_i^r = \frac{EIS_i}{EIS_{total}} \tag{5}$$

$$\mathrm{EIS}_i^c = \sum_{i=1}^{I} \mathrm{EIS}_i^r \,|\, OT = identical \tag{6}$$

Where: EIS_j = environmental impact score of material j (€); Q_j = quantity of the material j (m^3 or ton); D_j = distance of the supplier of material j (km); $EIS_{j,CON}$ = environmental impact score of material j in construction phase (€/Q); f_j = life time factor representing the ratio of project life to the life of element j; LT_p = design life time of the project (years); LT_j = design life time of the material j (years); $EIS_{j,EOL}$ = environmental impact score of material j at the end-of-life (€/Q); $EIS_{j,O\&M}$ = environmental impact score of material j in operation and maintenance phase; EIS_i = environmental impact score of element i (€); J = Total number of materials in element i; EIS_{total} = environmental impact score of the total project (€); I = Total number of elements in the project; EIS_i^r = relative environmental impact score of element i (€); EIS_i^c = cumulative relative environmental impact score of element i (€); OT = object type of the model element.

2.4 Visualization

In the proposed framework, two different types of information will be provided to the designer, namely the EIS report and the visualization of the EIS in the BIM model. The EIS report presents the absolute and relative EIS of each element and allows designers to identify which elements are more critical in terms of environmental impact. The designer can use this information to develop element-level strategies to improve the environmental score of the overall design. Regarding the visualization of EIS in the BIM model, a colour coding scheme is used to display the BIM model according to either the no cumulative relative EIS values (EIS_i^r) or the cumulative relative EIS values (EIS_i^c).

2.5 Workflow Process

The proposed framework allows the workflow process to move from the current fragmented approach characterized by several communications loops between the designer and the sustainability expert (Figure 3a), to a new and integrated approach where the designer can immediately perform the LCA analysis at any moment during the design phase (Figure 3b). In this way, not only he/she is able to identify on-the-fly points of attention through the direct visualization of the LCIA results on the model, but also to perform quick sensitivity analysis through which he/she can observe immediately the results of his/her design changes.

Figure 3: LCA analysis workflow based on (a) current fragmented approach, (b) proposed integrated approach

3. Implementation

The proposed framework was materialized through a tool developed as a plugin in Revit by means of Dynamo (Autodesk, 2019) (Figure 4). As mentioned before, the Dutch National Environmental Database (NMD) (Stichting Bouwkwaliteit, 2019) is used in combination with DuboCalc (Rijkswaterstaat, 2018), although it can be adapted and modified according to different purposes in the future. The structured quantity take-off data is generated by Dynamo and transmitted to an Excel sheet. Through a VBA script, quantity take-off, EIS values, and project management data are structured as shown in Figure 2. Then, through another macro in Excel, the EIS is calculated based on the structured data and the report is generated. The EIS of different materials are then retrieved by Dynamo, which adds EIS values as parameters and enable the visualization of the results in the model. The LCA database adopted in the implementation of the tool was compiled by a sustainability expert using DuboCalc software (Rijkswaterstaat, 2018) and contains 70 different construction materials with their corresponding individual EIS. Table 2 shows a section of this EIS database.

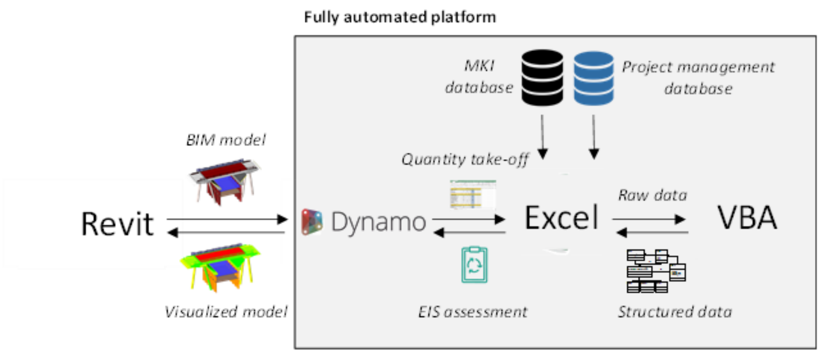

Figure 4: Architecture of the developed tool

Table 2: Section of the LCA database

Material/Element	Unit	Lifetime (years)	EIS_{CON} (€)	$EIS_{O\&M}$ (€)	EIS_{EOL} (€)
Asphalt (ZOAB)	ton	12	10,621	84,63	0,92
Asphalt (SMA, 0/11)	ton	16	10,372	59,28	0,92
Concrete mortar C20/25 (CEMIII)	m^2	100	29,48	0,00	3,21
Concrete mortar C30/37 (CEMIII)	m^3	100	15,14	0,00	6,34
Steel sheet pile	ton	100	96,43	0,00	-13,90
Composite sheet pile	ton	30	881,391	2168,32	47,89
Grout anchor	m^3	100	28,345	0,00	1,12

4. Case Study

In order to ascertain how the accuracy and calculation time of the automatic LCA analysis compares to those of the manual counterpart, the tool was tested through a real case study consisting of an infrastructure design project in the province of Utrecht, The Netherlands. The project comprises several concrete bridges, a highway and a large amount of steel sheet piles.

Given the substantial model size (i.e., approximately 1800 elements), this project is well suited to investigate the calculation time of the tool when it is employed on a large model. The results of the automatic LCA analysis are presented in the BIM model by means of a colour scheme as illustrated in Figure 5. The colour scheme can be based on the absolute, relative or the cumulative relative EIS. The cumulative EIS combines the individual scores of identical object types, i.e. sheet piles, to create a more realistic presentation. The colours range from red (highest EIS) to green (lowest EIS). From the analysis of Figure 5 it can be concluded that the road on top of the bridge contributes the most to the total EIS. Moreover, the sheet piles as a group have a relatively high contribution to the total EIS. This application illustrates how a colour scheme like this allows the design team to quickly identify the elements of the infrastructure that contribute the most to the EIS and use this information in the decision-making process of infrastructure design projects.

Table 3 shows the results of the comparison of the manual LCA analysis and the LCA analysis performed by the tool for several elements of the infrastructure considered in the case study. The results presented in this table show that overall the tool presents the same results as the manual calculation of the EIS. The small, insignificant, differences observed for the Bridge deck are a consequence of rounding errors.

Table 3: Accuracy of the EIS calculations

Model	**EIS manual (€)**	**EIS tool (€)**	**Accuracy (%)**
Sheet piles	117.034	117.034	100
Bridge deck	55.160	55.170	99,98
Approach slabs	2873	2873	100
Tubular piles	21.453	21.454	100

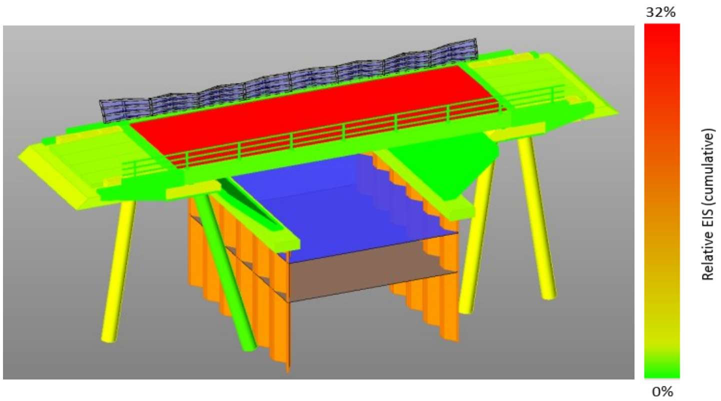

Figure 5: Colour scheme in BIM model presenting the cumulative relative EIS

To determine the extent to which the developed tool enables the reduction of the total cycle time of the LCA analysis of infrastructure design projects, the calculation time of the automatic LCA analysis was compared to that of the manual counterpart performed by a set of experts of the Dutch engineering and consulting firm Witteveen+Bos. The manual LCA analysis performed by Witteveen+Bos's experts was estimated to take between 1,5 to 3,5 working days, while the tool performed the required operations in approximately 35 minutes. This illustrative application shows that the calculation time of the traditional, time consuming and highly fragmented assessment process can be pulverized to a few minutes by using the developed tool.

The last step in the validation process of the tool consisted of assessing how the Witteveen+Bos's experts perceived the usefulness of the tool according to four categories: (1) functionality/applicability, (2) ease of use, (3) scalability and (4) sustainability consciousness. For that purpose, a workshop involving experts in the areas of infrastructure design, BIM coordination, sustainability, cost calculation, and project management was organized. During the workshop, an introductory presentation was given about the development and the functionalities of tool. Next, the tool was demonstrated, and experts were given the opportunity to ask questions about those functionalities. Finally, the experts were asked to fill out a questionnaire comprising a total of 16 questions divided among the four categories presented previously. The scores ranged from 1 (completely disagree) to 5 (completely agree). Moreover, the experts were also asked to give a general score to the tool varying between 1 (bad) and 10 (good).

The results of the questionnaires were presented in a spider diagram shown in Figure 6. This diagram presents a comparison between the performance of the current situation (orange) and the performance of the tool (blue). It is shown that the tool scores significantly higher on all four criteria compared to the current situation. This means that experts think that the application of the proposed framework can significantly improve the integration of environmental sustainability in infrastructure design. Moreover, Figure 6 also shows that a strong majority of the experts agreed that the developed tool is a good method to evaluate and improve the environmental performance of the infrastructure design (with average scores of 4,7 and 4,3), especially when compared to the current situation that is valued with scores of 2,8 and 2,4 respectively. During the workshop, experts identified that the developed tool has numerous potential applications within the infrastructure design process, i.e. evaluating design alternatives, optimizing designs, and presentation to clients. Similarly, the tool is easier to use, and results are easier to interpret comparatively to the current situation (3,5 and 4,1 against 2,0 and 2,0). Additionally, the developed tool fosters the designers' environmental sustainability consciousness significantly better than the current situation (with a score of 4,4 against 1,9).

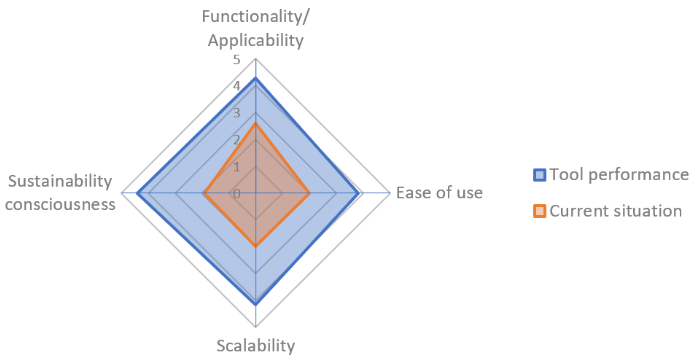

Figure 6: Comparison of the usefulness of the proposed tool with the conventional EIA assessment according to four categories: (1) functionality/applicability, (2) ease of use, (3) scalability and (4) sustainability consciousness

5. Conclusion

In the construction industry, the need for delivering environmentally sustainable infrastructure is of utmost urgency. An environmental sustainability assessment framework is therefore required to understand the interactions among subsystems, infrastructures characteristics and design-related decisions. However, this is a complex process and an integrated approach to implement sustainable aspects in the decision-making process of infrastructure design is currently lacking. The research work described in this paper presents a framework that aims to provide the infrastructure designer with on-the-fly information about the potential environmental impact of his/her design choices. An application of the proposed framework was developed and tested on a case study to investigate the capabilities of the framework in enabling a sustainability-driven decision-making process. The usefulness of the developed tool was posteriorly assessed and validated by means of an expert panel workshop.

From this case study it can be concluded that: (1) the proposed framework and its application have shown that the BIM environment is able to facilitate an automated and integrated LCA analysis of infrastructure design projects; (2) the BIM-based LCA analysis is accurate and much faster than the current, highly fragmented, LCA processes; (3) the visual presentation of the LCIA results allows designers to easily pinpoint high contributing model elements to the total EIS and use this information in the decision-making process. Finally, the BIM-based approach was found to foster the designers' sustainability consciousness by showing them the potential environmental impact of their design choices.

Future research work on integrating sustainability aspects in the design process of infrastructure through BIM will be focused on: (1) calculating and presenting the environmental performance of an infrastructure design by means of multiple impact category indicators; (2) including more sustainability aspects such as social and economic pillars and the information required from the BIM model to achieve this; (3) developing a direct connection between BIM-software and the environmental database to further improve the integration of the platforms; and (4) extending the applicability of the proposed framework to other geographical contexts.

References

Abidin, N. Z. (2010). Sustainable Construction in Malaysia – Developers ' Awareness, Proc. World Acad. Sci. Eng. Technol., vol. 5, no. 2, pp. 122–129.

Autodesk, (2019). Revit. Autodesk.

Basbagill, J., Flager, F., Lepech, M., Fischer, M. (2013). Application of life-cycle assessment to early stage building design for reduced embodied environmental impacts, Build. Environ., 60, pp. 81–92.

Bribián, I., Usón, A., Scarpellini, S. (2009). Life cycle assessment in buildings: State-of-the-art and simplified LCA methodology as a complement for building certification, Build. Environ., vol. 44, no. 12, pp. 2510–2520.

Bryde, D., Broquetas, M., Volm, J. M. (2013). The project benefits of Building Information Modelling (BIM), Int. J. Proj. Manag., vol. 31, no. 7, pp. 971–980.

Bueno, C., Fabricio, M. M. (2018). Comparative analysis between a complete LCA study and results from a BIM-LCA plug-in, Autom. Constr., 90, pp. 188–200.

Bueno, C., Pereira, L. M., Fabricio, M. M. (2018). Life cycle assessment and environmental-based choices at the early design stages: an application using building information modelling, Archit. Eng. Des. Manag., vol. 14, no. 5, pp. 332–346.

Carvalho, J., Bragança, L., Mateus, R. (2019). Optimising building sustainability assessment using BIM, Autom. Constr. 102, pp. 170–182.

Cavalliere, C., Hollberg, A., Dell'Osso, G. R., Habert, G. (2019). Consistent BIM-led LCA during the entire building design process, IOP Conf. Ser. Earth Environ. Sci., vol. 323, p. 012099.

Doan, D. T., Ghaffarianhoseini, A., Naismith, N., Zhang, T., Ghaffarianhoseini, A., Tookey, J. (2017). A critical comparison of green building rating systems, Build. Environ., vol. 123, pp. 243–260.

EN 15804, 2012. Sustainability of construction works—environmental product declarations—core rules for the product category of construction products.

van Harmelen, A. K., Korenromp, R. H. J., Ligthart, T. N., van Leeuwen, S. M. H., van Gijlswijk, R. N. (2004). Toxiciteit heeft zin prijs: Schaduwprijzen voor (eco-)toxiciteit en uitputting van abiotische grondstoffen binnen DuboCalc.

Hollberg, A., Genova, G., Habert, G. (2020). Evaluation of BIM-based LCA results for building design, Autom. Constr., vol. 109, pp. 102972.

ISO, 2006a. ISO International Standard 14040: environmental management – life cycle assessment – principles and framework. International Organization for Standardization, Geneva, Switzerland.

ISO, 2006b. ISO International Standard 14044: environmental management – life cycle assessment – requirements and guidelines. International Organization for Standardization, Geneva, Switzerland.

Rijkswaterstaat, (2018). DuboCalc. Available: https://www.rijkswaterstaat.nl/zakelijk/zakendoen-met-rijkswaterstaat/inkoopbeleid/duurzaam-inkopen/duurzaamheid-bij-contracten-en-aanbestedingen/dubocalc/index.aspx, accessed October 2019.

Santos, R., Costa, A. A., Silvestre, J., Pyl, L. (2020). Development of a BIM-based Environmental and Economic Life Cycle Assessment tool, J. Clean. Prod., 121705.

Soust-Verdaguer, B., Llatas, C., Moya, L. (2020). Comparative BIM-based Life Cycle Assessment of Uruguayan timber and concrete-masonry single-family houses in design stage, J. Clean. Prod., 121958.

Soust-Verdaguer, B., Llatas, C., García-Martínez, A. (2017). Critical review of bim-based LCA method to buildings, Energy Build., vol. 136, pp. 110–120.

Soust-Verdaguer, B., Llatas, C., García-Martínez, A. (2016). Simplification in life cycle assessment of single-family houses: A review of recent developments, Build. Environ., vol. 103, pp. 215–227.

Stichting Bouwkwaliteit, (2019). Nationale Milieudatabase. Available: https://www.milieudatabase.nl/viewNMD/, accessed November 2019.

A conceptual framework for more efficient simulation of the interplay between road pavements and the Urban Heat Island phenomenon

Monica Pena Acosta, Faridaddin Vahdatikhaki, João Santos, Andries G. Dorée
Construction Management and Engineering Department, University of Twente
m.penaacosta@utwente.nl

Abstract. There have been thirty-eight heat waves in Europe in the last century, seventeen of which were in the last decade. In urban areas, the effects of global warming are intensified because air and surface temperatures are, on average higher than in the surrounding areas, a phenomenon is known as Urban Heat Island (UHI). This research, therefore, investigates how road pavement design, construction, and maintenance can play an important role in the formation of UHI's while proposing a conceptual framework for a data-driven simulation of the interaction between road pavements and UHI's, moving one step closer towards smarter and sustainable solutions for asphalt road pavements.

1. Introduction

There have been thirty-eight heat waves in Europe in the last century, seventeen of which were in the last decade (Steeneveld *et al.*, 2011). Climate projections for the next decades show that the frequency and severity of heatwaves will further increase unless immediate actions are taken. Greenhouse gas (GHG) emissions need to drop globally by 45 percent until 2030 to keep global warming below 1.5 degrees Celsius (First, 2019).

In urban areas, the effects of global warming are intensified because air and surface temperatures are, on average higher than in the surrounding areas. This phenomenon is known as Urban Heat Island (UHI), which is understood as one of the main contributors to urban energy use and urban GHG emissions (Mirzaei, 2015). With half of the world's population living in urban areas, GHG emissions are likely to increase further, as cities continue to grow (U.N., 2018). Since the 1800s, scholars across various fields have studied urban heat islands. While governments, engineers, and city planners are urged to design and implement mitigation strategies to both reduce the heat trapped in the cities and increase urban climate resilience, up to date, there is no consensus about how to deal with its effects (Grimmond *et al.*, 2010, 2011).

Due to the complexity of urban geometry, the focus has primarily been on buildings and how they contribute to UHI. In doing so, the significant impact and role played by large urban infrastructures, particularly asphalt road infrastructure in the formation of UHI, remain mostly overlooked. Given the fact that road infrastructures can account for up to 45 percent of the urban area, this can be a significant oversight (Akbari and Rose, 2008).

Studies of road infrastructure have been carried out from the perspective of urban connectivity, in order to guarantee accessibility and efficient access to all spaces in the urban area, while reducing construction and maintenance costs (Sharifi, 2019). In recent years, due to the urgency of climate change, the current body of knowledge has also expanded to the sustainable design, construction, and maintenance of roads. This has been achieved through the implementation of green strategies such as the increased use of recycled materials, as well as the incorporation of new technologies for the design and application of fresh pavements with high thermal emissivity and water retention (permeable) pavements. However, the distinctive contributions of urban roads and their design and construction parameters to the formation of urban heat islands have not been clearly identified. (US EPA, 2008).

The research work presented in this paper proposes a framework for the study of the interplay between road pavements and UHI. The focus is specifically on the investigation of how road pavement design, construction, and maintenance can play a major role in the formation of UHI. To this end, we propose a conceptual framework that harnesses the advances in data science and machine learning along with the ever-increasing computing power to develop a data-driven modeling technique that can accurately simulate the impacts of road pavement design, construction, and maintenance on UHI. The proposed framework can be used to develop strategies and policies for mitigation of road pavement-induced impacts on UHI, moving a step closer towards smarter and sustainable solutions for asphalt road pavements.

2. Literature Review

Luke Howard first used the concept of the Urban Heat Islands in his book *The Climate of London* (Howard, 1833). The book outlines and discusses the effects of the built environment on the climate. Even though Howard was not able to take simultaneous measurements in different points in London and its surroundings, he was able to correctly point out the existence of an urban phenomenon causing the difference in temperature (ΔT_{u-r}). Centuries later, his findings were confirmed when geospatial information became available. The urban island effect then was mapped, revealing itself as a "pool" of warmer air that dwells in the built area. Recent literature points to Howard's findings as a "canopy effect" on the air temperature (Oke, 1982). The canopy layer is the air that lies below the roof level. The properties of the outdoor canopy layer are determined by exchanges of heat between vertical surfaces (building walls and roads), indoor air across building openings and outdoor spaces.

Howard describes four causes for the differences in temperature in the canopy layer as 1. anthropogenic sources of heat, 2. the geometry of urban surfaces trapping the radiation and blocking its reflection back to the sky, 3. the effect of urban "roughness" impeding the passage of the "light winds of summer," and 4. the availability of moisture to evaporate.

More recent literature on the understating of the urban effect translates Howard's findings in terms of the energy budget of the urban canopy layer, which is defined as:

$$Q^* + Q_F = Q_H + Q_E + \Delta Q_S \quad (1)$$

Where: Q^* = net radiation; Q_F = heat that anthropogenic activities add to the urban fabric; Q_H= transfer of heat from the surface to the air (sensitive heat exchanges); Q_E = latent heat exchanges; ΔQ_S = variation in energy added or taken from the urban fabric.

From Howard's findings, it is possible to conclude that the variation of urban temperature is mainly drawn as a function of the cooling effect driven by the loss of long-wave radiation to the sky, which is counterbalanced by the release of heat from storage. Under the canopy layer, building walls and urban roads will store and release this heat, and under the limited view of the sky given by the specific urban geometry, this heat, therefore, will remain trapped.

3. Approaches to assessing and model UHIs

Over the past centuries, both academia and industry have dedicated their efforts to measure the impact of UHIs. However, given the complexity of the problem, different types of modeling approaches and methodologies have been proposed, utilizing different parameters and scale of application. This has resulted in inconsistent outcomes and lack of a uniform methodology in the field (Grimmond *et al.*, 2010, 2011; Stewart, 2011).

For instance, balloons, tall T.V. towers, or helicopters were widely used before the 1980s, aiming to collect data for empirical statistical models (Roth, 2013). The most common statistical analysis compared time trends from the observations of two or three different environments. The primary emphasis at that time was to compare the average temperature in the urban boundary layer (UBL). However, these early studies were subject to a particular site and observation, and lacking the statistical significance to elicit a generic insight about UHI vis-à-vis urban geometries and contexts, particularly, energy surface characteristics, such as solar radiation balance and energy fluxes.

The shortcomings of statistical implementations were lessened by Oke and the development of an Urban Canopy Model (UCM). The model focusses on the energy transition between surface and air temperature in the urban canopy layer by averaging geometries of building height, width, impervious surfaces, and roads to represent urban surfaces and reduce the computational cost.

There are two main categories in the UCMs: 1) the single-layer urban canopy model (SLUCM) and 2) the multilayer canopy models (MLUCM). The main advantage of the UCM is the calculation of the energy budgets for roofs, walls, and roads to combine them later at the canopy level. These energy representations give more detailed information about the radiative budgets, turbulent heat, and momentum fluxes. The most advanced MLUCM models incorporate 3D urban environments, considering the impacts of vertical surfaces (walls) and horizontal surfaces (roofs and pavements) and consider urban canyon shadows, reflections, and radiation trapping (Garuma, 2018). Nonetheless, the complexity of the energy transfer processes at the surface temperatures and the turbulent surface exchanges create a significant challenge in assessing the impact of different parameters in the overall temperature difference. Consequently, there is no consistency among the measurements, and the outcomes are not replicable (Grimmond *et al.*, 2010, 2011; Mirzaei, 2015).

On the other hand, numerical models offer a more accurate simulation of the temperature and airflow conditions in the urban canopy (Bruse, 1999; Porson *et al.*, 2009; Garuma, 2018). These numerical models are mostly used to calculate sensible heat fluxes inside the buildings (i.e., the wall to the floor, and from the floor to the roof) and how environmental factor affects the energy composition of the building. Moreover, numerical models can be implemented to simulate parameters in the canopy layer, such as temperature, wind speed, and precipitation. Despite the greater complexity of the factors incorporated in these models, they are still limited to the spatial domain, and thus separated at different scales. This is because atmospheric and canopy scale turbulences cannot be modeled on the same temporal scale of time and length, and therefore the simplification made to the models is significantly different due to the scale of the study (Mirzaei and Haghighat, 2010).

Nowadays, satellite remote sensing techniques have proved useful in the detection of thermal patterns in urban areas receiving enough attention in the last three decades. Researchers around the globe (Golden and Kaloush, 2006; Buyantuyev and Wu, 2010; Cao *et al.*, 2010; Zhou *et al.*, 2014) have investigated more detailed scales using remotely sensed or ground-based imageries. Regardless of advances in the thermal remote sensing technologies and methods, many challenges arise when studying the thermal response of the urban surface, given the heterogeneity of the urban morphology. For instance, the measured surface temperature depends on the viewing geometry and solar orientation due to the orientation of the infrastructure (thermal anisotropy). In general, shaded areas are colder than average temperatures. However, the average pixel surface temperature depends on the perceived shadows and the sampled facets (Hu *et al.*, 2016; Li and Li, 2020). Moreover, the different types of materials used in the built environment required different corrections when processing the sensed imagery, creating significant discrepancies in the temperatures obtained, measured, and predicted. Therefore, the most common approach is the satellite-based observations in combination with statistical analysis to find correlations between land and temperature distributions (Zhou *et al.*, 2014).

Nevertheless, in the current state of the art, there is no single modeling approach or adaptive technique that meets all the needs and demands of urban areas. Furthermore, there is no single rule that maintains the level of detail and specificity that a model should contain.

3.1 Parameters and drivers that contribute to UHIs

While there is no consensus on modeling approaches or methodology for the assessment of urban heat islands (Grimmond *et al.*, 2010, 2011), the relevant parameters and driving forces affecting these heat islands can be derived from the literature. For example, Stanganelli and Soravia (2012), have shown that there is a direct relationship between the land coverage coefficient and temperatures; increasing the land coverage ratio will, therefore, increase urban temperatures too. In addition, increasing the average height of buildings will also increase temperatures. This can be attributed to the decrease in long-wave radiation capacity at night in densely populated areas.

Likewise, the urban geometry, which is a factor in the height, length and spacing of buildings, as well as the street profile (orientation, view factors and the relationship between the height and width of buildings), plays an important role in the formation of UHI, as demonstrated by Oliveira, Andrade, and Vaz (2011) and Mohajerani, Bakaric and Jeffrey-Bailey (2017).

The interaction between open spaces, buildings, and urban roads is a characteristic of urban geometry that influences the increase in air temperatures. This interaction creates a street canyon that affects air temperature and forms wind vortices (Vardoulakis *et al.*, 2014). In turn, since sidewalks are mostly on the surface, they are often shaded in an urban environment by buildings and trees and therefore overlooked. However, these street canyons, along with the urban fabric (materials), can have an impact on solar reflections, and on the amount of heat that is absorbed and released by the paved surfaces (Chen *et al.*, 2016). Recent investigations have shown that in large cities when viewed from above the urban canopy, paved surfaces (urban roads, sidewalks, and parking lots) typically cover between 29 and 39 percent of the city's surface area. However, when viewed from below the canopy, this percentage can increase to between 36 and 45 percent (Akbari and Rose, 2008).

Another important parameter is the type of materials used in the built environment. Depending on the thermal efficiency of the materials, they absorb and reflect the heat radiated by the sun in various ways and therefore affect the thermal comfort conditions of buildings and open spaces differently. The fraction of the incident radiation that is reflected from a surface is called albedo, and it plays a significant role in the energy balance on the surface of the earth since it defines how much solar radiation is absorbed (Mohajerani, Bakaric and Jeffrey-Bailey, 2017). Therefore, albedo is a significant parameter to consider in the study of heat islands. For example, fresh asphalt concrete can absorb up to 95 percent of the sunlight (5 percent albedo). In general, paved surfaces are comprised of materials with very low albedo and, therefore, roughly about 45 percent of urban areas have the unintended ability to store heat.

Yaghoobian and Kleissl (2012), found that although a small reduction in urban air temperature could be achieved by increasing the albedo, high pavement reflectivity contributed to increased use of building energy for summer cooling. This, in turn, carries a negative impact with regards to CO2 emissions. Experimental results from (Li, 2012) showed that a more reflective surface reduced the paved surface temperature by 15 degrees Celsius compared to a less reflective surface on a hot summer day. However, it was also observed that the adjacent painted wall temperature with albedo about 0.3 was 3 degrees Celsius warmer for the reflective surface versus the non-reflective pavement surface. This highlights the importance of context-specific mitigation strategies to address UHIs.

The following table summarizes the main contributing factors affecting UHIs based on the literature.

Table 1: Main contributing factors to UHIs

Category	Factor	Calculation method
Urban morphology	Anthropogenic heat (Q.F.)	The function of distance to a road and the road length
	Building fraction	The ratio between buildings and land area
	Non-permeable surfaces	Non-permeable Surfaces Index
	Sky view factor	A value between 0 to 1 expressing the radiation received by a flat surface
	Surface cover	The ratio between built area and land area
	Urban canyon	Measure between the two facing walls above the road
	Vegetation coverage	Normalized difference vegetation index (NDVI)
Material properties	Road albedo	Solar reflectance index (SRI)
	Road emissivity	
	Roof albedo	
	Roof emissivity	
	Wall albedo	
	Wall emissivity	
Urban context	Air temp	Measuring air temperatures (usually 2 m)
	Land surface temperature	Remote sensing
	Rainfall	Meteorological stations
	Specific humidity	Meteorological stations
	Urban climate zone	The classification proposed by (Stewart and Oke, 2012)
	Wind temp	Measuring air temperatures (usually 2 m)
	Wind velocity	

While the road fraction occupies a large percentage of a city's surface area, the literature shows that its explicit contribution to the formation of the heat island is not measured or modeled on its own. As shown in table 1, road albedo and emissivity are calculated as part of the solar reflectance index, which does not take into account neither the city sky view factor nor the canyon effect, thus leading to a more accurate SRI relative to flat surfaces with a ski view factor close to 1. However, in high-density urban environments, this is never the case.

4. Proposed Framework

This paper proposes a conceptual framework that addresses the need for a more explicit understanding of the contribution of road infrastructure in the UHI. In a nutshell, this framework intends to elaborate on the development of a data-driven approach to finding a correlation between road design parameters (e.g., geometry, material, texture, etc.) and UHI. As shown in Figure 1, this data-driven model is expected to use a machine learning method to identify the correlations between a set of input variables and UHI. This model can be used to gain a better understanding of the impact of the road network on the UHI phenomenon and also to develop a mitigation strategy for reducing UHI through enhanced road design.

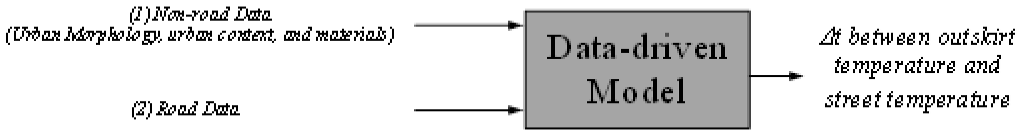

Figure 1: Schematic representation of the scope of the data-driven model

Figure 2 presents the overall framework for the development of the data-driven model. As shown in this figure, the proposed framework consists of 5 steps, namely, (1) Data Collection, (2) Data Integration, (3) Data Preparation, (4) Model Development, and (5) Analysis and Decision making. The remainder of this section is dedicated to the elaboration of each phase of this framework.

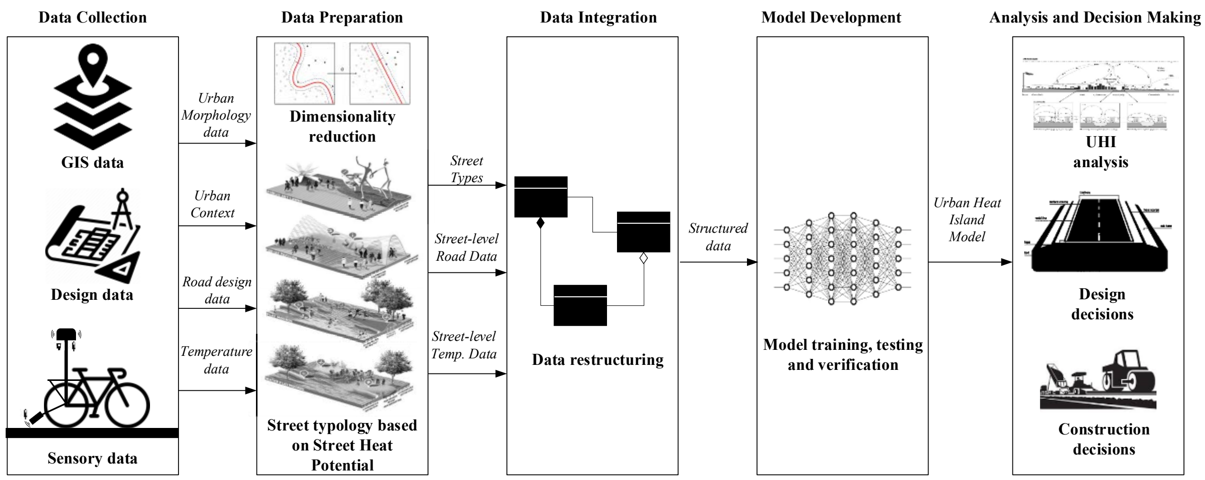

Figure 2: Conceptual framework for the development of data-driven Urban Heat Island model

4.1 Data Collection

As the first step in this methodology, a dataset consisting of input and output variables need to be prepared. The input variable consists of the road design data and all the influential parameters on UHI, as indicated in Table 1. The output variable encompasses high-resolution time-stamped data about the UHI, i.e., Δt between the temperature of each urban street and the baseline temperature in the outskirt of the city.

The first type of data pertains to the urban morphology. Urban morphology involves such data as anthropogenic heat, building height and density, surface, and vegetation cover. These data can be retrieved from the national cadastre databases, CityGML models, and public municipal and geoinformation data.

Urban context data pertains to the overall climate of the city at a given point in time. This includes data about the baseline temperature of the region, rainfall, specific humidity, wind temperature, and wind velocity. The time-stamped urban context data can be obtained from meteorological databases.

The next data type required for the data-driven model is the data about the design and construction of roads. This includes data about the physical properties of the road (asphalt type, density, layer thickness, etc.). This data type is available from the contract document at the municipality. From these documents, the specifications of different roads need to be extracted and structured.

Finally, the heat differential data need to be collected. This data pertains to the difference between the baseline temperature (i.e., the temperature in the outskirt of the city) and the micro-temperature at the street level. Although municipalities have recently started to deploy sensor technologies to collect temperature data from several strategic locations of their jurisdiction, the available data is insufficient for the scope of a data-driven model. To this end, a data collection method is developed to collect fill this gap. In this method, a sensorized bicycle is used to roam around the city and collect geo-referenced and time-stamped temperature data at (1) the level of road surfaces and (2) above the ground level, as shown in Figure 3. The sensor kit would include a microprocessor (e.g., Raspberry Pi), a GPS rover, a mobile weather station, and an infrared camera. The infrared camera, weather station, and GPS rover are connected to the microcontroller that is responsible for (a) registering, (b) synchronizing, and (c) storing the data.

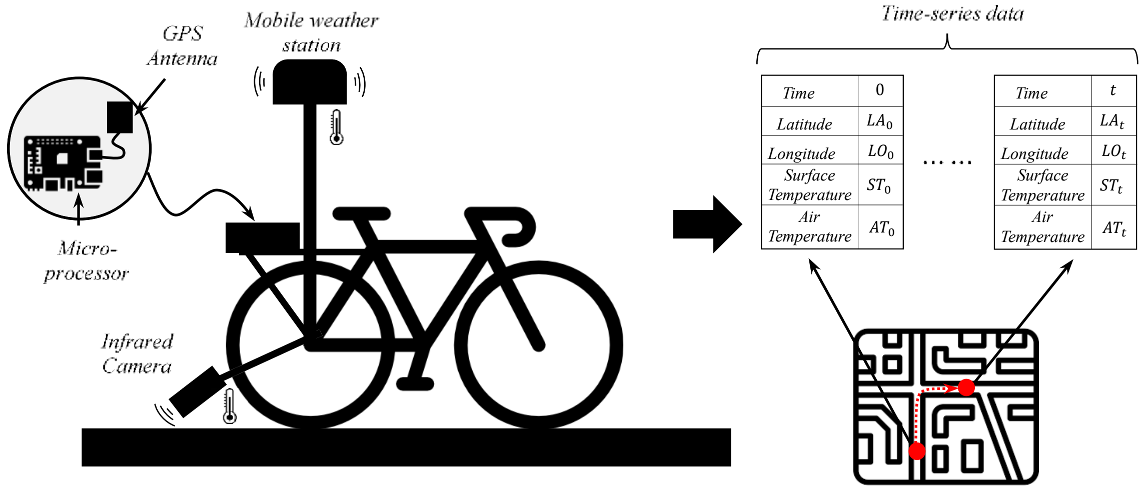

Figure 3: Data collection approach for street-level surface and air temperature data

4.2 Data Preparation

The sheer number of variables identified in the literature renders the application of the machine learning approach difficult since it requires a very large data set. Two preparatory and sequential measures will be implemented to address this issue. (1) The first step is to reduce the dimensionality of the data as much as possible. To that end, a multivariate analysis will be conducted to identify the variables (i.e., characteristics) that can best explain the variance in the data. This will help remove variables with a lower contribution to the internal structure of the data and thus simplify the training of the model.

(2) Next, to better distinguish between road-related and non-road-related variables, it is suggested first to develop a street typology based on the Street Heat Storage Potential (SHSP), as shown in Figure 4. To develop SHSP, all the non-road related variables (i.e., urban morphology, urban context, and urban material) that are not filtered out in the previous step are used to perform cluster analysis. It is proposed to use a centroid-based clustering method (e.g., K-means clustering) to identify a K number of street types that can explain the variance in UHI. As shown in Figure 4, at the end of this step, the thresholds of different variables that define different street types will be identified. The entire city can be categorized in terms of a finite number of street types using those thresholds.

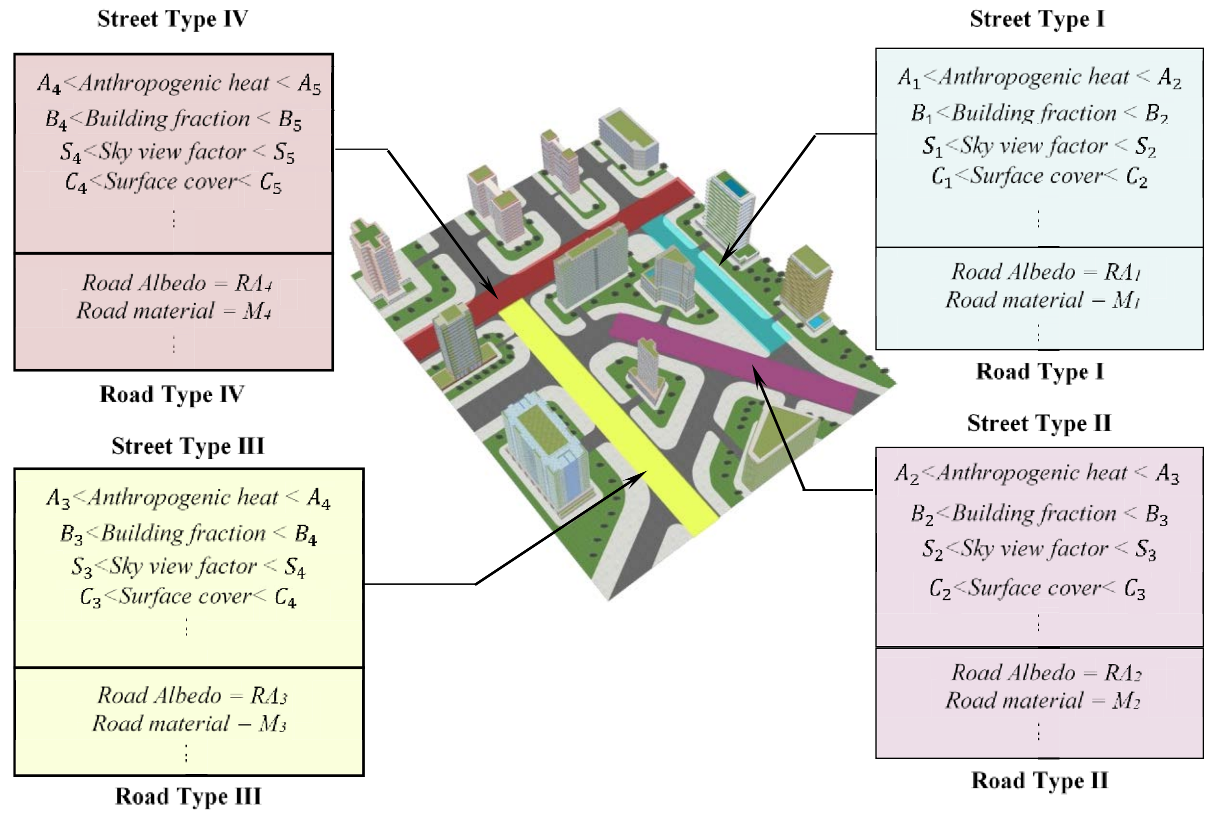

Figure 4: Schematic representation of street typology

4.3 Data Integration

In the next step, all the input variables need to be synchronized and integrated to form a consistent database for the development of the model. Figure 5 represents the data structure proposed for the modeling. As shown, all the data are categorized into three main classes, namely road data, context data, and street type. The resolution of the data will be at the street level. With regards to non-road related data, since they are all translated into street typology, the data is already in scale for the modeling. However, temperature data (as a sub-set of road data) need to be rescaled.

Depending on the frequency of the data collection and the traveling speed, several temperature data points can be collected from the same street. Therefore, all the data consequently registered in one street need to be averaged. Assuming that the entire street has uniform pavement, the road design data are considered constant throughout the street.

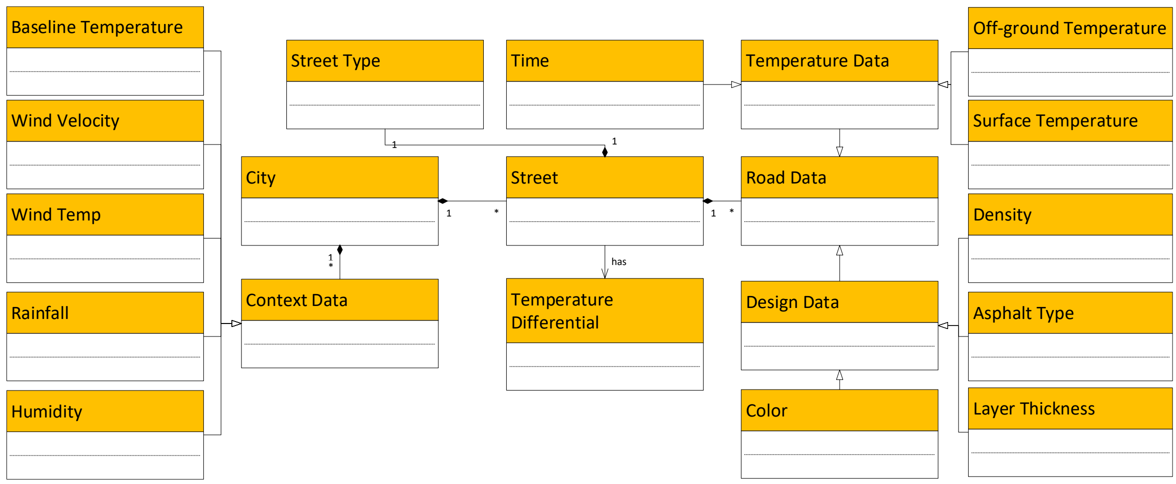

Figure 5: Data structure for the integration of data

4.4 Model Development

For this conceptual framework, we propose to use a convolutional neural network (CNN) to build a model that can capture the interaction between input variables and IHU data. Given the spatial nature of the data, a CNN and its locally connected layers would be efficient in managing the complexity of this problem by learning the spatial hierarchies of the non-road and road-related data sets in combination with street typology.

A CNN architecture typically consists of several convolutions, clustering, and fully connected layer. The proposed CNN architecture for this conceptual framework is a variant of the LeCun network, which takes advantage of two convolutional layers, two pooling layers, and an output layer. Each convolutional layer uses a 3x3 kernel. The convolution and pooling layer will perform the feature extraction; from these extracted features, the ΔT and the street temperature can be mapped. Metaheuristic methods will be used to optimize the internal parameters of CNN.

4.5 Analysis and Decision Making

Once the model is developed, it can be used for three main different purposes: (1) improving the design of new roads in an urbanized area, (2) developing mitigation strategies to reduce the impact of UHI, and (3) developing energy harvesting solutions.

Given that this data-driven model captures the interplay between road design parameters and UHI, it can be used to optimize the road design from the perspective of UHI. City planners can use this model to make decisions about such properties of the road as asphalt type, layer thickness, color, and density considering the characteristics of the road location (e.g., urban morphology, street type, etc.). Needless to say, this model can serve the additional objective of reducing UHI impacts on top of the conventional road design objectives (e.g., mechanical properties, service life, safety, and sustainability).

The model can also be used to develop several mitigation strategies for reducing UHI impacts. City planners can use this model to pinpoint potential areas where more vegetation and green facades/roofs can be of assistance. Also, they can make decisions about repainting roads that contribute most to UHI.

Finally, this model can be used to determine which part of the urban context energy harvesting methods can be used. Examples of such technologies are the use of pipe-pavement thermoelectric generators. The city planners can identify streets with the highest potential for the application of such technologies. This can be especially useful, considering the current cost of thermoelectric energy harvesting technologies.

5. Conclusion

In this paper, a conceptual framework for a more efficient, context-specific, and data-driven simulation of the interaction between road pavements and UHIs is proposed. It harnesses the advances in data science and machine learning to develop a data-driven modeling technique that enables the simulation of the impacts of road pavement design, construction, and maintenance on UHI. By taking into account the heat storage potential of the streets, the proposed framework will provide municipalities and policymakers with a computational platform to develop more effective UHI mitigation policies and programs that address the most vulnerable urban heat spots in a city, thereby moving a step closer towards smarter and sustainable solutions for asphalt road pavements within an urban context.

References

Akbari, H. and Rose, L. S. (2008) 'Urban Surfaces and Heat Island Mitigation Potentials', *Journal of the Human-Environment System*, 11(2), pp. 85–101. doi: 10.1618/jhes.11.85.

Bruse, M. (1999)' Modelling and strategies for improved urban climates', *Biometeorology and urban climatology at the turn of the millenium, Sydney, 8-12 novembre 1999*, p. 6.

Buyantuyev, A. and Wu, J. (2010) 'Urban heat islands and landscape heterogeneity: Linking spatiotemporal variations in surface temperatures to land-cover and socioeconomic patterns', *Landscape Ecology*, 25(1), pp.17–33. doi: 10.1007/s10980-009-9402-4.

Cao, X. *et al.* (2010) 'Quantifying the cool island intensity of urban parks using ASTER and IKONOS data', *Landscape and Urban Planning*. Elsevier B.V., 96(4), pp. 224–231. doi: 10.1016/j.landurbplan.2010.03.008.

Chen, L. *et al.* (2016) 'Intra-urban differences of mean radiant temperature in different urban settings in Shanghai and implications for heat stress under heat waves: A GIS-based approach', *Energy and Buildings*. Elsevier B.V., 130, pp. 829–842. doi: 10.1016/j.enbuild.2016.09.014.

First, P. J. (2019) *Global Warming of 1.5 C An IPCC Special Report on the Impacts of Global Warming of 1.5 C Above Pre-Industrial Levels and Related Global Greenhouse Gas Emission Pathways, in the Context of Strengthening the Global Response to the Threat of Climate Change.*, *Sustainable Development, and Efforts to Eradicate Poverty*. doi: 10.1017/CBO9781107415324.

Garuma, G. F. (2018) 'Review of urban surface parameterizations for numerical climate models', *Urban Climate*. doi: 10.1016/j.uclim.2017.10.006.

Golden, J. S. and Kaloush, K. E. (2006) 'Mesoscale and microscale evaluation of surface pavement impacts on the urban heat island effects', *International Journal of Pavement Engineering*, 7(1), pp. 37–52. doi: 10.1080/10298430500505325.

Grimmond, C. S. B. *et al.* (2010) 'The international urban energy balance models comparison project: First results from phase 1', *Journal of Applied Meteorology and Climatology*, 49(6), pp. 1268–1292. doi: 10.1175/2010JAMC2354.1.

Grimmond, C. S. B. *et al.* (2011) 'Initial results from Phase 2 of the international urban energy balance model comparison', *International Journal of Climatology*, 31(2), pp. 244–272. doi: 10.1002/joc.2227.

Howard, L. (1833) 'The Climate of London, vol I', *Harvey and Darton*, p. 285.

Hu, L. *et al.* (2016) 'A first satellite-based observational assessment of urban thermal anisotropy', *Remote Sensing of Environment*. doi: 10.1016/j.rse.2016.03.043.

Li, H. (2012) *Evaluation of Cool Pavement Strategies for Heat Island Mitigation*.

Li, N. and Li, X. (2020) 'The Impact of Building Thermal Anisotropy on Surface Urban Heat Island Intensity Estimation: An Observational Case Study in Beijing', *IEEE Geoscience and Remote Sensing Letters*, pp. 1–5. doi: 10.1109/lgrs.2019.2962383.

Mirzaei, P. A. (2015) 'Recent challenges in modeling of urban heat island', *Sustainable Cities and Society*. Elsevier B.V., 19, pp. 200–206. doi: 10.1016/j.scs.2015.04.001.

Mirzaei, P. A. and Haghighat, F. (2010) 'Approaches to study Urban Heat Island - Abilities and limitations', *Building and Environment*. Elsevier Ltd, 45(10), pp. 2192–2201. doi: 10.1016/j.buildenv.2010.04.001.

Mohajerani, A., Bakaric, J. and Jeffrey-Bailey, T. (2017) 'The urban heat island effect, its causes, and mitigation, with reference to the thermal properties of asphalt concrete', *Journal of Environmental Management*. Elsevier Ltd, 197, pp. 522–538. doi: 10.1016/j.jenvman.2017.03.095.

Oke, T. R. (1982) 'The Energetic Basis of the Urban Heat Island', *Quarterly Journal of the Royal Meteorological Society*, 108, pp. 1–24.

Oliveira, S., Andrade, H. and Vaz, T. (2011) 'The cooling effect of green spaces as a contribution to the mitigation of urban heat: A case study in Lisbon', *Building and Environment*. Elsevier Ltd, 46(11), pp. 2186–2194. doi: 10.1016/j.buildenv.2011.04.034.

Porson, A. *et al.* (2009) 'How many facets are needed to represent the surface energy balance of an urban area?', *Boundary-Layer Meteorology*, 132(1), pp. 107–128. doi: 10.1007/s10546-009-9392-4.

Roth, M. (2013) 'Urban Heat Islands', in *Handbook of Environmental Fluid Dynamics, Volume Two: Systems, Pollution, Modeling, and Measurements*, pp. 143–159. doi: doi:10.1201/b13691-13.

Sharifi, A. (2019) 'Resilient urban forms: A review of literature on streets and street networks', *Building and Environment*. Elsevier, 147(July 2018), pp. 171–187. doi: 10.1016/j.buildenv.2018.09.040.

Stanganelli, M. and Soravia, M. (2012) 'Connections between urban structure and urban heat island generation: An analysis trough remote sensing and GIS', *Lecture Notes in Computer Science (including subseries Lecture Notes in Artificial Intelligence and Lecture Notes in Bioinformatics)*, 7334 LNCS(PART 2), pp. 599–608. doi: 10.1007/978-3-642-31075-1_45.

Steeneveld, G. J. *et al.* (2011) 'Quantifying urban heat island effects and human comfort for cities of variable size and urban morphology in the Netherlands', *Journal of Geophysical Research Atmospheres*, 116(20), pp. 1–14. doi: 10.1029/2011JD015988.

Stewart, I. D. (2011) 'A systematic review and scientific critique of methodology in modern urban heat island literature', *International Journal of Climatology*, 31(2), pp. 200–217. doi: 10.1002/joc.2141.

Stewart, I. D. and Oke, T. R. (2012) 'Local climate zones for urban temperature studies', *Bulletin of the American Meteorological Society*, 93(12), pp. 1879–1900. doi: 10.1175/BAMS-D-11-00019.1.

U.N. (2018) *World Urbanization Prospects, United Nations Press*. doi: 10.4054/demres.2005.12.9.

US EPA (2008) 'Reducing Urban Heat Islands: Compendium of Strategies. Cool Pavements', *Epa*, pp. 1–23. doi: 10.1175/1520-0450(2002)041<0792:THFIUA>2.0.CO;2.

Vardoulakis, S. *et al.* (2014) 'Modelling air quality in street canyons : a review To cite this version : HAL Id : ineris-00961872'.

Yaghoobian, N. and Kleissl, J. (2012) 'Effect of reflective pavements on building energy use', *Urban Climate*. doi: 10.1016/j.uclim.2012.09.002.

Zhou, D. *et al.* (2014) 'Surface urban heat island in China's 32 major cities: Spatial patterns and drivers', *Remote Sensing of Environment*. Elsevier Inc., 152, pp. 51–61. doi: 10.1016/j.rse.2014.05.017.

Natural Language Generation from Building Information Models for Intelligent NLP-based Information Extraction

Ning Wang, Raja R.A. Issa
University of Florida, United States
n.wang@ufl.edu, raymond-issa@ufl.edu

Abstract. As more data is aggregated in building information models during the project preconstruction and construction phase, further use of the building information to support building construction, operation, and maintenance activities becomes important. For the reuse of information from the BIM models, this study aims to develop an automated information extraction method to process the data from BIM/IFC models into an NLP-based data representation to generate natural human language for BIM users who can understand BIM data easily. A prototype application is developed to validate the developed method using several BIM/IFC models. The results indicate that the developed information extraction (IE) method is valid for processing the BIM data into an NLP-based natural language representation for BIM users. The contributions of this study will serve as a basis for intelligent BIM information extraction and the further use of BIM data within different domains of interest.

1. Introduction

One of the major goals of Building Information Modeling (BIM) is to support data interoperability between different knowledge domains. Inefficient data interoperability costs the facilities industry around $15.8 billion annually (Gallaher et al., 2004). BIM aims to provide information support to on-site and off-site construction practitioners, such as project managers, estimators, and inspectors. A BIM system is developed to extract relevant project and building information for those construction practitioners to solve the data interoperability issue within the Architecture, Engineering, Construction, and Operations (AECO) industry. However, the outcomes of the current information extraction from BIM models are limited to a data spreadsheet, an information list, and other data representations which are difficult to be understood by BIM users who have limited BIM experience. One of the major challenges of current information extraction (IE) research is how to extract building information from BIM and transform the building information into semantic logic-based representation (Zhang and El-Gohary, 2015). Moreover, existing BIM IE efforts are limited in generating natural human language which can be easily understood by BIM practitioners.

In the Fourth Industrial Revolution (Industry 4.0), Artificial Intelligence (AI) has become more and more popular in the AECO industry, and AI provides more opportunities for improving the productivity and performance in the construction industry (Darko et al., 2020; Patrício and Rieder, 2018). AI aims to make a computing machine think and reason like a real human (Studer et al., 1998). According to Sacks et al (2018), AI BIM will become a trend in the future. Natural language processing (NLP), as a part of AI applications, is used to enable a machine to imitate natural human language capabilities and is used to build a virtual assistant to support human activities in daily life (e.g. Siri). A virtual assistant for a BIM system aims to provide knowledge and information support for construction practitioners. In order to build such a virtual assistant for a BIM system, an NLP-based IE framework is necessary and indispensable. An intelligent NLP-based BIM information extraction framework requires: (1) recognizing the natural human language and transforming it into a machine-readable request (i.e. natural language understanding); (2) retrieving or locating relevant structure building data from BIM data repository, according to the above request or query; and (3) transforming the requested structured building data or information into an NLP-based text data structure to generate natural human language which can be easily understood by BIM users (i.e. natural language generation). In order to easily understand the information or data extracted from BIM models, the knowledge or information representation for the BIM data structure is necessary. Natural language generation (NLG) is an application of syntactic NLP, which aims to transform structured data into the natural language for mimicking human language capabilities, which is the foundation of corpus linguistics for a virtual assistant for BIM.

This study aims to develop an automated NLP-based BIM information extraction (IE) method to generate natural human language for the intelligent BIM IE framework, and the outcomes are in the format of language sentences stored in a text file that can easily be understood by BIM users. To achieve this goal, this study started with a literature review to explain all terminology and background knowledge used in this study and state of the art of research on IE. Based on the literature review, an automated NLP-based BIM IE methodology was used. The developed methodology utilized the Industry Foundation Classes (IFC) data format as the information repository for BIM models, which is a widely supported specification in the AECO industry. The advantages of the BIM/IFC models are that they are open-source and easily accessible like a text file. The BIM/IFC information is extracted by the developed methodology, by implementing IfcOpenShell, an IFC API (application programming interface), to access data from an IFC file because the IFC file can be read by the IFC API for the purpose of the high efficiency of data read and information organization. An algorithm is designed in this study to transform the structured BIM/IFC data into the NLP-based natural language representation. A python-based prototype application was developed to validate the developed methodology by using sample and actual BIM/IFC architectural models. A comparison was conducted to demonstrate the differences between the developed NLP-based IE method and existing IE. The proposed automated NLP-based BIM IE methodology is the foundation for developing the virtual assistant for a BIM system.

2. Literature Review

2.1 Artificial Intelligence and Natural Language Processing

Al is "the ability of a digital computer or computer-controlled robot to perform tasks commonly associated with intelligent beings" (Copeland, 2019). AI research was born in 1956, in general, and the research on AI for the AECO industry started from the 1970s (Darko et al., 2020). The applications and research of AI are becoming more and more popular in the AECO industry. Current research and utilization of AI in the construction management and engineering area are mostly focused on project management, construction engineering, entity and activity recognition, and estimation and cost control (Chao et al., 2018). Since BIM can be used along the whole life cycle of a construction project, the application of AI on BIM can facilitate the performance and efficiency of the information exchange during different stages of project management. AI-based applications are a future trend of BIM research and development (Sacks et al., 2018).

NLP, as a part of AI applications, aims to process natural language which enables a machine to mimic human language capabilities (Cherpas, 1992; Zhang and El-Gohary, 2015). The major research on NLP is focused on semantic features and syntactic rules and structures within a sentence of natural human language. Ontology is widely used to share a common understanding of the domain knowledge between different information systems for the semantic NLP process of natural human language and knowledge representation (Studer et al., 2007; Wu et al., 2019).

Since NLG is part of syntactic NLP, semantic NLP is not necessary for this study. NLG enables a machine to generate human language based on structure and machine-readable data, and the syntactic sentence structure is the key to NLG. The underlying sentence structure of natural human language in English is the subject-verb-object (S-V-O) syntactic word order. The S-V-O structure is one of the predominant word orders in the languages of the world, and other languages, such as Spanish, French, Cantonese, and colloquial Egyptian Arabic languages, also follow the S-V-O structure (Celce-Murcia et al., 1999).

In linguistics, syntax defines the rules, principles, and processes in the structure of sentences. The categories of syntax in a sentence include noun (NN), determiner (Det), noun phrase (NP), adjective (ADJ), verb phrase (VP), verb (V), transitive verb (TV), ditransitive (DTV), sentential compliment verb (SV), adverb (Adv), preposition (P), and prepositional phrase (PP). A phrase structure is a fundamental ingredient to form the S-V-O sentence structure, and the phrase structure provides rules to demonstrate three indispensable parts of the S-V-O sentence structure. NP and VP are the two basic phrase structures to represent a sentence (i.e. NP + VP), in which NP stands for the subject and VP summarizes the verb and object parts. A grammar tree is utilized to visualize the phrase structure in a sentence. For example, Figure 1 illustrates an example sentence of "*The instance name of IfcWallStandardCase173 is Basic Wall:Exterior - Brick on CMU:354883.*" In this grammar tree, the root is the sentence (S), and there are several routes from the root to the leaves. The underlying phrase structure is the type of NP + VP, while forming a phrase structure is based on the end node, which are word types, such as noun (NN), determiner (Det), and preposition (P). The syntactic structure or sentence segmentation is the fundamental linguistic and grammatic basis for NLP (Lin et al., 2016; Wu et al., 2019). Therefore, this research implemented the phrase structure of NP + VP to process natural language, especially to generate natural human language based on the BIM/IFC model data.

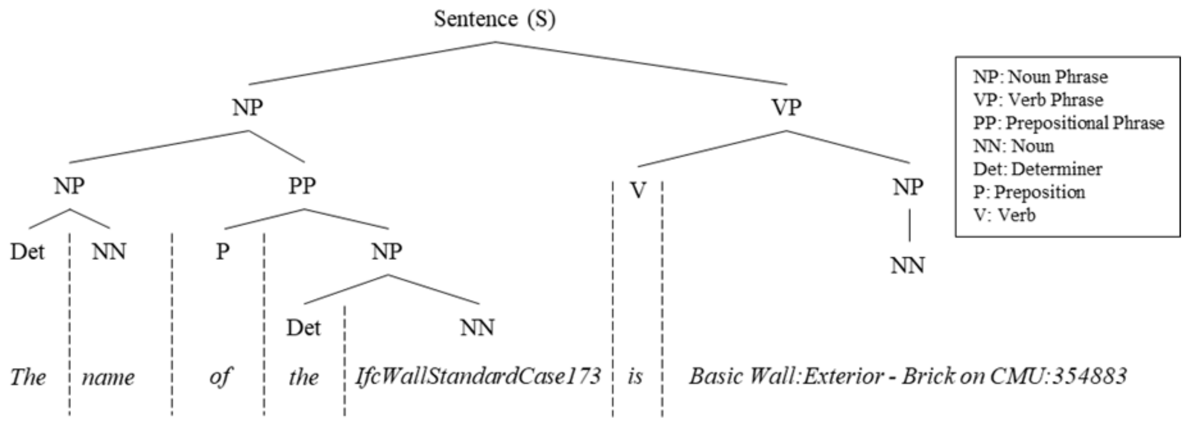

Figure 1: Grammar Tree: Phrase Structure in a Sentence

2.2 State of the Art of BIM Information Extraction

With the adoption of Information Technology in the AECO industry, BIM has become an indispensable and contributing factor for providing information support to construction practitioners. Industry Foundation Classes (IFC) is one of the most popular BIM data exchange formats for different BIM platforms in the AECO industry. BuildingSMART International proposed IFC as the international standard (ISO 16739) for BIM data format. IFC is based on the ISO-STEP (Standard for the Exchange of Product model data) EXPRESS data modeling language (buildingSMART, 2019). EXPRESS language is a product data specification language defined by ISO standard (ISO, 2004). The information in a BIM/IFC model can be accessed, checked, and freely modified without any license restrictions from software products.

As a result, any IFC file can be opened and edited by any free notepad-supported software. For these reasons, the BIM/IFC specification has become the most popular BIM file exchange medium for research use. Therefore, this study utilized IFC as the BIM data repository for NLG-based information extraction.

Building information searching and retrieval involve many time-consuming tasks (Sacks et al., 2018). Information extraction is one of the most important information support methods of BIM for practical construction use and research applications. The application areas of IE from BIM include model compliance check (Zhang and El-Gohary, 2016, 2015), model comparison (Ghang et al., 2011; Shi et al., 2018), information retrieval (IR) (Lin et al., 2016; Liu et al., 2016), partial model extraction (Jongsung et al., 2013; Zhang and Issa, 2013), data interoperability and integration (Karan et al., 2016; Nepal et al., 2013). The outcomes of current research and applications for BIM IE can be summarized into three categories: (1) spreadsheets which contain requested building information based on the different ontology domains; (2) partial BIM/IFC model codes for the purpose of sharing, visualizing and comparing; (3) organized and retrieved information representation and data structure for model checks, data interoperability, or information retrieval.

Research on the intelligent NLP-based information extraction from BIM, especially BIM NLG research, is limited. Some research used RDF (Resource Description Framework) and OWL (Web Ontology Language) as BIM/IFC repositories and SPARQL (SPARQL Protocol and RDF Query Language) as the query language to get relevant BIM data spreadsheet from the BIM RDF or OWL database for information retrieval (Karan et al., 2016; Liu et al., 2016; Studer et al., 2007). However, SPARQL and ontology structures are not easy to be understood for unexperienced construction personnel. Their methodology requires transforming data from BIM/IFC into an RDF or OWL database, which is a time-consuming and complicated process. Moreover, the storage size of an RDF or OWL file is much larger than its corresponding BIM/IFC file (buildingSMART, 2019; Krijnen and Beetz, 2018). Lin et al. (2016) proposed an NLP-based intelligent BIM framework for information retrieval. Their research utilized syntactic NLP as a tool to extract keywords from human language requests by natural language understanding (NLU). However, the outcome of their research on intelligent BIM IE is mainly in the format of spreadsheets and model visualization, instead of natural human language (i.e. NLG). Zhang and El-Gohary (2015) developed an automated IE from BIM transforming into semantic logic-based data representation for automated compliance checking (ACC) of BIM models. The methodology of their research was based on first-order logic (FOL), which is the most prominent and fundamental logical formalism for semantic NLP use. Their research outcome is a logic-based information representation, which is close to natural language. However, their IE is mainly for the use of ACC instead of intelligent IE, so the outcome is not considered as a natural language sentence but an information or data representation. An intelligent NLP-based IE method aims to mimic human language capabilities, including NLU and NLG. This study compared the proposed IE methodology with the research of Zhang and El-Gohary (2015), Lin et al. (2016) and Karan et al. (2016) in Section 4. The reason for comparing the proposed methodology with the aforementioned studies is that they focused on retrieval or extraction of requested information from BIM models, which is similar to the BIM information extraction in this study.

3. Methodology

The methodology for NLP-based BIM IE includes three major steps: (1) read information from BIM/IFC models, (2) transform IFC structure data to syntactic NLP-based natural language, and (3) write generated natural language into a text data file for storage. Figure 2 shows the main process of the methodology developed. The inputs of the methodology are IFC2x Edition 3 Technical Corrigendum 1 (IFC2x3 TC1) MVD (Model View definition) BIM/IFC models. In order to contain more semantic information about the building, the relevant IFC base quantity take-off data is exported from the BIM authoring tool (i.e. Autodesk Revit). The first step is to implement a read module to access information within the IFC file by using an IFC API. The read model aims to extract relevant IFC file data or IFC instance information. For example, the information of one instance of the *IFCWALLSTANDARDCASE* includes the *IFC instance ID, instance type, GlobalId, OwnerHistory, Name, Description, ObjectType, ObjectPlacement, Representation, Tag*, according to IFC2x3 schema (buildingSMART, 2020).

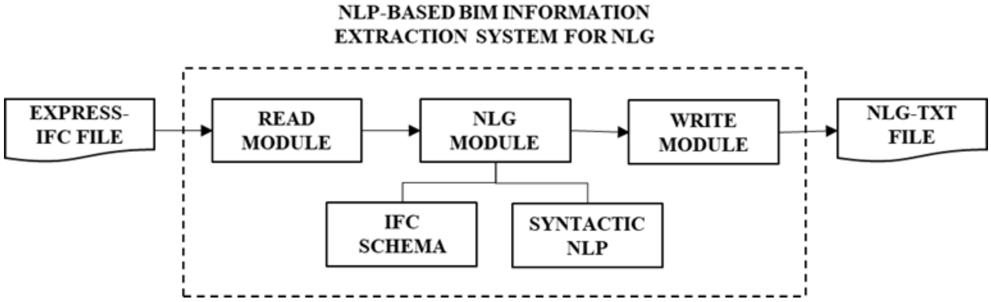

Figure 2: Developed Methodology

The second module aims to generate natural human language. After the information is read from each IFC instance, the corresponding NLG module is executed. The IFC schema is used to classify the types of IFC instances to generate natural language because the data structure of each IFC instance is different. For example, the data structure of *IFCPERSON* is "*#Instance ID = IFCPERSON*(*Id, FamilyName, GivenName, MiddleNames, PrefixTitles, SuffixTitles, Roles, Addresses*)", while that of *IFCORGANIZATION* is "*#Instance ID = IFCORGANIZATION*(*Id, Name, Description, Roles, Addresses*). In order to generate natural language, the attribute names of each IFC instance (e.g. *GlobalId*) are required. For example, the attribute name of "*GlobalId*" is required to generate the sentence of "*The* GlobalId *of the IfcWallStandardCase173 is 3XQgPac3bDUAgywXAYG0xW*". The IFC2x3 TC1 schema is complied with to get corresponding attribute names for each IFC instance. The NLG pattern is also based on the different data structures of each IFC instance. Table 1 shows the syntactic NLG pattern and NLG examples. The NLG pattern of the IFC header data is "Det NN V NN" based on the data structure of the header (e.g. * *Schema: IFC2X3*). The data structure of the IFC data part is "*#ID = IFC type (...);*" (e.g. *#1= IFCORGANIZATION($,'Autodesk Revit 2020 (ENU)',$,$,$);*), so the NLG pattern of the IFC data part is "Det NN P Det NN V NN" to generate natural language. In pattern P1, the X_1 is the instance name of one header data and the X_2 stands for the corresponding value. In pattern P2, *Y* represents the attribute name complied from IFC2x3 schema. X_1 is the combination of instance type and instance ID and X_2 is the corresponding attribute value. The rest of the NLG format is the preset language pattern shown in bold format.

Table 1: Syntactic NLG Pattern and Format

Pattern Number	IFC Type	NLG Pattern	NLG Format	NLG Example
P1	Header	Det NN V NN	**The** X_1 **is** X_2**.**	**The** *Schema* **is** *IFC2X3***.**
P2	Data	Det NN P Det NN V NN	**The** *Y* **of the** X_1 **is** X_2**.**	**The** *name* **of the** *IfcWallStandardCase173* **is** *Basic Wall:Exterior - Brick on CMU:354883***.**

Based on the syntactic NLP pattern and IFC schema, the NLG module converts the structured BIM/IFC data into natural human language for BIM practitioners to easily read and understand. The generated natural human language is written into an NLG-based text file, which is the outcome of the proposed methodology. However, the reference ID of natural language generated from each IFC instance is not easily understood by BIM users. For example, the value of *OwnerHistory* is a reference ID instead of a noun in an *IfcWallStandardCase* instance. Therefore, the referenced IFC instances are located by the proposed methodology for each IFC instance and the instance data is appended to the generated natural language sentence for users to understand necessary referenced information (e.g. *OwnerHistory*). Figure 3 shows the details BIM NLG algorithm. The first step is to input an IFC file and initialize all variables and generated language patterns. The type of IFC instance is an indispensable and contributing factor to determine the format of the NLG patterns. If the IFC instance belongs to the header part, pattern P1 is utilized to generate natural language. After getting the required instance name and value, the corresponding natural language sentence is generated and written into the outcome file. If the IFC instance is within the data part, the IFC schema is implemented to acquire the corresponding attribute names of the instance values. According to the type of each instance read from an IFC instance, the attribute names are located from the IFC schema by the algorithm. The natural human language sentences are generated based on the NLG pattern P2 and written into the text file for storage.

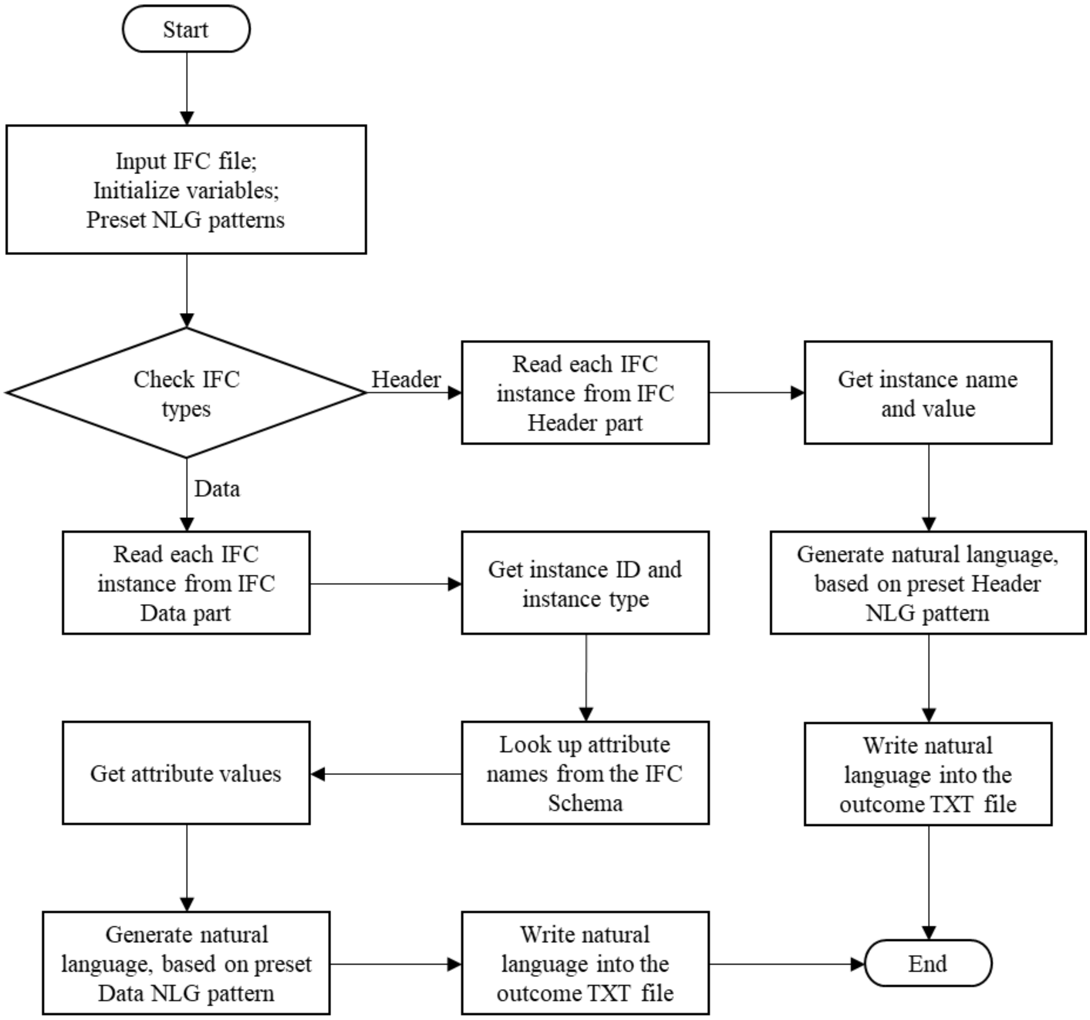

Figure 3: BIM NLG Algorithm

4. Results and Discussion

A python-based prototype application was developed based on the IfcOpenShell repository to validate the proposed research methodology. Three BIM/IFC sample models (i.e. sample model 1, IfcOpenHouse, VDC Center), and one actual architectural model (i.e. Rinker building) were utilized to validate the prototype application to reflect the efficiency and accuracy of the NLP-based IE algorithm. The computer used to validate the prototype application was an Intel i7-9700 CPU of 3.00 GHz with 8 cores and 32.0 GB RAM. The integrated development environment (IDE) was PyCharm 2019.3, and the python interpreter was python 3.5 distributed by Anaconda. The IfcOpenShell for python 3.5 was implemented to access and parse the input IFC file. Figure 4 illustrates the differences between input IFC data structure and outcome NLG-based natural language pattern via an example. According to syntactic NLP, each generated natural language sentence is mainly comprised of NP and VP phrase structures. In the NP part of generated natural language, the phrase structure is "the (attribute name) of the (instance name)". The attribute name was acquired from IFC2x3 TC1 schema, and the instance name was the combination of IFC instance type and instance ID. VP represents the verb phrase structure of "is (attribute value).", which is the rest of the generated natural language. The attribute value was attained via the IfcOpenShell. In the outcome NLG file, all reference IDs were converted into the corresponding IFC instances. Compared to the original input IFC file, the reference information from each IFC instance is much easier to be located by BIM users.

Input IFC:

```
ISO-10303-21;
HEADER;

/******************************************************************************************
...
* Database creation date:         Sun Feb 23 20:48:31 2020
* Schema:                         IFC2X3
...
******************************************************************************************/

DATA;
#1= IFCORGANIZATION($,'Autodesk Revit 2020 (ENU)',$,$,$);
#5= IFCAPPLICATION(#1,'2020','Autodesk Revit 2020 (ENU)','Revit');
...
#173= IFCWALLSTANDARDCASE('1kZG_d3tH6x9RIywCldq7U',#41,'Basic Wall:Exterior - Brick on CMU:354728',$,
'Basic Wall:Exterior - Brick on CMU',#142,#169,'354728');
...
```

⇩

Outcome NLG:

```
Header:
...
The database creation date is Sun Feb 23 20:48:31 2020.
The schema is IFC2X3.
...

Data:
The id of the IfcOrganization1 is None.
The name of the IfcOrganization1 is Autodesk Revit 2020 (ENU).
The description of the IfcOrganization1 is None.
The roles of the IfcOrganization1 is None.
The addresses of the IfcOrganization1 is None.
The applicationDeveloper of the IfcApplication5 is #1=IfcOrganization($,'Autodesk Revit 2020 (ENU)',$,$,$).
The version of the IfcApplication5 is 2020.
The applicationFullName of the IfcApplication5 is Autodesk Revit 2020 (ENU).
The applicationIdentifier of the IfcApplication5 is Revit.
...
The globalid of the IfcWallStandardCase173 is 1kZG_d3tH6x9RIywCldq7U.
The ownerhistory of the IfcWallStandardCase173 is #41=IfcOwnerHistory(#38,#5,$,.NOCHANGE.,$,$,$,1582508913).
The name of the IfcWallStandardCase173 is Basic Wall:Exterior - Brick on CMU:354728.
The description of the IfcWallStandardCase173 is None.
The objecttype of the IfcWallStandardCase173 is Basic Wall:Exterior - Brick on CMU.
The objectplacement of the IfcWallStandardCase173 is #142=IfcLocalPlacement(#129,#141).
The representation of the IfcWallStandardCase173 is #169=IfcProductDefinitionShape($,$,(#148,#166)).
The tag of the IfcWallStandardCase173 is 354728.
```

Figure 4: An example illustrating differences between input IFC and outcome NLG

The results indicated that the developed methodology is valid to generate natural human language. Table 2 illustrates the preliminary experimental results of the python-based prototype based on the presented research methodology. All BIM/IFC models were exported in the IFC2x3 TC1 schema from Autodesk Revit 2020. The test IFC files are from 16KB to 11MB to validate the response time and accuracy of the prototype application. For an IFC file with a small size of 16KB, the python program responded in 0.04s, while for a larger IFC file, the program can respond in 7.59s. The test results indicated that the developed python-based prototype application enabled the transformation of BIM/IFC EXPRESS data into NLG-based natural human language within 10s. The prototype application can quickly respond to the IFC-NLG transformation process. The measurement of accuracy was to compare the numbers of lines of the generated natural language sentences with the total numbers of all attribute values from the IFC file, which was conducted within the python program. The preliminary experimental results indicated that the proposed generation methodology of natural human language from BIM IFC data was accurate.

Table 2: Preliminary Experimental Results

Results	**Sample Model 1**	**IfcOpenHouse Model**	**Rinker Building Model**	**VDC Center Model**
IFC file size	16KB	102KB	10MB	11MB
Number of lines	260	2,700	195,397	207,448
NLG-TXT file size	71KB	399KB	37MB	42MB
Number of generated lines	939	4,358	299,725	359,389
Accuracy	100%	100%	100%	100%
Response time	0.04s	0.21s	6.89s	7.59s

A comparison between the developed methodology and the existing IE approaches was conducted to show the differences (see Table 3). Although those studies were not focused on generating natural human language from BIM models, their aim was to extract building information from BIM systems which is similar to this study. The developed methodology used IFC file as the BIM data repository which can save more storage space than other databases (DB) and OWL/RDF formats. The BIM/IFC API was implemented in this study for the purpose of higher efficiency of data read and better information organization, compared to a direct read from IFC files. The proposed methodology is mainly focused on syntactic NLP to generate natural human language, while some research utilized semantic NLP to generate different information representations. The final outcome of the NLP-based IE algorithm is natural human language sentences, while other research utilized different BIM information representations for the purposes of model checks (Zhang and El-Gohary, 2015), information retrieval (Lin et al., 2016), or data interoperability and integration (Karan et al., 2016). However, the format of natural language sentences is the foundation of corpus linguistics for the intelligent NLP-based BIM IE framework. In order to build a virtual assistant for BIM, the generation of natural human language is necessary. The proposed methodology for IFC to NLG still has limitations. The generated natural human language sentences are focused on the data representation of the fundamental data of IFC instances, which means the proposed NLG methodology aims to transform each line from the IFC file into natural human language, instead of summarizing the information acquired from the BIM/IFC model into sentences. In some cases, the summary information is required by BIM users, for example, to acquire the total numbers of walls with a specified name or total floor height, while the proposed methodology was designed to provide the basic data, such as descriptions and object types of the requested wall. To illustrate the summarization information or to generate summarized natural human language is also a future research direction of this study.

Table 3: Comparison between Proposed IE and Other related IE

Categories	Proposed Methodology	Zhang and El-Gohary (2015)	Lin et al. (2016)	Karan et al. (2016)
Input	IFC	IFC	IFC	IFC
BIM Repository Type	IFC	IFC	MongoDB (IFC Serialization)	OWL/RDF
BIM Repository Size	Standard	Standard	Much Larger than Standard	Much Larger than Standard
BIM/IFC API	Yes (IfcOpenShell)	Yes (JSDAI)	Yes (MongoDB)	Not Necessary
Semantic NLP	Not Necessary	Yes (FOL)	Yes (NLU)	Not Necessary
Syntactic NLP	Yes (NLG)	Not Necessary	Yes (NLU)	Not Necessary
Outcome	Natural Language	Data Representation (Logic Facts)	Spreadsheets Model Visualization	Spreadsheets

5. Conclusion

A virtual assistant for BIM aims to provide comprehensive information support for construction practitioners via extracting relevant project and building information. Most existing IE methods require BIM users possessing necessary BIM knowledge and experience, but BIM involves users from different domains of interest and many construction practitioners with limited BIM experience require BIM information support for their daily construction and operation activities. The representation in natural human language makes it easier for those BIM users to understand BIM information and data, but previous BIM IE research has been limited to provide natural human language. An intelligent BIM IE framework aims to generate such natural human language based on original and raw BIM data. Therefore, this study developed a methodology to transform the structured BIM/IFC building information into NLP-based natural human language for BIM users to easily understand BIM information. The initial results indicated that the developed prototype was valid for generating natural language based on extracted BIM/IFC information, and very efficient and accurate. The outcomes of this study are the foundation of corpus linguistics for the NLP-based intelligent BIM IE framework. It is expected that the developed methodology would lead to the improvement of Artificial Intelligence in the AECO industry. The developed methodology still has limitations to generate natural language sentences with summarization information. The future direction of this study aims to refine the developed methodology for the NLP-based intelligent BIM IE framework and enrich the generated natural language sentences to contain more information regarding the BIM models.

References

buildingSMART, 2020. IFC Specifications Database [WWW Document]. URL https://standards.buildingsmart.org/IFC/RELEASE/IFC2x3/TC1/EXPRESS/IFC2X3_TC1.exp (accessed 6.10.19).

buildingSMART, 2019. Industry Foundation Classes (IFC) [WWW Document]. URL https://technical.buildingsmart.org/standards/ifc (accessed 6.10.19).

Celce-Murcia, M., Larsen-Freeman, D., Williams, H.A., 1999. The grammar book : an ESL/EFL teacher's course., 2nd ed. ed. Heinle & Heinle.

Chao, X., Yang, L., Amin, A., 2018. Bibliometric Review of Artificial Intelligence (AI) in Construction Engineering and Management, in: International Conference on Construction and Real Estate Management 2018, Proceedings. pp. 32–41. https://doi.org/doi:10.1061/9780784481721.004

Cherpas, C., 1992. Natural language processing, pragmatics, and verbal behavior. Anal. Verbal Behav. 10, 135. https://doi.org/10.1007/bf03392880

Copeland, B.J., 2019. Artificial intelligence [WWW Document]. Encycl. Br. URL https://www.britannica.com/technology/artificial-intelligence (accessed 12.1.19).

Darko, A., Chan, A.P.C., Adabre, M.A., Edwards, D.J., Hosseini, M.R., Ameyaw, E.E., 2020. Artificial intelligence in the AEC industry: Scientometric analysis and visualization of research activities. Autom. Constr. 112, 103081. https://doi.org/10.1016/J.AUTCON.2020.103081

Gallaher, M.P., O'Connor, A.C., John, L., Dettbarn, J., Gilday, L.T., 2004. Cost Analysis of Inadequate Interoperability in the U.S. Capital Facilities Industry. Natl. Inst. Stand. Technol. U.S. Department of Commerce Technology Administration, Gaithersburg, MD.

Ghang, L., Jongsung, W., Sungil, H., Yuna, S., 2011. Metrics for Quantifying the Similarities and Differences between IFC Files. J. Comput. Civ. Eng. 25, 172–181. https://doi.org/10.1061/(ASCE)CP.1943-5487.0000077

ISO, 2004. ISO 10303-11:2004 Industrial automation systems and integration — Product data representation and exchange — Part 11: Description methods: The EXPRESS language reference manual [WWW Document]. URL https://www.iso.org/standard/38047.html (accessed 2.17.20).

Jongsung, W., Ghang, L., Chiyon, C., 2013. No-Schema Algorithm for Extracting a Partial Model from an IFC Instance Model. J. Comput. Civ. Eng. 27, 585–592. https://doi.org/10.1061/(ASCE)CP.1943-5487.0000320

Karan, E.P., Irizarry, J., Haymaker, J., 2016. BIM and GIS Integration and Interoperability Based on Semantic Web Technology. J. Comput. Civ. Eng. 30, 04015043-1-04015043–11. https://doi.org/10.1061/(asce)cp.1943-5487.0000519

Krijnen, T., Beetz, J., 2018. A SPARQL query engine for binary-formatted IFC building models. Autom. Constr. 95, 46–63. https://doi.org/10.1016/j.autcon.2018.07.014

Lin, J., Hu, Z., Zhang, J., Yu, F., 2016. A Natural-Language-Based Approach to Intelligent Data Retrieval and Representation for Cloud BIM. Comput. Civ. Infrastruct. Eng. 31, 18–33. https://doi.org/10.1111/mice.12151

Liu, H., Lu, M., Al-Hussein, M., 2016. Ontology-based semantic approach for construction-oriented quantity take-off from BIM models in the light-frame building industry. Adv. Eng. Informatics 30, 190–207. https://doi.org/10.1016/j.aei.2016.03.001

Nepal, M.P., Sheryl, S.-F., Rachel, P., Jiemin, Z., 2013. Ontology-Based Feature Modeling for Construction Information Extraction from a Building Information Model. J. Comput. Civ. Eng. 27, pp. 555–569. https://doi.org/10.1061/(ASCE)CP.1943-5487.0000230

Patrício, D.I., Rieder, R., 2018. Computer vision and artificial intelligence in precision agriculture for grain crops: A systematic review. Comput. Electron. Agric. 153, pp. 69–81. https://doi.org/10.1016/J.COMPAG.2018.08.001

Sacks, R., Eastman, C.M., Teicholz, P.M., Lee, G., 2018. BIM handbook : a guide to building information modeling for owners, designers, engineers, contractors, and facility managers, Third edit. ed. John Wiley & Sons, Inc., Hoboken, New Jersey.

Shi, X., Liu, Y.S., Gao, G., Gu, M., Li, H., 2018. IFCdiff: A content-based automatic comparison approach for IFC files. Autom. Constr. 86, pp. 53–68. https://doi.org/10.1016/j.autcon.2017.10.013

Studer, R., Abecker, A., Grimm, S., 2007. Semantic Web Services: Concepts, Technologies, and Applications, Springer e-books. Springer, Berlin.

Studer, R., Benjamins, V.R., Fensel, D., 1998. Knowledge Engineering: Principles and methods. Data Knowl. Eng. 25, pp. 161–197. https://doi.org/10.1016/S0169-023X(97)00056-6

Wu, S., Shen, Q., Deng, Y., Cheng, J., 2019. Natural-language-based intelligent retrieval engine for BIM object database. Comput. Ind. 108, pp. 73–88. https://doi.org/10.1016/J.COMPIND.2019.02.016

Zhang, J., El-Gohary, N.M., 2016. Extending Building Information Models Semiautomatically Using Semantic Natural Language Processing Techniques. J. Comput. Civ. Eng. 30, pp. 331–346. https://doi.org/10.1061/(ASCE)CP.1943-5487.0000536

Zhang, J., El-Gohary, N.M., 2015. Automated Extraction of Information from Building Information Models into a Semantic Logic-Based Representation, in: Computing in Civil Engineering 2015. pp. 173–180. https://doi.org/10.1061/9780784479247.022

Zhang, L., Issa, R.R.A., 2013. Ontology-Based Partial Building Information Model Extraction. J. Comput. Civ. Eng. 27, 576–584. https://doi.org/10.1061/(asce)cp.1943-5487.0000277

A Deep-Learning Method for Evaluating Semantically-Rich Building Code Annotations

Ruichuan Zhang, Nora El-Gohary
University of Illinois at Urbana-Champaign, USA
rzhang65@illinois.edu

Abstract. Existing automated code checking (ACC) methods require the extraction of requirements from building codes and the representation of these requirements in a computer-processable form. Although these methods have achieved different levels of performance, all of them are still unable to represent all types of building-code requirements. There is, thus, a need to enhance the semantic representations of building codes towards facilitating the representation of all requirements. To address this need, this paper first proposes a new approach to annotate and represent building-code sentences using requirement units that consist of semantic information elements and simple logic operators. To evaluate the proposed building-code annotation approach, this paper also proposes a new natural language generation (NLG)-based method for evaluating annotation quality. The proposed method consists of four steps: data preparation, data preprocessing, NLG model development and training, and sentence evaluation. Sentences from the International Code Council (ICC) building codes were used in the evaluation.

1. Introduction

To reduce the time, cost, and errors of compliance checking, various automated code compliance checking (ACC) systems have been developed and implemented. Most of the existing ACC systems require the extraction of requirements from building-code sentences and the conversion of the extracted requirements into a semantic representation. Semantic representations of building codes aim to represent the natural language requirements in computer processable forms. Different semantic representations of requirements have been developed in the construction domain for supporting compliance checking. Examples of semantic representations proposed in research efforts include the requirement, applicability, selection and exception (RASE) semantic markups proposed by Hjelseth and Nisbet (2011), the semantic information elements proposed by Zhang and El-Gohary (2013), and the visual language for compliance checking proposed by Preidel and Borrmann (2016). Examples of semantic representations used in commercial ACC applications include the predefined templates used in the Solibri Model Checker and the hardcoded building-requirements in the SMARTreview.

However, two knowledge gaps still exist. First, although existing ACC methods and applications have achieved different levels of automation, representativeness, and accuracy, they are still unable to represent all building-code requirements. For example, the RASE markups can be used to annotate nested clauses and exceptions in building-code sentences, but cannot represent "requirements that include alternatives and preferences" (Hjelseth and Nisbet 2011). Similarly, the predefined templates in Solibri Model Checker can only represent a limited number of requirements in a few building codes, such as the clearance requirements in the Standards for Accessible Design by Americans with Disabilities Act, and the dimension requirements in the International Building Code (IBC). There is, thus, a need to enhance the semantic representations or annotations of building codes towards facilitating the representation of all requirements. Second, most of the existing semantic representations were developed without sufficient evaluation in terms of their representativeness of building-code regulatory information. There is a lack of well-defined quantitative metrics and methods for evaluating the semantic representations and/or annotations of building codes.

To address the first knowledge gap, this paper proposes a new approach to annotate and represent building-code sentences using requirement units that consist of semantic information elements and simple logic operators. To address the second gap and evaluate the proposed annotation approach, this paper then proposes a natural language generation (NLG)-based method for evaluating annotation quality, where the building-code annotations are first used to generate new building-code sentences, and then the comprehensibility of the generated sentences are evaluated. Two metrics were used to evaluate the comprehensibility of the generated building-code sentences: bilingual evaluation understudy (BLEU) and recall-oriented understudy for gisting evaluation (ROUGE).

2. Background

2.1 Natural Language Generation

Natural language generation (NLG) is the process of representing the semantic information contained in the input data – which could be in various forms such as tables, images, or formal languages – in the form of natural language for the purpose of information digestion and communication (Arria NLG 2020). NLG plays a core role in many intelligent systems and applications such as spoken dialogue systems (Wen et al. 2015), image captioning (You et al. 2016), and business intelligence dashboards (Arria NLG 2020).

NLG methods range from template, rule, and heuristic-based methods to recent deep learning-based methods. Template, rule, and heuristics-based methods rely on manually-developed templates and rules to fill in the templates. Examples of template-based systems in the construction domain include the web-based document management system proposed by Ryoo et al. (2010); and commercial software such as e-Specs (Avitru 2018) and BIMdrive (Digicon 2018), which use premade templates (e.g., templates based on the National Master Specifications) to facilitate the development and maintenance of construction specifications. Deep learning-based methods use deep neural networks to automatically learn the syntactic and semantic patterns in the input data, which are later used to generate new text (e.g., semantically conditioned deep neural network-based text generation approach by Wen et al. 2015).

2.2 Deep Learning

Deep learning methods use computational models such as deep neural networks to learn multiple levels of information representations from large-scale data (LeCun et al. 2015). Deep learning methods have drastically improved the state-of-the-art performance in the natural language processing domain, and have eliminated a lot of the manual effort in feature engineering compared to traditional machine learning methods. In the construction domain, deep learning methods have been used to solve text analysis problems such as building-code requirement extraction (Zhang and El-Gohary 2019), building information modeling log data mining (Pan and Zhang 2020), and regulatory document semantic analysis (Zhang and El-Gohary 2020).

The most commonly used deep neural networks for dealing with sequential data such as text data are recurrent neural networks (RNNs). RNNs have recurrent connections between neurons in the neural networks to cycle the input information in order to learn the patterns of sequential data (Mikolov et al. 2010). To tackle the shortcoming of original RNNs, which is being less capable and less computationally efficient to learn from long-term dependencies in the sequential data, variants of RNNs have been designed and adopted such as long short term memories (LSTMs) and gated recurrent units (GRUs).

3. Proposed Approach to Annotate Building-Code Sentences for Supporting Automated Compliance Checking

This paper proposes a new approach to annotate building-code sentences using requirement units. Each requirement unit consists of semantic information elements and simple logic operators. The semantic information elements include the essential semantic information elements proposed by Zhang and El-Gohary (2013), as shown in Table 1, in addition to a new element, "subject relation", which describes a relation between two subjects in one requirement unit. The simple logic operators include conjunction (e.g., "and"), disjunction (e.g., "or"), and negation (e.g., "not"). Each requirement unit describes a requirement or condition on a subject and/or a compliance checking attribute, or a pair of subjects, and thus is easily processable by most of the existing semi-automated or automated compliance checking applications and systems. Figure 1 shows an example building-code sentence that is annotated with requirement units.

Table 1: Essential semantic information elements for representing requirements for compliance checking purposes (Zhang and El-Gohary 2013).

Semantic information element	Definition
Subject	An ontology concept representing a thing (e.g., building element) that is subject to a particular requirement
Compliance checking attribute	An ontology concept representing a specific characteristic of a "subject" that is checked for compliance (e.g., width)
Quantitative relation	A term/phrase that defines the type of relation for the quantity (e.g., extend)
Deontic operator indicator	A term/phrase that indicates the deontic type of the requirement (i.e., obligation, permission, or prohibition)
Comparative relation	A term/phrase for comparing quantitative values, including "greater than or equal to," "greater than," "less than or equal to," "less than," and "equal to"
Quantity value	A numerical value that defines the quantity
Quantity unit	The unit of measure for a "quantity value"

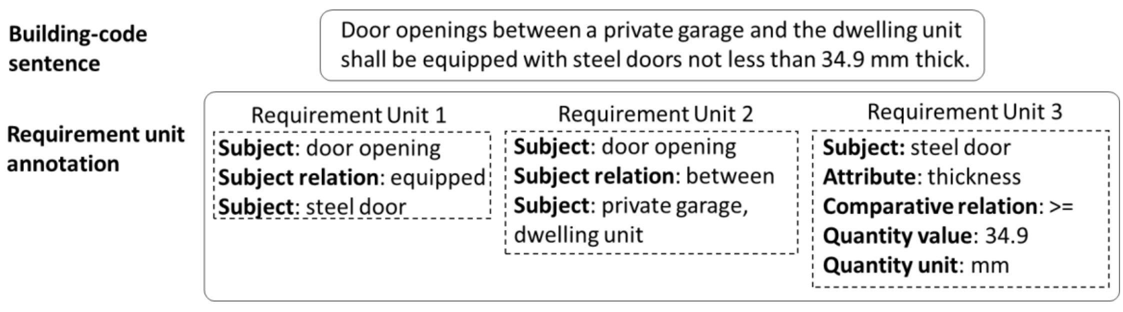

Figure 1: Example of Proposed Building-Code Sentence Annotations with Requirement Units

4. Proposed Deep Learning Natural Language Generation Method for Evaluating the Proposed Building-Code Annotation Approach

To evaluate the proposed building-code annotation approach, this paper proposes a deep learning natural language generation (NLG) method for evaluating annotation quality, where the annotations are first used to generate new sentences, and then the comprehensibility of the generated sentences are evaluated. The proposed method consists of four main steps (as per Figure 2): (1) preparing the training and testing data (i.e., pairs of natural language building-code sentence and the corresponding annotations); (2) preprocessing the data; (3) developing and training the deep learning model for generating building-code sentences; and (4) evaluating the comprehensibility of the generated building-code sentences using two sets of metrics: bilingual evaluation understudies (BLEU) and recall-oriented understudies for gisting evaluation (ROUGE).

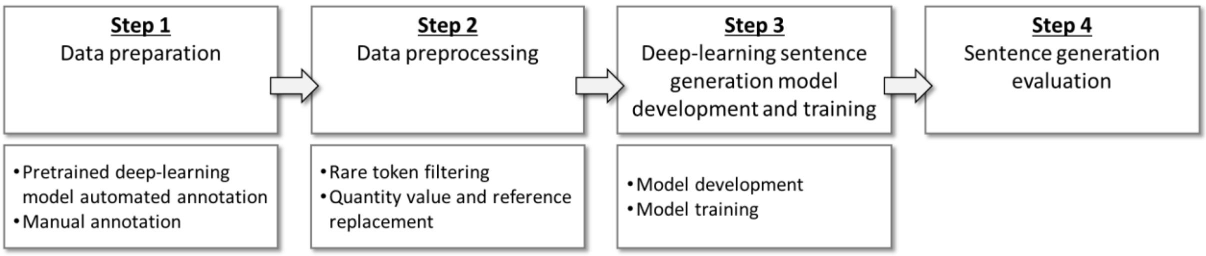

Figure 2: Proposed Deep Learning Natural Language Generation (NLG) Method for Evaluating the Proposed Building-Code Annotations

4.1 Data Preparation

Two datasets were used for training and testing the deep-learning building-code sentence generation model, which were annotated using two different methods. For training, to reduce the human effort, a relatively large dataset of sentences was collected and automatically annotated using a pretrained deep-learning model. For testing, a smaller dataset was collected and manually annotated by human annotators.

Automated Annotation of Training Data Using Pretrained Deep-Learning Model. A total of 80,000 sentences were collected from multiple regulatory documents including the International Energy Conservation Code, the International Residential Code, and the American National Standards for Accessible and Usable Buildings and Facilities. The pretrained deep information extraction model by Zhang and El-Gohary (2020) was used to automatically annotate the dataset with the proposed annotations.

Manual Annotation of Testing Data. A total of 100 sentences were collected from multiple chapters of the IBC 2009 and the Champaign 2015 IBC Amendments. The sentences were manually annotated by three different annotators.

4.2 Data Preprocessing

To further improve the quality of the training data and the robustness of the deep-learning sentence generation model, two data preprocessing steps were conducted: rare-token filtering, and quantity value and reference replacement.

Rare-Token Filtering. To reduce the effect of the noise in the training data, and to improve the model's ability to deal with words that are missing from the training data, rare tokens were filtered. First, the token frequencies in the entire corpus of building-code sentences were counted. Then, the tokens with frequencies less than the threshold were replaced by the single missing-word token.

Quantity-Value and Reference Replacement. Quantity values share similar semantic and syntactic patterns, and so do references (e.g., the index of a chapter, table, or building code). Thus, two single tokens, “quantity value” and “reference”, were used to replace tokens annotated as quantity values and tokens annotated as references, respectively, aiming to reduce the number of parameters to be learned in the sentence generation model and thus the possibility of overfitting.

4.3 Deep-Learning Sentence Generation Model Development and Training

The sequence to sequence (Seq2Seq) model (Sutskever et al. 2014) was modified and trained to automatically generate the sentences based on the building-code annotations.

Model Development. The Seq2Seq model consists of two main parts: the encoder and the decoder, each consisting of several components, as illustrated in Figure 3. The encoder transforms the input (i.e., the sequence of annotated input words) into a vector representation, which captures the syntactic and semantic information of the entire input word sequence. The encoder consists of two components: the embedding layer for vectorizing the input words, and at least one LSTM layer. The decoder further transforms the vector representation generated by the encoder into the output word sequence. The decoder consists of two components: at least one LSTM layer, and the output layer for making final word prediction and thus generating the sentence.

The LSTM layers in both the encoder and the decoder aim to learn the feature representations that capture the semantic and syntactic information of the words. Each LSTM layer consists of several stacked LSTM units – each computing the feature representations based on the input information fed to the current LSTM unit, and the information propagated from the last LSTM unit so that the information from previous words could be captured. To improve the ability of the LSTM layer to deal with long-term dependencies in the building-code sentences, the bidirectional architecture was used – both the forward and backward LSTM units were considered when learning the feature representations (Huang et al. 2015). To determine the best model size for the specific training data used and the specific building-code sentence generation task, models with three different depths were tested: shallow (one LSTM layer in each of the encoder and the decoder), medium (two LSTM layers in each of the encoder and the decoder), and deep (four LSTM layers in each of the encoder and the decoder).

Model Training. Perplexity was minimized to train the deep learning model and obtain the optimal model parameters. Perplexity is defined as the inverse probability of the corpus (e.g., a group of sentences) given a language model (e.g., the Seq2Seq model), normalized by the number of words in the corpus (Jurafsky and Martin 2014).

Several training strategies were adopted. For improving computational efficiency, the training was stopped at 20 epochs or when the change of the perplexity between two consecutive training epochs was smaller than a threshold. For improving the sentence generation performance, the training practices suggested by Sutskever et al. (2014) were followed, including uniform initialization of the model parameters and gradually decreasing the model learning rate. The model was implemented in Python 3, and was run on top of Pytorch.

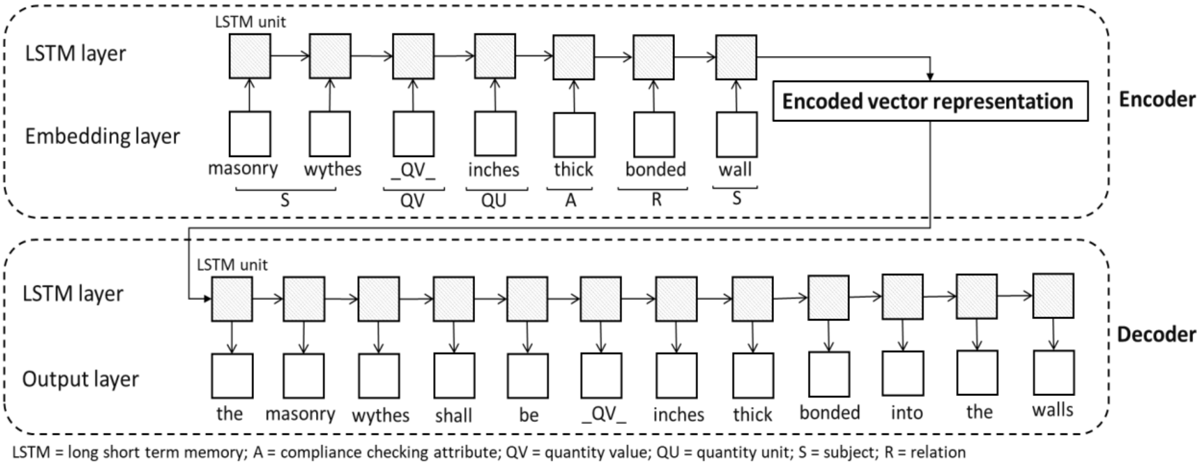

Figure 3: Sequence to Sequence (Seq2Seq) Model for Automatically Generating Building-Code Sentences

4.4 Evaluation of Generated Sentence

Two metrics were used to evaluate the comprehensibility of the generated building-code sentences: bilingual evaluation understudy (BLEU) and recall-oriented understudy for gisting evaluation (ROUGE).

BLEU is defined as the correspondence between the machine-generated text and the gold standard text (Papineni 2002), where p_n is the precision computed based on a contiguous sequence of n words, w_n is the weight corresponding to p_n, N is the longest sequence considered in calculating the metric, and c is a predefined scaling factor. BLEU_1 and BLEU_2 were used in this evaluation. A high BLEU indicates that the generated sentences correspond to the original sentences and thus the annotations used to generate these sentences are able to capture the semantics of the original sentences.

$$\text{BLEU}_N = c \exp\left(\sum_{n=1}^{N} w_n \log p_n\right)$$

ROUGE is defined as the overlap between the machine-generated text and the gold standard text (Lin 2004), where r_n is the recall computed based on a contiguous sequence of n words, w_n is the weight corresponding to r_n, and N is the longest sequence considered in calculating the metric. ROUGE_1 and ROUGE_2 were used in this evaluation. A high ROUGE indicates that the generated sentences overlap with the original sentences and thus the annotations used to generate these sentences are able to capture the semantics of the original sentences.

$$\text{ROUGE}_N = \sum_{n=1}^{N} w_n r_n$$

5. Preliminary Experimental Results

For the preliminary experiments, the size of the LSTM layers in the sentence generation model was set as 500, the dropout rate was set as 0.2, and the maximum length of the input data was set as 50. The sentence generation model optimization was performed using Adagrad, with a training data batch size of 64.

5.1 Comprehensibility with Different Types of Input Data

Two sentence generation models (of medium depth) were developed and used in the evaluation: one trained using data without preprocessing, and the other trained using preprocessed data. The evaluation results are shown in Table 2. The comprehensibility of the sentences was higher when the generation model was trained using preprocessed data, showing 4%, 3%, 3%, and 6% increase in $ROUGE_1$, $ROUGE_2$, $BLEU_1$, and $BLEU_2$, respectively. The results indicate that the two data preprocessing techniques adopted (rare-token filtering and quantity-value and reference replacement) help in generating more comprehensible building-code sentences by reducing the noise in the training data and increasing the robustness of the model.

Table 2: Comprehensibility (with medium-depth deep learning model) using different types of training data[1]

Type of training data	**ROUGE**		**BLEU**	
	$ROUGE_1$	**$ROUGE_2$**	**$BLEU_1$**	**$BLEU_2$**
Training data without data preprocessing	82%	75%	77%	67%
Training data with data preprocessing	**86%**	**78%**	**80%**	**73%**

[1]Bolded font indicates the highest performance.

5.2 Comprehensibility Using Deep-Learning Models of Different Depths

Three sentence generation models, with three different depths – shallow, medium, and deep – were developed and used in the evaluation. The evaluation results are shown in Table 3. The medium-depth model that has two LSTM layers each in the encoder and the decoder resulted in the highest comprehensibility, higher than the shallow-depth model by 6% in $ROUGE_1$, 5% in $ROUGE_2$, 3% in $BLEU_1$, and 3% in $BLEU_2$, and higher than the deep-depth model by 4% in $ROUGE_1$, 4% in $ROUGE_2$, 3% in $BLEU_1$, and 2% in $BLEU_2$. The results may indicate that the medium-depth model was most suitable for the size of the training data used – 80,000 samples, about 1,000,000 tokens. For much smaller/larger datasets or for a different type of text (e.g., different domains, different syntactic and semantic patterns, etc.), the other model depths could be used for evaluation.

Table 3: Comprehensibility with deep learning models of different depths (using preprocessed data)[1]

Deep learning building-code sentence generation model depth	**ROUGE**		**BLEU**	
	$ROUGE_1$	**$ROUGE_2$**	**$BLEU_1$**	**$BLEU_2$**
Shallow (one LSTM layer each in the encoder and the decoder)	80%	73%	77%	70%
Medium (two LSTM layers each in the encoder and the decoder)	**86%**	**78%**	**80%**	**73%**
Deep (four LSTM layers each in the encoder and the decoder)	82%	74%	77%	71%

[1]Bolded font indicates the highest performance.

5.3 Errors in Sentence Generation

Three main sources of sentence generation errors were identified based on an analysis of the experimental results. First, the building-code sentences that were used to create the training data were automatically annotated by a pretrained machine learning model, which did not achieve 100% accuracy and thus created annotation errors. Second, the building-code sentences were collected from multiple sources including text files crawled from webpages and converted from PDF files, and noise was added during the data crawling and conversion processes. Third, the building codes contain a significant amount of non-textual data such as tables and equations, some of which are difficult to be separated from the text and thus might have contaminated the building-code sentences used to create the training data.

6. Conclusions

This paper proposed a new building-code annotation approach and a new deep learning natural language generation (NLG)-based method for evaluating annotation quality, both for supporting automated checking. The annotation approach uses requirement units that consist of semantic information elements and simple logic operators. The annotation evaluation method, which was used to evaluate the proposed building-code annotation approach, first utilizes the annotations to generate new sentences, and then evaluates the comprehensibility of the generated sentences using BLEU and ROUGE. A $ROUGE_1$ of 86%, $ROUGE_2$ of 78%, $BLEU_1$ of 80%, and $BLUE_2$ of 73% were achieved when the medium-depth sentence generation model was used, which was trained on preprocessed data. These preliminary evaluation results indicate good comprehensibility of the sentences that were generated using the proposed annotations.

This paper contributes to the body of knowledge in four primary ways. First, the paper proposed a new building-code annotation approach for supporting automated compliance checking, which uses requirement units for coverage and simplification. Second, the paper proposed a new deep learning NLG-based method for evaluating building-code annotation quality, which helps provide a well-defined method and a set of quantitative metrics for evaluation. Third, the paper leverages large-scale unlabeled data to train the deep learning models by using a pretrained domain-specific sentence annotator, which greatly reduces the manual effort needed for creating labeled data. Fourth, the experimental results show that the data preprocessing techniques and the structure of the sentence generation model could affect the comprehensibility of the generated building-code sentences and thus affect the building-code annotation evaluation.

In their future work, first, the authors plan to improve the proposed building-code annotation approach by including more complex semantic relations such as exceptions and restrictions, in order to more accurately model the relations between requirement units. Second, the authors plan to improve the proposed deep learning NLG-based annotation evaluation method by improving the quality of the training data (e.g., using rule-based or machine learning-based preprocessing methods) and testing different sentence generation model architectures. Third, and most importantly, the authors plan to integrate the proposed annotation approach with a domain ontology to help improve the performance of existing automated compliance checking systems.

Acknowledgment

The authors would like to thank the National Science Foundation (NSF). This material is based on work supported by the NSF under Grant No. 1827733. Any opinions, findings, and conclusions or recommendations expressed in this material are those of the authors and do not necessarily reflect the views of the NSF.

References

Arria NLG, (2020). Arria NLG platform, https://www.arria.com/core-tech/core-tech-overview, accessed Feb 2020.

Avitru, (2018). Spec Editor, https://avitru.com/software/spec-editor, accessed May 2018.

Digicon Information Inc., (2018). BIMdrive Specification Management Software, http://www.digicon.ab.ca/services.aspx, accessed May 2018.

Hjelseth, E. and Nisbet, N. (2011). Exploring semantic based model checking. Proc. 2010 27th CIB W78 Int. Conf., http://itc.scix.net/data/works/att/w78-2010-54.pdf, accessed Feb 2020.

Huang, Z., Xu, W. and Yu, K. (2015). Bidirectional LSTM-CRF models for sequence tagging. arXiv preprint arXiv:1508.01991.

Jurafsky, D. and Martin, J.H. (2014). Speech and language processing (Vol. 3). US: Prentice Hall.

LeCun, Y., Bengio, Y. and Hinton, G. (2015). Deep learning. Nature. 521(7553), pp. 436.

Lin, C.Y. (2004). Rouge: a package for automatic evaluation of summaries. Proc. of ACL-04 Workshop. 8, pp. 74–81.

Mikolov, T., Karafiát, M., Burget, L., Černocký, J. and Khudanpur, S. (2010). Recurrent neural network based language model. Proc. of 11th Annual Conf. of ISCA. 2, pp. 1045–1048.

Pan, Y. and Zhang, L. (2020). BIM log mining: Learning and predicting design commands. Automat. Constr. 112, p.103107.

Papineni, K., Roukos, S., Ward, T. and Zhu, W.J. (2002). BLEU: a method for automatic evaluation of machine translation. Proc. 40th Annual Meeting on ACL. pp. 311–318.

Preidel, C. and Borrmann, A. (2016). Towards code compliance checking on the basis of a visual programming language. ITcon. 21(25), pp.402–421.

Ryoo, B.Y., Skibniewski, M.J. and Kwak, Y.H. (2010). Web-based construction project specification system. J. Comput. Civ. Eng. 24(2), 212–221.

Sutskever, I., Vinyals, O. and Le, Q.V. (2014). Sequence to sequence learning with neural networks. Adv. Neur. In. pp. 3104-3112.

Wen, T.H., Gasic, M., Mrksic, N., Su, P.H., Vandyke, D. and Young, S. (2015). Semantically conditioned lstm-based natural language generation for spoken dialogue systems. arXiv preprint arXiv:1508.01745.

You, Q., Jin, H., Wang, Z., Fang, C. and Luo, J. (2016). Image captioning with semantic attention. Proc. CVPR IEEE. pp. 4651–4659.

Zhang, J., and El-Gohary, N. (2013). Semantic nlp-based information extraction from construction regulatory documents for automated compliance checking. J. Comput. Civil Eng. 30(2), p.04015014.

Zhang, R., and El-Gohary, N. (2019). A machine learning-based approach for building code requirement hierarchy extraction. Proc. 2019 CSCE Annual Conf., Montreal, Canada.

Zhang, R., and El-Gohary, N. (2020). A Machine-Learning Approach for Semantically-Enriched Building-Code Sentence Generation for Automatic Semantic Analysis. Proc. 2018 ASCE CRC, Tempe, USA.

Compliance checking on building models with the Gherkin language and Continuous Integration

Dion Moult, Thomas Krijnen [1]
[1] Delft University of Technology
t.f.krijnen@tudelft.nl

Abstract. In this paper we document our approach on applying Behaviour-Driven Development (BDD) and Continuous Integration (CI) from the software industry to the construction sector. We have provided a freely available open software toolset for the application of rules in the Gherkin syntax to an IFC building model. A prominent aspect of BDD and contrary to mvdXML, the formalization of rules in plain-test human-readable scenarios provides a basis for collaborative formalization of rules among stakeholders. At the same time our approach includes imperative program code that is fully extensible to incorporate for example external data sources and geometrical reasoning. Runnings test on every model revision (the CI concept) as opposed to, for example, upon model delivery ensures a proactive approach to compliance. Reusing existing open source frameworks allowed us to build a comprehensive solution for continuous and automated model checking, visualization and reporting in several hundred lines of program code.

1. Introduction

The Industry Foundation Classes (IFC) cover a wide variety of subdomains in the construction industry and offer a considerable degree of freedom to modellers and implementers. Model View Definitions (MVD) can be used to formulate additional requirements on top of the rules and specifications defined in the IFC schema. The use of MVD is intended to specify requirements for certification purposes within the standardization organisation as well as requirements that are specific to individual projects or organizations. In short, it is assumed that if a model is delivered that complies with an MVD, it is fit for the purpose of a defined user.

Various MVDs are published as an international standard, four official standards for the IFC2X3 schema, and six standards for the IFC4 schema, four of which are still in draft form. Due to the limited publication, the current selection of MVDs do not account for the full variety of subdomains in the construction industry. Even within a published MVD standard, a recipient will often have different requirements compared to what is in the official standard. In addition, only one of these MVDs has an mvdXML available for distribution. Without a distributed mvdXML, it is complex to automatically validate deliverables against MVD requirements. Should the user wish to modify an MVD to their needs, they are required to modify the underlying mvdXML, or write their own.

The language to define MVD, mvdXML, has four main issues (a) the semantics are not precisely defined, (b) there is a variation in schemas and versions supported by tools, as such there is very limited interoperability, (c) the process of authoring mvdXML files is complex and requires extensive knowledge of the IFC schema, and (d) since the language is invented from scratch it's a large implementation effort for a vendor to implement support for mvdXML. Currently, the only free or open tool to compose mvdXML definitions is IfcDoc, which is not cross-platform. If an author wants to create their own mvdXML, this becomes problematic.

The published MVDs are primarily concerned with whether IFC entities are within the scope of a domain. Although possible within the mvdXML schema (using TemplateRules and in newer revisions of the standard: Constraints), the published MVDs do not help match attribute or parameter values to project-specific information requirements, which is often the priority to a recipient of a BIM model. Therefore, the published MVDs are not sufficient to establish whether a model produced with an MVD is fit for purpose.

Most of the published MVDs include a large portion of the IFC schema. As MVDs are also used for certification purposes, this requires vendors seeking certification to be able to support the import or export of a large portion of the schema. This complicates the certification process, and discourages the development of smaller, Unix-like, targeted tools that manipulate a specific subset of the IFC model, such as geometry, or asset management metadata. This requirement for a monolithic implementation acts as a barrier against smaller vendors attempting to enter the market.

Currently, buildingSMART, the standardisation organization behind IFC and mvdXML is contemplating to embrace more industry-standard tools1. This paper provides an exploration of the application of an industry standard tool in validation and testing of software. This is the Gherkin language as implemented in software tools (such as Cucumber, JBehave, Lettuce, Behat, and Behave) for Behaviour- or Test-Driven Development (BDD/TDD). BDD principles include to obtain a shared understanding of how the application should behave by means of conversation and concrete examples. The authors believe that this practice is just as relevant to building codes as it is to software.

2. State of the art

2.1 Schema languages

The IFC schema is published in the EXPRESS modelling language, with programmatically derived copies in XSD and OWL. The need for model schema subsets has been described in the introduction. Both the EXPRESS and the XML families of standards include parts to define model transformations and views. EXPRESS-X (Baily et al. 1996) defines SCHEMA_MAP and VIEW constructs and reuses the procedural rule language in EXPRESS to further qualify or derive attribute types. Within the IFC community there are infrastructure domain extensions developed in UML. That family of standards include QVT for transformations and OCL for constraint languages. The Semantic Web standards include SPARQL for querying and transformation using SPARQL CONSTRUCT and SWRL for rules and SHACL for constraints.

As noted, the buildingSMART organisation put forward mvdXML[2] for this purpose and implementations of mvdXML exist, such based on SPARQL SPIN in Zhang et al. (2015)by which portability of rule execution increases, but at the same time a dependency on linked data technology creates additional indirection due to the mapping to OWL, in particular for lists (Pauwels et al. 2017). An effort to simplify the MVD definition language starting from mvdXML semantics is given in (Liu et al. 2019).

In this context it's necessary to appreciate the distinction between declarative and imperative languages. Where the imperative focuses on how something is to be executed the declarative focuses on a specification of the outcomes. Examples of declarative programming languages include the query and rule languages above, imperative languages are most of the contemporary programming languages such as C++ and Python. Pichler et al. (2011) concluded in their tests in the field of business process modelling that the imperative modelling approach was more comprehensible (although notes that this observation may be skewed by familiarity of the subjects). Intuitively one might argue that incremental changes are easier to apply to imperative

[1] This is seen in initiatives such as https://github.com/buildingSMART/NextGen-IFC
[2] https://standards.buildingsmart.org/MVD/RELEASE/mvdXML/v1-1/mvdXML_V1-1-Final.pdf

statements, but declarative approaches might have a higher degree of composability, the ability to combine statements is less hindered by imperative considerations such as variable names.

2.2 Bespoke IFC model validation

The typical nature of model validation in the construction industry is well-described in literature (Eastman et al. 2009). There are applications that focus on (a) data completeness/correctness and exchange requirements, sometimes called pre-checking and (b) validation of the model with respect to design requirements. The process is outlined in four phases: rule interpretation, model preparation, rule execution and reporting. For the first part, existing legal documents can be annotated for example using RASE (Hjelseth and Nisbet 2011) to subdivide statements in requirements and applicable types.

As MVDs main aim is to check data exchange requirements in models and the complexity of using mvdXML is high due to required schema knowledge, industry has mostly embraced bespoke and closed solutions. One example is the Solibri Model Checker (SMC)[3]. Part of SMC's popularity arises from its ability to add its own classifications on top of IFC classes (i.e. the model preparation phase), which makes it very forgiving in the quality of input data, and allows people to test expectations on top of that. However, this leniency may be seen as detrimental to high quality OpenBIM adoption as it is ambiguous as to how exactly its tests relate to the IFC schema. In addition, its black-box nature makes it hard to guarantee that tests remain unchanged from version to version, or even persist in the next version, and commercial nature may make it impractical to require from BIM authors. As a parallel, proprietary unit testing frameworks are rare in the software industry. Nevertheless, its popularity demonstrates that there is market demand.

Alternative open source implementations exist, such as the IfcValidator[4] tool, which offers added transparency due to its open-source nature, and stays truer to the IFC schema, but requires precompiled test definitions and a dependency on BIMServer. This requirement increases the barrier to entry for most BIM authors, as BIMServer is not widely used, and to author a test requires the ability to set up a development environment, code compilation, and an understanding of BIMServer and the Java programming language. It is also restricted to data originating within a BIMServer, which can be problematic when data can some from multiple sources and formats from many disciplines. However, its ability to integrate into the model submission pipeline is beneficial for deployment and governance of BIM testing.

It is worth mentioning that there are other types of testing, such as collision and clash testing, auditing paper documentation, as-built verification, and manual design intent checks, but do not overlap significantly with the scope of an MVD, and are not addressed in this paper.

2.3 Software engineering

Within software engineering, the concept of testing and test suites are well established to guarantee that a deliverable is fit for purpose for a particular user. These test suites form part of the quality control procedure, project documentation, issue management process, deployment process, contractual requirements, and are often automated. Unlike the AEC industry, where data testing is fragmented, many software engineering test suites follow the procedures set out by the xUnit[5] framework.

[3] https://www.solibri.com/

[4] https://github.com/opensourceBIM/IfcValidator

[5] https://xunit.net/

One subset of test suite practices is known as Behaviour Driven Development (BDD). The characteristics of BDD are summarized in (Solis and Wang 2011). The first and foremost is that tests are written in a ubiquitous language so that customers and developers speak the same language and can collaboratively edit and review the body of rule definitions.

The software engineering discipline has largely embraced the paradigm of Continuous Integration / Continuous Delivery, meaning that tests are ran automatically and after every change or on a fixed interval.

3. Contribution

In this paper we apply the Behaviour Driven Development practice to a real-world project and construction company (both kept private). In our case, and many others, we used the Gherkin language which provides the benefit of expressing technical BIM concepts in real, human language that document project requirements for multiple stakeholders.

It is well established that mvdXML duplicates the pre-existing standards on model transformations and subset declarations. Further detailing that is not the aim of this paper. What is interesting to conclude from the state of the art is that in the languages described in previous sections there is often a different language for (a) validation and (b) declaration of subsets, but mvdXML aims to do both. Also, in BDD test sets are written in human readable, clearly understandable scenarios so that engineers, managers and auditors all verbally comprehend the rules. The technical focus on data modelling definition and tight coupling with the IFC schema renders mvdXML unsuitable as a basis for discussion with less technically proficient stakeholders. In this paper we elaborate on and discuss our experiments with Behaviour Driven Development (BDD) and testing of building models using the Gherkin syntax.

3.1 Rule translation

In our project, requirements are translated into scenarios written in Gherkin syntax, which are tested against the model. The characteristics of human readability and the ability to build up a complex vocabulary of building requirements render it suitable for application in the construction sector. An example of statements produced by various parties involved in a construction project is outlined in Table 1.

Table 1: Example of rule definitions from an (a) architect (b) lighting designer (c) asset manager and (d) the mvdXML specification.

The project must be geolocated All furniture must be contained in a room All walls must have a material and colour All wall type names must follow the naming convention of "XXXYYY" All wall types must have a fire rating
All spaces must have space lighting requirements All coverings must have a surface style All objects with a material with the name Glass must have an externally defined surface style containing BRDF data
All maintainable assets from the COBie list of assets must have warranty properties All warranty properties must have a point of contact and warranty end date as a minimum All maintainable assets must have an associated document which links to our maintenance document server
All sensors must have at least one port that submits signals

Unlike the typical usage of the MVD standard, these statements are created on a project by project basis, but common ones may be re-used, similar to how design patterns are re-used in software. These statements may be both internationalised and localised to account for different practices around the world. These statements are organised into scenarios, and parsed by a test runner. The Gherkin language can be parsed by a variety of test runners in a variety of programming languages. Once parsed, the test runner may invoke any software to validate the requirements of the test. It is possible, at this stage, to then generate mvdXML and use an mvdXML validator to check the model. However, it is proposed that writing model queries using a native programming language and an IFC library has benefits over mvdXML. In this paper, we use the IfcOpenShell library and write test implementations in Python, which is interpreted at runtime.

The mvdXML documentation provides a simple example enforcing that sensors have at least one port that submits signals. This can be represented by the single domain specific sentence in Table 1d.

The sentence is unchanged from the everyday domain language of the authors and recipients. The sentence may then be used in test suites and enforced contractually. The implementation in Python using the IfcOpenShell library is 10 lines of code (including line breaks for readability) and is shown below. In contrast, the corresponding implementation shown in the mvdXML documentation is 89 lines of code, excluding line breaks for readability. The Python code also has a certain natural readability, allowing non-programmers to understand what it is describing.

Table 2: The 10 lines of imperative Python code required to check the sample from the mvdXML specification. The equivalent mvdXML requires 89 lines.

```
for sensor in ifc_file.by_type("IfcSensor"):
    if not hasattr(sensor, "IsNestedBy") or not sensor.IsNestedBy:
        assert False
    for relation in sensor.IsNestedBy:
        for port in relation.RelatedObjects:
            if port.Name == "Output" \
                    and port.SystemType == "SIGNAL" \
                    and port.FlowDirection == "SOURCE":
                return
    assert False
```

3.2 Implementation

The BlenderBIM Add-on[6] (Figure 1) was used as an open source, visual BIM authoring and auditing tool. The BlenderBIM Add-on is part of the IfcOpenShell project, and uses IfcOpenShell, an established IFC library to read and write IFC2X3 and IFC4 schemas. Unlike other BIM authoring tools, which historically have emerged from fabrication and CAD industries, the BlenderBIM Add-on runs on Blender, a popular content creation suite in the creative computer graphics industry. This makes it adept at modifying and visualising mesh data, which is exceptionally useful for auditing, as in practice there is almost zero lag in displaying even the heaviest of models. It also has an interactive Python shell to query the model live. The internal data model is also designed specifically to mirror the IFC schema, to minimise data translation during import and export, and treat the IFC data as a native model. Because there is no rigid internal data model such as in the case of the pre-existing BIM authoring tools there is very little reinterpretation needed when opening an IFC file at the expense of the mesh-based nature being unable to mimic the parametric interfaces in such tools such as a

[6] https://blenderbim.org

representation of a wall by two movable end-points and a wall thickness (although parametric functionality in Blender is provided by other add-ons).

This approach to testing project and organisation specific exchange requirements by specifying domain specific Gherkin syntax, alongside a Python implementation in IfcOpenShell was implemented on real world BIM data in Australia to judge its suitability. IFC data was audited from architectural, MEP, landscape, and structural disciplines. The test runner implementation used was Behave[7]. An open-source tool called BIMTester was written as a thin wrapper around Behave. BIMTester would package Behave and the IfcOpenShell library into a single standalone executable, using pyinstaller, to allow users to easily run the tests cross-platform without needing a prior understanding of unit testing or how to install Python or its modules. Behave would return test results in JUnit XML, which is compatible with many available systems that understand xUnit testing. The BIMTester wrapper would then provide additional HTML formatting to the JUnit XML, presenting the test results in a colourful and friendly HTML report to BIM authors. BIMTester is under 150 lines of code.

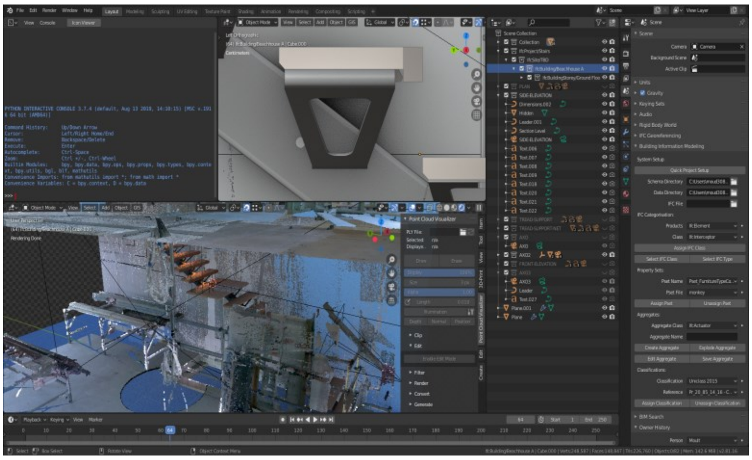

Figure 1: Visualization of a model in the BlenderBIM Add-on with the Blender user interface elements: Python console, renderings, outliner (model decomposition) and properties panel.

The first test suite performed was to check whether an IFC file was of a particular IFC schema. The schema version is often specified in contracts and in digital execution plans, in identical domain language to the sentence used in the test. A domain specific sentence to describe this exchange requirement is given in Table 3a.

Table 3: Two example Gherkin scenarios assessed in BIMTester

Given the IFC file "foo.ifc" Then the file should be an IFC2X3 file
The element {global_id} is an {ifc_class}

The first sentence specifies to the test runner which IFC dataset subsequent tests will be performed on. This is stored in the test environment, which persists across subsequent tests. This notion of persistence allows tests to depend on one another, leading to efficient test execution. Loading an IFC file is a one-liner in IfcOpenShell, as is the check for the schema.

Another fundamental test is to check whether BIM objects are assigned to the correct IFC class. From a contractual and BIM governance perspective, the IFC class determines portions of the digital strategy and execution plans, such as what LOI/LOD applies, which consultant has the

[7] https://behave.readthedocs.io/en/latest/

scope of a particular object, and what objects are to be included in deliverables, such as for the COBie MVD for maintainable assets. From a technical perspective, many of the properties and attributes available to an object in IFC depend on the IFC class, can be used as a guide to check whether the right classification system reference has been applied, and a used as filtered in processes, such as construction sequencing, prioritising clash detection, and scheduling for quantity take-off. Unfortunately, a lot of BIM authoring platforms tightly couple the geometry modelling capabilities with the class assignment, resulting in incorrect classifications. Similarly, a lack of industry knowledge around OpenBIM has led to an over-reliance on default BIM authoring tool IFC class mappings, with little evidence seen of processes in place to ensure correct IFC classes. A domain specific sentence to describe this exchange requirement is given in Table 3b.

In this case, the sentence contains two variables: {global_id} and {ifc_class}. Prior to the models being built, it is not known what IFC classes would be checked, nor what the element GUIDs would be. Therefore, contractually the sentence would be presented as a generic requirement, with an understanding that BIM authors may expect to be audited for any {global_id} or {ifc_class}. An implementation in IfcOpenShell is again one line of code.

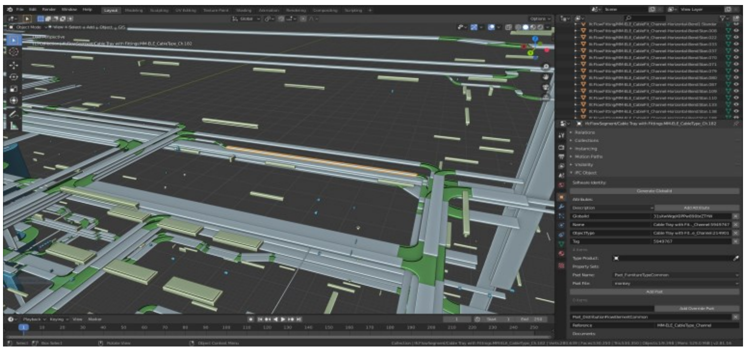

Figure 2: A model from the electrical discipline with objects colour coded by their IFC class value. Small dark blue objects are IfcBuildingElementProxy objects, which are easy to spot.

IFC classes usually require a visual check. Although some can be determined programmatically, such as by testing the aspect ratios of bounding boxes for slabs, columns, and beams, this method is generally less reliable. It is also not sufficient to check for the correct type product, as not all IFC products are typed, and a single generic type may be abused to create multiple different products. Approaches to check correct element class associations based on geometrical properties and proximity to other objects is given in Krijnen and Tamke (2015).

To allow efficient testing, the BlenderBIM Add-on was used with the ability to colour code a model by the IFC class and use drop-downs to select valid IFC classes. IFCs created by BIM authoring programs generally have various patterns in their export, and each firm tends to have their own style based off their internal BIM asset library. Together, these two characteristics allow one to quickly use bulk selection tools based on wildcard names and object attributes to quickly audit hundreds of objects at a time. The Blender modelling package has features for object isolation, hiding, and x-ray vision, allowing for further efficiencies in the test generation process. Objects could be selected in bulk and either have their current IFC class approved, or another IFC class specified as the correct IFC class (Figure 2).

3.3 Continuous Integration

The above results in over a hundred thousand of these tests created in a typical large project prior to construction detailing. As IfcOpenShell builds an indexed list of element global IDs, it is able to very efficiently retrieve any object in the IFC file once it has loaded. Execution of a single one of these tests is in the range of a millisecond, allowing to test the entire project in seconds. The testing bottleneck lies in the disk's capability to load the IFC file through IfcOpenShell, with an IFC file in the hundreds of megabytes taking between 10-20 seconds to load. However, once a file is loaded, the tens of thousands of tests which follow are completed in mere seconds. The entire process taken to spin up a new virtual testing machine with a clean environment, download the latest revision of all of the IFC files, download and install the testing dependencies, and run the tests for half a gigabyte of IFC data and hundreds of thousands of elements, and produce HTML reports for download is approximately 3-4 minutes on a single threaded, standard build server. This full set-up and tear-down process is typical of the process that a software company might have to perform QA. The process is fully automated and executed on a post-receive Git hook.

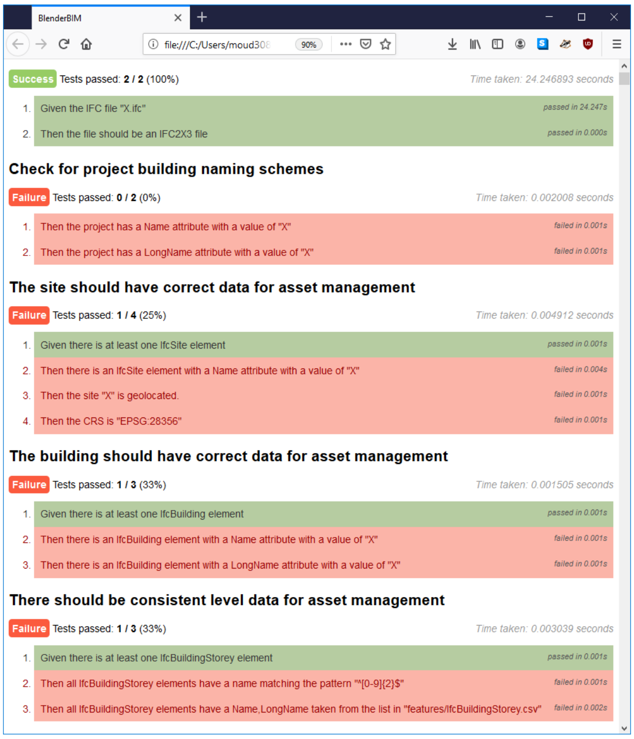

Figure 3: Overview of the test reporting page (somewhat censored). The time taken to load the file (24s) is significantly greater than test execution. The "scenario" syntax of the "given", "when", and "then" prefix is used as a convention, but may be omitted.

Once the test suite is created, it persists throughout all future model submissions. Models are often submitted on a regular basis, so in a week's time a proportion of elements would have been added, removed, or modified. Elements that are modified are already considered by the test suite, and so if the element IFC class changes, the test suite will continue to recheck its class, preventing the possibility of regressions, just as in software engineering. If an element is removed, the BIMTester tool has a purge option, which detects any {global_id} variables in the test suite and deletes all the corresponding tests prior to running the test suite. This is done through simple text file manipulation, as the test suite is a plaintext file, and has a negligible bearing on execution time. The test suite is version controlled with Git, allowing any test deletions to be undone, for example due to an errant export by a BIM author who may have disabled various categories of elements by mistake. Similar to detecting element removals, element additions are determined by identifying all elements in the model without a corresponding test, which is done using the BlenderBIM Add-on. This has the additional benefit of serving a similar purpose to a model compare, which directs the auditor's attention to new or changed portions of the model. This also means that subsequent audits are much faster, despite this being fundamentally but necessarily a manual process. An initial audit would take approximately 2 days to audit 30 IFC files, but subsequently would only take a few hours.

Once a test is performed and a report produced, it is not always straightforward to correlate the report results (Figure 3) back to a live model to fix the results. For example, not all BIM authoring tools make it easy to select an element by its IFC GlobalId attribute - requiring multiple steps and a specific procedure to be followed. Some OpenBIM viewers do not have this capability at all. Some elements that are composed into an aggregation are hard to select, and some elements are parametrically created (such as arrays) and cannot be individually selected in the native authoring tool. An element may have also been deleted since the audit was performed, resulting in confusion. Guides and plug-ins had to be produced to ensure that this process was smooth.

3.4 Summary and findings

The project documented in this paper had a total of 21 rule sentences implemented. Bridging the nouns in the Gherkin syntax to imperative operations on the IfcOpenShell Python IFC parser took 243 lines of code, averaging 11.5 lines of code per Gherkin syntax. This shows how by embracing existing open source solutions we were able to build an advanced system for automatically and continuously assessing the state of the building model with relation to an evolving body of rule definitions. Executing the rules was almost instantaneous on a test set of 35 files totalling 2.9GB, parsing the data took most time. The imperative implementation in Python and the “batteries-included” nature of its module ecosystem allowed for some interesting side effects, such as being able to cross reference data from an CSV file. This type of integration with external data is currently not feasible in mvdXML. Python also allowed for the usage of math primitives and trigonometry for the validation of latitude longitude. In addition, future work might make use of the fully evaluated geometry provided by IfcOpenShell and the validation n-ary predicates and relationships.

From a political perspective, people were not always used to data being audited to such a detailed level and sometimes the information requires were underspecified to be suitable for automated testing.

4. Conclusion

In this paper we have provided a freely available open source software toolset for the application of rules in the Gherkin syntax to an IFC building model and reporting on the validation outcomes. The coupling of BIM and code opens possibilities within the AEC industry. Several professionals with extensive experience have participated indirectly in the experiments and have since changed their previously negative conceptions of IFC, now considering it as the foundations for seamless, non-deprecating, and lossless data exchange. IFC enabled to take full ownership of data, provide ruthless automation and data integration.

Current implementations of rule checking on BIM models are hindered by the following limitations (a) lack of portability of rules (b) black box implementation (i.e. subject to change, unclear exact behaviour and (c) automatic inference (of quantities, subtypes, relationships) which is forgiving to end-user on the short term, but will hurt interoperability on the long term due to diverging implementations. We identified that existing ecosystems and frameworks typically have different languages for (a) validation/certfication and (b) model subset declaration. With mvdXML attempting to do both there is not a clear focus, uncertainty in industry and evaluating alternatives is problematic. We have therefore focussed only on model validation by embracing Behaviour-Driven Development approaches.

The trifecta of governance language (to be reused in contractual documents), cheap test creation (the majority of test sentence implementations are under 20 lines of code), and flexible pipeline integration (plaintext definitions and xUnit reporting) suggest that a Gherkin language based approach towards auditing BIM data is useful in the industry. Participants were willing to adapt business processes and easily understood the requirements being audited and imposed. Having automated testing integrated into the model submission process removed all barriers to entry, and the simultaneous provision of open-source test definitions, plain-text test definitions, and cross-platform, small utilities allowed the more curious participants to gain a deeper understanding of OpenBIM, without the need for prior programming experience.

The tests performed only focused on data exchange requirements. However, it is believed that these tests may be extended to cover design intention through the IfcObjective entity or to query spatial requirements. Further research will focus on the interaction of the results of xUnit tests within a BIM authoring tool and connecting to initiatives such as the BCF API and OpenCDE specifications.

References

Bailey, I., Hardwick, M., Laud, A., & Spooner, D. (1996). Overview of the EXPRESS-X Language. In Proceedings of the Sixth EXPRESS Users Group Conference, Toronto, Canada

Eastman, C., Lee, J. M., Jeong, Y. S., & Lee, J. K. (2009). Automatic rule-based checking of building designs. Automation in construction, 18(8), pp. 1011–1033.

Hjelseth, E., & Nisbet, N. (2011). Capturing normative constraints by use of the semantic mark-up RASE methodology. In Proceedings of CIB W78-W102 Conference.

Krijnen, T., & Tamke, M. (2015). Assessing implicit knowledge in BIM models with machine learning. In Modelling Behaviour (pp. 397–406). Springer, Cham.

Liu, H., Gao, G., Zhang, H., Liu, Y. S., Song, Y., & Gu, M. (2019). MVDLite: A Light-weight Representation of Model View Definition with Fast Validation for BIM Applications. arXiv preprint arXiv:1909.06997.

Pauwels, P., Krijnen, T., Terkaj, W., & Beetz, J. (2017). Enhancing the ifcOWL ontology with an alternative representation for geometric data. Automation in Construction, 80, pp.77–94.

Pichler, P., Weber, B., Zugal, S., Pinggera, J., Mendling, J., & Reijers, H. A. (2011). Imperative versus declarative process modeling languages: An empirical investigation. In International Conference on Business Process Management. pp. 383–394. Springer, Berlin, Heidelberg.

Solis, C. and Wang, X. (2011). A Study of the Characteristics of Behaviour Driven Development. In: 2011 37th EUROMICRO Conference on Software Engineering and Advanced Applications, Oulu, 2011, pp. 383–387.

Zhang, Chi, Jakob Beetz, and Matthias Weise. "Interoperable validation for IFC building models using open standards." Journal of Information Technology in Construction (ITcon) 20.2 (2015), pp.24–39.

A computational model for product cycling of modular buildings

Christopher Rausch[1]*, Benjamin Sanchez[2], Chloe Edwards[1], Carl Haas[1]
[1]University of Waterloo, Canada
[2]Tecnologico de Monterrey, México
*chris.rausch@uwaterloo.ca

Abstract. Advances in industrialized building systems are creating reliable solutions for traceability across a project. However, there is an increasing demand to expand traceability to more dimensions than just the materials, processes and stakeholders involved in a project. Social demands for a circular economy, in which parts, products and materials can flow within open resource loops, are necessitating the need for lifecycle-based traceability of our built assets. This paper presents a computational model for "product cycling" of modular buildings. Given their innate assembly and disassembly attributes, modular buildings offer a unique advantage to building owners and building stock managers for cycling of modules (i.e., adding modules in future adaptations, or redistributing, reusing and repurposing of modules into new assets). We present the basis for a computational model containing considerations for module topology, lifecycle costs and lifecycle impacts. We demonstrate the result of this model in a product configurator, which serves as a tool for expanding state-of-the-art traceability from being project-based to product-based across multiple lifecycles.

1. Introduction

While industrialized construction has been relied upon as a favorable approach for project delivery, modular and prefabricated assets present a unique opportunity for promoting a circular economy (Minunno, O'Grady et al. 2018). The nature of how modular assets are assembled in the field leads to an enhanced ability for disassembly, reuse and circular resource flows. However, current design and delivery methodologies are optimized for singular use of modular assets. Social demands for a circular economy – global natural resource depletion, increasing waste, environmental load, energy use, etc. – require innovative approaches to constructing our built environment (Adams, Osmani et al. 2017). With significant developments being realized in the manufacturing industry regarding the circular economy (Lieder, Rashid 2016), there is a need to expand this concept to industrialized construction. This research presents a computational model for promoting the concept of "product cycling" in modular buildings. The key to this model is optimizing design for multiple lifecycles, rather than a single lifecycle. The model contains analytical expressions for lifecycle costs and impacts, which are enumerated across multiple lifecycles (i.e., initial build, n number of adaptions and an End of Life stage). The proposed model is demonstrated in a configurator of a modular prototype (Figure 1).

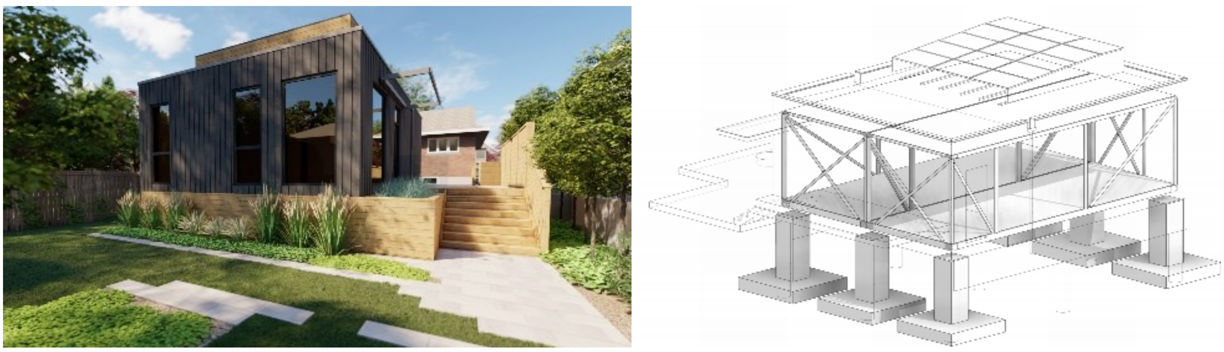

Figure 1: Two-module accessory dwelling unit used for demonstrating product cycling model

2. Background

Despite the fact that current impediments to BIM integration within modular construction and prefabrication stem largely from resistance to business change (Mostafa, Kim et al. 2018), this is rapidly changing, due in large part to advances from digital technologies and configuration platforms (Smith, Rupnik 2019). Product configurators in industrialized construction can be grouped into three typologies: (1) planning-based, (2) design-based, and (3) DfMA-based (Cao, Hall 2019). The principle of a configurator is to codify constraint-based logic for the topology of a manufacturable system, in order to define rules for how components and modules can be combined into products (Jensen 2010). Since product configurators rely on computational processes to generate and iterate assemblies, they can be used across a range of projects, thus reducing project-specific effort and resources required for BIM production (i.e., since this can be largely automated). The value of codifying construction systems extends beyond just the pragmatic harmonization of complex design-to-construction relationships. Increasingly, computational processes can also be used to address vital social imperatives such as sustainable development, embodied and operational energy reduction and resource preservation.

Lifecycle Assessment (LCA) is a methodology that accounts for the materials and energy involved in a product or service along its lifecycle and quantifies its environmental impacts (International Standard Organization 1997). By applying this methodology to the building and construction industry, it is possible to make important decisions during the design stages of a building, based on a holistic approach that involves the stakeholders of a global society. LCA represents a rational standardized approach that can evolve with the development of knowledge, and it also helps stakeholders to agree upon common strategies. LCA is now considered as one of the main tools used to help achieve sustainability in the building industry (Cabeza, Rincón et al. 2014, Azari, Abbasabadi 2018, Sanchez, Esfahani et al. 2019). When LCA is incorporated into the decision-making process for buildings, stakeholders can scientifically assess the lifecycle impacts of building subsystems, materials, and components, and then select alternatives that reduce overall net environmental impacts. Several national jurisdictions already have, or plan to soon implement, requirements and building practices for reporting LCA upfront in design (TAF 2017). In some cases, monetary benefits or penalties are associated with a building's embodied energy. As LCA monetization of built assets is shifting towards being a project mandate, there is an increasing need to develop tools to forecast expected LCA impacts and costs in order to facilitate optimized lifecycle solutions.

Previous research has quantified the advantages that modular buildings have in terms of LCA impacts over traditionally constructed buildings. Modular construction is superior from both a production standpoint (Lawson, Ogden et al. 2014), and from an operational standpoint (Kamali, Hewage 2016). Despite the range of studies either documenting or improving the innate opportunities of modular assets (either from cost, time, quality or environmental perspectives), no studies to date explore multi-lifecycle scenarios for buildings. Instead of exclusively focusing effort on adapting derelict assets that may not have up-to-date asset information nor the ability for easy adaptation, there is a growing opportunity to embed adaptability upfront in new assets. In this way, we can optimize for design scenarios that facilitate product cycling of buildings that are justified from cost and LCA perspectives.

3. Proposed Model

The proposed model consists of three key components to facilitate product cycling of modular buildings: (1) codification of a reconfigurable topology (i.e., ability for modules to be added or removed from building iterations), (2) derivation of lifecycle cost functions and (3) derivation of LCA impact functions. Collectively, these components comprise the computational core for a product cycling model for modular buildings. For demonstration purposes, the derivation of lifecycle costs and impacts in this paper is done assuming modules are added to an existing building over discrete adaptations and fully disassembled at the End of Life (EoL) stage. Future research will explore mixed cases of how modules can be added or removed from existing building configurations (both in a vertical and horizontal manner). The proposed methodology is based on the existing work by Sanchez et al. (2020) for the development of a multi-objective optimization approach to adaptive reuse of buildings.

3.1 Codification of Reconfigurable Topology

In order to facilitate reconfigurability of modular buildings, key design considerations need to be derived and codified. Codification in this case refers to the development of computational logic and rules behind how modules can be added or removed from each other or to/from site interfaces. It also refers to corresponding design details required to make a building functional when adding or removing modules (e.g., details for egress and access, details to close off or open interior spaces, details for adding or removing enclosure subassemblies, etc.). This codification is categorized into structural, constructability and architectural-based topologies.

Structural topology outlines the necessary requirements for ensuring a building can meet its load cases as required by the building code. Specifically, configuration of structural topology relates to the structure of each module and the building substructure (foundation). In the case of adding subsequent modules to an existing building, the building substructure and existing modules need to handle the additional loads of added modules. In this way, the initial lifecycle might have an overdesigned structural topology in order to anticipate future module cycling applications. Developing structural topology in a computational manner (i.e., distilling the overall design to a series of dimensional and system-based inputs complete with necessary structural checks) is becoming common practice in structural design firms since design iterations can be computed and updated in an efficient manner (Greenough, Smith et al. 2019).

Constructability topology needs to be embedded in the design to enable easy adaptability of a modular building. This requires both design for manufacture and assembly (DfMA) and design for disassembly (DfD) principles in order to increase the flexibility and reconfigurability of modular buildings. A popular approach for this is the use of kit-of-part connections that are nearly universal in application across platform configuration (Jensen, Lidelöw et al. 2015). Many modular companies are already investing in kit-of-part structural systems in order to optimize structural design, fabrication and onsite assembly (e.g., Z Modular's patented VectorBloc connection). It naturally follows that the use of these 'universal connections' are highly favorable for promoting the addition of more modules to a building, or for easing the processes of disassembly since processes can be repeated in a standardized manner.

Architectural topology is the last major design consideration that needs to be thoroughly examined in order to promote product cycling of modular buildings (Nunez 2010). For instance, kit-of-part connectors can also be used to promote mass customization of architectural features such as doors, windows, overhangs and balconies. These connectors can be as simple as engineered structural brackets that mount to the structural system that can be used for exterior mounted assemblies or balconies. The key difference between constructability and architectural-based topology is that architectural topology outlines how a module can be reconfigured to account for varying types of product cycling. One example is how a single-story modular building can be adapted from within to have a staircase for a second-story addition in a subsequent lifecycle (this is an example of vertical adaptability). Another example is how an existing building exterior could be adapted to allow same-level module additions (this is an example of horizontal adaptability).

3.2 Lifecycle Costs

Lifecycle costs are divided into three separate functions: (1) an initial capital costs (for the first lifecycle), (2) adaptation costs for each additional lifecycle, and (3) an End of Life (EoL) cost and reimbursement function. These costs are amalgamated into a net present value cost function, which can be compared against the monetization of LCA impacts.

Capital Cost Function. The initial capital cost function has components that are independent (or *quasi*-independent) of the number of modules such as costs for geotechnical evaluation, trenching/installation of building services (e.g., electrical, water, communications, etc.). Other costs are based on a minimum design case (single story, or single-module assembly) such as design, foundation, inspections/tests, and construction administration costs. Finally, certain costs are directly proportional to the number of modules, such as modular fabrication, delivery and installation. The proposed capital cost function, (C) is derived in Equation 1.

$$C(n,s) = (d + nD) + nM + R + F\left(\frac{n}{s}\right) + sf + O + (i + nI) + nA \tag{1}$$

where n is the number of modules, s is the maximum number of stories for future lifecycles (e.g., to influence design of foundation), d are fixed design costs, D are variable design costs, M is variable costs related to module fabrication, delivery, and installation, R are costs related to supply and installation of the roof module, F are scaled costs according to building footprint (n/s), f are incremental foundation costs based on the number of stories, O are costs for building service/utility supply, i are fixed costs for tests and inspections, I are variable costs for tests and inspections, and A are variable costs for project administration.

Adaption Cost Function. Adaptation costs are derived in Equation 2, where modules can be added in subsequent adaptation stages.

$$A_l(n_l) = r + n_l D + n_l M + n_l A + n_l I + (s_l - s_{l-1})o \tag{2}$$

where l is the adaptation of interest, n_l are the number of modules added for the adaptation, s_l is the number of stories added for the adaption, o are incremental site based costs (e.g., such as staircase/railings) and r is cost related to removal and reinstallation of the roof module. While this function only considers the addition of modules, a future (more comprehensive) adaption cost function can be derived to account for removing modules from an existing building.

End of Life Cost Function. The EoL function (Equation 3) considers costs associated with disassembly, module deconstruction, and component reuse for future building applications.

$$EoL(n) = nT - nU - nV \tag{3}$$

where T is the deconstruction cost per module (including site disassembly, transportation to facility and costs for disassembly of all components outside of the structural system), U is the reuse value for harvesting the structural system (which can be reused in new modular buildings), and V is the salvage value for non-structural components for each module.

Amalgamated Net Present Cost Function. Finally, all cost functions can be amalgamated into a net-present cost function according to Equation 4.

$$NPC(n,s,n_l,i,l) = C(n,s) + \sum_{l=0}^{j} \frac{A_l(n_l)}{(1+i)^l} + \frac{EoL}{(1+k)^g} \tag{4}$$

where i is the compounded interest/return rate over the number of adaptation period(s) l, and k is the interest rate for the number of time periods, g, between the end of life to present time. The purpose of this NPC function is to serve as an estimation tool to account for total lifecycle costs. As such, it assumes equal time periods between each adaptation (for simplicity), however a more complex function could be developed to anticipate different timeframes.

3.3 Lifecycle Impacts

In their work, Sanchez et al. (2019) proposed an LCA BIM-based methodology for evaluating the net environmental impacts for adaptive reuse of buildings. A consequential LCA approach is used to quantify the environmental impacts per subsystem and the building's operational and construction phase is dismissed from the LCA system boundaries since the study is focused on the quantification of embodied resources. Then, the environmental impacts that are estimated and monetized are Primary Energy Demand (PED) in Mega Joules and Global Warming Potential (GWP) in equivalent kilograms of CO_2. For the purposes of this study, the same approach is used in order to estimate the environmental impacts on the design for multiple lifecycles of modular building projects. Figure 2 shows the proposed methodology and system boundaries for evaluating the net environmental impacts. Equation 5 shows the derivation of net environmental impacts (EI) in the proposed LCA cradle-to-cradle framework. For a comprehensive breakdown of each component in the following equation, the reader is directed to Sanchez et al. (2019) – a summarized version is provided here for succinctness.

$$EI(n,s) = LCA_{substructure} + \sum_{i=1}^{i=n} LCA_{module} + \sum_{i=1}^{i=s-1} LCA_{building}^{adaptation} \quad (5)$$

where n are the number of modules, s are the number of stories (assumed to correlate to the number of building adaptations), $LCA_{substructure}$ are impacts associated with the raw resources related to the building substructure (assumed to be constant over the course of multiple lifecycles), LCA_{module} are impacts associated with each additional module added to the building and $LCA_{building}^{adaptation}$ are impacts associated with the additional resources and processes associated with each building adaptation. It is important to note that within each expression in Equation 5 are both LCA disbursements (i.e., negative impacts) and reimbursements (i.e., benefits associated with reuse, recycling and energy recovery). While Equation 5 is reported for each subsystem, it can also easily be reconfigured to report LCA impacts per lifecycle stage.

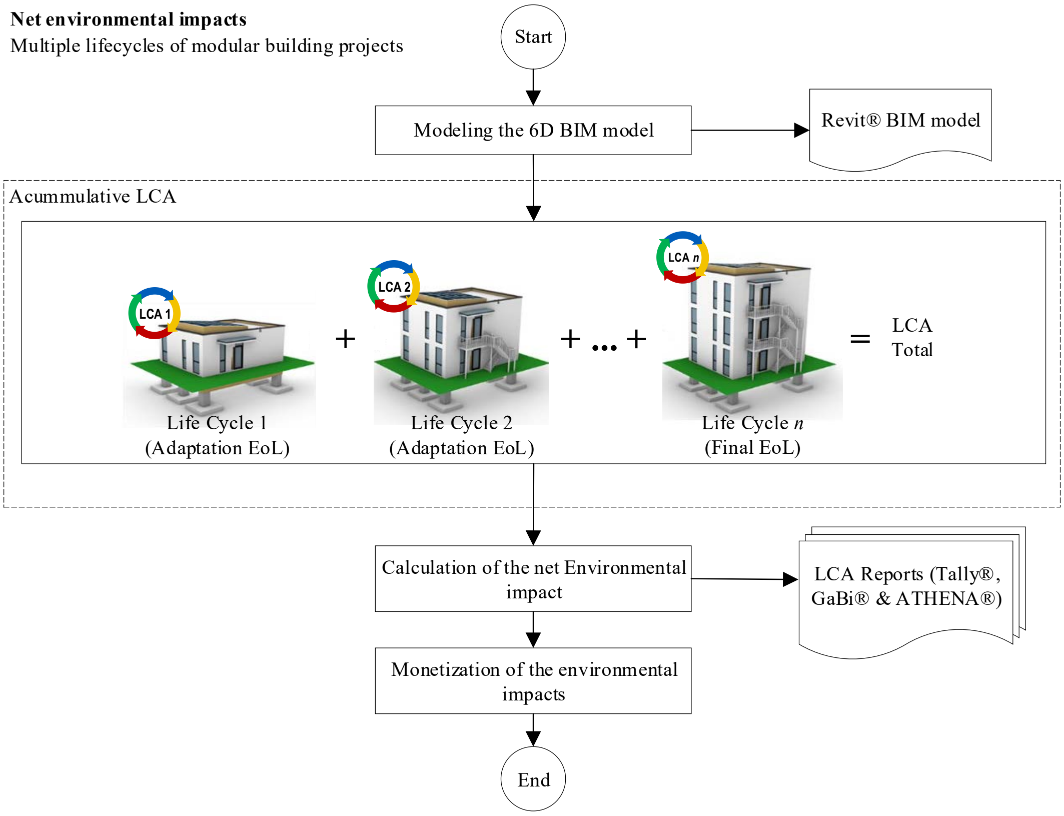

Figure 2: Methodology for evaluating the net environmental impacts in the proposed model

4. Conceptual Demonstration: A Modular Building Product Cycling Configurator

A modular prototype project located in Kitchener, Ontario (Canada) was carried out by Edge Architects in conjunction with Z Modular. The aim of this project was to provide supportive housing for a local nonprofit organization in the form of a 2-module backyard accessory dwelling unit, while simultaneously piloting an apartment layout for an upcoming midrise affordable housing complex. Data collected from this project is used herein to develop a conceptual configurator in order to demonstrate the proposed computational model. The prototype project includes several kit-of-parts features (e.g., VectorBlocs for the structural system to enable easy stacking and connection of modules, and adaptable entryway standoffs above the door which have the ability to be used for a canopy or for supporting a balcony). While actual project costs cannot be disclosed, the values reported in this paper are close to the actual values and are based on the detailed budget.

The conceptual configurator is based on a story-by-story iteration of the 2-module prototype project layout (Figure 1). This configurator was programmed using Grasshopper® visual programming interface using computational topology, and Equations 1 through 5. The configurator allows a user to select the number of stories in the first building iteration (i.e., lifecycle 1) and a maximum number of stories (i.e., lifecycle *n*). The maximum number of stories is used to computationally populate a foundation suitable for a building of this height. Then, based on the difference between the maximum number of stories and the initial number of stories, discrete adaption periods are presented to the user in terms of lifecycle costs and lifecycle impacts. Costs and LCA impacts are developed according to the material and system-outputs of the computational topology. Figure 3 depicts the configurator after a user has selected an initial building height of 1-story, with the ability to add modules in the future up to 4-stories. With these toggles selected, a rendered image of lifecycle 1 and lifecycle *n* are computationally generated. The lower part of Figure 3 has charts outlining the net-present costs and LCA impacts for each lifecycle (values in green outline LCA savings or reimbursements).

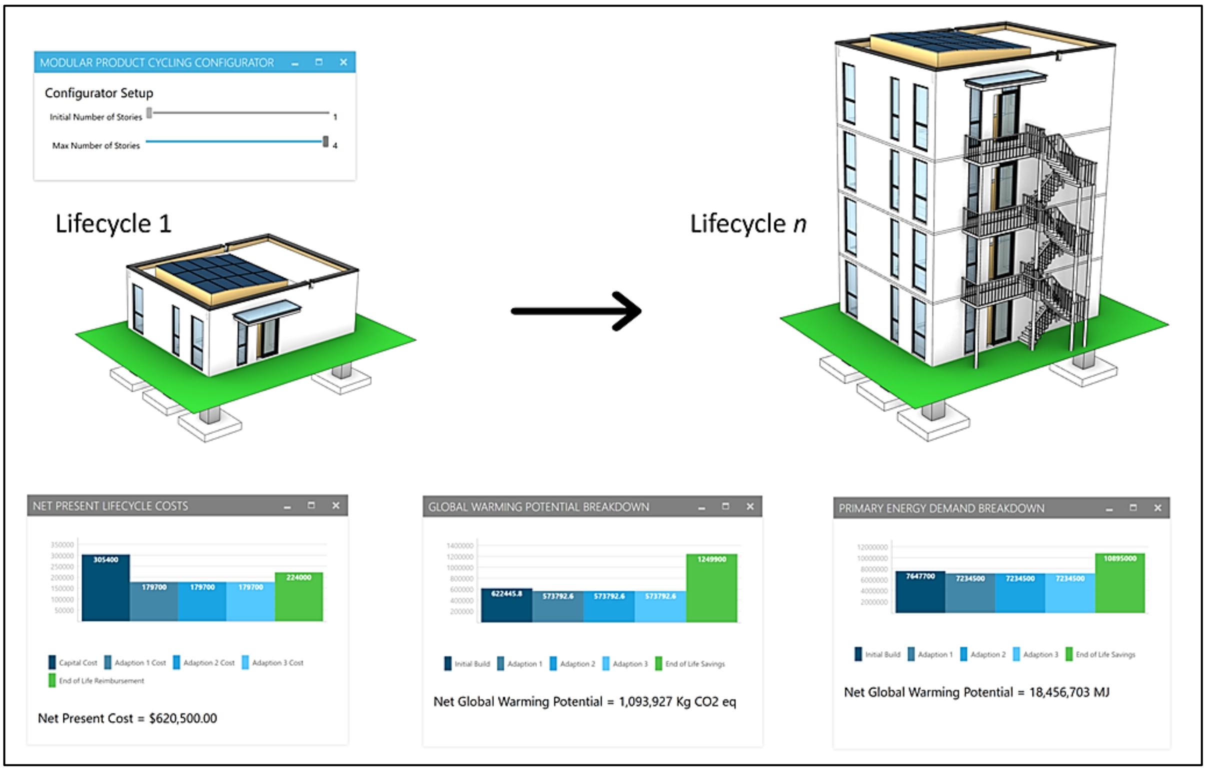

Figure 3: Product Cycling Configurator Graphical User Interface

The development of the structural topology focused on populating optimized foundations (concrete footings and piers) depending on the maximum story height since the structural system of each module (based on the kit-of-part VectorBloc connections) can facilitate stacking above the 4-story maximum height considered in this configurator. Based on geometry populated in Grasshopper®, a series of inputs are fed into a back-end spreadsheet in order to iterate, check and optimize design parameters corresponding to footing depth and area dimensions, and pier area dimensions (Figure 4). Constructability and architectural topology are programmed to add modules vertically, by removing the roof assembly and the insulated floor assembly for each module added to the top story. Then, two different staircase assemblies are populated as needed for each additional story being added. The interior layout of each story remains identical in order to simplify the reconfiguration process for each additional lifecycle. Finally, a kit-of-parts connection above the entryway is adapted from a canopy to a balcony when a story is added. The result of all codified topology is a detail-rich and accurate building layout driven by only two user inputs (i.e., initial and maximum number of stories).

Preliminary Design Calculations and Footing Parameters

Building Parameters		
Building Area	839.5	sq. ft
Trib Area Corner	104.9	sq. ft
Trib Area Int	209.9	sq. ft
Area of interest	C	C or I
Pier Dimensions	2.42 x 2.42	ft
Footing Dimensions	7.67 x 7.67 x 1.33	ft
Cover	0.2	ft

Reinforcement		
Pier r/w	12-20 vert	
	10 @ 12" ties	
Footing r/w	-20 T & B EW Hooked	
Spacing (in)	12	in
Spacing (mm)	294	mm

Loading	lb	kg
DL Per Unit	37500	17025
Storeys	3	
Units per storey	2	
DL total	225000	102150
Load Case 1 (Floor)	**lb**	**kg**
Live Load	33580	15245.3
DL: Partitions	16790	7622.7
DL: Floor finish	4197.5	1905.7
DL: M&E	4197.5	1905.7
Load Case 2 (Roof)	**lb**	**kg**
Snow Load	35259	16007.6
DL: Solar panel	12592.5	5717.0
DL: Roofing	4197.5	1905.7
DL: M&E	4197.5	1905.7
DL: Ceiling	4197.5	1905.7

Input Parameters *refer to diagram			
Loading			
ULS Applied Load	P_ULS	1402.9	kN
SLS Applied Load	P_SLS	1002.1	kN
ULS Bearing	q_ULS	180.0	kPa
SLS Bearing	q_SLS	120.0	kPa
Dimensions			
Pier*	h_p	900.0	mm
	b_p	900.0	mm
Footing *	H_f	3500.0	mm
	B_f	3500.0	mm
	t_f	450.0	mm
Material Properties			
Concrete Compressive Strength	f'c	4000	psi
	f'c	27.6	MPa
Concrete Cover	d_c	60.33	mm
Reinforcement Yield Strength	fy	60	ksi
	fy	413.7	MPa

Footing Area

Unfactored Loads from Preliminary Calculations	
Dead Load	1002.1 kN
Live Load	149.6 kN
Snow Load	157.0 kN

Loading Combinations			
ULS	Pf	1555.5	kN
SLS	Pf	1151.6	kN

Compute Minimum Footing Area			
ULS	Af	8.64	m2
	B_f	2.94	m
SLS	Af	9.60	m2
	B_f	3.10	m

Check			
	Actual	Min	
Footing Area (m2)	12.3	9.60	OK
Footing Width (m)	3.5	3.10	OK

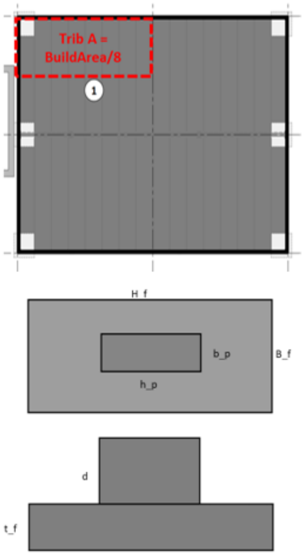

Shear - Minimum Footing Thickness

One-way Shear

Parameters		
Factored Reaction (qsf)	126.98	kPa
Dimension a_b	1300	mm
Beta	0.18	CL 11.3.6.2(a)
Theta	35	CL 11.3.6.2
lambda	1	CL 8.6.5
phi_c	0.65	CL 8.4.2
fc	27.6	MPa

Calculate minimum thickness of footing		
dv	243.5	mm
Min thickness	270.5	mm
Actual thickness	450.0	mm
Check Actual > Min	OK	

Two-way Shear

Parameters		
Column Type: Input I (internal) or E (edge) or C (corner)	c	
Punching perimeter (b0)	5400	mm
Beta_C	1	
alpha_s	1	
vc	1.30	Min of eqn 13.5-13.7
he	900.0	mm
Calculate minimum thickness of footing		
If d < 300 solve quadratic:		
If d > 300, check a_b < 2d	Apply CL13.3.4.3	
A = 4vc + qsf	5.3	
B = 4hevc + 2qsf*he	4898.3	
C = - qsf(Af - he^2)	-1452615.2	
dv	236.08	mm
Min thickness	262.31	
Check Actual > Min	OK	

Determine governing thickness		
One-way or Two-way Shear?	One-way shear governs	
Min thickness	262.3	mm

Figure 4: Output of Structural Load Calculations for Populating Optimal Foundation Design

Lifecycle costs are populated using construction costs (in CAD currency) from the prototype project and estimates for costs associated with roof removal/reinstallation, staircase assembly, reconfiguration of the canopy and additional costs associated with a larger foundation using a sliding scale based on the prototype project. EoL reimbursements are estimated according to the production cost of the structural system of each module (since they are assumed to be directly reused in new buildings), and other reimbursements associated with the subsystems, fixtures and raw materials (i.e., wood framing, copper piping, etc.). These reimbursements are offset by estimated costs for deconstruction which include site mobilization, transportation and labour required for deconstruction processes.

LCA impacts and reimbursements are computed automatically using the plugin Tally® in Revit® (note: while the configurator is programmed in Grasshopper® which natively runs in Rhinoceros®, we employ the use of Rhino.Inside® to access Grasshopper® directly in the Revit® environment). Detailed LCA results for each lifecycle stage are computed for the substructure, modules, and building adaptation of the case study. The organization of building lifecycle stages are described according to the normativity EN 15978 (Sanchez et al., 2019): product stage (A1. raw material supply, A2. transport, and A3. manufacturing), construction stage (A4. transport), Use stage (B2. maintenance and B4. replacement), EoL stage (C2. Transport to disposal, C3. waste processing, and C4. disposal) and Module D (D. benefits and loads beyond the system boundary from reuse, recycling, and energy recovery). The environmental impact categories estimated for the purposes of this study were Global Warming Potential (GWP) reported in Kg CO_2 equivalent units and Primary Energy Demand (PED) reported in MJ.

4.1 Comparison of Lifecycle Configurations

Using the configurator, we can explore the lifecycle configurations for an initial 1-story building. By selecting various maximum story values in lifecycle n (from 2 to 4), there are three distinct lifecycle configurations (A, B, C). Configuration A, for instance, has a foundation designed to handle up to a 2-story building, and as such has two primary lifecycle stages (an initial 1-story configuration and an adapted 2-story configuration), and a secondary EoL lifecycle. In the EoL lifecycle, subsystem deconstruction, recycling and reuse of modules occur (Figure 5). This same logic can be carried out for Configuration B and Configuration C.

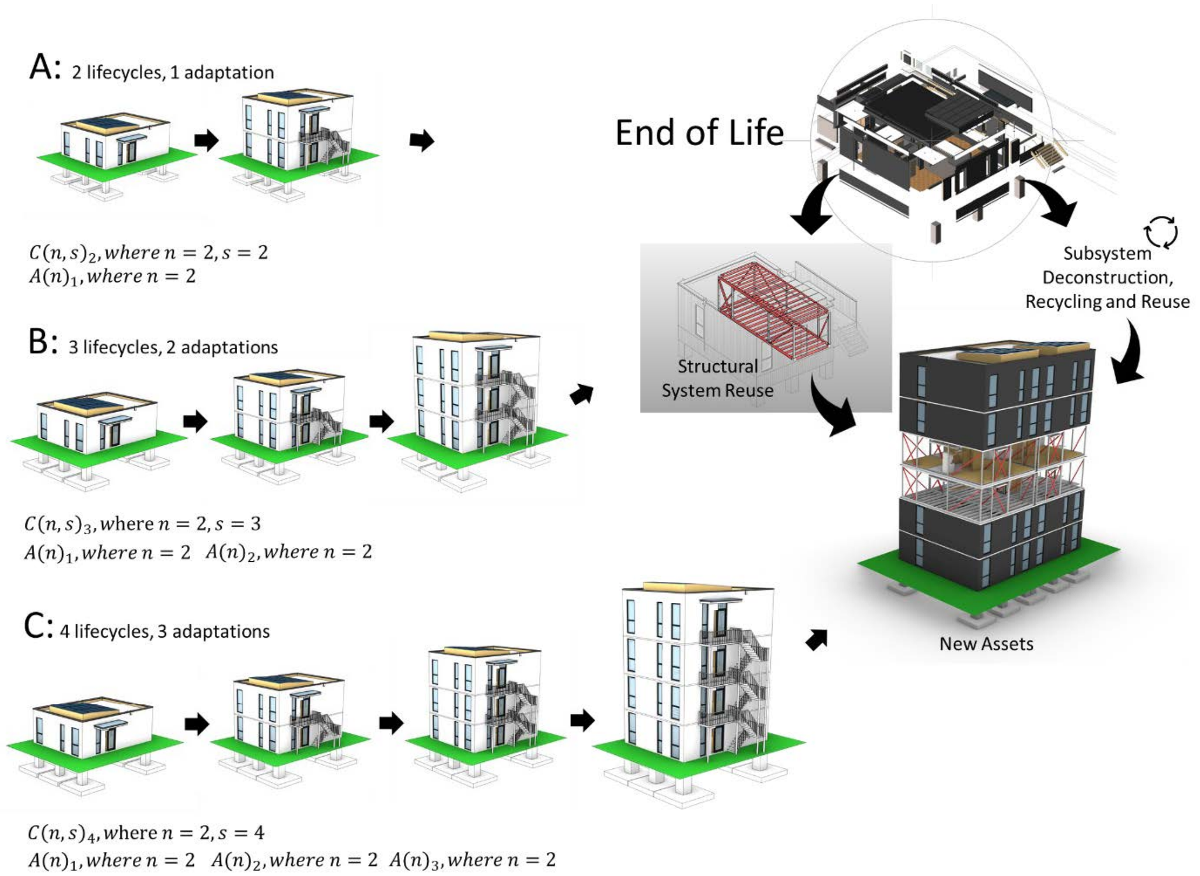

Figure 5: Lifecycle Configurations (A, B, C) for an Initial 1-Story Building Using the Configurator

Apart from exploring the potential ways in which a 1-story building can be reconfigured across multiple lifecycles, it is useful to compute the economic and environmental advantages of investing in reconfigurability. For demonstration purposes, we can compare Configuration A in Figure 5 with an alternative approach (Configuration A'): building a 1-story modular building, then deconstructing that building and foundation to erect a new 2-story building on the same site. The primary difference between Configuration A and A' is the structural topology in the foundation (both are modular buildings). By over-designing the foundation to allow reconfiguration which costs an additional \$4,000, net savings of \$66,250 can be achieved when scaling to a 2-story building (assuming the first foundation cannot be modified in-situ). In a similar manner, environmental savings of 19,295 Kg CO_2 eq. and 134,540 MJ can be achieved by investing upfront in reconfigurability as shown in Table 1.

Table 1: Comparison of Configuration A (1-Story up to 2-Story) and Configuration A' (Two Separate 1- and 2-Story Buildings) in Terms of Cost, Global Warming Potential and Primary Energy Demand

	Item	Cost	GWP (Kg CO2 eq.)	PED (MJ)
Configuration A	1-story up to 2-story	\$365,100	541,709	9,180,537
Configuration A'	1-story up to 1-story	\$237,400	270,291	4,582,789
	2-story up to 2-story	\$360,300	540,670	9,166,335
	Roof removal	\$4,800	1,039	14,202
	Existing foundation removal	\$6,250	9,873	134,918
	Existing module savings	-\$177,400	-260,869	-4,583,168
	Net	\$431,350	561,004	9,315,077
Savings	Configuration A over A'	\$66,250	19,295	134,540

5. Conclusion

Paired with computational tools for lifecycle traceability, modular buildings are uniquely poised to address vital social imperatives associated with sustainability and the circular economy. In this paper we propose a novel "product cycling" model for modular buildings as one way to work towards reaching these social imperatives. The proposed model consists of computational components to generate modular topology (i.e., materials and systems), lifecycle costs and LCA impacts. The configurator developed for demonstration purposes considers a prototype modular project, in which subsequent lifecycles can be introduced by adding modules to an existing building. A comparison of distinct lifecycle configurations and their alternatives (i.e., deconstructing existing buildings and demolition foundations) is shown to result in significant economic and environmental savings. This likely stems from the fact that certain costs in the construction of foundations for modular buildings are not significantly influenced by the quantity of materials used (e.g., volume of concrete and quantity of rebar). Some of these quasi-independent costs include building permits, soil investigation, structural design/analysis, excavation, surveyor, etc., all of which are almost independent of the foundation structure itself. This means that over-designing the foundation to handle future addition of modules can bring some cost savings over the long run, despite the additional up-front costs. Similarly, the lifecycle impacts of adding additional materials to the current use can be distributed over many future lifecycles, lowering the overall impact. This concept of over-designing the structural system to anticipate in-situ adaption is particularly relevant for property owners who foresee the need for adaptability across their assets (i.e., single-story applications being converted into mid-rise applications, or for home-owners who might "grow" their house as their family grows).

5.1 Limitations

An obvious point of contention when presenting economic comparisons for alternative investments is lost opportunity cost. While we do not directly account for lost opportunity cost in the proposed model (i.e., the additional investment required to enable a modular building to be reconfigured), based on our findings, we show that the additional investment in the foundation is low (< 2% of the total project cost). Another limitation relates to the exclusion of costs and LCA impacts related to the operation and maintenance of the building. Instead, we have focused exclusively on capital, adaptation and EoL stages for demonstration purposes.

Acknowledgements

The authors would like to acknowledge the financial support of the Natural Sciences and Engineering Research Council of Canada (NSERC), Mitacs Accelerate and Edge Architects.

References

Adams, K., Osmani, M., Thorpe, T. and Thornback, J., (2017). Circular economy in construction: current awareness, challenges and enablers.

Azari, R. and Abbasabadi, N., (2018). Embodied energy of buildings: A review of data, methods, challenges, and research trends. Energy and Buildings, 168, pp. 225–235.

Cabeza, L.F., Rincón, L., Vilariño, V., Pérez, G. and Castell, A., (2014). Life cycle assessment (LCA) and life cycle energy analysis (LCEA) of buildings and the building sector: A review. Renewable and sustainable energy reviews, 29, pp. 394–416.

Cao, J. and Hall, D., (2019). An overview of configurations for industralized construction: typologies, customer requirements, and technical approaches, , 07/10 2019, pp. 295–303.

Greenough, T., Smith, M. and Mariash, A., (2019). Integrating Computational Design to Improve the Design Workflow of Modular Construction. Modular and Offsite Construction (MOC) Summit, pp. 165–172.

International standard organization, (1997). ISO 14040: Environmental management-Life cycle assessment-principles and framework.

Jensen, P., (2010). Configuration of modularised building systems, Lulea tekniska universitet.

Jensen, P., Lidelöw, H. and Olofsson, T., (2015). Product configuration in construction. International Journal of Mass Customisation, 5(1), pp. 73–92.

Kamali, M. and Hewage, K., (2016). Life cycle performance of modular buildings: A critical review. Renewable and sustainable energy reviews, 62, pp. 1171–1183.

Lawson, M., Ogden, R. and Goodier, C., (2014). Design in modular construction. CRC Press.

Lieder, M. and Rashid, A., (2016). Towards circular economy implementation: a comprehensive review in context of manufacturing industry. Journal of Cleaner Production, 115, pp. 36–51.

Minunno, R., O'Grady, T., Morrison, G., Gruner, R. and Colling, M., (2018). Strategies for applying the circular economy to prefabricated buildings. Buildings, 8(9), pp. 125.

Mostafa, S., Kim, K.P., Tam, V.W. and Rahnamayiezekavat, P., (2018). Exploring the status, benefits, barriers and opportunities of using BIM for advancing prefabrication practice. International Journal of Construction Management, , pp. 1–11.

Nunez, J.G., (2010). Prefab the FabLab: rethinking the habitability of a fabrication lab by including fixture-based components.

Sanchez, B., Esfahani, M.E. and Haas, C., (2019). A methodology to analyze the net environmental impacts and building's cost performance of an adaptive reuse project: a case study of the Waterloo County Courthouse renovations. Environment Systems and Decisions, 39(4), pp. 419–438.

Sanchez, B., Rausch, C., Haas, C. and Saari, R., (2020). A selective disassembly multi-objective optimization approach for adaptive reuse of building components. Resources, Conservation and Recycling, 154, p.104605.

Smith, R.E. and Rupnik, I., (2019). 10 Productivity, innovation and disruption. Offsite Production and Manufacturing for Innovative Construction: People, Process and Technology.

TAF, (2017). Embodied Carbon in Construction: Policy Primer for Ontario.

BIM-enabled Design for Manufacture and Assembly

Tan Tan[1], Grant Mills[1], Eleni Papadonikolaki[1], Weisheng Lu[2], Ke Chen[3]
[1]University College London, United Kingdom
[2]The University of Hong Kong, Hong Kong SAR
[3]Huazhong University of Science and Technology, China
tan.tan.17@ucl.ac.uk

Abstract. Design for Manufacture and Assembly (DfMA) has been introduced into the construction industry to enhance production efficiency. DfMA is a design approach and evaluation system for improving manufacturability and assemblability. This paper outlines the past and ongoing Artificial Intelligence (AI) development in manufacturing-oriented DfMA, and provides a literature review of the concept and the use of DfMA in the construction. The applications, challenges and barriers of design optimization through DfMA and BIM-enabled DfMA are summarized. This desk study shows that studies related to construction-oriented DfMA are still in infancy. At present, articles about DfMA are focused on optimizing design and engineering for manufacturability and assemblability, but rarely describe its digital enablement. This study makes up for the lack of literature review in the evaluation of DfMA with concluding a preliminary application framework, and proposes a future-oriented study and new direction for BIM-enabled DfMA.

1. Introduction

The energy consumption and greenhouse gas emissions caused by buildings accounts for about one-third of emissions and may double in 2050 (Abergel et al., 2017), while the United Nations estimates that the urban population in 2050 will increase by 2.5 billion. But today construction delays, cost overruns, and productivity have not significantly changed (Trauner et al., 2017). A strategic approach to increase construction productivity and sustainability is therefore critical. DfMA has been regarded as Circular Economy solutions for sustainable development (Sanchez and Haas, 2018). The United Kingdom (UK), Singapore, and Hong Kong have identified DfMA as the way to transform the construction industry. Leading organisations and institutions are collaborating around DfMA as a philosophy and a methodology whereby products are designed in a way that is as amenable as possible for downstream manufacturing and assembly (O'Rourke, 2013; Balfour Beatty, 2018). The Royal Institute of British Architects (2013), Singapore's Building and Construction Authority (2016), UK's Infrastructure and Project Authority (2018), and Hong Kong's government (2018) are laying out the principles, processes and standards to achieve DfMA, but digital-enabled platforms for DfMA (P-DfMA) a just starting to emerge.

This study is focused on the evaluation of DfMA during design-review (Gao et al., 2019; Yuan et al., 2018) and the use of Building Information Modelling (BIM) policies, principles, rules, tools, technologies and processes (Eastman et al., 2011) to support the development, delivery, management and maintenance of built assets to achieve BIM-enabled DfMA innovation and collaboration (RIBA, 2013; BCA, 2016). Intelligent technologies originated from manufacturing-oriented DfMA are listed and discussed. This paper aims to investigate previous BIM-enabled DfMA studies and their impact on design optimization, and point the way for DfMA intelligent transformation. Firstly, this study investigates current practices and studies of DfMA design optimization. Secondly, the implementation of BIM-enabled DfMA (e.g. as a process, tool and information source). Thirdly, the intelligent technologies in manufacturing-oriented DfMA (e.g. expert systems, case-based reasoning, neural network). Finally, this study proposed future research direction of BIM-enabled DfMA in the construction.

2. Methodology

A two-step method was conducted. The first step is to investigate the state-of-art research of DfMA in construction. Google Scholar, Scopus and Web of Science were searched using the following keywords: "Design for Manufacture and Assembly" OR "Design for Manufacture" OR "Design for Assembly" OR "DfMA" AND "construction industry". The search was limited to peer-reviewed published articles in last 10 years, as most relevant policies and studies of DfMA in construction were produced during this time. Knowing these criteria, the search was performed in December 2019; articles published by then and appearing in the database were considered. Finally, Google Scholar has 739 results; Scopus has 138 results; Web of Science has 344 results. A total of 1221 hits resulted from the initial search. Next, inclusion and exclusion criteria were set. The former includes (1) articles written in English and produced by peer-reviewed articles; (2) articles published in Architectural Engineering and Construction (AEC) – related journals or conferences, and (3) regard DfMA as the key concept in studies. The exclusion criteria include (1) lacking focus on the construction industry and (2) only mention of DfMA rather than in-depth apply or discuss DfMA in studies. Then, conducting snowballing to filter out more related papers which also satisfy the inclusion and exclusion criteria. Snowballing iterated until no new papers were found. Finally, there were 28 articles.

The second step is to retrieve research of intelligent technologies in DfMA. This step is to summarize the common technologies and their application scenario rather than fully list all possibilities, thus the search is limited to peer-reviewed journal articles. Web of Science was used as it can screen out Science Citation Index Expanded journal articles directly. The searching keywords are: ("DfMA" OR "Design for manufacture and assembly" OR "Design for manufacture" OR "design for assembly") AND ("Intelligent Systems" OR "Artificial Intelligence" OR "Expert Systems" OR "Fuzzy Systems" OR "Genetic Algorithms" OR "Knowledge-Based Systems" OR "Neural Networks" OR "Context Aware Applications" OR "Embedded Systems" OR "Human–Machine Interface" OR "Sensing and Multiple Sensor Fusion" OR "Ubiquitous and Physical Computing" OR "Case-based Reasoning"). Finally, Web of Science has 38 results. All these filtered articles are related to DfMA in manufacturing industry. Finally, this study combined the study of BIM-enabled DfMA and Intelligent-enabled DfMA for a prototype framework.

3. Design for Manufacture and Assembly

Originated from manufacturing industry, DfMA combines Design for Manufacture (DfM) and Design for Assembly (DfA) (Bogue, 2012). The main purpose of DfMA is to assist designers in optimizing and increasing productivity by integrating downstream knowledge and information into the design stage. Evaluation of DfMA manufacturability and assembly is critical, to facilitate objectivity in team-based decision making (Leaney, 1996), and simulating it value (Gao et al., 2019).

DfMA is often realised through offsite construction/manufacture. Nevertheless, recently on-site “construction laboratories” have been used to deliver DfMA with local craftspeople, materials, machineries and advanced technologies (Watts, 2018). The need for BIM-enabled DfMA manufacturing and assembly has universal significance, regardless of the difference adoption of construction methods. Bogue (2012), Emmatty and Sarmah (2012) and Safaa et al., (2019) prioritise simple design, minimizing precast component types, using standard and off-the-shelf components, minimizing connector types and quantity, using as similar materials as possible, using as environmental friendly materials as possible, considering modular designs, standardizing handling and logistics, aiming for mistake-proof designs, and considering design for mechanized or automated assembly. Further attention is need to DfMA manufacturability and assemblability evaluation (Gao et al., 2019). Figure 1, shows potential BIM actions for DfMA that require further research and development.

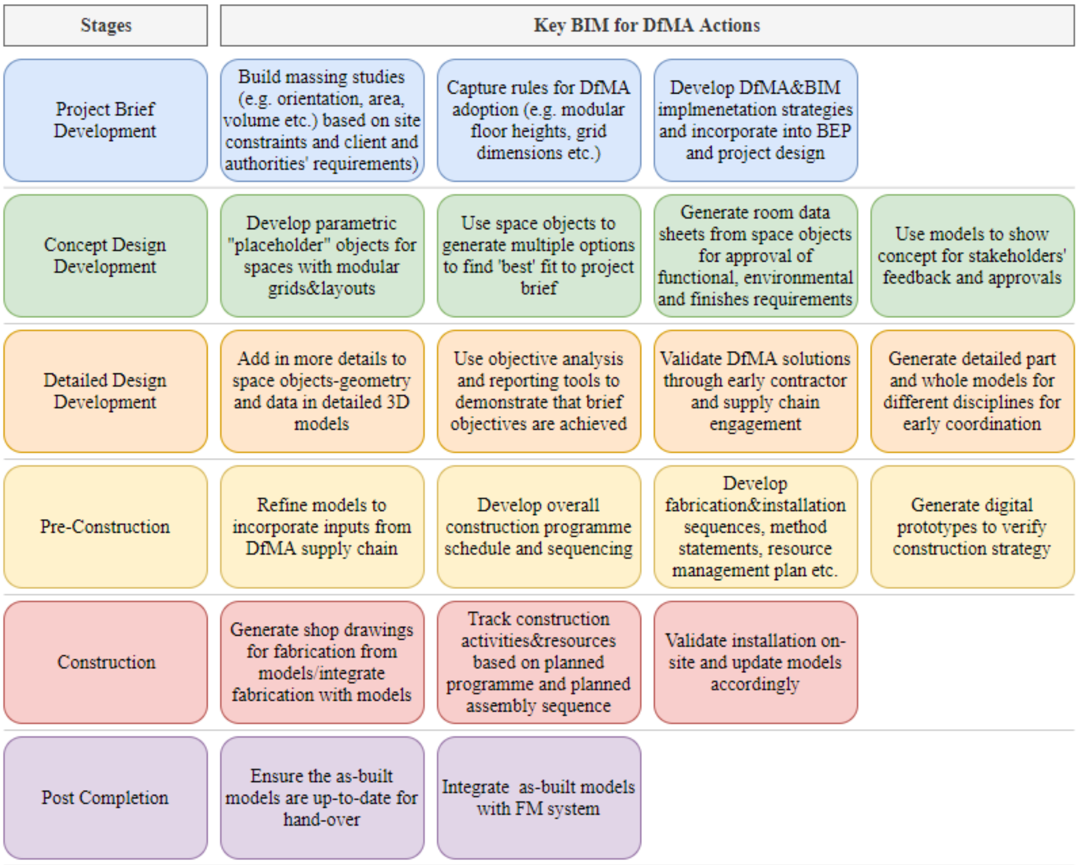

Figure 1: Key BIM actions for the DfMA approach (Derived from BCA, 2016)

4. DfMA Optimization Methods in Construction

Table 1 shows the 11 articles related to DfMA optimization methods and the evaluation of engineering choices or alternatives during design. Significant in this state of the art review is DfMA use for building façades (Montali et al., 2018; Montali et al., 2019; Giuda et al., 2019; Azzi et al., 2011; Başarır and Altun, 2018), weatherproof seals (Orlowski et al., 2018), and modular components (Rausch et al., 2016). Few studies focus on design optimization of the whole built project, although some such as Yuan et al., (2018) have established a process information model for DfMA-oriented prefabricated buildings. While Gerth et al., (2013) combined DfMA, constructability and waste management for the purposes of optimization of housing design.

Table 1: Optimization methods based on DfMA Since 2009

Name	Theory Base	Knowledge Elicitation Methods	Data Analysis Methods	Perspective		Specialize	Reference
				DfM	DfA		
BIM-Based optimizer	DfMA and lean construction	Literature review and questionnaire	Voting-Analytic Hierarchy Process		✓	Building elements and materials	Gbadamosi et al., (2018)

Design for Construction	Constructability, DfMA, and waste management theory	Workshop	Logical argumentation		✓	Housing wall	Gerth et al., (2013)
Knowledge-based engineering	DfMA	Literature review and interview	N/A	✓		Façade	Montali et al., (2018)
Knowledge-rich optimisation	DfMA	Semi-structured interview	N/A	✓		Façade	Montali et al., (2019)
DfMA-based evaluation	DfMA	Questionnaire, interview and observation	Analytic Hierarchy Process	✓	✓	Bridge	Safaa et al., (2019)
BIM-based Approach to Façade Cladding Optimization	Geometry, DfMA, and waste management theory	Project owners	Multi-criteria methodology	✓		Façade	Giuda et al., (2019)
DFMA-oriented prefabricated building information model optimization	DfMA	Expert consultation	N/A	✓	✓	Prefabricated buildings	Yuan et al., (2018)
Optimum assembly planning	DfMA	3D imaging (laser scanning)	Proposed Algorithm	✓	✓	Modular components	Rausch et al., (2016)
Variability-oriented assembly system	Design for assembly and group assembly	Project dataset, interview and site survey	Complete-linkage clustering		✓	Façade	Azzi et al., (2011)
Methodological approach to Design and Development of waterproof seals	DfMA	Expert consultation	N/A	✓	✓	Weatherproof seals	Orlowski et al., (2018)
Redesign procedure to manufacture adaptive façades	DfMA and Theory of Inventive Problem Solving (TRIZ)	Designers and experts	Weighted decision matrix method	✓	✓	Façade	Başarır and Altun, 2018

Optimizing design almost always involves a design trade-off as it needs considering numerous criteria. Multi-criteria methodology was used by the vast majority of these studies. Most are designed to simplify data acquisition. For example, through applying Analytic Hierarchy Process (AHP) or an evolutionary method based on AHP, such as Voting-AHP to apply a criteria weighting. Root cause analysis and cause and effect analysis were also used as the basis of weights (Gerth et al., 2013). Partial limitation of all these methods is the process of subjectively assigning relevance and weighting to assessment criterion. What are more weighting judgements may vary from project to project and may be dependent on different domain knowledge.

Optimization algorithms are also applied to the design process to judge potential alternatives. For example, Rausch et al., (2016) proposed an algorithm to optimally plan, order and arrange components and assess geometric variability and rework. Montali et al., (2019) created a "meta-domain" of analysis to find trade-offs between performance and architectural intent, while allowing for maximum compliance to manufacturing, logistic and design constraints. Manufactured products (such as specific modular components or facades) have been optimized using this method, but rarely whole architectural building solutions (combining strategies to integrate manufacturability and assemblability).

5. BIM-enabled DfMA

BIM has potential to extend the innovative and collaborative use of DfMA at both the object and integrated collaborative environment level (RIBA, 2013; BCA, 2016). Table 2 shows those that have applied BIM and DfMA. Some integrated BIM, DfMA process and strategies for implementation. For example, Machado et al., (2016) establish BIM-based collaborative strategy for DfMA, while Yuan et al., (2018), Kremer (2018) and Samarasinghe et al., (2016) integrate BIM into the design process.

Table 2: BIM-enabled DfMA

Author	Year	BIM application in DfMA
Yuan et al.,	2018	Integrate BIM in design process
Rausch et al.,	2016	Collect geometric data and identify critical points for the assembly from BIM model
Gbadamosi et al.,	2018	Collect geometric data and material information from BIM model
Machado et al.,	2016	Establish BIM-based collaborative strategy
Kremer	2018	Integrate BIM in design process
Lee et al.,	2014	Use BIM tool to process data
Tresidder and White,	2017	Use BIM to develop a checking and review tool
Giuda et al.,	2019	Collect geometrical information from BIM model, and process data using BIM plug-in
Samarasinghe et al.,	2016	Integrate BIM in design process

BIM provides an effective tool for review, checking, and data processing (Lee et al., 2014, Tresidder and White, 2017; Giuda et al., 2019). Open Application Programming Interfaces (APIs) can support BIM software vendors and help third party developers to program advanced software modules for the specialized information process service (Lee et al., 2014). BIM, digital DfMA models, components and connections can be used to streamline the processes of manufacture and assemble. Data-rich models and standardize DfMA elements, such as Prefabricated Prefinished Volumetric Construction (PPVC), Prefabricated Bathroom Unit (PBU), precast components, can support the adoption of a more systematic BIM-enabled DfMA process (BCA, 2016).

The BIM model is an important source of information, which can be analysed and optimised. This could include asset data, geometric data (Rausch et al., 2016; Gbadamosi et al., 2018; Giuda et al., 2019), material information (Gbadamosi et al., 2018), and assembly information (Rausch et al., 2016). These physical BIM properties can be combined with process information and downstream DfMA activities (such as procurement, manufacturing, transportation, installation). These can also be linked to upstream activities (such as briefings, option evaluations, and conceptual design) and increasing consensus among all project stakeholders (BCA, 2016). The structure of BIM and DfMA has been proposed, but under developed.

A BIM-based DfMA process has been established by Yuan et al., (2018). This linear evaluation process has been applied to understand prefabricated building manufacture and assemble. Although most studies are limited in that they focus on either DfM or DfA on industrial manufactured products, rather than architectures. A fully integrated DfMA decision support tool is needed to digitally evaluate across stages of the project lifecycle.

6. Intelligent-enabled DfMA

The application of intelligent technology in the process of DfMA is not a new move. In the past thirty years, with the origin of DfMA theory, related researches have continuously appeared. Commonly used intelligent technologies are shown in Table 3. They are applied for the improvement of process modelling, design estimation and evaluation, assembly/manufacture planning and optimization, recommendations generation, selections comparison, production uncertainty reduction and so on. These issues are also encountered in the process of construction-oriented DfMA. These efforts are for three aspects: (1) design evaluation; (2) design improvement; (3) manufacturing modelling; and (4) assembly planning. However, these intelligent technologies born for manufacturing-oriented DfMA have not been introduced into the construction industry for intelligent upgrading.

Table 3: Intelligent technologies in DfMA

Name	Type	Function	Reference
Experts systems/knowledge-based systems	DfA	Assembly sequence generation	ElMaraghy and Knoll 1991; Li and Chow, 1994; Zha et al., 1999
		Assemblability assessment	Chen et al., 1998; Zha et al., 1999; Mei and Robinson, 2000; Zha et al., 2001b; Shehab and Abdalla, 2006; Sanders et al., 2009
		Satisfying assembly requirements	Mo et al., 1999; Zha et al., 1999
		Flexible assembly planning	Zha et al., 2001a; Zha and Du, 2001; Zha, 2002
		Assembly cost estimation	Shehab and Abdalla, 2006; Sanders et al., 2009
		Assembly technique selection	Shehab and Abdalla, 2006
	DfM	Identifying manufacturing violations	Miller and Colton, 1992
		Modelling DfM process	Bayliss et al., 1995
		Manufacturability assessment	Jung and Billatos, 1993; Yang and Yuan, 1995; Chen et al., 1998; Chan, 2002; Valentinčič et al., 2007
		Facilitating material selection	Shehab and Abdalla, 2001
Case-based reasoning	DfA	Redesigning products with Improved assemblability	Kim, 1997
	DfMA	Machining fixture design in a virtual reality	Gaoliang et al., 2010
Rule-based reasoning	DfMA	Machining fixture design in a virtual reality	Gaoliang et al., 2010
Genetic Algorithms	DfA	Evaluating and selecting parts	Liang and Grady, 1997; Fazio et al., 1999
		Assembly sequence choices	Fazio et al., 1999
	DfMA	Fine-tunes attribute values of the selected design	Changchien and Lin, 2000
Neural network	DfM	Feature recognition	Onwubolu et al., 1999; Marquez et al., 1999
		Material and process parameter selections	Cherian et al., 2000

	DfA	Assembly time estimation	Namouz and Summers, 2013; Owensby and Summers, 2014
Fuzzy logic	DfA	Fuzzy assessment	Zha et al., 1999; Zha and Du, 2001; Zha, 2002
	DfMA	Generate accurate cost estimates	Shehab and Abdalla, 2001
Multi-agent system	DfA	Assembly planning	Zha, 2002

7. Discussion

This literature was mainly concentrated on the level of engineering efficiency of manufacturability and assemblability. Both BIM and intelligent technologies show the ability to facilitate the improvement of evaluation and decision-making for choices or alternatives. The application of BIM includes: (1) to enable the process of DfMA; (2) as a tool for DfMA; (3) as an information source / model for DfMA. Together with BIM, construction-oriented DfMA can adopt intelligent technologies which has been introduced into manufacture-oriented DfMA. A framework of BIM-enabled DfMA with intelligent technology was summarized from the review. As shown in Figure 2, BIM-enabled intelligent toolkit and BIM sources can support the DfMA for a multi-criteria methodology. A more integrated intelligent decision system can be built on this basis to help achieve better manufacturability and assemblability.

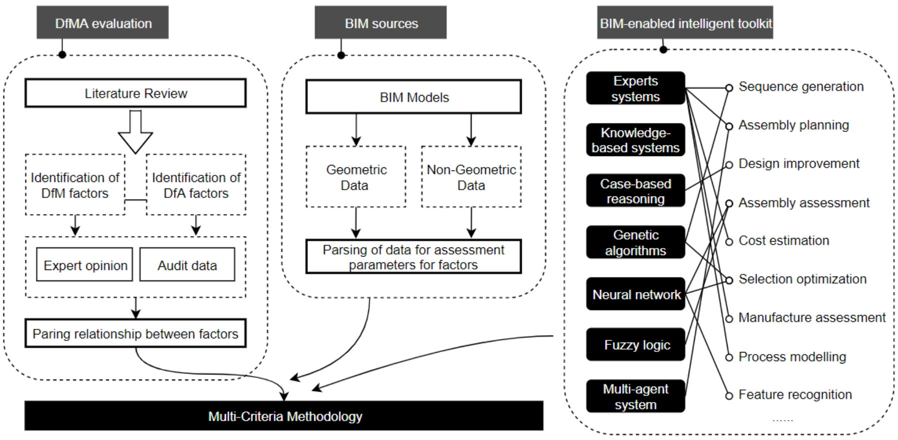

Figure 2: Prototype of BIM-enabled DfMA

However, DfMA intelligent technologies in the manufacturing industry have gone through more than twenty years of development, whereas the corresponding research in construction industry is still in its blank. These mature technologies have not been applied to the design of the construction industry. Due to the characteristic of construction, the process of digital enablement for DfMA cannot be directly transforming from the knowledge of the manufacturing industry. The construction industry does not simply rely on large-scale factory production to complete the entire production process as construction always needs on-site completion. With the development of construction industrialization, it provides an opportunity for the introduction of intelligent technologies. Especially in some building types, such as hospital, factory and house, the application prospect of these intelligent technologies will be more extensive. However, the limitation is that most of these studies in manufacturing were carried out about 20 years ago. The construction industry can get some inspiration for transformation from these mature applications, but still needs to be combined with the technological context of today's era. Further research is needed to bridge these applications to establish a new approach to BIM-enabled design optimization. Researchers need to go beyond the perspective of building components to explore the optimization of the entire building process. At the same time, different prefabrication ratios will result in different workloads at the factory and on-site, and all these factors need to be considered during the optimization method generation.

8. Conclusion and Future Work

This study reviewed previous studies DfMA design optimization studies, and explored their combination with BIM and intelligent technologies. This literature was mainly concentrated on the level of engineering efficiency of manufacturability and assemblability. Uses of BIM-based DfMA included the use of BIM: (1) to enable the process of DfMA; (2) as a tool for DfMA; (3) as an information source / model for DfMA. In addition, construction-oriented DfMA can adopt intelligent technologies which has been introduced into manufacture-oriented DfMA to tackle similar issues. Further research is needed to bridge these applications to establish a new approach to BIM-enabled design optimization. This could include:

• The integrated consideration of manufacturability and assemblability, rather than linear process evaluation and current multi-objective optimization methods.

• Advanced data and pairing to allow expert judgment. The use of historical data and machine learning algorithms may be supplemented by expert opinions to form a hybrid approach.

• Optimization for whole building architectures (e.g. complex healthcare, airport, transportation hub and so on), rather than single building components.

• Comparing different BIM-based DfMA strategies at different prefabrication levels (e.g. the higher the prefabrication, the higher the demand for manufacturing, and less on-site assembly). How to establish a corresponding design optimization method based on the changes in the proportions of these two aspects should be considered.

References

Abergel, T., Dean, B., & Dulac, J. (2017). Towards a zero-emission, efficient, and resilient buildings and construction sector: Global Status Report 2017. UN Environment and International Energy Agency: Paris, France.

Azzi, A., Battini, D., Faccio, M., & Persona, A. (2011). Variability-oriented assembly system design: a case study in the construction industry. Assembly Automation, 31(4), pp.348–357.

Balfour Beatty (2018). Streamlined construction: Seven steps to offsite and modular building.

Başarır, B., & Altun, C. M. (2018). A Redesign Procedure to Manufacture Adaptive Façades with Standard Products. Journal of Facade Design and Engineering, 6(3), pp.77–100.

Bayliss, D. C., Akueson, R., Parkin, R., & Knight, J. A. G. (1995). Concurrent engineering philosophy implemented using computer optimized design. Proceedings of the Institution of Mechanical Engineers, Part B: Journal of Engineering Manufacture, 209(3), pp.193–199.

BCA (2016). BIM for DfMA Essential Guide. Building and Construction Authority, Singapore.

Bogue, R. (2012). Design for manufacture and assembly: background, capabilities and applications. Assembly Automation, 32(2), pp.112–118.

Chan, D. S. (2003). Expert system for product manufacturability and cost evaluation. Materials and Manufacturing Processes, 18(2), pp.313–322.

Changchien, S. W., & Lin, L. (2000). Concurrent design of machined products: a multivariate decision approach. IEEE Transactions on Systems, Man, and Cybernetics, Part C (Applications and Reviews), 30(2), pp.252–264.

Chen, K. H., Chen, S. J. G., Lin, L., & Changchien, S. W. (1998). An integrated graphical user interface (GUI) for concurrent engineering design of mechanical parts. Computer integrated manufacturing systems, 11(1-2), pp.91–112.

Cherian, R. P., Midha, P. S., Smith, L. N., & Pipe, A. G. (2001). Knowledge based and adaptive computational techniques for concurrent design of powder metallurgy parts. advances in engineering software, 32(6), pp.455–465.

De Fazio, T. L., Rhee, S. J., & Whitney, D. E. (1999). Design-specific approach to design for assembly (DFA) for complex mechanical assemblies. IEEE transactions on robotics and automation, 15(5), pp.869–881.

Di Giuda, G. M., Giana, P. E., Masera, G., Seghezzi, E., & Villa, V. (2019). A BIM-based approach to façade cladding optimization: geometrical, economic, and production-control in a DfMA perspective. In 2019 European Conference on Computing in Construction (Vol. 1, pp.324–331). European Council on Computing in Construction.

Eastman, C., Teicholz, P., Sacks, R., & Liston, K. (2011). BIM handbook: A guide to building information modeling for owners, managers, designers, engineers and contractors. John Wiley & Sons.

ElMaraghy, H. A., & Knoll, L. (1991). Design and automatic assembly sequence generation of a dc motor. International Journal of Vehicle Design, 12(5-6), pp.672–683.

Emmatty, F. J., & Sarmah, S. P. (2012). Modular product development through platform-based design and DfMA. Journal of Engineering Design, 23(9), pp.696–714.

Gao, S., Jin, R., & Lu, W. (2019). Design for manufacture and assembly in construction: a review. Building Research & Information, pp.1–13.

Gaoliang, P., Guangfeng, C., & Xinhua, L. (2010). Using CBR to develop a VR-based integrated system for machining fixture design. Assembly Automation, 30(3), pp.228–239.

Gbadamosi, A. Q., Mahamadu, A. M., Oyedele, L. O., Akinade, O. O., Manu, P., Mahdjoubi, L., & Aigbavboa, C. (2019). Offsite construction: Developing a BIM-Based optimizer for assembly. Journal of cleaner production, 215, pp.1180–1190.

Gerth, R., Boqvist, A., Bjelkemyr, M., & Lindberg, B. (2013). Design for construction: utilizing production experiences in development. Construction Management and Economics, 31(2), pp.135–150.

Infrastructure and Projects Authority (2018). National infrastructure and construction pipeline. Available at https://bit.ly/2QoJxYn.

Jiang, L. (2016). A constructability review ontology to support automated rule checking leveraging building information models (Doctoral dissertation, The Pennsylvania State University).

Jung, J. Y., & Billatos, S. B. (1993). An expert system for assembly based on axiomatic design principles. Journal of Intelligent and Robotic Systems, 8(2), pp.245–265.

Kim, G. J. (1997). Case-based design for assembly. Computer-Aided Design, 29(7), pp.497–506.

Kremer, P. D. (2018). Design for Mass Customised Manufacturing and Assembly (DfMCMA): A Framework for Capturing Off-site and On-site Efficiencies in Mass Timber Construction. Mass Timber Construction Journal, 1(1), pp.9–13.

Leaney, P. G. (1996). Case Experience with Hitachi, Lucas and Boothroyd-Dewhurst DFA Methods. In Design for X (pp. 41–71). Springer, Dordrecht.

Lee, S. K., Georgoulas, C., & Bock, T. (2014). Towards 3-D Shape Restructuring for Rapid Prototyping of Joining Interface System. In ISARC. Proceedings of the International Symposium on Automation and Robotics in Construction (Vol. 31, p. 1). IAARC Publications.

Liang, W. Y., & O'Grady, P. (1997). Genetic algorithms for design for assembly: the remote constrained genetic algorithm. Computers & industrial engineering, 33(3-4), pp.593–596.

Machado, M., Underwood, J., & Fleming, A. (2016). Implementing BIM to streamline a design, manufacture, and fitting workflow: a case study on a fit-out SME in the UK. International Journal of 3-D Information Modeling (IJ3DIM), 5(3), pp.31–46.

Marquez, M., Gill, R., & White, A. (1999). Application of neural networks in feature recognition of mould reinforced plastic parts. Concurrent Engineering, 7(2), pp.115–122.

Mei, H., & Robison, P. A. (2000). Adding expert support to assembly-oriented computer aided design tools. Proceedings of the Institution of Mechanical Engineers, Part B: Journal of Engineering Manufacture, 214(1), pp.81–88.

Miller, G. S., & Colton, J. S. (1992). The complementary roles of expert systems and database management systems in a design for manufacture environment. Engineering with computers, 8(3), pp.139–149.

Mo, J., Cai, J., Zhang, Z., & Lu, Z. (1999). DFA-oriented assembly relation modelling. International Journal of Computer Integrated Manufacturing, 12(3), pp.238–250.

Montali, J., Overend, M., Pelken, P. M., & Sauchelli, M. (2018). Knowledge-Based Engineering in the design for manufacture of prefabricated façades: current gaps and future trends. Architectural Engineering and Design Management, 14(1-2), pp.78–94.

Montali, J., Sauchelli, M., Jin, Q., & Overend, M. (2019). Knowledge-rich optimisation of prefabricated façades to support conceptual design. Automation in Construction, 97, pp.192–204.

Namouz, E. Z., & Summers, J. D. (2014). Comparison of graph generation methods for structural complexity based assembly time estimation. Journal of Computing and Information Science in Engineering, 14(2), 021003.

Onwubolu, G. C. (1999). Design of parts for cellular manufacturing using neural network-based approach. Journal of intelligent manufacturing, 10(3-4), pp.251–265.

Orlowski, K., Shanaka, K., & Mendis, P. (2018). Design and Development of Weatherproof Seals for Prefabricated Construction: A Methodological Approach. Buildings, 8(9), 117.

Ou-Yang, C., & Yuan, Y. (1995). An approach to find the minimum wall thickness of a part from its B-Rep model. International journal of production research, 33(5), pp.1339–1355.

Owensby, J. E., & Summers, J. D. (2014). Assembly time estimation: assembly mate based structural complexity metric predictive modeling. Journal of Computing and Information Science in Engineering, 14(1), 011004.

O'Rourke, L. (2013). The future of DfMA is the future of construction. Engineering Excellence Journal, 77.

Rausch, C., Nahangi, M., Perreault, M., Haas, C. T., & West, J. (2016). Optimum assembly planning for modular construction components. Journal of computing in civil engineering, 31(1), 04016039.

Royal Institute of British Architects. (2013), RIBA Plan of Work 2013. RIBA Publishing.

Safaa, Y. P., Hatmoko, J. U. D., & Purwanggono, B. (2019). Evaluation of the use of prefabricated bridge elements with Design for Manufacture and Assembly (DfMA) criteria. In MATEC Web of Conferences (Vol. 270, p. 05006). EDP Sciences.

Samarasinghe, T., Mendis, P., Aye, L., & Vassos, T. (2016). Applications of design for excellence in prefabricated building services systems. In Proceedings of the 7th International Conference on Sustainable Built Environment.

Sanchez, B., & Haas, C. (2018). Capital project planning for a circular economy. Construction Management and Economics, 36(6), pp.303–312.

Sanders, D., Chai Tan, Y., Rogers, I., & Tewkesbury, G. E. (2009). An expert system for automatic design-for-assembly. Assembly Automation, 29(4), pp.378–388.

Shehab, E. M., & Abdalla, H. S. (2001). An integrated prototype system for cost-effective design. Concurrent Engineering, 9(4), pp.243–256.

Shehab, E. M., & Abdalla, H. S. (2006). A cost-effective knowledge-based reasoning system for design for automation. Proceedings of the Institution of Mechanical Engineers, Part B: Journal of Engineering Manufacture, 220(5), pp.729–743.

The Government of Hong Kong SAR Development Bureau. (2018). Construction 2.0. Available at https://www.hkc2.hk/booklet/Construction-2-0-en.pdf.

Trauner, T. J., Lowe, S., Nagata, M. F., & Manginelli, W. A. (2017). Construction delays. Elsevier Science & Technology Books.

Tresidder, M., & White, P. (2018). Briefing: Design for manufacture and off-site construction at Woolston Wastewater Treatment Works (UK). In Proceedings of the Institution of Civil Engineers-Management, Procurement and Law, 171(4), pp.137–140.

Valentinčič, J., Brissaud, D., & Junkar, M. (2007). A novel approach to DFM in toolmaking: a case study. International Journal of Computer Integrated Manufacturing, 20(1), pp.28–38.

Watts, A. (2018). Using robots to help close the gap between designing and making. In Proceedings of the Institution of Civil Engineers-Civil Engineering (Vol. 171, No. 3, pp.100–100). Thomas Telford Ltd.

Yuan, Z., Sun, C., & Wang, Y. (2018). Design for Manufacture and Assembly-oriented parametric design of prefabricated buildings. Automation in Construction, 88, pp.13–22.

Zha, X. F., Lim, S. Y., & Fok, S. C. (1999). Integrated knowledge-based approach and system for product design for assembly. International Journal of Computer Integrated Manufacturing, 12(3), pp.211–237.

Zha, X. F., Du, H., & Lim, Y. E. (2001a). Knowledge intensive Petri net framework for concurrent intelligent design of automatic assembly systems. Robotics and Computer-Integrated Manufacturing, 17(5), pp.379–398.

Zha, X. F., Du, H. J., & Qiu, J. H. (2001b). Knowledge-based approach and system for assembly oriented design, Part I: the approach. Engineering Applications of Artificial Intelligence, 14(1), pp.61–75.

Zha, X. F., & Du, H. (2001). Mechanical systems and assemblies modeling using knowledge-intensive Petri nets formalisms. AI EDAM, 15(2), pp.145–171.

Zha, X. F. (2002). A knowledge intensive multi-agent framework for cooperative/collaborative design modeling and decision support of assemblies. Knowledge-Based Systems, 15(8), pp.493–506.

A BIM-based approach towards additive manufacturing of concrete structures

Patricia Peralta Abadia*, Sebastian Heine, Horst-Michael Ludwig, Kay Smarsly
Bauhaus University Weimar, Germany
patricia.peralta.abadia@uni-weimar.de

Abstract. Additive manufacturing (AM) of concrete structures, a technology to automate the architecture, engineering, and construction industry, has been gaining relevance over the past decade. Current data models employed for AM of concrete structures have been evolving slower than AM technologies, most of which relying on solutions that are not suitable for concrete. Current data models insufficiently support complex inter-process relationships within concrete printing. Taking advantage of building information modeling (BIM), a semantic modeling approach, referred as "printing information modeling" (PIM), is proposed in this paper. The PIM model describes the parameters necessary to execute concrete printing jobs, taking into account processes, material, and geometry information. From the results achieved in this study, it is concluded that integrating PIM into BIM models has the potential to provide complete information models advancing AM of concrete structures.

1. Introduction

Additive manufacturing (AM) of concrete structures, also known as concrete printing, allows producing structures and structural components without using formwork, while reducing manufacturing costs, material costs, and waste (Buswell et al., 2007). Concrete components are manufactured from 3D models by computer-controlled processes in a layer-by-layer basis by extruding and precisely placing concrete. In contrast with fix materials such as polymers or metals, using concrete as printing material implies a strong dependency of the material properties on printing processes and strategies, due to the slow chemical reaction hardening the concrete (Bos et al., 2016). However, current data models employed for AM of concrete structures are derived in the same way as conventional AM, not taking into account the unique conditions specific to concrete printing.

Data modeling for AM is mainly based on traditional solutions, such as standard tessellation language (STL) for geometric representation and G-code (ISO 6983-1) for hardware control (Bonnard et al., 2018). The digital thread from 3D models to printed components is composed of five steps, where data is decomposed into several data formats:

i. design of 3D models as computer-aided design (CAD) models,
ii. conversion of 3D models to STL file format,
iii. generation of computer-aided manufacturing (CAM) models or build files and slicing,
iv. generation of G-code files, and
v. building and post-processing of components.

Information breaks along the digital thread, together with the limitations of the different formats used, cause redundancy, information loss, and inconsistencies, as shown by Lu et al. (2015) and Bonnard et al. (2018). Current data models for AM are insufficient to additively manufacture concrete structures and/or components with adequate structural performance and with geometric precision. Changes in the fresh material properties of concrete and problems with manufacturing processes during printing have a negative effect on the AM process and may diminish the performance of the printed components (Buswell et al., 2018). The inconsistency and unreliability in concrete printing, mainly related to unaccounted inter-process relationships between process, material and geometry, hampers the robustness of the technology. Expertise is required in the AM processes and in material science, from setting ideal process parameters to the preparation and formulation of printable concrete. Geometry and material design, process planning, and process monitoring in concrete printing jobs should go hand-by-hand, allowing traceability along the digital thread. In these respects, deficiencies regarding AM data modeling for concrete structures, such as a lack of knowledge of the relationships between AM parameters and information breaks occurring between 3D models and printing processes, limit the concrete printing process to a long trial-and-error learning curve, as also noted by Salet et al. (2017).

In AM of concrete structures, the material behavior of printable concrete, as a function of time, plays an important role in defining process settings, toolpaths, and computer numerical control (CNC) commands in G-code or CNC code. A new data model containing the main information regarding processes, material, and geometry is required to allow standardization of additive manufacturing in civil engineering. Therefore, the main challenge is to formally describe the relationships of AM processes, material, and geometry parameters to enhance the digital thread currently employed for concrete printing. A new AM data model that takes advantage of building information modeling (BIM) may support the standardization of AM in the architecture, engineering, and construction (AEC) industry. A widely used standardized open BIM exchange format in the AEC industry are the Industry Foundation Classes (IFC). However, a formal description of AM processes using IFC has not yet been reported.

To compensate for the deficiencies and to enhance AM data modeling for concrete structures, a semantic model to be integrated with BIM has been developed in this paper. The semantic modeling approach, referred to as “printing information modeling” (PIM), formally defines the parameters necessary to execute concrete printing jobs regarding processes, material, and geometry. By integrating PIM into BIM, i.e. onto the IFC schema, data generated in the AM digital thread can be stored without losing semantic information. The remainder of the paper is organized as follows. First, a background of joining BIM with AM is presented. Second, the semantic modeling approach is described, presenting the PIM model for AM of concrete structures. Third, the integration of the PIM model with BIM is proposed, where the PIM model is mapped onto the IFC schema to provide a comprehensive information model for additive manufacturing. Fourth, the integration is validated by a case study with an IFC model containing printing information, including slicing and toolpath generation. Finally, the paper concludes with a summary and an outlook on potential future research.

2. Background

BIM is a semantic modeling approach to digitally represent buildings and infrastructure, from planning and design phases to construction and facility management phases (Lu et al., 2015). BIM contains information regarding geometry, material, lifecycle, and compliance checking. The IFC describe basic information of buildings and infrastructure, and may be extended to support domain-specific information (Theiler & Smarsly, 2018). Several extensions have broadened the IFC schema to support point clouds (Krijnen & Beetz, 2017), sensor systems (Theiler & Smarsly, 2018), and cyber-physical systems (Fitz et al., 2019). In the manufacturing domain, an initiative has been started in 2016 to integrate BIM and prefabrication processes, known as IFC4precast. The initiative IFC4precast is currently under development to align precast CAD systems, manufacturing execution systems, and production planning systems (buildingSMART, 2020).

The idea of joining BIM and AM for construction as a digital planning method has been studied by Teizer et al. (2015) and Paolini et al. (2019). In a review, Gradeci et al. (2019) have identified promising potential for integrating BIM and AM, where standardization and documentation of life-cycle data will accelerate the acceptance of AM in the AEC industry. Studies that provide proof of concept for integrating BIM and AM have been developed, using BIM data as input for small-scale study cases (Ding et al., 2014; Correa, 2016; Davtalab et al., 2018). The BIM models, stored in IFC files, are used to transfer the data from BIM software applications to process planning software applications. In Ding et al. (2014), BIM models are manually sliced and data, such as geometry representations, material types and colors, are extracted from the IFC files to generate CNC code. Correa (2016) has developed a computer-aided design system for robot-oriented design of BIM models. The geometry data is extracted from the IFC files and processed according to constraints and limitations of 3D printers, such as printing size and resolution, using proxy elements. Davtalab et al. (2018) proposes to customize BIM models using user-defined property sets for additional material parameters and proxy elements to describe printers. The data is extracted from the IFC files of the customized BIM models and processed for process planning. However, using proxy elements and user-defined property sets to customize BIM models may cause a loss of semantic information (Theiler & Smarsly, 2018).

Formal descriptions of the information necessary for AM of concrete structures are required to preserve the semantic information generated during design and manufacturing. Formal descriptions are represented in the form of semantic models. Recently, semantic models have been developed for conventional AM, focusing on the AM product lifecycle (Lu et al., 2015) and to describe AM technology and operation based on the ISO 14649 standard (Bonnard et al., 2018). Semantic models for conventional AM cannot properly describe the interdependencies within concrete printing. Therefore, a semantic model that describes AM of concrete structures, which can be integrated with BIM, is needed. In the following section, a semantic modeling approach to describe the interdependencies within concrete printing is presented.

3. Printing information modeling

The PIM model defines all parameters relevant to AM of concrete structures for systematically representing specifications of concrete printing jobs. Classes are defined to group the main parameters describing processes, material, and geometry. The relationships between the parameters documented in literature are used as basis for developing the PIM model (Bos et al., 2016; Bonnard et al., 2018; Paul et al., 2018; Salet et al., 2017; Buswell et al., 2018). The PIM model is shown in Figure 1 as a unified modeling language class diagram, describing the printing information required for concrete printing jobs. In this section, elements of the PIM model are printed in *italics* when describing the semantic model.

The PIM model comprises three main abstract classes, *ProcessInformation*, *MaterialInformation*, and *GeometryInformation*. The process information is categorized into subclasses describing printing settings for the pump system and the printhead (*PumpSystemData* and *PrintheadData*), filament properties (*FilemantData*), printing strategy and toolpaths (*ToolpathData*), and monitoring data (*ControlData*). The material information includes subclasses to describe reinforcement (*ReinforcementData*) and concrete (*ConcreteData*). The geometry information may be inherited from BIM models, which incorporate geometry information by nature, and it is categorized into subclasses describing dimension definition (*Dimension*), point definition (*Point*), and geometric object definition (*GeometricObject*) as well as contour lines data (*ContourLine*) as a result of slicing. A detailed description of the semantic model is presented in Smarsly et al. (2020). In Figure 1, the gray-colored elements are used to illustrate the IFC mapping of the semantic model in the following sections.

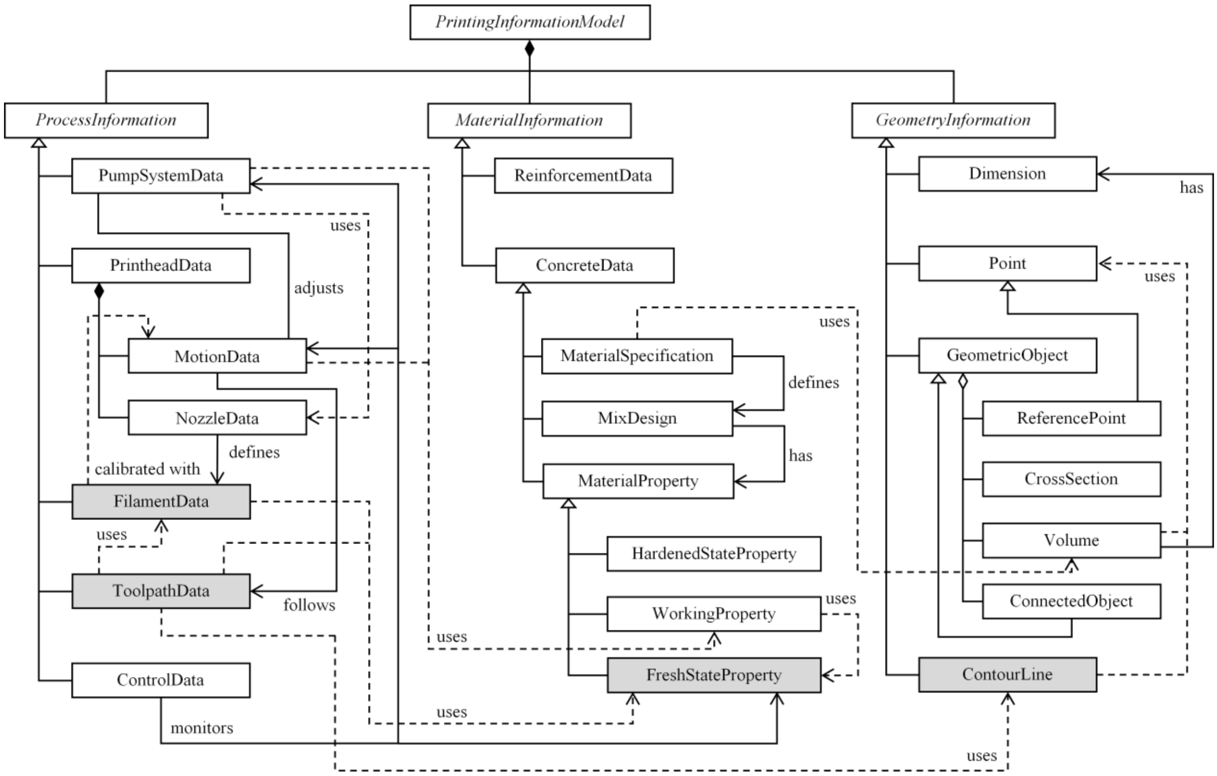

Figure 1: Extract of the PIM model.

4. IFC-based printing information modeling

A BIM approach towards concrete printing that aligns the PIM model and the IFC schema for IFC-based printing information modeling is presented in this section. Geometry parameters and material parameters that describe specifications required for AM are already specified in common BIM models compliant to the IFC schema (Smarsly et al., 2020). In this study, by mapping all parameters and parameter relationships defined in the PIM model onto the IFC schema, a comprehensive BIM model describing the AM digital thread is achieved. The BIM model is used later to generate commands that control concrete printers as CNC code. Hence, a BIM-based file format for 3D printing integrates the digital thread in a single file, from slicing to CNC code generation.

The PIM model is mapped onto the current IFC version "IFC 4 – Addendum 2", or "IFC4" for short (buildingSMART, 2017). IFC schema elements (e.g. IFC entities and property sets) and core concepts that can be reused are identified based on the description presented in Borrmann et al. (2015) and on the documentation of IFC4. Aligning the PIM model with the IFC schema reduces the need to define new IFC entities and property sets, ensuring the maintainability of the IFC schema. In this section, when describing the mapping, elements of the IFC schema are printed in *italics* and elements of the PIM model are printed in ***bold italics***. In the following paragraphs, a description of the mapping of the abstract classes ***ProcessInformation***, ***MaterialInformation***, and ***GeometryInformation*** onto the IFC schema is presented.

The ***ProcessInformation*** describes specific information required for additive manufacturing. Therefore, a domain-specific schema extension must be integrated into IFC's domain layer. In Table 1, the mapping for the subclasses of the abstract class ***ProcessInformation*** is summarized. In the table, it is noted if new subentities, enumeration constants, or property sets are needed.

Table 1: Mapping of the subclasses of the abstract class *ProcessInformation* onto the IFC schema.

PIM class	IFC entity	Function
PumpSystemData	*IfcDistributionSystem*	Describes the pump system as a network to distribute concrete as an operational type. The mixer is described as an *IfcTank* holding a source port, the pump is described as an *IfcPump,* and the hose is described as an *IfcPipeSegement*. All entities are connected through the concept of port nesting. The sink port of the distribution system is the nozzle in the printhead.
PrintheadData	*IfcTransportElement*[1]	Describes an element that moves horizontally in the XY plane and vertically in the Z axis, and that transports concrete. It is related to an actuator (*MotionData*) and a terminal (*NozzleData*). A new enumeration constant of *IfcTransportElementEnum* is required to describe movement in XYZ axes.
MotionData	*IfcActuator*	Controls the motion of the printhead converting input signals into a motion output.
NozzleData	*IfcFlowTerminal*[1]	Describes the basic shape and dimensions of the nozzle. A new subentity for *IfcFlowTerminal* is required to describe a nozzle.
FilamentData	*IfcBuildingElementPart*[1]	The printed element is an assembly of filament layers. Similar to the approach used for precast elements, each filament layer is described as an *IfcBuildingElementPart*. A new enumeration constant of *IfcBuildingElementPartTypeEnum* is required.
ToolpathData	*IfcLinearPositioningElement*[1]	Describes the toolpath with a curve, similar to an alignment. Properties to define attributes of the toolpath, such as direction, change of velocity (in curves) and print pattern, must be defined.
ControlData	*IfcMonitor* (Theiler et al., 2018)	The IFC schema extension *IfcMonitor* proposed by Theiler et al. (2018) can be applied to monitor and control the printing process.

[1] New subentities, enumeration constants, or property sets are required.

The ***MaterialInformation*** is aligned with the *IfcMaterialResource* schema in IFC's resource layer. The materials are associated to the *IfcElements* with the relationship *IfcRelAssociatesMaterial*, and property sets are used to define material properties. In the case of ***ConcretData***, existing property sets, such as *Pset_MaterialConcrete,* may be used to describe one or a set of ***MaterialSpecification***. In a similar manner, *Pset_MaterialCommon* and *Pset_MaterialMechanical* may be used to describe one or a set of ***HardenStateProperty***. New property sets need to be created to describe the subclasses ***MixDesign***, ***FreshStateProperties***, and ***WorkingProperty***.

The ***GeometryInformation***, as mentioned earlier, may be inherited from BIM models, i.e. entities and property sets that exist in the IFC schema, to describe dimensions, points, and geometric objects. Instances of ***GeometricObject*** are defined in the *IfcProductExtension* in IFC's core layer, aligned with subentities of the entity *IfcElement*, and their geometry may be defined with *IfcShapeRepresentation* or *IfcTopologyRepresentation*. In the case of building elements, such as walls and columns, instances of ***GeometricObject*** are defined in the schema *IfcSharedBldgelements* in IFC's interoperability layer. The subclass ***ContourLine*** describes the 2D geometric representation of the layers resulting from slicing the geometric objects. In this case, the sliced geometric objects may be defined either with the layers being instances of *IfcElement* connected to each other by the relationship *IfcRelConnectsElements* or with the layers being instances of *IfcElementComponent* (i.e. *IfcBuildingElementPart*) aggregated to form an *IfcElement* or an *IfcElementAssembly*. An example of the aggregated relationships can be seen in the example of *IfcWallElementedCase* (buildingSMART, 2017) and in the progress reports of the initiative IFC4precast (buildingSMART, 2020). In the following section, a case study is presented to validate the mapping described herein.

5. Case study

A case study is devised to validate the IFC-based printing information modeling approach for AM of concrete structures and to test the feasibility of the proposed mapping. A test structure is modeled for concrete printing, from slicing to generating a toolpath. The classes *ContourLine*, *FilamentData*, *ToolpathData*, and *FreshStateProperty* of the PIM model are described using IFC entities. In this section, the elements of the IFC schema are printed in *italics*.

The test structure of one story height is modeled using an IFC-compliant BIM software application. The test structure, shown in Figure 2, is composed of five walls (*IfcWallStandardCase*) of 2000 mm height, 150 mm thickness, and different lengths. The test structure is sliced into layers of 40 mm height. For each wall, every layer is described as an *IfcWallStandardCase* connected to each other layer using the relationship *IfcRelConnectsElements*. The layers are associated to data regarding filament, toolpath, and fresh material properties of the printable concrete, which requires new subentities, enumeration constants, and property sets. The new IFC elements and the associations with the layers are shown in the object typing diagram given in Figure 3. The filament data is described with an *IfcBuildingElementPart* (with a user-defined enumeration constant), the toolpath data is described with an *IfcLinearPositioningElement*, and the fresh state property for green strength is described with an *IfcPropertyListValue* added to the *IfcMaterial* for concrete.

As a result of the case study, an IFC-based printing information model is obtained, describing data regarding contour line, filament, toolpath, and fresh state material properties of the printable concrete. Each layer has a layer height of 40 mm, and the contour line information is described by the geometry representation of each layer. The filament has a thickness of 150 mm and a height of 40 mm, equal to the dimensions of each layer.

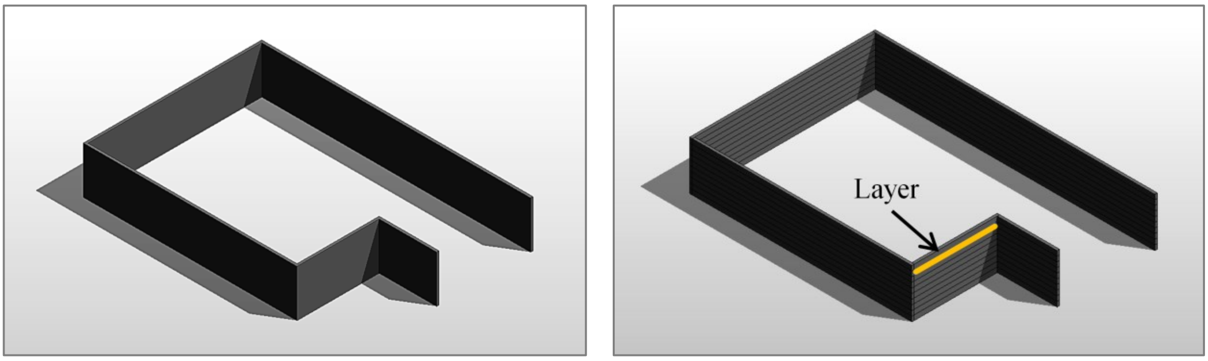

Figure 2: Model of the test structure (a) and sliced model (b).

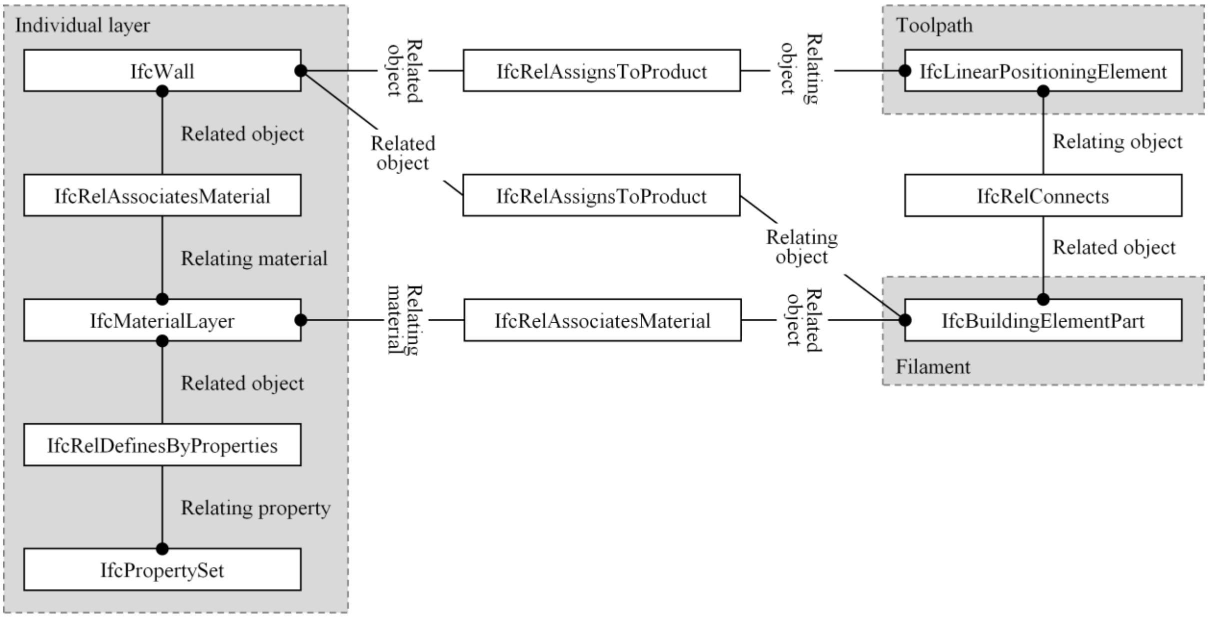

Figure 3: Object typing for a layer.

In the sliced model, each layer is represented as an *IfcSweptAreaSolid*, defined by a profile and an extrusion height. The profile describes the contour line of the layer, and the extrusion height describes the layer height. As shown in Figure 2, each wall is sliced into layers independently. Each layer has filament data, toolpath data, and the fresh material property "green strength". The geometry of the filament depends on the shape and dimensions of the nozzle (here 150 mm × 40 mm) and the composition of the concrete. By visualizing the filament data during the planning process, the tradeoff between printer resolution and geometric precision is addressed in case of the wall thickness being different from the filament thickness or in case of detailing. When the thickness of the wall and the filament are the same, the toolpath is defined by the centerline of the layer. The toolpath is later used to define the list of coordinates for the CNC code. It must be noted that for more complex layouts, fresh material properties, such as green strength, may affect the toolpath definition. In this case study, the green strength is described with a list since it is a function of time, i.e. it increases with time. Knowing the behavior of the green strength allows to accordingly modify the toolpath, improving the quality of the printed structure.

6. Summary and conclusions

A semantic modeling approach that takes advantage of BIM, referred to as "printing information modeling", has been developed, serving as a tool to define a new data model that provides a formal basis for standardizing additive manufacturing in civil engineering. The PIM model has been integrated into BIM by mapping its components onto the IFC schema. A case study has been devised to validate the mapping obtaining a comprehensive information model for AM of concrete structures. It has been demonstrated that the PIM model can be integrated with BIM to store the information necessary for data modeling of AM of concrete structures, showing potential of using IFC-compliant BIM models as sole formal basis for AM of concrete structures. Implementing the IFC-based PIM approach, besides advancing standardization in the AEC industry, allows collaboration between disciplines to integrate building services into the manufacturing process. However, the approach has only been tested with structures that have simple layouts, where toolpaths can be easily determined. In future work, the integration of AM into BIM documented in this paper may be improved by adding algorithms for toolpath optimizations and CNC code generation, known as "algorithmic BIM". Further studies are required to accurately describe the relationships between process information and material information in the IFC schema. Last, but not least, the integration of the PIM model into BIM may be formalized by an IFC schema extension.

Acknowledgments

The authors would like to acknowledge the financial support the German Research Foundation (DFG) through grant SM 281/7-1. Parts of this research have been conducted in the "Structural Health Monitoring Laboratory", sponsored by the European Union through the European Fund for Regional Development (EFRD) and the Thuringian Ministry for Economic Affairs, Science and Digital Society (TMWWDG) under grant 2016 FGI 0009. Any opinions, findings, conclusions, or recommendations expressed in this paper are those of the authors and do not necessarily reflect the views of DFG, EFRD, or TMWWDG.

References

Bonnard, R., Hascoët, J.-Y., Mognol, P. & Stroud, I., (2018). STEP-NC digital thread for additive manufacturing: data model, implementation and validation. International Journal of Computer Integrated Manufacturing, 31(11), pp. 1141–1160.

Borrmann, A., Beetz, J., Koch, C., Liebich, T. & Muhic, S., (2015). Industry Foundation Classes: A standardized data model for the vendor-neutral exchange of digital building models. In: Borrmann, A., König, M, Koch, C. & Beetz, J. (eds.), 2015, Building Information Modeling: Technology foundations and industry practice, Switzerland, Springer, pp. 81–126.

Bos, F., Wolfs, R., Ahmed, Z. & Salet, T., (2016). Additive manufacturing of concrete in construction: Potentials and challenges of 3D concrete printing. Virtual and Physical Prototyping, 11(3), pp. 209–225.

buildingSMART, (2017). Industry Foundation Classes 4.0.2.1, Version 4.0 – Addendum 2 – Technical Corrigendum 1. Retrieved January 20, 2020 at: https://standards.buildingsmart.org/IFC/RELEASE/IFC4/ADD2_TC1/HTML/.

buildingSMART, (2020). IFC4precast. Retrieved January 20, 2020 from www.ifc4precast.com.

Buswell, R. A., Leal de Silva, W. R., Jones, S. Z. & Dirrenberger, J., (2018). 3D printing using concrete extrusion: A roadmap for research. Cement and concrete Research, 112(2018), pp. 37–49.

Buswell, R. A., Soar, R. C., Gibb, A. G. F. & Thorpe, A., (2007). Freeform construction: Mega-scale rapid manufacturing for construction. Automation in Construction, 16(2007), pp. 224-231.

Correa, F. R., (2016). Robot-oriented design for production in the context of building information modeling. In: Proceedings of the 33rd International Symposium on automation and Robotics in construction. Auburn, AL, USA, July 18, 2016.

Davtalab, O., Kazemian, A., & Khoshnevis, B., (2018). Perspectives on a BIM-integrated software platform for robotic construction through Contour Crafting. Automation in Construction, 89(2018), pp.13–23.

Ding, L., Wei, R., & Che, H., (2018). Development of a BIM-based automated construction system. Procedia Engineering, 85(2014), pp. 123–131.

Fitz, T., Theiler, M. & Smarsly, K., (2019). A metamodel for cyber-physical systems. Advanced Engineering Informatics, 41(2019), 100930.

Gradeci, K. & Labonnote, N., (2019). On the potential on integrating building information modeling (BIM) for additive manufacturing (AM) of concrete structures [published online ahead of print date]. Construction Innovation. DOI: 10.1108/CI-07-2019-0057.

Krijnen, T., & Beetz, J. (2017). An IFC schema extension and binary serialization format to efficiently integrate point cloud data into building models. Advanced Engineering Informatics, 33(1), 473–490.

Lu, Y., Choi, S. & Witherell, P., (2015). Towards an integrated data schema design for additive manufacturing: Conceptual modeling. In: Proceedings of the ASME 2015 International Design Engineering Technical Conferences & Computer and Information in Engineering Conference. Boston, MA, USA, August 2, 2015.

Paolini, A., Kollmannsberger, S. & Rank, E., (2019). Additive manufacturing in construction: A review on processes, applications and digital planning methods. Additive Manufacturing, 30(2019), 100894.

Paul, S. C., van Zijl, G. P., Tan, M. J. & Gibson, I., (2018). A review of 3D concrete printing systems and material properties: Current status and future research prospects. Rapid Prototyping Journal, 24(4), pp. 784–798.

Salet, T. A., Bos, F. P., Wolfs, R. J. & Ahmed, Z. Y., (2017). 3D concrete printing – a structural engineering perspective. In: Proceedings of the 2017 fib Symposium – High Tech Concrete: Where Technology and Engineering Meet. Maastricht, NL, June 12, 2017.

Smarsly, K., Peralta, P., Luckey, D., Heine, S., & Ludwig, H.-M., (2020). BIM-based concrete printing. In: Proceedings of the International ICCCBE and CIB W78 Joint Conference on Computing in Civil and Building Engineering 2020. Sao Paolo, Brazil, June 2, 2020.

Teizer, J., Blickle, A., King, T., Leitzbach, O., Guenther, D., Mattern, H. & König, M., (2015). BIM for 3D printing in construction. In: Borrmann, A., König, M, Koch, C. & Beetz, J. (eds.), 2015, Building Information Modeling: Technology foundations and industry practice, Switzerland, Springer, pp. 421–446.

Theiler, M. & Smarsly, K., (2018). IFC Monitor – An IFC extension for modeling structural health monitoring systems. Advanced Engineering Informatics, 37(2018), pp. 54–65.

Metadata-based photo filtering for facility management

Thomas Czerniawski*, M.S., PhD student, Jong Won Ma, M.S., PhD student, Fernanda Leite, Ph.D., P.E., Associate Professor
University of Texas at Austin, USA
* tczernia@utexas.edu

Abstract. Facility management information systems are difficult to manage due to the enormous scope of buildings. We present a method for organizing and retrieving photos from massive facility management photo databases using photo-metadata. Providing an intuitive organizational scheme, location, camera orientation, and semantic content description metadata exploit the physical structure of the existing building their photos represent. Location is inferred using Bluetooth beacons. Camera orientation is inferred from the device's on-board inertial measurement unit (IMU). Image content is inferred using automatic object recognition. As a user traverses the interior of a facility, the photo library displayed on their mobile device is ordered by the proximity to the user's current location. A root mean square error (RMSE) of 1.1 meters is achieved for localization. This ordering is refined using a query image's camera orientation and image semantic content description. The presented photo management application reduces the time required to find relevant historical photos representing objects within a user's vicinity.

1. Introduction

Photographs are an underutilized resource in facility management. Several electronic reference texts in the facility management domain (Teicholz, 2014, Cotts, 1999, Talamo and Bonanomi, 2015, Wiggins, 2014, Teicholz, 2013, Finch, 2012, Gelfand, 2011) present virtually no search results for the terms: photos and photographs. With little guidance, facility management professionals are overwhelmed by enormous photo libraries collected over multiple decades, stored in scattered digital storage locations, and subjected to ephemeral categorization schemes (e.g. renovation or remodelling project identifiers).

In order to overcome these difficulties, the industry must improve their information stewardship; organizing, compiling, and maintaining photos in the most structured, integrated, and accessible manner possible (Smith and Tardif, 2009). It has been demonstrated that the search time required to find photos of interest was reduced by exploiting photo time-stamps in organizing photo libraries (Graham et al., 2002). In addition to the time-stamp, location is another useful form of metadata. Search engines have been refining the relevance of their search results using location data with great success (Crane et al., 2012). Rhodes (Rhodes, 2003) presented a systems called Just-in-Time Information Retrieval where old text notes are shown to a user based on their current location, people in their immediate area, and the subject-line and contents of any current notes being written. Evidently, metadata, including location and content description, has the potential to improve our ability to store and retrieve relevant information.

In this paper, we present a metadata-based photo filtering system for facility management. This metadata consists of location, camera orientation, and image semantic content description. Location is an important form of metadata because when performing work in a facility, facility managers are interested in idiosyncrasies of particular spaces and their histories. The accessibility of this information is a problem since relevant photos are often stored in dispersed project sorted folders, e.g. all files associated with renovation XYZ. Retrieving all location relevant photos would require remembering all projects that have taken place within a space and navigating through all associated folders. By tagging photos with location metadata, this search can be automated. In this work, location metadata is inferred from the Received Signal Strength (RSS) of Bluetooth Low Energy (BLE) beacon packets broadcast by anchor nodes and received by a BLE enabled mobile device. Bluetooth was selected as the localization hardware of choice because of the many reported benefits as compared to alternatives such as speed, energy-efficiency, mobile platform ease-of-development, and signal emitter positioning flexibility (Faragher and Harle, 2015).

Camera orientation is an important form of metadata because of the clues it provides about the relative position of the building component of interest compared to the user, e.g. above or beside. Camera orientation (heading and polar angle) is inferred from the mobile device's on-board inertial measurement unit (IMU). IMU data is easy to obtain as virtually all mobile devices are supplied with IMU's on-board.

Finally, image content description metadata is important because when diagnosing systemic problems within buildings, it is instrumental to be able to quickly analyse all similar building components within a facility. For example, if excessive moisture is being built up on the duct within the space the user is in, it would be informative to determine whether excessive moisture has been building up on ducts elsewhere in the building. Thus if all images with ducts, or more specifically ducts with pooling water, could be retrieved automatically, this analysis would be expedited. In this work, image content is inferred using automatic object recognition with a convolutional neural network.

Rather than relying on ad-hoc organizational schemes, photos stored and retrieved using location, camera orientation, and content description metadata exploit the intuitive physical structure of the existing building their photos represent. As a user traverses the interior of a facility, the photo library displayed on their mobile device is ordered by the proximity of each photo's captured location to the user's current location. This ordering is further refined using similarity of a query image's camera orientation and image content. This ultimately reduces the time required to find relevant historical photos representing object's within the user's vicinity.

2. Background

2.1 Indoor Localization

Indoor localization technologies, classified by measured physical quantity, fall into six categories (Torres-Solis et al., 2010), namely, (1) radio frequency waves, (2) photonic energy, (3) sonic waves, (4) mechanical energy (inertial or contact), (5) magnetic fields, and (6) atmospheric pressure. Radio frequency (RF) localization is selected for this work because of the availability of reliable low-cost commercial products, low processing requirements, privacy preservation, and the ability to provide adequate floor coverage using a small number of devices (Torres-Solis et al., 2010).

First, optimal beacon (RF signal emitter) locations are selected (Chawathe, 2008). Second, physical RSS measurements are translated to indoor location coordinates (x, y). This translation is achieved through geometric mapping or fingerprinting (Yang et al., 2013). In geometric mapping, distance relative to reference points is derived from RSS. Distances are then converted into locations using geometric algorithms (e.g., triangulation) (Yang et al., 2013). On the other hand, fingerprinting adopts a pattern-matching approach. Signal features of all possible locations in the area of interest are collected and stored in a fingerprint database (known as site survey or calibration). Localization is performed by matching the measured fingerprints at an unknown location with those in the database and returning the location corresponding to the best-fitted fingerprint (Yang et al., 2013).

Geometric mapping and fingerprinting contend with the following challenges. Materials such as wood and concrete attenuate RF signals, while metals and water cause reflections, scattering, and diffraction (Torres-Solis et al., 2010). These affects impact geometric mapping in particular due to multi-path radio wave propagation, which encumbers accurate calculation of distance. Another challenge involves the adverse effects of a changing physical environment on the propagation of radio waves. Changes such as the rearrangement of furniture, structural modifications or movement of personnel within a building. Signal properties measured at a certain point in time cannot be used to reliably localize without accounting for these dynamics (Torres-Solis et al., 2010).

2.2 Object Recognition

Object recognition is the process of categorizing subsets of input data into predefined classes. When applied on a pixel-level, it is called semantic scene segmentation. The success of emerging semantic scene segmentation methods is a result of the rapid progress of modern machine learning methods, such as convolutional neural networks. One requirement for applying these approaches successfully is the availability of large, labeled datasets. Several publicly available datasets related to building component recognition have been released in recent years. Notable RGB-D datasets include: ScanNet (Dai et al., 2017), 3DFacilities (Czerniawski and Leite, 2018), and Matterport (Chang et al., 2017). A convolutional neural network trained on 3DFacilities successfully recognized many building component categories in digital images automatically (Czerniawski and Leite, 2019). With this advance in object recognition technology, automated analysis of images using convolutional neural networks presents an opportunity for semantic-based retrieval of photos in the context of buildings. The method from (Czerniawski and Leite, 2019) will be used in this paper to generate photo content description metadata.

3. Methodology

An arrangement of three rooms in an institutional building are selected as the testbed (Figure 1). A custom photo taking and photo viewing software application is developed for a BLE enabled mobile device with on-board IMU (Figure 1). Metadata is captured with every photo (Figure 2). Metadata includes: a heading (degrees clock-wise from true-north), acceleration, and RSSs from all paired Bluetooth beacons.

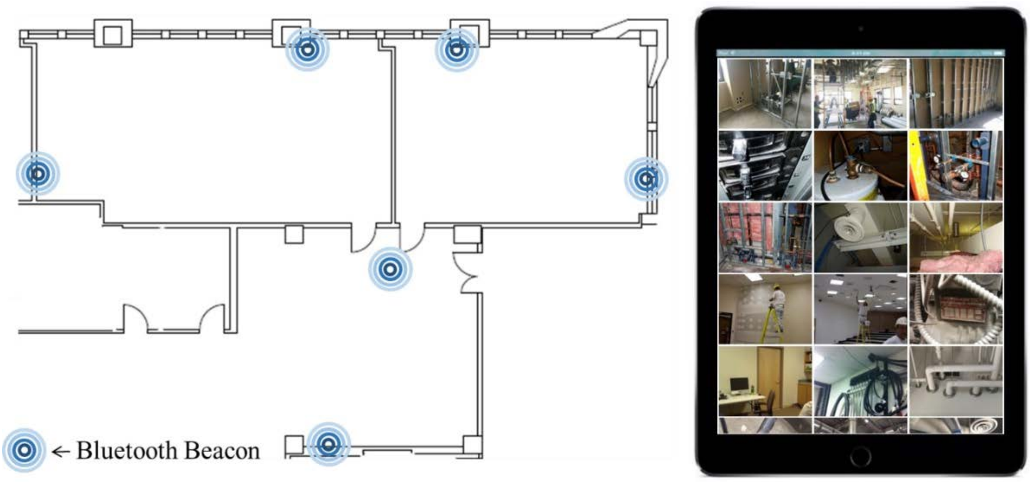

Figure 1: Testbed floorplan with beacon locations and mobile app screenshot with photos ordered by location

```
{"heading":236.4632568359375,
"acceleration":{"X":-0.8806915283203125,
                "Z":0.306976318359375,
                "Y":-0.0365447998046875},
"RSSIs":{"Beacon1":-94,-94,-100,-93,-95,-100, "Beacon2":-87,-87,-88,-89,-87,-86,
         "Beacon3":-77,-77,-77,-82,-88,-88, "Beacon4":-85,-100,-84,-89,-85,-85,
         "Beacon5":-63,-67,-67,-63,-64,-65, "Beacon6":-78,-83,-79,-76,-88,-79}}
```


Figure 2: Example captured image metadata: heading, acceleration, RSSIs

3.1 Localization

Bluetooth beacon locations were selected and the beacons were placed (Figure 1). The rationale behind the selected beacon locations was to maximize square footage of localizing scope using a minimal amount of beacons. The minimal amount of beacons was determined by the requirements of triangulation; each area of the floorplan should receive a relatively strong signal from at least three beacons. Beacon RSS measurements were then translated to indoor location coordinates (x_{photo}, y_{photo}) using a radio frequency (RF) fingerprinting pattern-matching approach (Yang et al., 2013). First, signal features of locations in the area of interest were collected and stored in a fingerprint database (known as site survey or calibration) along with their ground truth x and y coordinates. This floorplan canvasing was performed with a spacing of 1.3 meters. The resulting per-beacon signal strengths can be seen in Figure 3. The lighter the color, the stronger the signal strength, the darker the color, the weaker the signal strength.

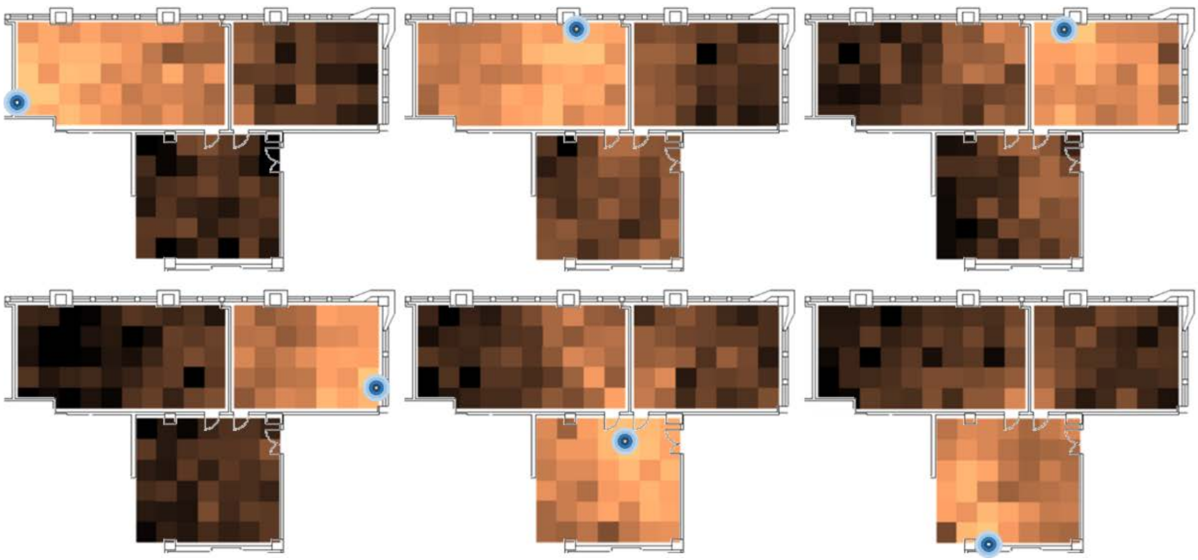

Figure 3: Beacon strength heat map for each of the six Bluetooth beacons

User localization (x_{user}, y_{user}) is performed by matching measured fingerprints at an unknown location with those in the database and returning the location corresponding to the best-fitted fingerprint. Each cell has a size of 1.3m by 1.3m and indoor location coordinates were calculated for the center of each cell to represent the dependent variables; for example, the dependent variables for the most upper-left cell would be x=0.65 and y=0.65. The regression algorithms were then designated to predict the location coordinates using 6 beacon signal features. Two regression algorithms, Artificial Neural Network (ANN) and Support Vector Regression (SVR) were deployed for estimating the location from sensor signals.

For ANN, a classic two hidden layer feed-forward neural network model was employed with the scaled conjugate gradient for back-propagation algorithm. We experimented to find the optimal model structure by generating 100 models by increasing the number of neurons in each hidden layer from 10 to 100 with interval of 10 units.

SVM maps the input training data into a higher dimensional feature space through function and creates a hyperplane with the margin which separates the feature space. SVR is a regression algorithm that maintains the main features of Support Vector Machine (SVM). In this process, kernel functions play an important role which transform the data into a higher dimensional feature space to make it possible to perform the linear separation. We've experimented with four common kernel functions (i.e., linear, polynomial, radial basis function, sigmoid) for our dataset.

The performance of both ANN and SVM are evaluated using root mean square error (RMSE).

3.2 Camera orientation

The camera orientation during image capture is inferred using heading and acceleration data. Acceleration data captures the direction of gravity and is used to calculate the polar angle of the camera.

3.3 Semantic Segmentation

The neural network from (Czerniawski and Leite, 2019) is used to semantically segment collected images. Pixels are classified into one of 18 building component classes. Number of pixels per class are divided by the total number of pixels in the image. This provides the portion of the image comprised by each class. Due to class imbalance, these feature space needs to be normalized by the natural distribution of classes in building images. The average per-image pixel class distribution is calculated for 3DFacilities. The pixel class distribution for each image is divided by the 3DFacilities average per-image pixel class distribution. The result is a per-class percent of average class presence. For example, door 210% means there are 210% the amount of door pixels as compared to an average image in 3DFacilities.

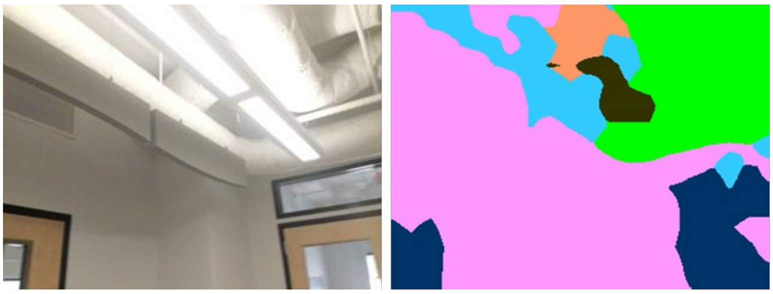

furniture	0%	railing	0%
door	210%	light fixture	0%
wall	142%	elevator	0%
floor	0%	plumbing	173%
window	0%	duct	227%
ceiling	19%	diffuser	0%
column	0%	sprinkler	0%
beam	0%	cable tray	0%
stairs	0%	conduit	154%

Figure 4: Example semantic segmentation by deep neural network and tabulated percent of average class presence

These 18 features provide a high-dimensional feature space wherein photos are organized based on the similarity of their semantic content Figure 5. During image retrieval, images will be ordered by proximity to a query image in this high-dimensional space.

3.4 Application use

Photo retrieval and ordering is performed in two stages. First, photos are ordered based on location proximity to the current location of the user. Search results can be further refined by the user capturing a photo of the building component of interest. The captured image provides additional camera orientation and content metadata for image retrieval and ordering.

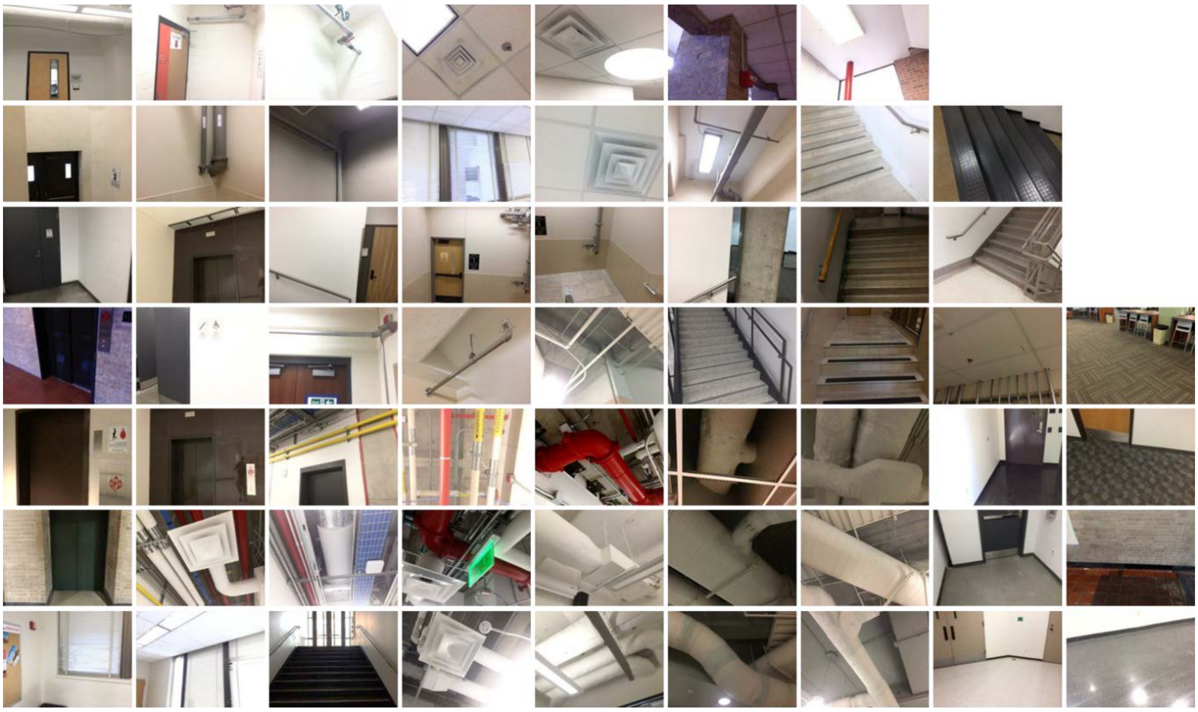

Figure 5: Image content feature-space projected to two dimensions using t-sne (Maaten and Hinton, 2008).

4. Results and Discussion

Historical photo retrieval is performed in two stages. As a user of the mobile applications travels through the interior of a facility, the photo library displayed on their mobile device is first ordered by the proximity of each photo's captured location to the user's current location. Then, the user can further refine retrieved photos by capturing a query image of their building component of interest and refine the search using similarity of retrieved images to the query image based on camera orientation and image content description.

4.1 Localization

Two regression algorithms, Artificial Neural Network (ANN) and Support Vector Regression (SVR) were deployed for localization. Of the 100 ANN models we tested, the best performance was observed when using 30 hidden neurons for each layer. For SVM, of the four common kernel functions tested, the best performance was achieved using the radial basis function. In this experiment, 5-fold cross validation was conducted to assess the generalizability of each prediction model and the root mean square error (RMSE) was calculated as an accuracy metric for 127 locations. As a result, average RMSE from SVM was lower than that from ANN, showing 1.103 meters and 1.151 meters respectively. The local RMSE values can be seen in the heat maps in

Figure 6. The two methods generally performed poorly in the same regions, and so there appears to be little opportunity for a boost in performance through an ensemble. Corners were areas for poor localization. Regions near beacons demonstrated the highest accuracy.

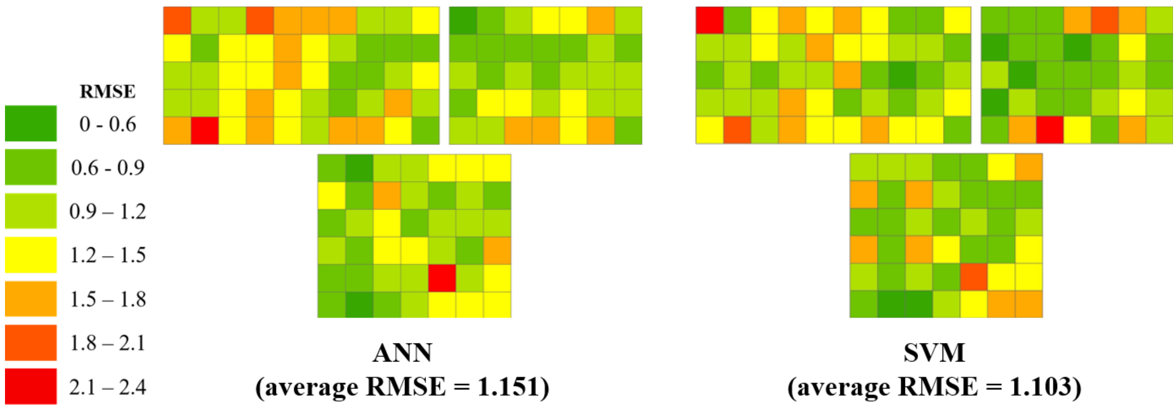

Figure 6: Localization error heat map

4.2 Camera orientation and Content Similarity

The user had the additional option of retrieving images with similar camera orientation and content to a query image. In Figure 7, the two search result images on the right-hand side share the same location metadata and so are both retrieved when the user is at that location. However, if the user is interested in the HVAC within that location, they capture the query image on the left-hand side of Figure 7. The convolutional neural network attached semantic metadata. Then the search results are further ordered by similarity to the query image.

Figure 7: Location metadata-based search results refined using query camera orientation and content metadata

4.3 Practical Benefits of the Mobile Application

The simplicity of a meta-data ordered photo gallery overcomes many of the difficulties involved in managing building facility information systems. Due to their enormous scope, both spatially and temporally, maintaining building information requires a lot of time and discipline. This requirement has prevented the adoption of many more capable yet complex information solutions in the facility management space. The presented application relies on photos, which are an incredibly easy form of data to collect. The presented application relies on automated meta-data tagging, removing the user and therefore the limitations of requiring prolonged and consistent discipline. Therefore, the presented application has a much higher probability of long-term sustainable adoption and use.

5. Conclusions

Facility management professionals are overwhelmed by enormous photo libraries collected over multiple decades, stored in scattered locations, and subjected to ephemeral categorization schemes. In this paper, we presented a method for organizing and retrieving photos from massive facility management photo databases using photo-metadata including: location, camera orientation, and semantic content description. Location was inferred from the Received Signal Strength of Bluetooth Low Energy beacons. Camera orientation was inferred from the device's on-board inertial measurement unit. Image content was inferred using automatic object recognition. As a user traversed the interior of the facility, the photo library displayed on their mobile device was ordered by the proximity of each photo's captured location to the user's current location. This ordering was refined using a query image's camera orientation and image content.

Localization was performed using a fingerprinting approach. First, signal features of locations in the area of interest were collected and stored in a fingerprint database along with their ground truth x and y coordinates. User localization was performed by matching measured fingerprints at unknown locations with those in the database and returning the location corresponding to the best-fitted fingerprint. The root mean square error (RMSE) for localization using SVM was lower than the RMSE for ANN, 1.103 meters and 1.151 meters respectively. The content of images was classified into 18 classes and provided a feature space were images of similar semantic content were proximal. This ultimately reduces the time required to find relevant historical photos representing objects within the user's vicinity.

References

Chang, A., Dai, A., Funkhouser, T., Halber, M., Nießner, M., Savva, M., Song, S., Zeng, A. & Zhang, Y. (2017). Matterport3d: Learning from RGB-D data in indoor environments. arXiv

Chawathe, S. S., (2008). Beacon placement for indoor localization using bluetooth. 11th International IEEE Conference on Intelligent Transportation Systems, 2008. IEEE, pp. 980–985.

Cotts, D. G. (1999). *The facility management handbook,* New York, AMACOM.

Crane, A. S., Pastusiak, A. & Zhiyanov, D. V. (2012). Using location for determining relevance between queries and advertisements. Google Patents.

Czerniawski, T. & Leite, F. (2018). 3DFacilities: Annotated 3D reconstructions of building facilities. *In:* SMITH, I. & DOMER, B. (eds.) *Advanced Computing Strategies for Engineering. EG-ICE 2018.* Cham: Springer.

Czerniawski, T. & Leite, F. (2019). Semantic Segmentation of Images of Building Facilities. *26th International Workshop on Intelligent Computing in Engineering.* Leuven, Belgium.

Dai, A., Chang, A. X., Savva, M., Halber, M., Funkhouser, T. A. & Nießner, M. (2017). ScanNet: Richly-annotated 3D reconstructions of indoor scenes. arXiv.

Faragher, R. & Harle, R. (2015). Location fingerprinting with bluetooth low energy beacons. *IEEE journal on Selected Areas in Communications,* 33**,** pp. 2418–2428.

Finch, E. (2012). *Facilities change management,* Hoboken, N.J, Blackwell.

Gelfand, L. (2011). *Sustainable Renovation,* Hoboken, John Wiley & Sons.

Graham, A., Garcia-Molina, H., Paepcke, A., Winograd, T. & Winograd, T., (2002). Time as essence for photo browsing through personal digital libraries. Proceedings of the 2nd ACM/IEEE-CS joint conference on Digital libraries, 2002. ACM, pp.326–335.

Maaten, L. V. D. & Hinton, G. (2008). Visualizing data using t-SNE. *Journal of Machine Learning Research,* 9**,** pp.2579–2605.

Rhodes, B. (2003). Using physical context for just-in-time information retrieval. *IEEE Transactions on computers,* 52**,** pp.1011–1014.

Smith, D. K. & Tardif, M. (2009). *Building information modeling: a strategic implementation guide for architects, engineers, constructors, and real estate asset managers*, John Wiley & Sons.

Talamo, C. & Bonanomi, M. (2015). *Knowledge management and information tools for building maintenance and facility management*, Springer.

Teicholz, E. (2014). *Technology for facility managers : the impact of cutting-edge technology on facility management,* Hoboken, New Jersey, John Wiley & Sons, Inc.

Teicholz, P. (2013). *BIM for facility managers*, John Wiley & Sons.

Torres-Solis, J., Falk, T. H. & Chau, T. (2010). A review of indoor localization technologies: towards navigational assistance for topographical disorientation. *Ambient Intelligence.* IntechOpen.

Wiggins, J. M. (2014). *Facilities Manager's Desk Reference,* Hoboken, Wiley.

Yang, Z., Zhou, Z. & Liu, Y. (2013). From RSSI to CSI: Indoor localization via channel response. *ACM Computing Surveys (CSUR),* 46**,** 25.

Automated Detection of Information Anomalies in Bridge Inspection Reports for Bridge Deterioration Prognosis

Ying Shi[1], Zhe Sun[2], Wen Xiong[3], Pingbo Tang[1,*]
[1] Carnegie Mellon University, the United States
[2] Arizona State University, the United States
[3] Southeast University, China
yingshi@andrew.cmu.edu

Abstract. Changes of bridge defects (e.g., cracks) are indicators of bridge deterioration patterns. Discovering such patterns could be vital for effective bridge deterioration prognosis. Bridge inspection reports contain detailed filed observations documented by experienced bridge engineers. Comparing inspection reports from different times is a way of discovering such deterioration patterns and diagnosing bridge conditions. However, field observations documented could be subjective due to inspectors' experiences and knowledge. Abnormal information items due to data collection & processing errors or undocumented changes in structural conditions can exist in inspection reports. These unreliable information items often mislead bridge deterioration prognosis. Discovering the "true" bridge conditions are challenging by using inspection reports with abnormal information, even for experienced bridge engineers. This study established an automated information anomaly detection framework to identify anomalous information that results in conflict deterioration patterns inconsistent with the predicted deterioration patterns generated based on previous deterioration patterns within the inspection reports. The approach is to formalize representations of the bridge deterioration patterns and to use the formalized representations to assess the observations documented in inspection reports against domain knowledge models captured in the majority of historical data sources about the studied bridge. Specifically, the proposed method established a novel coding system for representing the deterioration patterns of Continuous Rigid Frame Bridges (CRFBs). The results indicate that the proposed method has the potential of automating the detections of suspicious CRFBs deterioration facts in the annual inspection reports of a CRFB.

1. Introduction

Bridge deterioration prognosis is essential in bridge management by diagnosing deterioration facts and predicting deterioration trends. Discovering such deterioration patterns based on the inspection data is vital for effective bridge maintenance planning. Bridge engineers often conduct visual inspections and capture bridge deficiencies, and use such field observations for detecting bridge deteriorations (Rens, Nogueira and Transue, 2005). Bridge engineers established bridge deterioration models based on condition ratings on bridge and bridge elements (Cochat and Zenker, 2011) as indicators to predict the deterioration patterns. Previous inspection reports provide valuable information for establishing bridge deterioration models (Huang, 2010). Bridge inspection reports often contain detailed information about bridge deficiencies, such as defects, locations of defects, deficiency causes, etc. (Kaijian and Nora, 2017). Using multiple inspection reports from different periods could reveal bridge deterioration patterns, which indicate the way that bridge conditions change. All such information provides bridge engineers a comprehensive view of the bridge's condition and deterioration pattern for bridge deterioration prognostics.

In the current practice of bridge maintenance, bridge engineers often manually search for bridge deficiencies from previous inspection reports and discover the deterioration pattern by comparing defects documented on reports (Li and Burgueño, 2010). However, inspection reports could have errors, or called abnormal information items, that could produce conflicting deterioration patterns that are inconsistent with deterioration trends captured in certain parts of the historical data. In practice, anomalous information can cause faulty bridge deterioration pattern diagnosis. Even experienced engineers could hardly identify anomalous information manually because comprehensively examining the many possible failure modes underlying defects scattered in different parts of the inspection reports is tedious. Automatically connecting the scattered defect records to generate deterioration patterns and revealing the underlying failure modes, therefore, is necessary for detecting and addressing anomalous information items in inspection reports and generating reliable bridge deterioration models. The analyses of the authors indicate that a summarization of the inconsistencies between observations scattered around multiple inspection reports could help formalize a few rules that allow computers to identify suspicious information items. For example, the sudden change of the bridge's condition different from the previously documented deterioration trend could be a rule for helping a computer algorithm for detecting suspicious records. Computer algorithms could potentially cross-check data patterns against certain rule to highlight information anomalies to help engineers focus on those suspicious data items that need in-depth investigation. Anomaly detection, therefore, is a significant step for integrating human and machine intelligence for achieving timely and comprehensive data quality checking in bridge management.

Anomaly detection has been a popular topic in the informatics domain. Anomaly detection is the identification of patterns that is inconsistent with well-defined normal behavior (Chandola, Banerjee and Kumar, 2009). The anomaly detection indicates the process of finding the patterns in a dataset whose behavior is not normal on expected (Agrawal and Agrawal, 2015). Reasons for malicious activity, data noise (Raginsky *et al.*, 2012), and novel patterns (Ma and Perkins, 2003) could induce an anomaly. Anomaly detection can thus provide valuable information in a variety of areas, such as network intrusion detection (Bhuyan, Bhattacharyya and Kalita, 2014), medical informatics (Wong and Wagner, 2001), sensor networks (Chang, Member and Chiang, 2002), traffic monitoring (Ringberg *et al.*, 2007) and so on.

Anomaly detection methods can be statistical models, cognition model-based approaches, cognition-based detection techniques, machine learning-based methods, kernel-based online anomaly detection methods, computer immunology-based methods, and user intention-based method (Jyothsna, V. Rama Prasad and Munivara Prasad, 2011). These methods generate normal behavior from a given normal training data set, and then classify a test instance into the anomalous group or normal group. Researches about anomaly detection in bridge engineering mainly focus on the structural anomalies, which indicate the significant development of defects that induces structural degradation. Some bridge damage monitoring practices use anomaly detection method to analyze the sensor data to monitor a bridge's damage in structural health monitoring. Some researchers detect anomalies of crack growth by detecting abrupt changes, a shift in mean values, and inclination of changes based on sensor data (Trichias, Pijpers and Meeuwissen, 2014). Such anomaly detection methods use simple empirical statistic rules that identify abrupt changes of the sensor data and abrupt changes of the data change trend as anomalies.

The goal of this study is to establish an anomaly detection framework to support automatic anomalous information detection from inspection reports using rules from domain knowledge. The proposed method predicts potential deterioration patterns and identifies anomalies by comparing deterioration trends documented in inspection reports with the predicted trends of structural deteriorations. Specifically, the authors summarized three rules that specify how the cracks of bridges should evolve. These rules will enable the prediction of bridge cracks based on the spatiotemporal trends of structural defect developments documented in annual inspection reports of bridges. Overall, the contents of the bridge inspection reports that are not following the deterioration trends predicted based on the three rules are thus anomalous. The authors established a novel coding system for representing the locations and deterioration patterns of

Continuous Rigid Frame Bridges (CRFBs). An automatic anomaly detection algorithm uses the encoded defect development patterns of bridges to identify which defects documented are not following the rules of defect developments. The following sections detail this approach.

2. Methodology

The overall method is to encode defects documented in historical inspection reports, predict potential deterioration trends based on encoded historical defects and domain knowledge rules. Then the algorithm compares deterioration facts in an inspection report with the predicted ones to identify anomalous defects in the inspection report. The defect coding approach enables the comparison of deterioration patterns based on those facts collected at different times. Such a comparison generates deterioration trends based on the cracks observed at different times. The deterioration trend prediction step uses the historical deterioration trends and domain knowledge about defect development patterns to derive expected defects, given the current trends. The anomaly detection step finally identifies specific cracks as outliers that deviate from the deterioration patterns predicted based on historical reports and domain knowledge.

Specifically, the authors extract and represent crack distribution and deterioration patterns by using the proposed coding approach. The authors summarized domain knowledge rules for predicting reasonable and unreasonable deteriorations according to experts' experiences and mechanical principles. The domain knowledge could specify rules about common deterioration trends. Once a new inspection report is released, the proposed method can compare the deterioration patterns obtained from the new inspection reports with the predicted possible deterioration patterns and determine whether the new deterioration patterns are abnormal. In this method, the deterioration model can be continuously updated by new deficiencies information, so that the dynamic prediction model can follow up the real changes of the bridge's deterioration pattern and reflect real-time deterioration trend. Figure 1 shows the process of the anomaly detection method.

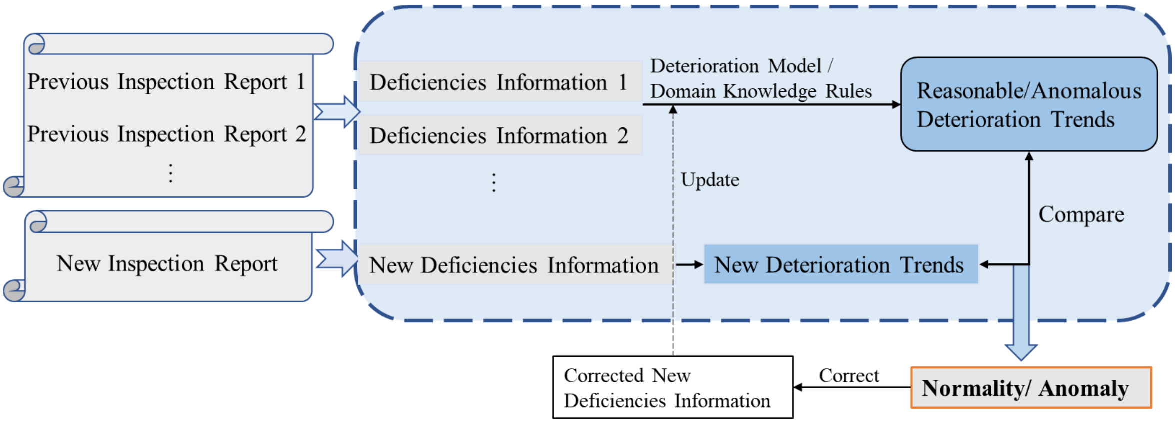

Figure 1: Process of the Anomaly Detection Method

2.1 Information Coding System

The authors proposed a novel information coding system for representing the crack deterioration facts and trends since inspection reports provide detailed information about cracks. The proposed encoding system focuses on extracting deterioration facts and examining cracking trends of Continuous Rigid Frame Bridges (CRFBs). The coding system allows a computer algorithm to automate the comparison of deterioration facts of CRFBs across multiple inspection reports and capture the CRFB deterioration trends represented by that coding system. The algorithm then uses the same coding approach to represent the facts and deterioration trends documented in new inspection reports to decide whether any significant deviation from the main deterioration trends exists or not. Those significant deviations are thus anomalies detected by the proposed algorithm that use the new coding approach.

Figure 2 shows the encoding approach using a matrix to represent a bridge's cracks distribution. This representation has each row to represent the distribution of the cracks by encoding information about the number of the span, location, type, and the number of cracks in the same type. The code number of each span is the number of the span in inspection reports. The method divides each span into five areas of the area around the left side of the span, the area around 1/4 of the span, the area around 1/2 of the span, the area around 3/4 of the span, and the area around the right side of the span. The area division stores the numbers of cracks in multiple areas of a span. Considering the related components (top slab, web slab, and bottom slab) and crack directions (transverse, longitudinal, diagonal, and vertical directions), there are nine types of cracks. The proposed representation approach counts the number of each type of cracks.

With the defined encoding rule, the extraction method searches five areas in each span and returns the number of each type of cracks in each area cracks to the encoding matrix in Figure 2. The deterioration pattern between two years can be represented by the matrix resulted from the subtraction between two crack distribution matrixes generated from different years' inspection reports.

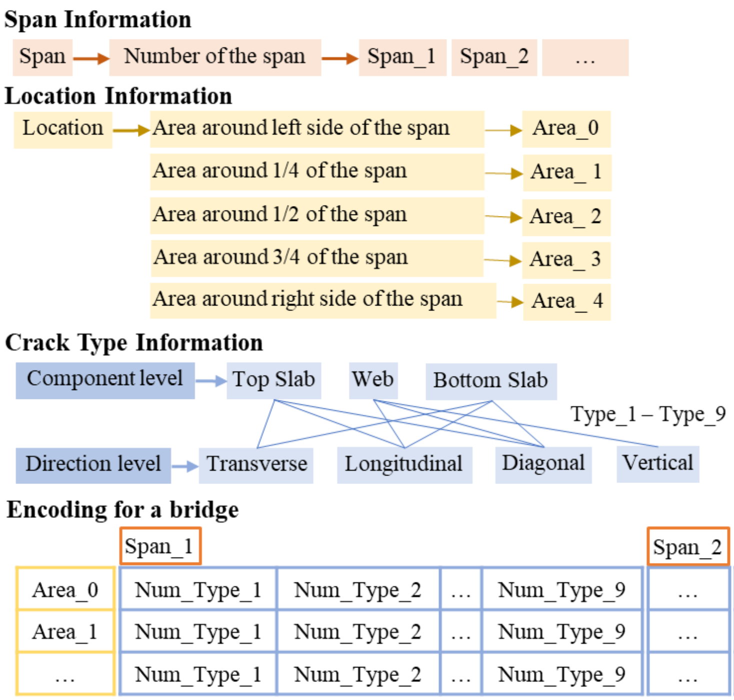

Figure 2: Crack Information Encoding Method

2.2 Anomaly Detection

The proposed anomaly detection method predicts potential deterioration patterns based on previous field observations and domain knowledge rules. A comparison between the deterioration pattern generated from inspection reports and the predicted deterioration patterns identifies anomalous patterns and tracks corresponding anomalous information. Bridge deterioration prediction uses two types of models extensively, 1) statistical and 2) mechanical deterioration models. The statistical deterioration models use previous observations of service life to predict future conditions (Kobayashi, Kaito and Lethanh, 2012). The statistical deterioration models are established based on the deterioration pattern of multiple bridges at a network level. The mechanistic deterioration models provide the prediction of service life based on mathematical descriptions of the phenomenon involved in element degradation, such as understanding the microstructure of concrete before and during degradation (Nickless and Atadero, 2018). The mechanistic deterioration models are used to predict a bridge's deterioration based on micro-response of bridge components (Morcous, Lounis and Cho, 2010).

This study synthesized three bridge deterioration rules based on expert experiences and domain knowledge to identify suspicious information in the inspection report shown in Table 1. First, if the new crack caused by a factor is also the factor of a crack in previous inspection reports, the appearance of the new crack should seem to be reasonable. However, a new crack that is caused by a new factor which never caused cracks observed before could be an anomaly, because the new factor indicates there is a recording error in the new report or an abnormal structural change. In the case of the CRFB in this study, the authors reviewed a large number of documents about such CRFB, including inspection reports and papers, and summarize the potential causes of each type of cracks.

Table 1: Three Rules for Determining Anomalous Deterioration Trends

	Reasonable deterioration patterns	**Anomaly**
Causes group	Cracks with the same cause could happen together. 1. Caused by negative bending: transverse crack in the top slab (type 1), the longitudinal crack in the top slab (type 2), the diagonal crack in the top slab (type 3) 2. Caused by positive bending: vertical crack in the web (type 6), the transverse crack in the bottom slab (type 7), the longitudinal crack in the bottom slab (type 8), the diagonal crack in the bottom slab (type 9) 3. Caused by shrinkage of concrete segments at different ages: longitudinal crack in the top slab (type 2) 4. Caused by torsion and distortion: longitudinal crack in the web (type 4) 5. Caused by shear: diagonal crack in the web (type 5) 6. Caused by tension stress at prestressing reinforcements' anchor area: diagonal crack in the web (type 5) 7. Caused by radial component force of longitudinal prestress in the bottom plate of curved bridges: longitudinal crack in the bottom slab (type 8), the diagonal crack in the bottom slab (type 9)	New types of cracks caused by new factors.
Causes collision	1. Vertical crack in the web (type 6) should happen after the transverse crack in the bottom slab (type 7) or the transverse crack in the top slab (type 1). 2. Transverse/ diagonal crack in the top slab (type 1/ type 3) should not happen with transverse/ diagonal crack in the bottom slab (type 7/ type 9).	Crack combinations contrary to reasonable deterioration patterns.
Symmetry	Cracks distribution is symmetric in a symmetrical span/ bridge.	Crack distribution is asymmetric in a symmetrical span/ bridge.

Table 2 lists nine types of cracks mentioned above and the corresponding causes. The nine types of cracks can be classified into seven groups according to the causes. The new crack with a factor the same as old cracks is reasonable, while the new crack with a new factor different from old cracks is an anomaly.

Second, there could be conflicts between the factors of different types of cracks. For example, vertical crack in the web should happen after the transverse crack in the bottom slab or the transverse crack in the top slab because the vertical cracks in the web are normally the extension of transverse cracks in the bottom slab or the top slab. Another conflict could be between the transverse/diagonal crack in the top slab and transverse/diagonal crack in the bottom slab, which indicates that they cannot occur at the same time. If the occurrence of a new crack induces such two conflicts, the new crack might be an anomaly.

The third rule is that the crack distribution is often symmetrical in a span or a bridge with symmetrical geometries. If the distribution of a certain type of crack is not symmetrical, the number of the kind of cracks might be a piece of abnormal information because such non-symmetrical distribution is different from a normal distribution in expert experiences. The three rules could help determine whether the generated deterioration pattern belongs to the unusual ones and whether there is an anomaly.

Table 2: Causes of Each Type of Cracks

	Type	**Causes**
1	Top Slab + Transverse	Negative Bending
2	Top Slab + Longitudinal	Negative Bending/ shrinkage of concrete segments at different ages
3	Top Slab + Diagonal	Negative Bending
4	Web + Longitudinal	Torsion and distortion
5	Web + Diagonal	Shear /Tension stress at prestressed reinforcements' anchor area
6	Web + Vertical	Positive Bending
7	Bottom Slab + Transverse	Positive Bending
8	Bottom Slab + Longitudinal	Positive Bending/ Radial component force of longitudinal prestress in the bottom plate of curved bridges
9	Bottom Slab + Diagonal	Factors combination of type 7 crack and type 8 crack

3. Case Study: Identifying Anomalous Facts in the Inspection Reports of a CRFB

The authors conducted a case study using a high-pier CRFB in China to examine the developed anomaly detection algorithm. The studied bridge locates within a complex terrain surrounded by mountains and wide rivers. The complex surrounding environment and the bridge's high latitude raise the difficulty of detailed bridge inspection. The bridge has a length of 612m (66m+4*120m+66m) with six spans, and the highest pier has a height of 83m.

In this case study, the authors took the intermediate span of the studied bridge as an example. The inspection report numbered the intermediate span as span 11, as shown in Figure 3. The inspection report in 2016 shows that the middle area of the span has two diagonal cracks in the web and one transverse crack in the bottom slab, and other areas have no cracks. The inspection report in 2017 shows that for the middle area of the span, the number of the diagonal cracks in the web and the transverse cracks in the bottom slab remain unchanged, but three longitudinal cracks appear in the top slab. Areas except for the middle area still have no cracks.

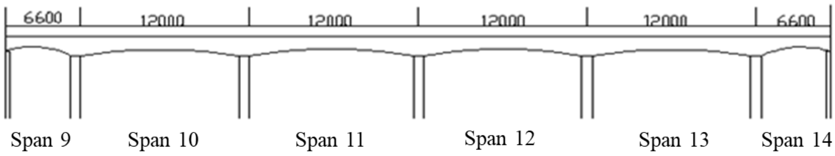

Figure 3: Overview of the High-pier Continuous Rigid Frame Bridge in China (cm)

Table 3 shows the distribution and number of cracks extracted from inspection reports in 2016 and 2017. The occurrence of three longitudinal cracks in the top slab represents a baseline of deterioration pattern, which could be compared with further deterioration patterns to detect the anomaly. The left part of Figure 3 represents the distributions of different types of cracks and the deterioration pattern from 2016 to 2017 by using the encoding system illustrated in Section 2.1. The expected deterioration pattern in the future could be the increase of longitudinal cracks in the top slab, which can also be called type 2 cracks according to the encoding system.

Table 4 shows the distribution and number of different types of cracks extracted from the 2019 inspection report. The right part of Figure 4 displays the distribution information and the deterioration trend generated based on the coding system. For the middle area of the span 11, the number the longitudinal cracks in the top slab (type 2 cracks) increases as the expected deterioration trend based on the previous deterioration trend from 2016 to 2017. However, novel crack types of the longitudinal, diagonal, and transverse crack in the bottom slab occur in the middle area of the span, and the number of these cracks has a significant increase, which is inconsistent with the expected deterioration trend. The significant change inconsistent with the expected deterioration trend is an anomaly.

Table 3: Crack Distribution of Span 11 in 2016 and 2017

Year	Area	Cracks		
2016	Area 0	None		
	Area 1	None		
	Area 2	Bottom Slab + Transverse, 1	Web + Diagonal, 2	None
	Area 3	None		
	Area 4	None		
2017	Area 0	None		
	Area 1	None		
	Area 2	Bottom Slab + Transverse, 1	Web + Diagonal, 2	Top Slab + Longitudinal, 3
	Area 3	None		
	Area 4	None		

The authors checked the cracks in 2019 inspection reports against the three rules illustrated in the anomaly detection method. For the first rule, the new type of cracks, which are longitudinal cracks in the web, might be an anomaly because its cause is different from the causes of all the previously observed cracks documented in the past reports. The cracks of type 4 might indicate a data error or a mechanic change that the girder starts to bear torsion and distortion. Besides, the factor of type 7 cracks causes the new cracks of type 8 and 9, so the new cracks of type 8 and 9 could be reasonable and normal.

Table 4: Crack Distribution of Span 11 in 2019

Area	Cracks					
Area 0	None					
Area 1	None	Web + Diagonal, 1	Top Slab + Longitudinal, 3	None		
Area 2	Bottom Slab + Transverse, 6	Web + Diagonal, 2	Top Slab + Longitudinal, 14	Bottom Slab + Longitudinal, 9	Bottom Slab + Diagonal, 8	Web + Longitudinal, 2
Area 3	None		Top Slab + Longitudinal, 9	None		
Area 4	None		Top Slab + Longitudinal, 1	None		

For the second rule, the cracks all follow the reasonable deterioration pattern, and there is no anomaly detected. According to the third rule, the cracks distribution and deterioration pattern should be symmetrical in the span, which means that the number of each type of cracks in the Area_1 (the area around 1/4 span) and Area_3 (the area around ¾ span) should be similar. Also, the number of each type of cracks in the Area_0 (the area around the left end) and Area_4 (the area around the right end) should be similar. However, for the area_1 and area_3, the cracks deterioration trends of type 2 and 5 are not symmetric, and for the area_0 and area_4, the cracks deterioration trend of type 2 is not symmetric. Such anomaly might indicate a data error or a sign of the appearance of this kind of crack in its symmetrical area. Though the crack distribution and deterioration are not symmetrical now, the mechanic is symmetric, and the new type of crack would appear in its symmetrical area in the future. For the symmetry of cracks' distribution and deterioration in a symmetrical bridge, the cracks in span 11 should compare with those in span 12, which is the symmetrical span of span11 at the bridge level.

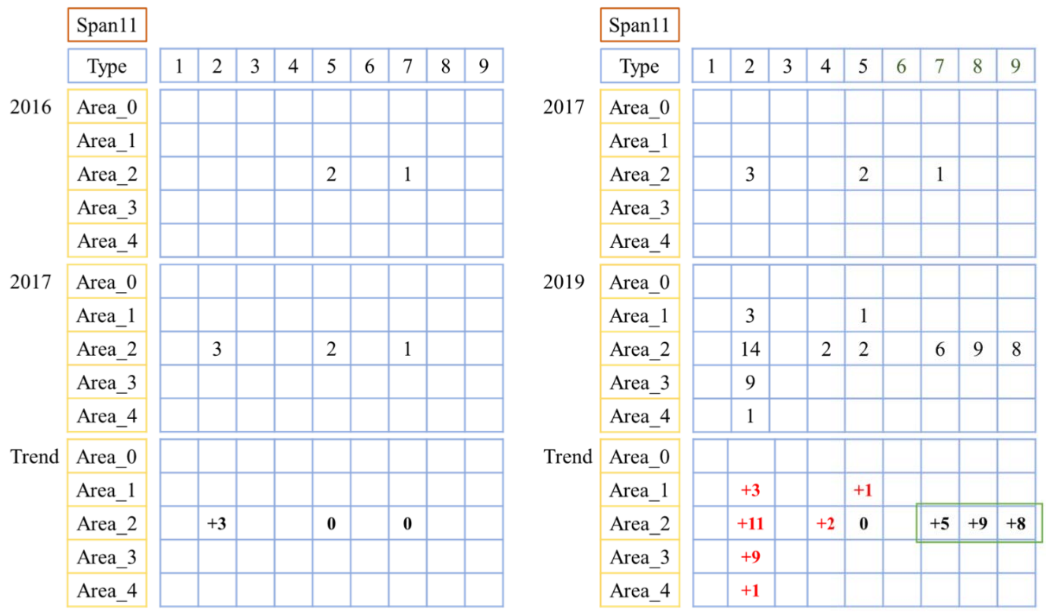

* Notes: Area (0: left end, 1: 1/4 span, 2: midspan, 3: 3/4 span, 4: right end);
Type (1: top slab + transverse, 2: top slab + longitudinal, 3: top slab +diagonal, 4: web + longitudinal, 5: web + diagonal, 6: web + vertical, 7: bottom slab + transverse, 8: bottom slab + longitudinal, 9: bottom slab + diagonal);

Figure 4: Deterioration Pattern of Span 11 from 2016 to 2019

4. Conclusion and Future Research

This study established an anomaly detection framework to identify information anomalies of cracks in bridge inspection reports. This method integrated three bridge engineering rules for guiding the detection of anomalous information by checking whether the deterioration pattern is reasonable or anomalous. Authors established a coding system that allows a computer algorithm to compare the deterioration facts across multiple annual inspection reports and formed the deterioration pattern by a matrix. Then, check the deterioration patterns in different years according to the proposed three rules. The results show that the proposed method can detect anomalous information in inspection reports. The detected anomalies need to be verified by the next year's crack information in the future. The prediction rules would be more reliable and comprehensive if generating rules by simulating the deterioration trends in a finite element model. Combining expert experiences, mechanics knowledge, and finite element simulation to generate anomaly detection rules is a critical part of further works.

In the bridge inspection process, incorrect data recordings could mislead the diagnosing process for revealing the "true" bridge condition. Abnormal changes in mechanical characteristics on bridges could also induce anomaly. The detected anomalies caused by such two factors can help bridge engineers to remove inaccurate data in inspection reports and assessing the bridge condition only based on reliable data. Therefore, future research should try to interpret the causes of the detected anomalies as incorrect data recordings or abnormal changes of the bridge. Then the research would try to resolve the anomalies caused by incorrect inspection report recordings to ensure the information validity for reliable deterioration prognostics. With the valid inspection reports, future research can interpret the mechanical mechanism underlying the true anomalies caused by the changes of abnormal mechanical behaviors to decide whether the bridge is still in good condition.

Acknowledgment

This material is based on work supported by the science and technology project on transportation construction by the U.S. National Science Foundation (NSF) under Grant No. 1454654 and the Ministry of Transport of the People's Republic of China (Project No. 2013318223380, 2014318J14250). The supports are gratefully acknowledged.

References

Agrawal, S. and Agrawal, J. (2015) 'Survey on anomaly detection using data mining techniques', *Procedia Computer Science*. Elsevier Masson SAS, 60(1), pp. 708–713. doi: 10.1016/j.procs.2015.08.220.

Bhuyan, M. H., Bhattacharyya, D. K. and Kalita, J. K. (2014) 'Network Anomaly Detection : Methods , Systems and Tools'. IEEE, 16(1), pp. 303–336.

Chandola, V., Banerjee, A. and Kumar, V. (2009) 'Anomaly Detection : A Survey', 41(3), pp. 1–58. doi:10.1145/1541880.1541882.

Chang, C., Member, S. and Chiang, S. (2002) 'Anomaly Detection and Classification for Hyperspectral Imagery'. IEEE, 40(6), pp. 1314–1325.

Cochat, P. and Zenker, M. (2011) 'Le syndrome de Pierson, Michel Pierson', *Archives de Pediatrie*, 18(11), pp.1127–1129. doi: 10.1016/j.arcped.2011.08.002.

Huang, Y. H. (2010) 'Artificial neural network model of bridge deterioration', *Journal of Performance of Constructed Facilities*, 24(6), pp.597–602. doi: 10.1061/(ASCE)CF.1943-5509.0000124.

Jyothsna, V., V. Rama Prasad, V. and Munivara Prasad, K. (2011) 'A Review of Anomaly based Intrusion Detection Systems', *International Journal of Computer Applications*, 28(7), pp. 26–35. doi: 10.5120/3399-4730.

Kaijian, L. and Nora, E.-G. (2017) 'Ontology-based semi-supervised conditional random fields for automated information extraction from bridge inspection reports', *Automation in Construction*, 81, pp. 313–327. doi:10.1016/j.autcon.2017.02.003.

Kobayashi, K., Kaito, K. and Lethanh, N. (2012) 'A statistical deterioration forecasting method using hidden Markov model for infrastructure management', *Transportation Research Part B: Methodological*. Elsevier Ltd, 46(4), pp. 544–561. doi: 10.1016/j.trb.2011.11.008.

Li, Z. and Burgueño, R. (2010) 'Using soft computing to analyze inspection results for bridgre evaluation and management', *Journal of Bridge Engineering*, 15(4), pp. 430–438. doi: 10.1061/(ASCE)BE.1943-5592.0000072.

Ma, J. and Perkins, S. (2003) 'Time-series Novelty Detection Using One-class Support Vector Machines', in *Proceedings of the International Joint Conference on Neural Networks*, pp. 1741–1745. doi:10.1109/ijcnn.2003.1223670.

Morcous, G., Lounis, Z. and Cho, Y. (2010) 'An integrated system for bridge management using probabilistic and mechanistic deterioration models: Application to bridge decks', *KSCE Journal of Civil Engineering*, 14(4), pp.527–537. doi: 10.1007/s12205-010-0527-4.

Nickless, K. and Atadero, R. A. (2018) 'Mechanistic Deterioration Modeling for Bridge Design and Management', *Journal of Bridge Engineering*, 23(5). doi: 10.1061/(ASCE)BE.1943-5592.0001223.

Raginsky, M. *et al.* (2012) 'Sequential Anomaly Detection in the Presence of Noise and Limited Feedback'. IEEE, 58(8), pp. 5544–5562.

Rens, K. L., Nogueira, C. L. and Transue, D. J. (2005) 'Bridge Management and Nondestructive Evaluation', 19(February), pp. 3–16. doi: 10.1061/(ASCE)0887-3828(2005)19.

Ringberg, H. *et al.* (2007) 'Sensitivity of PCA for Traffic Anomaly Detection', pp. 109–120.

Trichias, K., Pijpers, R. and Meeuwissen, E. (2014) 'A new approach for structural health monitoring by applying anomaly detection on strain sensor data', in *Health Monitoring of Structural and Biological Systems 2014*. SPIE, p. 90640A. doi: 10.1117/12.2045745.

Wong, W. and Wagner, M. (2001) 'Rule-Based Anomaly Pattern Detection for Detecting Disease Outbreaks', pp.217–223.

Inspecting structural components of a construction project using laser scanning

Linh Truong-Hong[1*], Roderik Lindenbergh[1]
[1]Department of Geoscience and Remote Sensing,
Delft University of Technology, The Netherlands
[*] l.truong@tudelft.nl

Abstract. In construction projects, inspection of structural components mostly relies on typical measurements (e.g. measuring tapes, levelling or total stations). Additionally, with those methods, only a few points on the structure can be measured, and resulted inspection may not fully reflect the actual, detailed condition. Laser scanning is emerging a remote sensing technology to capture the structures' surfaces in high details accurately and quickly. However, because of complex, massive data points acquired from the construction project, in practice, data processing is still manual work with support of computer aided program. To improve current workflows, this paper proposes a method automatically extracting structural components of the concrete building and subsequently inspects them in a term of deformation. The proposed method explores both spatial information of a point cloud and contextual knowledge of structures (e.g. orientation or shape). Additionally, based on the fundamental design of the structures, component's boundaries are automatically extracted to establish un-deformed surfaces of the components for deformation measurement.

1. Introduction

In construction projects, defects of structural components are inevitable. The construction cost can be up 16% of the total cost of the project when the defects were fixed at the last stage (Burati and Farrington, 1987). The rework costs can be minimized if any defect of the component can be identified at an early phase of the project. In current practice, defect inspection is mostly manual interpretation of geometric data acquired from measuring tapes, levelling or total stations. Therefore, project managers cannot identify the defects timely, accurately and objectively. In addition, inspection results in hard copies are cumbersome to use digital tools to improve efficiency of the project management.

A terrestrial laser scanning has ability to capture visible surfaces accurately, quickly and efficiently, which has been used at many construction projects in recent years for construction progress monitoring, surface defect detection, as-built BIM, and dimensional quality control (Bosche, 2010; Kim et al., 2014). As the point cloud represents multiple objects in a scene, a point cloud processing is often required to extract the point cloud of each object and/or objects' surfaces, but this is a nontrivial task. In practice, users often use commercial software (e.g. Revit, and ClearEdge 3D) to manually extract a point cloud of the components by using software functions like crop, segmentation and fitting. That is time consuming and is required experience users to handle a massive, complex data set of the construction project.

Recent effort in automatically extracting the structural components from the point cloud, Bosche (2010) mapped a 3D CAD model to the point cloud to extract members of an as-built model. Dimitrov and Golparvar-Fard (2015) proposed a region growing based on surface roughness estimated for each point by using multi-scale neighborhood to extract building objects. The method still had some drawbacks, for example over-segmentation, intensive computation demand. Kim et al. (2014) extracted data points of surfaces, and edges and corners to determine the dimensions of a reinforced concrete panel, and then as-design model was mapped to the point cloud to assess a construction deviation. Additionally, in supporting quality assurance and control of reinforced structures, Wang et al. (2017) extracted individual rebars in concrete structures by using one-class support vector machine approach based linearity, planarity and red-green-blue colors of the point cloud. Laefer and Truong-Hong (2017) used kernel density estimation (KDE) to detect primary surfaces of a steel cross-section to determine its shape and dimensions, and subsequently a correct section was identified by comparing the standard sections to the point cloud-based section for generating a 3D model of a steel member. In extracting structural members of a regular building, Maalek et al. (2019) extracted roughly horizontal planes (floor and ceiling) using a histogram based on points' elevation and then a hierarchical clustering method was segmented based on planar and linear features of each points computed from a robust principal analysis. Next, the planar surfaces with normal vectors perpendicular to main axes of the building were considered as columns' surfaces if they make to adjacent surface a symmetric section. In summary, existing methods are requirement of an as-design model, certain assumption to extract the structural components and time consuming. This paper proposes a new method to automatically extract point clouds describing the building components and inspect construction quality in a term of deformation.

2. Proposed method

The proposed method consists of two parts: extraction and inspection of structural components (Fig. 1), in which the first part includes 3 consecutive moduli: (i) floor/ceiling and wall, (ii) column and (iii) beam. The algorithm is based on a synergy between a point cloud, and contextual knowledge of structures. In a construction project of reinforced concrete buildings, structural elements of the story must be inspected before starting a next one. That implies a point cloud of one story is input data for the proposed method rather than those of an entire building. Moreover, contextual knowledge of the structures used in this method includes: (1) floor/ceiling and wall is a planar surface; (2) columns' orientations are vertical; (3) a beam is connected between two columns or a column and wall; (4) the minimum cross-section of the column and beam is 0.2mx0.2m while the columns' height and the beams' length is 2.0m and 1.0m, respectively.

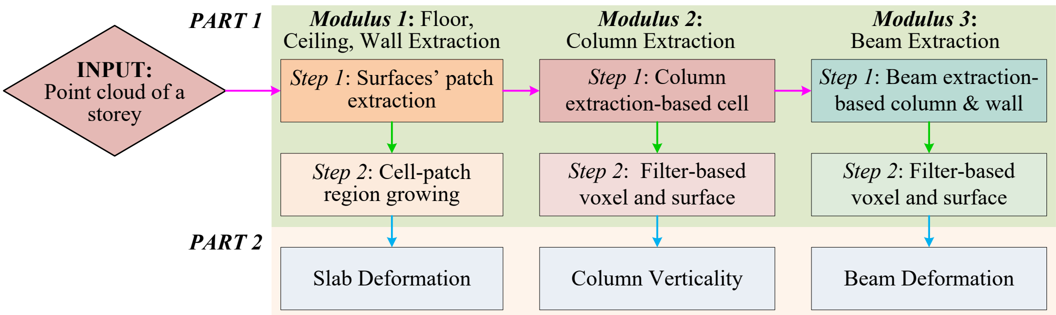

Figure 1: Workflow for inspecting structural components in reinforced concrete buildings

3. Structural component extraction

3.1 Modulus 1: Floor/ceiling and wall extraction

Cell-based segmentation method proposes to extract floor, ceiling and wall as they are planar surfaces in either horizontal or vertical direction. The method consists of two steps: extract the point cloud surfaces' patches through two-dimensional (2D) cells (*Step 1*), and segment a point cloud of a planar surface (*Step 2*).

Step 1: The algorithm employs a quadtree to recursively subdivide an initial 2D bounding box of a point cloud ($P = p_i \in R^3$) into 2D cells ($C = \{c_1, . . . c_i, c_N\}, i = [1, N]$) along the *x*- and *y*-directions in a Cartesian coordinate system until the cell size is no larger than the predefined cell size (*cell_size*). The cell c_i is classified as the "*full*" cell if it occupied the number of points larger than a predefined minimum number of the points (*min_ptc*), otherwise, it is an "*empty" cell.* Notably, only full cells are used in a further process. As the cell c_i may contain a point cloud of multiple components (e.g. floor, ceiling, beam or column) in elevation, kernel density estimation (KDE) generated from the *z*-coordinates of the points is used to extract the data points affiliated to a surface's patch ψ_{ij} (Laefer and Truong-Hong, 2017). The points belonging to the patch are located within two consecutive valleys of KDE (Fig. 2).

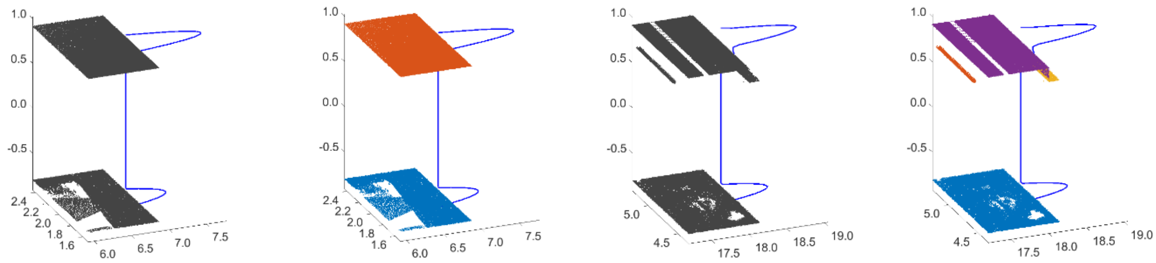

a) Case 1: A cell contains data points of a floor and ceiling

b) Case 2: A cell contains data points of a floor, ceiling and beam

Figure 2: Extracting data points of patches within a 2D cell

Step 2: Cell-patch region growing (CpRG) is developed to segments patches representing slabs of the floor and ceiling. CpRG consists of 3 sub-steps: patch-patch region growing (*Step 2.1*), patch filtering (*Step 2.2*), and patch-point region growing (*Step 2.3*).

Step 2.1: Patch-patch region growing

First, the proposed method computes salient features of each patch ψ_{ij}, which include a fitting plane $\psi_{ij}(p_{ij,0}, n_{ij})$, where $p_{ij,0}$ is a centroid of the points $p_{ij} \in \psi_{ij}$ and n_{ij} is a normal vector, and a residual value (r_{ij}) defined as a root mean square of distances $d(p_{ij}, \psi_{ij}(p_{ij,0}, n_{ij}))$. Next, patch-patch region growing starts to segment the patches with an initial seeding patch $\psi_{ij} \in c_i$ owning the smallest residual value to search neighbouring patches ($\psi_{kl} \in c_k$). The patch ψ_{kj} is added to a region (R_k) if it satisfies Eq. 1 and is added to the seeding patch set for next iterations if its residual value r_{kl} is smaller than the residual threshold (r_0). The growing process is completed when all predefined patches are checked. For details of the patch-patch region growing can refer to (Rabbani et al., 2006, Truong-Hong et al., 2018).

$$\begin{cases} \angle n_{ij}, n_{kl} \leq \alpha_0 \\ d\left(p_{kl,0}, \psi_{ij}(p_{ij,0}, n_{ij})\right) \leq d_0 \end{cases} \tag{1}$$

where $d\left(p_{kl,0}, \psi_{ij}(p_{ij,0}, n_{ij})\right)$ is a Euclidean distance between the centroid of the patch ψ_{kj} to $\psi_{ij}(p_{ij,0}, n_{ij})$, and α_0 and d_0 are the angle and distance thresholds.

However, the patches can contain the data points of other components, and/or points of the surface are possessed by unsegmented patches or an adjacent region. These issues can be solved in *Step 2.2* and *Step 2.3*, respectively.

Step 2.2: *Patch filtering algorithm*

For each region, the filtering algorithm extracts a boundary patch ($\psi_{ext,ij}$) of a region R_m and its neighbour interior patches ($\psi_{int,kl}$). Data points of the patches $\psi_{int,ij}$ are used to estimate a local surface (S_{ij}) by using a principal component analysis (PCA). Subsequently, the points $p_{ij} \in \psi_{ext,ij}$ are considered as inlier points $p_{int,ij}$ if the distance $d(p_{ij}, S_{ij}(p_{ij,0}, n_{ij}))$ is no larger than the distance threshold d_0, and remaining points are eliminated.

Step 2.3: *Patch-point region growing*

The process starts with a boundary patch $\psi_{ext,ij} \in c_i$ of a region R_m to search adjacent patches $\psi_{kl} \notin R_m$. Next, points p_{kl} are added to the region R_m if the distance $d(p_{kl}, \psi_{ij,ext}(p_{ij,0}, n_{ij}))$ is less than the distance threshold d_0. The patch ψ_{kl} is considered as a boundary patch for next searching iterations if more than 50% of the points of the patch ψ_{kl} is added to the region R_k.

Once the data points of the floor and ceiling are extracted, the remaining points cloud are used to extract vertical walls by using a similar process, in which the quadtree is used to generate 2D cells in the *yz* and *xz* planes, respectively. Moreover, details of cell-based segmentation can refer to Truong-Hong and Lindenbergh (2020).

3.2 Modulus 2 - Column Extraction

After extracting floor, ceiling and wall, 2D cells in *xy* plane used for extracting the floor and ceiling are recalled but the segmented points are discarded out of the cells. The algorithm has two main steps (Fig. 3).

In *Step 1*, for each cell c_i, the cell height (H_{ci}), which is computed from *z*-coordinates between the lowest and highest points, and the maximum gap (ΔH_{ci}), which is different *z* coordinates of two consecutive points in an elevation are computed. Next, the cells can possess points of the column if $H_{ci} \geq H_0$ and $\Delta H_{ci} \leq 0.5H_0$, where H_0 is the minimum column height. Subsequently, the remaining cells are clustered based on their connectivity and each cluster contains candidate points of columns (Fig. 3 a and b).

In *Step 2*, a voxel-based growing segmentation (VRG) (Vo et al., 2015) is adopted to segment points of a cluster. In this method, the point cloud is subdivided into the small voxel with the voxel size is no larger than the threshold (*voxel_size*), and then a fitting plane is estimate through points of the voxel to determine voxel's features: a normal vector and residual. VRG operates similar CpRG, in which the voxels associated with salient features used instead of the patches (Fig.3c).

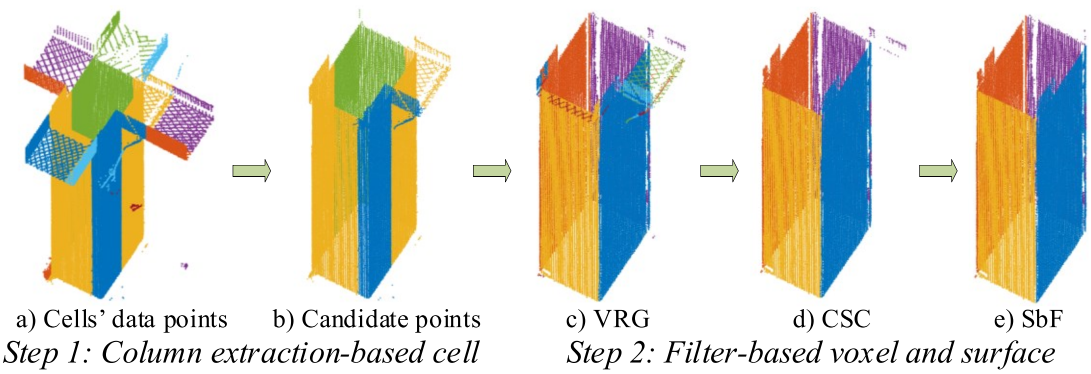

Figure 3: Illustration of Column extraction workflow

As the cluster in *Step 1* may contain points of other components adjoined to the column or may not represent to a real column, a connected surface component (CSC) algorithm is proposed to determine segmented surfaces are parts of the column (Fig. 3d). This is based on the hypothesis is that the component' surfaces connect together in a form of a close loop. The CSC algorithm starts with the initial segment, which is herein the largest surface in a term of an area. Two surfaces are connected if the angle between two normal vectors is larger than the angle threshold α_1, and the overlap length is no less than H_0 (Fig. 4a). Notably, lines $P_{i1}P_{i2}$ and $P_{j1}P_{j2}$ are respectively line segments generated from projected points of the surfaces S_i and S_j on the intersection line L_{ij}.

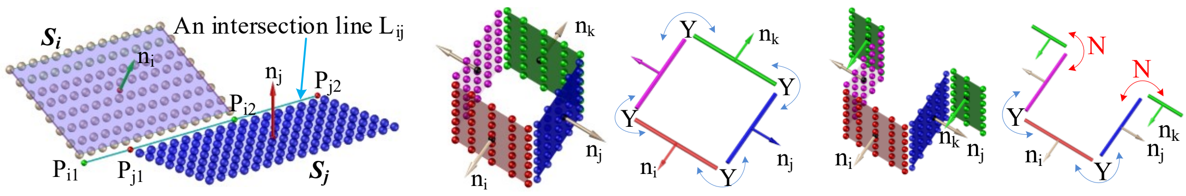

a) Surfaces connected　b) Case 1: all planes accepted　c) Case 2: 2 planes rejected

Figure 4: Illustrate the CSC algorithm

Once the connected segments are obtained, their segments are projected on a plane perpendicular to the surface of the reference segment. Subsequently, the segments that do not make a close loop are rejected (Fig. 4b and c). Finally, the column is considered as the real column if they are in a form of at least two surfaces. This criterion is applied to avoid missing the column at the building corner.

Finally, surface-based filtering (SbF) proposes to remove outlier points of the segments, which are points of co-planar surfaces of adjacent components including in the segment. This is based on an observation that the surface's points are bounded by intersection lines with the adjoined surfaces. For the surface S_i, the intersection line L_{ij} divides the points $p_i \in S_i$ into inlier ($p_{inl,i}$) and outlier ($p_{ext,i}$) groups, which is determined based on signs of sign distances $d(p_i, L_{ij})$. The outlier group has small number of the points ($|p_{ext,i}| < |p_{inl,i}|$), and the outlier points $p_{ext,i}$ are then discarded (Fig. 3e).

3.3 Modulus 3 - Beam Extraction

In a building structure, a primary beam connects between two columns or a column and a shear wall, and a beam connects to a side of a column. Moreover, the columns' shapes are mostly rectangular or square, which implies a beam's width is smaller or equal to the column's width. Notably, in this study, the secondary beam connecting two primary beams, is out of a scope of work. Similar the column extraction, the algorithm also consists of two Steps: rough and fine extraction of the beam.

Step 1: From each surface S_{ij} of a column Col_i, the fitting plane $S_{ij}(p_{ij,0}, n_{ij})$ is estimated using PCA, in which a direction of the normal vector is set outward the column (Fig. 5). A beam can connect between the column Col_i and Col_k, if the surface $S_{kl}(p_{kl,0}, n_{kl})$ of the column Col_k satisfies Eq.2. The first constrain is to ensure S_{ij} and S_{kl} parallel, the second constrain checks if Col_i and Col_k are on the same grid, and the last one finds S_{kl} is the closest surface of S_{ij}.

$$\begin{cases} \angle n_{ij}, n_{kl} \leq \alpha_1 \\ \left| d\left(p'_{kl,0}, L_{ij}\left(p'_{ij,0}, n'_{ij}\right)\right)\right| \leq S_{ij}.w \\ d\left(p_{kl,0}, S_{ij}(p_{ij,0}, n_{ij})\right) < 0 \wedge \left| d\left(p_{kl,0}, S_{ij}(p_{ij,0}, n_{ij})\right)\right| \rightarrow min \end{cases} \quad (2)$$

where α_1 = 5 degrees is the angle threshold, $p'_{ij,0}, p'_{kl,0}$ and $n'_{ij}$are projection of $p_{ij,0}, p_{kl,0}$ and n_{ij} on a *xy* plane, $S_{ij}.w$ is the width of the surface S_{ij}, which is a short side of a 2D minimum bounding box (*mbb*) of the points of the surface S_{ij} projected on its fitting surface, and the distance is a sign distance.

Subsequently, candidate points (PB_i) of the beam B_i are given in Eq. 3. The first condition is to obtain the points between two columns. The second condition is based on the beam's width no larger than the column's width. Moreover, when the surface S_{kl} is not available, which implies the wall supports the beam, the distance $d\left(p_{kl,0}, S_{ij}(p_{ij,0}, n_{ij})\right)$ is set as an infinity, and only $S_{ij}.w$ is used in the second condition.

$$p_i \in PB_i \; if \begin{cases} 0 \leq d\left(p_i, S_{ij}\left(p_{ij,0}, n_{ij}\right)\right) \wedge d\left(p_i, S_{ij}\left(p_{ij,0}, n_{ij}\right)\right) \leq d\left(p_{kl,0}, S_{ij}(p_{ij,0}, n_{ij})\right) \\ \left|d\left(p_i, L_{jl}\right)\right| \leq \max\left(S_{ij}.w, S_{kl}.w\right) + tol \end{cases} \quad (3)$$

where $d\left(p_i, L_{jl}\right)$ is a sign distance from the points p_i to the line $L_{ij} = p'_{ij,0}\, p'_{kl,0}$, $S_{kl}.w$ is the width of the surface S_{kl}, and tol = 0.1m is a tolerance compensating data errors or imperfect structures.

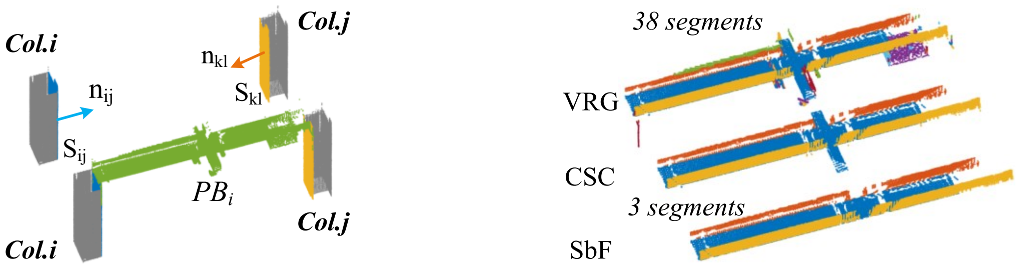

Step 1: Beam extraction based column & wall *Step 2: Filter-base voxel and surface*

Figure 5: Illustration of beam extraction

Step 2: Similar *Step 2* of the column extraction, VRG is to extract points of planar surfaces, CSC algorithm is to determine the final surfaces and SbF filters outlier points (Fig. 5). Notably, the initial surface for CSC algorithm is the bottom surface defined as the largest surface with the smallest angle between its normal vector and a unit vector of the oz axis (n_z = [0, 0, 1]).

4. Structure Inspection

This section is to inspect main structural components (ceiling slabs, columns and beams) in terms of deformations. A deformation is defined as a distance between the point cloud of the components' surfaces to the reference surface (S_{ref}) considering as the un-deformed surface.

4.1 Ceiling slab deformation

In concrete buildings, ceiling slabs are often supported by the beams and/or shear walls, and the slabs' edges are fixed. As such, intersection lines (L_{int}) between the slab's surface and supported element's surfaces (S_{SE}) are used to determine the reference surface (S_{ref}). Moreover, S_{SE} is perpendicular to the slab's surface. Thus, the algorithm identifies L_{int} to determine S_{ref} and computes slab's deformations.

For each slab $Slab_i$, the algorithm starts with boundary patches ($\psi_{ext,ij} \in c_i \subset Slab_k$) to retrieve adjacent cells c_j sharing an edge with c_i. Notably, c_j does not possess any patch of the slab $Slab_i$. Next, candidate points p_i of $S_{SE,i}$ are given in Eq. 4. Subsequently, VRG is employed to segment $p_i \in S_{SE,i}$, and the final surface of $S_{SE,i}$ is the closest surface , perpendicular to $\psi_{ext,ij}$.

$$p_i = \begin{cases} (p_{ci} \in c_i) \wedge (p_{cj} \in c_j) \; where \; p_{ci} \notin \; Slab_i \wedge p_{cj} \notin \; Slab_i \\ \qquad \left| d\left(p_{SSEi}, \psi_{ij.boundext}(p_{ij,0}, n_{ij})\right)\right| \leq d_1 \end{cases} \quad (4)$$

where d_1 = 0.3m is the distance threshold.

An intersection line segment $L_{int,i}$ between $\psi_{ext,ij}$ and $S_{SE,i}$ is determined, and the middle point of $L_{int,i}$ is considered as the edge point. The reference surface $S_{ref,i}(p_{ref,i},\ n_{ref,i})$ of $Slab_i$ is fitted through all edge points using PCA and the deformation of $Slab_i$ is expressed in Eq. 5.

$$d\left(p_i \in Slab_i, S_{ref,i}(p_{ref,i}, n_{ref,i}\right) = \frac{(x_i - x_0)n.x + (y_i - y_0)n.y + (z_i - z_0)n.z}{\sqrt{n^2.x + n^2.y + n^2.z}} \quad (5)$$

where $p_{ref,i} = (x_0, y_0, z_0)$ and $n_{ref,i} = (n.x, n.y, n.z)$ is the centroid of the edge points and the normal vector, and $p_i = (x_i, y_i, z_i) \in Slab_k$.

4.2 Column verticality

The column verticality is measured as out-of-plumbness of the column against a perfectly vertical surface (called the un-deformed surface, S_{ref}) through of the column top. The surface S_{ref} is determined through an intersection line L_{int} between the column's surface and the surface of the connected component (S_{CC}). The column often supports the beams (Case 1) and/or the ceiling slabs (Case 2), which can be automatically identify based on results from *Modulus 3*. The algorithm starts to determine L_{int} and then compute verticality.

For each surface S_{ij} of the column Col_i, PCA is employed to estimate unit vectors (n_{ij} – a normal vector, t_{ij} – a small tangent vector, tt_{ij} – a large tangent vector) while the 2D *mbb* is used to determine its width ($S_{ij}.w$) and height ($S_{ij}.h$).

For *Case 1*, from *Modulus 3*, if a beam B_k connecting to the column Col_i is available, the bottom surface S_{kl} of the beam B_k is retrieved. A sub-data set of S_{kl} given in Eq. 6 is representing $S_{CC,kl}$.

$$p_i \in S_{kl} \rightarrow p_{SCC,ij} \; if \; 0 \leq d\left(p_i, S_{ij}(p_{ij,0}, n_{ij})\right) \wedge d\left(p_i, S_{ij}(p_{ij,0}, n_{ij})\right) \leq S_{ij}.w \quad (6)$$

where $p_{ij,0}$ is a centroid of the points of the surface S_{ij}, and the distance here is a sign distance.

In *Case 2*, if a ceiling slab $Slab_k$ connects the column Col_i, only a subset of the slab expressed in Eq. 7 is considered to represent $S_{CC,kl}$.

$$p_i \in Slab_k \rightarrow \; p_{SCC,ij} if \begin{cases} 0 \leq d\left(p_i, S_{ij}(p_{ij,0}, n_{ij})\right) \wedge d\left(p_i, S_{ij}(p_{ij,0}, n_{ij})\right) \leq S_{ij}.w \\ \qquad \left| d\left(p_i, S^t_{ij}(p_{ij,0}, t_{ij})\right)\right| \leq 0.5 S_{ij}.w \end{cases} \quad (7)$$

Subsequently, the intersection line, $L_{int,jl}(p_{int,jl},\ t_{int,jl})$ is determined from the surface S_{ij} and $S_{CC,kl}$. Next, the reference surface $S_{ref,ij}$ is defined by a normal vector $n_{ref,ij}$ as a cross product of $t_{int,jl}$ and n_z. Finally, the verticality is distances $d(p_i \in S_{ij},\ S_{ref,ij}(p_{int,jl},\ n_{ref,ij})$ as given in Eq. 5.

4.3 Beam deformation

In concrete buildings, the deformation of a beam can express as the distance between the bottom surface S_{ij} of the beam B_i and the reference surface $S_{ref,i}$ through the beam supports. That is because the beam supports are assumed to be fixed. Moreover, as mentioned above, the end beams are supported by column (*Case 1*) and/or a shear wall (*Case 2*), which is automatically identified based on results of beam extraction in *Modulus 3*. For the bottom surface S_i of the beam B_i, unit vectors (n_{ij} – a normal vector, t_{ij} – a small tangent vector, tt_{ij} – a large tangent vector) and the surface dimensions ($S_{ij}.w$ - width and $S_{ij}.h$ - height) are respectively estimated by PCA and the 2D *mbb*. Notably, the direction of n_{ij} is the same to one of n_z.

For *Case 1*, the surface S_{kl} of the column Col_k connecting to the beam B_i is extracted, and then a sub-data set of the surface S_{kl} is to represent $S_{SE,ij}$, which is expressed in Eq. 8.

$$p_i \in S_{kl} \rightarrow p_{SSE,kl}\ if - S_{ij}.w \leq d\left(p_i, S_{ij}(p_{ij,0}, n_{ij})\right) \wedge d\left(p_i, S_{ij}(p_{ij,0}, n_{ij})\right) \leq 0 \quad (8)$$

where $d\left(p_i, S_{ij}(p_{ij,0}, n_{ij})\right)$ is a sign distance

In *Case 2*, the walls extracted from Modulus 1 closed to the end of the beam B_i is extracted. A sub-data set of the wall $Wall_k$ determined based on Eq.9, is used to determine $S_{SE,k}$.

$$p_i \in Wall_k \rightarrow\ p_{SCE,k} if \begin{cases} -S_{ij}.w \leq d\left(p_i, S_i(p_{ij,0}, n_{ij})\right) \wedge d\left(p_i, S_{ij}(p_{ij,0}, n_{ij})\right) \leq 0 \\ \left|d\left(p_i, S_{ij}^t(p_{ij,0}, t_{ij})\right)\right| \leq 0.5 S_{ij}.w \end{cases} \quad (9)$$

The intersection line, $L_{int,jl}(p_{int,jl},\ t_{int,jl})$ is determined from the surface S_{ij} and $S_{SE,k}$, and the reference surface $S_{ref,ij}$ is the surface through two intersection lines at the ends, in which the direction of $n_{ref,ij}$ is the same n_z. Finally, the distance $d(p_i \in S_{ij},\ S_{ref,ij}(p_{int,jl},\ n_{ref,ij}))$ given in Eq. 5 is the beam deformation.

5. Experiments and Results

To demonstrate the proposed method, a ground storey of a office building on Pham Ngu Lao st., Vietnam is selected. The storey is about 18.5m wide x 29.5m long x 3.45m high, and was scanned by a Trimble TX8 with a maximum scanning range at 120m and an angular accuracy of 8µrad in both vertical and horizontal (Trimble, 2020b). A point spacing of 11.3mm at a range of 30m and a total of 11 scanning stations was established to capture an interior storey with a maximize data coverage (Fig. 6a). The point clouds were registered by the Trimble RealWork software v11.2 (Trimble, 2020a) with the registration error about 1.57mm. Finally, 23.5 million points with x-, y- and z- coordinates was exported as input data for the proposed method. Notably, parts of a MEP system were installed, which obstructs to capture surfaces of several structural elements.

A set of parameters for the proposed method as following. For 2D cell decomposition, *cell_size* =1.0m and *min_ptc* = 10 are selected to ensure at least one cell representing the smallest slab by 2mx2m. The bandwidth of 0.2m is set for patch extraction by KDE, which allows to separate two surfaces of the thinnest component. Moreover, the thresholds α_0 = 5 degrees, d_0 = 10mm, r_0 = 10mm and *voxel_size* = 0.1m are selected for CpRG and VRG. Although the surfaces of the building components are almost perpendicular, the small angle threshold is selected to prevent points of the MEP components including in the ceiling segments. Notably, the distance and residual thresholds can adjust based on data errors and the surface roughness. Finally, the selected *voxel_size* is to ensure one voxel can representing a surface of the column and beam.

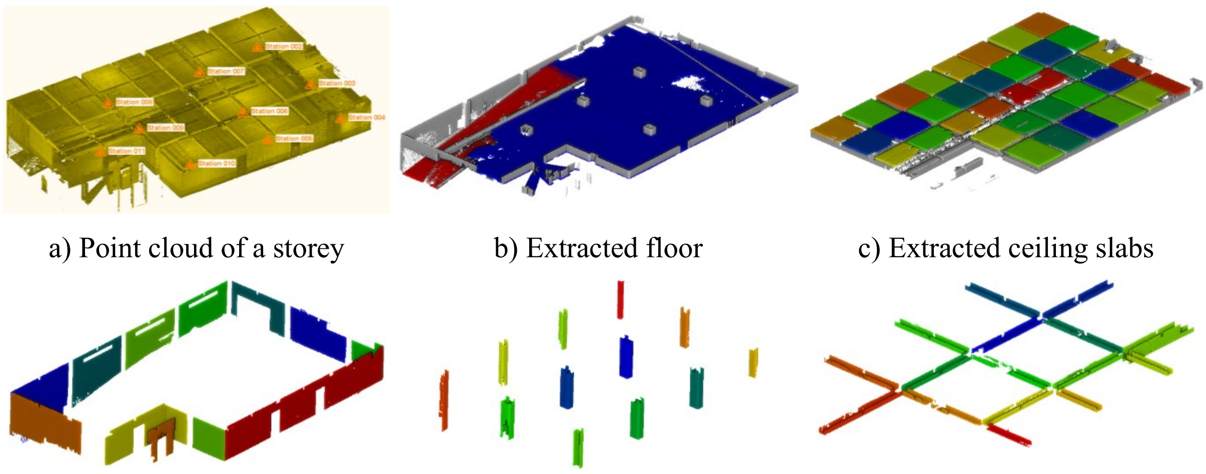

a) Point cloud of a storey b) Extracted floor c) Extracted ceiling slabs

d) Wall e) Column f) Primary beam

Figure 6: Point cloud of a storey from an internal scan and resulted component extraction

As a point cloud of one storey captured used as an input data for the proposed method, patches belonging to the floor and ceiling are mostly the first and last patches of a cell in the vertical direction, respectively. Thus, the first and last patches are respectively set as seeding patches for *Step 2.1* in floor and ceiling extraction, while all remaining patches use for Step 2.2 and 2.3. Once the points are assigned for the components, they are immediately deactivated, and only remaining points are used in subsequent steps. Results of the component extraction are shown in Fig. 6b-e. That can be seen all surfaces of the components (floor and ceiling slabs, columns and beams) are successfully extracted. However, in future work, additional experiemental tests and the quantitative elevation including the level of locational deviation, shape similarity and positional accuracy are implemeting to give detailed the perfromance of the proposed method.

Additionally, as only parts of the data sets are used in extracting the components, it shows that the proposed method is efficiently accommodates a large data set. For example, with a current data set, the processing time is 412.1 seconds including 166.9 seconds for floor and ceiling, 58.3 seconds for wall, 41.1 seconds for column and 145.8 seconds for beam. An executing time of the beam is larger than other components because the voxel size of 0.1m is set for VRG. This value can be adjusted based on the actual component size rather than a fixed value. This performance is based on an implementation of the proposed method in MATLAB 2019b (2019b) and processing on Dell Precision Workstation with a main system configuration as follows: Intel(R) Xeon(R) W-2123 CPU @ 3.6GHz with 32GB RAM.

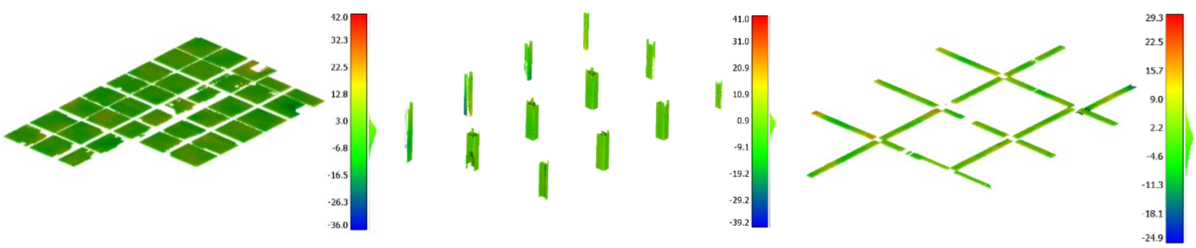

a) Ceiling slab deformation b) Column verticality c) Beam deformation

Figure 7: Results of building component inspection through deformation

Resulted inspection of the ceiling slabs, columns and beams are shown in Fig. 7. The slab deformations vary in a range from -36.00mm to 42.00mm, but deformations of 99.0% points are in a range a mean deformation (μ) ± 3 times of a standard deviation (σ) ($\mu \pm 3\sigma \equiv$ [-13.62mm, 10.54mm]. Large hogging deformations occurs around the lift where the point cloud of the lift's wall does not fully eliminate out of the slab segment. For the columns, the report shows that 98.0% of the points having the verticality varies in a range from -15.4mm to 14.2mm ($\mu = -0.62$mm and $\sigma = 4.94$mm), where the maximum and minimum verticality are -39.2mm and 41.0mm (Fig. 6b). Similarly, the beam deformations also change from -24.9mm to 29.3mm, but about 98.9% of the point deformations is in a range -13.35mm to 13.35mm ($\mu = 0.0$mm and $\sigma = 4.45$mm). In several beams, the large deformations are found in edges of the bottom surfaces because of an over-segmentation when extracting the points of the bottom surface. Thus, these points must be filtered to avoid miss-leading deformation report.

6. Conclusions

This paper presents an efficient, automatic method to extract structural components of a construction project of a reinforced concrete building. In structural component extraction, the proposed method consists of 3 consecutive moduli to extract the building components in a sequent order: floors, ceilings and wall, columns and beams, in which both spatial information of a point cloud and contextual knowledge about the structures are used. One of advantages of this methods is to roughly extract potential data points of components (floors, ceilings, columns and beams) before using cell-patch and voxel-based region growing to segment final surfaces of the components. As such, the proposed method only processes less complex, small sub-data set to extract the components, which makes the method efficient to a big data encountered in practice. This can be seen through a report of an experimental test on a 23.5 million points of one building storey, in which the proposed method successes to extract all surfaces of the building components with an executing time about 412.1 seconds. Moreover, by implementing the fundamental design of the structure, the component's boundaries can be automatically identified to establish un-deformed surfaces of the components for deformation measurement. In future work, the proposed method is going to test different types, layouts of the buildings and quantitative elevation strategy is implementing to give a detailed evaluation report. In addition, although the proposed method is developed for structure inspection, it could be extended for as-built BIM reconstructions.

Acknowledgements

This work was funded by the generous support of the European Commission through H2020 MSCA-IF, "*BridgeScan: Laser Scanning for Automatic Bridge Assessment*", Grant 799149. The first author is graceful for this support. The authors also thank Dat Hop Company Limited and Ceotic., JSC for their providing the laser scanning data.

References

Bosché, F. (2010). Automated recognition of 3D CAD model objects in laser scans and calculation of as-built dimensions for dimensional compliance control in construction. *Advanced Engineering Informatics,* 24**,** pp.107–118.

Burati Jr, J. & Farrington, J. (1987). Construction industry institute–Costs of quality deviations in design and construction. *Clemson University, Source Document,* 29.

Dimitrov, A. & Golparvar-Fard, M. (2015). Segmentation of building point cloud models including detailed architectural/structural features and MEP systems. *Automation in Construction,* 51**,** pp.32–45.

Kim, M.-K., Sohn, H. & Chang, C.-C. (2014). Automated dimensional quality assessment of precast concrete panels using terrestrial laser scanning. *Automation in Construction,* 45**,** pp.163–177.

Laefer, D. F. & Truong-Hong, L. (2017). Toward automatic generation of 3D steel structures for building information modelling. *Automation in Construction,* 74**,** pp.66–77.

Maalek, R., Lichti, D. D. & Ruwanpura, J. Y. (2019). Automatic recognition of common structural elements from point clouds for automated progress monitoring and dimensional quality control in reinforced concrete construction. *Remote Sensing,* 11**,** 1102.

Mathworks (2019b). MATLAB Function Reference. 2019b ed.

Rabbani, T., Heuvel, F. V. D. & Vosselmann, G. (2006). Segmentation of point clouds using smoothness constraint. *International Archives of Photogrammetry, Remote Sensing and Spatial Information Sciences,* 36**,** pp.248–253.

Trimble. (2020a). *Trimble RealWorks v11.2* [Online]. Trimble. Available: https://geospatial.trimble.com/products-and-solutions/trimble-realworks [Accessed 01/15 2020].

Trimble. (2020b). *Trimble TX8 LASER SCANNER* [Online]. Trimble. Available: https://geospatial.trimble.com/products-and-solutions/trimble-tx8 [Accessed 01/15 2020].

Truong-Hong, L., Chen, S., Cao, V. L. & Laefer, D. F. (2018). Automatic bridge deck damage using low cost UAV-based images.

Truong-Hong, L. & Lindenbergh, R. (2020). Quantitative assessment of structural components for construction management using laser scanning data. FIG Working Week 2020, 10-14 May 2020 Amsterdam, Netherlands. 15.

Vo, A.-V., Truong-Hong, L., Laefer, D. F. & Bertolotto, M. (2015). Octree-based region growing for point cloud segmentation. *ISPRS J Photogramm Remote Sens,* 104**,** pp.88–100.

Wang, Q., Cheng, J. C. P. & Sohn, H. (2017). Automated estimation of reinforced precast concrete rebar positions using colored laser scan data. *Computer-Aided Civil and Infrastructure Engineering,* 32**,** pp.787–802.

Towards a Unifying Domain Model of Construction Safety: SafeConDM

Carl Schultz, Beidi Li, Jochen Teizer
Aarhus University, Denmark
cschultz@eng.au.dk , beidi.li@eng.au.dk , teizer@eng.au.dk

Abstract. Specific occupational construction safety related knowledge and information are scattered and fragmented. Despite technological advancements of information and knowledge management, a link between safety management and information models is still missing. In this paper we present first steps towards a **unifying** formal (logic-based) domain model of construction safety, called *SafeConDM*, that consists of: (1) a semantically rich ontology of hazard, safety concepts, and concept relationships that builds on, and integrates with, existing construction safety ontologies and building information models; (2) a hierarchy of first-order *if-then* rules linking construction site states with the potential for specific hazards to occur that we define in a novel way using *spatial artefacts*. We present a prototype software tool based on *SafeConDM* for construction hazard analysis and safe construction planning decision support. We present an empirical evaluation on two real-world construction building models.

1. Introduction

Although significant research has been undertaken in construction safety and automated hazard analysis of construction plans (Zhang et al. 2013; Melzner et al. 2013; Zhang, Sulankivi, et al. 2015; Zhang, Boukamp & Teizer 2015; Schwabe et al. 2019), there is a lack of standardization of safety concepts and software tools within the architecture, engineering, and construction (AEC) research community. This lack of standardization makes it difficult to reliably integrate different areas of construction safety research in a way that can be readily exploited in practice on real construction projects. Among other reasons, such as the seriousness of project owners and contractors demanding such software tools, an extensible, integrated suite of safety analysis software tools for construction is currently still missing. Therefore, most of the existing approaches are done manually, and are thus prone to error or not performed at the right time (Teizer 2016).

Example: Like in many countries, falls on construction sites account for about one third of all fatalities and numerous more severe accidents leading to tragic loss of lives, serious or minor injuries (OSHA 2020). Consider the German construction safety regulation B100 for prevention illustrated in Figure 1 (left) (BG Bau 2019). The code states that any platform from which a worker could fall more than 2m requires a guard rail, or a covering if the drop is a hole in the platform greater than 9m^2 (additional rules exist for applying coverings on smaller openings on ground surfaces). Now suppose we seek to develop a software tool that can automatically assess this code on a given building information model (BIM). The standard approach, that we have also previously adopted (Zhang et al. 2013), is to formalize this code directly as a software algorithm, as illustrated in Figure 1 (right). The algorithm is then executed on a given BIM and an assessment report is generated, typically in addition to some modified version of the BIM, e.g., with guardrails and coverings added in order to satisfy the safety regulation.

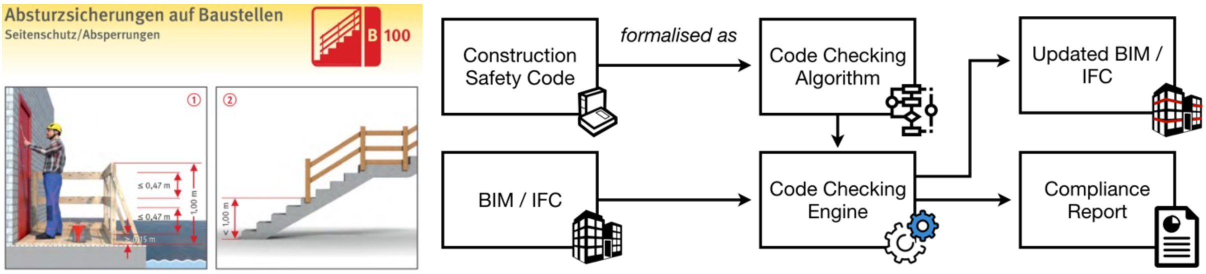

Figure 1: Example of safety regulation for fall prevention (BG Bau 2019) (left) and standard approach for formalizing and automating safety code compliance in construction (right).

There are numerous serious problems with this approach that become apparent when we attempt to scale up the formalization to cover a large portion of a safety code set in a unified way, and when we attempt to execute the formalized regulations (i.e., algorithms) on large, real-world BIMs.

Firstly, we distinguish the following concepts (Eastman et al. 2009; Solihin et al. 2017): Code *formalisation* is the task of representing or expressing the natural language code in a precise, unambiguous way so that it can be unambiguously interpreted by software (Zhang & El-Gohary, 2016). Code *execution* is the computational task of actually checking whether a BIM satisfies the code, and (optionally) modifying an uncompliant BIM in order to satisfy the code. Observe that in the given standard workflow, formalisation and execution are deeply entangled, having been combined into one step by going directly from natural language code to executable algorithm. The leads to a number of key problems (Schwabe et al. 2019; Solihin et al. 2017):

Lack of Transparency: the logic underlying the algorithm is only accessible to engineers with an information and communication technology (ICT) background, and even then may take some time if the algorithm is complicated, and may not even be possible if the algorithm is not open source nor otherwise documented. Third party formal verification of the algorithm becomes difficult or impossible, i.e. proving that it is correct for all possible input BIMs, within some predefined scope. Thus, as the software system's precise definition of code compliance is not readily accessible to engineers for either comprehension or verification, the value of safety assessment provided is significantly reduced.

Lack of Extensibility: What if an algorithm needs to be changed in some way, e.g. due to a change in the original codes, a need to improve runtime performance, or to adapt the algorithm to apply to a new region or context? What if a new code needs to be formalized and added to the code set? The standard workflow does not provide any support for community-based development and commonly treats code compliance software as a use-only black box. This significantly limits both the applicability of the code set, and its development and growth over time.

Confounding code semantics with execution concerns: Because such algorithms are intended to be directly executed on large and complex BIMs, they will necessarily need to implement a range of runtime optimizations that have nothing to do with the *meaning* and *intent* of the natural language code, i.e. the code's semantics. Examples of optimizations that can greatly complicate an algorithm include bounding box tests, organizing geometries into data structures such as quadtrees and R-trees, testing for a long list of special cases that can be handled more efficiently than the general case, etc. This is perhaps the most common and egregious problem with the standard approach where the logic underlying such algorithms **obscures the *intent* of the natural language code** by attempting to capture code semantics and suitable runtime performance in a single implementation step.

Supports a limited range of decision support services: In the workflow illustrated in Figure 1, the only way that the algorithm can be used without modification is: given a BIM, check if the code is satisfied. But what if we want to assess code compliance in a different way, for example: given a *partially complete* 4D BIM that evolves over time or is based on a construction schedule and a set of incomplete construction plan options. Each could provide the missing details from the 4D BIM, find which is the least/most hazardous plan, or least/most costly plan to ensure safety compliance. Alternatively, what if some plans still leave the BIM with certain key details missing, e.g. a specific wall may, or may not be, fully erected at a given construction stage. In principle, we are still relying on the *intent* of the original code for compliance assessment, but in both cases the algorithm that implements the code, e.g. for detecting fall hazards, will either need to be re-written, or the code checking engine will need to altered significantly. This further restricts the applicability of a given code compliance software tool.

We address these issues by strongly decoupling code *formalisation* and *execution* as illustrated in Figure 2. Our first key insight is to introduce new kinds of objects into BIMs, called *spatial artefacts* (Bhatt, Schultz, Huang 2012; Bhatt, Hois, Kutz 2012; Bhatt & Freksa 2015), that capture rich semantics of perception and behaviour in the form of objects that *occupy regions of empty space* that are necessary to reason about hazards. Some previous work has described adding geometries as a step, e.g. see (Schwabe et al. 2019; Solihin & Eastman 2015); also about enriching semantics of a model see (Belsky et al. 2015).

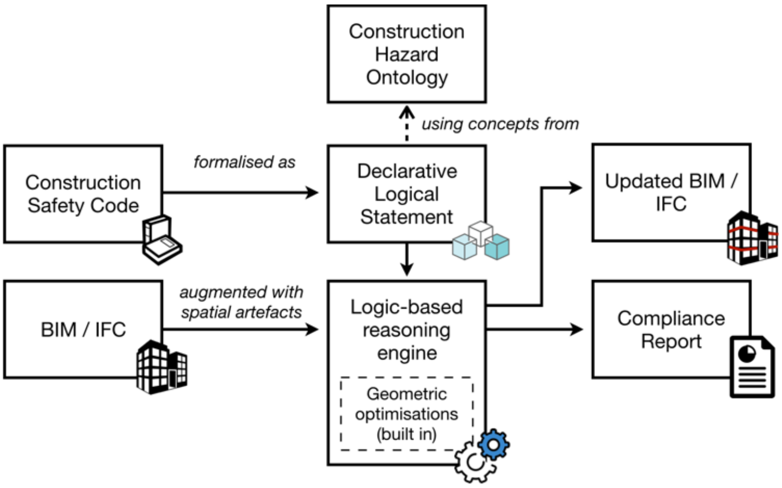

Figure 2: Our new workflow decouples code formalisation from execution via an ontology, spatial artefacts, and an enhanced reasoning engine.

Our second key insight is to use general logic-based reasoning engines with native spatial reasoning support built in, rather than developing our own ad hoc custom algorithms, to implement code execution so as to exploit their versatility (in the range of decision support services provided), reasoning efficiency (runtime performance), and solid mathematical foundations (formal rigour to support verification and soundness of compliance analysis).

Importantly, our key contribution here is to **extend** such reasoning engines with **in-built native support for spatial reasoning and geometric processing optimisations** which is necessary to manage large, real-world BIMs. We specifically build on the logic programming language Answer Set Programming (Walega et al. 2017).

Contribution 1. The shape of *empty space* in construction safety: Consider the region of empty space around an object such as a fuse box or valve; this region is meaningful because a person must be located in that region to perform a particular act (e.g. operate on the fuse box).

The geometry of this *functional space* region depends on properties of the person (consider electrician, mechanic, etc.), the task, and the object. Agents (e.g. workers and vehicles) have a *movement space* which are the regions in which they can move (travel) within. Excavators, for example, have an *operational space* required for rotating and depositing dug up material. People and sensors have *range spaces* (which can be further refined: *visibility space*, *hearing space*, *reach space*), and so on. These are examples of *spatial artefacts*, a concept that was pioneered by Bhatt et al. in the context of architectural analysis (Bhatt, Schultz, Huang 2012; Bhatt, Hois, Kutz 2012; Bhatt & Freksa 2015): regions of empty space that are rich with perceptual-locomotive semantics. Spatial artefacts "elevate" these semantically meaningful regions of empty space to become first-class objects, on the same ontological level as doors, walls, slabs, etc. Concretely, in a BIM such as IFC, spatial artefacts form an abstract class that can be defined as a subclass of `IfcSpace`.[1]

Example. Consider the previously discussed natural language code about a specific fall hazard: *"A platform that has a leading edge to a drop of more than 2m must be secured by a guardrail."*

We define a new *spatial artefact* called *Fall Space*, parametrically defined as: the region in which a person will fall by at least height `DANGEROUS_DISTANCE`, i.e. in the German code example the parameter is set to 2m. The dangerous platform edges can now be precisely, formally defined as: *"where Movement spaces horizontally meet (touch) a Fall Space"*.

This formalization is (a) very faithful to the original natural language code (semantics only), (b) easy to understand and verify (transparent); (c) directly applies to different contexts without changing the declarative statement that formalizes the code, i.e. the geometry of *Fall Space* is customized according to the project and context, whereas the concept "dangerous edge" as defined above does not need to change. Importantly, this provides a **uniform approach** for modelling a **large range of human-centered concepts** (movement, visibility, performing tasks etc.) that can seamlessly be integrated within a BIM, and are **effective "building blocks" for formalizing a broad range of hazards** in a clear and transparent way.

Contribution 2. Extending general logic-based reasoning engine with optimized spatial reasoning: Our idea here is to "push" the responsibility of runtime performance of code *execution* into the (general purpose) reasoning engine rather than dealing with runtime performance at the code *formalisation* stage, i.e. how the code is represented. In the context of construction and BIM a major bottleneck in runtime performance is evaluating the spatial relationships between a large number of complex geometries. For example, suppose a formalisation of the fall hazard code above is as follows, stating that if a movement space *M* and fall space *F* intersect, then their intersection defines a new *Fall Hazard Space* object:[2]

```
For all M,F in Objects :
  Movement_Space(M) and Fall_Space(F) and intersects(M,F) →
    Fall_Hazard_Space( @intersection(M,F) )
```

If a BIM has *n* movement spaces and *m* fall spaces then a naïve reasoning engine will perform $n \cdot m$ polyhedron intersection tests to execute this statement, which is prohibitively expensive for large BIMs. We may seek to solve this problem by changing the code formalisation to include additional conditions that "help" the reasoning engine by eliminating pairs of objects that are certainly not intersecting, e.g. by asserting that *M*,*F* must occupy the same building floors, and

[1] Currently spatial artefacts are not part of the Industry Foundation Classes (IFC) standard; compliance with IFC is straightforward by defining a new class `IfcSpatialArtefact` as a subclass of `IfcSpace`.

[2] In logical notation snippets we use the @ symbol to denote functions (e.g. @*intersection*(*A*,*B*)). Also note that the intersection of two polyhedra that are touching flush against each other (externally connected) is their shared surface.

that they occupy the same cell in our chosen spatial partition scheme such as quadtrees, R-trees, etc.:

```
For all M,F in Objects :
  Movement_Space(M) and Fall_Space(F) and same_floor(M,F) and same_quad_cells(M,F) and
  intersects(M,F) →
    Fall_Hazard_Space( @intersection(M,F) )
```

While this formalisation will have improved runtimes on larger BIMs, it comes at the cost of *transparency* and *extensibility*, and thus will not scale up well: the formalisation is less understandable and obscures the intent of the original natural language code, i.e. the original code does not describe quadtree partitioning schemes or even building storey partitioning. There is now also a problem of *portability*, as the formalisation now relies on the particular (arbitrary) spatial data structure used, i.e. in this case quad tree partitioning.

We address this by a novel extension of Answer Set Programming that integrates geometric processing optimisations and spatial reasoning *natively* within the general-purpose logic-based reasoning engine. This enables the code formalisation to stay as the first simpler form in the above example, while achieving good runtime performance on large BIMs.

2. SafeConDM: an Ontology of Construction Safety

Our approach has been developed based on previous research in ontological and logic-based approaches to Construction Safety including (Zhang et al. 2013; Zhang, Sulankivi, et al. 2015; Zhang, Boukamp & Teizer 2015; Schwabe et al. 2019). To illustrate this we integrate our approach into a broader existing ontological framework for construction safety. Figure 3 (left) illustrates the Construction Safety Ontology by Zhang, Boukamp & Teizer (2015) extended with new (abstract) classes: *spatial artefact* and *hazard space*. The authors distinguish the following three modelling layers: (1) *Construction Product Model:* building products and relations, such as doors, walls, storeys, slabs, and so on; (2) *Construction Process Model:* the construction plan including resources (equipment, materials, labour); (3) *Construction Safety Model:* construction safety knowledge (potential hazards, regulations, mitigating steps).

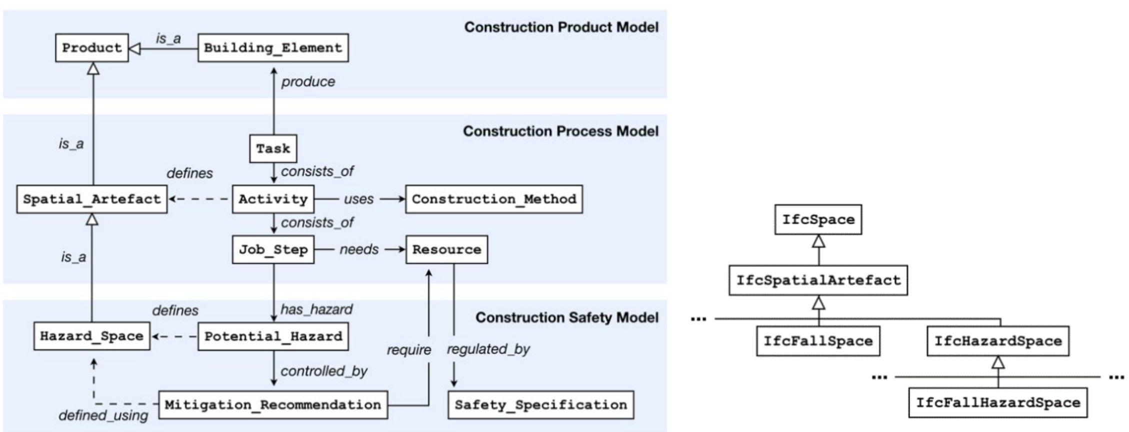

Figure 3: Construction Safety Ontology from (Zhang, Boukamp & Teizer 2015) extended with spatial artefacts to create SafeConDM (left); extract of IFC class hierarchy with spatial artefact subclasses (right)

We define pertinent spatial artefacts that capture semantic information about regions of empty space based on construction site activities, and human perception and behaviour (movement, visibility, falling spaces, function, etc.). Similarly, we model hazards as spatial artefacts whose existence and (geometric) definition is often a simple expression involving topological relations and Boolean operations between regions (intersection, union, offset etc.) – i.e. the "algorithm" for hazard detection is often as simple as clash detection. Spatial artefacts are modelled on the same ontological level as any other object in the product model, i.e. as illustrated in Figure 3 (left) they inherit from the abstract class *Product*. E.g. spatial artefacts are integrated within IFC as a subclass of `IfcSpace`, as illustrated in Figure 3 (right).

The shape of meaningful "empty spaces" in construction safety: In this paper we focus on *fall from height* hazards (leading edges and holes, see Figure 4). In Tables 1 and 2 we list the spatial artefacts that we use to define fall hazards. We develop two new classes of spatial artefacts: *Falling* spaces and *Hazard* spaces. We ground the geometry of the spatial artefacts in our models based on the specific context of *construction*. We encode rules about hazards as the spatial definition of specific (subclasses of) *Hazard spaces*.

Table 1: Construction site spatial artefacts

Spatial Artefact	Description
Movement Space	Regions in which an agent (e.g., construction worker, manager, visitor) can travel.
Movement corridor	Specific pathways along which a group of agents is moving (e.g., crowds).
Functional Space	Region in which an agent must be located to perform a given function or use a given object.
Work area	Area where an agent is occupied with a given task (e.g. electrician working on a fuse box).
Range Space	Regions carrying information about how an object can be detected by an agent.
Fall Space	Region in which an object or agent will fall by a dangerous distance.

Table 2: Construction site hazards defined as spatial artefacts

Subclass of Hazard Space	Hazard Category	Description	Spatio-Temporal Definition
Fall Hazard Space	Slips, trips, and falls	A person located in these regions is at risk of falling from a dangerous height.	Subset of movement spaces within 0.2m distance where the movement space meets (touches) a broad fall space.
Sprain Ankle Hazard Space	Slips, trips, and falls	A person in this region is at risk of twisting their ankle by walking into the small hole.	Intersection of movement space and narrow fall space.
Travelling Vehicle Strike Hazard Space	Struck by	A person located in these regions is at risk of being hit by a moving vehicle.	Intersection of vehicle movement space (or corridor) and worker movement space (or corridor).

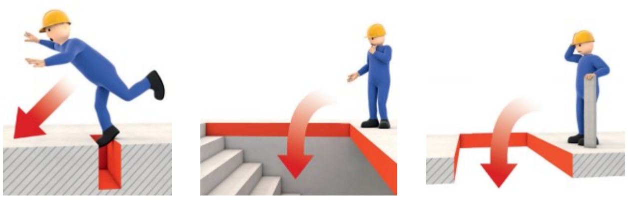

Figure 4: holes in which a worker may twist their ankle (*left*); leading edge onto an open stairway (*centre*); leading edge onto a hole through which a worker may fall a hazardous height (*right*).

3. Given a declarative formal encoding of construction safety codes, we can evaluate the Rule execution via Answer Set Programming

Given a declarative formal encoding of construction safety codes, we can evaluate the consistency of such statements on a given BIM using off-the-shelf solvers that have spatial reasoning support; we opt for using a logic programming paradigm where the knowledge base consists of Horn clause rules of the form: $h \leftarrow b_1, \ldots, b_n$, where proposition h is true (the rule head) if propositions $b_1, \ldots, b_n$ are all true (the rule body). Horn clauses strike a balance between being sufficiently expressive to capture logical *IF-THEN* relationships between symbolic terms, while still being computable (unlike full first-order logic). We specifically use Answer Set Programming (ASP), a logic-programming paradigm developed within the artificial intelligence community, that supports both deduction and other forms of non-monotonic reasoning (default reasoning, abduction) are decidable and computationally efficient.[3] We use our extension of ASP that also supports spatial reasoning, called ASPMT(QS) (Walega 2017), by encoding a building information model and derived artefacts as ASP *facts*, encoding the inference of hazards and responses as ASP *rules* and *constraints*, and implementing safety checking via ASP's *answer set search*. Our contribution in this paper on advancing ASPMT(QS) is the introduction of an internal geometry database for managing large amounts of geometric data (3D meshes and polygons), integrated natively within ASP; we have implemented ASPMT(QS) based on *clingo* (Gebser et al. 2016), a complete ASP system composed of a grounder (*gringo*) and a solver (*clasp*).

Example. The following ASPMT(QS) rule states that, for all movement spaces that meet flush (touch horizontally) with a fall space, then deduce a fall hazard space object. Its geometric representation is the intersection of the movement with the fall space offset by a given threshold e.g. 0.2m in this example.

```
define_fall_hazard_space_(Id, RepFallHazard) :-
   movement_space(M), representation(M, RepM),
   fall_space(F),     representation(F, RepF),
   meets_flush(RepM, RepF),
   unique_guid(Id),
   OffsetRepF = @offset(RepF, 0.2),
   RepFallHazard = @intersection(RepM, OffsetRepF).

fall_hazard_space(Id) :- define_fall_hazard_space_(Id, _).

representation(Id, RepFallHazard) :-
  define_fall_hazard_space_(Id, RepFallHazard).
```

Similarly, movement spaces are created as the volume 2m directly on top of slabs, subtracted by walls, columns and other movement obstacles. Fall spaces are the volume of space between the top surface of each object, and the next surface directly above (or the "sky") with the lower 2m subtracted. For this first prototype we simplified the calculation of movement spaces as the top surface of slabs subtracted by movement obstacles (columns and walls with voids where windows and doors will be placed), and we simplified fall spaces by taking a 2D bounding box of the site on each building storey and subtracting the slabs on that storey.

[3] Similar to Prolog, ASP has a knowledge base of facts and rules of the form: "Head :- Body." meaning that if the Body is true, then the Head must also be true. Rules with no Head are ASP *integrity constraints*, written: ":- Body." meaning that the Body must not be true (i.e. as a logical expression: Body implies False). Head and Body expressions consist of literals, representing propositions that can be either True or False, and ASP reasoning engines are specifically designed to rapidly find combinations of deduced facts that are consistent with all given domain rules (referred to as models or answer sets). We have extended the base language of ASP beyond propositions so that a set of consistent facts must also be spatially consistent, e.g. a 2D point P can never be both inside, and outside, of a given circle C (Walega et al. 2017).

4. Empirical Evaluation

In this section we execute the falling hazard rules on two real world, large construction BIMs (Figure 5). Navitas is a large four storied multi-purpose building in Aarhus, Denmark. The second BIM project is of a large 9 storey office building in Germany.

We generate 3D mesh representations of all BIM products (doors, walls, etc.) using IfcConvert from the IfcOpenShell project that we modified to also generate geometries for IfcOpening objects.[4] Table 3 presents statistics on the size of the BIM projects, number of spatial artefacts generated, and the runtime taken to (a) generate 3D meshes using IfcConvert and (b) generate all spatial artefacts using our software, based on ASPMT(QS).

Our system generated 184 spatial artefacts for Navitas in less than 1 second, and 890 spatial artefacts for the office building in 8 seconds. Figure 6 illustrates floors 2-5 of the office building as an example. In particular, our system detected particularly problematic situations such as doorways leading to empty elevator shafts, leading edges over a drop onto a stairway, and window openings (Figure 7).

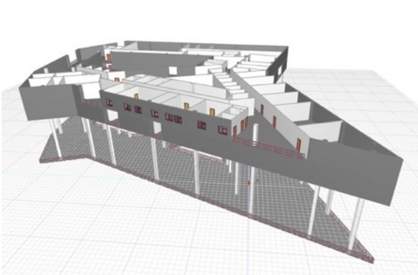

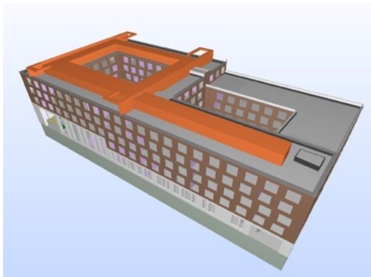

Figure 5: Two buildings used for empirical evaluation: (left) Navitas, Denmark; (right) a large office building in Germany.

Table 3: Statistics of the BIM projects (size and computation runtimes) in the empirical evaluation.

BIM Project (IFC)	**Number of BIM objects**	**Number of generated spatial artefacts**				**Time to generate 3D meshes from IFC via IfcConvert (seconds)**	**Time to generate all spatial artefacts (seconds)**
		Fall space	*Movement Space*	*Falling Hazard space*	**Total**		
Navitas	**707**	30	142	26	**184**	**19.0 sec**	**0.79 sec**
Office Building	**5415**	70	175	645	**890**	**99.0 sec**	**7.98 sec**

The results show that our prototype system with ASP rules executes in a practical amount of time (and is roughly two orders of magnitude faster than our previous implementations of fall hazard space solvers (Melzner et al. 2013)). This initial evaluation demonstrates that our prototype system can handle real-world sized buildings with an appropriate spatial resolution. Furthermore, assuming that a reader has a basic familiarity with logic, the definitions are arguably significantly simpler and more comprehensible than a C++ or Java (etc.) algorithm that iterates over BIM objects and geometries, builds data structures for faster geometric processing, etc.

[4] http://www.ifcopenshell.org/ifcconvert

Figure 6: Stories 2-5 (left to right) of the office building in Germany. *Top row*: movement spaces (green). *Bottom row*: fall spaces (green), fall hazard spaces (red).

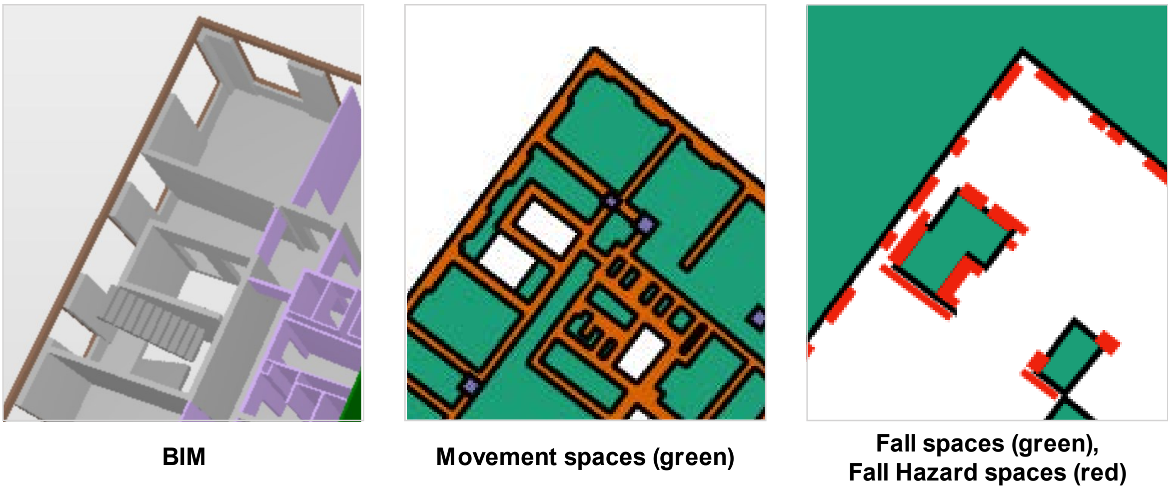

Figure 7: A stairway and adjacent elevator shaft on floor 5 (left image) creates a fall space with two dangerous leading edges where the two doors open onto the empty elevator shaft (right image).

5. Conclusions and Future Work

We have presented a novel approach to formalising safety construction rules via spatial artefacts, and have demonstrated safety rule checking on two real-world BIMs using our prototype rule checking system, implemented in Answer Set Programming extended to natively support spatial reasoning. In this paper we have focused on identifying fall hazards, however, our approach can be applied in a uniform way across a wide range of hazard categories. We are currently extending our system to include vehicle strike hazards, electrocution, vehicular blind spots, and so on, in the same way using a combination of spatial artefacts and logic programming with spatial reasoning. Another aspect that we have omitted to describe in the present paper is implementing *mitigation strategies* e.g. deciding to install guard rails, coverings, and so on and modifying the BIM accordingly. Mitigation steps are handled in the same way in our system, i.e. via logic programming rules. As future research we are also investigating non-monotonic reasoning features provided by Answer Set Programming as a means to check the safety of a plan that includes a temporal component i.e. 4D BIM.

Acknowledgements

The authors gratefully acknowledge the Independent Research Fund Denmark for their financial support of the project "Intelligent Software Healing Environments" (DFF FTP1).

References

Belsky, M., Sacks, R., & Brilakis, I. (2016). Semantic enrichment for building information modeling. Computer-Aided Civil and Infrastructure Engineering, 31(4), pp. 261–274.

BG Bau (2019). Absturzsicherungen auf Baustellen, https://www.bgbau.de/fileadmin/Medien-Objekte/Medien/Bausteine/b_100/b_100.pdf (Last accessed February 28, 2020).

Bhatt, M., Schultz, C. & Huang, M. (2012). The Shape of Empty Space: Human-centred cognitive foundations in computing for spatial design. IEEE Symposium on Visual Languages and Human-Centric Computing, VL/HCC.

Bhatt, M., Hois, J., & Kutz, O. (2012). Ontological modelling of form and function for architectural design. Applied Ontology, 7(3), pp.233–267.

Bhatt, M., & Freksa, C. (2015). Spatial computing for design - an artificial intelligence perspective. In: Studying visual and spatial reasoning for design creativity (pp. 109–127). Springer, Dordrecht.

Eastman, C., Lee, J. M., Jeong, Y. S., & Lee, J. K. (2009). Automatic rule-based checking of building designs. Automation in construction, 18(8), pp.1011–1033.

Gebser, M., Kaminski, R., Kaufmann, B., Ostrowski, M., Schaub, T., & Wanko, P. (2016). Theory solving made easy with clingo 5. In Technical Communications of the 32nd International Conference on Logic Programming (ICLP 2016). Schloss Dagstuhl-Leibniz-Zentrum fuer Informatik.

Melzner, J., Zhang, S., Teizer, J., & Bargstädt, H. J. (2013). A case study on automated safety compliance checking to assist fall protection design and planning in building information models. Construction Management and Economics, 31(6), pp.661–674.

OSHA (2019). Commonly used statistics, www.osha.gov/data/commonstats, (Feb. 28, 2020).

Schwabe, K., Teizer, J., König, M. (2019). Applying rule-based model-checking to construction site layout planning tasks, Automation in Construction, Elsevier, 97, pp.205–219.

Solihin, W., Eastman, C. (2015). Classification of rules for automated BIM rule checking development, Automation in Construction, 53, pp.69–82.

Solihin, W., Dimyadi, J., Lee, Y. C., Eastman, C., & Amor, R. (2017, July). The critical role of accessible data for BIM-based automated rule checking systems. In Proceedings of the joint conference on computing in construction (JC3) (Vol. 1, pp.53–60).

Teizer, J. (2016). Right-time vs. Real-time Pro-active Construction Safety and Health System Architecture, Construction Innovation: Information, Process, Management, Emerald, 16(3), pp.253–280.

Wałęga, P. A., Schultz, C., & Bhatt, M. (2017) Non-monotonic spatial reasoning with answer set programming modulo theories. Theory and Practice of Logic Programming, 17(2), pp.205–225.

Zhang, J., and El-Gohary, N. (2016). A prototype system for fully automated code checking. 16th International Conference on Computing in Civil and Building Engineering, Osaka, Japan, pp.535–542.

Zhang, S., Teizer, J., Lee, J. K., Eastman, C. M., & Venugopal, M. (2013). Building information modeling (BIM) and safety: Automatic safety checking of construction models and schedules. Automation in Construction, 29, pp.183–195.

Zhang, S., Sulankivi, K., Kiviniemi, M., Romo, I., Eastman, C. M., & Teizer, J. (2015). BIM-based fall hazard identification and prevention in construction safety planning. Safety science, 72, pp.31–45.

Zhang, S., Boukamp, F., & Teizer, J. (2015). Ontology-based semantic modeling of construction safety knowledge: Towards automated safety planning for job hazard analysis (JHA). Automation in Construction, 52, pp.29–41.

Data exchange analysis for property valuation on sustainability perspective

Tengxiang Su, Haijiang Li
Cardiff University, Cardiff, United Kingdom
SuT2@cardiff.ac.uk

Abstract. In real-estate domain, sustainable valuation and sustainable procurement are gradually accepted by different institutions all over the world. A large amount of research shows positive relationships between buildings' sustainable variables and observed property market values. However, the sustainability criteria in property valuation process is still lacking support data and standard information exchange methods. To enrich the fundamental database for sustainability assessment in property valuation and improve information exchange among different actors, this research proposes a holistic data interpretation of the information needed for the integration of property valuation and sustainability assessment. A standard information exchange method is further explored by referring to Building Information Modelling (BIM) related concepts (IFC/IDM/MVD). In this way, the comprehensive quantitative analysis of sustainability-related information in property valuation becomes tangible, and the accuracy and efficiency of property valuation will be improved.

1. Introduction

A plethora of research has shown that green buildings have a premium market price. Based on over 1200 green-rated buildings including office, retail, industrial buildings, hospitality and others, CoStar Group used standard regression analysis models and concluded the average LEED impact and Energy Star impact on sales price per square foot is a positive 9.94% and 5.76% respectively (Miller, Spivey and Florance, (2008)). Similar studies in Switzerland and UK found that property markets were increasingly paying premium price for the value-relevant sustainability features (Salvi, et al., (2008); RICS, (2013)). Therefore, research on the integration of sustainability assessment in property valuation process was required by real estate professionals and other market actors. Researchers and valuers tried to quantify the effects of sustainability-related features on property values directly (Kats, (2007)). However, the interpretation and application of sustainability measurement are still limited. This is because there is no available sustainability-related data on market values of properties or real estate professionals have limited knowledge and skills of sustainability assessment. To perform the sustainability assessment in property valuation more effectively, the current property valuation methods and procedures need to be improved and further developed.

Building information modelling (BIM), as a new technology for lifecycle project information exchange and management, has been developed by a great number of researchers and industrial professionals for sustainability assessment of buildings and infrastructure in the Architecture, Engineering, Construction and Facility Management domain (Eastman, (2008)). The application of BIM models in nature has the capability to create, collect, store and manage sustainability-related information for property valuation use. In addition, since no robust standard defines the specific requirements for data exchange of sustainability assessment in property valuation, current property valuation professionals have to acquire related information manually. This time-consuming process can be partly automated by using BIM related technologies: Industrial Foundation Class (IFC) standards, Information Delivery Manual (IDM) and the domain-specific Model View Definition (MVD).

In view of the potential benefits of BIM for sustainable property valuation, this research aims to provide a holistic data interpretation for sustainability assessment in property valuation and a standard information exchange framework for different actors. To achieve the above goal, this paper firstly reviewed 174 related documents and concluded sustainability-related parameters from them. After that, related information was defined in IFC format and extracted from BIM models using IDM standards. Finally, a case study based on advanced property valuation method was conducted and the trained machine learning model tested with lower prediction error. A valuation API was further proposed for the integration of machine learning models and BIM platform. This approach has the potential to reshape the hedonistic models already existed in property valuation.

2. The Current Status of Sustainability Assessment in Property Valuation

2.1 Systematic literature research on the integration of property valuation and sustainability assessment

In order to get a comprehensive understanding of current status of sustainability assessment in property valuation, this paper did a systematic literature which collected from 4 main academic databases namely Web of Science, Google Scholar, Science Direct & Scopus. The search criterion was devised as using two groups of keywords: (Property Valuation **or** House Price **or** Real Estate Appraisal) **and** (Sustainability Assessment **or** Green Certification) within (Title or Keywords). The initial search results – 715 documents (raw findings before removal of duplicates) breakdown into 6 search groups: Property valuation & Sustainability Assessment (217 documents); Property Valuation & Green Certification (76); House Price & Sustainability Assessment (72); House Price & Green Certification (133); Real Estate Appraisal & Sustainability Assessment (77); Real Estate Appraisal & Green Certification (140). In order to get rid of the duplicates, the 715 documents were imported into the same Mendeley Library folder with the number reduced to 234. After that, the 234 documents were manually checked by the authors and approved as relevant with sustainability assessment in property valuation, with the number reduced to 174 (Figure 1). These 174 files were further used for the holistic data interpretation regarding the database of property valuation and sustainability assessment in section 4.

According to the Appraisal Institute (2001), there are four fundamental forces influencing the property values: physical forces, economic forces, political and governmental forces and social forces. Recently, within the property valuation process, growing interest is shown on the social responsibility, financial benefit and potential risk reduction that sustainable development may bring into property valuation domain (Lorenz and Lützkendorf, (2008)). Figure 1 shows that the awareness of reflecting sustainability-related impacts in the traditional property valuation method is high and constantly growing among the general public in many countries. The complexity of sustainability and taking account this into different traditional property valuation methods require a significant change in the data collection and information exchange of property valuation professionals and other related market actors (Lorenz, Lützkendorf and Trück (2007)). Research and projects have been conducted to explore the possibility of characterizing the sustainability of a building by its environmentally related parameters (such as energy efficiency and lifecycle costing) according to the a specific internationally renowned green building labelling scheme such as LEED or BREEAM, but this is recognized as too short sighted due to the lack of holistic sustainability assessment consideration (Meins et al., (2010a)). Apart from energy efficiency and building ecology, social aspects and economic issues which also have parts to play in determining the sustainability assessment in property valuation.

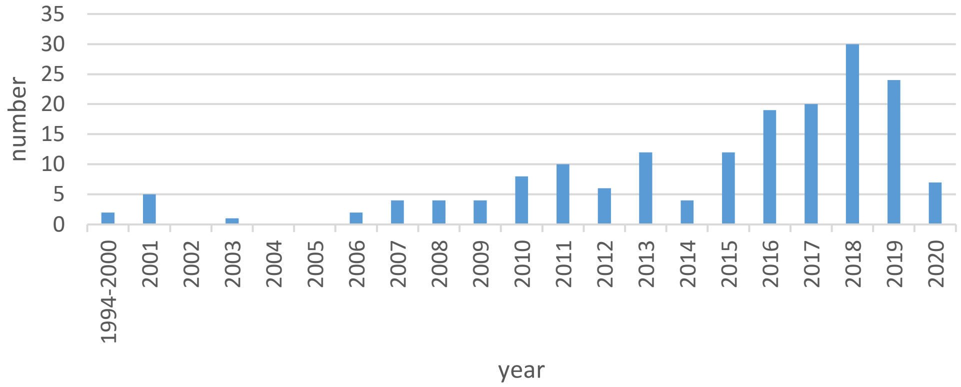

Figure 1: 174 research documents on sustainability assessment in property valuation from 1994-2020

2.2 Analysis of Quantitative Sustainability Assessment in Property Valuation

The environmental, social and economic benefits of sustainable buildings are generally accepted and extensively researched in the literature, which recognized as low lifecycle energy cost, energy efficiency, increased health comfort of tenants and being profitable and marketable than traditional buildings (Lorenz and Lützkendorf, (2008)). Researchers try to quantify the sustainable features by referring to direct or indirect financial gains or reduced property risks. For instance, Miller, Spivey and Florance (2008) compared the effects of sustainable features to LEED certificated buildings and Energy Star rated buildings in terms of rent and occupancy rate gains, increased sale price and lower cap rates. CASBEE system created a direct link between sustainability assessment and property valuation, taking into consideration of environmental quality and load reduction factors such as indoor heating and cooling, health and safety, indoor brightness and quietness, consideration of the landscape, water conservation and recycling, maintenance and operation schemes (Wong and Abe, (2014); IBEC, (2007)). Lorenz, Lützkendorf and Trück (2007) used property rating systems to economically assess the relationship between characteristics and attributes of sustainable buildings and reduced property specific risks, such as the flexibility and adaptability to reduce risks of market changes, environmentally friendly building components and materials to reduce the litigation risks. Lützkendorf and Lorenz (2007) tried to find the effects and benefits of different sustainable design features on different actors – developers and owners, tenants, society and environment.

3. System Design and Methodology

Building upon the research from the literature review, a novel system is proposed which enables the exploration of information management for property valuation on sustainability perspective. Figure 2 below illustrates the conceptual system framework, along with the adopted methodology for its development. In the next two sections, firstly, holistic data interpretation for the integration of property valuation and sustainability assessment will be achieved from quantitative analysis of related research publications and projects, industry standards and procedures. Secondly, related IFC datatypes will be defined based on the fundamental database and required information will be extracted from BIM models referring to IDM standards. Finally, a valuation API based on machine learning will be integrated into the BIM platform to achieve semi-automated property valuation on sustainable perspective.

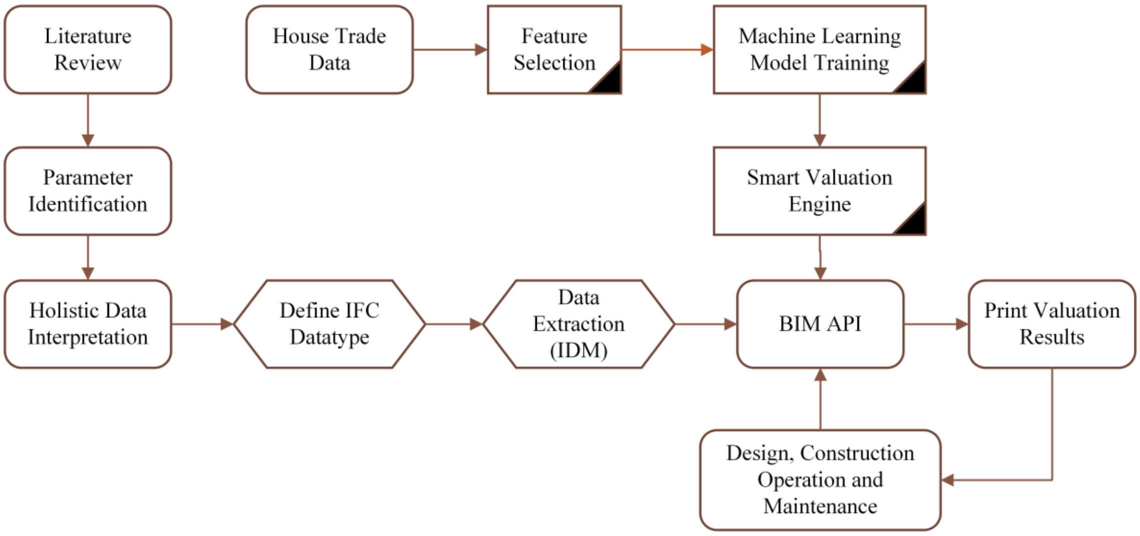

Figure 2: Conceptual system framework - data exchange analysis for sustainable property valuation

4. Data Exchange Analysis for the Integration of Sustainability Assessment in Property Valuation

4.1 Holistic Data Interpretation for Property Valuation on Sustainability Perspective

Collected from the 174 research documents including research paper, research projects and popular sustainability rating systems (LEED, BREEAM, DGNB and CASBEE) from different countries, the list of information contained in Table 1 (appendix) has been classified with 6 different types of information related to property valuation and sustainability assessment: information related to environmental quality, social and economic quality, functional quality, process quality, technical quality and site quality. Information included in traditional property survey and sustainability assessment are compared with information achievable within BIM related process. The yellow color stands for information needed for traditional property valuation and the green color stands for information needed for sustainability assessment, both of which may come from various sources. The light red in the 4th column means information required by both traditional property valuation and sustainability assessment. The dark red in the 3rd column means information can be defined and developed in the BIM related platform, which is the core for semi-automated property valuation.

4.2 Information exchange based on BIM related concepts – IFC/IDM/MVD

According to Ventolo (2015), the data collection in the traditional building survey can come from more than 40 data sources: regional government officials, property managers, professional journals, financial institutions, building architects, contactors, engineers and so on. All market actors in property markets can create their own sets of raw data in the building lifecycle, or they can collect and process information from other information source suppliers. Different market actors use different descriptive ways to interpret information in different data formats, which means information exchange issues will inevitably happen. These problems also exist in the integration of sustainability assessment and property valuation process.

To facilitate information exchange, this research uses standard information exchange technology referring to related BIM concepts. Firstly, related IFC concepts are defined for the integration of sustainability assessment in property valuation. The IFC data model, contains geometric information and semantic information, is an open and neutral object-based data format for standard description of architectural, building and construction industry (Liebich, (2013)). Table 2 in the appendix lists an example that shows IFC 4 entities and data attributes covering related information from the enriched database. The classifications of components and units are based on the rules of measurement for capital building works from RICS (2012). The definition of IFC entity and IFC attribute datatype refers to the IFC4 standard from buildingSMART International (Liebich, T. (2013)).

Secondly, required information is delivered using process map, which is created to cover the knowledge mapping of BIM models and property valuation on sustainability perspective. Figure 3 shows the process map for information exchange between architects, HVAC engineers and property valuers on sustainability perspective. The holistic data interpretation collected from literature and defined IFC standards provide guidelines for Architects, HVAC engineers and property valuers to create information when they are preparing the valuation models. The sustainability-related information is semi-automatically extracted from the enriched data models for sustainable property valuation.

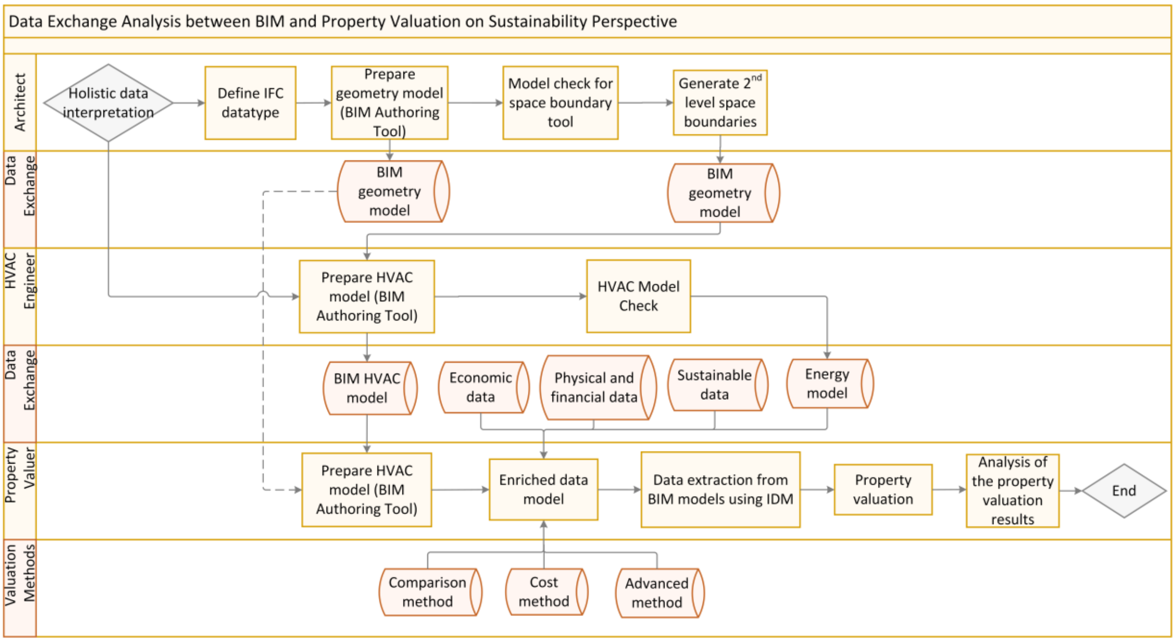

Figure 3: Process map for the information exchange between BIM and property valuation on sustainability perspective

5. Implementation and Demonstration – Case Study Based on Advanced Valuation Method

As Pagourtzi et al. (2003) concluded, there are traditional valuation methods (sales comparison method, DCF method) and advance valuation methods (data analysis methods). To fully perform the automatically information exchange, this research explores the use of the advanced valuation method using ensemble machine learning algorithms. The machine learning engine is trained with 700 traded houses from 47 different cities in America. The dataset contains 17 predicting variables, selected from 63 attributed by using gradient descent optimization algorithm. The dataset is divided into two groups: 70% for training dataset, 30% for testing dataset. After that, in order to find the best learning speed and the suitable complexity of the decision trees, the model hyperparameters are tested on Pycharm platform–which is an integrated development environment (IDE) specifically for the Python language. The model hyperparameters are finally set for training the ensemble machine learning engine: 1000 decision trees, learning speed at 0.1, maximum depth at 6, minimum sample leaf at 9. The code for the training model is showed below.

Code for the training model:

```
# Create the X and y arrays
X = features_df.as_matrix()
y = df['sale_price'].as_matrix()
# Split the data set in a training set (70%) and a test set (30%)
X_train, X_test, y_train, y_test = train_test_split(X, y, test_size=0.3,
random_state=0)
# Fit regression model
model = ensemble.GradientBoostingRegressor(
    n_estimators=1000, learning_rate=0.1, max_depth=6, min_samples_leaf=9,
    max_features=0.1, loss='huber', random_state=0)
model.fit(X_train, y_train)
```

Code for the prediction model:

```
from sklearn.externals import joblib
# Load the model we trained previously
model = joblib.load('trained_house_classifier_model.pkl')
house_to_value = [
    2006,# year_built          1,    # stories          4,# num_bedrooms
    3,   # full_bathrooms      2200, # livable_sqft     0,# garage_sqft
    0,   # half_bathrooms      2350, # total_sqft       0,# carport_sqft
    True,# has_fireplace       False,# has_pool
    True,# has_central_heating True, # has_central_cooling
    # Garage type: Choose only one
    0,   # attached            0,    # detached         1,# none
    # City: Choose only one
    1,      # Brownport ]
homes_to_value = [house_to_value]
predicted_value = predicted_home_values[0]
print("This house has an estimated value of ${:,.2f}".format(predicted_value))
```

After the machine learning model training, a Revit API is proposed to connect the smart valuation model to the BIM platform. The API helps extract IFC data from BIM models semi-automatically. The related data extracted from BIM is further tested by the trained machine learning model, with the prediction value of $587091.02, testing mean absolute error (MAE) at $59225.13, testing mean absolute percentage error (MAPE) at 10.08%. The MAE is the average of the absolute values of the prediction errors according to their magnitude. The MAPE, a measure of accuracy in a series value and usually expresses accuracy as a percentage, is calculated as formula 1:

$$MAPE = \frac{1}{n}\sum_{t=1}^{n}\left|\frac{A_t - F_t}{A_t}\right| \quad (1)$$

where A_t is the actual value and F_t is the forecast value. McCluskey et al., (2013) conducted a research on prediction accuracy of different modern approaches for mass appraisal, in terms of mean absolute percentage error, showing 10.40% for geographically weighted regression (GWR), 11.97% for ANN, 13.69% for spatial simultaneous autoregressive (SAR), and 12.27 for model regression modelling (MRM). Compared with these statistic models whose mean absolute percentage error are greater than 10.40%, this research shows the superiority of 10.08%.

Code for the testing:

```
# Find the error rate on the training set
mse = mean_absolute_error(y_train, model.predict(X_train))
print("Training Set Mean Absolute Error: %.4f" % mse)
# Find the error rate on the test set
mse = mean_absolute_error(y_test, model.predict(X_test))
print("Test Set Mean Absolute Error: %.4f" %)
```

6. Conclusions and future work

In this paper, firstly, a comprehensive database is collected from related literature for the integration of sustainability assessment in property valuation. Taking into consideration of the unique sustainability assessment method used in different regions or countries, this enriched database can be further developed for different sustainability rating systems as well as complying with the specific demand of the customers. Secondly, an efficient data exchange framework by using BIM related technology (IFC/IDM) is proposed for the efficient and cost-saving data collection and information sharing among different market actors. Lastly, a case study using advanced valuation method is further explored to connect the property valuation to BIM platform, and tested with the improved prediction accuracy. With this new information management framework, most of the information needed for property valuation on sustainability perspective can be semi-automatically extracted from BIM models. Consequently, fundamental improvements and changes can be made to property appraisal methods. In addition, the holistic data interpretation using bibliography analysis and information exchange framework under BIM platform presented in this paper has the potential for the information management of any further domain applications related to building and construction industry.

References

IBEC (2007). CASBEE Property Appraisal Manual.

Lorenz, D. and Lützkendorf, T. (2008). Sustainability in property valuation: Theory and practice Journal of Property Investment and Finance.

Lorenz, D.P., Lützkendorf, T. and Trück, S. (2007). Exploring the relationship between the sustainability of construction and market value: Theoretical basics and initial empirical results from the residential property sector, Property Management. 25(2), pp.119–149.

Lützkendorf, T. and Lorenz, D. (2007). Integrating sustainability into property risk assessments for market transformation, Building Research and Information. 35(6), pp.644–661.

McCluskey, W.J., McCord, M., Davis, P.T., Haran, M. and McIlhatton, D. (2013). Prediction accuracy in mass appraisal: A comparison of modern approaches, Journal of Property Research. 30(4), pp.239–265.

Meins, E., Wallbaum, H., Hardziewski, R. and Feige, A. (2010). Sustainability and property valuation: A risk-based approach, Building Research and Information. 38(3), pp.280–300.

Miller, N., Spivey, J. and Florance, A. (2008). Does green pay off?, Journal of Real Estate Portfolio Management. 14(4), pp.385–399.

Pagourtzi, E., Assimakopoulos, V., Hatzichristos, T. and French, N. (2003). Real estate appraisal: a review of valuation methods, Journal of Property Investment & Finance. [online] 21(4), pp.383–401. Available at: <http://www.emeraldinsight.com/doi/10.1108/14635780310483656>.

RICS (2013). Sustainability and commercial property valuation: RICS Professional Guidance, Global.

Wong, S.C. and Abe, N. (2014). Stakeholders' perspectives of a building environmental assessment method: The case of CASBEE, Building and Environment. 82, pp.502–516.

Appraisal Institute, (2001). The Appraisal of Real Estate, 12th ed. Chicago: Appraisal Inst.

Eastman, (2008). BIM Handbook: a guide to building information modelling for owners, managers, designers, engineers and contractors. New Jersey: John Wiley &Sons, Inc.

Salvi, M., Horejajova, A. and Muri, R. (2008). Minergie machtsich bezahlt. Zurich: Centre for Corporate Responsibility and Sustainability (CCRS) and Zurcher Kantonalbank.

Ventolo, (2015). Fundamentals of real estate appraisal, 12th ed. La Crosse: DF Institure, Inc.

Liebich, T. (2013). IFC4 – The new buildingSMART Standard. buildingSMART International.

Kats, G. (2007). The Costs and Benefits of Green. Capital E Analytics.

RICS (2012). RICS new rules of measurement: order of cost estimating and cost planning for capital building works, 2nd ed. Coventry: RICS.

Appendix

Table 1: Database for property valuation including sustainability-related information

Type of Information	Subtype	Performance indicator and attribute	A	B	C	D
Environmental Quality	Local Environmental Impact	Climate Change				
	Pollution	Noise from transport service and building service equipment, water pollution, land contamination, electromagnetic pollution				
	Land Use	Soil Characteristics				
		Layout, size, inclination, topography				
	Sustainable Resource	Rainwater use				
		Green area				
		Sunlight/Shading				
	Waste Water Volume	Waste water disposal				
Social and Economic Quality	Commercial Viability	Policy and economic situation				
		Demographic structure and development				
		Purchasing power, letting prospects, expected rates of return				
		Rental growth potential, inflation expectations, rental payments, other payments				
		Payments for construction, acquisition, disposal, payments for operating costs, marketing / letting fee, payments for revitalization				
		Number of tenants, Duration and structure of rental contracts				
		Vacancy rate, tenant fluctuation				
	Safety and Security	Location regrading natural hazards (risk of floods, landslides, collapse)				
	Lifecycle Cost	Water demand and price, energy demand and price				
Functional Quality	Indoor Air Quality	Sufficient natural air flow				
	Acoustic Comfort	Sufficient natural light				
	Visual Comfort	Good scene view				
	Flexibility and Adaptability	Flexibility of use (residential, office, medical practice), adaptability to users				
		Wheelchair accessibility				
		Wheelchair accessible washrooms				
		Usability of outside space				

		Elevators (for all stories or not)
		Wide doors and wide halls
		Floor plan, storey height
	Brand Value	Green certification
		Famous designer
	User Control	Individual temperature controls
	Design/Aesthetic Quality	Architectural quality, Holistic monument
Process Quality	Sustainability Aspects in Tender Phase	Ecological construction materials, risks and impacts for the local environment and residence
	Documentation for Sustainable Management	Documented maintenance and servicing activities
	Urban Planning and Design Procedure	Public accessibility, quality of layout,
	Construction Process/Site	Quality control during construction (air-tightness, thermography, sound insulation)
	FM-compliant Planning	
Technical Quality	Basic Information	Structure, age, size, construction type, main construction materials
		Availability of green roofs/green facades
		Degree of revitalization
		Building equipment and appliances
	Sound Insulation	Noise Protection Techniques and Components
	Quality of the Building Envelope	Heat insulation
		Moisture proofing of the thermal building envelope
	Ease of Cleaning Building Components	Ease of conducing cleaning, building services and maintenance works
	Recyclability and Energy efficiency	Ease of recovery and recycling, efficiency of heating ventilation, air conditioning, rainwater use
	Immission Control	External and internal accessibility
	Infrastructure	Fitness
	Quality of Indoor and Outdoor Spaces	Balcony, storage space
	Safety and Security	Clear arrange routes for escape
		Protection against burglary
		Fire Protection

		Quality of sanitary and electronic fixtures				
		Structural Safety				
		Durability of building components				
Site Quality	Local Environment and Policy	Visual context, building permission and planning regulations				
	Transport Access	Public transport, bicycle parking				
	Amenities	Area and distance to facilities (shopping, social and medical)				

A. Information included in traditional valuers' investigation
B. Information contained in sustainability assessment process
C. Information achievable within BIM related platform (design, planning, operation and maintenance process)
D. Information included in both property valuation and sustainability assessment

Table 2: IFC datatype response to sustainability assessment for property valuation

Type of data	Performance indicator and attribute	Component	Unit	IFC entity	IFC attribute datatype
Social and Economic Quality	Payments for construction, acquisition, payments for operating costs	General equipment	Weeks/ nr	IfcConstructionEquipmentResource	IfcQuantityTime
		Site Formworks	Weeks/ nr	IfcConstructionProduct Resource	IfcQuantityCount
Process Quality	Urban Planning and Design Procedure	Planning costs	m²/km²	IfcSite	IfcQuantityArea
		Design costs	m²	IfcBuildingStorey; IfcSlab	IfcQuantityArea
Technical Quality	Structure, age, size, construction type, main construction materials, building equipment and appliances	Superstructure	m²/nr	IfcSlab; IfcColumn; IfcBeam; IfcRoof; IfcStair; IfcRamp; IfcWall; IfcDoor; IfcWindow	IfcQuantityArea; IfcQuantityLength; IfcQuantityCount
		Fittings/furnishings	Nr	IfcFurnishing	IfcQuantityCount
Site Quality	Area and distance to facilities (shopping, social and medical)	Services	m²/nr	IfcBuilding; IfcSpace; IfcBuildingStorey; IfcTransportElement	IfcQuantityArea

Seeing the Risk Picture: Visualization of Project Risk Information

Irem Dikmen[1], Timo Hartmann[2]
[1]METU, Turkey, [2]TU Berlin, Germany
idikmen@metu.edu.tr

Abstract. Risk assessment is carried out to understand uncertainties and estimate how they may affect a project. Although there are various studies on alternative methods to quantify risk in projects, limited research exists about how the results are utilized to make sense of project risk by the decision-makers. Probabilistic methods such as Monte Carlo Simulation involve an additional complication as probability is an abstract concept and hard to interpret. We argue that blurred risk pictures as well as lack of familiarity of the users with the concept of probability may lead to misleading interpretations during risk assessments. The aim of this paper is to present the underlying theoretical ideas behind a planned empirical research project with the goal to explore how results of probabilistic risk assessment can be represented in a way that help decision-makers to understand risk in a project and develop visuals that can be used by the decision-makers to see the entire risk picture. Within the study we plan to analyze data from a case study on a mega tunnel project carried out in Turkey, hypothesizing that interactive visualizations may help the user to understand the inputs, outputs and assumptions in quantitative risk models, and help risk managers to understand how project outcomes may change with changes in the risk picture. We hope that the outcomes of the empirical research will allow us to develop better visuals for users to understand the potential scenarios in a project, probability, variation and model uncertainty.

1. Introduction

Managing risk in projects that involve high level of uncertainty and complexity requires a formal process to minimize threats and maximize opportunities. The normative guidelines such as ISO 31000 and PMBoK define phases of formal risk management (RM) process as; risk management planning, risk identification, assessment, analysis, response, monitoring and communication. Risk assessment (RA) is carried out to predict possible scenarios about risk events and their impacts on the project so that response strategies can be formulated. RA is a knowledge-intensive process that requires collection of statistical data as well as lessons learned from previous projects and knowledge elicitation from experts about magnitude of risks and possible scenarios. The Society of Risk Analysis (SRA) defines RA as a systematic process to comprehend the nature of risk and to express the risk, with the available knowledge. By engaging in quantifying the uncertainties, RA contributes to the understanding of risk and provides information useful for its management (Zio, 2018). Aven (2016) highlights that the way we understand and describe risk strongly influences the way risk is analyzed and hence it may have serious implications for risk-informed decision-making. Although construction project management literature is very rich in terms of quantitative methods that can be used for risk assessment (such as probabilistic, possibilistic or hybrid methods) (Taroun, 2014), limited number of studies exist about “knowledge” utilized and produced during RA as well as its communication.

Willumsen et al. (2019) point out that the underlying assumption behind all normative guidelines for RM and proposed RA methods/tools is “risk management creates value”. Among the limited studies that investigate how RM creates value in practice, Senesi et al. (2015) found that value creation by RM is usually attributed to the function of risk communication where the major benefit of RM from the eyes of practitioners is its facilitation of internal collaboration/discussion with the project team and organization. Ad hoc, dialogue-based RM during project meetings with upper and lower management is perceived as the main contributor to project success. Major benefits of RM are gained through communicating risk knowledge. The motivation of our research stems from the idea that more research is needed to understand the knowledge/information dimension within the RA process and how its effective communication may create value within the RM context.

Rickard (2019) points out the aim of pragmatic risk communication as transmission of information, which includes simplification of risk model outputs so the decision-makers “comprehend” the level of uncertainty. On the other hand, risk communication has a constitutive function as risk is not an objective phenomenon, thus risk communication has a role to enable decision-makers to interact with risk information and create shared meaning. According to Bostrom and Lofstedt (2003) “risk communication is more art than science”. Although there are no generic rules and guidelines about communication of risk information, Eppler and Aeschimann (2009) argue that due to its cognitive and communicative advantages, visualization can play a significant role in conveying risk information. In this research, we aim to focus on communication of probabilistic risk information and explore whether visualization methods can improve the communication process during RA.

2. Understanding Probability and Seeing the Risk Picture

Within the construction project management practice, most of the risk information are depicted in reports, such as progress reports and risk management plans. Risk assessment results (mainly risk ratings of probability - P and impact – I) are usually summarized in these reports by risk cards, matrices, checklists and maps. However, P-I based assessment is criticized because it is very simplistic and cannot demonstrate the real risk picture as interrelations between the risk factors and underlying assumptions cannot be explored further (Qazi and Dikmen, 2019). These problems are further inflated if sophisticated risk models are used. While probabilistic methods such as Monte Carlo Simulation (MCS) and Bayesian Belief Networks (BBN) are utilized for better understanding of likelihood of occurrence of risk scenarios and their impacts, holistic risk pictures get even more complex to understand.

These practical problems also have been well discussed within the academic literature. Zio (2018) argues that for more than 35 years, the probabilistic analysis has provided the basis for the quantification of risk in project-based industries. However, quantitative risk analysis is often criticized due to the difficulty of assigning probabilities (e.g., due to human errors or software failures), the difficulty of verifying the assumptions behind the models, and the inherent uncertainty involved in the phenomena of interest. Senesi et al (2015) questioned that, given the existence of probabilistic risk analysis and guidelines written to encourage the use of probabilistic risk analysis, why are these probabilistic methods not being used more often? As a result of their study, one of the major reasons was found as the difficulty in interpreting the results. The interpretation of results from probabilistic analysis requires knowledge of basic probability and statistics. This barrier refers to the difficulty that some project managers and team members may have in comprehending and using the outputs of probabilistic tools which was initially identified in the interviews as “lack of familiarity or understanding.” Several interviewees stated the importance of illustrating the probabilistic risk analysis results in a manner that employees and other project stakeholders could understand and interpret. In this research, we also argue that, the difficulty of interpreting probabilistic findings may also be due to blurred risk pictures as well as lack of familiarity with probabilistic terms, as will be discussed in the next section.

2.1 Understanding Probability

Understanding probability, as an abstract concept is usually identified as a difficult task. There are different ways to interpret probability; the frequentist view (randomness) and the subjective view (Bayesian). The Probability A of occurrence of a specific risk event reflects the fraction of times the event A is likely to occur if the situation is repeated infinite number of times (as a frequency), or as an expression of uncertainty that reflects the "degree of belief" of the assigner, based on his/her knowledge and assumptions (subjective view). Subjective probabilities that are based on expert judgement are utilized during RA, which demonstrate "degree of belief" about an uncertain issue based on personal experience and values (Aven, 2017). These judgments are conditional on a specific background knowledge, which covers data, information, and justified beliefs often formulated as assumptions. If subjective probabilities are used to express the uncertainties, the knowledge that supports the probabilities should also be reflected during the evaluation of RA results, thus, SoK (strength of knowledge) should also be considered while evaluating the model outputs (Aven, 2016). The knowledge and assumptions during RA which are usually "hidden" in numbers should be revealed so that a meaningful interpretation can be done to evaluate probabilistic findings. In the past, the subjective view was more applicable to construction projects as there was usually not enough data on previous projects to estimate frequencies. As more and more data is becoming quickly available with the quick digitization of the industry, the frequentist view becomes more prominent as well. To analyze frequentist risk information other factors become more prominent, such as the quality and quantity of the data the probabilistic risk information was extracted from. Equally important during the analysis are information about biases and generality of the collected data.

Gigerenzer (1991) argues that inability to understand statistical information is not a mental deficiency but also due to poor presentation of probabilistic information. "Correct probabilistic reasoning" may not be possible due to conceptual differences (rather than cognitive illusions). His theory on "probabilistic mental models" suggests that decision-makers first construct a mental model to arrive at a reasonable guess that consists of a "reference class" and probability cues (learned frequencies of co-occurrences). The difficulty of understanding probabilistic risk information may stem from lack of understanding of mental models leading to ambiguity about the context. Anjum and Rocca (2019) argue that how to understand probability is a controversial issue in philosophy, as well as in the risk field. Local context is important when interpreting probability and we make predictions about the future. The local context or "risk picture" depends on experience, knowledge, imagination and assumptions of the person/group of people who are trying to explore what may happen in the future due to uncertainties (Dikmen and Birgonul, 2018; Dikmen et al., 2018). In this study, we call the complex network of risk sources and events, consequences and background information as the "risk picture" and argue that decision-makers can make sense of the outputs of risk assessment considering this risk picture. Thus, we not only search for ways to simplify probabilistic results of MCS but also aim to visualize the risk picture.

2.2 Monte Carlo Simulation

Taroun (2014) stresses that Monte Carlo Simulation (MSC) has been the most frequently used RA method starting from 1970s and still continues to dominate risk assessment practices despite its difficulties. When MSC is used, the variability of the parameter under question (such as return of return, time and cost) is demonstrated by a probability distribution derived from the quantitative risk model. To develop the risk model, risk analysts determine the input variables, interrelate them with output variables, assign probability distributions to introduce uncertainty/variability to input variables and also define correlations (covariance) if variables are affected from the same risk sources. Then, using the random number generator, alternative scenarios are generated (usually thousands of iterations) and results are presented as probability distribution of the output, which approximates to Normal Distribution due to Central Limit Theorem. Statistical findings such as mean, median, variance, interquartile range are tabulated. At the moment, the software used for Monte Carlo Simulation (such as @RISK) produces several graphs such as histograms, cumulative curves, sensitivity tornado charts, scatter plots, box plots, overlays and trend graphs to demonstrate the level of uncertainty, expected values and contributions of risk factors (or risk-prone variables) to the variability of the output parameter. However, information depicted in various formats such as probability distribution charts, tornado graphs and statistical data tables makes it difficult for decision-makers to interpret MCS results (Naderpour, 2019). In this research, we question whether these outputs provide relevant information for decision-makers so that they create a shared meaning about the risk picture of the project. It is hypothesized that visual methods and aids can be developed to better communicate probabilistic outputs of MSC.

2.3 Visualization

Visuals are cognitively advantageous compared to representation of information in text or tabular formats leading to effective reduction of cognitive load. Van der Hoorn (2020) mentions that although there are various studies on the positive impact of visualization on cognitive load, there are limited studies on how visuals can affect sense-making. Moreover, Henike et al. (2019) investigate whether visualization can create response and attention framing bias and found that visuals may even affect managerial cognition in a negative way depending on cognitive load sources and cognitive impacts. Cognitive fit theory explains that when there is a match between the type of information presented by the system and required by the task, users' cognitive processes are augmented by the available information. Luo (2019) conducted a study to understand the effect of information presentation format on task performance (considering task type, complexity and domain) and argued that external representations of information (by graphs, maps, tables etc.) and internal mental models work together in a complementary fashion to solve problems. In our study, the requirements of the task (particularly, risk assessment), risk information (probabilistic as well as subjective risk input data) and performance of alternative visuals will be explored based on the cognitive fit theory and referring to various studies that depict performance criteria (such as interactive, purposeful, truthful, efficient, aesthetically pleasant etc.) for mindful use of visuals (such as Geraldi and Arlt, 2015)

Probabilities are usually visualized in grids, quantiles with dot plot representation, boxplots, violin plots, strip charts which actually are all about "frequencies". To foster probabilistic thinking, sometimes, alternative scenarios regarding risk events are shown by tree diagrams and stacked bar charts. Spiegelhalter et al. (2011) argue that first, it has to be decided why visualization is used to convey probabilistic information by understanding user needs. Some of the recommendations regarding visualization of probabilities include utilization of multiple formats, designing graphs to allow part-to-whole comparisons with an appropriate scale, ensuring interactivity and animations for increased adaptability of graphics to user needs (Spiegelhalter et al., 2011).

3. Research Objectives and Methodology

Based on the above theories, the research objective in our planned exploratory study is to develop visualization formats and methods to simplify complex probabilistic models and risk pictures for the decision-makers. Our research questions are:

- How can we best describe and represent results of probabilistic risk assessment, mainly Monte Carlo Simulation in a way that help decision-makers to make sense of risk in a project?
- What kind of visualizations can be used for decision-makers to understand the entire risk picture?

The key questions about risk visualization in this study are depicted in Figure 1.

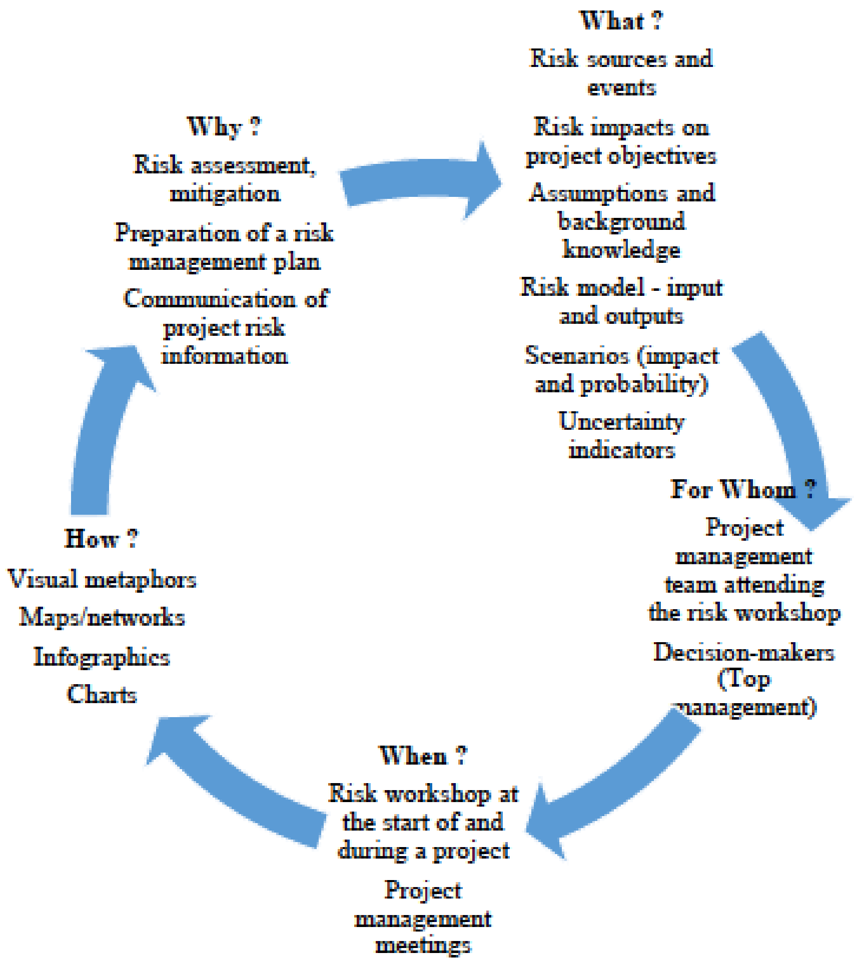

Figure 1: Key questions about risk visualization

The research will follow three phases: needs analysis – elicitation of requirements; development of methods and formats for better visualization of risk information and testing of visuals. It will be conducted by eliciting expert knowledge through workshops. Initially, several risk management plans will be investigated to understand the risk information and outputs of Monte Carlo Simulation usually presented in these documents. Then, a workshop will be conducted with domain experts to understand benefits and shortcomings of the current format of risk management reports as well as their expectations. In this paper, we present some of the initial findings based on evaluation of a risk report prepared for a mega project carried out in Turkey.

4. Initial Observations from the Case Project

The case project is a mega tunneling project carried out in Turkey. It is abbreviated as ISRC project and name is withheld due to confidentiality reasons. It had an investment cost of 1.1 billion USD. It was a BOT project where the JV was responsible for construction, operation and maintenance of the facility for around 25 years. The ISRC project covered construction of tunnels, cut and cover structures as well as roads. For the tunneling part of the project, where the tunnels are 3340 m long and have 13.2 m diameter, a risk plan/report was prepared by an international consultancy company. The report includes a risk checklist/register produced as a result of a risk workshop conducted with company experts and outputs of Monte Carlo Simulation carried out to assess schedule risks in the tunneling part of the project. The expected duration of the tunneling part of ISRC was 49 months (risk-free estimate). "Reasonable assessment of the JV's risk exposure" was conducted by the Consultant with the objective "to assist the JV in a more informed decision making process".

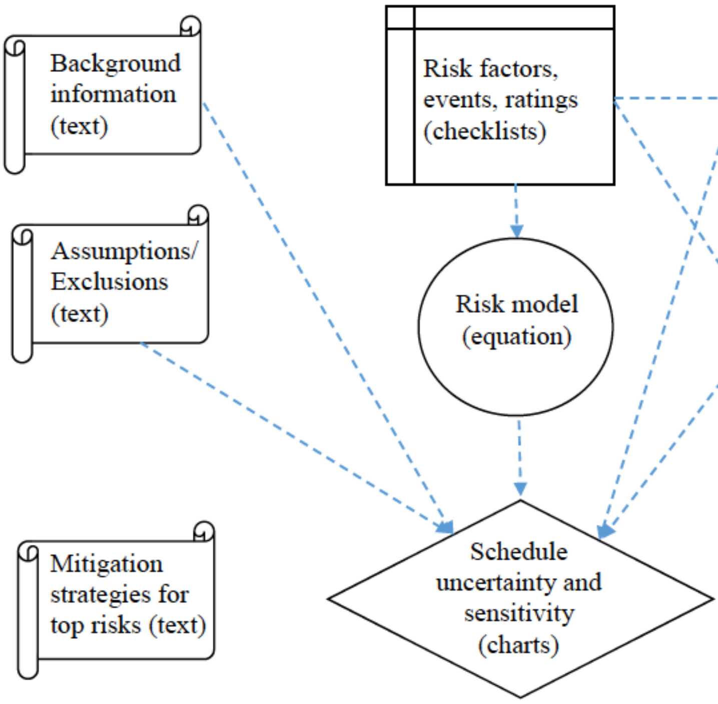

Figure 2: Risk-related information clusters (Note : The dashed lines indicate a missing link between information clusters)

First, a qualitative risk assessment was conducted using P-I ratings (on a scale of 1-3), then risks were prioritized and mitigation strategies were formulated for the significant risk events. The JV requested the consultant to quantify the impact of risks on project duration. Schedule risk analysis was performed using Primavera Risk Analysis to answer the following questions:

- What is the likelihood of JV achieving their planned construction duration (49 months as risk-free duration) and tender schedule (55 months)?
- What are the parameters, activities and risk events that schedule is most sensitive to?

The risk register includes 84 risk factors/events that may have an impact on cost and/or schedule of the project. High probability and high impact risks cover unrepairable/serious damage to TBM cutterhead and late delivery of TBM affecting advance rate whereas some low probability-high impact risks are earthquake induced liquefaction during construction and environmental constraints. In addition to the risk register given in a tabular format, there are other risk-related information given in different formats. Figure 2 summarizes the risk-related information depicted in the report, which may provide the basis of the "risk picture" for our detailed empirical study.

Although the report involves various pieces of information in different formats, the probability distribution chart and sensitivity chart are hard to interpret as how different risk-related information are combined to determine probability distributions is vague. The dashed lines in Figure 2 represent the missing links between information clusters. A statistics table presenting standard deviation, quartiles etc. that is usually presented in these kind of reports is not given.

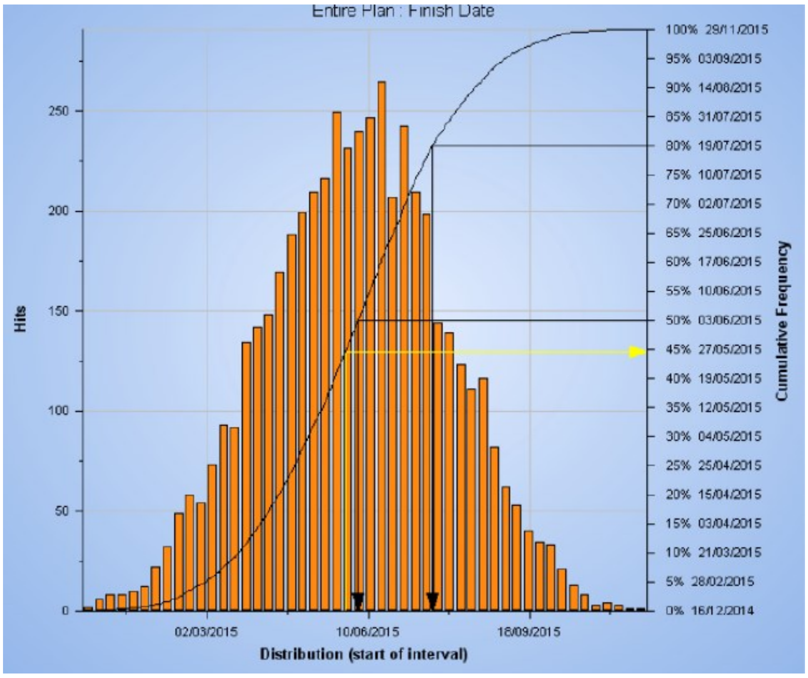

Figure 3: Probability distribution of schedule (completion dates)

Figure 3 presents the probability distribution of project duration when uncertainties in activity durations due to risk factors are considered as well as discrete risk events. The major finding given in the risk report is;

"When discrete risk events identified by the project team are taken into consideration along with the general uncertainty surrounding key construction activity durations, the confidence level in completing the project within 55 months is 90%. There appears to be a 50% confidence level that the project could be completed within 51 months"

The confidence level of 90% implies that in 90% of the scenarios generated during simulation by random sampling, the duration was calculated below 55 months, thus it reflects probability. Actually, this probability is purely epistemic-based expression of uncertainty estimated by considering variability of activity durations due to risk factors. The risk analyst is highly confident that the project will be completed in less than 55 months. A very common misunderstanding about probability is that decision-makers sometimes conceive 90% as an objective/frequentist value based on statistical information on previous projects and assume that 90% of similar projects (tunnel projects subjected to same risk factors) were completed in 55 months. Moreover, 90% does not indicate anything about the level of uncertainty or variability of project duration which could be evaluated by statistical indicators such as standard deviation and coefficient of variation, if presented in the report. Figure 3 shows the frequency of project durations calculated as a result of random sampling from individual probability distributions and its shape/steepness gives an indication of uncertainty of duration. However, the level of uncertainty is hard to interpret by the user if he/she is not knowledgeable about variation indicators such as standard variation and coefficient of variation.

In addition to the difficulties in the interpretation of probability and variability, decision-makers may experience difficulties in understanding how the risks and assumptions are related with this output. The probability distribution and probabilities associated with different project completion dates could be interpreted better if the links identified in Figure 2 were known by the user. While evaluating the MCS output, the decision-maker must consider that;

1. Some of the risks identified in the risk checklist are not taken into account (Assumptions: Financial, administrative, contractual risks are not taken into account, catastrophic events are not included, approvals from the client are assumed to be obtained in a timely manner, design will not change and also actual geological conditions will be the same as given in the geological report). Assumptions/background information that resulted in this probability distribution are not visible from this figure.
2. Risks are propagated into the schedule through project activities, which are assigned most likely, pessimistic and optimistic durations (triangular probability distributions) and discrete recent events (uniform probability distributions) based on subjective judgements of the risk analysts. However, how the risk factors in the risk checklist are interrelated with variability of activity durations is not clear. Thus, which risk factors are considered during probabilistic assessment is rather vague.
3. Probabilities can change significantly if probabilities assigned to activities and events are changed and correlations are defined between the parameters (if their probability of occurrence is interrelated). Several scenarios can be created considering implementation of alternative mitigation strategies, relaxing some assumptions and defining correlations. The probability distribution chart should not be treated as if it depicts the future with 100% reliability as alternative scenarios are also possible. For example, if the black swans (extreme events such as an earthquake etc.) were included into the analysis, there would be a "tail" in the distribution towards right.
4. Although sensitivity results are presented (most sensitive parameter is found as advance rate of TBM) it is difficult for a user to understand how the results may change if probability distribution for advance rate is changed. Results may also change when multiple risk factors/parameters are considered simultaneously.

It is evident that potential problems in understanding the level of risk and improvements should be explored by user studies. The initial analysis of the risk report from the case project gives some initial ideas what can be done to facilitate understanding of the risk picture. It is hypothesized that users may need to see the links between different pieces of information and outputs. Interactive visualizations are necessary to experiment with inputs of the risk model (risks, variables, assumptions, probability distributions etc.) to monitor impacts on project objectives. Interactivity and animations may provide opportunities for adapting to user needs. Better visuals that demonstrate model outputs considering both quartiles (probabilities or confidence levels) and level of uncertainty (deviations or confidence ranges) in an easy to understand format can help decision-makers who do not have necessary statistics background. If users want to associate risks with spatial and geographical information, GIS, 3D and 4D visualizations could provide further reference information to help risk managers to grasp the entire risk picture. As suggested by Spiegelhalter et al. (2011), multiple formats should be tried because no single representation can suit the needs of all users.

5. Conclusions

Effective communication of probabilistic risk information by using visuals has a potential to assist decision-makers while making sense of project risk. Visuals can be designed to portray the risk picture of the project and simulate project outcomes under different scenarios. Preliminary investigation of a risk report prepared for a tunnel project carried out in Turkey shows that various pieces of information are given in different formats (text, tables and graphics) and makes it difficult for the user to understand how the probability distribution curves are drawn and quartile values are calculated. It may be difficult for users to interpret the meaning of probabilities and other uncertainty indicators such as variation and sensitivities. In the forthcoming parts of this study, user studies will be carried out to understand what, why, for whom, when and how risk information should be visualized during risk assessment of construction projects.

In summary, the paper introduces the basic ideas behind an on-going research project about visualization of probabilistic risk information together with its research background and design. Some initial thoughts about problems that could be experienced by users while evaluating Monte Carlo Simulation results are shared. In the further steps of the project, user studies will be conducted to assess visualization needs and alternative formats (including metaphors such as roulette wheels, infographics etc.) will be developed to represent the project risk picture as well as probabilistic findings of RA.

References

Anjum, R.L and Rocca, E. (2019). From Ideal to Real Risk: Philosophy of Causation Meets Risk Analysis, Risk Analysis, 39(3), pp. 729–740.

Aven, T. (2016). Risk assessment and risk management: Review of recent advances on their foundation, European Journal of Operational Research, 253(1), pp.1–13.

Aven, T. (2017). Improving risk characterizations in practical situations by highlighting knowledge aspects, with applications to risk matrices, Reliability Engineering and System Safety, 167, pp.42–48.

Bostrom, A. and ,Lofstedt, R.E. (2003).Communicating Risk: Wireless and Hardwired,Risk Analysis, 23(2), pp. 241–248.

Dikmen, I. and Birgonul, M.T. (2018). Assumption-based Thinking for Risk Assessment. In: 16th Engineering Project Organisation Conference, 2018, Brijuni, Crotia, pp. 805–816.

Dikmen, I., Yildiz, E., Eken, G. and Ozbakan, T. (2018). An Experimental Study on Impact of Risk Data Visualization on Risk Evaluations. In: 5th International Project and Construction Management Conference (IPCMC 2018), Northern Cyprus, pp. 1419–1427.

Dikmen, I., Budayan, C., Hayat, E. and Birgonul, M.T. (2018). Effects of Risk Attitude and Controllability Assumption on Risk Ratings: An Experimental Study about International Construction Projects. ASCE Management in Engineering, 34(6), 04018037.

Eppler, M.J. and Aeschimann, M. (2009). A systematic framework for risk visualization in risk management and communication. Risk Management Journal, 11, pp. 67–89.

Geraldi J.G., and Arlt,M. (2015). Visuals matter! Designing and Using Effective Visual Representations to Support Project and Portfolio Decisions. Pennsylvania: Project Management Institute, Inc, Newtown Square.

Gigerenzer, G. (1991). How to Make Cognitive Illusions Disappear: Beyond "Heuristics and Biases". European Review of Social Psychology, 2(1), pp. 83–115.

Henike, T., Kamprath, M. and Hölzle,K. Effecting, but effective? How business model visualisations unfold cognitive impacts. Long Range Planning, https://doi.org/10.1016/j.lrp.2019.101925

Luo, W. (2019). User choice of interactive data visualization format: The effects of cognitive style and spatial ability. Decision Support Systems, 122, 113061.

Qazi, A. and Dikmen, I. (2019). From Risk Matrices to Risk Networks in Construction Projects. IEEE Transactions on Engineering Management, DOI: 10.1109/TEM.2019.2907787

Senesi, C., Javernick-Will, A. and Molenaar, K.R. (2015). Benefits and Barriers to Applying Probabilistic Risk Analysis on Engineering and Construction Projects. Engineering Management Journal, 27(2), pp. 49–57.

Rickard, L. N. (2019). Pragmatic and (or) Constitutive? On the Foundations of Contemporary Risk Communication Research. Risk Analysis (early access), https://doi.org/10.1111/risa.13415

Spiegelhalter, D., Pearson, M. and Short, I. (2011). Visualizing Uncertainty About Future", Science, 333(6048),1393-1400.

SRA (2015). SRA glossary. http://www.sra.org/sites/default/files/pdf/SRA_glossary_20150622.pdf.

Taroun, A. (2014). Towards a better modelling and assessment of construction risk: Insights from a literature review. International Journal of Project Management, 32, pp.101–115.

Willumsen, P, Oehmen, J., Stingl, V. and Geraldi, J. (2019). Value creation through project risk management. International Journal of Project Management, 37(5), pp.731–749.

Zio, E. (2018). The Future of Risk Assessment, Reliability Engineering and System Safety, 177, pp. 176–190.

An approach to process geometric and semantic information as open graph-based description using a microservice architecture on the example of structural data

Tim-Jonathan Huyeng[1], Christian-Dominik Thiele[1], Anna Wagner[1], Meiling Shi[1], André Hoffmann[1], Wendelin Sprenger[2], Uwe Rüppel[1]
[1]Institut für Numerische Methoden und Informatik im Bauwesen, Technische Universität, Darmstadt, Germany
[2]Zentrale Technik, Direktion Digitalisierung und Software-Engineering (DS)-BIM.5D,
Ed. Züblin AG, Stuttgart, Germany
huyeng@iib.tu-darmstadt.de – orcid.org/0000-0003-2347-2388

Abstract. The advancing digitalization in the building industry highlights weak points in the digital infrastructure. Due to heterogeneous software landscapes, cross-application data exchange, in particular, is a frequently criticized process for which no satisfying solution exists, so far. To overcome interoperability difficulties, open and application-independent data formats are necessary and the communication between software applications needs to be standardized. For the first aspect, the current research project SCOPE investigates the extent to which Semantic Web can be used as an alternative to conventional approaches. The ontologies developed and applied in the research project focus on geometry descriptions, the linking of geometric and non-geometric contents and the abstract description of building products. The second, overarching aspect is addressed by defining an underlying architecture. Hence, a microservice structure is proposed that allows the data to be extended and enriched with the help of the aforementioned ontologies.

1. Introduction

In the AEC industry, heterogeneous data sets resulting from different requirements are a challenge for interoperability and consistency of data management (Borrmann et al., 2018a). This is partly due to the fact that independent participants from different disciplines work together and also to the heterogeneous software solutions used in this field. There is currently no open, expandable and flexible data schema for this problem (Terkaj & Pauwels, 2017). To use and benefit of such a data schema, a software architecture is required, which allows to connect the heterogeneous software landscape.

The process of extracting geometric and semantic information and the preprocessing as well as the storing of these data is included in the overall approach of the research project SCOPE (SCOPE, 2018). The project proposes an approach to structure and store data in an openly described format for building processes. For this, the Semantic Web and its features are used to create graph-based building data. The SCOPE project is researching a software-independent, loss-free project data environment and a federal self-describing parametric modelling of multifunctional building products based on the Semantic Web with a focus on the building envelope.

This paper proposes a semantic web-based approach as a data schema, which differs from conventional Big Open BIM approaches that apply the Industry Foundation Classes (IFC) for data storage. The underlined data schema of SCOPE is based on ontologies which can be expanded individually. To interconnect different stakeholders and the heterogeneous software, we propose a microservice architecture based on core services. With microservices, which are defined as small processes that communicate with other services via HTTPS or a REST API (Dragoni et al., 2017), large software applications can be broken down into several smaller software applications that can be combined and reused independently. These smaller applications can be applied flexibly, replaced or organized as containers.

2. Related Work

To overcome the heterogeneous requirements and software landscapes, buildingSmart proposed the IFC. In this schema, it is possible to describe semantic and geometric information for the building industry (Borrmann et al., 2018a). Also, an official standard, the ifcOWL, serializes the IFC data schema graph-based. To use the IFC in a collaborative manner, the BIMServer was developed which is storing the information in a database according to the IFC-schema (Beetz et al., 2010).

In the field of microservice architecture in connection with product data and the building industry, different approaches exist, such as Speckle, BIMSWARM (planen-bauen 4.0, 2018) and the related research project *SolConPro* (SolConPro, 2015), which are briefly explained and delimited in the following.

Speckle, which is being developed as a modular platform, focuses, in addition to document and user management, on the connection of different platforms, so-called streams, which includes the extraction of data from authoring software (currently Autodesk Revit, Rhino, Grasshopper and Dynamo). For this purpose, a novel data format was developed in JSON schema and is based on object-oriented programming. The Speckle server can be extended by plugins and provides a REST API for communication. These plugins are addressed by the clients, such as web applications, CAD applications and automation scripts (Stefanescu, 2015).

To create standardized interfaces and open platforms, the BIMSWARM research project is developing a platform that provides certified tools and services (such as the evaluation, testing and visualization of building models). The API is based on open BIM standards (planen-bauen 4.0, 2018).

The research project SolConPro looked into data descriptions based on Semantic Web Technologies and a distributed product catalog. SolConPro focused mainly on solar construction processes and the integration of those into the buildings and products design and planning phases (Wagner et al., 2018).

3. Analysis

The established formats, in particular IFC, which is supported by over 250 software applications (buildingSMART, 2020), attempt to cover as many use cases occurring in the construction industry, such as building construction, civil engineering or infrastructures, simultaneously. The resulting complex data format leads to lengthy software licensing and rigid specifications (Borrmann et al., 2018a; Steinmann, 2018). To integrate novel, not yet described products, planners have to create their own, unspecified objects, e.g., by using IfcBuildingElementProxys or IfcPropertySets, which may not be interpreted or evaluated correctly by other authoring systems. Especially for multi-functional (facade) elements, hierarchically described product and project data are not suitable due to the lacking support for multi-inheritance (Wagner et al., 2018).

To exchange only required data for a certain use case from a complete model, it is possible to apply Model View Definitions (MVDs) onto IFC. With MVDs, a specific set of entities, attributes and properties are defined and subsequently extracted during data export. Therefore, redundant data based on different MVDs may be stored (buildingSMART, 2020).

Since the ifcOWL is an exact RDF serialization of the IFC schema, the restrictions and advantages of the IFC are valid for the ifcOWL, as well. Nonetheless, the ifcOWL can, due to its applied technologies, be extended more flexibly than the IFC schema itself. Yet, the translation does not simplify the objectified relations of IFC and thereby results in a rather verbose and over-complicated ontology for which several simplifications have been suggested (de Farias, Roxin, & Nicolle, 2015; Pauwels & Roxin, 2016).

Novel data platforms like Speckle and BIMSWARM are showing that a microservice architecture is a feasible concept. Still, these systems are not using graph-based data schemes and, therefore, a novel service architecture needs to be developed.

Currently, open standardizations for merging and exchanging data in the AEC sector are available but lack flexible, comprehensive and expandable schemes. In this context, research is experiencing a trend towards Linked Building Data to create open and flexible data schemes (Pauwels, Zhang, & Lee, 2017). Subsequently, the research presented in this paper is based on open graph-based building data and a microservice architecture to overcome the heterogeneous information and software landscapes in AEC.

4. Methodology

Based on the findings of the analysis, this paper proposes a methodology that is based on two elements, which are elaborated in more detail: Linked Data, graph-based building data and microservices to integrate software applications.

4.1 Data Structure

To comply with the best practices to publish Linked Data on the Web (Villazón-Terrazas et al., 2011), the data should be structured by applying several, concise ontologies for individual use cases. Hence, users can decide flexibly which data schemes are required for their use cases. Furthermore, core schemes should be utilized to harmonize the heterogeneous configurations of different use cases and stakeholders. As schemes exist for individual domains as well as core structures, no novel ontologies are introduced in this paper, much more a composition of several ontologies is proposed.

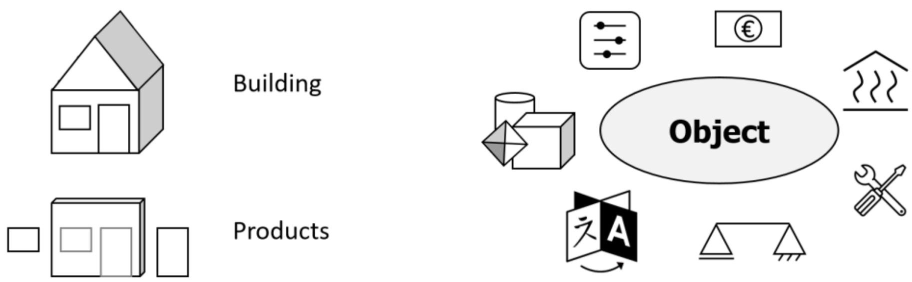

Figure 1: Differentiation between buildings and products (left) and perspectives for objects (right)

First, a differentiation between building and product level is considered, as visualized in Fig. 1, left. For building level data, the Building Topology Ontology (BOT, Rasmussen & Pauwels, 2019) is applied as core schema, whereas the product level relies on the Building Product Ontology (BPO, Wagner & Rüppel, 2019) for this purpose. Subsequently, a connection between BOT and BPO individuals needs to be realized.

Second, the different perspectives for objects should be distinguished. To minimize schema overhead and complexity while maintaining modularity, multiple, concise, domain-specific ontologies should be applied to the core structure of BOT and BPO. Thereby, each stakeholder may select their required configuration of data structures flexibly.

4.2 System architecture

The exchange of information between a wide landscape of software applications is an elementary component in the conventional construction and building process and also a major source of errors. To overcome this, a common openly accessible database is needed. The presented approach is proposing a triplestore as a common data storage. The idea is to describe the data as detailed as possible and provide access to it via one interface.

This also enables the connection of further software systems. The relevant services can extract the data required for their application from the graph or add results to it. In order to be able to access the data across services, a microservice architecture was developed (Fig. 2). As an overarching framework for the included microservices, the SCOPE Data Service offers the potential to add dedicated services for the respective actors involved in the life cycle of a building. Hence, this allows actors to individually extend and adapt the functionalities of the SCOPE Data Service (SCOPE, 2019).

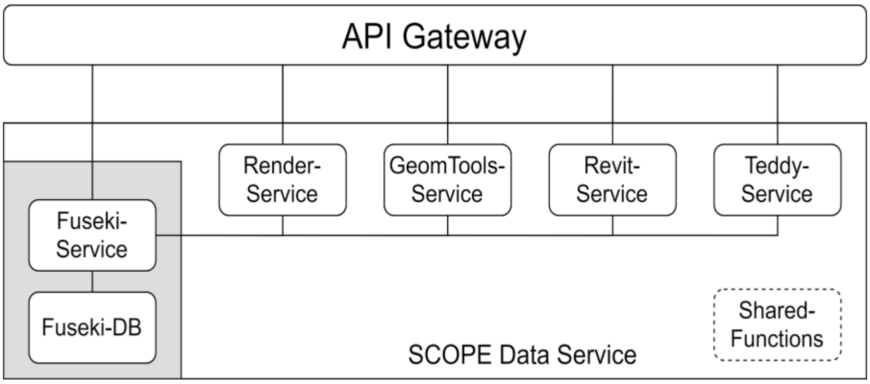

Figure 2: Example implementing the proposed microservice system architecture of SCOPE

An API gateway provides the entry point into the microservice structure, which is implemented via the administration tool *Kong* (Kong Inc., 2020). *Kong* is based on NGINX and serves as a reverse proxy server for the system. Communication between the services can be realized via HTTP(S) requests or further protocols and can be protected with *Kong* plugins like *Key Authentication* against external and unauthorized accesses.

Currently, each service runs in its own docker container. This allows adding new services easily in separate docker containers into the system. To set up the system a *docker-compose* file as well as a *make* script is recommended, which can deploy, start, stop and log all services combined. To ensure, that the service containers can communicate properly with each other, the containers are deployed in the same docker network. Within this network, the containers are accessible for other containers by their corresponding tag and port. The core services of the SCOPE Data Service are the Fuseki-Service as well as the Fuseki-DB. The Fuseki-Service is a microservice dedicated to manage communication with the corresponding triplestore (Fuseki-DB) that contains the product or project data. The data contained in the triplestore can be accessed via the connected Fuseki-Service, only, by using SPARQL queries. The Fuseki-Service, as a middleware, is able to check the user access rights as well as the query before routing this to the corresponding SPARQL-Endpoint of the Fuseki-DB.

5. Application

The suggested methodology of SCOPE is applied to the use case of structural engineering. For this purpose, an example scenario is considered, where a building model is created within an authoring tool, i.e., Autodesk Revit, which is uploaded to a server instance of the SCOPE Data Service. Within the instance, the data is structured graph-based. Subsequently, structural engineers can extract relevant information for their use cases that is pre-processed in accordance to the applied software application, i.e., SOFiSTiK. Following, the scenario will be discussed from the data perspective first, before elaborating on the implementation of the individual microservices.

5.1 Example Data

To give an expressive example on how data is structured in the proposed approach, the configuration for architectural and structural information is demonstrated on the example of a ground slab. For this configuration, several domains, aside the core structure, are needed.

Before elaborating on the applied modules, a connection between BOT elements and BPO products needs to be implemented. Thus, the presented approach suggests to model individual elements as BOT element, whereas their types and families are defined as BPO products. BPO products hold all properties and characteristics that are generally true for any individual of it, while the BOT elements may override deviating properties or have novel properties attached to them. The connection is realized with Schema.org's *model* property to indicate a relation between product models and individual products.

First, a taxonomy is required to define the types of the elements. Due to a lack of a full Linked Data taxonomy in AEC, the buildingSMART Data Dictionary is applied, as proposed in (Wagner & Rüppel, 2019). Another central component of building models is the geometry description. In contrast to common modelling approaches, the geometry does not serve as a core structure that is enhanced with non-geometric data. Instead, the Ontology for Managing Geometry (Wagner et al., 2019) and File Ontology for Geometry formats (Bonduel et al., 2019) are used to connect geometry descriptions to the non-geometric core structures. Hence, it is possible to exchange geometry descriptions or add multiple descriptions for different use cases while maintaining data integrity (Wagner et al., 2020).

The resulting data structure can be seen in Fig. 3. The slab is placed as BOT element within a BOT space and connected to a slab product, which is classified via the bSDD. The geometry description of the slab is attached to the BOT element, since slabs have individual geometries.

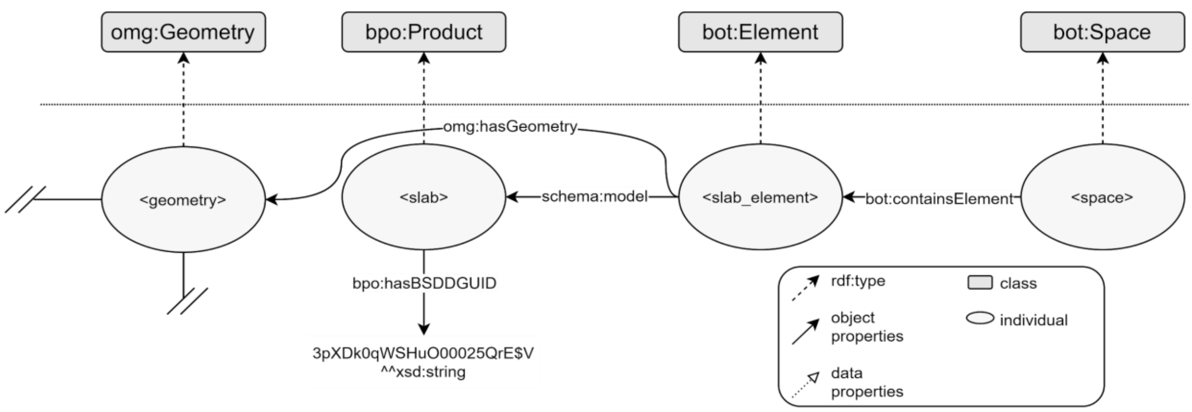

Figure 3: Core structure of the proposed approach using BPO and BOT

Next, a uniform data schema is necessary for the geometric description of objects. Proprietary authoring systems usually use a proprietary or adapted geometry kernel for the evaluation and creation of geometries which create geometrical objects based on mathematical functions (Borrmann et al., 2018b). To ensure application-independent geometry descriptions, the geometry kernel openCASCADE has been chosen for the description in the graph. This kernel is open source, therefore the methods and structure are openly described and can be interpreted outside of modelling tools. The geometric functions and operators of the kernel's Python library, PythonOCC (Paviot, 2017), are mapped in the developed Ontology for OpenCASCADE (OCC, Nothstein, Christian & Sprenger, Wendelin, 2019a). With the mapped kernel functions on the one hand, and the Ontology for Object-Oriented Programming (OOP, Nothstein, Christian & Sprenger, Wendelin, 2019b) to translate object-oriented source code into RDF on the other hand, Python code to create openCASCADE geometries can be translated into a Semantic Web context (see Listing 1). Hence, basic as well as complex geometry objects can be described in an RDF graph, according to the openCASCADE kernel functions.

For the example slab, Fig. 4 shows the geometry description according to the OCC and OOP ontology. The example slab geometry consists of one box (cube), only. This box is described by parameters which are represented in the form of an ordered list using the OOP. A method of the geometry description is the shape that is attached to the geometrical object via the OOP.

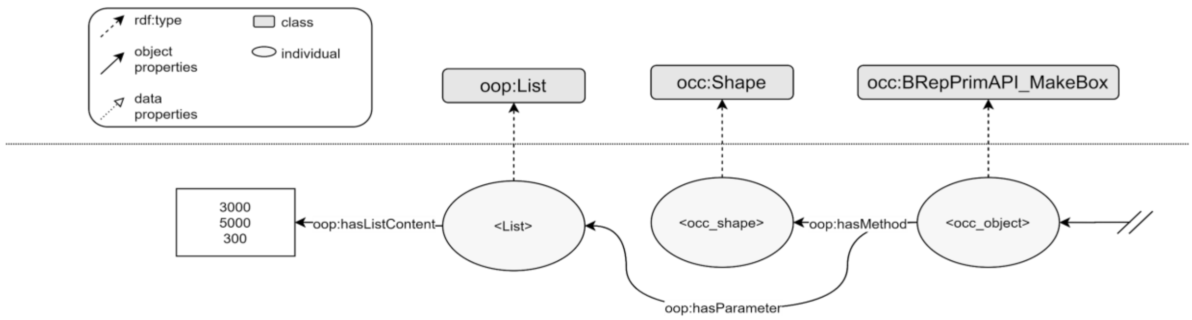

Figure 4: Detailed description of the OCC geometric representation

Listing 1: Geometric representation of the ground slab in Python with PythonOCC

```
occ_object = BRepPrimAPI_MakeBox(3000, 5000, 300).Shape()
```

With this detailed description of each step of an object's geometry creation, it is possible to observe or change individual stages afterwards. However, this also means that all steps for extracting the finished geometry from the graph must be carried out each time. To reduce the computational effort, a pickle serialization is integrated as additional geometry description, as suggested by the OMG/FOG approach.

The pickle serialization (connected in the graph via fog:asOccPickle) is used to increase the speed of queries of complex geometry objects (see Fig. 5). Therefore, a Python object is created by translating and executing the Python code from the graph-based OCC geometry description to be serialized as a pickle object and attached to the graph. Subsequently, queries of the geometry can be conducted on the pickle objects.

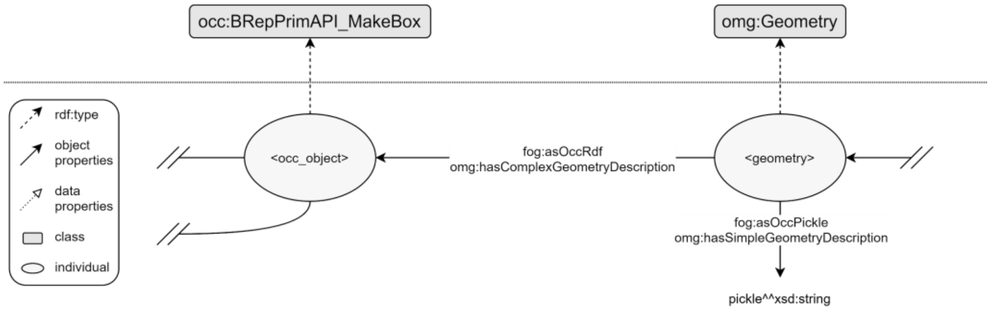

Figure 5: Structure of different geometric description of the example slab

Apart of geometry description, the example scenario requires structural information of the elements that is required by the structural engineer. Therefore, the Teddy Ontology (TDY, Thiele & Huyeng, 2020) is applied. As shown in Fig. 6, the relevant properties, such as the concrete strength and applied standard for the calculation are attached to the BPO product, as they are valid for any slabs that are of the same type. In contrast to that, the continuous elastic support is attached to the BOT element, as this may vary for individual slabs of the building.

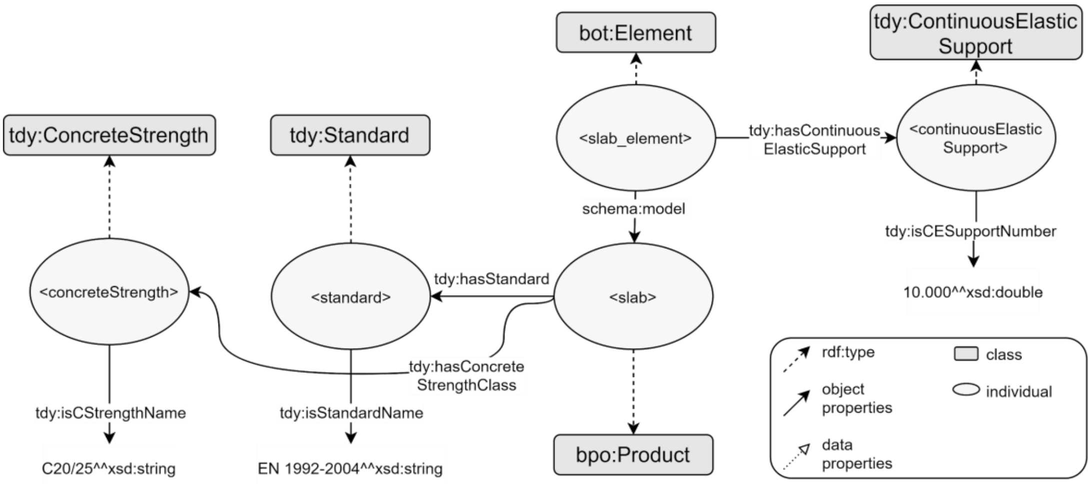

Figure 6: Example-slab using the teddy ontology for structural analysis

5.2 Microservice implementation

For the considered example use case, several microservices are applied. First, the building model is extracted from Revit via the Revit-Service. Moreover, essential functionalities like visualization via the Render-Service and such functionalities that are re-used by several services are extracted into specified services, such as the GeomTools-Service. Finally, the Teddy-Service is used to import the relevant structural data into SOFiSTiK.

In detail, the **Revit-Service** is developed which extracts the semantic and geometric description from the information of the authoring system and transfers it into the described open schema. The data from Revit is transferred to the service via HTTP(S) using a developed Revit plugin. This service disassembles the components and forms objects based on the given geometries according to the OCC ontology. The semantic information is currently stored in a graph on the same triplestore. Currently, the Revit-Service is only implemented for components of the shell form and can only export data into the graph, not vice versa.

For the visualization of the geometric and semantic data, a simple web interface is created - the **Render-Service** - which can be part of the service architecture if the user wishes so (see Fig. 7). The web interface displays the geometric data via WebGL. Besides the geometric representation, the corresponding graph can be displayed. In this case, the Render-Service is used for visualization as well as to increase the understanding of the method of data storage. The service also allows SPARQL queries to be executed. As an additional function, semantic attributes can be added to the geometric objects and, hence, attached to the graph, as well.

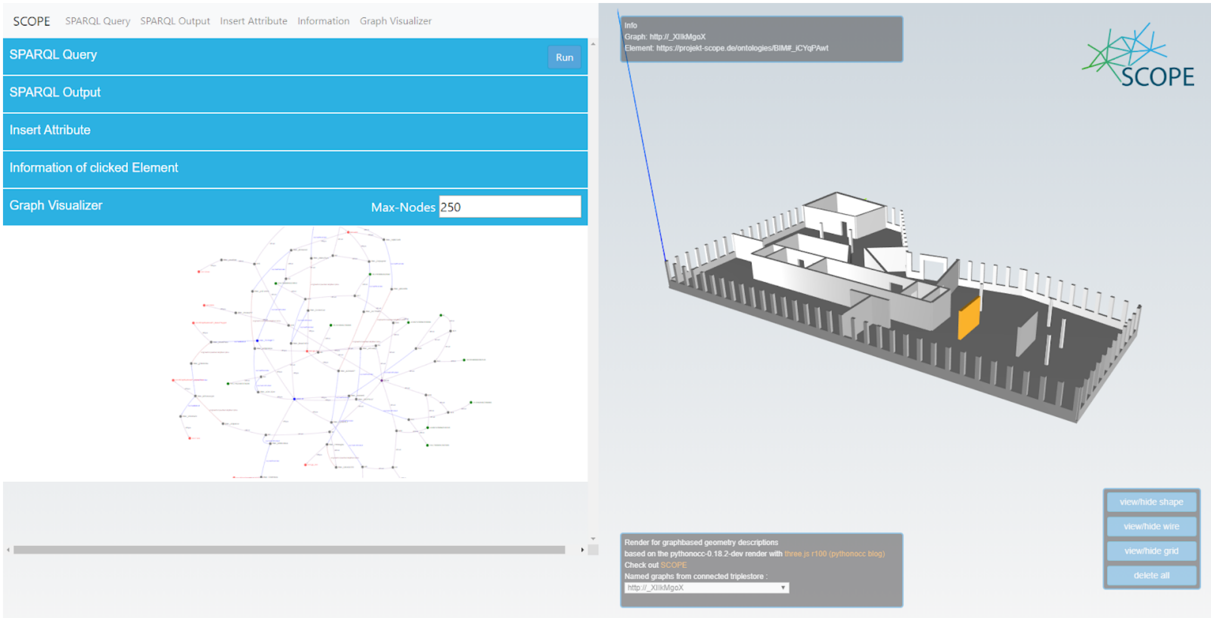

Figure 7: Render-Service shows geometric representation of a storey (right) and graph-based information (left)

As mentioned, the pickle serialization can be used to serialize complex geometric information in Python objects. To provide this functionality to all users, the **GeomTools-Service** is introduced. Besides the pickle serialization the service implements other geometry processing functions like the creation of bounding boxes. Similarly, the **Shared-Functions** microservice provides programming functions in Python and features that can be used across all services.

A structural engineer can, by means of the **Teddy-Service**, use relevant geometry descriptions and information for structural design that are both part of the graph. The service interprets the graph-based data and generates the input file for the calculation in SOFiSTiK. Based on the Teddy Ontology the relevant data for this specific, example sector of the building industry can be filtered from the graph.

6. Conclusion

The presented approach is demonstrated on the example use case and its functionalities are thereby verified. It is show that the data can be extracted from an authoring tool and subsequently filtered by microservices during the data processing. Hence, the proposed methodology shows advantages in comparison to the IFC and MVD method, where filtering takes places during data export. With the use of graph-based data schemes, it is possible to extend the configuration for graph-based building data considering individual domains that could be added in the future. Similarly, the microservice architecture allows users to include further services in regard of their applied software applications and use cases.

Regarding the Revit-Service, the service demonstrates that it is possible to extract structural data from Revit and store this data graph-based. However, for applications in the construction industry, the extraction of the entire model, synchronous collaboration, as well as the import of graph-based data is required.

Considering the data ownership, the microservice architecture supports both centralized and decentralized storage. On the one hand, the project information can be stored in a singular instance of the SCOPE Data Service, whereas a decentralized approach can be supported by dedicated microservices, see (Hoffmann et al., 2019), who propose a decentralized product catalog based on the presented microservice architecture.

The advantages of applying Linked Data, i.e., in the proposed graph-based building data, become more prominent with more applications, since more ontologies will be available and decentralized data storage more common. Furthermore, with a growing number of microservices and the application independently and exhaustively described data in triplestores, it will be possible to overcome the problems which are currently existing in the building industry related to data silos and proprietary software.

With the use of the graph-based data schemes and the microservice architecture it is possible to provide individual solution for the heterogeneous information and software landscape of the AEC domain. This stands in contrast of approaches that aim to address all use cases at once, e.g., the IFC. Subsequently, users can experience a well-tailored and less complex solution for their individual scenarios.

Acknowledgments

This work is part of the research project EnOB:SCOPE, founded by the German Federal Ministry for Economic Affairs and Energy (BMWi). The concepts of the ontology and the microservice were developed in collaboration with Fraunhofer Institute for Solar Energy Systems ISE and Ed. Züblin AG and implemented by the authors of this paper.

References

Beetz, J., van Berlo, L., R, L., Pim, H. (2010). Bimserver.org - an Open Source IFC model server. (https://www.researchgate.net/publication/254899282_Bimserverorg_-_an_Open_Source_IFC_model_server).

Bonduel, M., Wagner, A., Pauwels, P., Vergauwen, M., Klein, R. (2019). Including widespread geometry formats in semantic graphs using RDF literals. *2019 European Conference on Computing in Construction*. (https://research.tue.nl/en/publications/including-widespread-geometry-formats-in-semantic-graphs-using-rd, accessed May 2020).

Borrmann, A., Beetz, J., Koch, C., Liebich, T., Muhic, S. (2018a). Industry Foundation Classes: A Standardized Data Model for the Vendor-Neutral Exchange of Digital Building Models. In: Borrmann A, König M, Koch C, Beetz J, eds. *Building Information Modeling: Technology Foundations and Industry Practice*. Cham, Springer International Publishing,2018:81–126. (https://doi.org/10.1007/978-3-319-92862-3_5, accessed May 2020).

Borrmann, A., König, M., Koch, C., Beetz, J. (Eds.) (2018b). *Building Information Modeling: Technology Foundations and Industry Practice*. Cham, Springer International Publishing (http://link.springer.com/10.1007/978-3-319-92862-3, accessed February 2020).

buildingSMART (2020). Technical Resources website. Library Catalog: technical.buildingsmart.org (https://technical.buildingsmart.org/, accessed May 2020).

Dragoni, N., Giallorenzo, S., Lafuente, A.L., Mazzara, M., Montesi, F., Mustafin, R., Safina, L. (2017). Microservices: yesterday, today, and tomorrow. *arXiv:1606.04036 [cs]*. (http://arxiv.org/abs/1606.04036, accessed December 2019).

de Farias, T.M., Roxin, A., Nicolle, C. (2015). IfcWoD, Semantically Adapting IFC Model Relations into OWL Properties. *arXiv:1511.03897 [cs]*. (http://arxiv.org/abs/1511.03897, accessed May 2020).

Hoffmann, A., Wagner, A., Huyeng, T.-J., Shi, M., Wengzinek, J., Sprenger, W., Maurer, C., Rüppel, U. (2019). Distributed manufacturer services to provide product data on the web. *EG-ICE 2019 Workshop on Intelligent Computing in Engineering*. Leuven, Belgium.

Kong Inc. (2020). Kong: Next-Generation API platform for Microservices website. (https://konghq.com/, accessed February 2020).

Nothstein, Christian, Sprenger, Wendelin (2019a). OCC: Ontology for openCASCADE website. (https://www.projekt-scope.de/ontologies/occ/, accessed February 2020).

Nothstein, Christian, Sprenger, Wendelin (2019b). OOP: Ontology for object oriented programming website. (https://www.projekt-scope.de/ontologies/oop/, accessed February 2020).

Pauwels, P., Roxin, A. (2016). SimpleBIM : from full ifcOWL graphs to simplified building graphs. *11th European Conference on Product and Process Modelling (ECPPM)*. CRC Press (http://hdl.handle.net/1854/LU-8041826, accessed May 2020).

Pauwels, P., Zhang, S., Lee, Y.-C. (2017). Semantic web technologies in AEC industry: A literature overview. *Automation in Construction*, 73, pp.145–165.

Paviot, T. (2017). pythonOCC - 3D CAD/CAE/PLM development framework for the Python programming language website. (http://www.pythonocc.org/, accessed May 2020).

planen-bauen 4.0 (2018). BIMSWARM. *Das Portal für Bau-IT Produkte*. (https://www.bimswarm.de/, accessed January 2020).

Rasmussen, M.H., Pauwels, P. (2019). Building Topology Ontology website. (https://w3c-lbd-cg.github.io/bot/, accessed February 2020).

SCOPE (2018). SCOPE – Semantic Construction Project Engineering. (https://www.projekt-scope.de/, accessed January 2020).

SCOPE (2019). projekt-scope/scope-data-service website. (https://github.com/projekt-scope/scope-data-service, accessed December 2019).

SolConPro (2015). SolConPro - Solar Construction Process website. (http://www.solconpro.de/, accessed February 2020).

Stefanescu, D. (2015). Speckle: Data Platform for AEC website. (https://speckle.systems/, accessed January 2020).

Steinmann, R. (2018). IFC Certification of BIM Software. In: Borrmann A, König M, Koch C, Beetz J, eds. *Building Information Modeling: Technology Foundations and Industry Practice*. Cham, Springer International Publishing,2018, pp.139–153. (https://doi.org/10.1007/978-3-319-92862-3_7, accessed February 2020).

Terkaj, W., Pauwels, P. (2017). A Method to Generate a Modular ifcOWL Ontology. *Joint Ontology Workshop*.

Thiele, C.-D., Huyeng, T.-J. (2020). TDY: Teddy Ontology website. (https://w3id.org/tdy, accessed February 2020).

Villazón-Terrazas, B., Vilches-Blázquez, Luis.M., Corcho, O., Gómez-Pérez, A. (2011). Methodological Guidelines for Publishing Government Linked Data. In: Wood D, ed. *Linking Government Data*. New York, NY, Springer New York,2011, pp.27–49. (http://link.springer.com/10.1007/978-1-4614-1767-5_2, accessed May 2020).

Wagner, A., Bonduel, M., Pauwels, P., Rüppel, U. (2020). Representing construction-related geometry in a semantic web context: A review of approaches. *Automation in Construction*, 115:103130.

Wagner, A., Bonduel, M., Pauwels, P., Uwe, R. (2019). Relating geometry descriptions to its derivatives on the web. *2019 European Conference on Computing in Construction*. (https://research.tue.nl/en/publications/relating-geometry-descriptions-to-its-derivatives-on-the-web, accessed May 2020).

Wagner, A., Möller, L., Eller, C., Leifgen, C., Rüppel, U. (2018). SolConPro: An Approach for the Holistic Integration of Multi-Functional Façade Components into Buildings' Lifecycles.

Wagner, A., Rüppel, U. (2019). BPO: The Building Product Ontology for Assembled Products. In: CEUR-WS.org, ed. *Proceedings of the 7th Linked Data in Architecture and Construction Workshop - LDAC2019*.Vol2308. Lisbon, Portugal, pp.106–119.

A Visual Programming Approach for Validating Linked Building Data

Madhumitha Senthilvel, Jakob Beetz
Design Computation, Faculty of Architecture, RWTH Aachen University, Germany
senthilvel@caad.arch.rwth-aachen.de

Abstract. The upsurge in the development and availability of specialized BIM-based tools have enabled parsing of information from models into different formats for specific use cases. However, interoperability issues in IFC result in information loss during the conversion between formats, standards, and software. While Semantic Web technologies and Linked Data are promising approaches for representing and linking information spread across sources and formats, the problem of checking data consistency in the tool-chains remains. Approaches such as SPARQL, mvdXML are considered either too verbose or unable to handle non-IFC data. Since SHACL was only recently introduced (2017), visual interfaces for the creation of these rules are not investigated in the AEC domain. Current implementations of SHACL focus on the generation of validation reports and not on the creation of SHACL constraints themselves, which requires both Semantic Web knowledge and domain knowledge. This paper proposes a visual programming interface for creating SHACL shapes to improve the ease of creation and editing of constraints for non-semantic web experts with its focus on supporting AEC ontologies and use-cases. To aid that, this paper explores how constraints can be modularized in SHACL so that they are re-usable across use-cases. The proof of concept is demonstrated using a linked building data example. This work is an initial step towards connecting services, wherein, constraints can be created with minimal domain and expert knowledge, and these constraints facilitate checking the validity of information.

1. Introduction

Building Information Modelling (BIM) is being increasingly accepted as a valuable asset for the construction industry, in terms of design, planning, collaboration and constraint checking. With an upsurge in the development and availability of specialized BIM-based tools, it is now possible to parse information from models into different formats for specific use cases. However, due to interoperability issues in IFC (Industry Foundation Classes) and the checking tools that support it, information is lost during the conversion between formats, standards, and software.

Semantic Web technologies and Linked Data have been identified as promising approaches for representing and linking information spread across sources and formats (Beetz et al., 2009; Pauwels et al., 2011). Nonetheless, the problem of checking data consistency remains. Information still has to be checked for its consistency before being transferred between applications.

Numerous checking approaches such as XML, SPARQL Protocol and RDF Query Language (SPARQL), Shape Expressions (SHeX), Object Constraint Language(OCL), Shape Constraint Language(SHACL), its predecessor SPIN etc. have been employed to validate data. In the AEC domain, prevalent checking languages/standards are mvdXML and SPARQL. mvdXML is widely regarded as the go-to for constraint checking (Chipman et al., 2016). However, its support is limited for IFC based models, with little scope for checking other kinds of data such as photographs, textual information etc. Furthermore, existing implementations of mvdXML, SPARQL require both semantic and domain knowledge for modelling constraints; other modelling approaches such as SHACL, SHeX, OCL do not have implementations yet for AEC domain. The motivation for this research stems from this gap. This paper proposes and explores the implementation of an interface for creating constraints in SHACL using open-source API. The proposed approach focuses on a visual programming interface for creating SHACL shapes to improve the ease of creation and editing of constraints for non-semantic experts, to support AEC ontologies and use-cases.

To gain an understanding of the existing implementations of checking approaches, the next section focuses on mvdXML, and BIMSPARQL- the two most prevalent checking mechanisms in the AEC domain.

2. Existing methods for data validation: approaches, and implementations

The existing approaches for the creation of rules for data validation can be roughly categorized into proprietary methods and non-proprietary methods. Solibri Model Checker (SMC) is a widely-used checking tool for applications such as code compliance and clash detection falls under the Programming based approach (Zhang et al., 2015). While it is based on hard-coding rules, it is also customizable using the in-built Rule Manager option. However, proprietary definitions are employed to implement these rules. This reduces the flexibility of the tool for checking information beyond those envisioned by the tool developers. Such a situation is valid, especially in a linked data environment where non-IFC data would also have to be validated. Non-proprietary model checkers (for example, the mvdXML Checker) overcome vendor-lock-in.

This section begins with discussing the major non-proprietary implementations for data validation in AEC: IFCDoc, mvdXML generator for mvdXML and BIMSPARQL for SPARQL for creating constraints and contrasting them with SHACL. The section aims to give an overview of implementations of the above approaches and the challenges associated with using them. These challenges serve as a prologue to understanding the desired features of an interface for creating constraints for AEC use cases.

2.1 mvdXML

mvdXML is a standard introduced by buildingSMART. It is an electronic format representing the Model View Definitions (MVD), which themselves represent the information required during data exchanges. They are a subset of the data schema and can be obtained from Information Deliver Manual (IDM) and Exchange Requirement (ER). mvdXML documentation describes its application to IFC data schema only (Chipman et al., 2016).

However, mvdXML has some drawbacks, most of which stem from the complex nature of IFC itself. For example, it lacks logical formalisms, it only considers IFC schema, and MVD-based view constructors are not flexible and dynamic (Roxin, 2016). However, implementations for generating rules and checking them have been developed.

The mvdXML Checker is an implementation developed by Zhang et. al which checks for IFC data conformation which uses mvdXML rulesets (Zhang et al., 2015). To function it needs: a mvdXML generator for creating rulesets (*IFCDoc*), the checker itself which checks the generated rulesets against given IFC data, and lastly an output viewer which shows the validation in BCF (Building Collaboration Format). For brevity, *IFCDoc* will be briefly discussed. *IFCDoc* is a tool which creates XML rulesets preloads all the IFC schema releases. It enables checking the existence of a value/entity/attribute, whether it is present in the correct entity type and subtype and finally, the accuracy of the attribute value and cardinality of the said attribute. van Strien gives a comprehensive practical guide to *IFCDoc* (van Strien, 2015).

However, it requires domain end-user to have knowledge of IFC, mvdXML and *IFCDoc* (Weerink, 2016). Currently, *IFCDoc* tool has limited support since it is not being updated. Consequently, the mvdXML generator and checker was hence developed by implementing a user-interface for generating the XML rulesets using spreadsheet-based requirement documentation along with Zhang et. al's original Checker (Weerink, 2016). This generator works specifically for a set of specifications and hence is not generic to accommodate other use-cases.

2.2 SPARQL

SPARQL, which has been implemented for querying and validation in BIMSPARQL, is regarded as complex and has a high threshold for learning due to its verbosity and flexibility to define a constraint in multiple ways (Zhang et al., 2018). However, SPARQL's inherent flexibility for querying a query in multiple ways demands that the user be well aware of the syntax of the language. Additionally, current implementations of SPARQL still necessitate the user to enter queries according to SPARQL syntax, with no masking of the complexities of the language.

3. SHACL as an alternative data validation language

In section 2, existing implementations for checking information were discussed. As of now, only *IFCDoc* exists to generate mvdXML rulesets. While there are limited open-source options for editors/tools to check AEC information, there exists an even more dire shortage of tools for generating the rules which are necessary for the checking process. These tools will need to be able to cater to checking non-IFC data as well. SHACL (Shape Constraint Language), a domain-agnostic constraint language is still not yet investigated for the AEC domain, partially due to it being a recent development[1]. SHACL uses the concept of shapes graphs (rulesets) to define constraints. When a given input (termed as data graph) is validated against shape graphs, a validation report is generated containing the classes violating the rules. SHACL is considered a more general-purpose validation language since it can be used for any information encoded in the JSON/turtle format.

At present, SHACL has a few implementations such as *TopBraid's SHACL API*[2], *SHACL Playground*[3], *pySHACL*[4] and *unSHACLed*[5] etc. The former 4 focus on the validation of data against the shapes, and not on the creation of the constraints (shapes) themselves. Only *unSHACLed* implements a prototype based on an interface for a drag-and-drop option for creation of SHACL shapes (Meester et al., 2019). This feature of drag and drop helps mask the complexity of the language and make it easy for all levels of users to utilize the tool.

However, in the AEC domain, the challenge in integrating SHACL in practice with other tools is that such constraint definition languages require not only expert semantic web knowledge but also knowledge on assessing the applicability of these rules for AEC ontologies and use-cases. In a visual programming approach, the syntax of SHACL can be masked by the code blocks. General purpose visual programming languages have been shown to be more user-friendly and accessible for non-domain users (Catarci and Santucci, 1995).

The partially pre-programmed editable code-blocks (called nodes) can be connected non-linearly, hence facilitating the quicker generation of SHACL shapes. In this approach, the code blocks contain the reusable SHACL shapes (constraints) and the associating data object against

[1] Introduced as a standard in 2017.
[2] https://github.com/TopQuadrant/shacl
[3] https://shacl.org/playground/
[4] https://pypi.org/project/pyshacl/
[5] http://ecodalo.ilabt.imec.be:8980/#/

which it is being validated. Thus the user only has to determine the type of constraints (such as cardinality, data type, range etc.), and the associated class and property for which these constraints apply can be determined through the API itself.

4. Implementation Approach

Beyond commercial add-ons such as *GrassHopper* and *Dynamo*, there exists numerous open-source APIs for visual programming such as *Node-RED, noflo, PyFlow* etc. Libraries such as *Node-Red* and *noflo* are based on JavaScript and can be deployed on the web, but they lack an interface for visualizing models, including IFC models. *PyFlow*, on the other hand, can be deployed as a stand-alone and also in conjunction with an open-source 3D modeller called *FreeCAD*. Thus, models can be visualised, information can be extracted from *FreeCAD* and used in visual programming. In this work, we have chosen to develop the SHACL module with *FreeCAD* and *PyFlow* so that information can be extracted from *FreeCAD* for easier modelling in *PyFlow*.

4.1 FreeCAD and PyFlow

FreeCAD is an open-source general-purpose modelling tool, with emphasis on parametric modelling("FreeCAD: Your own 3D parametric modeller," n.d.). Originally, it began with support for mechanical and product design, it now supports Architectural and Civil Engineering modelling also, by making use of *IfcOpenShell*. *FreeCAD* implementation closely resembles the work proposed by Preidel et.al, in which a Visual Code Compliance Language based on graphical notation is described (Preidel and Borrmann, 2016).

FreeCAD splits its tools into workbenches, thus making modularized parts, which can be mix-matched by users for creating models. All of these run on the scripting language Python, giving end-users flexibility to create their tools and functionalities. Additionally, it also supports 3rd party tools and libraries for a variety of applications, thus making it possible to run tools inside tools. One such tool is *PyFlow*, a general-purpose visual scripting framework for python ("wonderworks-software/PyFlow," 2020). It contains editable node packages, which can be user-defined. A more customized version of the *PyFlow* is the *NodeEditor*, which customises the *PyFlow* nodes for interaction with files loaded in *FreeCAD*.

Figure 4.1 shows a general workflow of the SHACL Constraint creator using the above open-source applications. *FreeCAD*, the information visualization interface, interacts with *PyFlow* (the Visual programming interface). In the current set-up of *PyFlow*, two existing modules: an in-built *Pyflow module* and a *FreeCAD NodeEditor module* is pre-loaded. The in-built *PyFlow* module contains basic nodes for manipulation of any data. The *FreeCAD NodeEditor* contains pre-defined nodes for interacting with the *FreeCAD* environment. In this paper, a new module called "SHACL Constraint Creator" is added to the above modules in *PyFlow*. This module contains SHACL shape nodes which take minimal non-syntactical input from the user, to create

SHACL shapes(rulesets) based on information loaded in the *FreeCAD* module. As shown in the figure, all SHACL Shape nodes can take their base input (such as the Class to be checked, the property to be checked etc.) from the model loaded in *FreeCAD*.

In this paper, we take a use-case, where an IFC model "HelloWall.ifc" is loaded in *FreeCAD*. The wall has a property: *label* with value "Wall". The other properties of this wall can be accessed in *PyFlow* giving this input to the node *FreeCAD_Object2 (refer to Figure 4.2)*. This node after execution is shown in Figure 4.3. This node is used as a reference for creating constraints using the *SHACL Constraints Creator module*, explained in the next section.

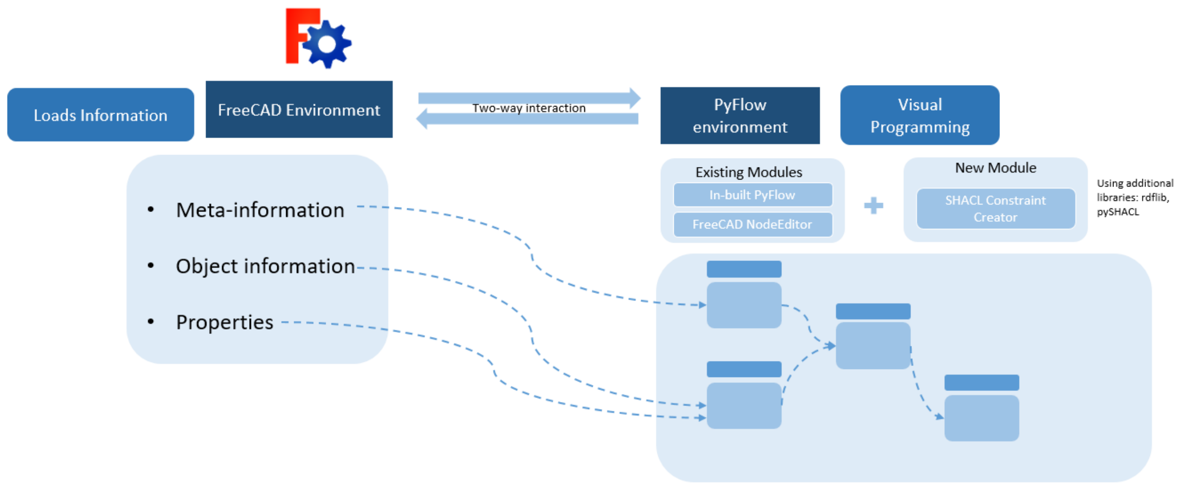

Figure 4.1: Implementation approach for SHACL Constraint Creator using FreeCAD and PyFlow

4.2 SHACL Constraints Creator module

A typical SHACL shape graph in *.ttl* serialization contains three parts: The first part defines the prefixes, followed by the testing node which defines the targeting class(Entity being checked) for the checking in the data graph, and finally the property for which the constraint is specified (property being checked). The *SHACL Constraints Creator module* is designed in the same structure.

The composition of a mvdXML ruleset, and a SHACL Shape is shown in Figure 4.4. An overview of how constraints in SHACL differs from constraints in mvdXML is shown in Listing 4.1. In this example, we check if in the entity *IfcWallCommon* there exists a value for the property *Thermal Transmittance*. First, the mvdXML-based formulation in *IFCDoc tool* is shown along with definition of the components of the file/s (Chipman et al., 2016). Below this, for the same example, the formulation in SHACL is shown.

Concept Templates->	<...> *(excluded, refer to* (Chipman et al., 2016)*page 43 for details)*
Concepts->	<Concept uuid="e9941408-82a6-4c00-a397-11087e6c5d1f" name="load bearing external walls required to have property 'ThermalTransmittance'"> <Definitions> <Definition> <Body lang="de"><![CDATA[For all load bearing external walls the property 'ThermalTransmittance' shall be applied]]></Body> </Definition> </Definitions> <Template ref="5c252c86-5bff-4372-9a27-b794069f9fbb"/> <Requirements> <Requirement applicability="export" exchangeRequirement= "ae70f764-938b-4cf7-9814-c29a47f56b0e" requirement="mandatory"/>

	</Requirements>
	<TemplateRules operator="or">
Target Class->	<TemplateRule Parameters="O_PsetName[Value]='Pset_WallCommon' AND
Target property->	O_PName[Value]='ThermalTransmittance' AND O_PSingleValue[Exists]=TRUE"/>
Cardinality->	<TemplateRule Parameters="T_PsetName[Value]='Pset_WallCommon' AND
	T_PName[Value]='ThermalTransmittance' AND T_PSingleValue[Exists]=TRUE"/>
	</TemplateRules>
	</Concept>
Required Prefixes->	@prefix dash:<http://datashapes.org/dash#>.
	@prefix sh:<http://www.w3.org/ns/shacl#>.
	@prefix ifcowl:<http://www.buildingsmart-tech.org/ifcOWL/IFC2x3_TC1#>.
	@prefix inst:<http://www.linkedbd.net/resource11>.
	@prefix express:<http://www.w3id.org/express#>.
	@prefix rdf:<http:www.w3.org/1999/02/22-rdf-syntax-ns#>.
	@prefix xsd:<http://www.w3.org/2001/XMLSchema#
	@prefix owl:<http://wwww.w3.org/2002/07/owl#>.
Definition of Sample shape->	ifcowl:TestIfc
	a sh:NodeShape;
Target Class->	sh:TargetClass ifcowl:IfcWallCommon;
Target Property->	sh:property [
	sh:path ifcowl:ThermalTransmittance;
Cardinality->	sh:minCount 1;
	sh:datatype xsd:integer
	].

Listing 4.1: Comparison of rulesets in mvdXML, from IFCDoc tool(above)and SHACL shape file (below)

In the above example, *ifc:TestIfc* is a sample NodeShape in SHACL, which targets the entity *ifcowl:IfcWallCommon*, and specifies the property *ifcowl:ThermalTransmittance* is having a constraint that it should have at least one value and that value must be an integer (and not be empty). It has to be noted that the mvdXML file shown in Listing 4.1 is only a snippet, and the additional files which included the concept templates etc. will also have to be defined and created before checking.

Similar to the structure of SHACL shape in Listing 4.1, the SHACL Constraint Creator module in *PyFlow* contains a Prefix library, a *NodeShape library* and a *Constraints library*. While the *Prefix library* contains relevant prefixes, which the user can select, the *NodeShapeLib library* contains nodes which with input pins for the name of the sample node shape class, the targeted class for checking, and the property being checked.

In the *Constraints library*, value configurable nodes for checking cardinality, data type, relationship are defined. Figure 4.3 shows the *SHACL Constraint Creator module* in *PyFlow*. Upon running the workflow shown in Figure 4.3, a SHACL file is generated and saved, the contents of which are show in in Listing 4.2.

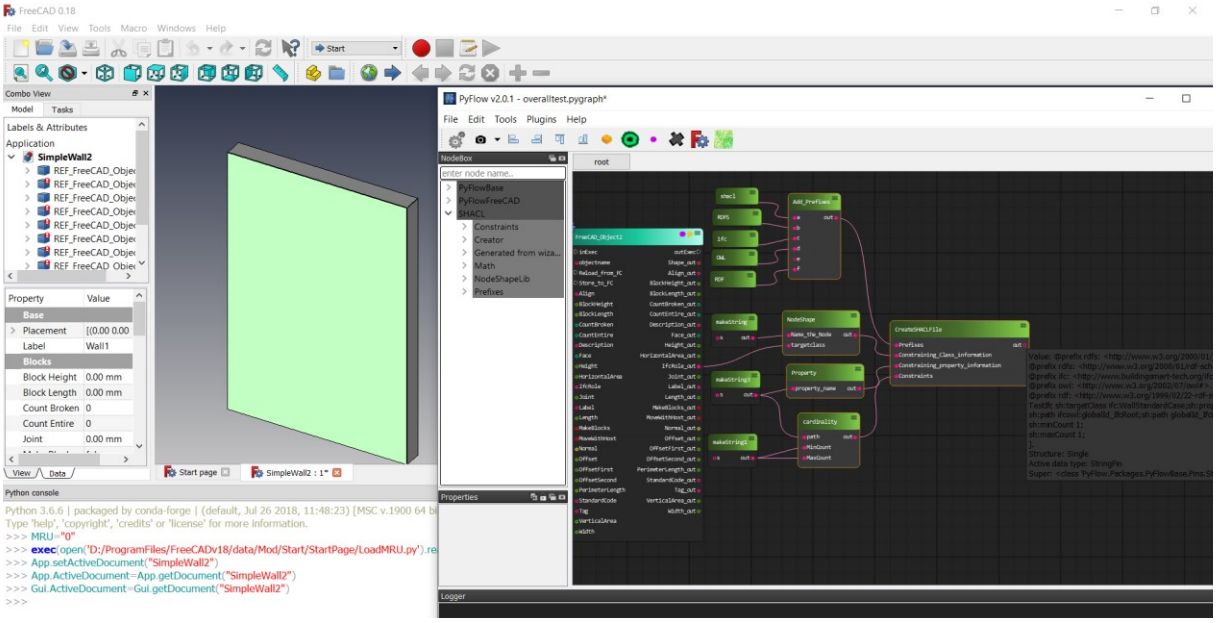

Figure 4.2: FreeCAD with sample file HelloWall.ifc loaded and PyFlow-the open source visual programming editor

```
@prefix rdfs: <http://www.w3.org/2000/01/rdf-schema#>.
@prefix rdfs: <http://www.w3.org/2000/01/rdf-schema#>.
@prefix ifcowl: <http://www.buildingsmart-tech.org/ifcOWL/IFC2x3_TC1#>.
@prefix owl: <http://www.w3.org/2002/07/owl#>.
@prefix rdf: <http://www.w3.org/1999/02/22-rdf-syntax-ns#>.

ifcowl:TestIfc sh:targetClass ifcowl:WallStandardCase;
sh:property [
sh:path ifcowl:globalId_IfcRoot;
sh:minCount 1;
sh:maxCount 1;
].
```

Listing 4.2: SHACL ShapeFile generated by the SHACL Constraints Creator

The nodes of *NodeShape* take input directly from the *FreeCAD_Object2* node (refer section 4.1). Additionally, an introspection feature is also implemented, which contains the IFC schema, which reads the relevant applicable inheritances and associated properties for the loaded object. Based on the information defined in the *FreeCAD_Object2* node, the search option displays only relevant *NodeShapes* and applicable property constraints, thus making it easier for the user to construct. All the nodes used in Figure 4.3 are reusable, meaning that they can be used as inputs for defining other constraints.

The SHACL Constraints Creator module is available on GitHub[6].

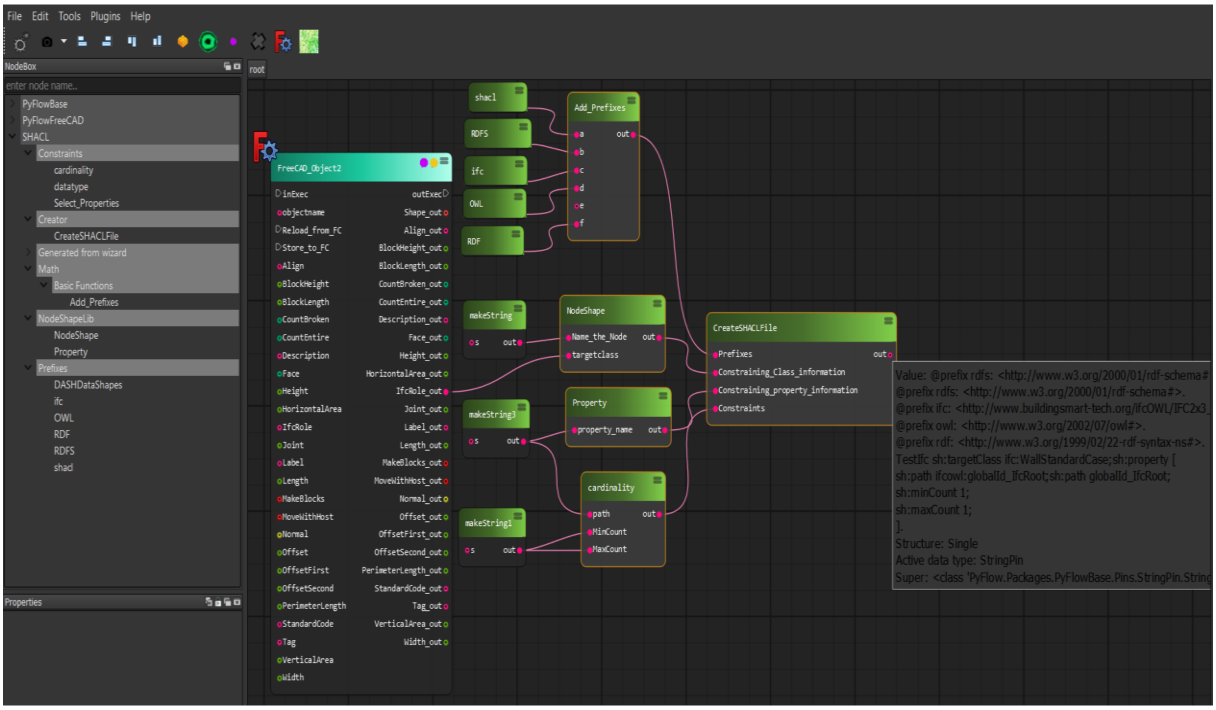

Figure 4.3: SHACL Constraint Creator module in PyFlow Environment

5. Discussion and Conclusion

Checking conformance of models finds application in situations beyond code compliance. As previously mentioned, such checking is necessary during file transfer between tools, formats and standards. The above situations are common-place when working in a collaborative environment, and hence access to an easy-to-use checking tool is necessary for all stakeholders involved.

From a stakeholder perspective, who has to create these constraints, the main task is to convert the text-based requirements into computer-executable rule-sets. The *SHACL Constraint Creator* facilitates this through an interface in which the user can drag and drop nodes, and populate the nodes with information from the text-based requirements. The computer-executable rulesets are then automatically generated from the information, which can then be used to validate any file. The *FreeCAD* environment supports multiple formats, including images, IFC, CAD/DWG etc., and hence constraints can be created for any type of information, thus it can be used for also checking the information in a linked data environment. In the example discussed in section 4.2, the model loaded in *FreeCAD* is a *.ifc* file, while the SHACL constraints are created for *ifcOWL*, to demonstrate the viability of using SHACL for linked building data checking. It has to be noted that the current implementation is still under development.

SHACL also supports querying, with SHACL Advanced Features focusing on SPARQL queries for extensions. Additionally, efforts are on for incorporating GraphQL with

[6] https://github.com/sbalot/SHACLConstraintCreator

SHACL("Publishing RDF/SHACL Graphs as GraphQL," n.d.; Taelman et al., 2019). Such querying can also be modularised as nodes (similar to the way constraints are in this paper) so that end-user directly inputs informal text-information, which is then converted to queries or used for further validation. FreeCAD also contains modules for connecting to BIMServer[7] and a BCF tool[8] for uploading/downloading and updating files in it. Further, if *PyFlow* can be wrapped with JavaScript or used with container solutions such as Docker, it can be deployed as a standalone on the web, thus enabling easier creation of constraints. Future work will be focusing on incorporating the functionalities of these in *SHACL Constraints Creator*.

Acknowledgement

This research was funded through a doctoral research grant by the *Deutscher Akademischer Austauschdienst (DAAD)*.

References

Beetz, J., Leeuwen, J. van, Vries, B. de, (2009). IfcOWL: A case of transforming EXPRESS schemas into ontologies. AI EDAM 23, pp.89–101. https://doi.org/10.1017/S0890060409000122

Catarci, T., Santucci, G., (1995). Are Visual Query Languages Easier to Use than Traditional Ones? An Experimental Proof. BCS HCI, pp. 323–338.

Chipman, T., Liebich, T., Weise, M., (2016). mvdxml: Specification of a standardized format to define and exchange Model View Definitions with Exchange Requirements and Validation Rules. Model Support Group (MSG) of buildingSMART International Ltd.

FreeCAD: Your own 3D parametric modeler [WWW Document], n.d. URL https://www.freecadweb.org/ (accessed 2.28.20).

Pauwels, P., Van Deursen, D., Verstraeten, R., De Roo, J., De Meyer, R., Van de Walle, R., Van Campenhout, J., (2011). A semantic rule checking environment for building performance checking. Automation in Construction 20, pp.506–518. https://doi.org/10.1016/j.autcon.2010.11.017

Preidel, C., Borrmann, A., (2016). Towards code compliance checking on the basis of a visual programming language. Journal of Information Technology in Construction (ITcon) 21, pp.402–421.

Publishing RDF/SHACL Graphs as GraphQL [WWW Document], n.d. URL https://www.topquadrant.com/graphql/shacl-graphql.html (accessed 3.8.20).

Roxin, A., (2016). A Semantic Web Approach for defining Building Views.

Taelman, R., Sande, M.V., Verborgh, R., (2019). Bridges between GraphQL and RDF, in: W3C Workshop on Web Standardization for Graph Data. Presented at the W3C Workshop on Web Standardization for Graph Data, p. 4.

van Strien, E., (2015). MVD Checker Guide.pdf. Technische Universiteit Eindhoven, Eindhoven, The Netherlands.

Weerink, J., (2016). Verifying the completeness of Building Information Models. Technische Universiteit Eindhoven, Eindhoven, The Netherlands.

wonderworks-software/PyFlow [WWW Document], 2020. URL https://github.com/wonderworks-software/PyFlow (accessed 2.28.20).

Zhang, C., Beetz, J., Weise, M., (2015). Interoperable validation for IFC building models using open standards 20, pp.24–39.

[7] https://www.freecadweb.org/wiki/Arch_BimServer
[8] https://github.com/podestplatz/BCF-Plugin-FreeCAD

BIM-based sizing of reactors in processing facilities

Heinrich Söbke*, Patricia Peralta Abadia, Dominik Heigener, Kay Smarsly
Bauhaus University Weimar, Germany
heinrich.soebke@uni-weimar.de

Abstract. Processing facilities, such as wastewater treatment plants or biogas plants, are complex engineering structures that convert input streams to output streams using physical, biological, or chemical processes. When planning, constructing, and operating processing facilities, a large number of experts are involved, typically collaborating by exchanging unstructured files or even physical hardcopies, rendering planning, constructing, and operating of processing facilities costly and error prone. A promising approach towards improving processing facilities planning, while reducing cost and errors, is based on building information modeling (BIM). Using standardized data exchange formats, such as the Industry Foundation Classes (IFC), BIM supports digital planning of buildings. However, the IFC are currently incapable of describing information required for planning processing facilities, particularly information required for sizing of reactors, which is a crucial task in planning processing facilities. Advancing BIM-based planning of processing facilities, an IFC schema extension to support sizing of reactors is proposed in this paper. With the IFC schema extension, a semantic basis is provided to enable BIM-based sizing of reactors, as exemplarily illustrated by means of biogas plants.

1. Introduction

Processing facilities are complex structures that convert input streams to output streams using physical, biological, or chemical processes. Processing facilities are part of technical infrastructure, such as wastewater treatment plants, incineration plants, waterworks, or biogas plants. By transforming natural resources or waste into usable or disposable materials, processing facilities fulfill vital services to society.

The core of each processing facility is a reactor that hosts the conversion processes. Sizing of reactors is a task required for planning processing facilities, which aims to determine appropriate sizes and output streams of processing facilities. Sizing of reactors, due to the complexity of the processes involved, requires close collaboration of experts ("planners") of fluid mechanics, environmental engineering, structural engineering, chemical engineering, and microbial engineering. Despite the advancements in digitalization recently made in the context of Industry 4.0, as discussed in Tay et al. (2018), planners of processing facilities still collaborate on a manual basis, using spreadsheets or hardcopies. The common procedure followed to plan processing facilities is characterized by information breaks caused by manual information exchange that is time-consuming and error-prone. In addition, not all types of processing facilities follow dedicated standards and guidelines that clearly define the planning procedures to be followed, i.e. the information requirements may vary even within a single discipline, depending on the experience of the planners. Thus, improved planning is required to minimize time and errors through enhanced information storage and exchange relevant to sizing of reactors to advance planning, construction, and operation of processing facilities.

Building information modeling (BIM) supports digital planning, construction, and operation of buildings. Sizing of reactors in processing facilities may be advanced by BIM-based information storage and exchange, in that various planning options may be documented, stored, and optimized, facilitating the collaboration between planners. The Industry Foundation Classes (IFC) are a standardized open BIM data exchange format (buildingSMART, 2018). The IFC, continuously being extended to broaden the scope of application, have originally been designed to exchange building information, primarily geometry and material information (Laakso & Kiviniemi, 2012). Recently, the IFC have been used to describe processing facilities, such as wastewater treatment plants (Söbke, et al., 2018) or related infrastructure, such as sewer systems (Bock & Michaelis, 2019). However, sizing of reactors in processing facilities based on the IFC has received limited attention.

This study aims to develop an IFC schema extension to support sizing of reactors in processing facilities. Although the concept proposed herein, thus the IFC schema extension, is generic and extensible towards several reactor types, this study, for the sake of clarity, will exemplarily focus on reactors (more precisely, anaerobic digestion reactors) in biogas plants. In the reminder of the paper, the methodology and the semantics of the IFC schema extension are presented, followed by the implementation and validation of the IFC schema extension and concluding summary.

2. Semantics of the IFC schema extension for sizing reactors

In a previous study conducted by Söbke et al. (2018), a framework for an IFC schema extension for BIM-based description of wastewater treatment plants has been proposed, hereinafter termed "WWTP IFC extension". Building upon the previous work, the WWTP IFC extension is used as a basis for describing information relevant to sizing reactors in processing facilities. As an example, the information needed for sizing an anaerobic digestion reactor (ADR) in a biogas plant is semantically described, showing that the approach presented herein qualifies as a basis to formalize sizing of reactors. In this section, a general approach for sizing of reactors is derived from the WWTP IFC extension, followed by a concise description of anaerobic digestion reactors. Then, the semantic model for conceptually describing anaerobic digestion reactors is presented and converted into the IFC schema extension for sizing reactors.

2.1 Sizing reactors in processing facilities

The WWTP IFC extension of the previous study is centered on an entity submodel, proposed to describe wastewater treatment plants based on a semantic model. The sizing of reactors in wastewater treatment plants is determined by the given loads (planning specifications), design decisions, and calculations defined by standards, such as the German DWA standard A 131 (DWA, 2000), or computational fluid dynamic (CFD) models. For example, the DWA standard A 131 describes different load cases with different wastewater volumes that define the technical capacity of the reactors, such as dry weather inflow, maximum inflow, or lowest temperature inflow. Each load case is used as input for the calculations, giving sizing results as output. Hence, sizing of reactors may be formalized as a semantic model representing a further abstraction comprised by loads and corresponding sizing results, analogous to a structural analysis model.

Figure 1 shows the semantic model, describing all information needed for sizing reactors in a processing facility, where the classes highlighted in grey are specific for one of the reactors in a wastewater treatment plant. As shown in Figure 1, the *ProcessSpace* interface corresponds to a reactor (i.e., a tank), and the entity *ProcessSpaceLoadModel* is intended to describe the loads and sizing results of a reactor. Using the *ProcessSpace* interface, one or more instances of the *ProcessSpaceLoadModel* may be assigned to a tank. The *ProcessSpaceLoadModel* contains aggregations to the *ProcessSpaceLoadGroup* and to the *ProcessSpaceResultGroup*. In the *ProcessSpaceResultGroup*, sizing results are stored, according to the loads described by the *ProcessSpaceLoadGroup*. A *ProcessSpaceLoadGroup* has an aggregation to one or more *ProcessSpaceLoads*, which are necessary for sizing in compliance with load cases defined in a distinct standard. In the semantic model, each load case is represented by a *ProcessSpaceLoad*, and the sizing results are stored in a *ProcessSpaceResult*. All load cases are combined using a *ProcessSpaceLoadGroup/ ProcessSpaceResultGroup* pair, entailing the final design specification of a specific reactor.

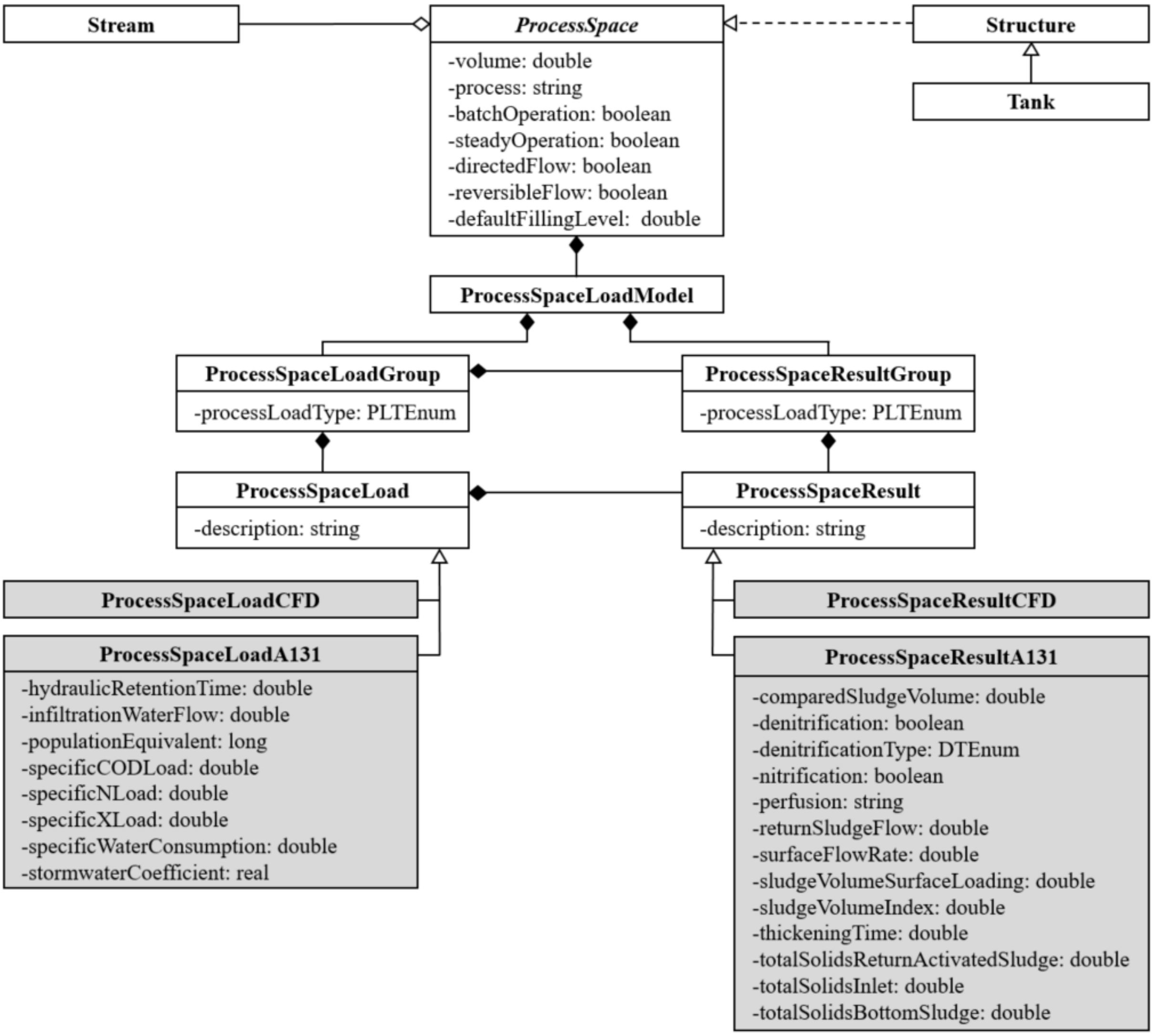

Figure 1: Extract of the semantic model for sizing reactors in a processing facility

Each reactor in a processing facility has specific input parameters (loads) and output parameters (sizing results) that may vary according to the different standards. Subclasses of *ProcessSpaceLoad* and *ProcessSpaceResult* may be defined to describe each standard. For example, in Figure 1, subclasses of *ProcessSpaceLoad* and of *ProcessSpaceResult* are defined to describe sizing according to CFD models and to the DWA standard A131.

2.2 Anaerobic digestion reactors for biogas plants

To describe the semantics of the IFC schema extension for sizing of reactors, an anaerobic digestion reactor for biogas plants, the illustrative example in this study, is formalized. The prevalence of biogas plants in Germany has considerably increased in the course of the so-called "Energy Revolution" (Renn and Marshall, 2016). With ongoing spreading of biogas plants, the demand for digitally supported planning (and, therefore sizing) is expected to further increase.

Anaerobic digestion is a sequence of microbiological processes that decompose biodegradable material ("biomass") by microorganisms under absence of oxygen. Anaerobic digestion is applied in waste management as a waste treatment method or for supplying regenerative energies. Anaerobic digestion has two main products, (i) biogas, consisting of methane and carbon dioxide, and (ii) digestate, a reduced-volume bacterial biomass. Biogas is an energy source that may be harnessed as regenerative energy via cogeneration of heat and electricity, while digestate may be used as fertilizer. The type of reactor hosting anaerobic digestion processes depends on the waste to be treated and on the final use to be given to the waste. A more detailed description of anaerobic digestion and types of reactors can be found in Mata-Alvarez (2003).

2.3 A semantic model for sizing anaerobic digestion reactors

The semantic model developed to support sizing of anaerobic digestion reactors, as mentioned earlier, is based on the semantic model derived from the WWTP IFC extension of the previous study conducted by the authors, as shown in Figure 1. To extend the semantic model towards anaerobic digestion reactors, in essence, specific subclasses of *ProcessSpaceLoad* for the input streams and specific subclasses of *ProcessSpaceResult* for the output streams are defined. To semantically describe further details relevant to sizing of anaerobic digestion reactors, sources that provide detailed knowledge are identified, analyzed, and formalized, complemented by expert interviews. Serving as knowledge sources, a plenitude of standards, guidelines, and research projects exist, such as simulation models of anaerobic digestion processes (Batstone et al., 2002). In addition, the Association of German Engineers (VDI, 2006) characterizes substrates and the influence on biogas formation, which is also outlined by Weinrich et al. (2018). Furthermore, sizing concepts have been proposed by Garcia-Heras (2003) and Paterson, et al. (2015), concluding that the current planning practice of anaerobic digestion reactors is strongly influenced by tacit knowledge gained by long-term experience. Similarly, standards of the German Association for Water, Wastewater and Waste (DWA) are implicitly related to anaerobic digestion reactors, although not explicitly addressing the reactor sizing. For example, the DWA-M 380 guideline describes co-fermentation of various substrates (DWA, 2009), the DWA-M 363 guideline describes origin, treatment, and utilization of biogas (DWA, 2010), and the M-372 standard (ATV-DVWK, 2003) describes sizing of anaerobic digestion reactors as a sub-aspect of the standard.

To create the semantic model, the sizing parameters determined from the above knowledge sources are defined and, in a subsequent step, formalized in the semantic model. Taking into account different anaerobic digestion reactor types, the sizing parameters are divided into three categories,

i. configuration parameters (representing the characteristics and operation of reactors),
ii. input parameters (representing input streams), and
iii. output parameters (representing output streams).

Table 1 shows the *configuration parameters* that define the characteristics and operation of anaerobic digestion reactors, such as type of anaerobic digestion and operating temperature.

Table 1: Sizing anaerobic digestion reactors: Configuration parameters

Configuration parameter	**Description**
methodOfDigestion	Enumeration describing the method applied for anaerobic digestion (enumeration values: wet, dry). In wet reactors, the substrate is liquid, and it is stirred or pumped, while in dry reactors the substrate is stacked.
modeOfOperation	Enumeration describing the method of operation (enumeration values: continuous, discontinuous). In continuous mode, the substrate is continuously fed into the reactor, with concurrent removal of processed substrate. In discontinuous mode (or batch mode), the reactor is filled to capacity and emptied once the process is complete.
typeOfReactor	Enumeration describing the reactor type (enumeration values: suspended, fixed film). In suspended reactors, the processes are executed in liquid, whereas in fixed film reactors, the anaerobic digestion processes take place on the surface of solids.
processTemperature	Temperature of the substrate being digested (double value, representing °C). Depending on the temperature, the process type is determined, either mesophilic (30 °C – 37 °C) or thermophilic (60 °C – 70 °C).

The *input parameters*, primarily required to characterize the substrate for calculating the expected gas yield, are shown in Table 2. In general, organic dry matter (OTS) is the most common parameter, while carbohydrates, lipids, and proteins allow a more accurate calculation of the biogas yield.

Table 2: Sizing anaerobic digestion reactors: Input parameters

Input parameter	**Description (data type, unit)**
substrateInputstream	Daily volume flow of the substrate (double, m^3/d).
oTS	Substrate parameter organic dry matter (OTS) (double, kg/m^3).
carbohydrates	Substrate parameter carbohydrates (double, kg/m^3).
lipids	Substrate parameter lipids (double, kg/m^3).
proteins	Substrate parameter protein (double, kg/m^3).
tC	Substrate parameter total organic carbon (TC) (double, kg/m^3).
dOC	Substrate parameter dissolved organic carbon (DOC) (double, kg/m^3).
cOD	Substrate parameter chemical oxygen demand (COD) (double, kg/m^3).
meanResidenceTime	Parameter of operation, residence time of the substrate in the reactor (double, days). For wet reactors, the mean residence time is the hydraulic retention time.
loadingRatePerUnitVolume	Ratio of the daily load to the fermenter volume (double, $kg/m^3 \cdot d$).

Table 3 describes the *output parameters*. Among the most relevant parameters with respect to the output stream is the effective reactor volume. The other parameters are related to the digestate and biogas production. The efficiency of a reactor is described by the digester gas efficiency, as a key performance indicator to evaluate the planning quality.

Table 3: Sizing anaerobic digestion reactors: Output parameters

Output parameter	Description
effectiveReactorVolume	Reactor volume required to process the input stream (double, m^3).
digestateOutputstream	Daily volume flow of the digestate (double, m^3/d).
digesterGasFlowRate	Daily volume flow of gas (double, m^3/d).
methane	Gas parameter methane (double, m^3/m^3).
oTS	Digestate parameter organic dry matter (OTS) (double, kg/m^3).
digesterGasEfficiency	Gas per OTS dry mass (double, m^3/kg).

Figure 2 shows the main classes of the semantic model for sizing anaerobic digestion reactors, developed based on analyzing the knowledge sources and, specifically, the parameters relevant to sizing anaerobic digestion reactors. The classes *ProcessSpaceLoad* and *ProcessSpaceResult* are known from the semantic model of the WWTP IFC extension. Extending these classes, the subclasses *ProcessSpaceLoadADR* and *ProcessSpaceResultADR* include the attributes required for sizing anaerobic digestion reactors.

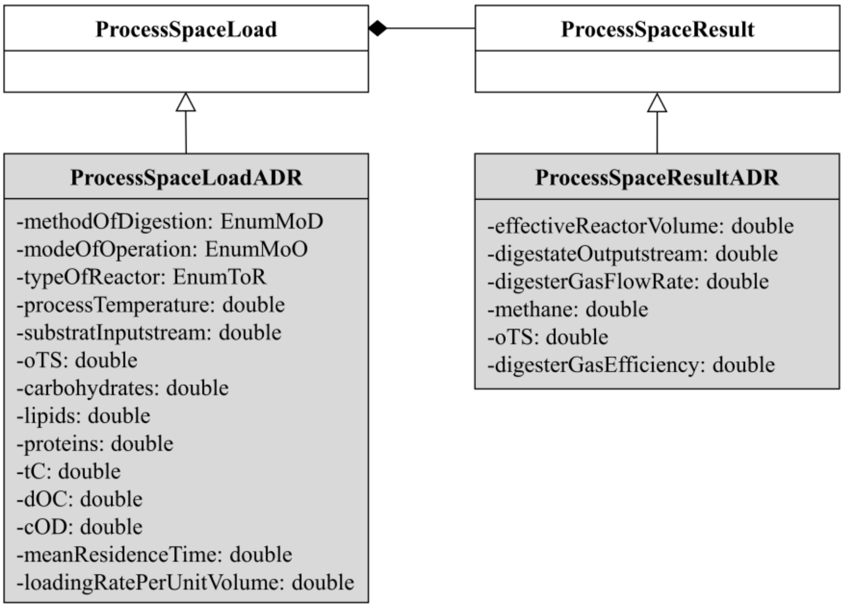

Figure 2: Main classes of the semantic model for sizing anaerobic digestion reactors

3. Implementation of the IFC schema extension for sizing reactors

In this section, the proposed sematic model is implemented into the IFC schema extension for sizing reactors. The IFC schema extension proposed in this study is compliant to IFC version “IFC 4 – Addendum 2”, or “IFC4” for short (buildingSMART, 2017). Figure 3 shows the IFC schema extension for sizing reactors, building upon the WWTP IFC extension proposed in Söbke et al. (2018). The extract shown in Figure 3 describes an IFC submodel, referred to as *IfcProcessSpaceLoadModel*, developed following the concept implemented in the IFC entity *IfcStructuralAnalysisModel* of the current IFC schema. Because of the analogy of the sub model and the existing IFC entity, ease of use is expected for users familiar with the entity *IfcStructuralAnalysisModel*. The IFC schema extension for sizing reactors extends the submodel *IfcProcessSpaceLoadModel* by creating new enumeration values for

IfcProcessSpaceLoadTypeEnum for sizing design methods and new IFC subentities of *IfcProcessSpaceLoad* to describe load cases defined by each design method and of *IfcProcessSpaceResult* to describe the resulting variants for each sizing design method.

The IFC schema extension for sizing reactors is implemented for one type of anaerobic digestion reactor with standard operating conditions. Figure 4 shows the entities of the IFC schema extension for sizing an anaerobic digestion reactor in biogas plants. The entities *IfcProcessSpaceLoad* and *IfcProcessSpaceResults* are defined according to the semantic model shown in Figure 2, where the configuration and input parameters are defined as process space loads, and the output parameters are defined as process space results. In the IFC schema extension for sizing reactors, the operational, input, and output parameters are described either with enumeration values or with double data types. Due to specific parameter types, new subentities of *IfcResourceMeasure*, such as *IfcMassVolumetricFlowRateMeasure* and *IfcDensityMassMeasure*, are introduced.

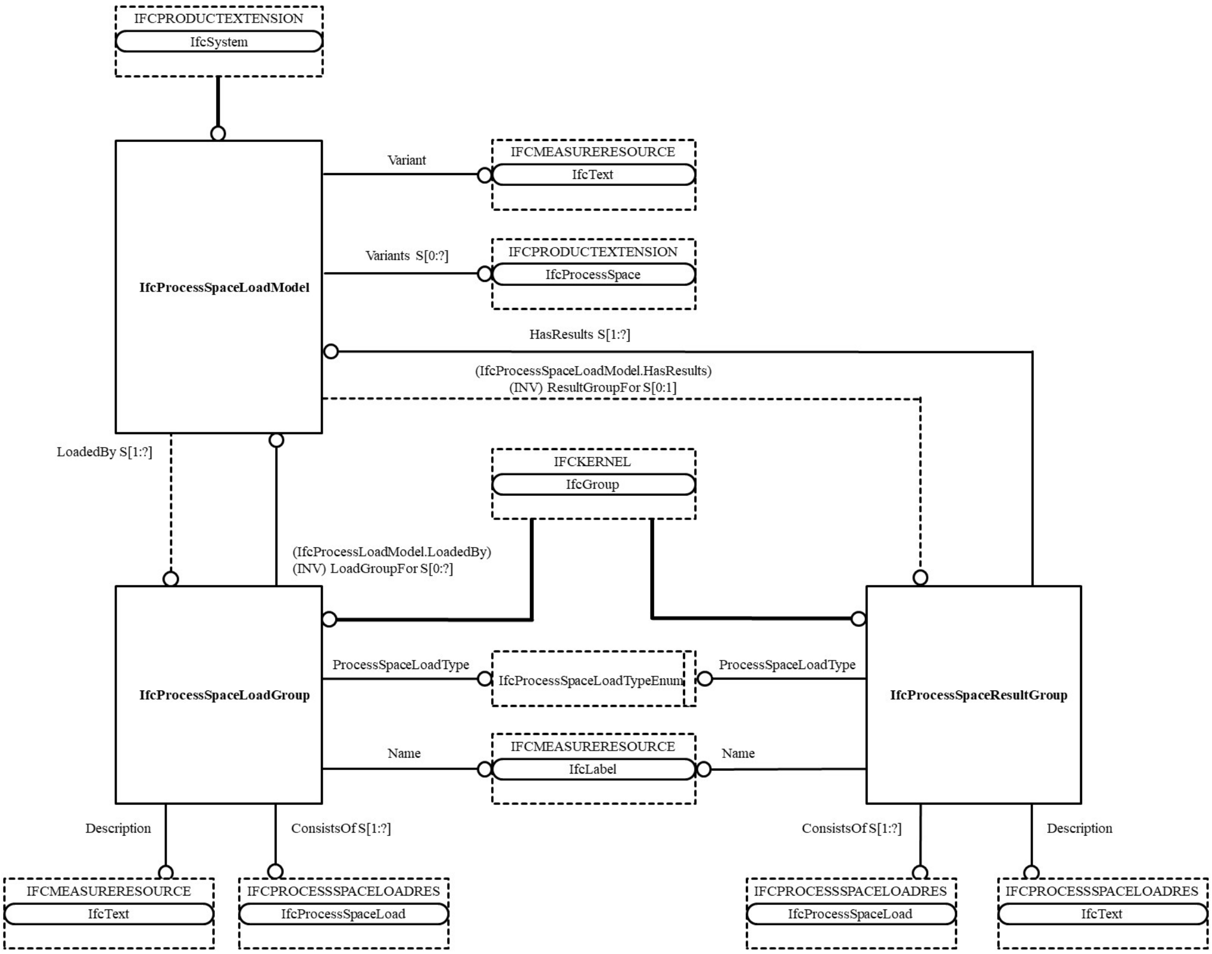

Figure 3: IFC schema extension for sizing reactors in processing facilities

The IFC schema extension introduced herein provides a procedure to formalize sizing of reactors supporting BIM-based planning of processing facilities, while minimizing the complexity of future IFC schema extensions, thus reducing the time required for standardization processes, which usually take up to five years. One example of efforts at making the standardization process in a reasonable time is the IFC scheme extension *IFC Bridge*, which was carried through in the fast-track (Borrmann, et al., 2019). The fast-track approach does not claim to cover all conceivable details, but rather to focus on frequently occurring manifestations of properties and entities. Therefore, with the concept of the *ProcessSpaceLoadModel*, a data model equipped with the specialized subclasses for reactors may be standardized in shorter times. In the following section, the IFC schema extension is validated with an illustrative example.

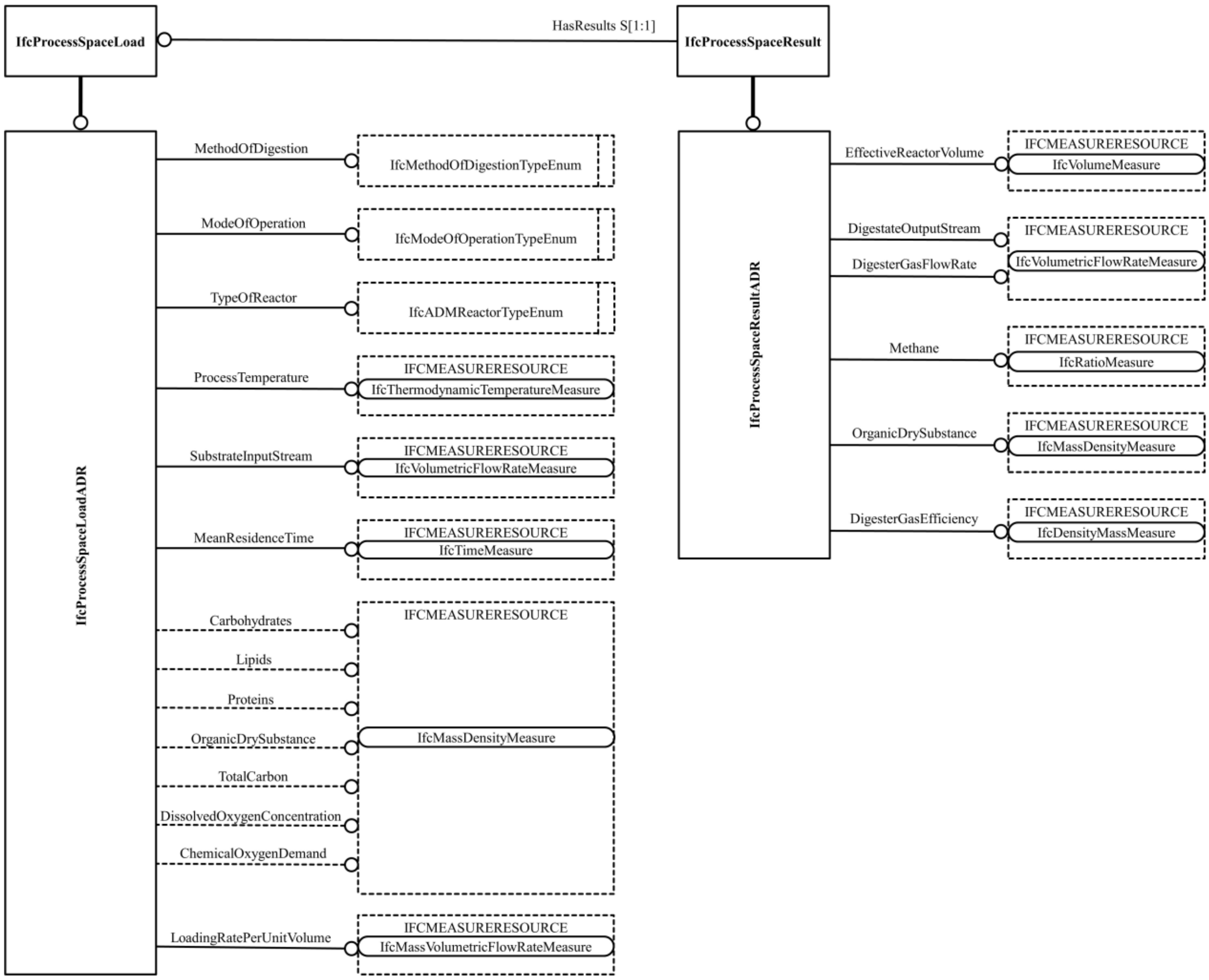

Figure 4: IFC schema extension for sizing anaerobic digestion reactors in biogas plants

4. Validation of the IFC schema extension for sizing reactors

To validate the IFC schema extension for sizing reactors, an IFC-compliant BIM model of an anaerobic digestion reactor is modelled (i.e., instantiated) from the IFC schema extension, as shown in Figure 5, to describe its sizing information. The reactor is first modeled using a BIM tool and then the corresponding IFC file is generated. Next, the IFC file is processed using a Java-based software application, capable of reading and editing IFC files, which incorporates the IFC schema extension. The Java-based software application extends the IFC file to incorporate the entity *IfcProcessSpaceLoadModel*, which describes the sizing information. Listing 1 shows an extract of the processed IFC file covering load and sizing results data for the anaerobic digestion reactor; the semantics of the attributes are annotated.

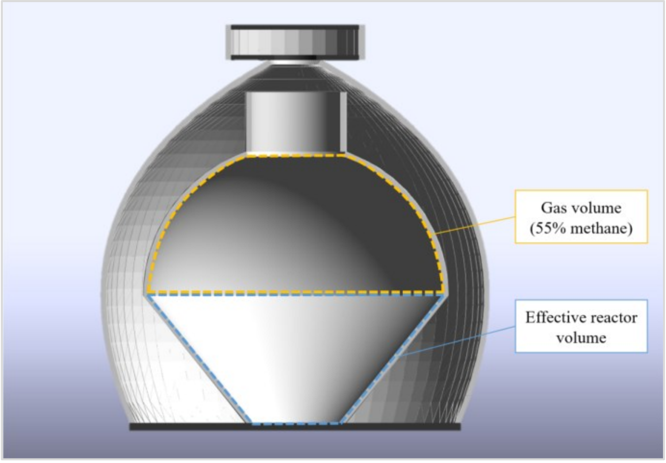

Figure 5: BIM model of the anaerobic digestion reactor

```
...
#61= IFCPROCESSSPACELOADADR(
      'Load for standard operation',    /* Name                        */
      .WET.,                            /* MethodOfDigestion           */
      .CONTINUOUS.,                     /* ModeOfOperation             */
      .SUSPENDED.,                      /* TypeOfReactor               */
      37.0,                             /* ProcessTemperature          */
      10.0,                             /* SubstrateInputStream        */
      30.0,                             /* MeanResidenceTime           */
      ...
      12.0,                             /* DissolvedOxgenConcentration */
      115.0,                            /* ChemicalOxygenDemand        */
      5.0                               /* LoadingRatePerUnitVolume    */
      );
...
#85= IFCPROCESSSPACERESULTADR(
      'Results  for standard operation'/* Name                        */
      340.0,                            /* EffectiveReactorVolume      */
      4.5,                              /* DigestateOutputStream       */
      400.0,                            /* DigesterGasFlowRate         */
      0.55,                             /* Methane                     */
      63.0,                             /* OrganicDrySubstance         */
      0.6,                              /* DigesterGasEfficiency       */
      );
```

Listing 1: Extract of the IFC file of the anaerobic digestion reactor, specifying load and sizing result data using the *IfcProcessSpaceLoadADR* and *IfcProcessSpaceResultADR* entities

5. Summary and conclusions

Enabling BIM-based planning of processing facilities, an IFC schema extension supporting sizing of reactors, a crucial task in planning processing facilities, has been presented. The IFC schema extension, designed in compliance with the current IFC schema, has exemplarily been illuminated by means of anaerobic digestion reactors in biogas plants. As a result, planning processing facilities is advanced through enhanced data exchange between planners while reducing errors and costs. The IFC schema extension has been implemented as a generic approach that may be applied to sizing of further types of reactors with other input and output parameters. As has been demonstrated in the validation of the IFC schema extension, the extension may be used as basis for BIM-based simulations of process facilities.

Acknowledgments

The authors would like to acknowledge the financial support of the German Federal Ministry of Education and Research (BMBF) through grant FKZ 01IS17007C. This work has also been partially supported by the German Research Foundation (DFG) under grant SM 281/7-1, which is gratefully acknowledged. Any opinions, findings, conclusions, or recommendations expressed in this paper are those of the authors and do not necessarily reflect the views of the sponsors.

References

ATV-DVWK, (2003). Merkblatt ATV-DVWK-M 372: Technische Rahmenbedingungen für die Vergärung von Abfällen [Technical requirements for the fermentation of waste]. Hennef, Germany: DWA.

Batstone, D. J., et al., (2002). The IWA Anaerobic Digestion Model No 1 (ADM1). Water Science and Technology, 45(10), pp. 65–73.

Bock, B., & Michaelis, E., (2019). Building Information Modeling in der Abwasserableitung mit openBIM [Building Information Modeling in wastewater treatment with openBIM]. Wasser und Abfall, 21(5), pp. 36–42.

Borrmann, A., et al., (2019). The IFC-Bridge project – Extending the IFC standard to enable high-quality exchange of bridge information models. In: Proceedings of the 2019 European Conference for Computing in Construction. Chania, Greece, July 10, 2019.

buildingSMART, (2017). Industry Foundation Classes 4.0.2.1, Version 4.0 - Addendum 2 - Technical Corrigendum 1. Retrieved January 2, 2020 at: https://standards.buildingsmart.org/IFC/RELEASE/IFC4/ADD2_TC1/HTML/.

buildingSMART, (2018). IFC Overview Summary. Retrieved March 25, 2018 at: http://www.buildingsmart-tech.org/specifications/ifc-overview.

DWA, (2000). Standard ATV-DVWK-A 131E: Dimensioning of Single-Stage Activated Sludge Plants. Hennef, Germany: DWA.

DWA, (2009). Merkblatt DWA-M 380: Co-Vergärung in kommunalen Klärschlammfaulbehältern, Abfallvergärungsanlagen und landwirtschaftlichen Biogasanlagen [Co-digestion in municipal sludge digesters, waste fermentation plants and agricultural biogas plants]. Hennef, Germany: DWA.

DWA, (2010). Merkblatt DWA-M 363: Herkunft, Aufbereitung und Verwertung von Biogasen [Origin, Treatment and Utilisation of Biogases]. Hennef, Germany: DWA.

Garcia-Heras, J. L., (2003). Reactor sizing, process kinetics and modelling of anaerobic digestion of complex wastes. In: Mata-Alvarez, J. (ed.). Biomethanization of the Organic Fraction of Municipal Solid Wastes. London, UK: IWA Publishing, pp. 21–62.

Laakso, M. & Kiviniemi, A., (2012). The IFC standard: A review of history, development, and standardization, information technology. Journal of Information Technology in Construction, 17(2012), pp. 135–161.

Mata-Alvarez, J., (2003). Fundamentals of the anaerobic digestion process. In: Mata-Alvarez, J. (ed.) Biomethanization of the Organic Fraction of Municipal Solid Wastes. London, UK: IWA Publishing London, pp. 1-20.

Paterson, M., et al., (2015). Realisierung einer Biogas-Kleinanlage Ein Handbuch für Landwirte [Realisation of a small biogas plant - A manual for farmers]. Darmstadt, Germany: Kuratorium für Technik und Bauwesen in der Landwirtschaft e.V. (KTBL).

Renn, O. & Marshall, J. P., (2016). Coal, nuclear and renewable energy policies in Germany: From the 1950s to the ‘Energiewende’. Energy Policy, 99(2016), pp. 224–232.

Söbke, H., Theiler, M., Tauscher, E. & Smarsly, K., (2018). BIM-based description of wastewater treatment plants. In: Proceedings of the 17th International Conference on Computing in Civil and Building Engineering. Tampere, Finland, June 5, 2018.

Tay, S. I., Lee, T. C., Hamid, N. Z. A., & Ahmad, A. N. A., (2018). An overview of Industry 4.0: Definition, components, and government initiatives. Journal of Advanced Research in Dynamical and Control Systems, 10(14), 1379–1387.

VDI, (2006). VDI 4630: Fermentation of organic materials: Characterization of the substrate, sampling, collection of material data, fermentation tests. Düsseldorf, Germany: VDI.

Weinrich, S., Schäfer, F., Bochmann, G. & Liebetrau, J., (2018). Value of batch tests for biogas potential analysis: Methods comparison and challenges of substrate and efficiency evaluation of biogas plants. In: Murphy, J. D. (ed.). IEA Bioenergy Task 37, (2018:10). Retrieved January 2, 2020 at: http://task37.ieabioenergy.com/files/daten-redaktion/download/Technical%20Brochures/Batch_tests_web_END.pdf

From point cloud to IFC: A masonry arch bridge case study

Ana Sánchez-Rodríguez [1], Sebastian Esser [2], Jimmy Abualdenien [2], André Borrmann [2], Belén Riveiro [1]
[1] Department of Materials Engineering, Applied Mechanics and Construction, School of Industrial Engineering, University of Vigo, Spain
[2] Chair of Computational Modelling and Simulation, Technical University of Munich, Germany
anasanchez@uvigo.es

Abstract. For the last several years, laser scanning has become one of the reference technologies when talking about the monitoring of assets. Nowadays, the trend is to use these data for creating semantically rich three-dimensional (3D) models, broadly known as digital twins. The bottleneck appears when processing the large amount of data acquired with the laser scanner. This paper tackles the creation of IFC data models using classified point cloud data. The point labelling methodology is based on one in the state-of-the-art, whose results have been improved. Then, each group of points is converted to a triangulated mesh, and the resultant geometrical objects are placed in an IFC-based model in a low and high level of detail. Moreover, the resultant IFC model allows the enrichment of the captured geometry with additional information.

1. Introduction

The modern society is increasingly dependent on digital representations of the environment. Since the majority of the assets are already built, there are usually no digital as-built representations of them available. Assets are likely to change during their life cycle due to deterioration caused by impacts or sudden events. Therefore, digital representations should represent assets during their entire lifecycle, from design to their end-of-life, so that periodic maintenance and analysis can be performed in order to evaluate their behaviour.

The digital replica of the real-world data is known as digital twin (El Saddik, 2018). This "twin" should contain not only 3D geometrical data, but also semantically rich information representing the characteristics associated with the asset (materials, safety, occupancy, relations between components, etc.). A digital twin (DT) of the infrastructure will ensure its normal functionality and operation, being able to detect changes in its condition due to the constant update of its information. This will decrease the disruption of service, the risk to which the end-users are subjected to, and costs savings for the infrastructures owners as a consequence of the previous (Lu and Brilakis, 2019a). It is important to highlight that the characteristics of DTs will depend a lot on their purpose, so a DT can have different levels of detail (LoD): from non-geometrical representation, to two dimensional (2D) geometry, or 3D data models (i.e. plans, B-reps, point clouds). In some cases, the geometry of the DT will not be required, being uniquely dependent on the semantic information. This calls for linked data approaches so that the needed information is easily available, accessible, and properly organised. One example of linking information could be the use of ontologies, useful for data hierarchies (Beetz, 2018).

Although the creation of DT during the design phase of an infrastructure is broadly extended, it is not the case during the rest of its life cycle. This is motivated by the resource consumption of this task in comparison with doing it the traditional way. This is where LiDAR technology comes into place. Point clouds provide geometrical information about the environment where the survey was performed, but it is not enough. This information needs to be processed and interpreted so that it can be used in a BIM (Building Information Modelling) model or as a DT. The paper aims to demonstrate a full toolchain from the capturing process to the validation of the IFC (industry foundation classes) data format. The proposed workflow shows the capability of IFC to store not only design data but also the results of processed point clouds. The definition of end-user requirements (EURs) for digital twins is not a defined task for this paper. Lu and Brilakis (2019b) prepared the fundamental information that a DT should contain in the form of six EURs. The present work has been developed in order to fulfil these requirements.

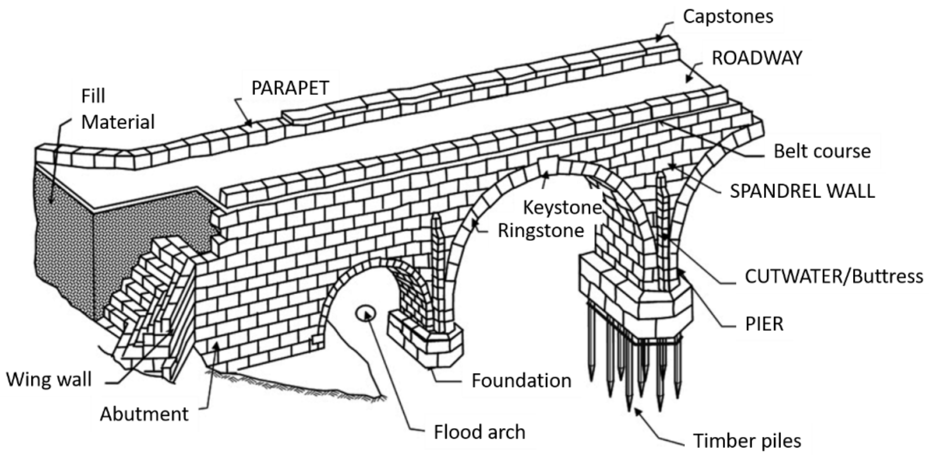

Figure 1: Main components of a masonry arch bridge (Ural *et al.*, 2008)

The bridge under study is to be divided into six different elements: spandrel walls, vaults, piers, cutwaters, roadway and parapet (Figure 1). The present article is divided as follows: Section 2 summarizes the state of the art in relation with the field of research; Section 3 introduces IFC as one of the most frequently used data structures for BIM processes; Section 4 describes the methodology developed from the point cloud classification to the IFC instance model creation; the results are presented in Section 5; and, finally, a summary of the conclusions extracted from this work is exposed (Section 6).

2. Literature Review

Point clouds acquisition can be performed using aerial laser scanning (ALS), mobile laser scanning (MLS), or terrestrial laser scanning (TLS) systems. Depending on the use of the point clouds in a later step, a different system is to be used. In this relation, Soilán *et al.* (2019) presented a review with the most relevant laser scanning technologies available in the market and their applications regarding transport infrastructures. Since the present work is focused on masonry arch bridges, the better approach is to use TLS systems to perform the survey. They usually work mounted on a stand or tripod and obtain high-resolution scans in a short period of time (in a range of minutes) (Olsen *et al.*, 2010).

In order to create a 3D data model of an asset using a point cloud, a first classification of points is needed so that the elements forming the asset are grouped. Over the years and thanks to the evolution of technology, numerous works concerning the automatic or semi-automatic classification of point clouds started to arise. When specifically talking about arch bridges, Walsh *et al.* (2013) started classifying points into different structural elements using laboratory specimens and testing real bridges. Later on, Riveiro, DeJong and Conde (2016) developed a methodology for automatically segment their structural elements. Concerning the inspection of masonry arch bridges, Sánchez-Rodríguez *et al.* (2018) showed an automatic processing method for laser scanning data in order to detect faults in their piers. The current trend for point cloud classification is to use algorithms that automatically predict the class of a point based on learning algorithms. Barrile, Candela and Fotia (2019) worked with an aerial survey of a concrete viaduct in order to apply photogrammetric reconstruction to classify the structural elements of the asset. They applied image analysis techniques and used the Mask-RCNN (Region-Based Convolutional Neural Network) (He *et al.*, 2017) to perform this classification.

After processing the point cloud data, the next step would be to create a 3D data model of the structure using that information. In this paper, the standard IFC is to be used. There are already some works developed in this respect. Ma *et al.* (2018) manually prepared the 3D model using Revit, tracing the points in the cloud. Later, a pipeline for going from point clouds to IFC models was presented in (Zhao and Vela, 2019). They detect and classify objects using a machine learning approach and then, each individual element is parametrized to create the IFC objects. Lu and Brilakis (2019a) created a method for creating DTs of reinforced concrete bridges from already labelled point clusters. Those clusters are sliced and projected to the XY-plane in order to fit a 2D ConcaveHull α-shape. The obtained contour is then transformed to 2D Cartesian points (*IfcCartesianPoint*) to create the IFC instances.

Another approach for the point cloud-to-IFC conversion is to make use of the (3D) laser scanning data reconstructing the geometric surfaces needed to produce a mesh. Numerous methods have been proposed to tackle this problem. Most commonly, the variational methods (Zhao *et al.*, 2000), tensor voting (Medioni, Lee and Tang, 2000), implicit surface (Hoppe *et al.*, 1994), and Delaunay triangulations (Cohen-Steiner and Da, 2004). Delaunay triangulations are greedy algorithms that reconstruct the surface as a result of the union of sequentially selected triangles. Such algorithms start with a seed triangle, and then the triangulated surface incrementally grows by using the previously selected triangles to select a new triangle for advancing the front. The idea presented in this paper is that IFC provides geometric representations within its geometry resources to store meshes like the created ones.

This paper examines whether and to what extent bridges can be better described using the latest schema extension proposal IFC4x2. Thus, a framework was developed which converts the captured geometries into an IFC4x2 based instance model. During the processing, two LoDs were considered to make the resulting model lightweight and easy to consume in various use case scenarios. Moreover, the models are enriched with semantic information that was extracted during the segmentation and processing of the point cloud.

3. Data Formats for Digital Twins

The way in which information is stored, exchanged, and shared between different parties in a project needs to be standardized. The use of data models ensures it's the success of data exchange processes, with information encoded using a specific data model. For the use of BIM models or DTs, they have to meet specific geometric and semantic requirements, which have been defined exemplarily by the BIM4INFRA2020 project (BIM4INFRA2020, 2018). Data models can provide geometric and semantic information or only geometric content. DXF and OBJ can be considered as the most representative ones when talking about geometric data models (Autodesk, 2017; Wavefront, 2019). Since in this work semantic information is also used, IFC2x3, IFC4, IFC4x1, IFC4x2 and CityGML should be the ones coming into place (buildingSMART International Alliance for Interoperability, 2007; buildingSMART International, 2018). In this work, IFC 4x2 is the data model to be used since it covers requirements for detailed geometric representations paired with specific product classifications for each component. This will avoid the need for re-implement a way of combining geometry with semantics in a formal way.

The IFC data model was initially designed to transfer digital models of buildings. Since the interest in BIM technology is constantly increasing during the last years, the international non-profit organization buildingSMART International (bSI) decided to extend the IFC data model for civil infrastructure assets. The first initiatives in this regard were the IfcAlignment project (buildingSMART International, 2018) and the IFC Overall Architecture report (Borrmann *et al.*, 2017). Upon these projects, the IfcBridge extension project has added new classes and types to enable a more detailed description of bridge structures. The final deliverables include a comprehensive requirements analysis as well as a schema extension proposal (Borrmann *et al.*, 2019). Besides IfcBridge, several other projects like IfcRoad, IfcPortsAndWaterways, and IfcTunnel are conducted inside the Infra room, which is a subsection of bSI. Additionally, the IfcRail project (located inside the RailwayRoom) proposed a schema extension for railbounded traffic. It is ongoing work to harmonize all proposals among the individual projects to deliver a harmonized infra extension in the end. This deliverable will most likely build the base for the next major release IFC5.

Even though the toolchain discussed in this paper was not in the primary scope of the IfcBridge extension project, data exchange scenarios of processed point cloud information can be realized using IFC classes.

4. Methodology

The methodology presented in this paper is in charge of creating IFC instance models in order to store bridge models created out of a laser scan. It is divided into three parts: (i) point cloud classification; (ii) point cloud-to-mesh conversion; and (iii) generation of the IFC model.

4.1 Point Cloud Classification

The point cloud classification methodology follows the steps previously stated in Riveiro, DeJong and Conde (2016), where a methodology for the segmentation of masonry arch bridges from TLS datasets was presented. In the present work, this method has been modified in order to improve the performance of the algorithms, as presented in Figure 2.

The method starts with a masonry arch bridge point cloud, already aligned and prepared for its processing. This point cloud $B = (x, y, z, I)$, is formed by the 3D spatial coordinates (x, y, z), and the reflected laser pulse intensity, I. In this case, only the geometrical information is to be used. The point cloud is oriented to the y coordinate axis, resulting $B_r = (x, y, z)$ applying principal component analysis (PCA), and taking the first component as basis to perform the rotation (Gressin *et al.*, 2013). Next step is to distinguish between points forming vertical and non-vertical elements. This is done calculating the elevation angle histogram of the points cloud, in which two main peaks are present. The points are thus classified in two classes: vertical elements $V = (x, y, z) \epsilon B_r$ and non-vertical elements $N = (x, y, z) \epsilon B_r$.

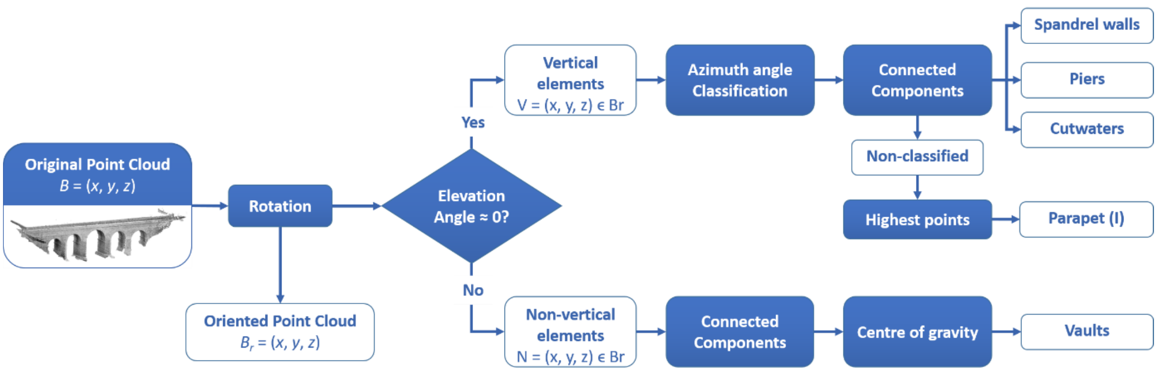

Figure 2: Proposed classification workflow

Working with the point cloud containing vertical bridge elements, *V*, a first classification based on the azimuth angle of each point is performed. As before, this angle was computed in a neighbourhood of 0.25 m. Then, a *k-means* clustering (Lloyd, 1982) is applied to the data, dividing the point cloud into four main classes: possible spandrel walls, possible piers, possible cutwaters, and non-classified points. Each of these new sections is specifically analysed so that the wrongly classified points are reclassified. A connected components detection algorithm is applied for this matter. Points belonging to the parapet of the bridge are present in both the vertical and non-vertical elements point cloud. In both classes, the parapet is detected as the highest points in the cloud.

Lastly, from the point cloud of non-vertical elements, points forming vaults are detected applying a connected components detection algorithm, and each individual one is isolated thanks to their center of gravity.

4.2 Point cloud-to-Mesh Conversion

Once the point cloud is segmented, multiple steps are performed to reconstruct the final mesh (as illustrated in Figure 3). First, each segment is preprocessed by omitting noise. Here the points are sorted in an increasing order of the average squared distance to their nearest neighbors, and the points with the largest value are deleted. The reconstructed mesh could be used for multiple different purposes, including performing simulations and renovation. Thereby, in some cases, a highly detailed or a coarse representation could fit more to the intended purpose.

Based on the purpose, a level of detail (Trimble, 2013) is selected. Accordingly, capturing reality (LoD 500), focuses first on reconstructing the outer surface of the geometric features by approximating its shape. Once the surface is reconstructed, an additional step is required to fill any remaining gaps / holes. These holes could result due to scanning or processing issues, which are hard to completely avoid, like because of defects in the scanning process or inaccuracies in the segmentation or noise omitting algorithms. On the other hand, selecting a low LoD requires much less processing as only rough placeholders that represent the overall dimensions are required. In this regard, based on the convex hull (Barber, Dobkin and Huhdanpaa, 1996) of each segment, a triangulated mesh, which does not suffer from any holes, is generated.

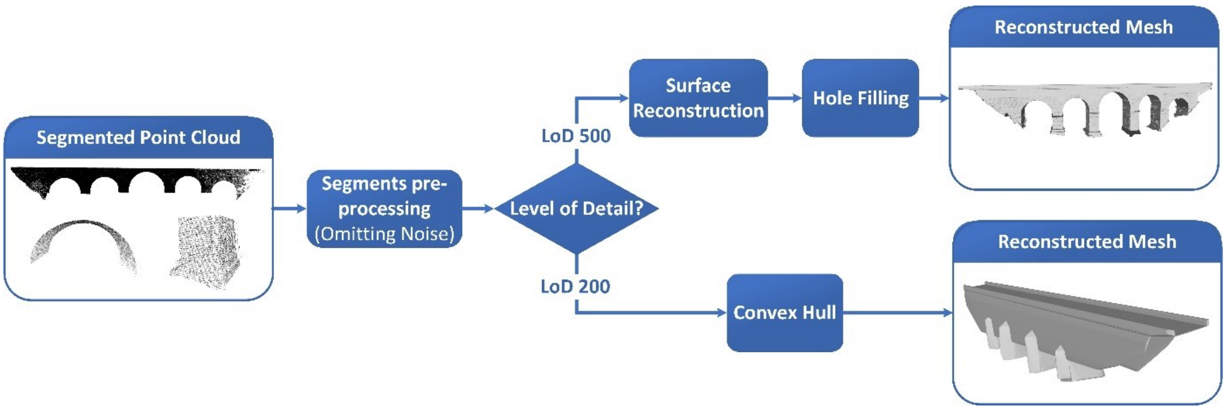

Figure 3: Proposed framework for transforming point cloud segments to 3D mesh. The framework provides two approaches, one for reconstructing surfaces with high details, and another for generating a coarse representation of each segment

4.3 Generation of the IFC Model

The IFC data model provides huge flexibility to model use-case specific requirements. An example of this is the flexibility to assign the best-fitting geometry representation for a given source geometry. Product representations can be modeled by using explicit or implicit (i.e. procedural) geometries. Besides, a huge advantage of IFC compared to other data models is the opportunity to represent several levels of details using the same data standard. This makes the results easier to consume in a variety of existing tools since IFC is widely adopted in the AEC (Architecture, Engineering, and Construction) market. The generation of the IFC instance model containing the captured bridge is done by a console app written on top of the IFC framework XBIM (Lockley, 2007). It creates a basic spatial structure typically used for bridges which splits the construction into logical parts (e.g., superstructure, substructure, foundation). Several products are assigned to these logical containers afterwards. A simple JSON-based dictionary enables the engineer to assign the segmented geometries to a suitable *IfcProduct* class.

The computed meshes are stored as instances of the class *IfcTriangulatedFaceSet* and linked to instances that are derived from *IfcProduct*.

5. Results

5.1 Case Study

The bridge selected to validate the presented process is a masonry arch bridge. It is the roman bridge of Segura, located on the border of Portugal and Spain and crossing the river Erjas. The bridge is used to communicate the provinces of Castelo Branco (Portugal) and Cáceres (Spain) by a national road (Durán, 1996). This bridge has been selected since it has already been studied in previous works (Arias *et al.*, 2010; Riveiro, DeJong and Conde, 2016).

Data Acquisition. Each survey has to be planned according to the needs given by the structure to be scanned and its environment. In this case, the survey is done in an outdoors environment, and so the meteorological conditions have also to be considered. The point cloud acquisition was performed using the TLS Riegl LMS-Z390i (*RIEGL*, 2020). The operations of recording point clouds with this RIEGL scanner were controlled with Riscan PRO Software (Riegl©). In order to perform the survey leaving as less non-scanned bridge parts as possible, the scans were taken from seven different positions from which a different point cloud was obtained. These were aligned thanks to the use of reflective targets placed over several planes in the surroundings of the structure. For the case of this paper, the point cloud was reused from a previous survey, which is described more in detail in (Arias *et al.*, 2010). The obtained point cloud is formed by 1,259,148 points.

Ground Truth Preparation. The ground truth used to compare the point cloud classification has been obtained using the software *CloudCompare* (v2.10.2) (*CloudComapre*, 2020), in order to manually segment the point cloud into seven different classes of points: roadway, parapet, spandrel walls, vaults, piers, cutwaters, and non-classified points.

5.2 Point Cloud Classification

The classification of points in masonry arch bridges point clouds has been proven as valid in a previous work by Riveiro, DeJong and Conde (2016). That methodology has been modified for this work in order to improve its performance. The dataset described in Section 5.1 is used to prove the validity of the classification methods proposed. This point cloud is segmented in seven categories depending on their geometrical characteristics, as exposed in Section 4.1. An overview of the results is presented in Figure 4. Figure 4(a) and (c) show the original point cloud (upstream and downstream, respectively), while in Figure 4(b) and (d), points are depicted with different colours depending on their specific group.

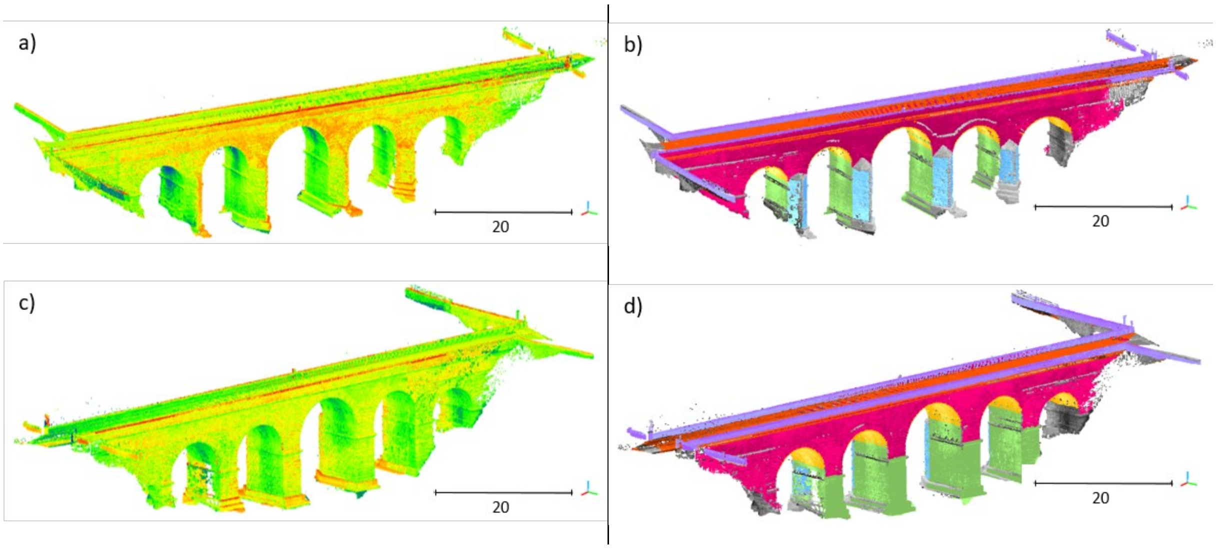

Figure 4: Original point cloud upstream (a) and downstream (c) compared with the classification results: roadway (orange), parapet (lilac), spandrel walls (magenta), vaults (yellow), piers (green) and cutwaters (blue)

The results obtained with this new methodology are compared quantitatively with the previously labelled ground truth. The same is done with the ones obtained by Riveiro, DeJong and Conde, (2016). The parameters chosen to summarise the performance of each method are the precision, recall, and F-Score metrics. The methodology developed for this work shows better results than the previous one presented in (Riveiro, DeJong and Conde, 2016).

Table 1: Performance metrics

Element	**Precision**	**Recall**	**F-Score**	**Precision**	**Recall**	**F-Score**
	Previous methodology			**New methodology**		
Spandrel walls	0.7694	0.1996	0.3170	0.8711	0.8956	0.8832
Vaults	0.9685	0.1147	0.2050	0.9452	0.7240	0.8199
Piers	0.7786	0.7563	0.7673	0.6794	0.9448	0.7904
Cutwaters	0.2016	0.1784	0.1893	0.9750	0.7444	0.8442
Roadway	0.8348	0.2975	0.4387	0.5427	0.9963	0.7026
Parapet	-	-	-	0.7512	0.6690	0.7078

5.3 Generation of the IFC Model

The model generation was performed by the developed methodology described in Section 4.2 and 4.3. The individual segments (vaults, piers, etc.) were preprocessed and reconstructed in both LoDs, 200 and 500. At the end, all segments are combined to represent the captured bridge as illustrated in Figure 5 and Figure 6. The resultant meshes were efficiently generated, producing models that are lightweight enough (in terms of the number of points per triangulated geometry) to be visualized in the common IFC viewers that support IFC4X2 (like *BIM vision* 2.23 or *FZK Viewer*).

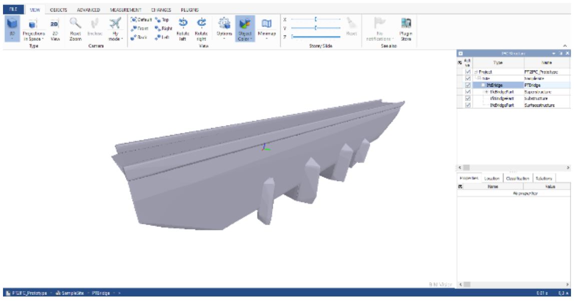

Figure 5: Resulting IFC Model in LoD 200

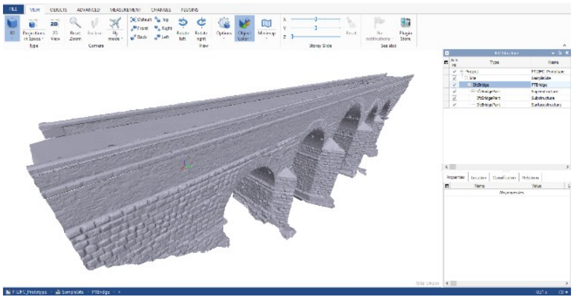

Figure 6: Resulting IFC Model in LoD 500

Additionally, the IFC models were semantically enriched by adding custom property sets to the *IfcProject* and *IfcSite* entities, incorporating the parameters used to capture the point cloud using the laser scanner as well as the parameters used to reconstruct the surfaces. This information enables the receiving engineer to roughly classify the quality of the given model. It is important to have such properties directly assigned to the model to enable a correct interpretation of the given geometry.

6. Conclusion

This paper presents an automatic methodology for transforming classified point clouds into IFC models for further applications. The presented methodology is divided into three main parts: (i) point cloud classification; (ii) point cloud-to-mesh conversion; (iii) mesh-to-IFC conversion. The methodology overcomes the gaps existing in the captured point cloud using advanced geometric reconstruction techniques and maps the segmented assets to the latest IFC schema. Furthermore, the IFC-based result is then ready to get further information attached to it, such as construction materials, structural health monitoring information, etc. This can be considered the first approach to transform masonry arch bridges' point clouds into Digital Twins.

The results presented show a good performance referring to point cloud classification, improving a previously published methodology. In addition, the models created using this information allow to present different level of detail, depending on the purpose of the DT. Finally, it is important to highlight that the end user's requirements are also fulfilled. This work proves that laser scanning systems can be considered as a tool for capturing the as-built environment and creating digital representations of it. Different aspects may be taken into consideration for future work regarding the transformation of point clouds into IFC. The results obtained in the classification of LiDAR data can always be improved. Nowadays, the use of deep learning algorithms is one of the latest trends developed, being in the state of the art for many applications. Progress is under way in the 3D data field, and it is foreseeable that the AI (artificial intelligence) is able of obtaining better results than heuristics for certain applications in the near future. Some works using specialized neural networks (kpconv, PointNet, PointNet++, splatnet, etc.) have already shown good results. Concerning the creation of IFC instance models, other techniques can be used to compare the results in the same datasets. Moreover, different bridge's typologies should be studied in order to prove a broader validity of the developed algorithms.

Acknowledgements

This work has been partially supported by the Spanish Ministry of Science, Innovation and Universities through the project Ref. RTI2018-095893-B-C21. This project has received funding from the European Union's Horizon 2020 research and innovation programme under grant agreement No 769255. This document reflects only the views of the author(s). Neither the Innovation and Networks Executive Agency (INEA) or the European Commission is in any way responsible for any use that may be made of the information it contains.

References

Arias, P. *et al.* (2010) 'Terrestrial Laser Scanning and Non Parametric Methods in Masonry Arches Inspection', *International Archives of Photogrammetry, Remote Sensing and Spatial Information Sciences*, XXXVIII.

Autodesk (2017) *Autodesk Developer Network - DXF Reference*. Available at: https://web.archive.org/web/20171019003526/http://usa.autodesk.com/adsk/servlet/item?id=24240325&siteID=123112 (Accessed: 3 March 2020).

Barber, C. B., Dobkin, D. P. and Huhdanpaa, H. (1996) 'The Quickhull Algorithm for Convex Hulls', *ACM Transactions on Mathematical Software*. doi: 10.1145/235815.235821.

Barrile, V., Candela, G. and Fotia, A. (2019) 'Point cloud segmentation using image processing techniques for structural analysis'. doi: 10.5194/isprs-archives-XLII-2-W11-187-2019.

Beetz, J. (2018) 'Structured Vocabularies in Construction: Classifications, Taxonomies and Ontologies', in *Building Information Modeling*. Aachen: Springer International Publishing, pp. 155–165. doi: 10.1007/978-3-319-92862-3_8.

BIM4INFRA2020 (2018) *Umsetzung des Stufenplans 'Digitales Planen und Bauen' AP 1.2 'Szenariendefinition' und AP 1.3 'Empfehlung'*. Available at: https://bim4infra.de/wp-content/uploads/2018/09/AP1.2-AP1.3_BIM4INFRA_Bericht-Stufenplan.pdf (Accessed: 3 March 2020).

Borrmann, A. *et al.* (2017) *IFC Infra Overall Architecture Project Documentation and Guidelines*, *buildingSMART*.

Borrmann, A. *et al.* (2019) 'The IFC-Bridge project – Extending the IFC standard to enable high-quality exchange of bridge information models', *Proceedings of the 2019 European Conference for Computing in Construction*, 1(July), pp. 377–386. doi: 10.35490/ec3.2019.193.

buildingSMART International (2018) *Industry Foundation Classes - Version 4.1.0.0*. Available at: https://standards.buildingsmart.org/IFC/RELEASE/IFC4_1/FINAL/HTML/ (Accessed: 26 February 2020).

buildingSMART International Alliance for Interoperability (2007) *IFC 2x3*. Available at: https://standards.buildingsmart.org/IFC/RELEASE/IFC2x3/TC1/HTML/.

CloudComapre (2020). Available at: https://www.cloudcompare.org/.

Cohen-Steiner, D. and Da, F. (2004) 'A greedy Delaunay-based surface reconstruction algorithm', *Visual Computer*. doi: 10.1007/s00371-003-0217-z.

Durán, M. (1996) 'Puentes Romanos Peninsulares: Tipología y Construcción', in *Actas del I Congreso Nacional de Historia de la Construcción*. Madrid.

Gressin, A. *et al.* (2013) 'Towards 3D lidar point cloud registration improvement using optimal neighborhood knowledge', *ISPRS Journal of Photogrammetry and Remote Sensing*, 79, pp. 240–251. doi:10.1016/j.isprsjprs.2013.02.019.

He, K. *et al.* (2017) 'Mask R-CNN', *Proceedings of the IEEE International Conference on Computer Vision*, pp. 2980–2988. doi: 10.1109/TPAMI.2018.2844175.

Hoppe, H. *et al.* (1994) 'Piecewise smooth surface reconstruction', in *Proceedings of the 21st Annual Conference on Computer Graphics and Interactive Techniques, SIGGRAPH 1994*. doi: 10.1145/192161.192233.

Lloyd, S. P. (1982) 'Least Squares Quantization in PCM', *IEEE Transactions on Information Theory*. doi:10.1109/TIT.1982.1056489.

Lockley, S. (2007) *xBIM Toolkit*. Available at: https://docs.xbim.net/index.html (Accessed: 29 November 2019).

Lu, R. and Brilakis, I. (2019a) 'Digital twinning of existing reinforced concrete bridges from labelled point clusters', *Automation in Construction*. Elsevier, 105(February), p. 102837. doi: 10.1016/j.autcon.2019.102837.

Lu, R. and Brilakis, I. (2019b) 'Generating bridge geometric digital twins from point clouds', *Proceedings of the*

2019 European Conference for Computing in Construction, 1, pp. 367–376. doi: 10.35490/ec3.2019.182.

Ma, L. *et al.* (2018) '3D Object Classification Using Geometric Features and Pairwise Relationships', *Computer-Aided Civil and Infrastructure Engineering*. Blackwell Publishing Inc., 33(2), pp. 152–164. doi:10.1111/mice.12336.

Medioni, G., Lee, M. and Tang, C. (2000) *A Computational Framework for Segmentation and Grouping*, *A Computational Framework for Segmentation and Grouping*. Elsevier Science. doi: 10.1016/B978-0-444-50353-4.X5000-8.

Olsen, M. J. *et al.* (2010) 'terrestrial Laser Scanned-Based Structural Damage Assessment'.

RIEGL (2020) *RIEGL, Laser Measurement Systems GmbH*.

Riveiro, B., DeJong, M. and Conde, B. (2016) 'Automated processing of large point clouds for structural health monitoring of masonry arch bridges', *Automation in Construction*. Elsevier B.V., 72, pp. 258–268. doi:10.1016/j.autcon.2016.02.009.

El Saddik, A. (2018) 'Digital Twins: The Convergence of Multimedia Technologies', *IEEE Multimedia*. IEEE Computer Society, 25(2), pp. 87–92. doi: 10.1109/MMUL.2018.023121167.

Sánchez-Rodríguez, A. *et al.* (2018) 'Detection of structural faults in piers of masonry arch bridges through automated processing of laser scanning data', *Structural Control and Health Monitoring*, 25(3), p. e2126. doi:10.1002/stc.2126.

Soilán, M. *et al.* (2019) 'Review of Laser Scanning Technologies and Their Applications for Road and Railway Infrastructure Monitoring', *Infrastructures*, 4(58).

Trimble (2013) *Project Progression Planning with MPS 3.0*. Available at: http://support.vicosoftware.com/FlareFiles/Content/KB/Trimble - Progression Planning V15.pdf.

Ural, A. *et al.* (2008) 'Turkish historical arch bridges and their deteriorations and failures', *Engineering Failure Analysis*. Pergamon, 15(1–2), pp. 43–53. doi: 10.1016/j.engfailanal.2007.01.006.

Walsh, S. B. *et al.* (2013) 'Data Processing of Point Clouds for Object Detection for Structural Engineering Applications', *Computer-Aided Civil and Infrastructure Engineering*. Wiley/Blackwell (10.1111), 28(7), pp.495–508. doi: 10.1111/mice.12016.

Wavefront (2019) *B1. Object Files (.obj)*.

Zhao, H. K. *et al.* (2000) 'Implicit and nonparametric shape reconstruction from unorganized data using a variational level set method', *Computer Vision and Image Understanding*. doi: 10.1006/cviu.2000.0875.

Zhao, Y.-P. and Vela, P. A. (2019) 'Scan2BrIM: IFC Model Generation of Concrete Bridges from Point Clouds', in *Computing in Civil Engineering 2019*. Reston, VA: American Society of Civil Engineers, pp. 455–463. doi:10.1061/9780784482421.058.

From Terrestrial Laser Scans to a Surface Model of a Building; Proof of Concept in 2D

Enrico Romanschek[1], Christian Clemen[1], Wolfgang Huhnt[2]
[1]HTW Dresden,
[2]TU Berlin, Germany
enrico.romanschek@htw-dresden.de

Abstract. A method for obtaining complete, gapless and non-intersecting two-dimensional surface models from the data of the terrestrial laser scanners (TLS) is presented. Terrestrial laser scanners offer the possibility to measure exact recordings of spatial situations at a specific point in time. The goal of numerous research projects is to detect building components in a point cloud using automated procedures and to aggregate them to a building model. We present an approach that uses the topology and information from the measurement of the original observation data (TLS) and provides as object description a complete, gapless and non-overlapping decomposition of the observation area. Round off errors are avoided because we use integer values as coordinates for all measured points and an exact approach to compute intersection points using rational numbers. The proposed paper presents essential steps and findings for problems in the two-dimensional space.

1. Introduction

Our assumption is that a complete spatial decomposition (in contrast to pure object modeling) opens up numerous and novel spatial analysis options. The main feature of our method is the complete modelling of the area covered (Kraft, 2016, p. 81). This means that not only the solid objects are modelled by a boundary representation (B-Rep), but also the empty space. Thus, there are no gaps in the model and each object in the model knows its neighborhood.

A precondition for these possibilities is exact computation, because numerous intersections have to be calculated: 3D objects (usually components) and the empty space touch and penetrate each other. When designing the algorithm, we tried to avoid purely geometrical calculations (e.g. intersection) and replaced them with topological data structures. This also enables fast and clear navigation through the modeled elements and the empty space in-between objects. Our method uses integer coordinates, so all topological queries to the model are unambiguous and respond with an exact geometry, similar to (Sugihara and Iri, 1990). The generation of the integer coordinates is done at the beginning of the algorithm with respect to the accuracy of the measured points; this guarantees that there are no ambiguities in the model already during the algorithm when establishing the topological relations. The advantages of integer computations in geometry were already described in (Fortune and van Wyk, 1996) or (Shewchuk 1997).

The methodological foundation of our approach was described in (Huhnt, 2018). Based on this, the presented algorithm in this paper extends the approach algorithmically and relates it to the use case "Surveying with TLS". We hope that this approach is practically important when generating building models (Scan-to-BIM) and building progress control (Scan-vs-BIM). A key feature of our approach is a basic topological data structure that represents the complete, gapless and non-intersecting space by including surfaces from the TLS data. The presented method serves as a basis for building models, but it is also adaptable for other applications with linear or planar boundaries, such as cadastral maps in Geographic Information Systems.

Topology plays a decisive role not only in space decomposition. We use the additional information "laser scanner stands in empty space". From this, two semantic properties, describing the substance of the space, can be derived: "solid" for the areas where the laser of the TLS is reflected, and "no solid" for the areas where the laser can penetrate. Since there are also areas that are not detected, these areas get the substance property "indeterminate".

This paper describes research that is in progress. We simplified the point clouds from 3D, using only detected 2D-segments, which are projected onto a horizontal plane. For simplification, we also set the instrumental center-points (tilt and turning axis of the scanner) of all scans to the same height. The methodical expansion of our approach to the three-dimensional space will be investigated in further research.

2. Motivation and Related Work

There are numerous research projects on the object reconstruction in a point cloud using automated methods (Weinmann, 2016) (Tang et al, 2010). The entirety of the identified components (walls, doors ...) then forms a building model. In general, a boundary representation (B-Rep) is chosen as the geometric representation type, since solids are measured on their outer surfaces. The challenge of these approaches is that complex and numerically error-prone geometric analyses are required to detect overlapping components. It is also common practice to work with preprocessed and unified point clouds of all TLS scan positions. Most of the relevant research approaches have in common that they are restricted to a specific geometry such as rectangular or vertical components, or they require specific user input and are semi-automated. There are approaches with similarities to our research. We focus in this literature review specifically on these approaches. However, we found that none of these approaches works with exact geometry and integer coordinates.

We work with line segments and plane patches that are generated directly from the non-unified point clouds of each scan. A similar technique is presented in (Mura et al, 2014). However, not all detected plane patches are processed there, but only the vertical ones, which are later, used to detect walls. Also, the procedure of (Xiong et al, 2013) works with plane patches. Contrary to our approach, the patches are created in the unified point cloud of voxels and they are directly intersected after a classification according to building components.

An approach for automatic semantic structuring of point clouds is described in (Ochmann et al, 2014) and extended to full building models in (Ochmann et al, 2016). Here they work with the unified point cloud, but additionally calculate the surface normal of the points, whose orientation is corrected by the TLS-view point positions. Using this information, the point cloud is segmented into the individual rooms. After that they generate the walls and openings of the building structure. This approach is similar to the first steps in our algorithm.

A generation of models from mobile scanning data shows (Turner et al, 2015). They consider the empty space between the scanner and surfaces of objects. Their procedure is based on voxels that are classified as inside and outside and then be used for subsequent model generation. However, this approach focuses on visualization, simulation and navigation. It is not intended for precise engineering needed for as-built models.

A method for automatic model reconstruction is presented in the work of (Budroni, 2013). The method presented there uses, in contrast to our approach, the unified point cloud and assumes a space decomposition, also known as Manhattan-World, which assumes that walls and ceilings are perpendicular to each other. The structure of the building is captured with sweep planes and then a building model is generated. Our approach work without this basic assumption of a Manhattan-World, because we use the information of the TLS point position and from which TLS-view point a point was measured.

3. The Algorithm

The algorithm is broken down into twelve steps building up on each other. The steps are described in the twelve subsections of this section.

3.1 Point Cloud Registration

TLS (Terrestrial Laser Scanner) or in general Lidar (Light Detection and Ranging) are instruments that scan their surroundings with a laser (Lemmens, 2011). If the laser hits a surface and is reflected, the distance and direction to this point can be determined (see Figure 1a,b). From the polar measurement values, two or three-dimensional Cartesian coordinates are calculated and stored, depending on the system. The many coordinates of a scan form a point cloud with the sensor centre as the coordinate origin. The point cloud approximately describes the discretized course and structure of the reflecting surface (Figure 1b). Since the coordinates are calculated from measured values, they have deviations from the actual positions of the reflected points, so they cannot be considered as error-free. This fact must be taken into account when evaluating the data generated by this algorithm.

For evaluation, all local point clouds must be transformed into a common coordinate system but are processed individually. The transformation will not be discussed in detail here, as it depends on the capturing device and process; and there are existing software solutions for this (technet, 2020) and (Faro, 2019).

3.2 Segment Detection

The second step checks whether adjacent points of a single point cloud lie on a straight line up to a maximum distance to be defined. If this is the case, a line segment is created over these points along the adjusted line (see Figure 1c).

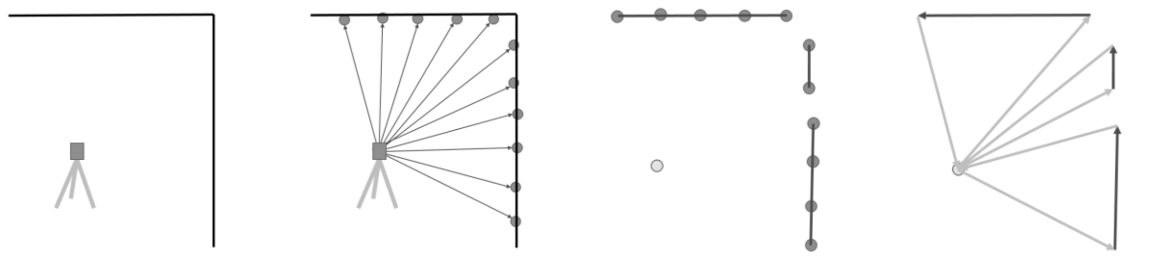

a) TLS in Room b) Capture c) Segment Detection d) Sector Formation

Figure 1: From Scan to Sector

The goal of this step is to reduce the amount of data and to identify line segments which form the surface of building components. These line segments are essentially necessary in the course of this algorithm as described in the next upcoming steps. The equivalent to line segments in a three-dimensional process would be plane patches, which are created, for example, according to the method of (Gielsdorf, 2009) directly during registration.

3.3 Sector Formation

The area between a scanner position and an associated detected line segment is empty at the time of measurement; otherwise, no measurement of the underlying points would have been possible. Therefore, the triangle of the centre of the scanner and the line segment is also empty and we give it the substance property "no solid". The side of the triangle consisting of the detected line segment is given the additional property of a separating layer between "solid" and "no solid", because the area behind this line segment, seen from the centre of the scanner, must have a different substance property.

Since the triangles describe a section around the scanner's centre point of view, they are called sector triangles in the following. In three dimensions, a pyramid or two tetrahedrons would be created between the scanner position and the plane patch. The detected line segments of a reference point form a group of triangles with the reference point as the common centre (see Figure 1d). Sector triangles are generated for each scanner position and the entirety of the sector triangles, which are present in a common coordinate system after registration, forms the data basis of the further steps (see Figure 2).

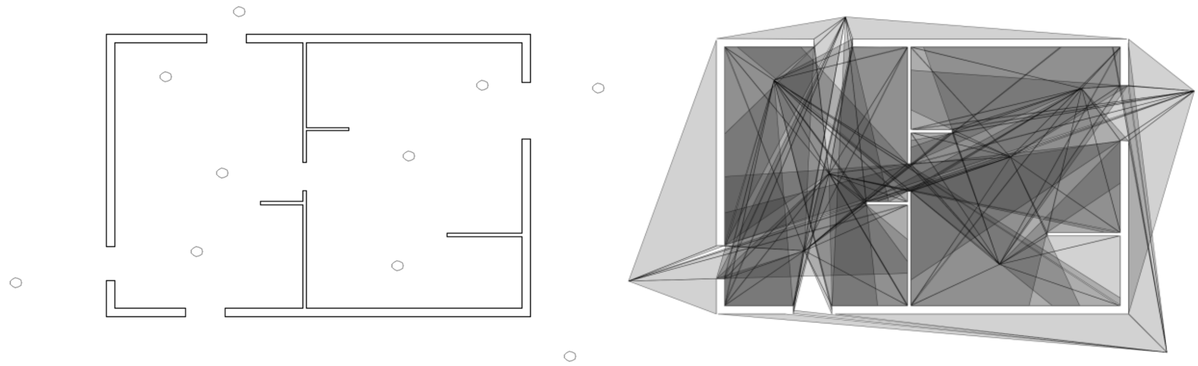

a) Floorplan with Scanner Positions b) Sector Triangles of all Scanner Positions

Figure 2: Floorplan and Generated Sector Triangles

3.4 Integer Coordinates

The algorithm is based on the use of integer coordinates, so the coordinates of the vertices of the sector triangles of floating point numbers must first be converted into integers. For the conversion, first the extent of the minimum enclosing rectangle ($bbox$) of the entire investigation area is determined. As further parameters, the minimum point distance or the positioning accuracy (d_{min}) and the number set of the integer type (n_{max}) must be known. The scaling value (s_{xy}) is either known or can be calculated with equation 1.

$$s_{xy} = \left\lfloor \frac{n_{max}}{max(x_{max_{bbox}} - x_{min_{bbox}}, y_{max_{bbox}} - y_{min_{bbox}})} \right\rfloor \quad (1)$$

If the inequality in equation 2 is not fulfilled or the scaling value is zero, the number range of the integer type is not sufficient for the desired positioning accuracy at the extent of the minimum enclosing rectangle.

$$d_{min} \geq \frac{\sqrt{2}}{s_{xy}} \quad (2)$$

Afterwards each individual coordinate of the sector triangle vertices is converted into integer coordinates.

$$\begin{bmatrix} x \\ y \end{bmatrix}_{int} = \begin{bmatrix} \left\lceil \left\lfloor s_{xy}\left(x_{float} - x_{min_{bbox}}\right) \right\rfloor \right\rceil \\ \left\lceil \left\lfloor s_{xy}\left(y_{float} - y_{min_{bbox}}\right) \right\rfloor \right\rceil \end{bmatrix} \quad (3)$$

3.5 Triangulation to Form the Basic Mesh

Next, all points with integer coordinates are triangulated. By using integer coordinates, it is possible to get precise statements of the relative position from a point to a line segment. For this purpose, the determinant of a matrix is calculated from the two points of the line segment (A,B) and the point (P) to be determined (similar to the 3d geometric predicates in (Fortune and van Wyk, 1996)). The integer type of the determinant in the following equation needs twice the size of the integer type of the coordinates.

$$det_{AB} = \begin{vmatrix} x_A & x_B & x_P \\ y_A & y_B & y_P \\ 1 & 1 & 1 \end{vmatrix} \tag{4}$$

For the determination of the position three cases are distinguished, if the determinant is zero then the point is collinear with the line segment, if it is negative then the point is to the right, if it is positive then the point is to the left of the line segment.

There are numerous algorithms for generating a two-dimensional (Delaunay) triangulation (Su 1995). However, the algorithm used must work with integer coordinates and to determine the position of a point to a line segment, the above shown method (with Equation 4) must be applied. We use a simple but reliable approach:

1) The convex hull of all points is calculated with the algorithm from (Andrew 1979) (Figure 3a).
2) The polygon of the hull is then divided into triangles by drawing lines from the point with the smallest x-value to the remaining vertices of the polygon (Figure 3b). For this, it is important that the convex hull does not contain double or collinear points.
3) The remaining points are then successively inserted into this initial mesh and new triangles are formed (Figure 3c).
4) We flip all edges between two triangles until all triangles meet the Delaunay criterion (Figure 3: Steps of Triangulation Figure 3d). Because detailed analyses (Vetter, 2019) have shown that it is advantageous if the triangles of the basic mesh meet the Delaunay criterion. Thus, the number of intersections can be reduced in the next step of the algorithm.

Once all the points have been inserted into the triangle mesh, it may not be changed. It is therefore given the name basic mesh.

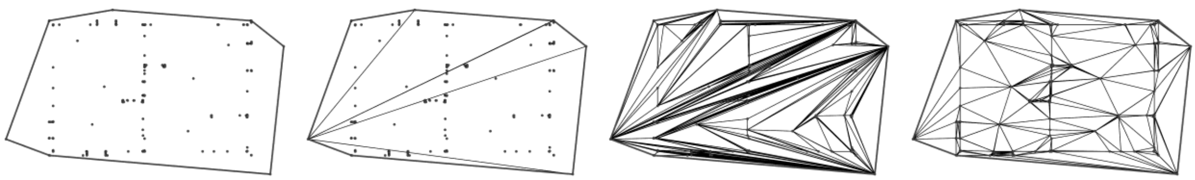

a) Convex Hull b) Initial Triangles c) Triangulation of all Points d) Basic Mesh (Delaunay)

Figure 3: Steps of Triangulation

3.6 Edges of Sector Triangles in the Basic Mesh

In this step, the paths of all edges of the sector triangles in the basic mesh are determined. These edges do not necessarily coincide with edges of the basic mesh. This has to be done separately for each sector edge.

The Path Algorithm

First, find a triangle whose vertex is the starting point of the sector edge. As all points were previously inserted into the triangle mesh, there is always a result here. This vertex gets the information that the sector edge starts here.

Edges of sector triangles can intersect edges of the basic mesh. As shown in Figure 4a and b, two situations can occur. The calculation starts based on the star of mesh triangles around the start of the edge or the sector triangle. The intersection of this edge with the star can either be a vertex of the basic mesh or it can be an intersection point with an edge of the basic mesh as shown in Figure 4a. The calculation continues with the result. The same situations can occur after an intersection with an edge of the basic mesh as shown in Figure 4b. The path calculation ends once the end of the sector edge is reached.

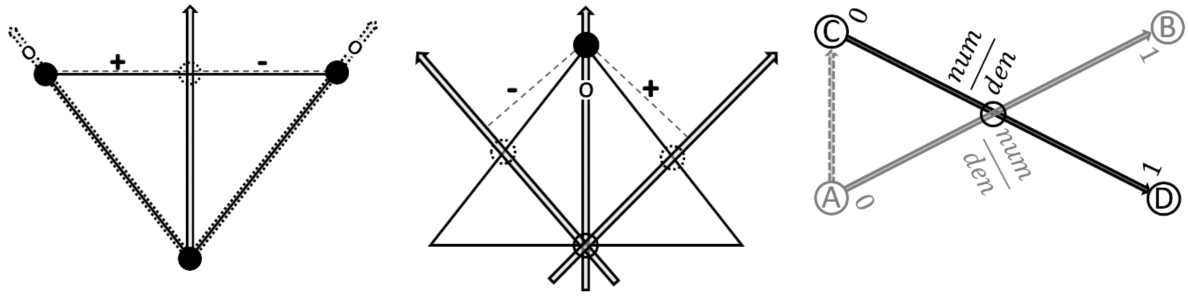

a) Sector Edge after Meeting a Vertex

b) Sector Edge after Meeting an Intersection with an Edge of the Basic Mesh

c) Intersection Calculation

Figure 4: Sector Edges in the Basic Mesh

Rational Numbers for Exact Computation

The positions of the intersection points on the mesh edges and the sector edges are stored as a rational number. The rational number is represented as a fraction of two integers (numerator and denominator) with twice the size of the integers of the coordinates. In our implementation, we use for the coordinates 32 bit integers and for the numerator and denominator 64 bit integers.

Calculation of an Intersection Point

To calculate the position of an intersection of two edges A-B and C-D we need the vectors AB, CD and AC as shown in Figure 4c. Both fractions have a common denominator.

$$denominator = \begin{vmatrix} x_{AB} & x_{CD} \\ y_{AB} & y_{CD} \end{vmatrix} \tag{5}$$

The numerators of the fractions of the positions on A-B and C-D are:

$$numerator_{AB} = \begin{vmatrix} x_{AC} & x_{CD} \\ y_{AC} & y_{CD} \end{vmatrix}, numerator_{CD} = \begin{vmatrix} x_{AC} & x_{AB} \\ y_{AC} & y_{AB} \end{vmatrix} \tag{6}$$

If the denominator is negative, the sign of all values must be changed. The intersection point is between the end points of the two edges if the two fractions ($numerator_{AB}/denominator$, $numerator_{CD}/denominator$) are positive and are proper fractions.

3.7 Intersection Points inside Mesh Triangles

After all intersection points of the sector edges with the basic mesh edges have been calculated, the intersection points within the triangles of the basic mesh can be calculated.

To do this, we iterate over all triangles and sort the vertices and all intersections on the corresponding mesh edges in the order of the vertices into a list. Since the outgoing and intersecting sector edges were saved for each point, the sector edges intersecting the triangle can now be determined. Please note that several sector edges may overlap (in Figure 5a between index 1 and 6) or intersect on an edge of a triangle (in Figure 5a index 3).

Now, using the indices on the edge of the triangle it can be determined whether there are intersections within the triangle – using the beforehand created topological relations only. To do this, check for each intersecting sector edge (or set of sector edges with the same indices) and search for those sector edges (sets) that have one index between the start and end index and the other index between the end and start index. If this is the case, an intersection point and its position on all involved sector edges can be calculated (Figure 5a indices 0-3 and 1-6). The intersection point also gets all intersecting sector edges stored. These can then be sorted according to the order on the edge of the triangle. The same is done with the points on the edge.

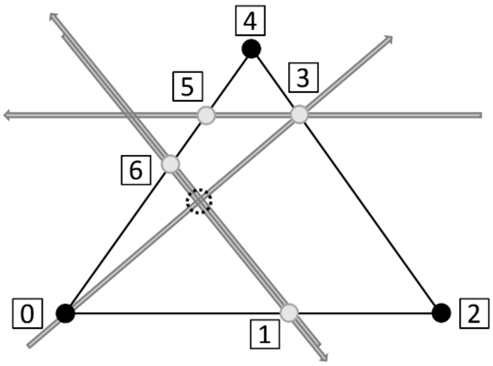

a) Intersection Inside Triangle

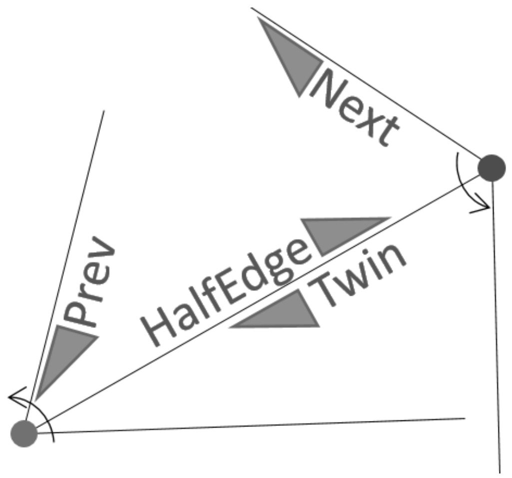

b) Connection of Half-Edges

Figure 5: Intersections and Connections

At the end of this step, each point (initial and intersection points) has a sorted list with all outgoing and intersecting mesh and sector edges (as a set if they have identical destination points). Also each mesh and sector edge has a sorted list with the points lying on it.

3.8 Creation of Half-Edges

In this step, the basic (triangle) mesh is transformed to a polygonal mesh consisting of convex polygons (see Figure 5a).

All points are considered and for each edge or respectively edge set in the corresponding list a half-edge with the point as start vertex is created. These half-edges get the adjacent sector edges that run in the same direction, saved in a list, and the half-edges are saved in an ordered list to the points.

Then these half-edges are linked. The scheme of the linking can be seen in Figure 5b. The previous (prev) is the twin of the half-edge in the list of half-edges of the point following the half-edge. The twin can be found in the list of the half-edges of the target point. In addition, the next one is the half-edge before the twin in the list of half-edges of the corresponding point.

At the end of this step only the half-edges with their vertices and the corresponding sector edges are needed. All data of the previous steps with reference to the basic mesh are now no longer required.

3.9 Creation of Polygonal Facets

Once all half-edges are created, each one has a successor (next), a predecessor (prev) and a twin. Thus, iterations can be made over them and a facet can be created and stored for each closed ring of half edges.

3.10 Detection and Unification of "no solid" Facets

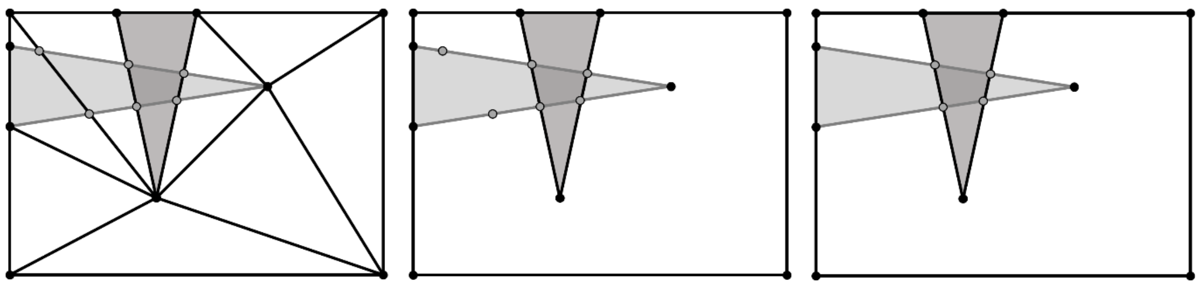

a) Original b) Edges Removed c) Vertices Removed

Figure 6: Removing of Unnecessary Elements

As depicted in Figure 6a, the newly created mesh of polygonal facets contains many unnecessary edges and vertices. These can now be removed if they do not belong to a sector triangle. Afterwards the remaining facets are checked whether they can be assigned to the substance type "no solid".

To remove unnecessary half-edges, iterate over all facets and in these over-all associated half-edges. If you find a half-edge that has a twin and both have no underlying sector edge and both do not belong to the same facet, then you can remove this pair safely and remove one of the associated facets (Figure 6b). Afterwards we check all half-edges if they have the same underlying edges as their next and if the next of the twin of the next is the twin of the current half-edge. If this is true, this vertex can be removed safely (Figure 6c).

Finally, we iterate over the remaining facets again and check whether all the corresponding half-edges have a sector edge underneath. In this case, the facet can be assigned to the substance type "no solid". All other facets keep the type "indeterminate". This test only works because each half-edge has only the sector edges assigned that run in the same direction, so the inside of a facet is also inside a sector triangle. If all half-edges of a facet have the flag of a separator between "solid" and "no solid", they can even be assigned to the substance type "solid", but this case is very unlikely.

Figure 7 shows a complete polygonal mesh after this step of the original floorplan and scanner constellation in Figure 2a.

3.11 Further Substance Detection

This step requires further research. The aim is to assign the substance type "no solid" and "solid" to further facets by analyzing the polygonal mesh using purely topological information and semantic annotations. In this context, it is also important to consider that the geometry is derived from measurements, so it has a stochastic nature.

A first algorithm searches all half-edges belonging to a sector triangle and then assigns the substance type "no solid" to all facets inside the closed ring of half edges found.

However, there are further algorithms and methods for topological inference that help to distinguish between "no solid" and "solid".

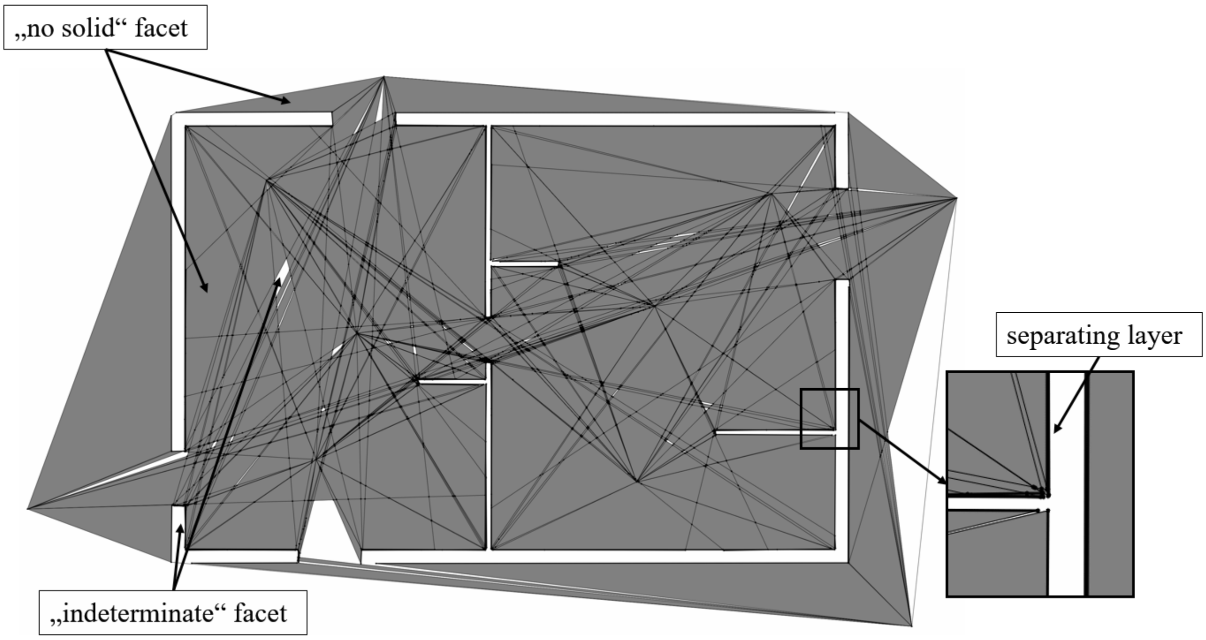

Figure 7: Polygonal Mesh before Further Substance Detection

3.12 Subsequent Analyses

Now, after all preceding steps, we have a half-edge structure of polygonal facets. The facets are "no solid", "solid" or "indeterminate". We also have two types of vertices, the (initial) points with the integer coordinate and the intersections, which usually do not have integer coordinates. These results can be used for further investigations such as object reconstruction (walls, openings, ceilings …) or clash detection.

4. Discussion, Conclusions and Outlook

As depicted in Figure 7, the presented procedure works error-free and with our generated test data. The polygonal mesh is generated from the mass of unstructured point cloud data. The concurrent reduction of the amount of data and high quality abstraction is an advantage. By using integer coordinates and a consistent topology, a higher numerical stability and uniqueness is achieved.

We hope that this method will lead in practical application to improve object recognition for measured building surveys and on-site monitoring with terrestrial laser scanners. Once having the space decomposition given with exact computation and having classified polygonal structures that are fast to navigate and easy to group as sets, it will be possible to better close gaps in the measured point cloud. Thus, object recognition is less sensitive to obstacles or non-reflecting objects. With the given algorithms and topological structure described in this paper, we will investigate if it is possible to separate and classify objects (walls, opening) in the point cloud and quantify differences between as-planned and as-build.

As next, the step presented in section 3.11 has to be worked out to get the remaining information of the original data into the polygonal mesh. Furthermore, the algorithm has to be tested on real measured data and against other Procedures. Therefore, it is necessary to adapt the detection of the line segments in section 3.2 for three-dimensional point clouds. This will probably happen basing on detected plane-patches intersected by a horizontal slice plane.

A further field of application of the presented method for the two-dimensional use case might be GIS data. For this purpose, it is necessary to adapt the algorithm, since these data do not consist of point clouds.

The most relevant step of further developments, however, is the extension of the algorithm for the three-dimensional space. The basis will then no longer be line segments but plane-patches and the result will be a mesh of polyhedra.

References

Andrew, A. (1979). Another efficient algorithm for convex hulls in two dimensions, Information Processing Letters 9, pp. 216–219.

Budroni, A. (2013). Automatic model reconstruction of indoor Manhattan-world scenes from dense laser range data.

Faro (2019). Faro Scene website, https://www.faro.com/de-de/produkte/3d-design/faro-scene, accessed February 2020.

Fortune, S., Van Wyk, C. J. (1996). Static analysis yields efficient exact integer arithmetic for computational geometry, ACM Trans. Graph. 15(3) (July 1996), pp. 223–248.

Gielsdorf, F. (2009). Ebenendetektion, Matching und verkettete Transformation von Laserscans. allgemeine vermessungsnachrichten (AVN) 12/2009 (11), pp. 391–395.

Huhnt, Wolfgang (2018). Reconstruction of edges in digital building models, Advanced Engineering Informatics 38, pp. 474-487.

Kraft, B. (2016). Ein Verfahren der Raumzerlegung als Grundlage zur Prüfung von Geometrie und Topologie digitaler Bauwerksmodelle.

Lemmens M. (2011). Terrestrial Laser Scanning, Geo-information. Geotechnologies and the Environment, 5 Springer, Dordrecht, pp. 101–121.

Mura, C., Mattausch, O., Jaspe Villanueva, A., Gobbetti, E., Pajarola, R. (2014). Automatic room detection and reconstruction in cluttered indoor environments with complex room layouts. Computers & Graphics 44, pp.20–32.

Ochmann, S., Vock, R., Wessel, R., Tamke, M., Klein, R. (2014). Automatic generation of structural building descriptions from 3D point cloud scans, 2014 International Conference on Computer Graphics Theory and Applications (GRAPP), Lisbon, Portugal. pp. 1–8.

Ochmann, S., Vock, R., Wessel, R., Klein, R. (2016): Automatic reconstruction of parametric building models from indoor point clouds. Computers & Graphics 54, pp. 94–103.

Shewchuk, J. R. (1997): Adaptive Precision Floating-Point Arithmetic and Fast Robust Geometric Predicates, Discrete Comput Geom 18 (3), pp. 305–363.

Su, P., & Drysdale, R. L. S. (1995). A comparison of sequential Delaunay triangulation algorithms, Proceedings of the eleventh annual symposium on Computational geometry, pp. 61–70.

Sugihara, K.; Iri, M. (1990). A Solid Modelling System Free from Topological Inconsistency. J. Inf. Process. 12 (4), pp. 380–393.

Tang, P., Huber, D., Akinci, B., Lipman, R., Lytle, A. (2010). Automatic reconstruction of as-built building information models from laser-scanned point clouds. A review of related techniques. Automation in Construction 19 (7), pp. 829–843.

technet GmbH (2020). Scantra website, https://www.technet-gmbh.com/produkte/scantra/, accessed February 2020.

Turner, E., Cheng, P., Zakhor, A. (2015). Fast, Automated, Scalable Generation of Textured 3D Models of Indoor Environments. IEEE J. Sel. Top. Signal Process. 9 (3), pp. 409–421.

Vetter, J. (2019). Eine Untersuchung zum Aufwand bei der Berechnung einer Raumzerlegung im 2D aus einer gegebenen Menge an Polygonen.

Weinmann, M. (2016). Reconstruction and Analysis of 3D Scenes – From Irregularly Distributed 3D Point Clouds to Object Classes.

Xiong, X., Adan, A., Akinci, B., Huber, D. (2013). Automatic creation of semantically rich 3D building models from laser scanner data. Automation in Construction 31, pp. 325–337.

A Rule Language Model for Subsurface Data Refinement

Ashley Caselli, Vincenzo Daponte, Gilles Falquet, Claudine Métral
Centre Universitaire d'Informatique (CUI), University of Geneva, Switzerland
ashley.caselli@unige.ch

Abstract. The automated regulation compliance checking in the domain of Architecture, Engineering, and Construction (AEC) still presents many challenges to face. The completeness and correctness of the input data affect the results of the compliance checking. Refinement operations on data represented through knowledge graphs can help the assessment of these data properties. In this work, a model to represent rules holding complex constraints is proposed and conveyed through an ontology. This model aims to overcome existing expressiveness limitations and to provide a conceptual tool to represent both compliance regulations and domain experts' knowledge encoded through heuristics. These heuristics are used to drive the refinement process needed prior the compliance checking. The proposed model is intended as the first step towards an automatic execution process of both types of rule instances. The model has been assessed by representing regulations issued by Swiss entities and domain experts' heuristics targeting data of an area of the city of Geneva.

1. Introduction

Nowadays the construction of an automated regulation compliance checking systems within the Architecture, Engineering, and Construction (AEC) domain is still a burning issue. The rationale behind such systems is the need for tools capable of (i) providing a compliance assessment on existing objects, and (ii) driving future developments. Such tools aim to assess whether the spatial configuration of the objects situated within an area of interest (AOI) fulfills a given set of constraints, namely construction codes, issued by the competent entities. In order to evaluate the compliance with such constraints both spatial reasoning and heterogeneous data integration capabilities are needed. Heterogeneous data involved in a compliance process range over two macro-categories: (i) geospatial and architectural data, and (ii) textual data, which define the spatial constraints. The latter should be expressed using a formal representation in order to be exploitable within such process. Regarding geospatial and architectural data, many efforts have been carried out to achieve their integration. However, geospatial data are intrinsically error-prone and characterized by uncertainty known as *spatial vagueness* (Schneider, 2011), which makes the integration not trivial. To cope with it an interest in modeling and processing data affected by spatial vagueness has grown in the last years (Schneider, 2011). Furthermore, there is another aspect to consider when designing a decision-making system that includes geospatial data as input: the possibility to face incomplete data in presence of multiple sources. It is safe to assume that the results of an automated compliance checking system are affected by the *completeness* and *correctness* of the input data. To assess these data properties, refinement operations are crucial to achieve more accurate results.

2. Background

(Paulheim, 2016) defines a *refinement* process on a knowledge graph as a process that tries to infer and add missing knowledge (*completion*) and identifies erroneous information (*error detection*). From a data quality perspective, the refinement operations point to increase the overall completeness and correctness of a knowledge graph. Current approaches differ along several dimensions, applying methods that range from machine learning to NLP-based ones.

(Paulheim, 2016) reveals that a holistic solution that targets both completeness and correctness is not handled by any of them. All the solutions discussed focus on automatically complete/correct the knowledge graph using it (internal approach) or additional data (external approach) as input. Semi-automatic approaches, that involve the human in the process, have also been proposed. However, they are mostly designed as games where human players unconsciously correct data while playing. The reviewed works do not present tools that formally express domain experts' knowledge (i.e. in the form of rules) for refinement purposes.

Regulatory compliance knowledge has been represented through different models and among these many were designed for the automatic execution of the rules represented. Studies in this domain focused on the expressiveness of these models and their capability to represent also nonstandard rules such as the refinement heuristics. An ever-increasing adoption of Resource Description Framework (RDF) (Miller and Manola, 2004) to represent architectural and urban data paved the way to the design and development of automated semantic rule compliance checking processes. Many attempts have been done in the construction domain, such as the checking of building envelope design (Tan, Hammad and Fazio, 2010), construction quality (Zhong *et al.*, 2012), and fire safety code (Balaban, Kilimci and Çagdas, 2012; Dimyadi *et al.*, 2014). In addition, many rule compliance tools have been developed by domain experts, such as SMARTCodes (Eastman *et al.*, 2009) and Solibri Model Checker. Consequently, an interest in a more open regulatory knowledge representation arose. As depicted by (Pauwels and Zhang, 2015), there exist three main approaches to tackle the issue of modeling the regulation knowledge within a semantic regulation compliance checking process: (i) hard-coded rules, (ii) rules expressed as queries, and (iii) usage of dedicated rule languages. Most compliance checking environments relied on hard-coded rules, which required technical programming skills to be managed. However, further research efforts have led to the development of domain-specific languages targeting the construction domain, such as the Building Environment Rule and Analysis (BERA) language (Lee, Eastman and Lee, 2015) and the Drools Rule Language (Beach *et al.*, 2013, 2015). A comprehensive approach to semantic compliance checking of underground utilities has been designed and developed by (Xu and Cai, 2020). Their manuscript presents a framework capable of: (i) mapping spatial data and underground utilities spatial constraints (textual information) to an RDF format, and (ii) detecting spatial noncompliance of underground utilities using SPARQL queries for spatial reasoning. The mapping process is carried out using a model formalized into four different ontologies to represent both spatial data and textual descriptions of spatial constraints (utilities' rules and specifications). Constraints are automatically extracted using NLP-based techniques and represented as a ten-elements tuple. Each tuple is expressed as a *spatialConfiguration* and the tuple's elements become objects related to the current configuration (a detailed description of such rule ontology is shown in Figure 1). Besides other conditions, each *spatialConfiguration* specifies the constrained objects on which it applies and the spatial relation that stands among them. Both the spatial relation and the target objects are expressed as literal (string) values. A dictionary-like resource of related-terms is then exploited to perform the mapping among the target objects and the real objects. Likewise, the spatial relation term is mapped to the correspondent SPARQL query. This approach, although effective in the presented use cases, presents limitations in terms of openness and expressiveness. The reliance on a dictionary-like resource leads the object mapping process to be an equality evaluation among words. This practice may represent an obstacle when the regulations to apply are issued by different entities and written in different languages, as in the Swiss case. In this circumstance, a semantic-based approach may ease the integration of concepts extracted from regulations issued by different entities. Moreover, in case of more complex regulation constraints, the related terms approach may lead to a loss of expressiveness, as for the case of the spatial constraints extracted by the NLP algorithm from the spatial cognitive-linguistics elements. The expressiveness limitations are visible, for instance, in the attempt to represent mathematical expressions or object's property-dependent constraints such as: *"direct distance between an electrical object and another object should be 0.5m per kA of short-circuit current to ground"*.

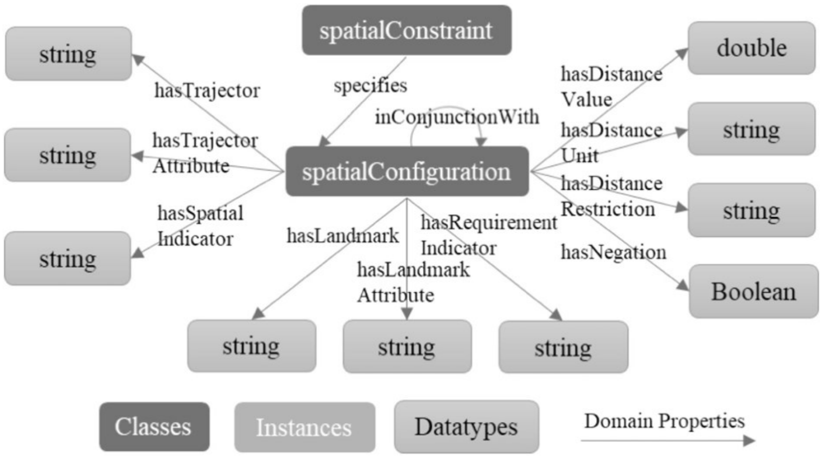

Figure 1: Utility spatial rule ontology used in the framework presented in (Xu and Cai, 2020).

3. Proposal

The main objective of this work is to provide a formal model to represent both regulatory knowledge, issued by several entities, and refinement rules. This model is conceived to be part of a process that applies both refinement and compliance rules, and it is designed to overcome the limitations in terms of expressive capability of the existing approaches. To achieve this purpose the proposed rule model provides the means for a high-level representation for both domain experts to define refinement rules and entities to formalize compliance regulation knowledge. The additional expressiveness allows to represent heuristics that handle the spatial vagueness gaps that cannot be addressed with other refinement rules. Spatial vagueness refers to the concepts of *spatial uncertainty* (Schneider, 2011) defined as (i) *positional uncertainty*: lack of knowledge about the position and shape (real boundary); and (ii) *measurement uncertainty*: inability to measure the object precisely. These gaps in the AEC objects are handled through heuristics that formulate calculated hypotheses, based on domain experts' knowledge, on the objects missing features. An example of such a heuristic is: *"if the depth value of a subsurface building is missing, then the depth is assigned to the value numberStoreysBelowGround * constantValue"*, that belongs to the analyzed refinement rules. This model may also serve as the abstract midpoint among a logic-based compliance rules representation (i.e. extracted by an NLP-based algorithm) and the rule execution (evaluation). In section 3.1 the research path that led to the proposed model is presented. The model's top level is based on two components: (i) the rule structure, and (ii) the expression structure. The rule structure, outlined in section 3.2, expresses the rule's context and domain. The expression structure, presented in section 3.3, represents the actual rule's constraint defined by the regulation or the heuristics that has to be applied.

3.1 Methodology

A model conceived to represent refinement and compliance rules should be able to represent several kinds of relations. Besides the well-known spatial relations, it should also include mathematical (i.e. *"for each data sample must be valid that the metric RAYON_RACINES does not exceed 20 m"*), logical (*"minimum spacing required between conducts or cables is 0.4m if* *they are insulated"*) and possibly combinations of the above ones. The steps taken to fulfill these requirements are the following. At first, the regulations issued by several Swiss entities (e.g. Swiss Society of Engineers and Architects (SIA), *Système d'Information du Territoire à Genève* (SITG), Swiss Confederation, Swiss Federal Roads Office (FEDRO)) that involve subsurface objects have been analyzed. The analysis focused on the study of their structure, rather than the content. In the second step, the rules have been split into basic components. These components have been analyzed and abstracted into higher level classes which are presented in section 3.2. Once identified, these classes have been structured into a unified model to represent compliance rules. On this preliminary model a validation process to assess its expressive capability has been carried out. The validation feedback served as tuning factor to refine the model in order to be suitable for representing both spatial constraints and domain expert heuristics. The validation process that helped to assess the expressiveness of the model is outlined in section 4.

3.2 Rule model Structure

The proposed model relies on the following basic components that were identified in the first stages of the development:

- **Rule** defines a binary relation among objects, or unary on a single object as in the case of the heuristics.
- **Condition** models the circumstances under which a rule is applicable and the implications it entails.
- **Expression** represents the constraints or the implications that a rule defines. It allows to represent different kind of relations (i.e. spatial, mathematical, logical, and combinations of the previous ones). Due to its expressiveness both compliance rules (mostly based on spatial relations) and refinement rules may be defined.

These components were then structured to build the model presented below and enriched with the additional concepts mentioned in the model outline.

The *Rule* class may represent a binary-relation where the two objects involved are referred to as *trajector* and a *landmark*. The *Rule* may also represent a unary relation referring to a single object (*trajector*) and to the evaluation of one or more of its properties. Figure 2 shows an overview of the rule model top-level. The terms *trajector* and *landmark* were proposed in (Langacker, 1987), where they refer to the universal asymmetry between the subject and the object of an action, state or relation. Both objects are expressed through an external vocabulary that formally defines them. This allows to decouple the rule model from any objects' representation. In this specific case, a subsurface objects ontology developed alongside the domain experts from HEPIA has been used. In Figure 3 it is shown the portion of the ontology, that defines the utility networks, aligned with the CityGML UtilityNetworkADE (Becker, Nagel and Kolbe, 2011). Any other subsurface objects ontology could have been used. The rule also specifies (*rules:validOn*) a *Validity Context* within which it applies and the *Entity* that issued it (*rules:issuedBy*). In addition, it defines (*rules:hasPrecondition*, *rules:hasPostcondition*) one or several conditions that must hold. They are represented by means of the *Condition* class.

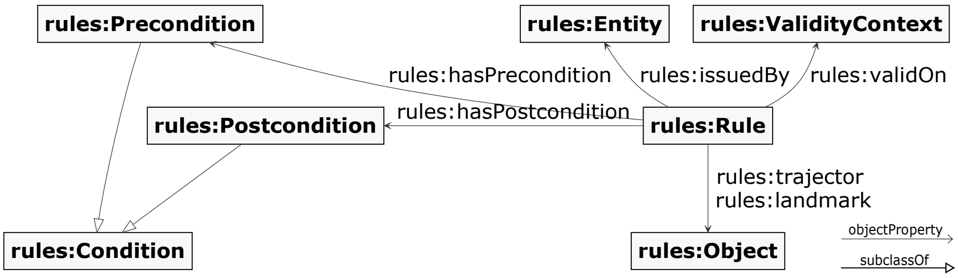

Figure 2: The Top-level of the proposed Rule representation model.

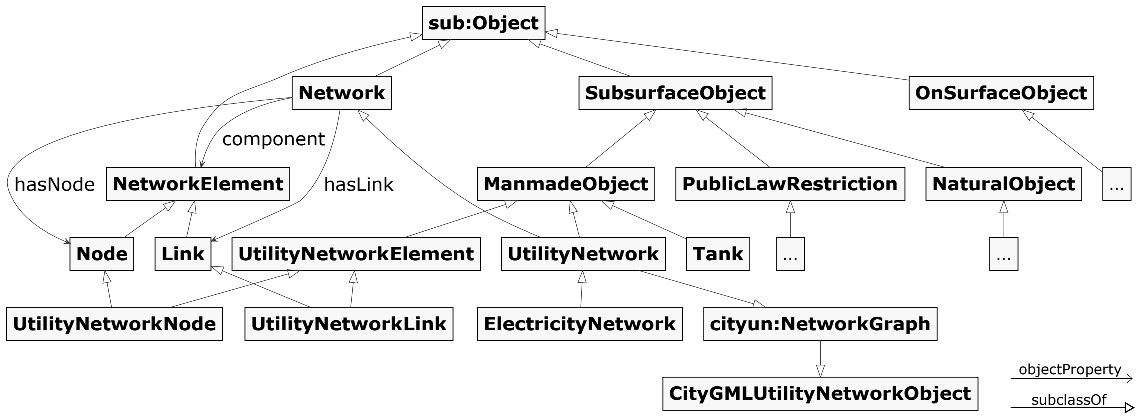

Figure 3: Portion of subsurface ontology aligned with CityGML UtilityNetworkADE ontology.

Validity Context

This class represents the temporal and spatial context within which the rule applies. Temporal context is crucial to identify the temporal validity window of the rule. Regarding the spatial context, it represents the macro-zone targeted by the rule (i.e. urban zone, building zone, industrial zone).

Condition

Besides the *Validity Context*, each rule specifies the circumstances under which it is applicable and the constraints it entails. They are represented and referred to as *Condition*. Figure 4 shows the condition hierarchy that includes two subclasses: *Precondition* and *Postcondition*. A Precondition is a condition that constrains the applicability domain of the rule, while a Postcondition is the condition that the rule entails. For this reason, a rule will always be represented with at least one Postcondition. This, conversely, does not apply for the Precondition, which may not exist for every rule. Finally, as shown in Figure 4, each *Condition* is related to an *Expression* that represents the actual constraint/implication.

3.3 Expression Structure

An *Expression* represents either the constraint or the implication that a rule defines. It may represent any kind of expression written in the form

Expression ::= Operand Operator Operand

An *Operand* can be one of the following: an element of the set *{"trajectory", "landmark"}*, a *Value*, a *PropVal*, an *Object* (i.e. Tank, TreeRoot), or another *Expression*. This representation allows the recursive definition of an *Expression*, without an upper-bound on the recursion depth. The two operands are identified as *LeftOperand* and *RightOperand*, as shown in Figure 4. An *Operator*, on the other hand, can be mathematical, logical, or spatial. A detailed overview of the Expression class structure is shown in Figure 5.

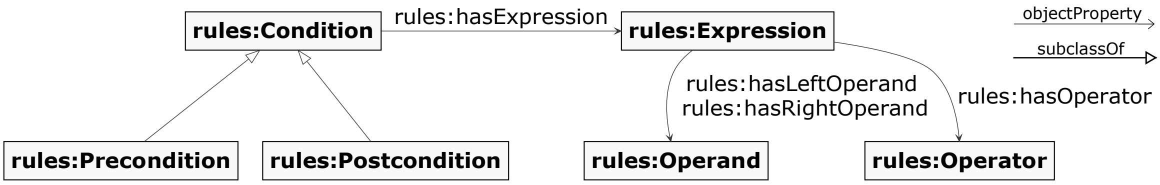

Figure 4: The overview on the rule's Condition part

Value (Operand)

It represents a value in terms of its actual value, the precision if any, the unit of measure, and possibly the degree of confidence of the value.

PropVal (Operand)

The *PropVal* class is used to represent the object's property involved in the expression and it has two properties: *onArg* and *onProp*. The first one is used to describe which rule's argument (*trajectory* or *landmark*) is the target object. The second one represents the property name.

SpatialOperator (Operator)

The *SpatialOperator* class represents the operators capable of evaluating a spatial relation among two objects. An ontology has been defined to represent the spatial relations implied in the compliance rules. The identified relations have been organized in three main categories: *topological* relations (contains, disjoint, touches, ...), *directional* relations (above, below, ...), and *distance* relations (horizontal, vertical, and direct distance). This ontology is intended to represent just those appearing in the compliance rules analyzed. If necessary, it can be extended for the needs of additional rules.

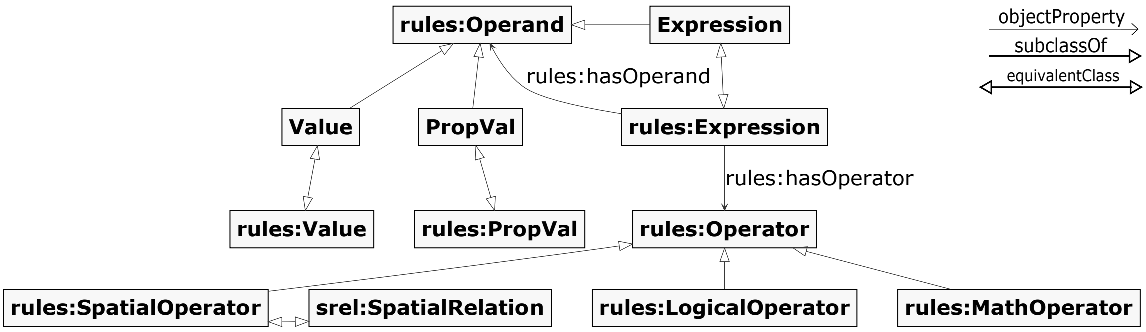

Figure 5: The structure details of the rule's Expression class.

4. Validation

The evaluation of this model was conducted by assessing its expressive capacity against a wide set of regulations issued by several Swiss entities and refinement heuristics from domain experts' knowledge. A set of heterogeneous rules and regulations were abstracted using the proposed model to create *Rule* instances.

The process was conducted following three steps:

1. Translate the original regulation texts from French (being from Geneva canton) to English using the terms identified in the model.
2. Map the top-level concepts of the rule structure model to the respective parts of the regulation.
3. Identify the syntactical structure of the conditions and represent it through *Expression* instances.

Most of the rules were taken from the *Ordonnance sur les lignes électriques* (Regulation on electrical power lines) and the Swiss Confederation. A concrete example of the validation process is reported below starting from an article on the positioning of grounding installations of electrical network. This particular article is the number 134.4 from the *Ordonnance sur les lignes électriques* regulation whose original text is:

En cas de rapprochement dans le sol, la distance directe entre les éléments reliés au dépôt de combustibles ou de carburants et les conducteurs de terre, les éléments mis à la terre de lignes ou d'installations électriques à courant fort étrangères au dépôt doit être de 0,5 m par kA de courant de court-circuit à la terre, mais jamais inférieure à 10 m.

1. The text has been translated as follows: *In the event of close proximity in the ground, the **direct distance** between the elements connected to the combustible or fuel tank and the electric ground conductors, grounded elements of **high current** electrical networks or installations not connected to the tank **must be 0.5 m per kA of short-circuit current to ground, but never less than 10 m**.*
2. Mapped towards the proposed model:

   Rule: Regulation on electrical power lines - article 134.4

   Entity: Swiss Confederation

   Validity context: From 30/03/1994

   Object - trajector: electric ground conductors, grounded elements of power lines or electrical installations

   Object - landmark: elements connected to the combustible or fuel ***tank***

   Precondition: The rule applies on high current ***electrical network*** ground conductors and elements connected to the combustible or fuel ***tank***

   Postcondition: the ***direct distance*** between ***Object - trajector*** and ***Object – landmark*** must be 0.5 m per kA of short-circuit current to ground, but never less than 10 m
3. Represent the syntactic structure of the conditions through expression instances:

   Precondition: Check the type of the input objects as shown in Figure 6.

   Postcondition: Build the expressions to evaluate the relations and the properties involved in both Postconditions as shown in Figure 7 and Figure 8.

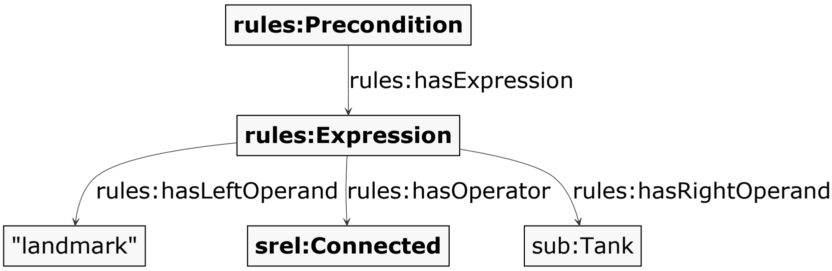

Figure 6: The representation of the Precondition from the example rule using the proposed expression model.

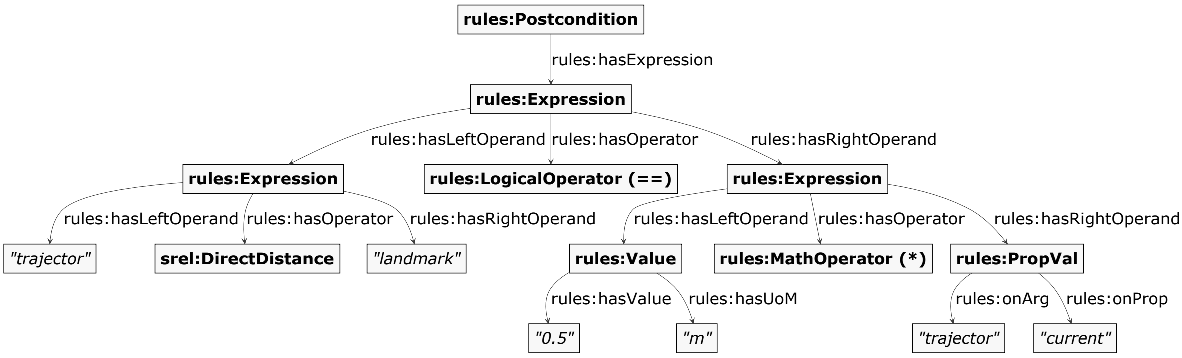

Figure 7: The representation of the first Postcondition associated to the compliance rule extracted from the article 134.4 on electrical power lines using the proposed model.

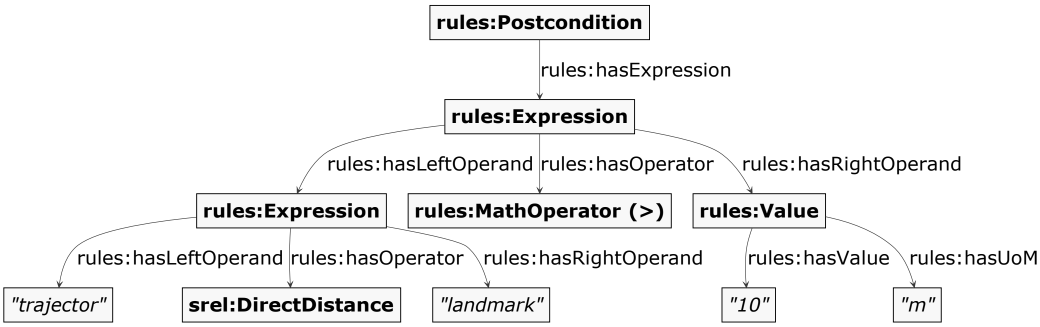

Figure 8: The representation of the second Postcondition associated to the compliance rule extracted from the article 134.4 on electrical power lines using the proposed model.

In addition to the regulation instances the evaluation process was also applied to heuristics from domain experts' knowledge. Heuristics on data processing and validation have been defined with the research group from Geneva's *Haute école du paysage, d'ingenierie et d'architecture (HEPIA)*. In the considered example the heuristics refer to the data imported from SITG (SITG, 2020). This entity provides a wide range of data on the Geneva canton through interactive maps and downloadable data. The following example concerns tree roots data, namely their radius value:

for each data sample must be valid that the metric RAYON_RACINES does not exceed 20 m.

These heuristics are represented through the proposed model and expressed using the Turtle syntax (Carothers and Prud'hommeaux, 2014):

```
rdf:type rules:Rule ;
rules:hasPostcondition [
```

```
            rules:hasExpression [
                 rules:hasLeftOperand [
                     rdf:type rules:PropVal ;
                     rules:onArg "trajector" ;
                     rules:onProp sub:radius ; ] ;
                 rules:hasOperator :lessEqualOperator ;
                 rules:hasRightOperand [
                     rdf:type rules:Value ;
                     rules:hasUoM "m" ;
                     rules:hasValue "20"^^xsd:int ; ] ; ] ; ] ;
         rules:trajector sub:TreeRoot ;
         rules:validOn [
             rdf:type rules:ValidityContext ;
             rules:fromDate "2020-01-08"^^xsd:date ] ;
```

Below is shown the representation of the structure of the postcondition through expression instances:

Precondition: None.

Postcondition: Build the expression to evaluate the values and the mathematical relation as shown in Figure 9.

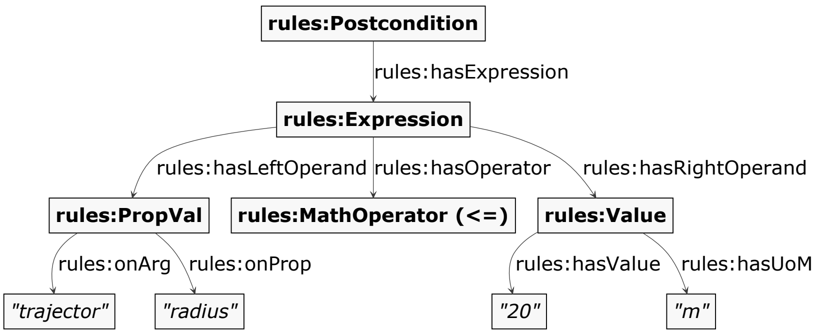

Figure 9: The representation of the Postcondition from the example heuristics using the expression model proposed.

5. Conclusions

Refinement operations are essential to increase data quality in terms of completeness and correctness. In the design of decision-making systems, such as one for automated compliance checking, these properties affect the accuracy of the results. In this article, a novel rule model has been presented wherewith both refinement and spatial rules for subsurface data may be formally expressed. In addition, the model allows to represent heuristics derived from domain expert's knowledge and compliance checking rules for refinement purposes. The model has been outlined and its classes and relationships presented. The expressive power is one of the key features that characterizes the proposed model and it has been assessed through a validation process. The validation has considered both regulation constraints including complex logical and mathematical expressions and heuristics from domain experts. Current developments focus on a rule execution engine that translates the rules represented as instances of the proposed model into SHACL rules (Kontokostas and Knublauch, 2017). These translated rules are then executed by a SHACL engine. Future works will focus on the development of a domain-specific language (DSL) (Fowler, 2010) to facilitate the specification of rules for both specialized and non-specialized personnel.

Acknowledgments

This research was supported by Innosuisse in the framework of the Subsurface project. The authors would like to thank Prof. Giovanna Di Marzo Serugendo as director of the CUI center, HEPIA and Topomat as partners of the project. The authors thank the HEPIA research group led by Prof. Dr. Bernd Domer with F. Boujon, K. Adouane and L. Neuenschwander for their support as domain experts.

References

Balaban, Ö., Kilimci, E. S. Y. and Çagdas, G. (2012) 'Automated Code Compliance Checking Model for Fire Egress Codes', in.

Beach, T. H. *et al.* (2013) 'Towards Automated Compliance Checking in the Construction Industry', in Decker, H. et al. (eds) *Database and Expert Systems Applications*. Berlin, Heidelberg: Springer Berlin Heidelberg, pp.366–380.

Beach, T. H. *et al.* (2015) 'A rule-based semantic approach for automated regulatory compliance in the construction sector', *Expert Systems with Applications*. Elsevier Ltd, 42(12), pp. 5219–5231. doi:10.1016/j.eswa.2015.02.029.

Becker, T., Nagel, C. and Kolbe, T. H. (2011) 'Integrated 3D Modeling of Multi-utility Networks and Their Interdependencies for Critical Infrastructure Analysis', in *Lecture Notes in Geoinformation & Cartography*. Springer, pp. 1–20. doi: 10.1007/978-3-642-12670-3_1.

Carothers, G. and Prud'hommeaux, E. (2014) *{RDF} 1.1 Turtle*. Available at: https://www.w3.org/TR/turtle/ (Accessed: 29 February 2020).

Dimyadi, J. *et al.* (2014) 'Regulatory Knowledge Encoding Guidelines for Automated Compliance Audit of Building Engineering Design', in *Computing in Civil and Building Engineering (2014)*. Reston, VA: American Society of Civil Engineers, pp. 536–543. doi: 10.1061/9780784413616.067.

Eastman, C. *et al.* (2009) 'Automatic rule-based checking of building designs', *Automation in Construction*. Elsevier, 18(8), pp. 1011–1033. doi: 10.1016/j.autcon.2009.07.002.

Fowler, M. (2010) *Domain Specific Languages*. 1st edn. Addison-Wesley Professional.

Kontokostas, D. and Knublauch, H. (2017) *Shapes Constraint Language ({SHACL})*. Available at: https://www.w3.org/TR/2017/REC-shacl-20170720/.

Langacker, R. W. (1987) *Foundations of cognitive grammar: Theoretical prerequisites*. Stanford university press.

Lee, J.-K., Eastman, C. M. and Lee, Y. C. (2015) 'Implementation of a BIM Domain-specific Language for the Building Environment Rule and Analysis', *Journal of Intelligent & Robotic Systems*. Kluwer Academic Publishers, 79(3–4), pp. 507–522. doi: 10.1007/s10846-014-0117-7.

Miller, E. and Manola, F. (2004) *{RDF} Primer*. Available at: http://www.w3.org/TR/2004/REC-rdf-primer-20040210/.

Paulheim, H. (2016) 'Knowledge graph refinement: A survey of approaches and evaluation methods', *Semantic Web*. Edited by P. Cimiano. IOS Press, 8(3), pp. 489–508. doi: 10.3233/SW-160218.

Pauwels, P. and Zhang, S. (2015) 'Semantic Rule-checking for Regulation Compliance Checking: An Overview of Strategies and Approaches', in *Proceedings of the 32nd CIB W78 Conference*, pp. 619–628.

Schneider, M. (2011) 'Fuzzy Spatial Data Types for Spatial Uncertainty Management in Databases', in *Handbook of Research on Fuzzy Information Processing in Databases*. IGI Global, pp. 490–515. doi: 10.4018/978-1-59904-853-6.ch019.

SITG (2020) *SITG | Le territoire genevois à la carte*. Available at: https://ge.ch/sitg/ (Accessed: 29 February 2020).

Tan, X., Hammad, A. and Fazio, P. (2010) 'Automated Code Compliance Checking for Building Envelope Design', *Journal of Computing in Civil Engineering*, 24(2), pp. 203–211. doi: 10.1061/(ASCE)0887-3801(2010)24:2(203).

Xu, X. and Cai, H. (2020) 'Semantic approach to compliance checking of underground utilities', *Automation in Construction*, 109, p. 103006. doi: 10.1016/j.autcon.2019.103006.

Zhong, B. T. *et al.* (2012) 'Ontology-based semantic modeling of regulation constraint for automated construction quality compliance checking', *Automation in Construction*, 28, pp. 58–70. doi: 10.1016/j.autcon.2012.06.006.

Developing a Framework for the Implementation of Robotics in Construction Enterprises

Makram Bou Hatoum, Hala Nassereddine
University of Kentucky, USA
mbh.93@uky.edu , hala.nassereddine@uky.edu

Abstract. As the fourth industrial revolution, Industry 4.0, continues to evolve, it becomes imperative for construction firms to seek, find, and adopt new technologies that transform the traditional, conservative construction industry into Construction 4.0. Autonomous Robotics, a pillar of Industry 4.0, have the potential to automate construction sites. In recent studies, researchers have explored potential applications for robotics in different project aspects such as structure works and safety monitoring, highlighting significant improvements on project performance. However, automating construction sites via robotics comes with major barriers, making it challenging for construction enterprises to adopt robots. Thus, this paper reviews recent studies to recapitulate the current state of robot implementation in construction and provide a list of recommendations for construction enterprises. Recommendations are presented in a simple framework that can serve as a roadmap to adopt robotics in the industry and a decision-making tool to guide companies in the implementation of robotics.

1. Introduction and Background

Since the early ages, humans sought and developed different structures to shelter themselves from the outside world. The evolution in their methods, materials, equipment, and types of structures formed what is long known as the construction industry. To this day, construction remains one of the strongest economic sectors through generating billions of dollars annually, employing millions of people all around the world, and contributing to 13-15% of the global Gross Domestic Product (GDP) (Schilling, 2013). However, when compared to other industries like manufacturing, construction currently trails behind, especially at the level of efficiency and productivity; it is estimated that $1.6 trillion of opportunity are needed to close the gap between both industries as of 2017 (McKinsey Global Institute, 2017). A major reason for this trail is that conventional construction reached its maximum ability to improve productivity and enhance quality and project performance as shown in, especially with the technology it currently utilizes (Bock and Linner 2015).

Bock and Linner (2015) applied Foster's S-curve to the construction industry. S-curves represent the development of product or technology over time in relation to a performance index or rate of technical adoption. S-curves aim to demonstrate the lifecycle of the innovation through three phases: (1) *innovation* – when knowledge is being built through research and development, different organization and technical problems are present, and first trails are being conducted; (2) *growth* – when the increase in knowledge leads to overcoming obstacles and developing products and services that get rapidly adopted by customers of the industry; and (3) *maturity* – when stagnation occurs due to the technology reaching technical, organizational, and economical limits. The study overlaid two S-curves: one that describes the limits of traditional technology, and one with the innovation, growth, and maturity of new approaches which start as a subordinate of the existing technology but gain momentum and adoption rate over time.

When applying the overlaying S-curve approach to the construction industry, the stagnation of the industry's conventional performance becomes visible. The world currently witnesses the "fourth industrial revolution", a revolution characterized by automating all the industries and spreading innovation. Thus, an automated construction industry serves as a solution to grow the productivity and efficiency of the current construction industry and improve its performance over time. The concept of automated construction initiated in 1970 in Japan, when analysis of the construction industry showed a significant decrease in productivity growth rate as compared to the manufacturing industry. As a result, extensive research in automated construction in the 1970s and 1980s caused breakthroughs in building component manufacturing, large-scale prefabrication, relatively simple single task construction robots, robot-oriented design, automated robotic on-site factories, and automated deconstruction. After nearly 40 years, the increased focus of construction companies on creating and adopting automated technologies and the sheer volume of research on automating the construction industry put automated construction in the growth phase (Bock 2015). Even though the application of robotics in the manufacturing industry created an "evolution", its application in the construction industry can best be described as an "unfinished revolution" (Balaguer and Abderrahim 2008). The physical implementation of robotics on construction sites is still minimal, despite the importance of utilizing robotics on construction projects and the growing research interest around it. Thus, as shown in Figure 1, this paper builds on existing research efforts that have investigated the challenges and benefits of implementing robotics in construction and presents a framework guide the construction industry and its decision-makers in the implementation of robotics.

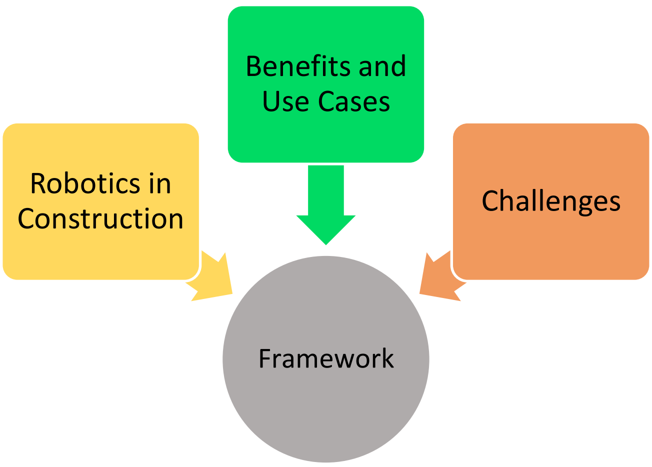

Figure 1: Structure of the Paper

2. Robotics in Automated Construction

Robotics is an important pillar of automated construction. Robotics is defined as the "science of designing, building, and applying robots" which aims to improve production quality and the life of workers in the industry through incorporating the "background, knowledge, and creativity of mechanical, electrical, computer, industrial, and manufacturing engineering" (Jackson 1990). Buswell *et al.* (2007) defined construction robots as intelligent machines operated by smart controls with a varying sophistication level and utilized by the industry to enhance speed and construction process precision. Implementing robotics in construction is stated to improve different aspects in construction especially productivity, safety, and quality (Bademosi et al. 2019). Thus, the opportunities that robotics can offer to construction has spurred researchers' interest.

Previous research endeavors have been conducted to identify the benefits of implementing robotics, categorize the associated challenges and barriers, and develop solutions to overcome these pain points. Aghimien et al. (2019) conducted an extensive literature review on the implementation robotics in construction between 2009 and 2019 and identified 91 papers varying between reviews, experiments, and case studies. They formed a keyword network analysis of 41 words that met the authors' required threshold of 4 co-occurrences. The words were further grouped in five clusters: *construction automation* which highlights the effort undertaken my researchers to explore robotics' potential benefits in construction in terms of productivity, cost, management and other factors; *industrial robots and application* which signifies the applications of automated construction in which robotics is being studied such as wielding, lifting, kinematics, sensing, improving project delivery; *robots systems and designs* which includes studies on the programming of robotics to perform their desired functions; *robotics in earthworks* which encompasses research done in the earthwork and foundation works which involve repetitive tasks and use heavy machinery, most of which can be automated – (Seo *et al.* 2011), for instance, developed a robotic excavator to enhance quality productivity and safety; *robots control and information system* which is mostly related to research that focuses on the control systems and programming of robots to perform work independently and autonomously, in addition to integrating Building Information Modeling (BIM) and 3D manufacturing with robots. Further benefits and use cases of the implementation robotics are explained in section 3.

3. Benefits and Use Cases of Robotics in Construction

The need for robotics in the construction industry is vital for different reasons as that it would yield different tangible and intangible benefits. As summarized and discussed by Carra *et al.* (2018), reasons to use robotics in construction include: the scarcity of building material resources (increase in cost while availability decreases), urbanization (construction within densely populated areas), ageing workforce (increase in fatigue and injuries while trades suffer from shortage of labor), enhanced connectivity and convergence (especially with workers becoming more familiar with technology and connectivity), environmental reasons (robots can be environmentally friendly and use green energy instead of electric power-strain systems), and safety purposes (reduce number of accidents on construction sites). Because of this, different studies tended to research the benefits of using robotics in the construction industry. Banik and Barnes (2002) saw automating the construction industry as a solution for the shortage in skilled labor. Elattar (2008) considered implementing robotics as a solution to deal with the increase in construction demand due to the heavy migration into cities worldwide.

Löfgren (2006) described the implementation of robotics as a financial investment with tangible benefits in the perspectives of *efficiency, effectiveness,* and *performance.* The technology's ability to improve the existing internal processes in the organization can lead to operational excellence and reduce the time and cost needed to perform tasks in the construction industry, and ultimately increasing efficiency. Effectiveness can be the result of the enhanced value achieved for the end-user by using technology, and the increase in the financial value of business activities and management. As for performance benefits, the technological innovation and enhanced learning would enable the development of the business and the organization itself for future orientations. Martinez *et al.* (2008) suggested that implementing robotics can increase productivity, increase costs savings, and enhance safety. Robots have the ability to increase production speed, eliminate human limitations, and reduce variability in operations, all of which reflect on the quality of the end product. Robotic operations can also grant engineers better control of the project, leading to faster problem detections and increase in quality.

In addition to that, robots decrease the dependency on human labor and increase cost savings as they have the potential to lower problems related to quality and rework. The decrease in dependency on humans can also decrease the number of human resources needed, which usually contribute to 30-50% of a total construction project cost, and therefore saves cost, besides improving time performance and better end quality (Balaguer 2000, Dabirian *et al.* 2016, Bakir and Balchi 2018). Researchers noted that even though implementing robotic on the short term would be expensive, companies can reap long term benefits through cost savings; these savings will be the result of replacing human resources will improve costs savings, especially that robots would reduce human errors and provide a "manufacturing type of controlled industry" which better controls the environment and adds focus on the end product (Kitahara and Takashi 2006, Kim *et al.* 2010). Martinez *et al.* (2008) also suggested that safety can be enhanced, especially with the robot's ability to work in dangerous and hazardous zones. This reinforces previous studies that indicated that robots could decrease human need in high risk activities and the incidence of trauma disorders in activities that need repetitive motion (Tucker 1998; Demsetz 1990).

While rating benefits of robotics, contractors considered decreasing human labor, cost savings and higher construction steadiness as the top three benefits followed by increasing productivity, enhancing quality, enhancing safety and reducing material disposal (Struková and Líška 2012). Elhouar *et al.* (2019) considered prefabricated components as the easiest construction aspect to automate as they are constructed by volumes in controlled manufacturing environment. Shop fabricated components are also easy to automate, such as structural and wood elements specific for a project that can be controlled in a shop environment. On the other hand, the authors indicated that some construction aspects are to automate. It is not easy to automate shop fabricated elements, for instance, because it is hard to automate lifting prefabricated components and assembling them. The hardest aspect to automate according to the study remains specialty trades of construction activities, which requires extensive research and development. The authors suggested the integration of 3D printing with robots to automate the construction of a reinforced beam. Bademosi *et al.* (2019) listed further research applications of robotics in construction such as nail and screw recycling (Wang *et al.* 2019), inspection and maintenance (Agnisarman *et al.* 2019), fabrication of building elements (Camacho *et al.* 2018, Zhang *et al.* 2018), masonry works (Goessens *et al.* 2018), earthwork processes (Kim *et al.* 2018), and maintenance and cleaning work for high rise buildings(Lee *et al.* 2018, Muthugala *et al.* 2020). Ruggiero *et al.* (2016) researched emerging robotic technologies that can be applied to construction applications, such as multi-tooled or hydro-powered demolition robots, 3D printing and contour crafting robots, surveying, crafting, monitoring or transportation drones , bricklaying robots whether in buildings or roads, welding robots, exoskeletons to support workers in heavy duty activities that require physical efforts, forklift robots, roadwork robots for repaving or repainting, and humanoids which remain under heavy research and development. The various robotics applications identified by researchers highlight the potential this technology has to transform the industry. However, researcher have also stated that there are challenges and obstacles that need to be overcome before reaping the benefits of automation in construction.

4. Challenges and Barriers for Robotics in Construction

Stewart *et al.* (2004) performed an extensive literature review and identified the information technology (IT) implementation barriers for robotics. The importance of these barriers relies on the fact that automating construction, especially by using robotics, will be heavily dependent on the use and expanding of IT across the construction industry. The authors studied barriers in a top-down effect that starts from the industry, then organization, down to the project. At the level of the *industry*, examples of barriers included the lack of client leadership, poor inter-operability between applications and organizations, fragmentation of the industry, and the low exposure to IT. At the level of the *organization*, barriers included limited resources especially for medium and small enterprises, traditional business practices and resistance to change, and redundancy for IT investments. As for the *project* level, fear of change, low technology literacy oh some key participants, project time tightness and security concerns were a few barriers listed by the study.

Mahbub (2008) organized the barriers into five categories: economic and cost, structure and organization of the industry, construction product and work processes, technology, culture and human factor. *Economic and cost* barriers include high cost of investment and implementation, high-risk investments, and high costs of owning and using. This adds to Fiatech (2004) who also highlighted economic factors such as the unwillingness to pay from owners, no guidance or standards, security, reliability and storage of large data from job site. *Structure and organization of the industry* barriers include the need for compatibility between robotics and existing design, management capabilities, labor practices and site operations. *Construction product and work processes* barriers include the complexity and standardization of construction products, and locational conditions like weather, labor supply, building codes. *Technology* barriers include the nature of construction projects and layout, causing robots to be robust and flexible with high mobility and versatility. Construction usually adopts robots from other industries, so they must be adjusted. Stein *et al.* (2002) suggested robots that move around the site with engines, batteries or motors, reprogrammed to meet changing conditions and changing site layouts (digital control with manipulators using coordinate systems in 3D motion), handle huge loads and adverse weather and site conditions (like dust and chemicals). Lack of repetitive activities in the construction projects is also a barrier, so the industry should perform a lot of reconfiguration to make construction tasks more repetitive and reconfigure construction site to make it more adjusted to robots. The high cost of robots also makes it uncalled for, especially that some countries employ construction labor with very low wages. *Culture and Human Factor* barriers calls for a need of new people with backgrounds in handling robots. First, the labor-intensive nature of the construction industry is also characterized by many small size contractors that have short term contracts that do not require money investment in expensive machineries and robots. Second, being a labor-intensive industry, introducing robots to construction can become a three wat talk between management, labor and unions. Labor unions in some countries refuse robots because they replace workers, while other countries excessively use robots pushing people away from the industry. This was also discussed by Romeo (2015) who considered that robots may be a threat to workers, especially that it is a one-time investment that pays itself and doesn't need worker unions, salaries or healthcare.

Bakir and Balchi (2018) also highlighted barriers such as the industry's high level of fragmentation, project planner's lack of integrating technology while planning to achieve high ROI and fear of risk and financial losses, and organizations' resistance to change the way they operate projects without integrating automation. The study also referenced the harsh working environment of the construction site (Van gassel, 2005) and the risk of cyber breach and low awareness level of technology (Kaivo-oja et al., 2016). Other social issues also affect the implementation of robotics (Burke 2015; Industrial Robots and Robot System Safety 2015; Ruggiero *et al.* 2016). These barriers include the worker and public privacy concerns that can may emerge due to using surveillance technologies like drones. Cyber hacking can also be a concern, whether directly or indirectly. For example, drones can be hacked through their Bluetooth communication network and transfer of data can easily happen from the drone to the hacking party. Some safety concerns also come into place, with some workers fearing on their safety in case of a random event where the robot breaks or gets out of control.

Struková and Líška (2012) conducted a survey to rank barriers against robotics. Contractors considered "high acquiring, maintenance and updating costs" as the biggest barrier, followed by local unavailability and difficulty to acquire, incompatibility with current practices and construction operations, not considered effective in construction sites, low workforce awareness, difficulty in using robots, and finally rejection from workers and/or management. Carra *et al.* (2018) listed different challenges at the level of the construction site, workers, supply chain and material markets. In contrast to the manufacturing industry, the construction site is very dynamic and not stationary. Different buildings are unique in different aspects such as shape, design, materials and locations, so technologies should be extra flexible and adaptive to change. Moreover, construction-project stakeholders are rather traditional, with a skeptical attitude towards changes especially on the technology side. The complexity of the supply chain is another challenge, especially that the construction supply chain is fragmented, so is the variety in markets. Regional markets have intrinsic differences when it comes to regulations, material and workforce costs, and desirable product qualities implying different requirements for robots.

Delgado *et al.* (2019) investigated the construction industry specific related challenges against implementing robotics. Using literature, the study divided the challenges across five themes: the aging, unskilled *workforce* and lack of training; *economic* including high capital investment, low return on investment intensive capital and stifle collaboration contracts; *cultural* challenges which include the industry being very well established and resistant to change, in addition to fear of job loss and robot-human interaction; *research and development* (R&D) challenges including the low investment in R&D and its narrow scope, weak innovation and complex implementation; and finally the *industry-intrinsic* challenges because of the industry's nature of being fragmented, project-based, intensively competitive, highly risky, poor communication, low profits, limited use of digital modelling, in addition to the predominance of the SME sector and the conflicting interests and subpar collaboration in the supply chain. The study then divided the challenges across four factors that limit the adoption of robotics: contractor's economic factors, client's economic factors, technical and work culture factors and the robotics' weak business case. At the level of the contractor, the easy access to labor, weak motivation to improve productivity and the domination of small subcontractors that don't have the resources to adopt and implement robotics play a big role in avoiding automation, in addition to the industry being high risk with low profit margins in compared to other industries (according to TCI (2018), the top 100 construction companies in the United Kingdom had an average profit margin of around 1.5% in 2017). As for clients, especially at the level of governments, the decrease in spending and the continuous search for the "lowest price" to award projects restricts the use of automation and limits creativity and critical thinking. Technical and work culture factors are related to the industry's culture that resists change, in addition to the workforce who are not trained on human-robot interactions, and the unproved effectiveness of robots and the immaturity of available technologies. Finally, the weak business case is simply because of the lack of strong evidence supporting the claims of time and cost savings due to robotics, especially that construction is low profit and high risk. Proof for high return on investment is needed from research to convince enterprises to utilize robots.

Challenges mentioned and described in this section did not come without suggestions to overcome them. Starting with Delgado *et al.* (2019) who recommended contractors to analyze the risk factors of utilizing robots to justify the high investment costs, urged governments to use their resources to incentivize the adoption of technologies, and asked for more research on the interaction between humans and workers. Bakir and Balchi (2018) recommended a four level robotization pyramid that companies can follow to shift from pure human-driven tasks, to using tools and equipment (current state), to semi-robotized machines reaching the ultimate goal of fully robot—driven activities. Bademosi *et al.* (2019) identified foundational knowledge, skills, and abilities (KSAs) that can be implemented in construction education to equip construction students for successful future in automaton. Carlos and Mohamed (2008) called for more integration between project stakeholders (such as architect, designers, structural, MEP), expanding the dependency om pre-fabrication technology, modify construction machinery to be more autonomous and develop user-friendly robots with easy to handle machine systems, and a heavier investment in research and development that target the culture and organizations to create change. Struková and Líška (2012) state that change should start by people then technology, and the most important factor to adopt robots is that the construction robots have to have a high system flexibility to adapt with the unstable environment of construction site. The study called for more focus on semi-automated systems that can be better monitored and controlled than fully automated systems, especially in tasks and activities with low safety risks. This can encourage small and medium sized construction companies to adopt this technology and utilize it; especially that robotics can be developed for tasks that endanger the health and safety of labor.

5. Recommendations for Robotics: Proposed Framework

Findings from previous sections show different challenges that need to be overcome to successfully implement robotics on construction projects. Most of these challenges focused on the short-term financial aspects of implementing robotics, resistance for change from organizations, and nature of the construction projects. However, research continues to weigh the perceived benefits of implementing robotics. Benefits such as productivity, quality, communication, innovation, and safety can result in rewarding long-term benefits at the organizational level. Moreover, the extant literature highlights that an organization that aims to implement automation and adopt robotics on their projects needs to have the support of its management. It is crucial that management commits to this change and promotes innovation, enabling the transformation of traditional processes, empowering employees, providing training, and investing in both new technologies and solid networks to handle this change.

The culminating effort of this study is a framework that aims to assist construction enterprises when deciding to implement robotics. The framework, displayed in Figure 1, presents essential recommendations for three different facets: organization (which includes management and processes), people (which encompasses engineers, construction labor and administrative staff working on and off construction sites), and technology.

As previously synthesized in this paper, each of these facets has several challenges that need to be overcome and addressed before moving forward with implementing robotics. For example, when making such a decision, selecting the appropriate software and hardware need to be considered, proper training need to be provided, alongside the full support of executives and management (has support of executives and management. Implementing robotics is a multi-dimensional decision and a one-size-fits-all strategy is not possible. The framework outlined in Figure 2 provides companies with a set of recommendations to implement robotics by addressing common robotics challenges encountered in all three facets. This implementation will ultimately result in short- and long-term benefits (outlined on the outer surface of the framework).

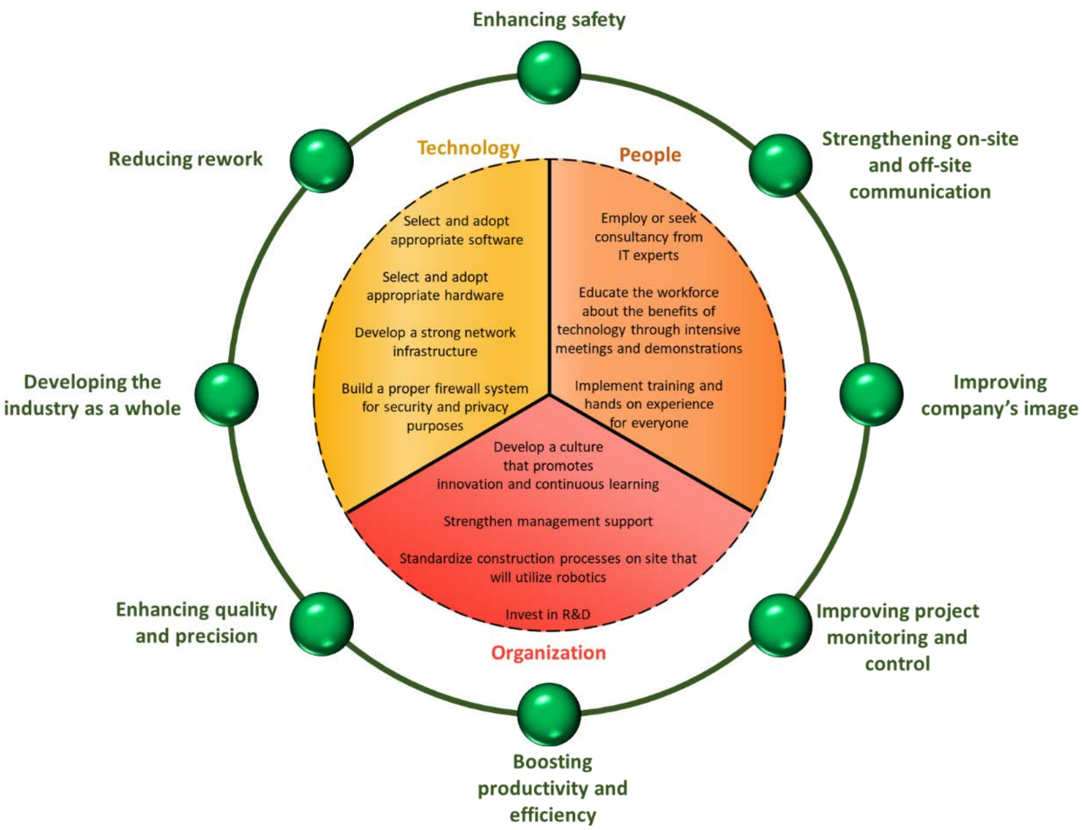

Figure 2: A Framework for the Implementation of Robotics in Construction

6. Conclusions, Limitations and Further Study

Implementing robotics is an integral part of automating the construction industry. Despite the different barriers standing against this implementation, research is being developed on different construction applications and tasks to slowly transition the world's most traditional industry into the new era of automation. This paper reviewed the different research done on topic, from benefits, use cases, and challenges. The different findings were transformed by the authors to a list of recommendations, presented in the form of a simple framework that can assist construction enterprises in their decision to adopt robots and implement robotic automation in their projects. The framework was limited to the papers reviewed in this research. It also presented general conditions that the enterprise should consider at the level of the organization, the technology being adopted, and the employees working inside the enterprise. Further studies can adopt this framework and expand on the technicalities of every aspect discussed. More facets can be added into it as well, such as the types of activities that can be automated and the current robots available to perform this automation. Other further studies can validate the framework through interviewing construction enterprises and presenting the framework to confirm, remove and/or add new aspects and recommendations.

References

Aghimien, D.O., Aigbavboa, C.O., Oke, A.E., and Thwala, W.D., (2019). Mapping out research focus for robotics and automation research in construction-related studies. *Journal of Engineering, Design and Technology*.

Agnisarman, S., Lopes, S., Madathil, K.C., Piratla, K., and Gramopadhye, A., (2019). A survey of automation-enabled human-in-the-loop systems for infrastructure visual inspection. *Automation in Construction*, 97, pp.52–76.

Bademosi, F.M., Tayeh, R., and Issa, R.R., (2019). Skills Assessment for Robotics in Construction Education.

Bakir, A. and Balchi, I., (2018). Development and Implementation of Robotics in Construction A Case Study of a Contractor Firm. Master's Thesis.

Balaguer, C., (2000). Open issues and future possibilities in the EU construction automation. *In*: *Proceedings of the IAARC International Symposium on Robotics and Automation, Taipei, Taiwan*. Citeseer.

Balaguer, C. and Abderrahim, M., (2008). Trends in Robotics and Automation in Construction, Robotics and Automation in Construction. *Tech, URL:* http://www.intechopen.com/books/robotics_and_automation_in_construction/trends_in_robotics_and_automation_in_construction

Banik, G. C., Barnes, W. C., (2002). Issues and Challenges for the Construction Community. *ASEE Annual Conference proceedings*, 5365-5372, ASEE.

Bock, T., (2015). The future of construction automation: Technological disruption and the upcoming ubiquity of robotics. *Automation in Construction*, 59, pp.113–121.

Bock, T. and Linner, T., (2015). *Robot oriented design*. Cambridge University Press.

Burke, C, (2015). Expert: Terrorists Hacking Into Robots, Drones to Use as Weapons. *Newsmax*, *N.p.*, 16 Apr. 2015. Web. 14 Oct. 2015.

Buswell, R.A., Soar, R.C., Gibb, A.G., and Thorpe, A., (2007). Freeform construction: mega-scale rapid manufacturing for construction. *Automation in construction*, 16 (2), pp.224–231.

Camacho, D.D., Clayton, P., O'Brien, W.J., Seepersad, C., Juenger, M., Ferron, R., and Salamone, S., (2018). Applications of additive manufacturing in the construction industry–A forward-looking review. *Automation in construction*, 89, pp.110–119.

Carlos, B. and Mohamed, A., (2008). Trends in Robotics and Automation in Construction. *Robotics and Automation in Construction, Balaguer Carlos and Abderrahim Mohamed, Eds. InTech*.

Carra, G., Argiolas, A., Bellissima, A., Niccolini, M., and Ragaglia, M., (2018). Robotics in the construction industry: state of the art and future opportunities. *In*: *ISARC. Proceedings of the International Symposium on Automation and Robotics in Construction*. IAARC Publications, pp.1–8.

Dabirian, S., Khanzadi, M., and Moussazadeh, M., (2016). Predicting labor costs in construction projects using agent-based modeling and simulation. *Scientia Iranica*, 23 (1), pp.91–101.

Delgado, J.M.D., Oyedele, L., Ajayi, A., Akanbi, L., Akinade, O., Bilal, M., and Owolabi, H., (2019). Robotics and automated systems in construction: Understanding industry-specific challenges for adoption. *Journal of Building Engineering*, 26, 100868.

Demsetz, L. (1990). Automated Construction: Manufacturing has become highly automated - so why not building construction*? Construction Dimensions*, pp.79-85.

Elattar, S., (2008). Automation and robotics in construction: opportunities and challenges. *Emirates journal for engineering research*, 13 (2), pp.21–26.

Elhouar, S., Alzarrad, M.A., and Elhouar, S., (2019). A Synopsis of 3D Printing and Robotics Applications in Construction.

Fiatech (2004). Intelligent & Automated Construction Job Site, 1-8, URL: http://fiatech.org/projects/roadmaps/jobsite.html

Goessens, S., Mueller, C., and Latteur, P., (2018). Feasibility study for drone-based masonry construction of real-scale structures. *Automation in Construction*, 94, pp.458–480.

Industrial Robots and Robot System Safety, (2015). *OSHA Technical Manual (OTM)*. Occupational Safety & Health Administration. United States Department of Labor. Web. 14 Oct. 2015.

Jackson, J.R., (1990). *Robotics in the Construction Industry*. FLORIDA UNIV GAINESVILLE DEPT OF CIVIL ENGINEERING.

Kim, J., Lee, S.S., Seo, J., and Kamat, V.R., (2018). Modular data communication methods for a robotic excavator. *Automation in Construction*, 90, pp.166–177.

Kim, T., Lee, U.-K., Yoo, W.S., An, S.-H., Cho, H., Lee, Y., and Doh, N., (2010). Benefit/cost analysis of a robot-based construction automation system. *In*: *ICCAS 2010*. IEEE, pp.616–621.

Kitahara, S. and Takashi, Y., (2006). Deployment of construction robots applying the information technology and network system. *In*: *Proc. Int. Symp. Automation and Robotics in Construction*. pp.19–23.

Lee, Y.-S., Kim, S.-H., Gil, M.-S., Lee, S.-H., Kang, M.-S., Jang, S.-H., Yu, B.-H., Ryu, B.-G., Hong, D., and Han, C.-S., (2018). The study on the integrated control system for curtain wall building façade cleaning robot. *Automation in Construction*, 94, pp.39–46.

Löfgren, A., (2006). ICT investment evaluation and mobile computing business support for construction site operations. *In*: *5th annual mobility roundtable conference, 1-2 June 2006, Helsinki*.

Mahbub, R., (2008). An investigation into the barriers to the implementation of automation and robotics technologies in the construction industry. PhD Thesis. Queensland University of Technology.

Martinez, S., Balaguer, C., Jardon, A., Navarro, J., Gimenez, A., and Barcena, C., (2008). Robotized lean assembly in the building industry. *In*: *Proceedings of the 25th International Symposium on Automation and Robotics in Construction, Vilnius, Lithuania*. pp.26–29.

McKinsey Global Institute, (2017). Reinventing Construction through a Productivity Revolution. URL: https://www.mckinsey.com/industries/capital-projects-and-infrastructure/our-insights/reinventing-construction-through-a-productivity-revolution

Muthugala, M., Vega-Heredia, M., Mohan, R.E., and Vishaal, S.R., (2020). Design and Control of a Wall Cleaning Robot with Adhesion-Awareness. *Symmetry*, 12 (1), p.122.

Romeo, N, (2015). Afraid of Robots Taking Your Jobs? You Should Be. *The Daily Beast*. Newsweek/Daily Beast, 3 June 2015. Web. 11 Oct. 2015.

Ruggiero, A.N., St Laurent, C.L., and Salvo, S.D., (2016). Robotics in construction.

Seo, J., Lee, S., Kim, J., and Kim, S.-K., (2011). Task planner design for an automated excavation system. *Automation in Construction*, 20 (7), pp.954–966.

Stein, J., Gotts, V., and Lahidji, B., (2002). Construction Robotics. *Eastern Michigan University*.

Stewart, R.A., Mohamed, S., and Marosszeky, M., (2004). An empirical investigation into the link between information technology implementation barriers and coping strategies in the Australian construction industry. *Construction Innovation*, 4 (3), pp.155–171.

Struková, Z. and Líška, M., (2012). Application of automation and robotics in construction work execution. *AD ALTA: Journal of Interdisciplinary Research*, 2 (2), pp.121–125.

The Construction Index (TCI), (2019). TCI Top 100 Construction Companies 2018. URL: https://www.theconstructionindex.co.uk/news/view/tci-top-100-construction-companies-2018

Tucker, R, (1988). High Payoff Areas fix Automation Applications*, Proc. of the Fifth International Symposium on Automation and Robotics in Construction,* 9-16, June 68, 1988. Tokyo.

Wang, Z., Li, H., and Zhang, X., (2019). Construction waste recycling robot for nails and screws: Computer vision technology and neural network approach. *Automation in Construction*, 97, pp.220–228.

Zhang, X., Li, M., Lim, J.H., Weng, Y., Tay, Y.W.D., Pham, H., and Pham, Q.-C., (2018). Large-scale 3D printing by a team of mobile robots. *Automation in Construction*, 95, pp.98–106.

A Review of Wall-Climbing Robots: Technical Analysis and Potential for Indoor Building Inspection

Leyuan Ma, Timo Hartmann
Technische Universität Berlin, Germany
leyuan.ma@campus.tu-berlin.de

Abstract. Regular inspection is indispensable during the operation period of existing buildings. However, the current approaches involve a high number of manual operations and are by large limited to the inspection of visible elements. Autonomous wall-climbing robot with through-wall imaging module to perform visual inspection of concealed components has the potential to overcome these problems. Towards this goal, this paper reports on a survey on different adhesion and locomotion technologies for wall-climbing robots. Doing so, we qualitatively evaluated available adhesion and locomotion approaches based on seven criteria: reliability, simplicity, payload capacity, velocity and continuity, transition dexterity, steering ability, and obstacle-overcoming ability. Finally, according to the prioritized requirements for indoor building inspection, pneumatic adhesion combining wheel-driven movement outperforms other combinations, which is applied to the prototype of the proposed indoor wall-climbing robot.

1. Introduction

Periodical inspection and preventive maintenance of existing buildings can reduce the possibility of unexpected failures in systems and equipment, and provide valuable information to all relevant parties. However, with the high number and complexity of building components in existing buildings, it is cumbersome for building owners and maintenance staff to conduct a thorough inspection and real-time surveillance during the operation period of a building. This has motivated extensive research on thermography-based building performance inspection (Ham and Golparvar-Fard, 2014), sensor-based indoor environmental monitoring (Ali et al., 2016), non-destructive testing for condition assessment of building structures (Venkatesh and Alapati, 2017), and automated fault detection and diagnostic for building systems with the help of building automation system (BAS) (Golabchi et al., 2016). Some of them also focused on improving the automation level using mobile-robot platforms (Rakha and Gorodetsky, 2018; Mantha et al., 2018). The main challenges facing the current research and implementation are as follows: 1) the installation of sensors for some old buildings without BAS is labor-consuming and the sensors are inadequate to provide sufficient monitoring information; 2) the output data are usually not intuitive and still need further professional analysis to detect and localize the fault; 3) the existing inspection techniques are limited to the surface level, some building components such as mechanical, electrical and plumbing systems (MEP) hidden in walls and ceilings cannot be detected. Although there are some wall scanning devices available in the market (e.g. Walabot, Bosch Wallscanner and DeWalt Hand Held Radar Scanner), they are manually operated, which limits their application for higher spaces in a building. All the challenges above lead to the need for developing an indoor wall-climbing robot system with on-board sensors to achieve a real-time visual inspection for concealed components.

Wall-climbing robots capable of moving on various types of surfaces and performing tasks on desired locations have been widely used in the remote examination and maintenance of hard-to-reach surfaces. With respect to its application on building inspection, scientific work mainly focused on wall-climbing robot aided crack inspection or deterioration estimation of exterior walls (Sekhar, 2014; Schmidt and Berns, 2013). There is still a dearth of studies in employing wall-climbing robots in monitoring internal building components. For the robot to achieve continuous motion and conduct the desired work on indoor horizontal or vertical surfaces, two essential elements including adhesion and locomotion mechanisms need to be taken into consideration. Several reviews for those mechanisms used in current wall-climbing robots were published over the last decade (Schmidt and Berns, 2013; Nansai and Mohan, 2016). Nevertheless, none of them was presented from the perspective of building inspection. The aim and the contribution of this paper is to provide a holistic survey and an adaptability assessment for existing attachment and movement methods in the context of indoor building inspection, which allows for realizing an optimal design of the indoor wall-climbing robot.

This paper first defines a set of criteria for the evaluation of different mechanisms. Then it summarizes adhesion and locomotion principles applied in existing wall-climbing robots, and analyses the advantages and disadvantages of different methods according to the criteria. Furthermore, this paper discusses which locomotion or adhesion technique is suitable for the indoor wall-climbing robot to accomplish building inspection. Finally, it concludes by a possible combination of the attachment and movement technology, and a prototype of the indoor wall-climbing robot.

2. Methodology

2.1 Evaluation Criteria Definition

A successful wall-climbing robot has to be specialized to the certain task and the field of application. In this paper, we define that a comprehensive building examination includes the inspection of building walls, roofs, structural components and major MEP systems. Since there are already some wall-climbing robots and drone-based instruments for the building exterior inspection, this work focuses on studying how a wall-climbing robot can move and conduct tasks on interior walls and ceilings. To this end, we suggest seven criteria in Table 1, with which we assess different existing wall-climbing technologies.

Table 1: Evaluation criteria of wall-climbing robot technologies

Number	Criterion	Implication	Remarks
1	Reliability	The degree of stability at which a robot can attach to the wall	The robot should remain stable while operating on surfaces associated with unevenness and dust
2	Velocity and continuity	The extent of speed and continuity the robot can reach	The robot should move continuously at a given speed
3	Obstacle overcoming ability	The height of a hurdle the robot can cross	The robot should be able to get over most obstacles that may appear on the surface
4	Steering ability	The ability of the robot to move omnidirectionally	The robot should flexibly change the direction of movement
5	Transition dexterity	The capacity of the robot to smoothly transfer between two orthogonal surfaces	The robot should autonomously move between two surfaces

6	Payload capacity	The weight of the auxiliary equipment the robot can carry	The robot should stay stably on the wall with the carried instruments
7	Simplicity	The workload for designing, assembling and controlling	A non-complex design makes the robot lightweight, compact and energy-saving

2.2 Review Strategy

The advanced search function in Web of Science was used to obtain a comprehensive and accurate literature list. The searching formula was TS= (maintenance OR examin* OR inspect* OR monitor* OR audit* OR check*) AND TI=(climbing robot), with which 730 publications were found. After reading the titles, abstracts and conclusions, 42 of them were selected for further review. From these 42 papers, we extracted four main adhesion principles and accordingly divided the papers into four groups. After that, we summarized movement modes applied in each group of articles, followed by the evaluation of existing technologies.

3. Adhesion Techniques

The main adhesion techniques reported in the scientific literature are 1) magnetic adhesion, 2) pneumatic adhesion, 3) bio-inspired adhesion, and 4) electrostatic adhesion. In terms of the magnetic adhesion, its requirement for ferromagnetic surfaces limits its application on most internal surfaces of the building. So the following investigation only focuses on the other three adhesion principles.

3.1 Pneumatic Adhesion

Pneumatic adhesion is the most common approach to press the robot on the desired surface. It can be achieved through vacuum suction or propulsion. Specifically, vacuum suction usually depends on suction cups to create partial vacuum. A suction cup is an elastic and flexible object using negative pressure to adhere to nonporous surfaces (Brusell et al., 2016). The vacuum suction can either be passively produced (Yoshida and Ma, 2010) or actively produced (Zhao et al., 2004; Schmidt et al., 2011). The passive suction simply relies on the physical pressure of the suction cup against the desired surface, which is simple and energy-saving. However, the passive suction cup only performs well on smooth surfaces like glass walls, the roughness of some interior walls or ceilings can easily lead to a loss of adhesion.

In active suction, suction cups along with on-board or external electrical vacuum pumps are commonly utilized. These active systems supply stronger adhesion, which enables the robot to work on rougher surfaces. But the seal leakage can still happen when crossing obstacles on the surface. This leads to the increasing number of suction cups (Schmidt et al., 2011), and at the same time adds complexity to the system. Besides, the on-board vacuum pump makes the system heavy, while the external device limits the operating range. Additionally, the system might be too noisy to be used indoors and demands high power consumption to maintain contact. The other available approach is based on the principle of the vacuum impeller. It consists of a short cylinder with an open inlet covering the blades, and a drive shaft connecting the motor and the blades (Liang et al., 2014). The high-speed rotation of the blades causes a rotational airflow, which then generates a negative pressure inside the cylinder shell to make the whole unit attach to the working surface. In this way, the noisy and energy-consuming vacuum pump can be replaced. Another advantage of this method is its applicability to a broad range of surface conditions as there can be no contact between the adsorption generator and the target surface. Meanwhile, the clearance height between the suction unit and the surface also makes it possible for the robot to pass over some bulges, although the robot designer needs to find the optimal clearance height to ensure both the adhesion and the obstacle-surmounting ability.

As for the propulsion-based adhesion, the presented robots are mainly equipped with propellers, which are open running devices with blades that convert the rotational motion into thrust force (Nishi and Miyagi, 1993). This method possesses all the strengths of the impeller-based apparatus and the robot can even fly over higher obstacles if its main structure is designed as a drone (Myeong et al., 2015). However, the common challenge facing these two techniques is the selection of proper types of blades, as well as motors to assure the stability and enough load capacity of the robot.

3.2 Bio-Inspired Adhesion

Some insects and vertebrate animals that can move smoothly along most surfaces in nature have become a source of inspiration for researchers. Synthetic dry adhesive's adhesion through van der Waals force (Aksak et al., 2008), and bionic grasping grippers like claws (Xu et al., 2012) or miniature spines (Liu et al., 2013) which form a force closure between the gripper and the rough wall, are two typical bionic techniques to create attachment. These biomimetic mechanisms do not need external energy to provide pressure difference. Besides, the bio-inspired robot can be assembled to be compact and light. However, firstly, the new bionic technology is still under development and has not achieved high performance as animals. For example, the gecko-driven fibrillar adhesives are sensitive to the dust and have no self-cleaning ability, which causes the decrease of the adhesion. Secondly, the complete imitation of the well evolved animal structure and the kinematics of their legs is still a tricky task. In other words, it usually requires a complex mechanical structure. Thirdly, since climbing animals usually carry their own weight when moving, bio-inspired robots also have low payload.

3.3 Electrostatic Adhesion

Electrostatic adhesion applies the principle of electrostatic induction to produce attraction force between the electrode panel and the traversed surface. Wall-climbing robots using this adhesion principle are usually equipped with electroadhesive foot pads (Chen, 2015). It shows excellent ability to clamp to various kinds of surfaces including wood, dry concrete, drywall, glass and steel (Schmidt and Berns, 2013). It is safe and energy-efficient, and can realize a lightweight structure. Unfortunately, the development of this technology is still at an early stage and has not been fully understood. Furthermore, its adhesion force is weaker than the other techniques and thus has low bearing capacity.

4. Locomotion Mechanisms

Different adhesion methods require different locomotion means. In general, there are three means of robot locomotion that we found in the literature: leg-based, wheel-driven, and track-based.

4.1 Leg-Based Locomotion

Leg-based mechanisms work in combination with suction cups (Guan et al., 2013), electroadhesive pads (Chen, 2015), or bio-inspired feet (Liu et al., 2013). This step-wise operation enables each foot to achieve attachment/detachment on/from the surface. In this way, the robot can easily step over an obstacle and move from one plane to another. Nevertheless, it requires time to alternately switch the idling and the supporting leg, which not only reduces the moving velocity and continuity, but also demands an advanced controlling system. Besides, it is hard to quickly change the climbing direction. With respect to the mechanical design, the number of limbs and the degree of freedom (DOF) for each limb are determined by the requirements of specific applications. Wall-climbing robots with biped (Guan et al., 2013), quadruped (Chattunyakit et al., 2019), hexapod (Spenko et al., 2008) and octopod (Xu et al., 2012) structure are available in the current research. Apparently, the increasing number of limbs and the larger DOF improves the mobility and the stability of the robot. However, this comes with a complicated and heavy structure. Therefore, a trade-off between the configuration and the performance needs to be made.

4.2 Wheel-Driven Locomotion

The wheel-driven climbing robot usually works together with the propeller or vacuum impeller. The attachment and movement can be accomplished via the combination of the pneumatic adhesion and wheel drive force with maximized friction between the wheel and the surface (Myeong et al., 2015). During climbing, wheels' motors generate the required torque either to stop the robot at any position or to move it to any place, which guarantees the stability and the flexibility of the whole system (Alkalla et al., 2015). This hybrid actuation system not only holds all the advantages of the pneumatic adhesion such as high performance in obstacle overcoming and adaptability to multiple surfaces, but also allows a higher velocity and continuity, as well as a compact size. However, a strong thrust force is required in order to drive the robot to transfer between two orthogonal surfaces especially from the vertical surface to the horizontal, which increases the difficulty of the design. EJBOT-II (Alkalla et al., 2019) added two arms to provide forces against the ground to help the robot raise up toward the wall. Unfortunately, there is no practical test to verify its ability to move from the wall to the ceiling.

4.3 Track-Based Locomotion

The track-based mechanism can be equipped with multiple suction cups (Lee et al., 2015) or bionic feet (Liu et al., 2019). Compared with the legged climbing robot, caterpillar treads on this kind of robot offer larger adhesion area, which enhances the adhesion property and the payload capacity. But its rotary motion makes it difficult to control pads to detach from or attach to surfaces. Besides, although the crawler-type robots provide more traction force than the wheeled structure, they are too bulky and hard to move omnidirectionally.

5. Discussion

Based on the above evaluation of present adhesion and locomotion techniques, we failed to identify a mechanism that performs equally well with respect to all criteria. To ensure an optimal design, a robot developer should prioritize the design requirements according to the area of application. For the purpose of visually inspecting indoor building components including MEP systems inside walls and ceilings, the basic requirement for the robot is a high reliability. In other words, the robot system has to be safe enough to assure its attachment, since an unexpected fall can be dangerous. Second, a compact and lightweight architecture can not only save a lot of energy, but also makes the robot easy to stably adhere to the wall. Third, the payload capacity, which is also related to the reliability, needs to allow the robot to carry multiple sensors for visual examination and power supply to support at least one-room inspection. Fourth, the robot should reach a velocity of about 10cm/s and move continuously for a fast through-wall detection of the electrical wiring, plumbing, structural components and wood-destroying insects. Fifth, to realize autonomous inspection, the robot should also be capable of smoothly transferring between indoor horizontal and vertical surfaces. Sixth, to conduct a thorough examination, robots need to harness benefits of arbitrary movements. Last, since the indoor surfaces are relatively flat, the robot is desired to pass over small obstacles like some protruding decorations on the wall.

Table 2 presents nine combinations of the attachment and movement mechanisms, and the qualitative evaluation of defined criteria according to the reported properties by literature. Based on the reported result of each alternative in the reviewed literature, we qualitatively assigned a binary value of “high” and “low” to represent the performance of alternative against each criterion. Considering the above prioritized requirements, it shows that the combination of pneumatic adhesion and wheel-driven movement outperforms other systems. Fig. 1 shows the prototype of the indoor wall-climbing robot we built. It is expected to function on plaster walls or drywalls and plaster ceilings in existing buildings or newly constructed buildings where interior furnishing is finished. The built prototype here illustrates the connection of the selected two mechanisms. In future work, we plan to firstly test the blades and motors to see whether it can provide enough thrust force for adhesion. Besides, we will conduct a thorough review of available non-destructive testing technologies and choose one that can inspect hidden components in existing buildings. Furthermore, we need to develop a stable structure that supports a smooth transition between the wall and the ceiling.

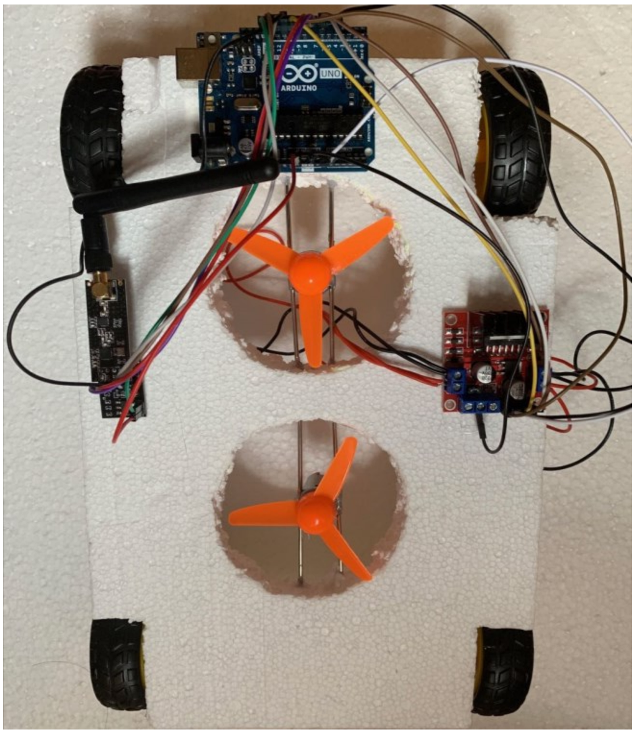

Figure 1: Indoor wall-climbing robot prototype

Table 2: Evaluation of available combinations of locomotion and adhesion mechanisms

<table>
<tr><th>Locomotion mechanism</th><th colspan="2">Adhesion mechanism</th><th>Reliability</th><th>Simplicity</th><th>Payload capacity</th><th>Velocity and continuity</th><th>Transition dexterity</th><th>Steering ability</th><th>Obstacle-overcoming ability</th></tr>
<tr><td rowspan="4">Leg-based locomotion</td><td rowspan="2">Pneumatic adhesion</td><td>Passive suction cups</td><td>Low</td><td>Low</td><td>Low</td><td>Low</td><td>High</td><td>Low</td><td>High</td></tr>
<tr><td>Active suction cups</td><td colspan="3">Depends on the configuration of the limbs</td><td>Low</td><td>High</td><td>Low</td><td>High</td></tr>
<tr><td rowspan="2">Bio-inspired adhesion</td><td>Synthetic dry adhesive</td><td>Low</td><td>Low</td><td>Low</td><td>Low</td><td>High</td><td>Low</td><td>High</td></tr>
<tr><td>Bionic grasping grippers</td><td>High</td><td>Low</td><td>Low</td><td>Low</td><td>High</td><td>Low</td><td>High</td></tr>
<tr><td rowspan="2">Wheel-driven locomotion</td><td rowspan="2">Pneumatic adhesion</td><td>Impeller-based adsorption</td><td>High</td><td>High</td><td rowspan="2">Depends on the performance of the impeller / propeller</td><td>High</td><td rowspan="2">Depends on the performance of the impeller/ propeller and the structure</td><td>High</td><td rowspan="2">Depends on the clearance height between the pneumatic unit and the surface</td></tr>
<tr><td>Propeller-based propulsion</td><td>High</td><td>High</td><td>High</td><td>High</td></tr>
<tr><td rowspan="3">Track-based locomotion</td><td>Pneumatic adhesion</td><td>Passive suction cups</td><td>High</td><td>Low</td><td>High</td><td>High</td><td>Low</td><td>Low</td><td>High</td></tr>
<tr><td rowspan="2">Bio-inspired adhesion</td><td>Synthetic dry adhesive</td><td>High</td><td>Low</td><td>High</td><td>High</td><td>Low</td><td>Low</td><td>High</td></tr>
<tr><td>Bionic grasping grippers</td><td>High</td><td>Low</td><td>High</td><td>High</td><td>Low</td><td>Low</td><td>High</td></tr>
</table>

6. Conclusion

This paper investigated the existing wall-climbing robots for inspection and maintenance tasks and found nine typical types of robot systems with different locomotion and adhesion mechanisms. Further, we assessed those nine systems based on the evaluation criteria defined for the indoor wall-climbing robot. The result showed that the motorized wheels along with the propeller or vacuum impeller could be a promising approach. However, further research is necessary to create a wall-climbing robot architecture which allows the robot to move from the vertical surface to the horizontal surface. It is also our aim to call the attention of professionals in robotics and building management to the application of wall-climbing robots indoors.

References

Aksak, B., Murphy, M.P., Sitti, M., (2008). Gecko inspired micro-fibrillar adhesives for wall climbing robots on micro/nanoscale rough surfaces, in: 2008 IEEE International Conference on Robotics and Automation. Presented at the 2008 IEEE International Conference on Robotics and Automation, pp. 3058–3063. https://doi.org/10.1109/ROBOT.2008.4543675

Ali, A.S., Zanzinger, Z., Debose, D., Stephens, B., (2016). Open Source Building Science Sensors (OSBSS): A low-cost Arduino-based platform for long-term indoor environmental data collection. Building and Environment 100, pp.114–126. https://doi.org/10.1016/j.buildenv.2016.02.010

Alkalla, M.G., Fanni, M.A., Mohamed, A.F., Hashimoto, S., Sawada, H., Miwa, T., Hamed, A., (2019). EJBot-II: an optimized skid-steering propeller-type climbing robot with transition mechanism. Advanced Robotics 33, pp.1042–1059. https://doi.org/10.1080/01691864.2019.1657948

Alkalla, M.G., Fanni, M.A., Mohamed, A.M., (2015). A novel propeller-type climbing robot for vessels inspection, in: 2015 IEEE International Conference on Advanced Intelligent Mechatronics (AIM). Presented at the 2015 IEEE International Conference on Advanced Intelligent Mechatronics (AIM), pp. 1623–1628. https://doi.org/10.1109/AIM.2015.7222776

Brusell, A., Andrikopoulos, G., Nikolakopoulos, G., (2016). A survey on pneumatic wall-climbing robots for inspection, in: 2016 24th Mediterranean Conference on Control and Automation (MED). Presented at the 2016 24th Mediterranean Conference on Control and Automation (MED), IEEE, Athens, Greece, pp. 220–225. https://doi.org/10.1109/MED.2016.7535885

Chattunyakit, S., Kobayashi, Y., Emaru, T., Ravankar, A.A., (2019). Bio-Inspired Structure and Behavior of Self-Recovery Quadruped Robot with a Limited Number of Functional Legs. https://doi.org/10.3390/app9040799

Chen, R., (2015). A Gecko-Inspired Electroadhesive Wall-Climbing Robot. IEEE Potentials 34, pp.15–19. https://doi.org/10.1109/MPOT.2014.2360020

Golabchi, A., Akula, M., Kamat, V., (2016). Automated building information modeling for fault detection and diagnostics in commercial HVAC systems. Facilities 34, pp.233–246. https://doi.org/10.1108/F-06-2014-0050

Guan, Y., Zhu, H., Wu, W., Zhou, X., Jiang, L., Cai, C., Zhang, L., Zhang, H., (2013). A Modular Biped Wall-Climbing Robot With High Mobility and Manipulating Function. IEEE/ASME Transactions on Mechatronics 18, pp.1787–1798. https://doi.org/10.1109/TMECH.2012.2213303

Ham, Y., Golparvar-Fard, M., (2014). 3D Visualization of thermal resistance and condensation problems using infrared thermography for building energy diagnostics. Vis. in Eng. 2, 12. https://doi.org/10.1186/s40327-014-0012-0

Lee, G., Kim, H., Seo, K., Kim, J., Kim, H.S., (2015). MultiTrack: A multi-linked track robot with suction adhesion for climbing and transition. Robotics and Autonomous Systems 72, pp.207–216. https://doi.org/10.1016/j.robot.2015.05.011

Liang, R., Altaf, M., Ahmad, E., Liu, R., Wang, K., (2014). A Low-Cost, Light-Weight Climbing Robot for Inspection of Class Curtains. International Journal of Advanced Robotic Systems 11, 106. https://doi.org/10.5772/58710

Liu, Y., Sun, S., Wu, X., Mei, T., (2013). A leg-wheel wall-climbing robot utilizing bio-inspired spine feet, in: 2013 IEEE International Conference on Robotics and Biomimetics (ROBIO). Presented at the 2013 IEEE International Conference on Robotics and Biomimetics (ROBIO), IEEE, Shenzhen, China, pp. 1819–1824. https://doi.org/10.1109/ROBIO.2013.6739732

Liu, Yanwei, Liu, S., Wang, L., Wu, X., Li, Y., Mei, T., (2019). A Novel Tracked Wall-Climbing Robot with Bio-inspired Spine Feet, in: Yu, H., Liu, J., Liu, L., Ju, Z., Liu, Yuwang, Zhou, D. (Eds.), Intelligent Robotics and Applications, Lecture Notes in Computer Science. Springer International Publishing, Cham, pp. 84–96. https://doi.org/10.1007/978-3-030-27532-7_8

Mantha, B.R.K., Menassa, C.C., Kamat, V.R., (2018). Robotic data collection and simulation for evaluation of building retrofit performance. Automation in Construction 92, pp.88–102. https://doi.org/10.1016/j.autcon.2018.03.026

Myeong, W.C., Jung, K.Y., Jung, S.W., Jung, Y.H., Myung, H., (2015). Development of a drone-type wall-sticking and climbing robot, in: 2015 12th International Conference on Ubiquitous Robots and Ambient Intelligence (URAI). Presented at the 2015 12th International Conference on Ubiquitous Robots and Ambient Intelligence (URAI), IEEE, Goyang, South Korea, pp. 386–389. https://doi.org/10.1109/URAI.2015.7358881

Nansai, S., Mohan, R.E., (2016). A Survey of Wall Climbing Robots: Recent Advances and Challenges. Robotics 5, 14. https://doi.org/10.3390/robotics5030014

Nishi, A., Miyagi, H., (1993). Propeller type wall-climbing robot for inspection use. https://doi.org/10.22260/ISARC1993/0025

Rakha, T., Gorodetsky, A., (2018). Review of Unmanned Aerial System (UAS) applications in the built environment: Towards automated building inspection procedures using drones. Automation in Construction 93, pp.252–264. https://doi.org/10.1016/j.autcon.2018.05.002

Schmidt, D., Berns, K., (2013). Climbing robots for maintenance and inspections of vertical structures—A survey of design aspects and technologies. Robotics and Autonomous Systems 61, pp.1288–1305. https://doi.org/10.1016/j.robot.2013.09.002

Schmidt, D., Hillenbrand, C., Berns, K., (2011). Omnidirectional locomotion and traction control of the wheel-driven, wall-climbing robot, CROMSCI. Robotica 29, pp.991–1003. https://doi.org/10.1017/S0263574711000294

Sekhar, P., (2014). Duct fan based wall climbing robot for concrete surface crack inspection, in: 2014 Annual IEEE India Conference (INDICON). Presented at the 2014 Annual IEEE India Conference (INDICON), IEEE, Pune, India, pp. 1–6. https://doi.org/10.1109/INDICON.2014.7030589

Spenko, M.J., Haynes, G.C., Saunders, J.A., Cutkosky, M.R., Rizzi, A.A., Full, R.J., Koditschek, D.E., (2008). Biologically inspired climbing with a hexapedal robot. J. Field Robotics 25, pp.223–242. https://doi.org/10.1002/rob.20238

Venkatesh, P., Alapati, M., (2017). Condition Assessment of Existing Concrete Building Using Non-Destructive Testing Methods for Effective Repair and Restoration-A Case Study. Civil Engineering Journal-Tehran 3, pp.841–855. https://doi.org/10.28991/cej-030919

Xu, F., Wang, X., Jiang, G., (2012). Design and Analysis of a Wall-Climbing Robot Based on a Mechanism Utilizing Hook-Like Claws. International Journal of Advanced Robotic Systems 9, 261. https://doi.org/10.5772/53895

Yoshida, Y., Ma, S., (2010). Design of a wall-climbing robot with passive suction cups, in: 2010 IEEE International Conference on Robotics and Biomimetics. Presented at the 2010 IEEE International Conference on Robotics and Biomimetics, pp. 1513–1518. https://doi.org/10.1109/ROBIO.2010.5723554

Zhao, Y., Fu, Z., Cao, Q., Wang, Y., (2004). Development and applications of wall-climbing robots with a single suction cup. Robotica 22, pp.643–648. https://doi.org/10.1017/S0263574704000517

Robot Construction Simulation using Deep Reinforcement Learning

Aiyu Zhu, Pieter Pauwels, Bauke de Vries
Eindhoven University of Technology, Netherlands
a.zhu@tue.nl, p.pauwels@tue.nl, b.d.vries@tue.nl

Abstract. Currently, various types of construction robots are introduced in prefabrication construction, leading to a new research domain of Robot-Oriented Design. Although construction robotics display huge potential, its application in real construction projects is still limited. One of the reasons is the lack of a framework for collaborative robots ('cobots') to complete more complex tasks. Its main intention is to integrate standalone Single Task Construction Robots (STCRs) into controlled environments that enable the implementation of networked robot systems, in which various robots can be used for different types of tasks in a (semi-)automated manner. Before putting this into practice, such innovation obviously needs to be tested in a simulation environment. In this paper, we present a training mechanism for the collaborative work of the Single Task Robots in the construction process to achieve cobots' construction simulation based on a deep reinforcement learning method.

1. Introduction

In recent years, there has been a growing interest in the prefabricated home industry from both investors and buyers, and it is quickly becoming a new standard in homebuilding (Lopez and Froese, 2016). Prefabrication, pre-assembly, modularization, system building, and industrialized buildings are the terms used for describing the rapid construction of buildings in which (structural) components are produced at a plant, and the construction site is used only for assembling (Generalova, Generalov and Kuznetsova, 2016). Prefabricated homes offer several attractive advantages compared to the traditional on-site construction method, such as a substantial reduction of construction time, higher quality control, and potential cost savings (Siggner, Rebecca & Yamashita, 2006).

Currently, various types of construction robots are introduced in prefabrication construction, leading to a well-defined domain of Robot-Oriented Design (ROD – (Bock, 2015)). Robotics and automated systems have the potential to revolutionize the industry and provide many advantages to Architecture, Engineering and Construction (AEC) area as a whole (Davila Delgado *et al.*, 2019). For example, the research resulted in an on-site digital fabrication robot with versatile functions (Buchli *et al.*, 2018), and a novel large-scale Digital Construction Platform (DCP) for on-site sensing, analysis, and fabrication (Keating, 2014).

Although construction robotics display huge potential for the AEC industry, their application in real construction projects is limited (Dawod and Hanna, 2019). One of the crucial reasons is the lack of the concept of robots working together ('cobots') to complete more complex tasks. Its main intention is to integrate standalone Single Task Construction Robots (STCRs) into controlled environments that enable the implementation of networked robot systems, in which various robots can be used for different types of tasks in a (semi-)automated manner (Davila Delgado *et al.*, 2019).

Another key challenge is the connection of robots with digital models, including Building Information Models (BIM) and digital twins. Industry domains and software developers have become more interested in organizing and sharing the 'semantics' of a building (Pauwels, Zhang and Lee, 2017). Robots need to use the data that is embedded in any virtual model and consume it to construct the building (semi-)automatically. Yet, the dataflow from a virtual model to the robot is often very tedious and labor-intensive and needs to be programmed.

Creating a simulation of the real construction environment for robots and training them to learn how to construct collaboratively is a considered method to optimize robot construction. The simulation environment allows us to explore how simulated robots can work together, learn, and interact with simulated objects starting from available data (e.g. BIM model). In this article, we particularly focus on the evaluation of learning algorithms that can be used by robots. Reinforcement learning is one of the methods that can be used in the cobots for learning how to collaborative work on one site. In Reinforcement learning, agents learn by interacting with their environment, using a scalar reward signal as performance feedback (Kaelbling and L., 1996). The simplicity and generality of this reinforcement learning method make it attractive also for multi-agent learning (Buşoniu, Babuška and De Schutter, 2006).

Since the exploration of the environment by reinforcement learning will produce a large amount of data, the introduction of deep learning has become a competent data processing method of reinforcement learning. The neural network connects logic regressions to process the output result through an activation function to realize the non-linear data processing, while deep learning allows multiple neural networks to be connected (Schmidhuber, 2015). DRL is a method to implement deep learning in reinforcement learning, which significantly improves the performance of reinforcement learning (Mnih *et al.*, 2013).

In this paper, we investigate using deep reinforcement learning as a training mechanism for a simulated Single-Task Construction Robot (STCR), assuming that this can be scaled to many robots. This paper looks specifically into the case of a simplified construction site in which a single robot is required to complete a transport task in the simulated environment. In the next section, we will first have a brief review of deep reinforcement learning. In Section 3, a framework is proposed for testing learning methods in collaborative robots, after which tests are documented in Section 4. The article ends with future work and conclusions.

2. Deep Reinforcement Learning for STCRs

Reinforcement learning is one of the machine learning methods that relies on reward and punishment values to let agents learn and improve their actions in a defined environment. In other words, agents are embedded in an environment; they go through a number of episodes; and at the start of every episode, the current environment is observed as a state; after which actions are made by the agent that lead to success or failure; and the agent finally learns. Every next episode can be handled more quickly.

There are four essential elements in reinforcement learning: state, action, reward and training policy (Mnih *et al.*, 2013). The state is the overall virtual representation of the current environment. The action can be any action that is made available to the agent (e.g. move, rotate, replace, pick, etc.). The training policy defines the behavior of the agent. In the training policy of reinforcement learning, the strategies are divided into model-free and model-based according to whether there is a pre-trained model. Also, according to the different methods of action selection, the policy is classified as value-based to solve discontinuous problems and policy-based to solve continuous problems (Sutton and Barto, 1998). In our case, we simplified the construction process to discrete actions without pre-trained, so we rely on the Q-learning algorithm (Bertsekas and Yu, 2012) to define that policy. Q-learning is an off-policy, model-free, value-based algorithm that allows an agent to improve his policy from the previous learning experience (previous episode). According to Q-learning, at the beginning of each episode, the agent observes the current environment as the state, after which it performs actions based on maximum Q-value. If the ε-greedy parameter which is used to control the agent's choice of action (Sutton and Barto, 1998) is activated, the agent is supported in taking random action, and then this Q-learning policy does not apply. Finally, the reward is a scalar value that is used by the agents to choose for one action over any other available action. This reward is used as feedback from a number of potential future states (next state), right before replacing the current state with the preferred future state (highest reward). By iterating through the learning episodes, Q-learning aims to figure out the optimal policy.

It has been suggested by Deepmind Technologies (Mnih *et al.*, 2013) to improve the way in which agents learn over the course of multiple episodes by using the Q-learning algorithm in combination with a deep neural network. This results in a Deep Q Network (DQN) for training, in which (1) the Q-learning algorithm is used for evaluating available action's rewards and (2) a neural network (NN) is used to maintain memory between each episode. In other words, this is a deep reinforcement learning algorithm based on a Q-learning trained convolutional neural network(Mnih *et al.*, 2013). While training the agent over several episodes, the NN will modify its parameters according to the reward given to the agent in each episode, in order to improve the agent's action towards its goal. Accuracy, normalized rewards, and loss are hereby used as quantitative evaluation measures to estimate the effectiveness of the training.

The above method can be used for simulating robots in a virtual environment that learn to navigate (actions) in a virtual construction site. The trained neural network can be used for simulation purposes in the user's construction layout and output of the transport workflow for robots.

3. Proposed DQN for STCRs

In this work, we have implemented a DQN in Python code for STCRs. We have used this DQN in a simplified 2D environment that stands apart from any Building Information Modelling (BIM) environment, even though we eventually plan to integrate our simulation environment with BIM data. In this article, we focus on the reinforcement learning algorithm itself and its usefulness to train STCR for construction processing simulation.

3.1 Simulation Environment Policy

In our work, we assume a simplified simulated construction site, which consists of a 2D rectangular grid (6 x 6 grid) bound by the boundary line of the virtual construction site (Figure 1). Each grid cell is one hundred pixels wide and high. A STCR is represented as a white square and has three functions: move one grid cell in any of four directions, pick up and place. A construction component is represented as a yellow square and can be picked and placed. A target location is represented as a red circle and can have a component placed on it. A forbidden area is represented as a black square which is inaccessible.

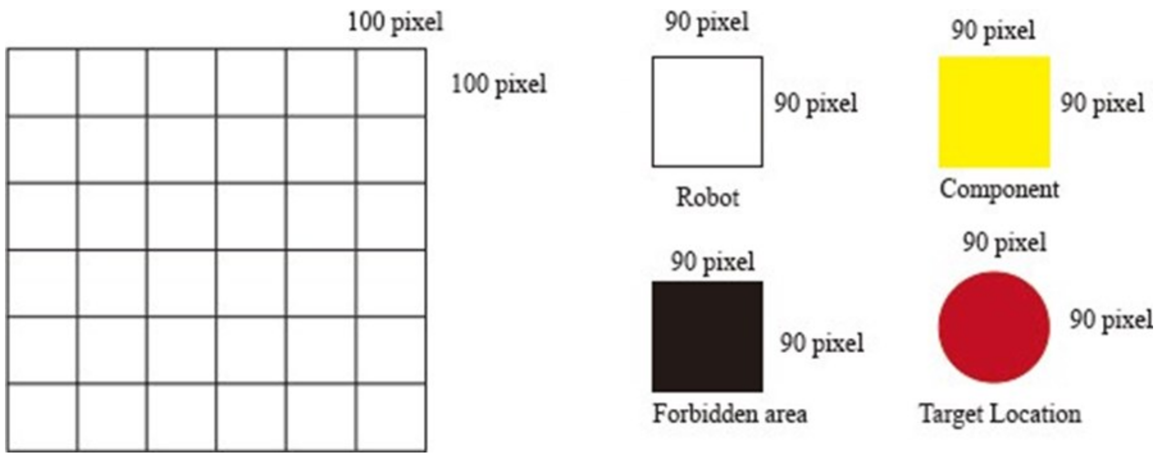

Figure 1: 2D Rectangular Grid Simulated Construction Site

In this simplified environment, we trained the robot to find the target construction component and transfer it to the target location. We have defined that the construction robot can move one grid cell at a time (action). When the construction robot moves to the grid cell containing a construction component, the pick action is activated. When the construction robot transports the construction component to the target location, the place action is activated. The pick and place actions have a positive reward value of +1; the regular move values have a reward value of 0. Meanwhile, a considerable negative reward of -100 is included for moving out of the boundary or for moving to the forbidden areas. Only when the robot achieves transportation of construction component to the target location, it gains a reward of +10.

3.2 System Architecture

In our work, we did implement not only the DQN, but also the 2D visualization environment, as shown in Fig. 1. The main purpose of this interactive system is to connect the simulation environment with the DQN, pass the state coordinates as an array in the environment to the DQN for calculation, and feed the results given by the DQN back to the environment. However, the simulation we need is not only to require the simulation environment to interact with DQN but also to allow the interactive system to provide optimized transport routes. To achieve our purpose, we designed the architecture of our interactive system in three parts: the learning part, the storage part and the evaluation and output part.

3.2.1 Learning

The implemented DQN trains a single STCR through several episodes to achieve transport work in a simulated construction site. We treat the simplified six actions (pick, place, up, down, left, right) of the STCR as actor actions. The STCR is trained using self-play, which acts to perform on the construction in different strategies based on the environment feedback rewards. The agent aims to move and place all the components in the correct position, which marks the end of each episode in training within the selected environment.

According to the DQN requirements, the agent position in the environment used as the input of the states to the neural network and the Q-value is estimated by rewards of current and previous actions in states. The agent implements the action with maximum Q-value in each step and gets reward feedback of this action.

In order to achieve learning in the robot, to find the component and to transport the component to the target location, we applied a distributed method to establish two single fully connect neural networks to connect the robot to component and target location respectively, as shown in Figure 2. Then, the independent learning situation is integrated into a complete learning system for different tasks of one robot. By evaluating the completion of each episode, the agent policy is optimized over time.

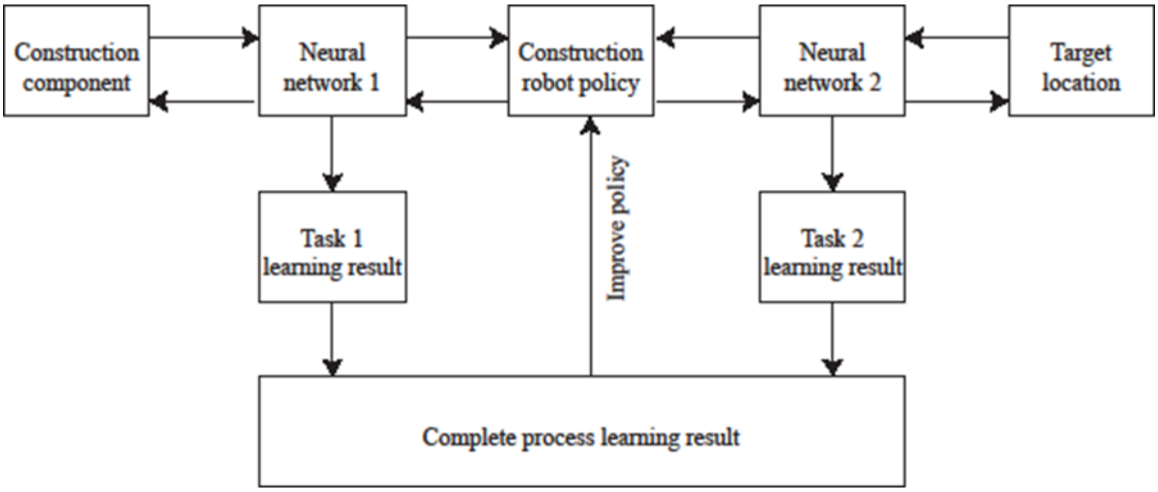

Figure 2: Two neural networks and a construction robot policy allow the SCTR to learn

3.2.2 Storage

The storage part is mainly divided into two parts, as shown in Figure 3. The first part is used to record the move actions (up, down, left, right) of agents in each episode, and the second part is only used to record the move actions of agents with higher rewards and fewer steps (best episode). Since the DQN algorithm we employed is an off-policy algorithm, the agent can optimize the neural network by learning from previous experience. Therefore, the stored data (first part) is mainly used to provide learning data to the agent. The second part of the storage (right in Fig. 3) is used to screen out the optimal solution for a given number of episodes. By analyzing the records in part two, we can evaluate the optimization efficiency of the neural network and give the optimal solution under the current training times.

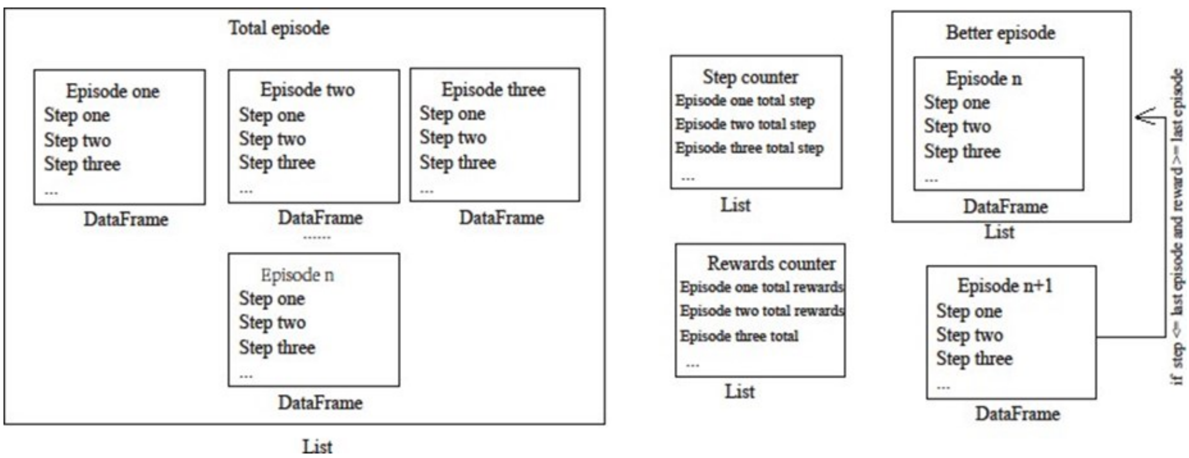

Figure 3: Storage Architecture

3.2.3 Evaluation and Output

In the actual construction, controlling time cost is one of the essential factors to optimize the construction process. In our simplified environment, we were looking for strategies to maximize rewards by taking the fewest steps. The evaluation system rates the action policy for each episode based on rewards and steps ratio (R/S ratio). The output system then selects the action policy with the highest score in the current training episodes as the suggested route. When there is more than one action policy with the same maximum score, the output system treats each action policy as the suggested route.

4. Experiments

In this work, we have used the above setup to train STCRs. To accomplish the purpose of simulation, we have set up two environments with the same network architecture, learning algorithm and hyperparameters settings to train the neural networks of the construction robot for learning the transportation and testing the reaction of the construction robot in an environment of various situations. We set the learning rate to 0.1 and the ε-greedy parameter to 0.1. At the same time, we used the AdamOptimizer algorithm(Kingma and Ba, 2015) with mini-batches of size 64.

In the training environment, randomly generated coordinates are given for the initial positions of construction robot, construction component and target location of each episode. The training was done with a total of one thousand episodes.

In the experimental environment (test set), fixed positions were assigned to construction robots, construction components, target locations, and the forbidden areas. An episode ends when either the transportation finished or when the robot moved to the forbidden area or out of the environment (violation). The experiment was done with one hundred episodes.

4.1 Training Environment

The training environment is mainly used to train the action strategy of construction robots, as shown in Figure 4(a). In the training environment, there is no forbidden area. The main task is to connect and train the robot with the neural network of the component and target location. In the case of a random initial position, the robot can find a better action strategy to complete the transport work. The result of the training is presented in Figure 4(b). It shows that, out of a thousand episodes, the transportation task succeeded about 800 times. At the same time, there is a linear relationship between the total number of episodes and episode success.

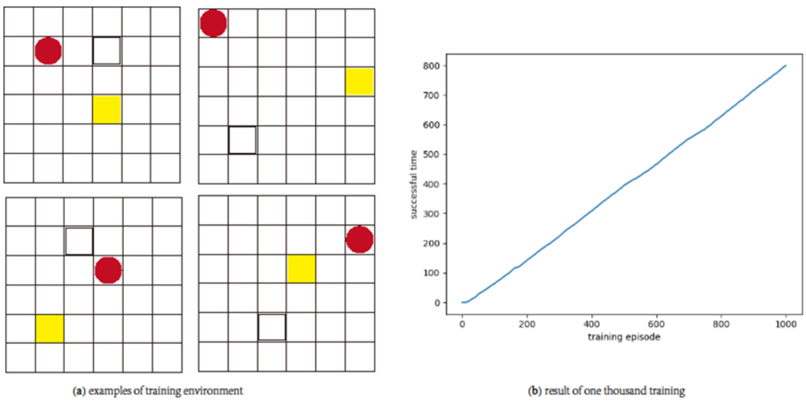

Figure 4: (a) Some Situations in the Training Environment and (b) Training Result

4.2 Experiment Environment

The experiment environment is used to evaluate the learning result of the robot in new construction sites. In the environment, the positions of construction robot, construction component and target location are fixed, and forbidden areas are set in different positions. Figure 5 presents three situations: (1) without forbidden areas, (2) containing one forbidden area and (3) containing two forbidden areas. We implement the trained neural network in three situations individually and evaluate learning results based on the evaluation strategy. After one hundred episodes of each situation, the system provides at least one suggested route based on evaluation results.

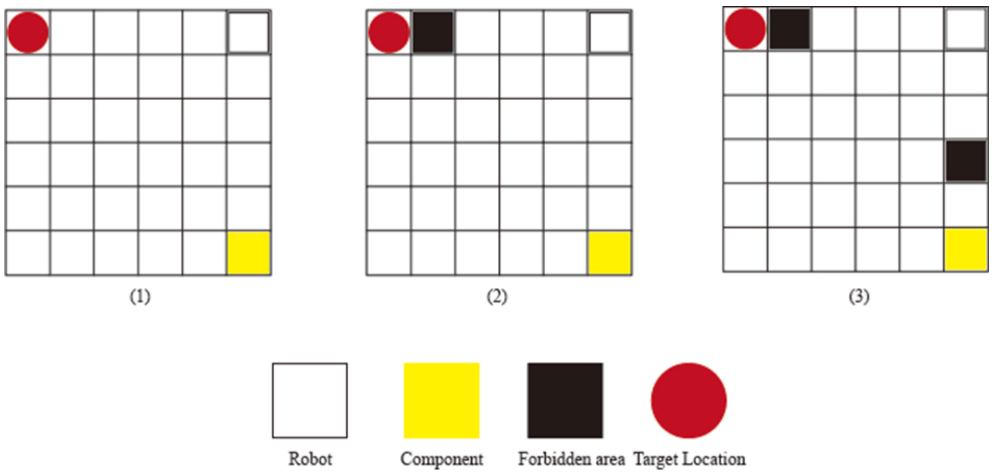

Figure 5: Experiments' Environments

4.3 Evaluation and Output

As illustrated in Figure 6, after running around 50 episodes, the ratio between the number of episodes and success reaches a more linear growth. Figure 7 shows the ratio between rewards and steps ratio (R/S ratio), over the number of episodes needed to obtain success. It shows the number of active learning episodes for the trained robot and the maximum ratio under current episodes. By tracking the maximum R/S ratio, the suggested route can be found as in the episode(s) which has the lowest number of steps and the highest reward. After 100 episodes, as shown in Figure 8, the Q-value of the robot on each state is printed out in the simulation environment, and a suggested route is planned for the construction robot.

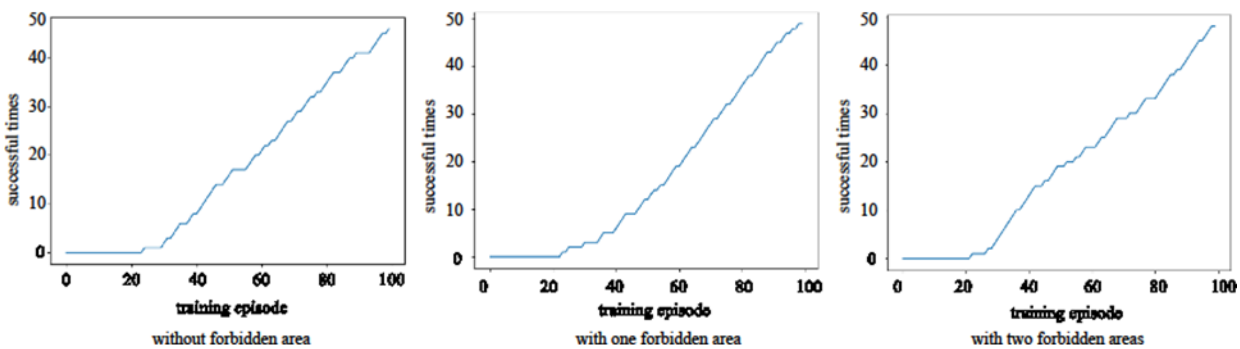

Figure 6: Successful Times in One Hundred Episodes

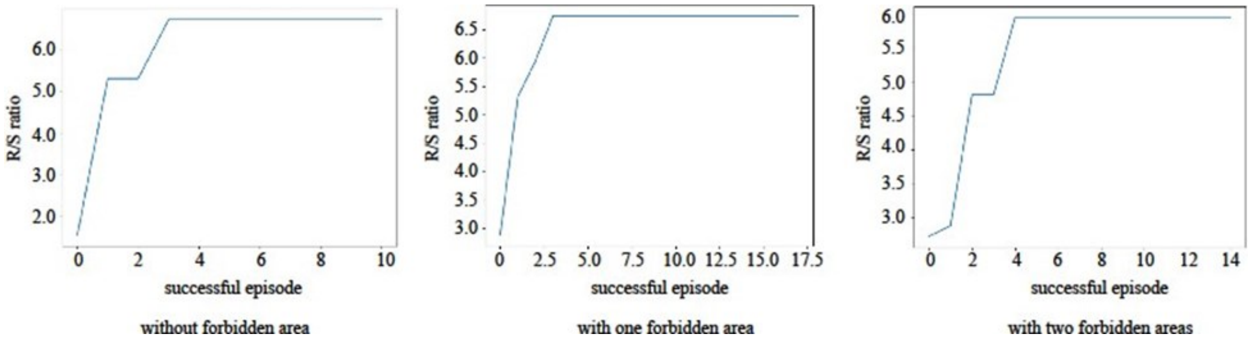

Figure 7: Rewards and Steps Ratio in Successful Episode

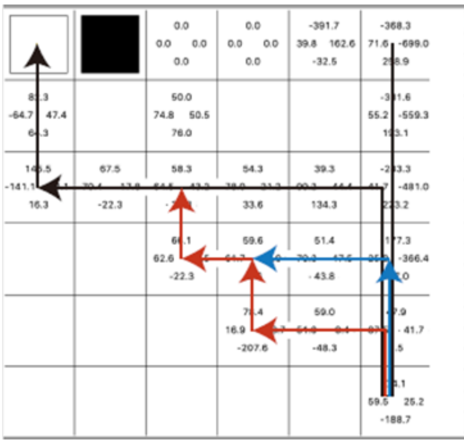

Episode number	Total rewards	Total steps	Total R/S ratio	Total States record
28	12	93	1.066021505	[array([0., -500.]), array([-100., -500.]), array([-1
32	12	37	2.72972973	[array([0., -500.]), array([-100., -500.]), array([-2
33	12	33	3.060606061	[array([0., -500.]), array([0., -400.]), array([
34	12	21	4.80952381	[array([0., -500.]), array([0., -400.]), array([-1
37	12	19	5.315789474	[array([0., -500.]), array([0., -400.]), array([
41	12	17	5.941176471	[array([0., -500.]), array([0., -400.]), array([
43	12	17	5.941176471	[array([0., -500.]), array([0., -400.]), array([
49	12	17	5.941176471	[array([0., -500.]), array([0., -400.]), array([
52	12	15	6.733333333	[array([0., -500.]), array([0., -400.]), array([
59	12	15	6.733333333	[array([0., -500.]), array([0., -400.]), array([
63	12	15	6.733333333	[array([0., -500.]), array([0., -400.]), array([
66	12	15	6.733333333	[array([0., -500.]), array([0., -400.]), array([
77	12	15	6.733333333	[array([0., -500.]), array([0., -400.]), array([
78	12	15	6.733333333	[array([0., -500.]), array([0., -400.]), array([
79	12	15	6.733333333	[array([0., -500.]), array([0., -400.]), array([
84	12	15	6.733333333	[array([0., -500.]), array([0., -400.]), array([
93	12	15	6.733333333	[array([0., -500.]), array([0., -400.]), array([
96	12	15	6.733333333	[array([0., -500.]), array([0., -400.]), array([
98	12	15	6.733333333	[array([0., -500.]), array([0., -400.]), array([

Figure 8: Suggested Routes for Construction Robot and Successful Episode Records

5. Future Work

In future work, to realize the collaborative construction simulation of multiple robots, we need to continue our research in three aspects. In the first place, this simulated environment needs to take into account and use data from a BIM model. In this experiment, we constructed a simplified simulated site plane. However, in the actual construction process, the construction environment is a sophisticated three-dimensional space. So, the next step is to explore how to connect the DQN with a BIM model so that the simulated robot construction environment is closer to the real construction environment.

Secondly, further work needs to study the different types of construction robots. In this experiment, we selected the transportation construction robot with simple functions for simulation; reality has much more diverse and complex robots. Next, we will simulate more types of construction robots in the simulated environment.

Finally, research on how to make construction robots work together is also one of our priorities in the future. In this experiment, we used a DQN to realize the construction process simulation of a STCR. Next, based on the experience of this experiment, we plan to study how to realize a collaborative construction process by two SCTRs using DQN.

6. Conclusion

In this paper, we propose the use of a deep reinforcement learning algorithm to train one simulated STCR in its goal to optimally transport construction site material within a bounded construction site layout. This simulation can realistically be modelled in a single-agent model-based environment that includes a deep reinforcement learning algorithm. With this DQN-supported simulated environment, we aim at finding an appropriate workflow of robot work under different construction layout strategies.

Through the experimental results, we can find that the deep reinforcement learning algorithm can simulate the process of robot construction under the same simplified simulated environment. Even if there are dynamic changes within the construction environment, the robot can still realize its goal in the construction process.

References

Bertsekas, D. P. and Yu, H. (2012) ‘Q-learning and enhanced policy iteration in discounted dynamic programming’, *Mathematics of Operations Research*, 37 (1), pp. 66–94. doi: 10.1287/moor.1110.0532.

Bock, T. (2015) ‘The future of construction automation: Technological disruption and the upcoming ubiquity of robotics’, *Automation in Construction*. Elsevier, 59, pp. 113–121. doi: 10.1016/j.autcon.2015.07.022.

Buchli, J. *et al.* (2018) ‘Digital in situ fabrication - Challenges and opportunities for robotic in situ fabrication in architecture, construction, and beyond’, *Cement and Concrete Research*. Elsevier Ltd, pp. 66–75. doi:10.1016/j.cemconres.2018.05.013.

Buşoniu, L., Babuška, R. and De Schutter, B. (2006) ‘Multi-agent reinforcement learning: A survey’, *9th International Conference on Control, Automation, Robotics and Vision, 2006, ICARCV ’06*, (May 2014). doi:10.1109/ICARCV.2006.345353.

Davila Delgado, J. M. *et al.* (2019) ‘Robotics and automated systems in construction: Understanding industry-specific challenges for adoption’, *Journal of Building Engineering*, 26, p. 100868. doi:10.1016/j.jobe.2019.100868.

Dawod, M. and Hanna, S. (2019) ‘BIM-assisted object recognition for the on-site autonomous robotic assembly of discrete structures’, *Construction Robotics*. Springer International Publishing. doi: 10.1007/s41693-019-00021-9.

Generalova, E. M., Generalov, V. P. and Kuznetsova, A. A. (2016) ‘Modular Buildings in Modern Construction’, *Procedia Engineering*. The Author(s), 153, pp. 167–172. doi: 10.1016/j.proeng.2016.08.098.

Kaelbling, L. P. and L., L. M. (1996) ‘Reinforcement Learning: A Survey’, *Journal of Artificial Intelligence Research*, 4 (9), pp. 237–285. doi: 10.1007/s11431-012-4938-y.

Keating, S. (2014) ‘Robotic Fabrication in Architecture, Art and Design 2014’, *Robotic Fabrication in Architecture, Art and Design 2014*, (March 2014). doi: 10.1007/978-3-319-04663-1.

Kingma, D. P. and Ba, J. L. (2015) ‘Adam: A method for stochastic optimization’, *3rd International Conference on Learning Representations, ICLR 2015 - Conference Track Proceedings*, pp. 1–15.

Lopez, D. and Froese, T. M. (2016) ‘Analysis of Costs and Benefits of Panelized and Modular Prefabricated Homes’, *Procedia Engineering*. Elsevier, 145, pp. 1291–1297. doi: 10.1016/J.PROENG.2016.04.166.

Mnih, V. *et al.* (2013) ‘Playing Atari with Deep Reinforcement Learning’, pp. 1–9. Available at: http://arxiv.org/abs/1312.5602.

Pauwels, P., Zhang, S. and Lee, Y. C. (2017) ‘Semantic web technologies in AEC industry: A literature overview’, *Automation in Construction*. Elsevier B.V., 73, pp. 145–165. doi: 10.1016/j.autcon.2016.10.003.

Schmidhuber, J. (2015) ‘Deep Learning in neural networks: An overview’, *Neural Networks*. Elsevier Ltd, pp. 85–117. doi: 10.1016/j.neunet.2014.09.003.

Siggner, Rebecca & Yamashita, K. (2006) ‘Modular Housing : Benefits , Challenges and Lessons Learned’, pp.1–4.

Sutton, R. S. and Barto, A. G. (1998) ‘Reinforcement Learning: An Introduction’, *IEEE Transactions on Neural Networks*, 9(5), pp. 1054–1054. doi: 10.1109/tnn.1998.712192.

An object-based conceptual model for ICT-based situational awareness of the construction process

Yuan Zheng [1], Seppo Törmä [1], Olli Seppänen [1]
[1] Aalto University, Finland
[1] VisuaLynk Oy, Finland
yuan.zheng@aalto.fi

Abstract. Due to the dynamic nature of the construction process, situational awareness (SA) is essential for the stakeholders to perceive, understand and project the real situation of the construction process to support their decision making. SA requires a collection, integration, and interpretation of information to reveal the occurrence of the real-world elements and environment. Nowadays, with the emerging ICT implementations in the construction domain, the volume, content, and quality of data and information that enables situational awareness for the construction process have increased. This provides the potential of establishing an ICT-based SA system for the construction process. However, SA information of construction process has been collected with point solutions so far, which does not allow true SA considering multiple information streams together. In order to integrate the information via multiple ICT systems to support the establishment of ICT-based SA system for the construction process, this paper presents an object-based conceptual model. This model offers an initiative of conceptualizing the objects in the construction process and intend to be a reference for integrating the information from various ICT systems.

1. Introduction

The concept of Situational Awareness (SA) has been an active study among the domains of military, aviation, and traffic controls, which aims to support timely decision making in highly dynamic environments (Endsley, 1995). Endsley (2000) defined SA as 'the perception of elements in the environment within a volume of time and space, the comprehension of their meaning, and the projection of their status in the near future'.

Construction is a dynamic process, which always has a high deviation between actual and as-planned execution (Park and Peña-Mora, 2003; Garcia-Lopez, 2017). Engineers, managers, and workers of the construction process thus need SA to promptly capture and understand the actual situation, for further decision making and action taking to respond to variability timely (Akinci, 2015; Reinbold, 2019). SA in the construction process can help stakeholders to have a better understanding of what is the status of their related activities, what is the status of relevant entities for these activities and what will be the status of activities and entities in near future. Specifically, the modern construction planning methods such as Takt time planning (Frandson et al., 2013; Binninger et al., 2017), Location Based Management System (Kenley and Seppänen, 2010) and Last Planning System (Ballard, 2000) also require detailed SA for supporting the accurate planning, resource allocation and activity constraints identification on the level of operation management.

The initial requirement of SA is to obtain information of the relevant elements from the real-world context (Tretmans and van de Laar, 2013). Historically, collecting information about the construction process has been a challenge in the construction domain (Akinci, 2015). Nowadays, numerous emerging Information and Communication Technologies (ICT) implementations in the construction industry have empowered automatic information collection and process monitoring. The prime examples are the sensing technologies (Akinci et al., 2006; Correa, 2018; Linares et al., 2019), including the Internet of Things (IoT) (Dave et al., 2016), indoor positioning (Zhao et al., 2019), and image processing (Zou and Kim, 2005). These ICT systems can collect events from real-world entities in the construction process, to provide real-time information that represents their situation.

Meanwhile, the mature implementations of Building Information Modelling (BIM), Enterprise Resource Planning (ERP) system and Electrical Document Management (EDM) system, have also enriched digitalized information content of the construction process. As a consequence, the information bottleneck of achieving SA of the construction process has been alleviated, which also provides a potential of the cross-system interaction among these ICT systems to establish an integrated SA system of the construction process from the information level.

The fundamental issue of such interaction is information integration. The aim of information integration is to improve the information interoperability among the systems, for reflecting and interpreting the comprehensive and integrated situations of the construction process. However, the information isolation is identified as a common problem in the construction domain (Kosovac et al., 2000; Dave et al., 2008; Reinbold et al., 2019). To achieve the successful integration, a common information model is required as a unified reference that formalizes the real-world objects and their relations based on construction domain knowledge, moreover, illustrates the exchange and provenance of the information through heterogeneous systems. Although several existing information models in the construction domain are sufficient to represent static or slowly evolving information of real-world objects, few of them can generically integrate the information from state of art ICT systems.

In this paper, we propose an object-based conceptual model of the ICT-based SA for the construction process. This model provides a coherent higher-level conceptualization of the real-world objects and information entities in the construction process, which is intended to be a generic reference of integrating the information from the various ICT systems, ultimately to support the establishment of the SA system of the construction process.

2. SA of the construction process

2.1 System requirement

SA requires a collection, integration, and interpretation of the information to reveal the occurrence in the environment and to be aware of the situation. Such information of the situation may be acquired via various information sources (Tretmans and van de Laar, 2013). Thus, to manage large amount of information acquired via various sources, Tretmans and van de Laar (2013) suggested that a computer-based system is indispensable to manage the information. Moreover, such a system is not a monolithic system but should be considered as a system of systems (SoS), due to SA needs to be maintained by several agents via different systems. Each system may provide distributed information of SA, but the information from one system may be not available from another system (Borth, 2013). Thus, the SA system should be built from various interacting constituent systems to perform multiple tasks and process heterogeneous data sources.

In terms of construction, even though the emerging ICT implementations have eased the digital information shortage, the information has been isolated to multiple systems, which is not able to be used by cross-system manners (Dave et al., 2016). Therefore, from the practical view, the SA of the construction process should be implemented as such SoS that integrates and maintains the information collected from various systems and ICT tools. This system covers the whole context of the construction process and specifically focuses on the operation management level. The constituent systems should provide detailed information about the real-world process, reflect the involved entities and indicate their situation. These systems may be independent but need to be networked on the information level to serve the goal of maintaining the SA of the construction process. Examples of constituent systems of the SA of the construction process are:

- BIM platforms
- Planning and scheduling systems
- ERP systems
- IoT/sensor systems
- Construction management tools to record progress information

2.2 Information model requirement and information input

From the information level, the major challenges of the SoS-based SA system include a large quantity of information, requiring historical data, heterogeneity and independence of data sources, information reliability and information interpretation for human operating (Tretmans and van de Laar, 2013). Froese (1996, 2003) emphasizes that standard information models is required as a cornerstone to support information management and systems interoperability. Meanwhile, the current initiatives of the information integration towards the model-based systems are structured data (Caldas et al., 2005). Therefore, to establish the ICT-based SA system aforementioned, an information model should be built up initially as a reference for integrating the information from various systems. Such an information model is a representation of domain knowledge and maintains as a central skeleton on the information that reflects the actual construction process and related entities in a centralized manner. Meanwhile, most of the detailed information is likely to remain in the original systems that provide it for the use of a SA system through standard interfaces.

With the respect of the current ICT implementations and the purpose of the SA for the construction process, the required information inputs of this ICT-based SA system are wide and various. We categorized the information inputs as three types: 1) Static or slowly evolving information. This type of information is constant or slowly changed, including the BIM models, organizational information, the master schedule of construction projects, etc. 2) Real-time or frequent information. Such dynamic information is mainly for capturing and updating the situation of the activities, actors, resources and external conditions, which could be obtained from sensors, monitors or status event reports.3) Regularly updated plans. The information from plans can provide detailed information about as-planned activities and workflow.

It should be noted that the information acquired through different systems has a very different nature and usage. First, slowly evolving information can be regarded as a background of the real-world objects in the construction process. Second, the real-time data from sensors and activity execution provides information describing how the activities got executed and what is the status of related building elements and resources. Overall, this kind of information flows in as a constant stream of small events. Finally, in terms of the plan, the role of this information is to coordinate and guide the work to be done and to compare with the actual situation for further understanding of the situation and adjustment of the plans.

3. Related modeling works

A conceptual model is a representation of an application domain with the abstraction of the domain objects to facilitate information systems development (Evermann and Wand, 2001). Using the object-oriented conceptual model to structure the information in the construction domain could be beneficial to formalize the information as a standardized model (Björk, 1992).

In the past decades, due to the emerging of the computer-integrated construction (CIC), several significant efforts of conceptual modeling the construction process information and data have been reported (Luiten et al., 1993; Luiten, 1994; Froese, 1996; Stumpf et al., 1996; El-Diraby et al., 2005). The major contribution of these works is focusing on the abstraction of the construction process and entities to provide references for managing the construction information, moreover, linking the construction information with the computer-based applications. Luiten et al. (1993) developed a construction information model that identifies the central concepts in the construction domain including product, activity, resource, and contract, along with their inter-concept relationships. This model is the initial contribution of the information reference model for AEC (IRMA) (Froese, 1996). Later, Luiten (1994) developed the Building Project Model (BPM), which focuses on integrating the information of product, activity, and resource. Froese (1996) reviewed a set of conceptual models of construction process information and proposed a core model of the construction process with the central elements and relationships. Meanwhile, Stumpf et al. (1996) developed an Object-Oriented model that integrates information of the construction process and product, which is an integrated model that defined the construction process components of construction processes and the relationships between them. El-Diraby et al. (2005) provided a domain taxonomy as a consistent semantic representation of construction knowledge, with defined higher-level concepts of the construction process. The main elements of the aforementioned models are as shown in Table 1.

Table 1: Main elements of the existing models of the construction process and entities.

Model	Author and Year	Main elements in the model
The information reference model for AEC (IRMA)	Luiten et al., 1993	Project Object, Product, Activity, Resource, Contract, and Agent
Building Project Model (BPM)	Luiten, 1994	Construction Activity, Construction Resource, Labour Force, Material, Equipment, Constructor, Product, Construction State
The core model of the construction process	Froese, 1996	Entity, Process, Constraint, Control, Production, Result, Method, Sequence Constraints, Utilization, Input, Physical Entity, Information, Person, Organization, Bulk Material, Equipment, Product Entity
Integrated Construction Information Model (ICIM)	Stumpf et al., 1996	Project, Component, Activity, Schedule, Construction Zone, Component Group, Resource Use
Domain taxonomy	El-Diraby et al., 2005	Process, Project, Actor, Product, Resource, Technical Topic, System

When compared to these previous models, although they can reflect the construction process and related entities, the demands of ICT-based SA of the construction process aims at a much higher level of detail and accuracy to represent not only the construction process and related entities, but also their real-time situation information. Moreover, information of real-world entities is obtained by the implementations of various ICT systems, thus, the modeling should also consider the linkage of the systems and data sources together. Simultaneously, more accurate modeling of the multiplicity of connections and conditions from which the execution of an activity depends on is required. From the Lean Construction perspective, such connections are referred to as flows. The view of flows was first introduced by Koskela (1999, 2000), which conceptualizes the construction activities as assembly type that enabled by seven major types of flow: Labor, Equipment, Location, External condition, Material, Information, Location, and Prerequisite.

4. Model development approach

The approach of model development is based on the framework presented in Fig. 1, which includes two phases: specification and conceptualization. The model specification aims to determine the scope of the model and analyze the requirement of the model. Following with the conceptualization, the existing models and relevant knowledge were reviewed to conceptualize the real-world objects and information entities.

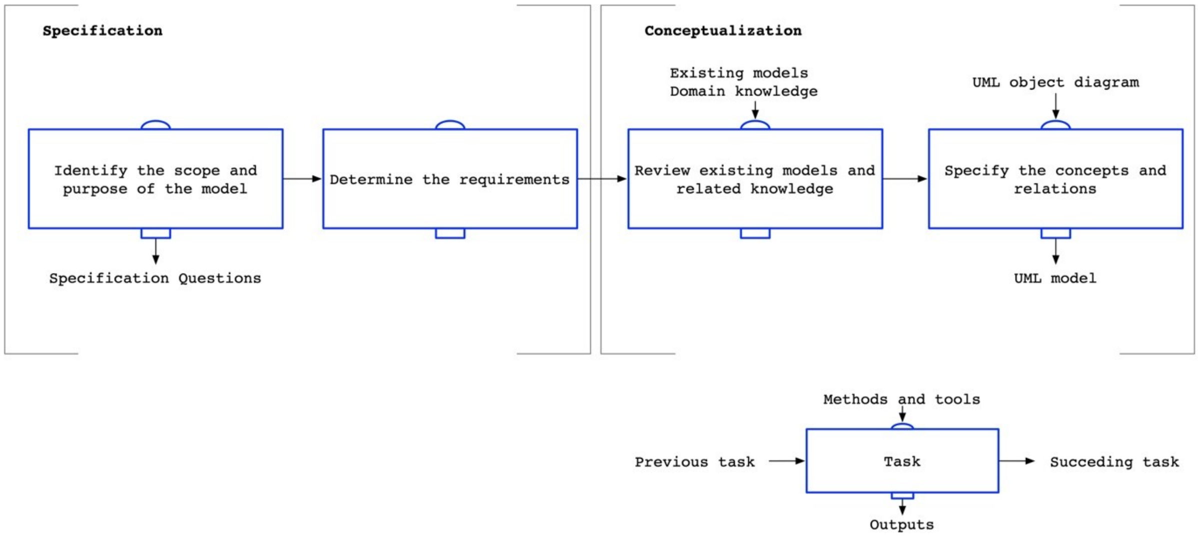

Figure 1: The model development framework

The specification part includes two tasks. Initially, it was important to determine the scope and purpose of the model. In this study, two specification questions are listed, whose answers are the formalization of the model specification. The questions include: 1) What is the scope of the model? 2) What is the purpose of the model? This was followed by identifying the model requirements, which provide a more detailed specification of the requirement of formalizing the content of the model, including the requirement of the information model and information input from various ICT systems

After defining the model specification, the next phase is the model conceptualization. This part aims to formalize the object classes as an abstraction of the construction process. The first task is to review the related domain knowledge and the existing models, which is followed the task of defining what classes should be modeled, what are the hierarchies of the classes (generalization relations), and what terms should be used for the classes, and what cross-class relations should be specified to represent the interaction between the classes in the construction process. The output of the step is a UML class diagram. UML modeling is widely applied in the software domain, which offers modeling constructs to describe the architecture of an information system.

5. The proposed conceptual model

Upon the previously described model development approach, the developed model is shown as a UML class diagram in Figure 2. The model includes the higher-level classes, along with the relations between the classes (or themselves). For the sake of concision and clarity, the attributes of the classes are omitted, and only major classes are shown in the diagram. The classes refer to the major objects and information entities found within the construction domain, along with their attributes that holds the detailed information and data of the objects. On the other hand, the relationships refer to the inter-class relations in the model, to describe the relations between classes. All the classes and relationships are defined by using general abstract terms based on domain knowledge or reusing the homogenous classes in the previous models. The main classes of the model are described in the following section.

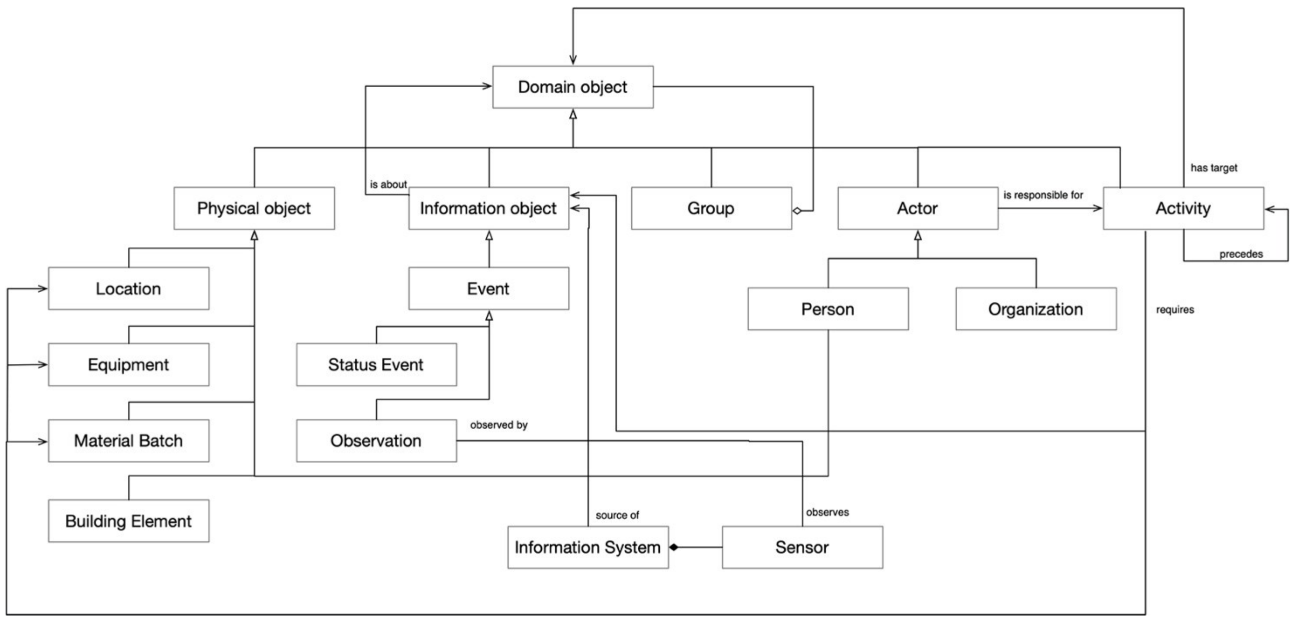

Figure 2: The overview of the conceptual model

5.1 Main classes in the model

5.1.1 Domain Object

Domain Object is the abstraction of all the central objects that are discussed in the construction process, such as entities, activities, resources, products and so on. Each of the *domain object* has a unique identifier that can be used to distinguish the object from others. Unique identifiers are essential in enabling linking between systems, data, and users, and are necessary for building more advanced functionalities on top of SA. Meanwhile, domain objects could have different classifications from various classification systems. Classifications codes make it possible to connect domain-specific type information to objects.

5.1.2 Physical Object

The class of *Physical Object* refers to any object that has physical dimensions and a position involved in the construction process. The hyponymies of the *Physical Object* include *Location*, *Building object*, *Equipment*, *Material batch*, and *Person*.

5.1.3 Information Object

Information Object is the entity that carries information, such as a BIM model, drawing, specification, message, and so on. In the construction activities, the *information objects* are required to provide necessary information about some other object.

5.1.4. Group

The group is the superclass for all kinds of groupings of objects, such as procurement packages, shipments, installation areas, fabrication lots, and so on. *Groups* are often created because some activity is carried out at the same time for all members of the group.

5.1.5 Actor

Actor refers to a resource capable of taking responsibility for activities. *Actors* are divided into *Persons* and *Organizations*. When construction robotics becomes more widespread, the concept of Persons can be expanded to include autonomous robots.

5.1.6 Activity

Activity refers to a superclass for all work or aggregations of works that are carried out in the construction process. *Activities* also have precedence relations with other activities.

5.1.7 Event

The event represents an occurrence that happens with a time instant for obtaining the information about the situation of an entity. The *events* are in the form of *sensor observations* or *status events*. *Sensor observations* can originate in a range of different kinds of sensors, measuring for various instance properties, for example: position, acceleration or temperature. The source of *status events* can be a human user, who updates status information using a construction management tool or the ERP systems. Another possible source of the *status events* are reality capture technologies based on computer vision and image processing. These technologies could provide an automatic *status event* update.

5.1.8 Information System

In the scope of this model, an *information system* is defined as the system that generates and manages information of the construction process, which is also known as the source of certain *information objects*. *Sensors* and other devices are the components of an *information system*.

5.2 Example of implementing the model

To validating the proposed model and specifically to illustrate the potential model implementation that integrates the information from heterogeneous ICT systems, an example scenario is considered as a case study. In this case, it is assumed that there is a concrete column casting process in the location of *Area1*, which consists of three activities in a sequence: *Activity1*, *Activity2, and Activity3*. *Activity1* aims to install the reinforcement bars of *Column1,* followed by *Activity2* to set up the formwork and at last *Activity3* is to pour concrete of the *Column1* for the casting. *Activity1* and *Activity2* have been completed with the inspection and now *Activity3* is in progress. In terms of the execution of *Activity3,* it requires the design information of *Column1* and resources of *Worker1, Equipment1, Area1,* and *MaterialBatch1.* Meanwhile, for ensuring the strength growth of the *Column1*, the temperature and relative humidity in the *Area1* are required in a certain range during the concrete pouring procedure (Park and Paulay, 1975). The project manager wants to monitor the situation of *Activity3* to ensure it could be executed normally as planned and take the prompt response when a variation happens during execution.

The systems and tools employed in this case including the BIM model, construction plans, quality inspection and progress report software, sensors and ERP system. For the *Column1*, its design information can be retrieved from the *BIM model1*. The information and the status of the activities is acquired from the latest construction plan *Plan1* and quality/progress reports. In terms of *Worker1, Equipment1,* and *MaterialBatch1* that are required by *Activity3*, their basic information is acquired from ERP system. Meanwhile, each of them is deployed with an indoor positioning sensor, the sensors track their real-time position to indicate their status. For the *Area1*, two sensors are deployed, one is observing the real-time average humidity in the Area1 and another is observing the temperature.

As conventional manner, each of the systems works individually to provide the partial information of the entities in the construction process. But in order to achieve SA, the information from these systems should be used collaboratively as a SoS to provide the integrated situation of the *Activity3*. Figure 3 is a UML object diagram of the scenario as an instance of the proposed conceptual model. The diagram comprises the related entities of *Activity3*, and the information of entities is acquired via multiple systems. Meanwhile, their situation is represented by related status events and observations. Based on the relations between entities and *Activity3*, an integrated situation of the process is illustrated. It is obvious that the resources are in the right position, but the relative humidity of *Area1* at that time instant is relatively lower (highlighted in red), which is a kind of variation that might impact the execution. Thus, if the humidity remains at that level, the project manager should take actions of increasing the relative humidity in the *Area1* to ensure the execution.

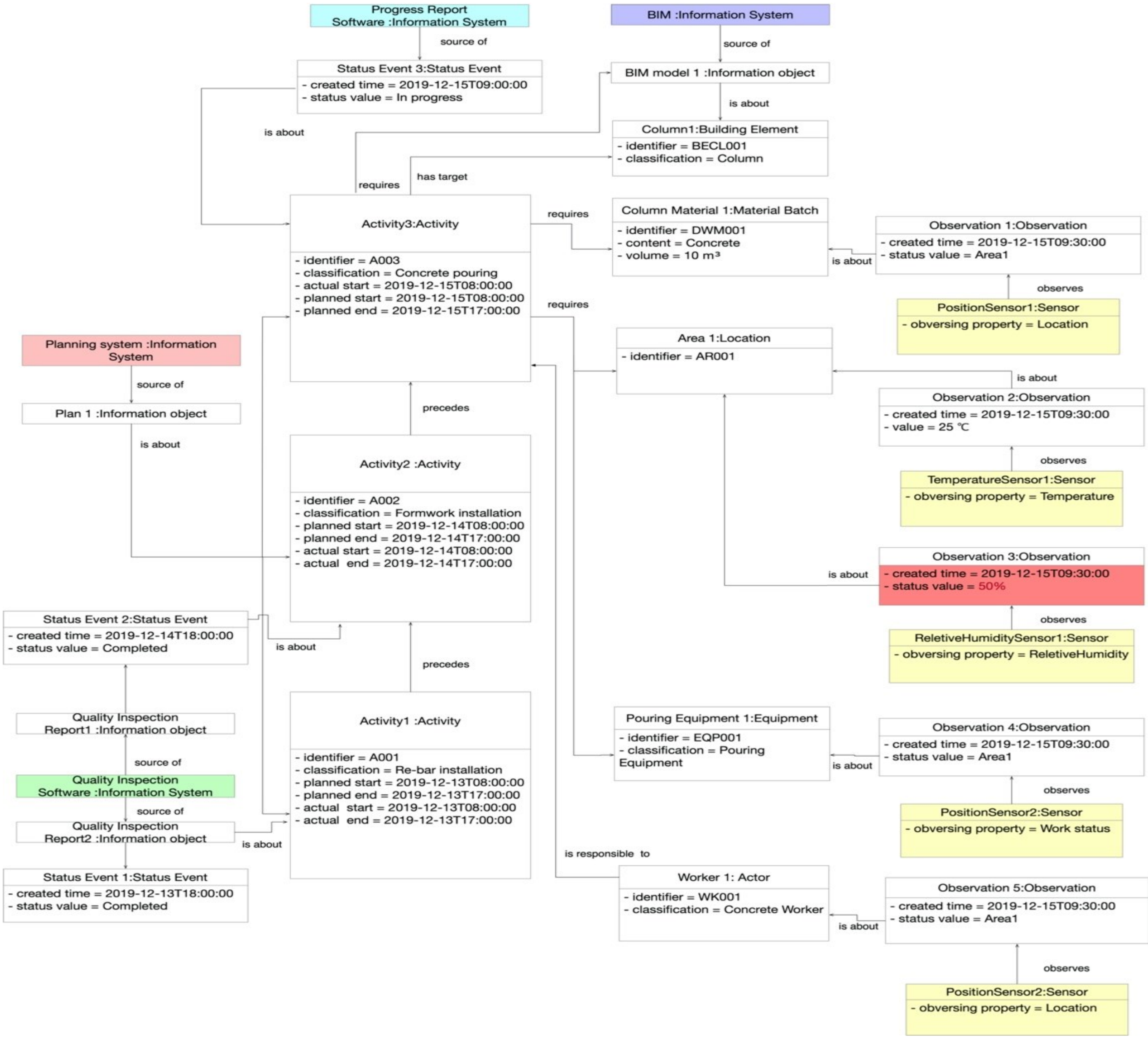

Figure 3: Object diagram of the example scenario

6. Conclusions

SA is essential for the stakeholders to perceive, understand and project the real situation of the construction process to support their decision making. The emerging ICT implementations will improve the SA of construction management from the information level. The SA of the construction process should be implemented as SoS that integrates and maintains the information collected from various systems and ICT tools to serve the goal of SA. This system requires a common information model to reflect the real-world context and integrate the information from heterogeneous systems.

This paper has addressed an object-based conceptual model, which offers a conceptualization of the objects in the construction process and integrates the information from various ICT systems to represent their situation for supporting the establishment of the SA system of the construction process. As has been demonstrated in the example part, the proposed model formalizes the entities in the construction process and is able to integrate the information from multiple systems, especially, the information of status events and real-time sensor observation to represent the situation of the entities. Furthermore, from connections between the entities and activities, the integrated situation of the construction process can be perceived.

However, the proposed model is intended to be a reference for information integration, which only provides the information-level support for establishing the ICT-based SA system of the construction process. It has a limitation that is not capable to provide a direct solution of SA. In terms of further application-level of achieving SA of the construction process, the knowledge-based model should be developed rather than the information model. Therefore, in further study, a structured knowledge model as Semantic Web ontology will be developed based on this model, and practical cases of the ICT-based SA will be conducted.

References

Akinci, B., Boukamp, F., Gordon, C., Huber, D., Lyons, C. and Park, K., (2006). A formalism for utilization of sensor systems and integrated project models for active construction quality control. Automation in construction, 15(2), pp.124–138.

Akinci, B., (2015). Situational Awareness in Construction and Facility Management. Frontiers of Engineering Management, 1(3), pp.283–289.

Ballard, H.G., (2000). The last planner system of production control (Doctoral dissertation, University of Birmingham).

Binninger, M., Dlouhy, J. and Haghsheno, S., (2017). Technical takt planning and takt control in construction. In 25th Annual Conference of the International Group for Lean Construction (Vol. 7, No. 09, p. 2017).

Borth, M., (2013). On the architecture of systems for situation awareness. In Situation Awareness with Systems of Systems (pp. 39–53). Springer, New York, NY.

Björk, B.C., (1992). A unified approach for modelling construction information. Building and Environment, 27(2), pp.173–194.

Caldas, C.H., Soibelman, L. and Gasser, L., (2005). Methodology for the integration of project documents in model-based information systems. Journal of Computing in Civil Engineering, 19(1), pp.25–33.

Correa, F.R., (2018), May. Cyber-physical systems for construction industry. In 2018 IEEE Industrial Cyber-Physical Systems (ICPS) (pp. 392–397). IEEE.

Dave, B., Koskela, L., Kagioglou, M. and Bertelsen, S., (2008). December. A critical look at integrating people, process and information systems within the construction sector. In Proceedings for the 16th Annual Conference of the International Group for Lean Construction (pp. 795–807).

Dave, B., Kubler, S., Främling, K. and Koskela, L., (2016). Opportunities for enhanced lean construction management using Internet of Things standards. Automation in construction, 61, pp.86–97.

El-Diraby, T.A., Lima, C. and Feis, B., (2005). Domain taxonomy for construction concepts: toward a formal ontology for construction knowledge. Journal of computing in civil engineering, 19(4), pp.394–406.

Endsley, M.R., (1995). Measurement of situation awareness in dynamic systems. Human factors, 37(1), pp.65–84.

Endsley, M.R. and Garland, D.J., (2000). Theoretical underpinnings of situation awareness: A critical review. Situation awareness analysis and measurement, 1, p.24.

Evermann, J. and Wand, Y., (2001), December. An ontological examination of object interaction in conceptual modeling. In Proceedings of the Workshop on Information Technologies and Systems WITS (Vol. 1, pp. 15–16).

Frandson, A., Berghede, K. and Tommelein, I.D., (2013), August. Takt time planning for construction of exterior cladding. In Proc. 21st Ann. Conf. of the Int'l Group for Lean Construction

Froese, T., (1996). Models of construction process information. Journal of Computing in Civil Engineering, 10(3), pp.183–193.

Froese, T., (2003). Future directions for model-based interoperability. In Construction Research Congress: Wind of Change: Integration and Innovation (pp. 1–8).

Garcia-Lopez, N.P., (2017). An activity and flow-based construction model for managing on-site work. PhD Dissertation.

Kenley, R. and Seppänen, O., (2006). Location-based management for construction: Planning, scheduling and control. Routledge.

Koskela, L.J., (1999). July. Management of production in construction: a theoretical view. In Proceedings of the 7th Annual Conference of the International Group for Lean Construction. Berkeley, California, USA.

Koskela, L., (2000). An exploration towards a production theory and its application to construction. VTT Technical Research Centre of Finland.

Kosovac, B., Froese, T. and Vanier, D., (2000). Integrating heterogeneous data representations in model-based AEC/FM systems. Proceedings of CIT, 2, pp.556–567.

Linares, D.A., Anumba, C. and Roofigari-Esfahan, N., (2019). Overview of Supporting Technologies for Cyber-Physical Systems Implementation in the AEC Industry. Computing in Civil Engineering.

Luiten, G.T., (1994). Computer-aided design for construction in the building industry.

Luiten, G., Froese, T., Björk, B.C., Cooper, G., Junge, R., Karstila, K. and Oxman, R., (1993). August. An information reference model for architecture, engineering, and construction. In First International Conference on the Management of Information Technology for Construction (pp. 1–10).

Park, M. and Peña-Mora, F., (2003). Dynamic change management for construction: introducing the change cycle into model-based project management. System Dynamics Review: The Journal of the System Dynamics Society, 19(3), pp.213–242.

Park, R. and Paulay, T., (1975). Reinforced concrete structures. John Wiley & Sons.

Reinbold, A., Seppänen, O., Peltokorpi, A., Singh, V. and Dror, E., (2019), July. Integrating indoor positioning system and BIM to improve situational awareness. In Annual Conference of the International Group for Lean Construction. International Group for Lean Construction.

Stumpf, A.L., Ganeshan, R., Chin, S. and Liu, L.Y., (1996). Object-oriented model for integrating construction product and process information. Journal of Computing in Civil Engineering, 10(3), pp.204–212.

Saltzer, J.H. and Kaashoek, M.F., (2009). Principles of computer system design: an introduction. Morgan Kaufmann.

Tretmans, J. and van de Laar, P., (2013). Introduction: situation awareness, systems of systems, and maritime safety and security. In Situation Awareness with Systems of Systems (pp. 3–20). Springer, New York, NY.

Zhao, J., Seppänen, O., Peltokorpi, A., Badihi, B. and Olivieri, H., (2019). Real-time resource tracking for analyzing value-adding time in construction. Automation in Construction, 104, pp.52–65.

Zou, J. and Kim, H., (2005), December. Image processing for construction equipment idle time analysis. In 22nd International Symposium on Automation and Robotics in Construction, ISARC 2005.

Common Data Environment within the AEC Ecosystem: moving collaborative platforms beyond the open versus closed dichotomy

David F. Bucher, Daniel M. Hall
ETH Zurich, Switzerland
bucher@ibi.baug.ethz.ch

Abstract. The Common Data Environment (CDE) is seen as an opportunity to increase collaboration and efficiency during project handling and act as a basis for *Industry 4.0* in the construction industry. CDE developments in industry and research use various approaches to collaboration and interoperability. Past attempts to conceptualize these approaches have been limited to an open versus closed dichotomy. This paper suggests a new conceptualization for interoperable CDE's is needed. A three-dimensional paradigm for interoperable CDE development is proposed. Such an understanding makes it possible to more clearly define CDE interoperability and conceptualize links between Building Information Modeling, the CDE, and enterprise-level platforms such as digital twins.

1. Introduction

The architecture, engineering, and construction (AEC) sector is in a state of change. Firms in the industry are eager to catch up with the speed of digital transformation in other industries. However, only a few construction firms have managed to fully digitize their operations (Jan Koeleman et al., 2019). Only small increases in productivity can be observed in the industry (von Tunzelmann, 2003). To increase productivity gains, academics and industry practitioners suggest the need to embrace *Industry 4.0* as a transition from the separation of the cyber and physical spaces to a unification of the cyber and physical (see Figure 1).

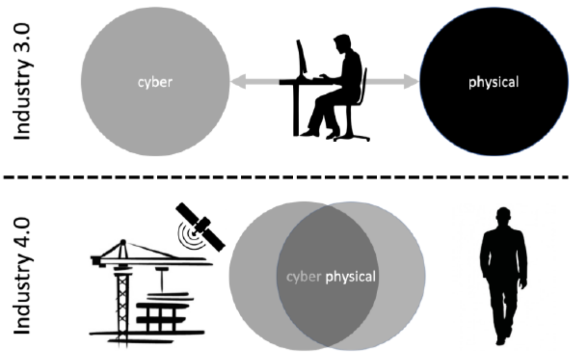

Figure 1: Unification of cyber-physical spaces (Klinc and Turk, 2019)

To help accomplish Industry 4.0 in construction, there is an emerging focus on the development of the Common Data Environment (CDE). A CDE is a tool based on the idea of linking a collaborative project space with cloud technology to form a collaborative platform. Using a CDE, it should then be possible for all project participants to move towards an integral and collaborative approach of project handling.

The CDE is seen as the next evolution of Building Information Modeling (BIM). In the current BIM environment, there has been emphasis on standard formats for data exchange. This helps with interoperability between different authoring software used throughout the project lifecycle by a highly-fragmented supply chain. Recent research and newer standards focus on describing the process and structure for information exchange (Radl and Kaiser, 2019). "OpenBIM" standards enable interoperable and open exchanges while "ClosedBIM" refers to authoring software that does not share data openly. As the concept of a collaborative CDE platforms have developed, the dichotomy between open and closed exchange standards has been extended to refer to the design of CDE's, with emerging references to the "ClosedCDE" and "OpenCDE" (International BuildingSmart, 2019). However, there are limitations to this approach. Such a conceptualization lacks a nuanced view of CDE interoperability, and may be overly reductionist and simplistic. There are different software solutions that can be used as CDE, and specific software for this application is under development.

Therefore, this paper attempts to understand the implications of developing CDE frameworks to interoperability and their resulting ecosystem. To do this, we have analyzed the current emerging CDE systems. We argue that existing terminology for interoperability (e.g., OpenBIM and ClosedBIM) cannot simply be extended to OpenCDE and ClosedCDE. Instead, we propose a new systems-of-systems conceptual paradigm to understand interoperability in consideration of the future requirements to develop such collaborative platforms. These requirements take into consideration underlying data structures and show how current research can possibly be helpful and interlinked. Finally, this paper aims to contribute to the understanding of the current situation and possible future ecosystem of the industry with regard to collaborative platforms.

2. Computer-aided processes to enable AEC collaboration

Collaboration and efficient inter-organizational interactions are key factors for successful project handling within the AEC sector. Construction project teams often consist of different specialist units, which are contributing to the final product within a specific project phase (Wu et al., 2019). Scholars suggest the need for teams to access new technologies that can improve cooperation (Homayouni et al., 2010) and increase efficiency with regard to process, product, and people (Gu and London, 2010).

Since the introduction of the computer-aided processes into the AEC industry, the methodologies used in construction have developed into three separate tracks: computer-based analysis and computing referred to as computational engineering, computer-based design, planning, and construction (CAD), and the computer-based operational, commercial planning and management. The integration of these three aspects into a common information sharing environment started in the early 1990s through document management systems referred to as project space (Borrmann et al., 2018). Later, it was envisaged that new digital tools such as Building Information Modeling (BIM) would enable more efficient collaboration. Many firms today view BIM as the crucial factor for embedding digital processes and digital execution of the project.

2.1 OpenBIM vs. ClosedBIM

Through three-dimensional modeling and semantic aggregation of data, BIM helps individual project participants to handle the information they need. However, these central repositories of building data still represent single silos of information. This makes it difficult for other project participants to access needed information (Lee et al., 2016). The term ***ClosedBIM*** can be used to describe scenarios where different authoring software do not share data openly

The need for data exchange during different stages of the project and between specific domains led to the emergence of a need for seamless collaboration and interoperability to achieve full integration of data (e.g., construction elements, tasks, contracts, costs, and duration). This data is sourced, connected and integrated between all participants involved in a project. Information exchanges occur continuously throughout the project at various levels of detail. This data exchange is possible through the development of the open standard exchange format Industry Foundation Classes (IFC) (Juan and Zheng, 2014). IFC enables different participants, provided with heterogenic systems and applications to simplify their exchange of information and enhanced the level of collaboration. This interoperable open standard exchange is known as ***OpenBIM.***

However, regardless of open or closed, BIM approaches have been limited to deal with data outside of project-specific information. BIM is mostly used through a file-based approach, where silos of information reside within files stored on local machines or common servers. One result of these silos of information is that BIM has been primarily implemented only in the design and construction phases. There has been limited adoption of BIM in the operation and maintenance phase. For large enterprises with multiple business units, the introduction of BIM is primarily carried out in the civil design, geotechnics, and architectural design departments. BIM is used far less in the organization management functions such as financial management, risk assessment, and health and safety organization (Heaton et al., 2019).

2.2 Common Data Environment

In recent years, the use of a ***Common Data Environment*** (CDE) has emerged. The term CDE refers to the use of cloud technology to create a project or central space to handle integral model-based project management. CDE is a collective term for such a framework given by the PAS 1192 (British Standards Institution), processed to the new ISO norm 19650. In a CDE, each stakeholder can call the information from the CDE and in turn store his own data into it. To avoid file-based collaboration, REST-based web interfaces are now increasingly used (Afsari et al., 2016). This enables the deposit of all domain-specific partial models and documents across all different project phases. CDE enables the efficiency and performance of the inter-organizational collaborative process by involving all actors during a project. The methods of the BIM process can be used more frequently in every project phase. The current development of CDE represents an evolution of interoperability in construction.

In particular, the use of CDE extends the methods of the BIM process to be more effective for data generation during later project phases. This can link with the emerging concept of digital twins. Digital twins combine the digital image of a building with sensors and the Internet-of-Things (IoT) to provide real-time data for the continuous recording and provision of data about a building. These digital twin platforms not only enable data preservation in the last life cycle of a building but enabling analytics to predict future events (Sallaba et al., 2017). Therefore, they become a decisive driver for new service concepts such as predictive maintenance and data mining. However, since the foundation of any data aggregation is made in the product's creation phase, the CDE should be considered an important predecessor in the creation of a digital twin platform.

2.3 OpenCDE vs. ClosedCDE?

At first glance, one can observe that the development of CDE is evolving in a similar way to the *open v. closed* BIM dichotomy. Market-leading software vendors, which are already strongly positioned in specific solutions, are already developing customized solutions (Autodesk, 2020). They are promising a high degree of interoperability and connectivity, but exclude any other CDE tools. Consequently, all project participants are bound to one specific product. This might be understood as a ClosedCDE approach.

Meanwhile, CDE solutions based on the IFC exchange format are proposed. These might be interpreted as an OpenCDE approach. Such an approach is based on OpenBIM guidelines and demand open standards for the data exchange of building models. As the primary data basis, this implies that the limitations of the IFC format are still valid. Tailored to the description of a complete building model, it is difficult to map individual products with a digital model. Comprehensive and flexible descriptions of building and product life cycle data are inadequate (Wagner et al., 2019).

As a further step towards improved interoperability between different CDE solutions, the international organization buildingSMART is pursuing a so-called OpenCDE API standardization. Based on the recently adopted DIN SPEC 91391-2 standard, the functional scope and data exchange between different collaborative platforms is defined on a generic basis (Block and Hagedorn, 2019). An Application Programming Interface (API) is a programming interface that serves to exchange information between different applications and individual program parts in a standardized way. The transfer of data and commands is structured according to a previously defined syntax. As a result, the data is delivered in an enterprise-wide environment.

To summarize, the current tendency in the field of CDE is similar to the situation of the interoperability of proprietary authoring file formats. Few industries encompass such diversity in terms of processes, systems, and stakeholders as the construction industry (Borrmann et al., 2018). So far, it seems the emergence of CDE has followed the same dichotomy similar to OpenBIM versus ClosedBIM.

However, there are limitations to this approach. OpenBIM and ClosedBIM are concepts used to establish specific processes for interoperability in a heterogeneous software environment with products from different vendors. To apply such a polarized conceptualization to CDE development may be too simplistic and reductionist. Instead, in the proceeding sections, an argument is made for a new CDE system-of-systems paradigm. This paradigm is evaluated based on degrees of interoperability and in consideration of emerging developments such as digital twin.

3. Proposal for a new CDE system of systems paradigm based on interoperability

As stated by Djuedja et al. (2019) and Poirier et al. (2014), it is primarily the interoperability that prevents a lossless and seamless data exchange within the BIM methodology. Therefore, it is reasonable to consider interoperability not only within BIM use cases but to extend it to the CDE subject. Here, the authors propose a new CDE paradigm based on the n-dimensional interoperability capability of CDE environments based on three dimensions of interoperability. By CDE environments, this paper refers not only to one specific collaborative platform, but also multiple CDE's operating within an ecosystem.

The first dimension is between the tools of one CDE. The second dimension is between the CDE's used within one firm boundaries. The third dimension is between collaborative platforms and digital twin platforms. Table 1 shows as an introduction an exemplary list of the different dimensions of interoperability.

Table 1: Exemplary list of dimensions of interoperability

Dimension of Interoperability	Example
1. Between Tools within one CDE	Using BIM360 with data coming from Navisworks and Revit
2. Between CDE's within a project or firm	Exchange data from tpCDE[1] to Oracle Aconex
3. Between collaborative and digital twin platforms	Delivering information from EPLASS CDE[1] to Bentley iTwin Services[2]

Using these three dimensions, it is possible to indicate in which dimensions a loss-free data exchange and a reversing information flow is possible. This also enables the terms OpenCDE and ClosedCDE to be redefined as a framework rather than a specific process, as will be discussed in detail below. This allows a clear separation of the terms without excluding the existing nomenclature. To demonstrate how this works, three example cases are presented with increasing levels of dimensional interoperability (e.g. 1D, 2D, and 3D).

3.1 One-Dimensional CDE

A one-dimensional CDE is based on the interoperability between tools within a single CDE (see Figure 2). Interoperability is marked as a red arrow in the following figures, while a one-way data exchange is shown with a blue arrow. The top layer (purple) shows a CDE that has been structured based on the OpenBIM approach. The connection between different tools, like design software, calculation, and simulation tools are established by the open standard IFC. The middle layer (blue) shows one-dimensional interoperability is achieved through a common data basis, a common data format, which can only be used by specific tools. An example of such a solution would be Autodesk's BIM 360, which is very restrictive regarding the accepted data formats. Examining the framework, which is simplified by these collaborative platforms as a tier, it can be seen that interoperability is only possible within one layer, within one dimension. Conceptualizing a collaborative platform as a specific layer, figure 2, we see that the five levels of interoperability developed by (Steel et al., 2012) are valid in the first dimension, i.e., within a specific layer.

However, the global structure implies that the system is closed. Interoperability between the different layers is only possible to a limited extent or on the basis of basic file exchange. Specific data records or data particles cannot be exchanged with each other, for example, based on an API. In a simplified scheme, no continuous data exchange is established when using different collaborative solutions within a project. For example, collaboration's CDE in the design phase and another solution for construction progress tracking. At the conclusion of a project phase, a hard-fork is made similar to a Git workflow, i.e., the data is frozen and transferred as a semantic model or information container. Using our proposed conceptualization, this should be called a one-dimensional CDE *regardless of whether the specific layer exchange is based on IFC or Autodesk BIM 360.*

In Figure 2, this methodology is conceptually represented by the light red arrows on the right project layer (orange). This results in a discrete data flow when considering the information flow within the project, which carries risks such as data loss and inconsistency. In addition, it is difficult to access information from a previous phase because the data stream only flows in one direction. This results in a discrete data flow when considering the information flow within

[1] Thinkproject offers two CDE solutions for construction and engineering projects. The tpCDE for construction and engineering projects of any kind and the EPLASS CDE, especially adapted for infrastructure projects.

[2] iTwin Services, developed by Bentley Systems, enables to create, visualize, and analyze digital twins of infrastructure projects and facilities.

the project, which carries risks such as data loss and inconsistency. In addition, it is difficult to access information from a previous phase because the data stream only flows in one direction.

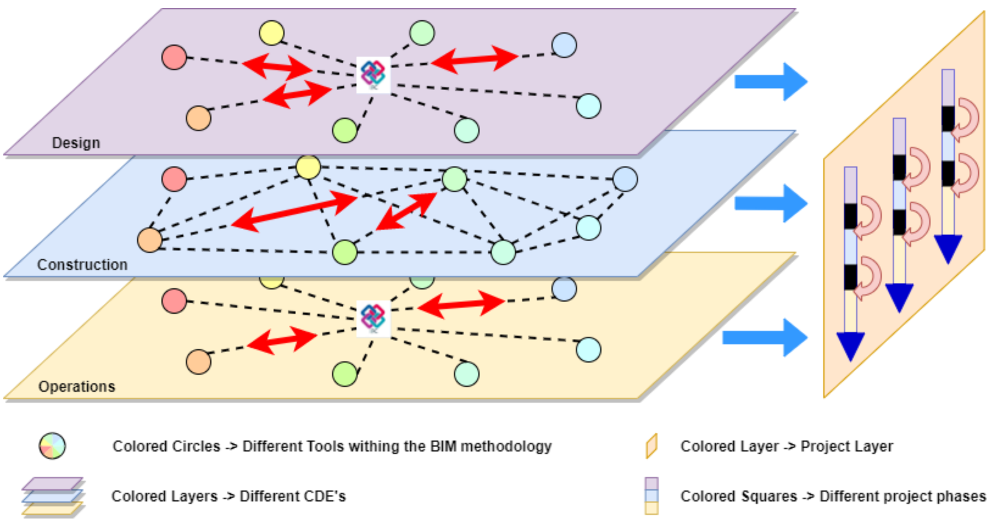

Figure 2: 1-Dimensional Interoperability System – ClosedCDE

3.2 Two-Dimensional CDE

A two-dimensional CDE is characterized by interoperability between CDE's (see Figure 3). A two-dimensional CDE is characterized by interoperability between CDE's. As discussed above, efforts are underway to define a standardized interface between these layers, between different collaborative platforms. The basic principles such as multi-model containers and metadata requirements, which are described in detail in the DIN SPEC 91391-2 standard, are not addressed in this paper. Nevertheless, this reformulated functionality is assumed to be an example of the methodology of a two-dimensional interoperability CDE environment.

The introduction of a common interface leads to the establishment of smooth cooperation in the context of project progress across phase but still within company boundaries. Apart from the underlying data schema of the individual CDE's, it is possible to exchange specific data packets with each other, regardless of which tool it is used by.

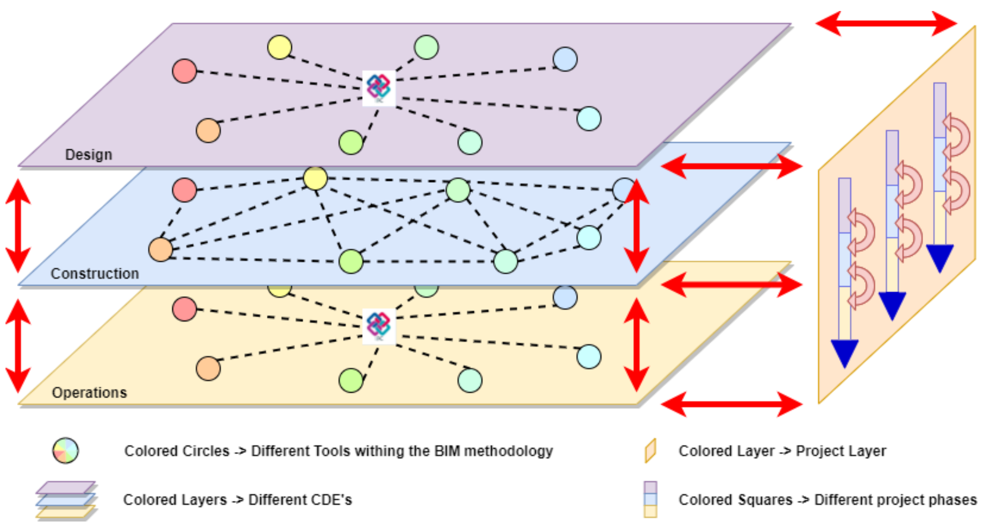

Figure 3: 2-Dimensional Interoperability System - OpenCDE

Data can thus be retrieved in any project phase, even if it originates from a different platform and has been aggregated in a different phase. However, these CDE's must have such an interface implemented to allow correct mapping. The resulting 2D framework refers to a project-level ecosystem of openness. In a global view, a system in which data generated by specific tools and stored in different collaborative solutions are seamlessly connected, again marked as red arrows.

3.3 Three-Dimensional CDE

A three-dimensional CDE is characterized by interoperability between enterprise-level platforms (see Figure 4). These platforms can be digital twins or asset information management platforms held at the enterprise level. While 1D and 2D CDE's are characterized by project-level interoperability, a 3D CDE represents stacks of these CDE's that are linked together. Two specific examples can illustrate the 3D CDE. First, take the provision of information by a general contractor to its subcontractors. Their applications depend on specific data from the collaborative environment and vice versa. This is leading to an ecosystem in which different companies are connected through their collaborative platforms and associated tools at more than a project-by-project basis (see Figure 5).

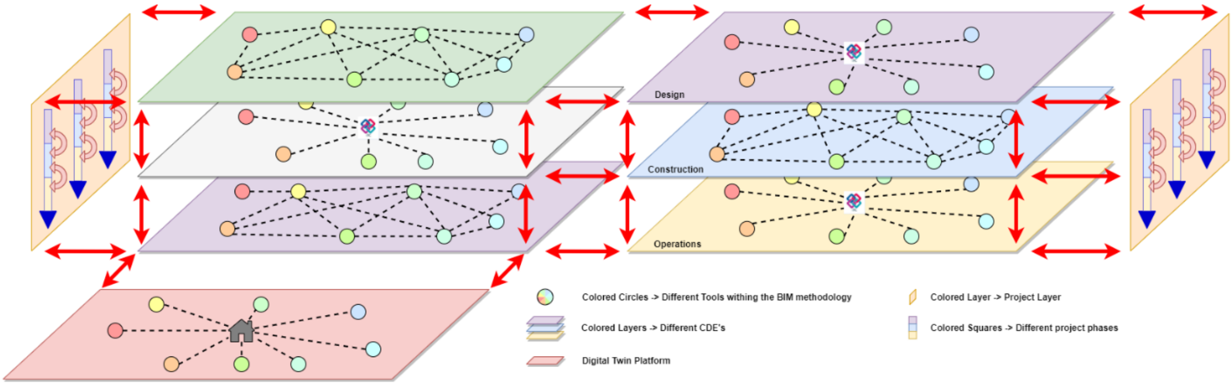

Figure 4: 3-Dimensional Interoperability System

Second, take the mapping of project information to a digital twin system. Digital twin platforms have a high demand for machine readability of data. There is need for interoperability and the ability to seamlessly exchange data is the key factor. Since they can be seen as an extension of the Common Data Environment, it is essential that sensor data as well as monitoring and maintenance information can be losslessly linked to existing data. Present data is very often highly integrated with geometry and semantics, which means that semantic data is linked to geometry through a hierarchical structure. This fact prevents a direct integration of continuous recording into such a schema, as it does not support non-compliant data. Therefore, this third typology, based on three necessary dimensions of interoperability, shows that the detailed study of the data flow and the underlying structure is essential to achieve real interoperability as a cornerstone to industry 4.0. Observing the resulting ecosystem, the countless edges are characteristic (see Figure 5). These represent the data flow between different tools, collaborative platforms, and digital twin platforms. However, there remain questions such as to what extent the complexity caused by the fact that each edge is ultimately also a specific API is conducive to interoperability.

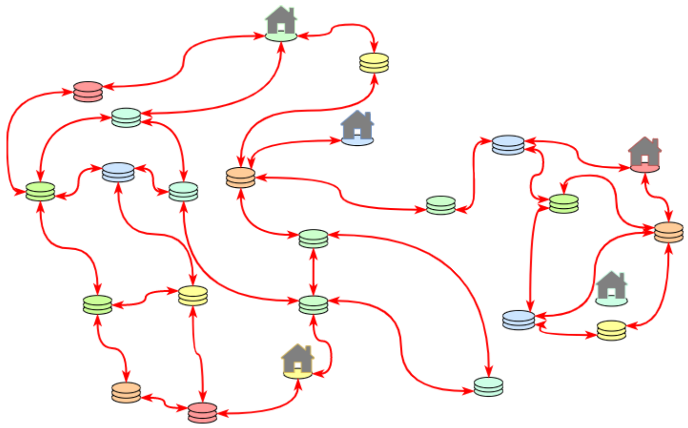

Figure 5: Emerging ecosystem consisting of CDE's and digital platforms

3.4 Discussion and Conclusion

As observed in the development of the described systems of different typologies, the higher the requirement for interoperability, the more important the data basis and its processing becomes.

The current situation is primarily a 1-dimensional interoperability system, regardless if an OpenBIM or ClosedBIM approach is used. Data exchange is mainly achieved within a specific solution. While it is possible for different tools to store their data in a collaborative environment, there is no way to link them further or connect them to external platforms. This makes the formulation and standardization of a common interface for CDE all the more interesting. With the 2-dimensional interoperability framework, a big step towards a real collaboration of different project participants can be achieved. Nevertheless, a common consensus on the data schema used, as conceived in research on the semantic web and linked data, is not established. There is still a need for human intervention to trigger actions. In contrast to this, as discussed by (Pauwels and Terkaj, 2016), when structuring the information base on the foundation of linked data and a web-wide graph, the possibility is opened up for digital agents to interpret this data semantically and use it with minimal human intervention (Werbrouck et al., 2019). This could results in the long-term, that the current trigger-based API, which is based on human actions, will be replaced by a partially self-organizing data set.

If two-dimensional interoperability in a system is possible to establish the loss-free exchange of data via an API, it becomes more difficult with more complex systems. These multi-typological environments, consisting of platforms for not only collaborative work but also for digital twin and others, have a much wider range of data formats, such as the binary data buffer. The resulting requirement on data systems to process a wide variety of formats in a continuous process requires a flexible data structure.

At this point, emerging approaches such as semantic web and linked data can help solve challenges from existing data islands across the digital life cycle in the AEC industry (Pauwels et al., 2017). By formulating a basic data schema, it becomes possible to link different information based on various formats (Pauwels et al., 2017). There is need to avoid restrictive and monopolized formats. Rather, a new basic linkage can be created conceptually (see Figure 7) which aims to solve the current fragmentation of schemas and achieve a higher level of interoperability. Furthermore, this layer also opens up the possibility of connecting data requirements that are still unknown today. While the majority of linked data scholarship has focused on overcoming the challenges of existing exchange formats, there could be future research opportunity to develop an ontology of the CDE with reference to the requirements for a collaborative platform.

With regards to industry 4.0, it is conceivable that today's data formats will never sufficiently support processes such as the interaction of cyber-physical systems (see Figure 6). Therefore, this basic CDE layer promises sufficient flexibility to link future information schemas that promote automation, self-managing systems, and decentralized decision-making processes.

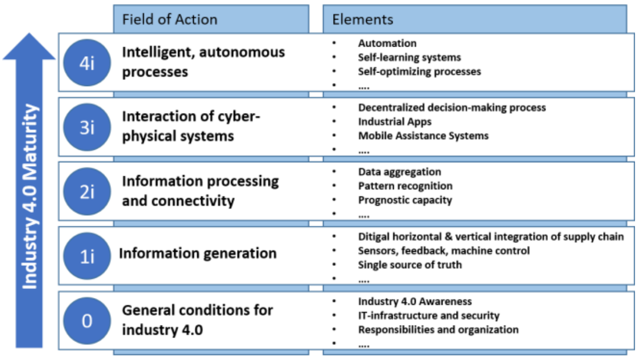

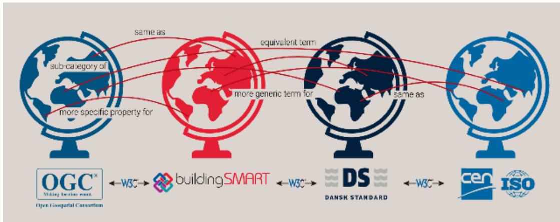

Figure 6 (left): Maturity levels of industry 4.0 (adapted from (Reuter et al., 2016))

Figure 7 (right): New basic linkage through linked data (Rasmussen, 2019)

In addition, we suggest that conceptualizing CDE as *only* a project platform will limit the potential developments of CDE. Instead, a three-dimensional CDE can also serve as the storage environment for design data, productivity, and efficiency at the firm and enable exchanges at the enterprise level. Future research could conduct case studies on the dimension developed for further refinement and assessment of the proposed three-dimensional paradigm.

In summary, there is great value to reconceptualize the interoperability of collaborative systems. From a systems-of-systems perspective, we propose a three-dimensional conceptual framework to move the conversation beyond the open versus closed dichotomy inherited by project-based BIM. The proposed 3D CDE is based on interoperability between Tools within one CDE (1D), between CDE's within a project or company (2D), and between enterprise-level platforms for digital twins and asset information management systems. Highlighting these possible environments and emerging ecosystems can give practice and research a better understanding and overview of the further development of the industry towards *Industry 4.0* and link future CDE work to ongoing research in linked data.

References

Afsari, K., Eastman, C.M., Shelden, D.R., (2016). Cloud-based BIM Data Transmission: Current Status and Challenges Cloud-BIM and Internet of Things (IoT) View project Cloud-based BIM Data Transmission: Current Status and Challenges.

Autodesk, (2020). Autodesk Construction Cloud. URL https://construction.autodesk.com/ (accessed 1.16.20).

Block, M., Hagedorn, P., (2019). Durchgängige Interoperabilität in BIM-basierten Workflows durch den Einsatz von Webschnittstellen. 31. Forum Bauinformatik.

Borrmann, A., König, M., Koch, C., Beetz, J., (2018). Building information modeling: Technology foundations and industry practice, Building Information Modeling: Technology Foundations and Industry Practice. Springer International Publishing, Cham.

Djuedja, J.F.T., Karray, M.H., Foguem, B.K., Magniont, C., Abanda, F.H., (2019). Interoperability challenges in building information modelling (bim). In: Proceedings of the I-ESA Conferences. Springer International Publishing, pp. 275–282.

Gu, N., London, K., (2010). Understanding and facilitating BIM adoption in the AEC industry. Autom. Constr. 19, pp.988–999.

Heaton, J., Parlikad, A.K., Owens, D., Pawsey, N., (2019). BIM as an Enabler for Digital Transformation 2019, pp.49–54.

Homayouni, H., Neff, G., Dossick, C.S., (2010). Theoretical categories of successful collaboration and BIM implementation within the AEC industry. In: Construction Research Congress 2010: Innovation for Reshaping Construction Practice - Proceedings of the 2010 Construction Research Congress. pp. 778–788.

International BuildingSmart, (2019). Oracle Joins as a Strategic Member of buildingSMART International. URL https://www.buildingsmart.org/oracle-joins-as-a-strategic-member-of-buildingsmart-international/ (accessed 5.10.20).

Jan Koeleman, Maria João Ribeirinho, David Rockhill, Erik Sjödin, Gernot Strube, (2019). Decoding digital transformation in construction | McKinsey. McKinsey Co.

Juan, D., Zheng, Q., (2014). Cloud and Open BIM-Based Building Information Interoperability Research. J. Serv. Sci. Manag. 07, pp.47–56.

Klinc, R., Turk, Ž., (2019). Construction 4.0 – Digital Transformation of one the oldest industries 21, pp.292–410.

Lee, D.Y., Chi, H. lin, Wang, J., Wang, X., Park, C.S., (2016). A linked data system framework for sharing construction defect information using ontologies and BIM environments. Autom. Constr. 68, pp.102–113.

Pauwels, P., Terkaj, W., (2016). EXPRESS to OWL for construction industry: Towards a recommendable and usable ifcOWL ontology. Autom. Constr. 63, pp.100–133.

Pauwels, P., Zhang, S., Lee, Y.C., (2017). Semantic web technologies in AEC industry: A literature overview. Autom. Constr.

Poirier, E.A., Forgues, D., Staub-French, S., (2014). Dimensions of Interoperability in the AEC Industry. American Society of Civil Engineers (ASCE), pp. 1987–1996.

Radl, J., Kaiser, J., (2019). Benefits of Implementation of Common Data Environment (CDE) into Construction Projects. IOP Conf. Ser. Mater. Sci. Eng. 471.

Rasmussen,M.H.,(2019)URLhttp://www.student.dtu.dk/~mhoras/presentations/defense.html#/8/11 (accessed 2.16.20).

Reuter, C., Gartzen, T., Prote, J.-P., Fränken, B., (2016). Industrie-4.0-Audit. VDI-Z.

Sallaba, M., Dr. Gentner, A., Esser, R., (2017). TMT_Digital_Twins_Studie_Deloitte.

Steel, J., Drogemuller, R., Toth, B., (2012). Model interoperability in building information modelling. Softw. Syst. Model. 11, pp.99–109.

von Tunzelmann, N., (2003). Historical coevolution of governance and technology in the industrial revolutions. Struct. Chang. Econ. Dyn. 14, pp.365–384.

Wagner, A., Nothstein, C., Rist, T., Hoffmann, A., Huyeng, T.-J., Shi, M., (2019). Zusammenführung Ontologien zur Beschreibung parametrischer, multifunktionaler Bauprodukte in einem Semantic Web Kontext. 31. Forum Bauinformatik.

Werbrouck, J., Pauwels, P., Beetz, J., van Berlo, LéonJeroen Werbrouck , Pieter Pauwels , J.B. and L. van B., (2019). Towards a Decentralised Common Data Environment using Linked Building Data and the Solid Ecosystem. In: Bimal Kumar, Farzad Rahimian, D.G. and T.H. (Ed.), 36th CIB W78 2019 Conference. Newcastle, UK, pp. 113–123.

Wu, G., Zhao, X., Zuo, J., Zillante, G., (2019). Effects of team diversity on project performance in construction projects. Eng. Constr. Archit. Manag. 26, pp.408–423.

Digital Twin in Construction: An Empirical Analysis

Mahmoud El Jazzar[1*], Melanie Piskernik[2**], Hala Nassereddine Ph.D.[1***]
[1] Construction Engineering and Project Management, University of Kentucky, USA
[2] Institute of Interdisciplinary Construction Process Management, Technical University of Vienna, Austria
[*] meljazzar@uky.edu, [**] melanie.piskernik@tuwien.ac.at, [***] hala.nassereddine@uky.edu

Abstract. Construction is one of the most information-intensive industries where information needs to be readily available, accurate, timely, and in a format that is understandable by the recipient. Information needs to be effectively exchanged throughout the lifecycle – from conceptual planning to decommissioning. As Industry 4.0 continues to evolve, it is imperative that construction adopts new technologies. A key element of the Industry 4.0 roadmap is Digital Twin, a digitization technology that allows the physical and virtual space to communicate. While Digital Twin is rapidly being adopted in multiple sectors, the technology has the potential to leverage construction data. This paper synthesizes the current state of practice of Digital Twin in construction by reviewing the extant literature and proposes a framework that classifies the level of integration in construction into three subcategories namely: Digital Model, Digital Shadow, and Digital Twin. A conceptual illustration of Digital Twin in construction is also presented.

1. Introduction

Construction is one of the most information-intensive industries where information needs to be readily available, accurate, complete, timely, and in a clear format that is understandable by the recipient (Xu et al., 2014). Massive data is generated throughout the project lifecycle of a construction project – from conceptual planning to decommissioning. The success of the construction project relies heavily on the management of flow of information and the ability to process the sheer volume of data and extract useful insights (Bilal et al., 2016). Researchers noted that information management is an integral part of the lifecycle of a construction project – from when the information is being generated, transmitted, and interpreted to when the information enables the project to be built, maintained, reused, and eventually recycled (Onyegiri and Nwachukwu, 2011). While the importance of information throughout the project lifecycle has been recognized, studies have focused on information management during design and construction. While these phases are critical, they only account for about 30 to 40 percent of the total project cost (Jiang, 2013). The operating and usage phase is the phase that accounts for the majority of the total project lifecycle (60 to 80 percent) (Jiang, 2013; Nicał and Wodyński, 2016).

Although the construction industry is often labeled as conservative regarding potential advancements in technology and technological applications, it has made significant strides over the past few decades to improve information management through the use of Building Information Modeling (BIM) (Nassereddine et al., 2019). BIM has transformed the traditional paradigm of construction industry from 2D-based drawing information systems to 3D-object based information systems (Arayici et al., 2011; BIM Alliance, n.d.). For more than a decade, BIM has been one of the most important innovation means to approach building design holistically, enhance communication and collaboration among key stakeholders, increase productivity, improve the overall quality of the final product, reduce the fragmentation of the construction industry, and improve its efficiency (Succar, 2009; Schweigkofler et al., 2018). One of the greatest benefits of BIM is its ability to represent in an accessible way the information needed throughout a project lifecycle, rather than being fragmented (Carlsén and Elfstrand, 2018).

While extensive research studies have been conducted to explore the use-cases of BIM and assess its benefits throughout the lifecycle of the construction project, BIM does not capture the data generated during the operating and usage phase (Khajavi et al., 2019). As the fourth wave of technological advancement (Industry 4.0) continues to evolve, it is imperative that construction adopts new technologies. A key element of the Industry 4.0 roadmap is Digital Twin, a digitization technology that is designed to monitor a physical asset and improve its operational efficiency through the collection of real-time data which enables predictive maintenance and results in well-informed decision-making (Khajavi et al., 2019).

Fenn and Raskino (2008) explained that there are five major stages in the growth, dissemination and development of a technology. Collectively, they are referred to as the 'innovation hype cycle,' as depicted in Figure 1. The hype cycle begins with the trigger (step 1) where a breakthrough event or prototype generates interest in an innovation. Once this trigger occurs, there is a rapid increase in hype as the cycle reaches the peak of inflated expectations (step 2). In this stage, advanced companies and consumers seek out the innovation and adopt it early. However, as time passes but before measurable results are returned, impatience produces the trough of disillusionment (step 3). The innovation does not simply waste away into nothingness at this point. Some early adopters and researchers overcome the challenges and begin to reap benefits, then commit to moving forward. This is the slope of enlightenment (step 4). Finally, after the aforementioned enlightenment, the applications of the technology to the real world are defined and the innovation reaches the plateau of productivity (step 5). The growth and lifecycle of Digital Twin can be plotted on the hype cycle, as shown in Figure 1. Per Gartner, who developed the hype cycle, Digital Twin is a promising technology that is still in its developmental phases. As of 2019, Gartner placed it at the peak of inflated expectation (Campos-Ferreira et al., 2019).

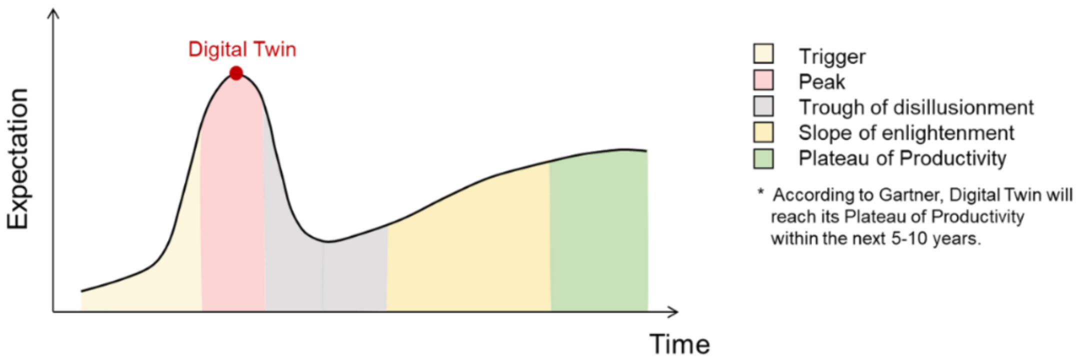

Figure 1: Innovation Hype-Cycle of Digital Twin
[Reproduced from (Campos-Ferreira et al., 2019)]

The main objectives of this research are to gain an understanding of the potential of Digital Twin in the construction industry and suggest a framework that outlines the applications of Digital Twin in construction, its perceived benefits, the challenges associated with its implementation, and the requirements needed to generate a Digital Twin.

The research objectives are achieved through an extensive and comprehensive review of the extant literature on Digital Twin. Research endeavors that have investigated the implementation of Digital Twin in non-construction industries were reviewed, examined, and analyzed to gain a thorough understanding of the origin, evolution, and capabilities of Digital Twin. Research efforts that have discussed the use of Digital Twin in the construction industry were then studied.

2. Digital Twin Concept

The concept of Digital Twin can be traced back to 2002 when Dr. Michael Grieves from the University of Michigan gave a presented on what he called Conceptual Ideal for Product Lifecycle Management (PLM) (Grieves and Vickers, 2016). The PLM concept, which has all the elements of the Digital Twin, considers that each system consists of two systems: the physical system or the real space that has always existed and a virtual system that contains all the information related to the physical system. These two systems are linked and thus, information flow is enabled between the physical and virtual systems (Grieves and Vickers, 2016). The first Digital Twin implementation was in 2010 when the National Aeronautics and Space Administration (NASA) on the Apollo program where at least two identical space vehicles were built to allow mirroring or twinning of the condition of the real space vehicle throughout the mission (Campos-Ferreira et al., 2019; Schleich et al., 2017). Schleich et al. (2017) stated the first formal definition of Digital Twin was provided by NASA where Digital Twin was described as “an integrated multiphysics, multiscale, probabilistic simulation of an as-built vehicle or systems that uses the best available physical model, sensor updates, fleet history, etc., to mirror the life of its corresponding flying twin”. Other researches provided a simplified definition of Digital Twin. For example, (Tao et al., 2018) stated that the idea and concept of Digital Twin is composed of the physical product, the virtual product, and the connected data that links the physical and virtual products. The various Digital Twin definitions focus on three components: the physical space, the virtual space, and the connected data.

Concepts and frameworks that contain these three components therefore correspond to the DT concept, but the literature also differs in the level of data integration. Some virtual representations do not allow bidirectional automatic data exchange, whereas this is the case with fully integrated DTs. In order to resolve the definition of uncertainty, (Kritzinger et al., 2018) suggests three subcategories in the DT classification. The Digital Model (DM) has the least data integration, the data flow between the physical object and the digital is done manually. Changes in the state of the digital or physical object have no direct impact on the state of the counterpart. When the data transfer between physical and digital objects takes place automatically, one speaks of the Digital Shadow (DS). With full integration of the data flow in both directions between the physical and digital object, it is DT in full expression of the concept.

3. Digital Twin in other industries

With the rapid advances in emerging technologies, industrial interest in Digital Twin has increased in the past decade. Campos-Ferreira et al. (2019) reviewed 644 publications related to Digital Twin between 2014 and 2019 and noted that the number of publications has been exponentially increasing indicating the increased interest in Digital Twin as a promising enabling technology. The analysis of these publications showed that most of the Digital Twin research has been in engineering (35.6 %) and computer science (23.5 %). These two areas include manufacturing, product development, robotics, simulation, communication, analytics and architecture validation. The authors also examined the impact Digital Twin can have and concluded that most of the previous research efforts showed that Digital Twin has the capabilities to improve the product, the design, and the production and to reduce logistics risks. They also noted that Digital Twin is not only used to simulate processes and increase efficiency, but also to predict process behaviors.

In manufacturing, (Kritzinger et al., 2018) argued that the current focus in Digital Twin research is on production planning and control as this area is considered the connecting data link in the production process. Qi and Tao (2018) discussed the application of Digital Twin for product design. They explained that Digital Twin-based product design that allows designers to view, optimize and verify functions of their product. Once the design is finalized and coordinated, the product is sent to the smart factory to be produced. From the input of the raw material to the output of the desired product, the entire process is managed and optimized through Digital Twin. The Digital Twin of the product remains in constant contact with the finished product to monitor it in real time. Subsequently, the Digital Twin can predict the future behavior of the product, which enables proactive maintenance. Using virtual and augmented reality technologies, the maintenance, repair and overhaul processes can also be optimized. Finally, in order to improve the next generation of the product, the data of the product life cycle is collected and inherited.

Another area where Digital Twin is currently being implemented is logistic (Dohrmann et al., 2019). The entire industry is moving towards open interfaces and cloud-based IT systems that enable machine learning and advanced analytics. Examples for the application of Digital Twin in logistics include the following: predicting the conditions inside a packaging using sensor data, the design of warehouses can be optimized by simulating the product, personnel and transport flows in it. Taking these applications a step further, logistics networks could be globally linked and simulated using Digital Twin and geographic information systems (GIS).

As the concept of DT is evolving other industries are adopting DT for increasing their efficiency as well as their product quality. Even though construction is not using DT in its full extend yet, the adoption process already started.

4. Digital Twin in Construction

4.1 Review of Existing Literature

With the increased interest in Digital Twin, the construction industry began to follow suit in this area. While the definition of Digital Twin might seem similar to BIM, construction researchers highlighted the differences between these two concepts. Khajavi et al. (2019) stated that although BIM and Digital Twin have similarities, they differ in multiple ways such as the purpose, technology, the end-users, and the facility life stage. The applications of BIM have been extensively investigated in the body of knowledge of construction. While BIM is used by the architects/engineers during the design phase of the project to perform clash detections and material take-off and by contractors to conduct production control, constructability analysis, site and safety management (Volk et al., 2014), it does not work with real-time data (Khajavi et al., 2019). Digital Twin, however, is implemented to monitor the physical asset and improve its operational efficiency by analyzing real-time parameters (Khajavi et al., 2019). The Digital Twin of a building for example can be used for operation and maintenance purposes by allowing facility managers to perform what-if analysis and ultimately enhance energy utilization and improve residents' comfort (Khajavi et al., 2019). The data collected using a Digital Twin during the operation and maintenance phase of the facility can be saved in a database to be used by architects on future projects (Qi and Tao, 2018). Most applications of Digital Twin in construction are in the operation and maintenance phase of the facility whether the project is residential or industrial.

Existing literature on Digital Twin in construction is not easily found because the term "Digital Twin" is not explicitly mentioned in most papers and, is occasionally referred to as BIM or BIM-FM (facility management).

Shen et al. (2012) presented a framework for an agent-based web service geared towards facility lifecycle information integration. The objective of this framework was to support facility management decisions using data collected throughout the project lifecycle – from planning, to design, to construction. The proposed information integration framework was built using BIM and real-time asset tracking and real-time asses monitoring technologies such as wireless sensors and Radio Frequency Identification (RFID). It is worth mentioning that this integrated approach has been successfully applied to two industrial projects, however, due to the nature of the industries, the authors were unable to share the results.

Dibley et al. (2012) proposed an ontology-based solution for sensor-based building monitoring. The authors developed an intelligent multi-agent software framework, OntoFM, to support real-time monitoring. The framework consisted of several ontologies such as building ontology, sensor ontology, topology ontology, and other supporting ontologies. The developed software was deployed for testing purposes and the results of the validation showed that the framework can address the current challenges facing the use of ontology for building monitoring.

Lee et al. (2013) suggested a system to advance urban facility management and perform status monitoring of urban facilities. This proposed approach can intelligently identify facility risks and prepare the urban facilities management for real-time emergency response. The authors developed and tested a prototype of the proposed Intelligent Urban Facilities Management System (IUFMS). Although the proposed system was performed on simple events of aboveground and underground urban facilities, the results demonstrated a promising approach for facility emergency risk management.

Ko et al. (2013) implemented a comprehensive facility management solution using RFID technology to enhance the efficiency of facility management. A web-based RFID facility management system was developed and consisted of four modules: a data management module to collect maintenance records, a statistical module to graphically display the collected data, a schedule module to ensure the facility functions are normal, and a forecast module to predict the lifetime of complements and avoid facility malfunction using fuzzy neural networks. The system was developed to accommodate the flexibility of the team in arranging maintenance time. The system can be used at different locations at different conditions by different crews on site. The authors concluded that the system minimizes the total operational time and prevents duplicate maintenance activities.

Lin et al. (2014) proposed a new mobile automated BIM-based facility management system (BIMFM) to be used in the operation and maintenance phase by facility management technicians. The mobile BIMFM system was tested on a commercial building project. The results demonstrated the effectiveness of the system, paving the way for improving the efficiency of facility management staff, and facilitating the data updates from facility management to the BIM environment.

Motamedi et al. (2014) provided a framework for generating BIM-based customized visualizations known as Facility management Visual Analytics System (FMVAS). The proposed framework utilizes various sources of building knowledge to assist facility management technicians in finding the root causes of failures. The system consists of four layers: the user interface, the engine, the knowledge base, and the database. FMVAS integrates inspection and maintenance data of the Computerized Maintenance Management System (CMMS) with BIM data and provides users with customized color-coded visualizations using users input, and stored data to show possible root causes of failures in the system.

Kang and Hong (2015) proposed a software architecture to support information interoperability and the effective integration of heterogeneous data obtained from BIM into a GIS-based facilities management system.

Shalabi and Turkan (2017) noted that existing facility management information systems shortcomings lack interoperability and visualization capabilities and highlighted the need for a new approach to optimize data collection for corrective maintenance. They proposed an approach to link BIM and present alarms reported by facility management systems. The automated process shows that data can come from different sources and can be integrated into BIM using IFC. While bidirectional data exchange between the systems still requires future research, this study shows potential for minimizing the lead time in corrective maintenance.

Peng et al. (2017) studied an airport terminal and shows how valuable the integration of data mining, data analysis and BIM can be for building operation and maintenance. The use of BIM and sensor data in the operation and maintenance phase of facilities generates a sheer volume of data that facility managers have access to. Often times, facility managers have to deal with increasingly non-intuitive data sets and also error-prone manual data entries, which results in various challenges. To address this problem, the authors suggested a BIM-based Data Mining approach to analyze the accumulated data and extract meaningful laws and patterns and detect improper records. In this proposed approached, the BIM database is first integrated into a data warehouse. Three different Data Mining methods are then performed one after the other, namely cluster analysis to find relationships of similarity among records, outlier detection technique to clean the database, and improved pattern mining algorithm to find deeper logic links among records. Facility managers work with a few high-quality data records rather than going over an unmanageable number of individual entries.

Arslan et al. (2017) introduced a Highly Archived Distributed Object-Oriented Programming (Hadoop) architecture, which merges BIM and real-time wireless sensor data to reduce safety hazards in facility management. The safety hazards considered in the study are ranked according to their severity for vacant properties fire, vandalism, burglary and undetected water damage. The authors developed a prototype where wireless sensors (motes) were programmed and initialized to record temperature, activity and water values. The raw sensor data was then processed and loaded in the Hadoop storage via Flume, same as the BIM data which was integrated with Scoop. The framework used Hive – a open-source solution to structure the already integrated storage data – to link the stored sensor data to the BIM data considering unique identification of the rooms. The framework can be used to build a proactive safety facility management system, in which facility managers of vacant properties are notified about hazards in real-time.

Suprabhas and Dib (2017) suggested integrating wireless sensor data into facility management. The collected sensor data should be linked and reported via the BIM model, using Construction Operations Building Information Exchange (COBIE) as the exchange format. COBIE is an IFC-based data exchange application that is usually integrated into the BIM modelling software via plugin. The suggested application was designed to assist facility management personnel with early detection of issues and maintenance checks.

Hu et al. (2018) noted that Mechanical, Electrical and Plumbing (MEP) information is currently being transferred to the operation and maintenance phase unstructured or in hard copy. The authors proposed a solution for the intelligent integration of MEP systems into the as-built BIM model. Therefore, an automatic logic chain between the MEP systems was generated by using an algorithm and the equipment is grouped and labeled according to a scheme. To support the delivery of the as-built model extended by MEP information, an algorithm for the generation of GIS maps was proposed. A cross-platform was developed using the extended as-built model and the operation and maintenance management system to perform routine tasks and to respond efficiently to MEP emergencies. The system presented was applied to a case study. The results show that the owners were able to reduce the time and costs by 20 % due to the presentation of the MEP information. Additionally, the maintenance staff was enthusiastic because the solution gives easy access to relevant information, real time visualization is possible, the response time to emergencies is optimized and the overall collaboration is promoted.

Chen et al. (2018) presented a framework which supports automatic scheduling of maintenance work orders to enhance facility maintenance management (FMM) and improve decision-making. The FMM framework was created by linking data from BIM and facility management systems (FMS) through proposing an IFC extension for maintenance tasks. Once BIM and FMS data were integrated, errors in components were visualized and geometrical and semantic information of the dialed component could be extracted from the BIM models. The maintenance work order schedule can be automatically generated using a modified Dijkstra algorithm. The algorithm considers four factors: problem type, emergency level, distance among complements, and location. The feasibility of the proposed framework was validated in indoor and outdoor 3D environments.

4.2 Discussion

After reviewing the literature, the authors noticed that although the concept of Digital Twin was not clearly mentioned in the reviewed publications – the title and abstracts only referred to BIM or BIM-FM – the content corresponds to the concept of Digital Twin. Therefore, the authors are proposing a framework for classifying the existing literature and help the construction industry better understand the level of maturity of Digital Twin in construction. The framework is based on the work of (Kritzinger et al., 2018) who outlined a classification of Digital Twin implementation in manufacturing. Their classification included three subcategories, each having a specific level of data integration. Digital Model is the digital representation of the physical space that does not involve any automated data exchange between the physical and virtual space. Digital Shadow builds on the Digital Model subcategory and enables an automated one-way data flow between the physical and virtual space. Digital Twin takes Digital Shadow a step further where the physical and virtual space are fully integrated in both directions.

Based on the research papers that have been examined and the three classification subcategories defined by (Kritzinger et al., 2018), it can be noted that the construction industry is moving beyond the current BIM practices, which mainly focus on the utilization of Digital Models in design and construction. The majority of the publications reviewed by the authors falls in the Digital Shadow subcategory, which, in the context of the construction industry, indicates that while data is being collected and linked to the BIM model, changes made to the digital models do not lead to changes in the physical space. For example, a MEP-system can be monitored using a Digital Shadow, in case of an emergency the Digital Model would highlight the problem but would not take any action. A fully integrated Digital Twin would not only shut the concerning part of the MEP-system down but would also predict a potential emergency before occurrence and suggest corrective measures. The concept of Digital Twin in construction is illustrated in Figure 2. To archive Digital Twin in its full potential, the initiation should be at an early project phase and throughout the whole lifecycle of a facility. The data collection should start in the design phase using a BIM model. Data should then be continuously updated and gathered throughout the construction project lifecycle to obtain a fully functional as-built model ready for the commissioning phase. In the operation and maintenance phase, the model aggregates data from various sensors (i.e. pressure, heat). The data is stored and analyzed using cloud-computing (i.e. data mining and big data). The virtual representation is then updated in real-time with the essential data and predictions of the behavior of the physical facility. This functionality gives the owner, the facility manager, and the operator of the facility the ability to make informed decisions. The bidirectional communication between the physical and virtual facility also enables proactive maintenance. Moreover, the long-term benefit of applying this concept is to improve the next generations of construction projects using the knowledge captured in the Digital Twin. The analysis of the literature review by subcategory is shown Figure 3.

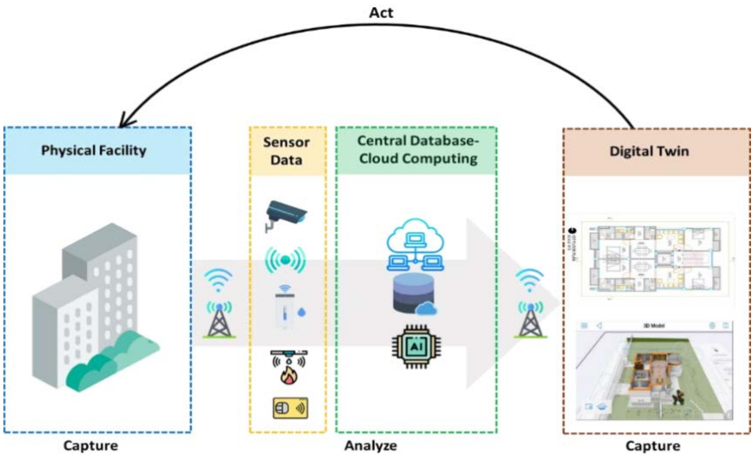

Figure 2: Framework for the implementation of Digital Twin in construction

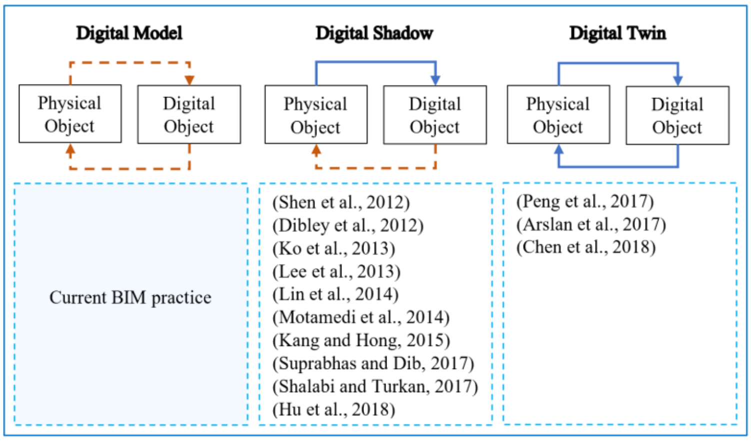

Figure 3: Classification of the existing literature based on Digital Twin integration

While Figure 3 shows that the construction industry is currently in the Digital Model subcategory, it also suggests that the industry is on its way to implement Digital Twin fueled by the increased interest in Digital Shadow, an intermediate step between the current state and the future state (i.e. Digital Twin). Additionally, (Dickopf et al., 2019) outlined the following three-step holistic approach to support this transition: 1) employ simulation tools to understand the facility and analyze various what-ifs scenarios, 2) use the simulated models to leverage the integration of Internet of Things (IoT) to enhance the accuracy and efficiency of predicting future real-data that is expected to be generated throughout the lifecycle of the facility, and 3) collect real-data and leverage it with what was simulated to enhance the performance of the actual facility and influence the early phases of future projects.

5. Conclusion

This paper provided an overview of the origins and definition of Digital Twin and briefly discussed some of the Digital Twin applications in manufacturing and logistics. The current state of Digital Twin in construction was then investigated via literature review and an illustration of the concept of Digital Twin in Construction was proposed. The culminating effort of this study is a framework for understanding the current state of implementation of Digital Twin in the construction industry. The framework was developed through the synthesis of the extant literature and divided the digital-twin related research into three subcategories: Digital Model, Digital Shadow, and Digital Twin. Digital Model has no automated links between physical object and virtual representation (i.e. BIM). Digital Shadow augmented on the Digital Model concept and has one directional link. Digital Twin represents the highest integration level using the bidirectional automated link. The analysis of the framework showed that although construction has made significant strides by going beyond Digital Model, the application of Digital Twin is still not fully accomplished in construction industry. However, it can be concluded that the focus of research is currently being shifted toward Digital Twin. The first step to achieve this shift is to have sufficient data collection and connection to BIM including sensing data by leveraging the research performed in the Digital Shadow subcategory.

References

Arayici, Y., Coates, P., Koskela, L., Kagioglou, M., Usher, C., O'Reilly, K., (2011). BIM adoption and implementation for architectural practices. Struct. Surv. 29, pp.7–25. https://doi.org/10.1108/02630801111118377

Arslan, M., Riaz, Z., Munawar, S., (2017). Building Information Modeling (BIM) Enabled Facilities Management Using Hadoop Architecture, in: 2017 Portland International Conference on Management of Engineering and Technology (PICMET). Presented at the 2017 Portland International Conference on Management of Engineering and Technology (PICMET), IEEE, Portland, OR, pp. 1–7. https://doi.org/10.23919/PICMET.2017.8125462

Bilal, M., Oyedele, L.O., Qadir, J., Munir, K., Ajayi, S.O., Akinade, O.O., Owolabi, H.A., Alaka, H.A., Pasha, M., (2016). Big Data in the construction industry: A review of present status, opportunities, and future trends. Adv. Eng. Inform. 30, pp.500–521. https://doi.org/10.1016/j.aei.2016.07.001

BIM Alliance, n.d. BIM Alliance on BIM. BIM Alliance. URL https://www.bimalliance.se/vad-aer-bim/bim-alliance-om-bim/ (accessed 12.19.18).

Campos-Ferreira, A.E., Lozoya-Santos, J. de J., Vargas-Martınez, A., Mendoza, R.R., Morales-Menendez, R., (2019). Digital Twin Applications: A Review 6.

Carlsén, A., Elfstrand, O., (2018). Augmented Construction: Developing a framework for implementing Building Information Modeling through Augmented Reality at construction sites. Luleå University of Technology.

Chen, W., Chen, K., Cheng, J.C.P., Wang, Q., Gan, V.J.L., (2018). BIM-based framework for automatic scheduling of facility maintenance work orders. Autom. Constr. 91, pp.15–30. https://doi.org/10.1016/j.autcon.2018.03.007

Dibley, M., Li, H., Rezgui, Y., Miles, J., (2012). An ontology framework for intelligent sensor-based building monitoring. Autom. Constr. 28, pp.1–14. https://doi.org/10.1016/j.autcon.2012.05.018

Dickopf, T., Apostolov, H., Müller, P., Göbel, J.C., Forte, S., (2019). A Holistic System Lifecycle Engineering Approach – Closing the Loop between System Architecture and Digital Twins. Procedia CIRP 84, pp.538–544. https://doi.org/10.1016/j.procir.2019.04.257

Dohrmann, K., Gesing, B., Ward, J., (2019). Digital Twins in Logistics - A DHL perspective on the impact of digital twins on the logistics industry.

Fenn, J., Raskino, M., (2008). Mastering the hype cycle: how to choose the right innovation at the right time, Gartner, Inc./Harvard Business School Press series. Harvard Business Press, Boston, Mass.

Grieves, M., Vickers, J., (2016). Origins of the Digital Twin Concept. https://doi.org/10.13140/RG.2.2.26367.61609

Hu, Z.-Z., Tian, P.-L., Li, S.-W., Zhang, J.-P., (2018). BIM-based integrated delivery technologies for intelligent MEP management in the operation and maintenance phase. Adv. Eng. Softw. 115, pp.1–16. https://doi.org/10.1016/j.advengsoft.2017.08.007

Jiang, H., (2013). A System Dynamics Model for Manpower and Technology Implementation Trade-off And Cost Estimation. Electronic Theses and Dissertations 202.

Kang, T.W., Hong, C.H., (2015). A study on software architecture for effective BIM/GIS-based facility management data integration. Autom. Constr. 54, pp.25–38. https://doi.org/10.1016/j.autcon.2015.03.019

Khajavi, S.H., Motlagh, N.H., Jaribion, A., Werner, L.C., Holmstrom, J., (2019). Digital Twin: Vision, Benefits, Boundaries, and Creation for Buildings. IEEE Access 7, pp.147406–147419. https://doi.org/10.1109/ACCESS.2019.2946515

Ko, C.-H., Pan, N.-F., Chiou, C.-C., (2013). Web-based radio frequency identification facility management systems. Struct. Infrastruct. Eng. 9, pp.465–480. https://doi.org/10.1080/15732479.2010.546804

Kritzinger, W., Karner, M., Traar, G., Henjes, J., Sihn, W., (2018). Digital Twin in manufacturing: A categorical literature review and classification. IFAC-Pap. 51, pp.1016–1022. https://doi.org/10.1016/j.ifacol.2018.08.474

Lee, Jaewook, Jeong, Y., Oh, Y.-S., Lee, J.-C., Ahn, N., Lee, Jaehong, Yoon, S.-H., (2013). An integrated approach to intelligent urban facilities management for real-time emergency response. Autom. Constr. 30, pp.256–264. https://doi.org/10.1016/j.autcon.2012.11.008

Lin, Y.-C., Su, Y.-C., Chen, Y.-P., (2014). Developing Mobile BIM/2D Barcode-Based Automated Facility Management System. Sci. World J. 2014, pp.1–16. https://doi.org/10.1155/2014/374735

Motamedi, A., Hammad, A., Asen, Y., (2014). Knowledge-assisted BIM-based visual analytics for failure root cause detection in facilities management. Autom. Constr. 43, pp.73–83. https://doi.org/10.1016/j.autcon.2014.03.012

Nassereddine, H., Veeramani, D., Hanna, A., (2019). Augmented Reality-Enabled Production Strategy Process. Presented at the 36th International Symposium on Automation and Robotics in Construction, Banff, AB, Canada. https://doi.org/10.22260/ISARC2019/0040

Nicał, A.K., Wodyński, W., (2016). Enhancing Facility Management through BIM 6D. Procedia Eng. 164, pp.299–306. https://doi.org/10.1016/j.proeng.2016.11.623

Peng, Y., Lin, J.-R., Zhang, J.-P., Hu, Z.-Z., (2017). A hybrid data mining approach on BIM-based building operation and maintenance. Build. Environ. 126, pp.483–495. https://doi.org/10.1016/j.buildenv.2017.09.030

Qi, Q., Tao, F., (2018). Digital Twin and Big Data Towards Smart Manufacturing and Industry 4.0: 360 Degree Comparison. IEEE Access 6, pp.3585–3593. https://doi.org/10.1109/ACCESS.2018.2793265

Schleich, B., Anwer, N., Mathieu, L., Wartzack, S., (2017). Shaping the digital twin for design and production engineering. CIRP Ann. 66, pp.141–144. https://doi.org/10.1016/j.cirp.2017.04.040

Schweigkofler, A., Monizza, G.P., Domi, E., Popescu, A., Ratajczak, J., Marcher, C., Riedl, M., Matt, D., (2018). Development of a Digital Platform Based on the Integration of Augmented Reality and BIM for the Management of Information in Construction Processes, in: Chiabert, P., Bouras, A., Noël, F., Ríos, J. (Eds.), Product Lifecycle Management to Support Industry 4.0. Springer International Publishing, Cham, pp. 46–55. https://doi.org/10.1007/978-3-030-01614-2_5

Shalabi, F., Turkan, Y., (2017). IFC BIM-Based Facility Management Approach to Optimize Data Collection for Corrective Maintenance. J. Perform. Constr. Facil. 31, 04016081. https://doi.org/10.1061/(ASCE)CF.1943-5509.0000941

Shen, W., Hao, Q., Xue, Y., (2012). A loosely coupled system integration approach for decision support in facility management and maintenance. Autom. Constr. 25, pp.41–48. https://doi.org/10.1016/j.autcon.2012.04.003

Succar, B., (2009). Building information modelling framework: A research and delivery foundation for industry stakeholders. Autom. Constr. 18, pp.357–375.

Suprabhas, K., Dib, H.N., (2017). Integration of BIM and Utility Sensor Data for Facilities Management, in: Computing in Civil Engineering 2017. Presented at the ASCE International Workshop on Computing in Civil Engineering 2017, American Society of Civil Engineers, Seattle, Washington, pp. 26–33. https://doi.org/10.1061/9780784480823.004

Tao, F., Cheng, J., Qi, Q., Zhang, M., Zhang, H., Sui, F., (2018). Digital twin-driven product design, manufacturing and service with big data. International Journal of Advanced Manufacturing Technology 94, pp.3563–3576. https://doi.org/10.1007/s00170-017-0233-1

Volk, R., Stengel, J., Schultmann, F., (2014). Building Information Modeling (BIM) for existing buildings - Literature review and future needs. Autom. Constr. 38, pp.109–127. https://doi.org/10.1016/j.autcon.2013.10.023

Xu, X., Ma, L., Ding, L., (2014). A Framework for BIM-Enabled Life-Cycle Information Management of Construction Project. Int. J. Adv. Robot. Syst. 11, 126. https://doi.org/10.5772/58445

Universitätsverlag der TU Berlin

eg-ice
European Group for Intelligent Computing in Engineering

EG-ICE 2020 Workshop on Intelligent Computing in Engineering

1st–4th July 2020, Online
Proceedings

The 27th EG-ICE International Workshop 2020 brings together international experts working at the interface between advanced computing and modern engineering challenges. Many engineering tasks require open-world resolutions to support multi-actor collaboration, coping with approximate models, providing effective engineer-computer interaction, search in multi-dimensional solution spaces, accommodating uncertainty, including specialist domain knowledge, performing sensor-data interpretation and dealing with incomplete knowledge. While results from computer science provide much initial support for resolution, adaptation is unavoidable and most importantly, feedback from addressing engineering challenges drives fundamental computer-science research. Competence and knowledge transfer goes both ways.

ISBN 978-3-7983-3155-6 (print)
ISBN 978-3-7983-3156-3 (online)

ISBN 978-3-7983-3155-6

http://verlag.tu-berlin.de